

THE ROAD TO THE HYDROGEN FUTURE: RESEARCH & DEVELOPMENT IN THE HYDROGEN PROGRAM

Catherine E. Gregoire Padró
National Renewable Energy Laboratory
1617 Cole Blvd.
Golden, CO 80401

KEYWORDS: hydrogen research; renewable energy; sustainable energy systems

INTRODUCTION

The U. S. Department of Energy (DOE) conducts R&D for the development of safe, cost-effective hydrogen energy technologies that support and foster the transition to a hydrogen economy. Of particular interest is the innovative research supported by the DOE's Hydrogen Program, focused primarily on exploration of long-term, high-risk concepts that have the potential to address large-scale energy needs.

Hydrogen can be produced directly from sunlight and water by biological organisms and using semiconductor-based systems similar to photovoltaics (PV), or indirectly, via thermal processing of biomass. These production technologies have the potential to produce essentially unlimited quantities of hydrogen in a sustainable manner.

Storage of hydrogen is an important area for research, particularly when considering transportation as a major user, and the need for efficient energy storage for intermittent renewable power systems. Although compressed gas and liquid hydrogen storage systems have been used in vehicle demonstrations worldwide, the issues of safety, capacity, and energy consumption have resulted in a broadening of the storage possibilities to include metal hydrides and carbon nanostructures. Stationary storage systems that are high efficiency with quick response times will be important for incorporating large amounts of intermittent PV and wind into the grid as base load power.

In addition to the extensive fuel cell development programs in other offices within DOE, the Hydrogen Program conducts fuel cell research focused on development of inexpensive, membrane electrode assemblies, and the development of reversible fuel cells for stationary applications. The Program also supports research in the development of hydrogen/methane blends and hydrogen-fueled internal combustion engines and generator sets.

A large hurdle to expanded use of hydrogen is public perception. Widespread hydrogen use represents an extraordinary educational challenge, as well as the absolute requirement that safety be intrinsic to all processes and systems. The development of reliable, low-cost hydrogen sensors is an important aspect of the Program, as is the development of codes and standards for the safe use of hydrogen.

DIRECT HYDROGEN PRODUCTION TECHNOLOGIES

The use of solar energy to split water into oxygen and hydrogen is an attractive means to directly convert solar energy to chemical energy. Biological, chemical, and electrochemical systems are being investigated within DOE as long-term (>10 years), high-risk, high-payoff technologies for the sustainable production of hydrogen.

Biological Systems

In nature, algae absorb light and utilize water and CO₂ to produce cell mass and oxygen. A complex model referred to as the "Z-scheme" has been identified to describe the charge separation and electron transfer steps associated with this process that ultimately drives photosynthesis. A number of enzymatic side pathways that can also accept electrons have been identified. Of interest is a class of enzymes known as hydrogenases that can combine protons and electrons obtained from the water oxidation process to release molecular hydrogen. These algal hydrogenases are quickly deactivated by oxygen. Researchers have identified mutant algal strains that evolve hydrogen at a rate that is 4 times that of the wild type, and are 3-4 times more oxygen tolerant [1,2].

Photosynthetic organisms also contain light harvesting, chlorophyll-protein complexes that effectively concentrate light and funnel energy for photosynthesis. These antenna complexes also dissipate excess incident sunlight as a protective mechanism. The amount of chlorophyll antennae in each cell is directly related to the amount of "shading"

experienced by subsequent layers of microorganisms in a mass culture. In a recent set of experiments, researchers have observed that green alga grown under high light intensities exhibit lower pigment content and a highly truncated chlorophyll antennae size. These cells showed photosynthetic productivity (on a per chlorophyll basis) that was 6-7 times greater than the normally pigmented cells [3], a phenomenon that could lead to significant improvements in the efficiency of hydrogen production on a surface-area basis.

These technical challenges are being addressed by a team of scientists from Oak Ridge National Laboratory (ORNL), the University of California Berkeley, and the National Renewable Energy Laboratory (NREL). Various reactor designs are under development for photobiological hydrogen production processes (single-stage vs two-stage, single organism vs dual organism). At the University of Hawaii's Natural Energy Institute (HNEI), a new, potentially low cost, outdoor tubular photobioreactor is under development to test a sustainable system for the production of hydrogen [4].

In addition to the photosynthetic production of hydrogen from water, the Program supports the development of systems to convert CO (found in synthesis gas) to hydrogen via the so-called water-gas shift reaction ($\text{CO} + \text{H}_2\text{O} = \text{CO}_2 + \text{H}_2$). This reaction is essential to the widely-used commercial steam methane reforming process for the production of hydrogen. In the industrial process in use today, high-temperature (450°C) and low-temperature (230°C) shift reactors are required to increase the overall hydrogen production efficiency and to reduce the CO content to acceptable levels. In this project, microorganisms isolated from nature are used to reduce the level of CO to below detectable levels (0.1 ppm) at temperatures of around 25-50°C in a single reactor [5,6]. This process, under development at NREL, has significant potential to improve the economics of hydrogen production when combined with the thermal processing of biomass or other carbon-containing feeds.

Photochemical Systems

Among the technologies that have been investigated, photocatalytic water splitting systems using relatively inexpensive, durable, and nontoxic semiconductor photocatalysts show promise. Supported catalysts such as Pt-RuO₂/TiO₂ have sufficient band gaps for water splitting, although the current rate of hydrogen production from these systems is too low for commercial processes. Modifications to the system are required to address issues such as the narrow range of solar wavelengths absorbed by TiO₂, the efficiency of subsequent catalytic steps for formation of hydrogen and oxygen, and the need for high surface areas. Binding of catalyst complexes that absorb light in the visible range to the TiO₂ should improve the absorption characteristics. Aerogels of TiO₂ as a semiconductor support for the photocatalysts have potential for addressing reaction efficiency and surface area issues. The University of Oklahoma is investigating these systems.

The Florida Solar Energy Center (FSEC), in conjunction with the University of Geneva, is investigating tandem/dual bed photosystems using sol/gel-deposited WO₃ films as the oxygen-evolving photocatalyst, rather than TiO₂. In this configuration, the dispersion containing the wider band gap photocatalyst must have minimal light scattering losses so that the lower band gap photocatalyst behind it can also be illuminated.

Photoelectrochemical Systems

Multijunction cell technology developed by the PV industry is being used to develop photoelectrochemical (PEC) light harvesting systems that generate sufficient voltage to split water and are stable in a water/electrolyte environment. The cascade structure of these devices results in greater utilization of the solar spectrum, resulting in the highest theoretical efficiency for any photoconversion device. In order to develop cost effective systems, a number of technical challenges must be overcome. These include identification and characterization of semiconductors with appropriate band gaps; development of techniques for preparation and application of transparent catalytic coatings; evaluation of effects of pH, ionic strength, and solution composition on semiconductor energetics and stability, and on catalyst properties; and development of novel PV/PEC system designs. NREL's approach to solving these challenges is to use the most efficient semiconductor materials available, consistent with the energy requirements for a water splitting system that is stable in an aqueous environment. To date, a PV/PEC water splitting system with a solar-to-hydrogen efficiency of 12.4% (lower heating value, LHV) using concentrated light, has operated for over 20 hours [7]. HNEI is pursuing a low-cost amorphous silicon-based tandem cell design with appropriate stability and performance, and is developing protective coatings and effective catalysts. An outdoor test of the a-Si cells resulted in a solar-to-hydrogen efficiency of 7.8% LHV under natural sunlight [8].

INDIRECT HYDROGEN PRODUCTION TECHNOLOGIES

These systems offer the opportunity to produce hydrogen from renewable resources in the mid-term (5-10 years). Using agricultural residues and wastes, or biomass specifically grown for energy uses, hydrogen can be produced using a variety of processes.

Biomass pyrolysis produces a bio-oil that, like petroleum, contains a wide spectrum of components. Unlike petroleum, bio-oil contains a significant number of highly reactive oxygenated components derived mainly from constitutive carbohydrates and lignin. These components can be transformed into hydrogen via catalytic steam reforming using Ni-based catalysts. By using high heat transfer rates and appropriate reactor configurations that facilitate contact with the catalyst, the formation of carbonaceous deposits (char) can be minimized. The resulting products from the thermal cracking of the bio-oils are steam reformed at temperatures ranging from 750-850°C. At these conditions, any char formed will also be gasified. At NREL and the Jet Propulsion Laboratory, research and modeling are underway to develop processing technologies that take advantage of the wide spectrum of components in the bio-oil, and address reactivity and reactor design issues [9, 10]. Evaluation of co-product strategies indicates that high value chemicals, such as phenolic resins, can be economically produced in conjunction with hydrogen [11].

Biomass is typically 50 weight % (wt%) moisture (as received); biomass gasification and pyrolysis processes require drying of the feed to about 15 wt% moisture for efficient and sustained operation, in addition to requiring size reduction (particle size of ~1 cm). In supercritical gasification processes, feed drying is not required, although particle size reduction requirements are more severe. A slurry containing approximately 15 wt% biomass (required size reduction ~1 mm) is pumped at high pressure (>22 MPa, the critical pressure of water) into a reactor, where hydrothermolysis occurs, leading to extensive solubilization of the lignocellulosics at just above the supercritical conditions. If heat transfer rates to the slurry are sufficiently high, little char is formed, and the constituents of biomass are hydrolyzed and solubilized in the supercritical medium. Increasing the temperature to ~700°C in the presence of catalysts results in the reforming of the hydrolysis products. Catalysts have been identified that are suitable for the steam reforming operation [12]. HNEL, Combustion Systems Inc., and General Atomics are investigating appropriate slurry compositions, reactor configurations, and operating parameters for supercritical water gasification of wet biomass.

HYDROGEN STORAGE, TRANSPORT, AND DELIVERY

The storage, transport, and delivery of hydrogen are important elements in a hydrogen energy system. With keen interest in mobile applications of hydrogen systems, and as intermittent renewables penetration of the electric grid increases, storage becomes essential to a sustainable energy economy. Light weight and high energy density storage will enable the use of hydrogen as a transportation fuel. Efficient and cost effective stationary hydrogen storage will permit PV and wind to serve as base load power systems.

Compressed Gas Storage Tanks

Currently, compressed gas is the only commercially available method for ambient-temperature hydrogen storage on a vehicle. Compressed hydrogen stored at 24.8 MPa in a conventional fiberglass-wrapped aluminum cylinder results in a volumetric storage density of 12 kg of hydrogen per m³ of storage volume and a gravimetric density of 2 wt% (grams of hydrogen per gram of system weight). Carbon fiber-wrapped polymer cylinders achieve higher densities (15 kg/m³ and 5 wt%), but are significantly below target values required for hydrogen to make major inroads in the transportation sector (62 kg/m³ and 6.5 wt%). Advanced lightweight pressure vessels have been designed and fabricated by Lawrence Livermore National Laboratory [13]. These vessels use lightweight bladder liners that act as inflatable mandrels for composite overwrap and as permeation barriers for gas storage. These tank systems are expected to exceed 12 wt% hydrogen storage (at 33.8 MPa) when fully developed.

Carbon-based Storage Systems

Carbon-based hydrogen storage materials that can store significant amounts of hydrogen at room temperature are under investigation. Carbon nanostructures could provide the needed technological breakthrough that makes hydrogen powered vehicles practical. Two carbon nanostructures are of interest – single-walled nanotubes and graphite nanofibers. Single-walled carbon nanotubes, elongated pores with diameters of molecular dimensions

(12 Å), adsorb hydrogen by capillary action at non-cryogenic temperatures. Single-walled nanotubes have recently been produced and tested at NREL in high yields using a number of production techniques, and have demonstrated hydrogen uptake at 5-10 wt% at room temperature [14]. Graphite nanofibers are a set of materials that are generated from the metal catalyzed decomposition of hydrocarbon-containing mixtures. The structure of the nanofibers is controlled by the selection of catalytic species, reactant composition, and temperature. The solid consists of an ordered stack of nanocrystals that are evenly spaced at 0.34-0.37 nanometers (depending on preparation conditions). These are bonded together by van der Waals forces to form a "flexible wall" nanopore structure. Northeastern University estimates that excellent hydrogen storage capacities are possible in these structures.

Metal Hydride Storage and Delivery Systems

Conventional high capacity metal hydrides require high temperatures (300-350°C) to liberate hydrogen, but sufficient heat is not generally available in fuel cell transportation applications. Low temperature hydrides, however, suffer from low gravimetric energy densities and require too much space on board or add significant weight to the vehicle. Sandia National Laboratories (SNL) and Energy Conversion Devices (ECD) are developing low-temperature metal hydride systems that can store 3-5 wt% hydrogen. Alloying techniques have been developed by ECD that result in high-capacity, multi-component alloys with excellent kinetics, albeit at high temperatures. Additional research is required to identify alloys with appropriate kinetics at low temperatures.

A new approach for the production, transmission, and storage of hydrogen using a chemical hydride slurry as the hydrogen carrier and storage medium is under investigation by Thermo Power Corporation. The slurry protects the hydride from unanticipated contact with moisture and makes the hydride pumpable. At the point of storage and use, a chemical hydride/water reaction is used to produce high purity hydrogen. An essential feature of the process is recovery and reuse of spent hydride at a centralized processing plant. Research issues include the identification of safe, stable and pumpable slurries and the design of an appropriate high temperature reactor for regeneration of spent slurry.

END USE TECHNOLOGIES

Proton exchange membrane (PEM) fuel cells could provide low-cost, high-efficiency electric power, and be operated "in reverse" as electrolyzers to generate hydrogen. There has been a significant increase in industry activity for the development of PEM fuel cells for vehicular applications, with a number of active demonstration projects. Improvements in catalyst loading requirements, water management, and temperature control have helped move these power units from mere curiosities to legitimate market successes. In order to increase the market penetration in both the transportation and utility sectors, additional improvements are required. Los Alamos National Laboratory is developing non-machined stainless steel hardware and membrane electrode assemblies with low catalyst loadings to achieve cost reductions and efficiency improvements [16]. The most important barriers to implementation of low-cost PEM fuel cells are susceptibility of the metal or alloy to corrosion, water management using metal screens as flow fields, and effective stack sealing. Operating the PEM fuel cell "in reverse" as an electrolyzer is possible, but optimum operating conditions for the power production mode and for the hydrogen production mode are significantly different. Design issues for the reversible fuel cell system include thermal management, humidification, and catalyst type and loading.

In an effort to promote near-term use of hydrogen as a transportation fuel, the Program is investigating the development of cost effective, highly efficient, and ultra-low emission internal combustion engines (ICE) operating on pure hydrogen and hydrogen-blended fuels. Research at SNL is focused on the development of a hydrogen fueled ICE/generator set with an overall efficiency of >40% while maintaining near zero NO_x emissions [15].

SAFETY

Hydrogen leak detection is an essential element of safe systems. The development of low-cost fiber optic and thick film sensors by NREL and ORNL, respectively, will provide affordable and reliable options for hydrogen safety systems. NREL is using optical fibers with a thin film coating on the end that changes optic properties upon reversible reaction with hydrogen. Changes in the reflected light signal is an indication of the presence of hydrogen. Sensitivity and selectivity are important research issues. ORNL is focused on the development of monolithic, resistive thick film sensors that are inherently robust,

selective to hydrogen, and easy to manufacture. Research issues include developing appropriate techniques for active (versus traditional passive) thick film applications.

Recognizing the importance of safe use of hydrogen, the DOE, in conjunction with Natural Resources Canada, has compiled a comprehensive document of prevailing practices and applicable codes, standards, guidelines, and regulations for the safe use of hydrogen. The *Sourcebook for Hydrogen Applications* is intended to be a "living document" that can be updated to reflect the current state of knowledge about, and experience with, safely using hydrogen in emerging applications. DOE also supports the development of codes and standards under the auspices of the International Standards Organization.

CONCLUSIONS

The DOE Hydrogen Program conducts R&D in the areas of production, storage, and utilization, for the purpose of making hydrogen a cost-effective energy carrier for utility, buildings, and transportation applications. Research is focused on the introduction of renewable-based options to produce hydrogen; development of hydrogen-based electricity storage and generation systems that enhance the use of distributed renewable-based utility systems; development of low-cost technologies that produce hydrogen directly from sunlight and water; and support of the introduction of safe and dependable hydrogen systems including the development of codes and standards for hydrogen technologies.

REFERENCES

- [1] Ghirardi, M.L., R.K. Togasaki, and M. Seibert, 1997, "Oxygen Sensitivity of Algal Hydrogen Production," *Appl. Biochem. Biotechnol.*, 63-65, 141-151.
- [2] Seibert, M., T. Flynn, D. Benson, E. Tracy, and M. Ghirardi, 1998, "Development of Selection/Screening Procedures for Rapid Identification of Hydrogen-Producing Algal Mutants with Increased Oxygen Tolerance," International Conference on Biological Hydrogen Production, Plenum, NY, in press.
- [3] Melis, A., J. Neidhardt, I. Baroli, and J.R. Benemann, 1998, "Maximizing Photosynthetic Productivity and Light Utilization in Microalgal by Minimizing the Light-Harvesting Chlorophyll Antenna Size of the Photosystems," International Conference on Biological Hydrogen Production, Plenum, NY, in press.
- [4] Szyper, J.P., B.A. Yoza, J.R. Benemann, M.R. Tredici, and O.R. Zaborsky, 1998, "Internal Gas Exchange Photobioreactor: Development and Testing in Hawaii," International Conference on Biological Hydrogen Production, Plenum, NY, in press.
- [5] Maness, P.-C. and P.F. Weaver, 1997, "Variant O₂-Resistant Hydrogenase from Photosynthetic Bacteria Oxidizing CO," Proceedings of the Fifth International Conference on the Molecular Biology of Hydrogenase, Albertville, France.
- [6] Weaver, P.F., P.-C. Maness, and S. Markov, 1998, "Anaerobic Dark Conversion of CO into H₂ by Photosynthetic Bacteria," International Conference on Biological Hydrogen Production, Plenum, NY, in press.
- [7] Khaselev, O. and J.A. Turner, 1998, "A Monolithic Photovoltaic-Photoelectrochemical Device for Hydrogen Production via Water Splitting," *Science*, 280, 425.
- [8] Rocheleau, R., 1998, "High Efficiency Photoelectrochemical H₂ Production using Multijunction Amorphous Silicon Photoelectrodes," *Energy & Fuels*, 12 (1), 3-10.
- [9] Wang, D., S. Czernik, and E. Chomet, 1998, "Production of Hydrogen from Biomass by Catalytic Steam Reforming of Fast Pyrolysis Oil," *Energy & Fuels*, 12 (1), 19-24.
- [10] Miller, R.S. and J. Bellan, 1997, "A Generalized Biomass Pyrolysis Model Based on Superimposed Cellulose, Hemicellulose and Lignin Kinetics," *Comb. Sci. and Technol.*, 126, 97-137.
- [11] Wang, D., S. Czernik, D. Montane, M.K. Mann, and E. Chomet, 1997, "Hydrogen Production via Catalytic Steam Reforming of Fast Pyrolysis Oil Fractions," Proceedings of the Third Biomass Conference of the Americas, Montreal, 845-854.
- [12] Matsunaga, Y., X. Xu, and M.J. Antal, 1997, "Gasification Characteristics of an Activated Carbon in Supercritical Water," *Carbon*, 35, 819-824.
- [13] Mititsky, F., and B. Myers, and A.H. Weisberg, 1998, "Regenerative Fuel Cell Systems," *Energy & Fuels*, 12 (1), 56-71.
- [14] Dillon, A.C., K.M. Jones, T.A. Bekkedahl, C.H. Kiang, D.S. Bethune, and M.J. Heben, 1997, "Storage of Hydrogen in Single-Walled Carbon Nanotubes," *Nature*, 386, 377-279.
- [15] Van Blarigan, P., 1998, "Advanced Hydrogen Fueled Internal Combustion Engines," *Energy & Fuels*, 12 (1), 72-77.
- [16] Cleghorn, S., X. Ren, T. Springer, M. Wilson, C. Zawodzinski, T. Zawodzinski, and S. Gottesfeld, 1997, "PEM Fuel Cells for Transportation and Stationary Power Generation Applications," *Int. J. Hydrogen Energy*, 23, 1137-1144.

HYDROGEN ENERGY: THE GOOD, THE BAD, AND THE ENVIRONMENTALLY ACCEPTABLE

Clovis A. Linkous
Florida Solar Energy Center
1679 Clearlake Road
Cocoa, FL 32922-5703

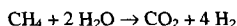
ABSTRACT

Hydrogen is in many respects the ultimate fuel: it is the most abundant element in the universe; as a molecular species it possesses the highest gravimetric energy density of any chemical substance; it can be burned cleanly to produce only water as a reaction product; and its simple and rapid electrode kinetics open the possibility of high efficiency fuel cell-driven power trains. On the other hand, as a gaseous substance under standard conditions, it is inconvenient to use as an on-board fuel without severe compromises with respect to distance between refueling stops; rapid rates of effusion and wide combustibility range limits give rise to safety concerns; and finally, under terrestrial conditions, H_2 is seldom found in Nature—it must be derived from other compounds, often at considerable expense. The various aspects of hydrogen energy combine to paint a picture that is compelling but also technologically challenging.

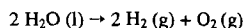
INTRODUCTION

Hydrogen is in many respects the ultimate fuel. First off, it is the most abundant element in the universe. It is estimated that hydrogen makes up 90% of all the atoms or 75% of the mass of the universe. While this fact has little bearing on our current energy economy on Earth, the recent revelation that abundant frozen water deposits may lie below the polar regions of the Moon has galvanized the space technology community over the possibility of producing hydrogen fuel from extraterrestrial sources [1]. While the elemental abundance of hydrogen on earth is also great, almost none of it is found in diatomic molecular form. Free H_2 can be found in the atmosphere at the 0.5 ppm level [2,3], but otherwise it exists principally in combined form with water, biomass, and fossil fuels. H_2 must then be derived from other materials; depending on the source, the energy cost of liberating the hydrogen as H_2 can be quite high, and becomes a major cost component in its manufacture.

For example, H_2 can be had from methane by reaction with steam at 500° C over a Ni catalyst:



The enthalpy of this process per mole of H_2 is only 10.33 kcal, and can be performed with a 65-75% energy efficiency (H_2 heating value out compared to energy input) [4]. In contrast, there is great interest in economically obtaining H_2 directly from liquid water:



Here one is essentially inputting the entire heat of combustion with the hope of getting the free energy back at a later time. The standard enthalpy per mole of H_2 here is 68.3 kcal, a more energetically challenging proposition. Nevertheless, the use of solar based, renewable energy sources to drive the reaction is conceptually very attractive, both from an environmental preservation and a long term sustainability point of view.

While H_2 as a fuel today seems relegated only to certain types of space travel, its energetic nature is in fact greatly in demand as a chemical commodity. US H_2 consumption is already something on the order of 9×10^6 tons/year [5]. Most of this represents internal consumption: the oil refineries account for half of the total, employing it for hydrocracking and hydrodesulfurization; another third is used for ammonia production; much of the remainder is used in methanol production, hydrogenation of polyolefins, and various other chemical and manufacturing processes. The electrolytic production of Cl_2 also yields an equimolar amount of by-product H_2 that is usually used internally for brine concentration or other process heat applications.

Only a few percent of the total is actually sold as a market commodity. Of that, NASA is by far the largest single consumer, requiring some 7000 tons of liquified H_2 per year [5]. Despite its major position in certain industries, annual non-refinery H_2 production (6.7×10^{12} l) represents only 2 day's US gasoline consumption [6].

In Table I, a comparison of relevant fuel properties of H_2 are compared to those of methane, methanol, and gasoline. Many of the superlative characteristics of H_2 are apparent. With the LHV heat of combustion of -57.8 kcal/mol (LHV= lower heating value: product water is left in the vapor state, so that the latent heat of vaporization is not included in the total reaction enthalpy), H_2 is certainly not an exceptional energy producer on a molar basis. However, because it is the lightest element in the Periodic Table, it has a gravimetric energy density of 1.20×10^5 kJ/kg, or 51,590 Btu/lb. This can be compared to jet fuel at about 18,400 Btu/lb, or coal and biomass at 7500 Btu/lb. H_2 has indeed been considered as a substitute for jet fuel: the US Air Force ran Project Bee from 1955-57, where a B-578 twin engine bomber containing a Curtis Wright J-65 turbo-jet engine ran on liquid H_2 [7].

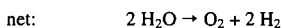
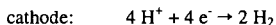
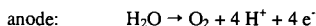
H_2 ELECTROCHEMISTRY

Another asset of H_2 lies in the simplicity of its chemistry. With relatively few bonds being broken and formed, its energy is quickly released. The high intrinsic rate constants enables one to consider the possibility of electrochemically releasing its energy. The exchange current density, or fundamental dynamic charge transfer rate at zero applied voltage, for H_2 discharge on a Pt electrode is 1.0×10^{-3} A/cm² [8]. One can operate a continuous flow hydrogen-air electrochemical cell, or fuel cell, by introducing H_2 to the anode or fuel compartment, and air or O_2 to the cathode or oxidant compartment. Product water is exhausted from the cathode compartment. By utilizing gas diffusion electrodes, where the reactant gases penetrate a thin, finely porous, hydrophobic matrix of fluorocarbon polymer, carbon fiber, and supported noble metal catalyst, current densities in the 100's of mA/cm² can be obtained. This translates to a specific power on order of 100 W/kg.

The free energy of reaction is manifested as a voltage that can be used to power an external load. One is then freed from the Carnot efficiency limitations of combustion engines. Fuel cells offer the possibility of obtaining operating fuel efficiencies of 40-50% for vehicular applications. This represents on order of a 50% improvement in fuel efficiency over internal combustion engines. As an example, to match the range of an average-sized vehicle equipped with an IC engine rated at 19 mpg and carrying 111 lb (18 gal) of gasoline, its H_2 fuel cell counterpart would only need to carry 15 lb of H_2 [9].

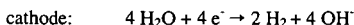
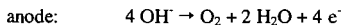
By the same token, one can electrolyze water and produce H_2 by application of a voltage sufficient to exceed its free energy of formation, or 1.23 V:

acidic electrolyte



The mechanism written above assumes an acidic electrolyte. While electrolysis using simple mineral acids is indeed possible, the leading technology at low pH is based on solid polymer electrolytes [10]. Alkaline electrolysis is also possible, and in fact is the most longstanding and least expensive electrolytic technology. The respective half cell reactions then become:

alkaline electrolyte



The energy efficiency of electrolysis is generally taken as 60-80%. These are practical, as opposed to theoretical, values. The basic relationship between current and applied voltage enables one to operate the cell at any desired efficiency. The determining factor is the relationship between current density and capital cost. Smaller voltages make for less energy per volume unit of H_2 , but the current density (H_2 evolution rate per unit area) is also less, and so the electrolyzer must be made larger and more costly for a given H_2 production capacity. An can be run at 99% efficiency, but the H_2 output would be so low as to be impractical.

While generally not as economical as steam reforming of natural gas, electrolysis has already carved out various market niches for H_2 production where the cost of electricity is low, the

availability of natural gas is poor, the required H₂ purity is high, or the required production rate is modest (< 10,000 scf/day).

H₂ STORAGE

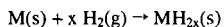
As a gaseous substance under standard conditions, it is inconvenient to use H₂ as an on-board fuel without severe compromises with respect to distance between refueling stops. This is perhaps its greatest limitation, and a large segment of the hydrogen community is committed to increasing the range limits of H₂-fueled travel by reducing the volumetric energy density of the stored material.

The simplest answer is to carry the H₂ as a pressurized gas; unfortunately, the H-content of a standard 2200 psi cast iron vessel is less than one percent [11]. It has been estimated that tank pressure must be increased to >10,000 psi using carbon fiber-reinforced cylinders in order for a H₂-powered vehicle to have the same range as a gasoline-powered one [12].

One can then consider liquifaction as a means of carrying H₂. As a liquid, it has one-tenth the weight of an equal volume of gasoline, but only one-quarter the energy as well. While this represents a tremendous improvement in volumetric energy density over the gaseous state, one should consider that the liquid must be stored at 20.3 K. As a result, vacuum-insulated, stainless steel storage tanks must be used. For vehicles such as NASA's space shuttle, the low surface-to-volume ratio of its 10⁵ plus gallon tanks minimize boil off losses. For domestic transportation, boil-off would be a greater problem, although it is estimated that boil-off could be held to 2% per day [13]. The resulting H-content of an insulated LH₂ storage system would be on order of 20%.

Since the freezing point of H₂ is only 6.5 degrees less than its liquifaction temperature, engineers have sought to increase the LH₂ density by about 15% by mixing solid and liquid to make a slurry, or "slush H₂". It is typically mixed as 50% solids at the triple point of H₂ (13.8 K, 52.8 torr). A further advantage of this approach is that the refrigeration heat capacity is increased by 82.7 kJ/kg, resulting in a 24% increase in the effective heat of vaporization [14,15].

Another way of storing H₂ in the solid state is to combine it with various electropositive metals to form metal hydrides:



There are a number of low molecular weight metal hydrides whose H-contents lie in the 4-7% range, such as CaH₂ and MgH₂. While the numbers may appear low, as noted above, they are well in excess of what can be obtained with conventional pressurized gas cylinder technology. These hydriding reactions are typically exothermic, so that to recover the stored H₂, the hydride must be heated to overcome the enthalpy of formation and shift the equilibrium back toward the free gas. This becomes a problem when the heat of formation of the hydride becomes comparable to the heat of combustion of H₂.

There are some metal alloys for which the hydride heat of formation is low enough that the equilibrium can be controlled at ambient temperature simply by pumping H₂ into and out of the hydride storage bed. Two families of metal alloys that have received much attention are the AB₂'s and the AB₃'s. The former group consists of some combination of low valency first row transition metals, such as Ti, V, and Fe. The latter group is represented by LaNi₅. With H-contents on order of 3%, they represent only a modest improvement over compressed gas. Nevertheless, because of their stability under negative potential in alkaline electrolyte, these materials have attracted great attention in the battery business, where Ni-metal hydride batteries are rapidly replacing Ni-Cd secondaries in high cost portable devices, such as laptop computers.

THE ENVIRONMENTAL IMPERATIVE

The idea of hydrogen energy has been with us since the days of Jules Verne, but events in recent years have begun to stimulate serious public discussion.

One was the push in California to mandate the used of zero emission vehicles. In 1991, California enacted legislation creating a market for clean vehicles that will require significant changes in the automobile of today. A series of categories defining progressively more stringent emissions standards were defined: Transitional Low Emission Vehicles (TLEV); Low Emission Vehicles (LEV); Ultra-Low emission Vehicles (ULEV); and Zero Emission Vehicles (ZEV) [16]. The TLEV will allow hydrocarbon emissions of 0.18 g/mile, 3.4 g/mile of CO, and 0.4 g/mile of NO_x. The ZEV is exactly what it says: 0.0 g/mile for the above pollutants. A H₂-powered fuel

cell vehicle is one of the few that could meet these standards. While the original legislation mandated that by 1998, 2% of all vehicles sold by major automakers must be ZEV's, the California Air Resources Board has since relaxed that requirement until 2003, at which time 10% of sales must qualify [17].

Another recent event is the signing of the Kyoto Protocol. This treaty requires industrialized countries to reduce greenhouse gas emissions on average by 5.2 percent below 1990 levels during the first "commitment period" between 2008 and 2012. There are differentiated targets ranging from 92 and 110 percent of 1990 levels. The US must reduce emissions by 7%. US greenhouse gas emissions in 1990 were estimated at 1.46×10^9 metric tons in carbon equivalent [18].

With the likelihood of future carbon tax assessments, clean burning H_2 is a clear advantage. In truth, H_2 does make for some NO_x formation, as does any fuel using air as oxidant in a combustion process. However, the extent of NO_x formation per energy unit is estimated to be some 80% less than for petroleum-based fuels [19].

SAFE H_2 ?

The H_2 flammability limits vary from 4 to 75% in air, the widest of any fuel. From a safety point of view this is thought to be a negative attribute: leaks that contain H_2 may ignite while other fuels would be too concentrated or too dilute. H_2 detectors should alarm when $[H_2] > 1\%$, at 20-25% lower flammability limit. On the other hand, a plume of H_2 gas leaking into the air quickly rises and dissipates because of its lower density. Engine tolerances must be made more precise to prevent significant blow-by during compression; pronounced "flashback" effects (engine backfire through intake system) require direct cylinder injection.

Just as with natural gas, safety codes will undoubtedly require that an odorant be added to H_2 to alert consumers to leakage. This is a matter of concern to fuel cell manufacturers, who need ultrapure H_2 to prevent poisoning of their noble metal electrocatalysts.

Regardless of the advances made in H_2 energy technology, to achieve widespread acceptance the public image of H_2 must change. Few public conversations on H_2 can go for very long without mention of the either the Challenger space shuttle or Hindenburg disasters. Recently, research by A. Bain has shown that the shell material of the Hindenburg was sufficiently flammable that it would have burned even if the dirigible had been filled with helium [20]. Indeed, there have been less publicized instances where He-filled balloons have caught fire. Burning H_2 produces a largely transparent flame, so that hydrogen's role in the enormous conflagration caught on film in 1937 could only have been indirect.

The economics of H_2 transport basically follow that of natural gas: for many users at close distance, pipeline is the preferred way of transporting H_2 ; for few users at longer distance, liquifaction is cheaper. Much effort has gone into determining whether the existing natural gas pipeline network could some day be used for transporting H_2 . The ability of H_2 to penetrate and embrittle metallic parts is a matter of concern. Carbon steel is embrittled by H_2 , making it more susceptible to stress fractures. The general view is that at modest pressures (< 700 psi) H_2 would be compatible; at higher pressure, seamless stainless steel piping would be necessary [4]. Actually, some 500 miles of pipelines dedicated to H_2 transport currently exist worldwide, with major concentrations in Germany's Ruhr Valley and near LaPorte, Texas [21].

CONCLUSION

While most consider H_2 to be a fuel of the future, it is actually all around us today as a basic chemical commodity. It will always be there when we need it, first from fossil fuels, then biomass, and finally from water. The obvious gravimetric advantage is tempered by its gaseous state. A number of storage technologies offer trade-offs between weight and volume. The simplicity of its chemistry invites the more efficient electrochemical option. Its widespread implementation may ultimately hinge on what levels of air quality our society is willing to accept.

ACKNOWLEDGEMENT

The author would like to thank the many co-workers at the Florida Solar Energy Center who assisted in the preparation of this report, as well as the U.S. Department of Energy, Office of Solar Thermal, Biomass Power, and Hydrogen Technologies, for their financial support.

REFERENCES

- 1- R.A. Kerr, Science, 1998, Vol. 279, 1628.
- 2- W. Zittel and M. Altmann, "Molecular Hydrogen and Water Vapour Emissions in a Global Hydrogen Energy Economy," Hydrogen Energy Progress XI, proceedings of the 11th World Hydrogen Energy Conference, T.N. Veziroglu, C.-J. Winter, J.P. Baselt, and G. Kreysa, eds, Schön and Weitzel GmbH, Frankfurt am Main, 1996, p. 71-81.
- 3- D.R. Lide, ed., CRC Handbook of Chemistry and Physics, 74th edn, CRC Press, Boca Raton, 1974, p. 4-14.
- 4- R.L. Mauro, "The Hydrogen Technology Assessment, Phase I," National Hydrogen Association, Washington, DC, 1994.
- 5- J.R. Birk, B. Mehta, A. Fickett, R. Mauro, and F. Serfass, Hydrogen Energy Progress IX, additive, proceedings of the 9th World Hydrogen Energy Conference, International Association of Hydrogen Energy, p. 101.
- 6- R.L. Bechtold, Alternative Fuels Guidebook. Properties, Storage, Dispensing, and Vehicle Facility Modifications, Society of Automotive Engineers, Warrendale, PA, 1997.
- 7- J.L. Sloop, "Liquid H₂ as a Propulsion Fuel," NASA report SP4404, 1978.
- 8- J.O'M. Bockris and S. Srinivasan, "Electroodic Reactions of Oxygen," ch. 8 in Fuel Cells, McGraw-Hill, New York, 1968.
- 9- "Feasibility Study of Onboard Hydrogen Storage for Fuel Cell Vehicles," US Department of Energy, Office of Transportation Technologies, January, 1993.
- 10- A.B. LaConti, A.R. Fragala, and D.L. Smith, in "Proceedings of the Symposium on Electrode Materials and Processes for Energy Conversion and Storage," J.D.E. McIntyre, S. Srinivasan, and F.G. Will, eds., The Electrochemical Society, Inc., Pennington, NJ, 1977.
- 11- A.J. Appleby, "Fuel Cells and Hydrogen Fuel," Hydrogen Energy Progress IX, proceedings of the 9th World Hydrogen Energy Conference, Paris, France, June 22-25, 1992, T.N. Veziroglu, C. Derive, and J. Pottier, eds, MCI, Paris, 1992, p. 1375-1383.
- 12- D.L. Block, S. Dutta, and A. T-Raissi, "Storage of Hydrogen in Solid, Liquid, and Gaseous Forms," Florida Solar Energy Center, FSEC-CR-204-88, June, 1988.
- 13- W. Strobl and W. Peschka, "Liquid Hydrogen as a Fuel of the Future for Individual Transport," BMW AG Presse, Munich, Germany.
- 14- Fujiwara, M. Yatabe, H. Tamura, M. Takahashi, J. Miyazaki, and Y. Tsuruta, Int. J. Hydrogen Energy, Vol 23, (1998) 333-338.
- 15- R.L. Mauro, "The Hydrogen Technology Assessment, Phase III," National Hydrogen Association, Washington, DC, 1994.
- 16- D.L. Smith, "Strategy for Fuel Cells in Vehicles," National Hydrogen Association, Washington D.C., March 4, 1994, p. 1.
- 17- "Guide to Alternative Fuel Vehicle Incentives and Laws," 2nd edition, November, 1996, U.S. Department of Energy, Clean Cities Program.
- 18- B. Hileman, Chemical and Engineering News, Vol. 74, Jan. 15, 1996.
- 19- "Liquid Hydrogen Powers Third EQHPP Demonstration Bus," Hydrogen and Fuel Cell Letter, P. Hoffmann, ed., Vol. 11, No. 5, May 1996, p. 4.
- 20- M. DiChristina, Popular Science, November 1997, p 71-76.
- 21- "Direct-Hydrogen-Fueled Proton-Exchange-Membrane Fuel Cell System for Transportation Applications," C.E. Thomas, Directed Technologies, Inc., Department of Energy, DOE/CE/50389-502.

Table I. Selected Fuel Properties of Hydrogen, Methanol, and Gasoline

| property | hydrogen | methane | methanol | gasoline |
|---|---|---|----------|-----------|
| molecular weight (g/mol) | 2.018 | 16.043 | 32.042 | 100-105 |
| carbon content (wt %) | 0 | 75 | 37.5 | 85-88 |
| specific gravity | 0.0838 g/l (g) 0.070 g/cm ³ (l) | 0.6512 g/l (g) 0.466 g/cm ³ (l) | 0.796 | 0.69-0.79 |
| boiling point (°C) | -252.87 | -162 | 65 | 27-225 |
| heat of combustion (HHV, kcal/mol) | 68.3 | 212.9 | 173.5 | 1307 |
| lower flammability limit (vol %) | 4.1 | 5 | 7.3 | 1.4 |
| upper flammability limit (vol %) | 75 | 15 | 36 | 7.6 |
| diffusion coefficient (cm ² /s) STP in air | 0.61 | 0.16 | - | 0.05 |

HYDROGEN PRODUCTION FROM HIGH MOISTURE CONTENT BIOMASS IN SUPERCRITICAL WATER

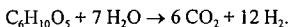
Michael Jerry Antal, Jr. and Xiaodong Xu

Hawaii Natural Energy Institute

University of Hawaii at Manoa, Honolulu, HI 96822

INTRODUCTION

The goal of this work is to define conditions which enable the steam reforming of biomass (represented below as cellulose $C_6H_{10}O_5$) to produce hydrogen:



Earlier work has shown that when biomass is heated quickly in water above its critical pressure, no char is formed. Instead, the biomass decomposes into simple organic molecules dissolved in the water, which further decompose to hydrogen, carbon dioxide, and some methane when exposed to a carbon catalyst at temperatures above 600 °C. In this paper we detail the conditions which evoke the biomass steam reforming chemistry, and we offer insight into the influence of the reactor's wall on the product distribution.

APPARATUS AND EXPERIMENTAL PROCEDURES

The two flow reactors (see Figures 1 and 2) used in this work are fabricated from Hastelloy C276 tubing with 9.53 mm OD x 6.22 mm ID x 1.016 m length. The reactant flow is quickly heated by an annulus heater (located along the reactor's centerline) and an entrance heater outside the reactor to temperatures as high as 800 °C. The annulus heater (3.18 mm OD x 15.2 cm heated length) delivers all its heat directly to the feed. The entrance heater is made from a split stainless steel tube that is held in good thermal contact with the reactor, and an electrical heater which is coiled around the outer surface of the stainless steel tube. Downstream of the entrance heater, the reactor's temperature is maintained in an isothermal condition by the furnace. The chief purpose of the furnace is to prevent heat loss. In fact, in some experiments the temperature setpoint of the furnace was below the lowest temperature measured along the reactor wall. Carbon catalyst is usually packed in about 60% of the heated zone of the reactor, as well as the downstream cold section of the reactor. The reactor's temperature profile is monitored by 12 fixed, type K thermocouples held in good thermal contact with the reactor along its outer wall. Also, in reactor #1 the reactant temperature is measured by a fixed, internal, annulus thermocouple which is located 5.08 cm upstream of the furnace (see Figure 1). Pressure in the reactor is measured by an Omega PX302 pressure transducer. A Grove Mity-Mite model 91 back-pressure regulator reduces the pressure of the cold, two phase, product effluent from 28 to 0.1 MPa. After leaving the back-pressure regulator, the reaction products pass through a gas-liquid separator. The liquid product is collected over a measured time period to calculate the liquid outlet flow rate. The gas flow rate is measured using a wet test meter.

The feeder consists of a cylinder, a movable piston, and two end-caps (High Pressure Equipment). The cylinder is first filled with the feedstock, then the piston is placed on top of the feed, and the two end-caps are installed. Both the feeder and the reactor are pressurized separately to 28 MPa at the beginning of a run. During the time that the system is being brought up to temperature, water is pumped into the reactor by a Waters 510 HPLC pump. When the main body of the reactor reaches the desired temperature (usually about 650 °C), the feeder is connected to the reactor. Thereafter, water flow to the reactor is terminated, and water flow to the feeder is initiated, displacing the sawdust paste feedstock into the reactor. Because the thermophysical properties of the paste are considerably different than those of water, and possibly also because of exothermic pyrolysis reactions associated with the decomposition of the paste, the temperature of the feed rises very rapidly in the entrance region of the reactor. To avoid excessively high temperatures, usually it is necessary to reduce the heat input to the feed from the annulus heater and the entrance heater.

RESULTS

In earlier work we reported the ease of gasification of glycerol in supercritical water. Table 1 confirms the earlier result. In it we see that the hydrogen content of the gas increases from 38% to 51% after 3.45 hr, while the methane content decreases from 20% to 11%. During this time the total gas yield increased from 1.18 to 1.6 L/g and all the carbon in the feedstock was converted to gas. The increasing gas yield is due to the consumption of water and methane by the steam reforming reaction. Evidently this reaction is catalyzed by the reactor's wall and/or the carbon catalyst, which become more active (i.e. "seasoned") as time passes. When the gas yield reached a steady state, the feed was switched and sawdust paste was fed to the reactor for 4

hours. After this, glycerol was again fed to the reactor. Table 1 shows that the sawdust paste causes the reactor's wall and/or the carbon catalyst to lose some activity towards the steam reforming reaction.

The waste product generated by the commercial production of biodiesel fuel contains glycerol and methanol. We prepared a mixture of these two alcohols with a composition identical to that of the industrial waste. The gas produced from this mixture (see Table 2) is very rich in hydrogen, and the yield (2.05 L/g) is high. The water leaving the reactor was clean with a pH of 4-5. Evidently, this waste product is a perfect feedstock for hydrogen production.

As mentioned earlier, we prepare a sawdust paste by mixing wood sawdust into a starch gel, and this paste is easily fed to our reactors. Large quantities of wood sawdust are available at \$30 per dry ton, and the quoted price of corn starch in bulk is \$0.12 per pound. Using these values, the price of a 10 wt % sawdust, 3.65 wt % starch paste is \$0.043 per pound. Similarly, the price of a 20 wt % sawdust, 3.65 wt % starch paste is \$0.031 per pound. For comparison, the price of low sulfur coal is about \$0.025 per pound.

Sawdust paste gasification results from three consecutive runs (no intervening experiments) on different days are displayed in Table 3. In all 3 cases, the reactor plugged after 2 to 3 hours on stream. Although the measured temperatures were similar on 3 and 10 July, the gas yield increased from 1.61 to 2.18 L/g, and the hydrogen content of the gas increased from 43 to 57%. Because fresh carbon catalyst was employed with each experiment, we assumed that the increase in gas yield was due to a seasoning effect of the high temperature in the entrance region on the reactor's wall. To see if the seasoned wall would provide a high gas yield at lower temperatures, we employed a lower entrance temperature in the next experiment (21 July). Remarkably, the results were effectively identical to those of the first experiment. This result, and others indicate that high temperatures are requisite to achieve high gas yields with high hydrogen concentrations from wood sawdust.

CONCLUSIONS

1. A semi-solid gel can be made from 4 wt % (or less) corn starch in water. Wood sawdust and other particulate biomass can be mixed into this gel and suspended therein, forming a thick paste. This paste is easily delivered to a supercritical flow reactor by a cement pump.
2. Above the critical pressure of water, wood sawdust can be steam reformed over a carbon catalyst to a gas composed entirely of hydrogen, carbon dioxide, methane, and a trace of carbon monoxide. There are effectively no tar or char byproducts. The liquid water effluent from the reactor has a low TOC value, a neutral pH, and no color. This water can be recycled to the reactor.
3. The wall affects the gasification chemistry. Products from wood sawdust paste gasification decrease the activity of the wall towards hydrogen production by improving methane yields. These wall effects are strongly temperature dependent. High entrance temperatures strongly favor the methane steam reforming reaction and result in the production of a hydrogen rich gas.

ACKNOWLEDGMENTS

This work was supported by NREL/DOE under cooperative agreement DE-FG36-94AL85804, and the Coral Industries Endowment of the University of Hawaii at Manoa. We thank for useful advice, and Neil Rosmeissl (DOE), Dr. Patrick Takahashi, and Dr. Richard Rocheleau (UH) for their interest in this work. We also thank Jose Arteiro (UH) for assistance with the experiments, Prof. Don Scott (U. Waterloo), Prof. Esteban Chomet (U. Sherbrooke), Prof. Jefferson Tester (MIT), Dave Nahmias, and William Hauserman, Prof. Angela Garcia (University of Alicante), and Professor Galen J. Suppes (University of Kansas) for useful advice.

Table 1. Gas composition from glycerol gasification in supercritical water at 28 MPa with coconut shell activated carbon catalyst using reactor #2 (exp. date: 2/19/98).

| | | | | | |
|--|-----------------------------|------|------|------|--------------------------|
| Feedstock | 18.72 wt% glycerol in water | | | | |
| Reactor peak temp / Catalyst bed temp | 560°C/ 665°C | | | | |
| Flow rate (g/min) | 2.0 | | | | |
| Time on stream (hr) | Before paste ¹ | | | | After paste ² |
| | 1.32 | 2.08 | 2.55 | 3.45 | 5.48 |
| Product | Mole fraction | | | | |
| H ₂ | 0.38 | 0.46 | 0.51 | 0.51 | 0.48 |
| CO | 0.02 | 0.03 | 0.03 | 0.03 | 0.03 |
| CO ₂ | 0.35 | 0.33 | 0.31 | 0.32 | 0.32 |
| CH ₄ | 0.20 | 0.13 | 0.12 | 0.11 | 0.16 |
| C ₂ H ₆ | 0.05 | 0.04 | 0.04 | 0.03 | 0.01 |
| Total gas yield (L gas / g of organics) | 1.18 | 1.40 | 1.49 | 1.60 | 1.60 |
| (g gas / g of organics) | 1.01 | 1.11 | 1.13 | 1.18 | 1.17 |
| C efficiency | 0.96 | 1.00 | 1.00 | 1.01 | 1.01 |
| Global mass balance | 0.99 | 1.01 | 1.01 | 1.02 | 1.02 |

1. Poplar wood sawdust/corn starch paste was fed to the reactor for 4 hours after the gas generation from glycerol reached a steady state.
2. Glycerol was fed to the reactor again after the reactor plugged with the sawdust/corn starch paste.

Table 2. Gas composition from gasification of glycerol/methanol mixture in supercritical water at 28 MPa with coconut shell activated carbon catalyst using reactor #2 (exp. date: 3/13/98).

| | | | | |
|--|-----------------------------------|------|------|------|
| Feedstocks | Simulated biodiesel waste product | | | |
| Reactor peak temp / Catalyst bed temp | 730°C/ 720°C | | | |
| Flow rate (g/min) | 2.0 | | | |
| Time on stream (hr) | 0.42 | 0.73 | 1.25 | 1.68 |
| Product | Mole fraction | | | |
| H ₂ | 0.64 | 0.64 | 0.65 | 0.64 |
| CO | 0.05 | 0.05 | 0.05 | 0.05 |
| CO ₂ | 0.21 | 0.21 | 0.21 | 0.21 |
| CH ₄ | 0.10 | 0.10 | 0.10 | 0.10 |
| Total gas yield (L gas / g of organics) | 2.05 | 2.05 | 2.05 | 2.05 |
| (g gas / g of organics) | 1.25 | 1.22 | 1.24 | 1.20 |
| C efficiency | 1.05 | 1.03 | 1.04 | 1.01 |
| H efficiency | 1.43 | 1.41 | 1.44 | 1.38 |
| O efficiency | 1.36 | 1.32 | 1.35 | 1.31 |
| H balance | 1.04 | 1.03 | 1.04 | 1.03 |
| O balance | 0.99 | 0.98 | 0.99 | 0.98 |
| Global mass balance | 0.98 | 0.97 | 0.98 | 0.97 |

Table 3. Gas composition from poplar wood sawdust / corn starch gasification in supercritical water at 28 MPa with coconut shell activated carbon catalyst on different dates using reactor #1.

| Experiment date | 7/3/97 | 7/10/97 | 7/21/97 |
|---|--|--|---|
| Feedstocks (dry basis) | 10.72 wt% sawdust/ 4.01 wt% corn starch | 11.17 wt% sawdust/ 4.19 wt% corn starch | 11.1 wt% sawdust/ 4.15 wt% corn starch |
| Reactor peak temp / Catalyst bed temp | 790°C/ 685°C | 790°C/ 700°C | 732°C/ 690°C |
| Flow rate (g/min) | 2.0 | | |
| Time on stream (hr) | 1.62 | 1.52 | 1.42 |
| Product | Mole fraction | | |
| H ₂ | 0.43 | 0.57 | 0.45 |
| CO | 0.03 | 0.04 | 0.03 |
| CO ₂ | 0.38 | 0.33 | 0.38 |
| CH ₄ | 0.17 | 0.06 | 0.15 |
| C ₂ H ₆ | 0.001 | 0.001 | 0.0 |
| Total gas yield (L gas /g of organics) | 1.61 | 2.18 | 1.57 |
| (g gas/ g of organics) | 1.37 | 1.65 | 1.48 |
| C efficiency | 0.96 | 1.01 | 1.01 |
| Global mass balance | 1.01 | 1.00 | 0.99 |

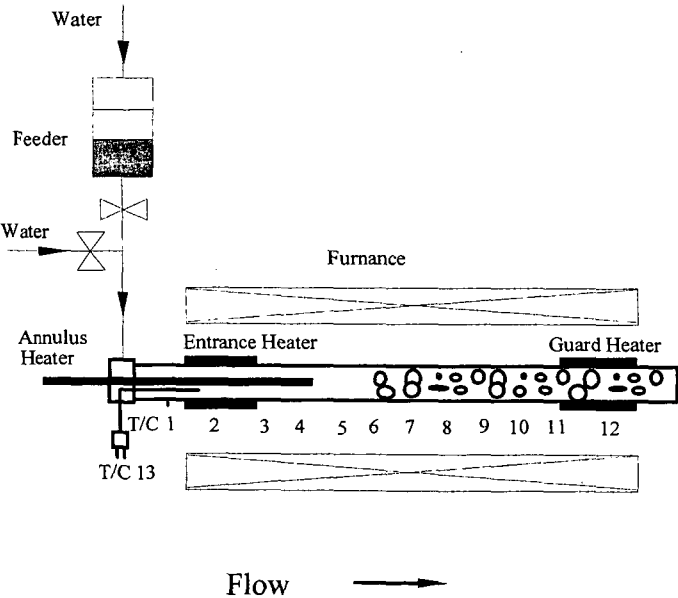


Figure 1. Reactor #1.

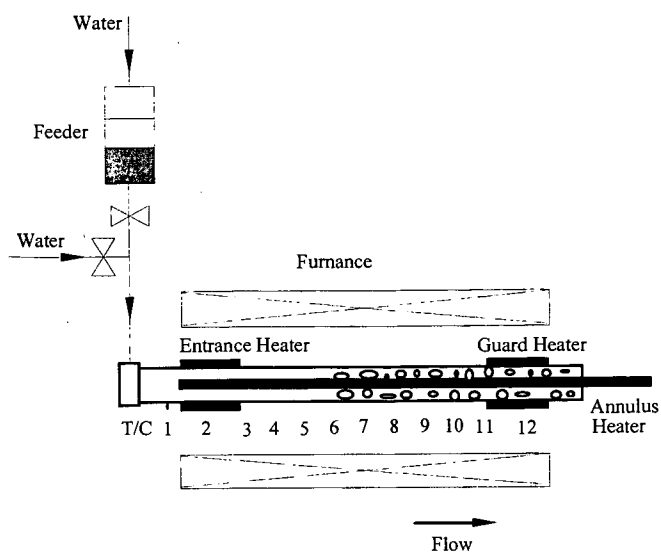


Figure 2. Reactor #2.

DEVELOPMENT OF HYDROGEN STORAGE SYSTEMS BASED ON GRAPHITE NANOFIBERS

C. D. Tan, R. Hidalgo, C. Park and N. M. Rodriguez
Chemistry Department, Hurtig Hall,
Northeastern University, Boston, MA 02115

KEYWORDS: HYDROGEN STORAGE, GRAPHITE NANOFIBERS, CARBON NANOSTRUCTURES

INTRODUCTION

The ever growing demand for energy, as well as the increase in environmental concerns, are exerting pressure for the development of cleaner fuels and more efficient engines. The conventional internal combustion engine currently used in most automobiles produces an array of pollutants including, particulate materials, nitrogen oxides, sulfur oxides, hydrocarbons and carbon monoxide as well as large amounts of carbon dioxide. Although reduction of toxic emissions has been achieved to some degree by the use of the catalytic converter unit, this approach puts great demands on supported noble metal systems, which are required to operate with maximum efficiency over extreme temperature ranges (1).

It has been predicted that oil reserves will peak in about 15 years and therefore, in order to sustain the energy demand it is necessary to find new fuels and more efficient processes. A new technology that is becoming the subject of increasing research effort, is that of fuel cells. In this method, direct conversion from chemical into electrical energy is realized, and consequently, the efficiency of the process is enhanced by almost a factor of three over that of the conventional internal combustion engine, where most of the energy is wasted as heat. Hydrogen and oxygen are the essential reactants for the PEM fuel cells that are being developed for electric vehicles (2,3). A number of factors contribute to the choice of hydrogen as a fuel, not least being the fact that it is one of the most abundant elements found in nature and during its reaction with oxygen the only product is water. Unfortunately, due to the lack of a suitable storage system and a combination of both volume and weight limitations, the driving range of electric vehicles is restricted to about 100 miles. This is one of the shortcomings that has prevented this very promising technology from reaching the commercial arena.

Currently, four methods are being considered for hydrogen storage in commercial applications; pressurized gas storage, liquefied hydrogen, selected metal hydrides and refrigerated super-activated carbon. Pressurized gas offers the advantage of being simple, however, in mobile applications the large volume coupled with the small capacity (8.7 wt. % at 5,000 psi and 7.6 wt. % at 10,000 psi) will limit its practicality. Liquefied hydrogen is expensive since it requires constant refrigeration and loss of the gas by evaporation is inevitable. While the latter two approaches may offer benefits over the other technologies with regard to safety aspects, they do however, have their own set of associated drawbacks. Metal hydrides are heavy, expensive, release heat during the hydrogen absorption process (4) and require the use of about one third of the stored energy during the release of the hydrogen fuel.

Because of their extremely high surface area, active carbons constitute without any doubt the preferred adsorbent in many processes (5-8). Carbon molecular sieves have been known for several decades (9-15) and present an alternative choice for many commercial gas separation processes. These structures are produced from a variety of carbonaceous solids of different origins, including active carbons, cokes, and chars. Activated carbons possess a wide pore size distribution, where the fraction of micro- and nanopores is rather small. While these materials are very effective for the adsorption of a variety of molecules, one has to consider that the interaction between the adsorbent and the adsorbate is only of a physical nature, and as a consequence, the retention of gases is only achieved at extremely low temperatures. The use of activated carbons for gas storage at high temperatures has been found to be ineffective since the solid takes up storage volume without appearing to add any substantial benefits to the overall capacity.

In more recent years there has been a growing interest in the effects of confinement and the influence of the walls of the solid on the gas adsorption process. Indeed, theoretical studies carried out by Gubbins (16-18) using modern statistical mechanic fluids theory indicate that when fluids are restricted within narrow pores, their behavior does not conform to that predicted by classical thermodynamic methods. Non local density functional theory method calculations and molecular simulations have been employed to determine the optimum pore size of carbons for gas adsorption and it was concluded that the ideal system consisted of slit pores bounded by parallel single layers of graphite (16). One of the reasons for this requirement is that in such a configuration, the solid will exhibit the highest ratio of nanopore volume to total volume and as a consequence void space will be eliminated.

In addition, since adsorption of gas molecules on the wall of the pore can cause profound perturbations in the system it is perhaps this aspect that might allow retention of the adsorbate at higher temperatures and at low pressures. It is well known that certain solids, particularly metals, chemisorb gases at room temperature and indeed, this property is routinely used to determine the metal surface area in supported catalyst systems (19). In contrast to physical adsorption, chemisorption requires energy in order to release the adsorbed molecules.

Graphite, is a layered solid in which the various planes are bonded by van der Waals forces where the minimum distance possible between the carbon layers for single crystal graphite is 0.335 nm. In this crystalline structure delocalized π -electrons form a cloud above and below the basal plane and it is this arrangement that imparts a certain degree of metallic character to the solid that results in a relatively high electrical conductivity across each carbon layer. The interlayer spacing in graphitic materials is a property dependent on a number of parameters including, the nature and the thermal history of the precursor, and can vary between 0.335 and 0.342 nm, which by appropriate intercalation procedures can be expanded up to values of 0.9 nm (20,21). Unfortunately, in its conventional form of flat sheets, graphite has an extremely low surface area (~ 0.5 m²/g) resulting from the very small number of edges that are exposed and this aspect has tended to limit its usefulness as a practical selective adsorption agent for small diameter molecules due to diffusion restrictions.

Graphite nanofibers, GNF, are a novel material that has been developed in our laboratory from the metal catalyzed decomposition of certain hydrocarbons (22,23). These structures possess a cross-sectional area that varies between 5 to 100 nm and have lengths ranging from 5 to 100 μ m (24). High-resolution transmission electron microscopy studies have revealed that the nanofibers consist of extremely well-ordered graphite platelets (25), which are oriented in various directions with respect to the fiber axis. The arrangement of the graphene layers can be tailored to a desired geometry by choice of the correct catalyst system and reaction conditions, and it is therefore possible to generate structures where the layers are stacked in a "ribbon", "herring-bone", or "parallel" orientation.

EXPERIMENTAL

Synthesis and Characterization of Graphite Nanofibers

GNF were prepared from the decomposition of ethylene, carbon monoxide and hydrogen mixtures over selected metal powders at temperatures between 500 and 700°C as described in previous publications (22,23). The solids were demineralized by immersing them in a mineral acid solution for a period of a week, washed and dried before testing. GNF were examined by high resolution transmission electron microscopy, temperature programmed oxidation, X-ray diffraction and nitrogen adsorption techniques.

Hydrogen Adsorption/Desorption

Hydrogen adsorption experiments were performed in a custom built unit that consists of two stainless steel vessels. The sample vessel, which is 100 cm³ in volume is connected to the hydrogen reservoir vessel via a high pressure bellows valve. GNF are loaded in the sample container and the entire system evacuated in an oil free

environment for about 5 hours at 150°C. The connecting valve is then closed and the sample cooled to room temperature for several hours. Hydrogen is permitted to enter the reservoir vessel and the pressure allowed to reach thermal equilibrium over a two hour period. The connecting valve is then opened and hydrogen immediately gains access to the sample and undergoes adsorption at room temperature. Blank experiments to determine the various parameters involved during gas expansion were conducted in the absence of GNF and also in the presence of other solids. Approximately 1 gram of GNF was placed in the adsorption unit and allowed to react with hydrogen at 1800 psi at room temperature for a several hours. Changes in pressure were carefully monitored as a function of time. Following adsorption hydrogen was allowed to exit the system and the volume carefully measured by displacement of water. Throughout these processes the adsorption unit was continuously monitored with a high sensitivity H₂ detector to ensure a complete absence of leaks in the system.

RESULTS

TEM examinations of the carbon deposited during the catalytic formation of GNF indicated that under the conditions described above, nanofibers were the only product of the reaction, with no other forms of carbon being present. A high resolution transmission micrograph of the typical appearance of the nanofibers is presented in Figure 1a, where the graphene layers that are separated at a distance of ~ 0.34 nm can be observed. A schematic rendition illustrating the arrangement of graphite platelets within the structure is shown in Figure 1b.

When samples of catalytically grown GNF were placed in the adsorption unit, hydrogen uptake to unprecedented levels was obtained. Certain types of graphite nanofibers were found to be capable of adsorbing and storing extremely high quantities of hydrogen at room temperatures in amounts that were over an order of magnitude higher than that found with conventional materials such as metal hydrides (26). Figure 2 shows two typical isotherms for the adsorption of the hydrogen over a selected sample of GNF. Following the first adsorption, hydrogen was released from the sample and a second adsorption was carried out. Based on the pressure drop of the second uptake it is estimated that this sample of GNF adsorbs over 40 wt % of hydrogen.

DISCUSSION

The extraordinary hydrogen adsorption behavior exhibited by GNF is believed to be due to the unique structure of this molecularly designed solid. The material consists of graphite platelets possessing a small cross-sectional area, which is estimated to be on average 20 nm, combined with an abundance of exposed edges. In addition, since hydrogen possesses a kinetic diameter of 0.289 nm, a value slightly smaller than that of the interlayer spacing in graphite nanofibers, 0.342 nm as measured by X-ray diffraction, adsorption occurs due to the gas being able to readily gain access to the inner regions of the solid. Another aspect of significance in this regard is that the solid consists entirely of non-rigid wall nanopores that extend across the nanofiber.

Following adsorption we found that a significant amount of hydrogen was still retained within the structure and the presence of this stored gas caused the lattice to expand as determined by X-ray diffraction. This finding leads us to conclude that during the adsorption process, the GNF lattice expands in order to accommodate a multi-layer configuration of H₂.

The interaction of hydrogen with graphite surfaces has been investigated using various techniques including neutron scattering (27). It has been concluded that a commensurate $\sqrt{3} \times \sqrt{3}$ structure is achieved at low coverage and an incommensurate layer is observed at monolayer coverage. Following the formation of a second monolayer, a lattice parameter of 0.35 nm is observed. This value is smaller than the measured bulk hexagonal closed packed of 0.376 nm, which suggests that the presence of graphite causes hydrogen to adopt an unusually highly packed structure, thus accounting for the high storage levels measured in the current experiments.

ACKNOWLEDGMENTS

Financial support was provided by the United States Department of Energy, Grant number DE-FC36-97GO10235

REFERENCES

1. K. C. Taylor, in *Automobile Catalytic Converters*, Springer-Verlag, New York, p. 120 (1984).
2. A. J. Appleby and F. R. Foulkes, *Fuel Cell Handbook*, (Van Nostrand) 1989.
3. K. V. Kordesch and G. R. Simader, *Cgem. Rev.* 25, 191 (1995)
4. F. E. Lynch, *J. Less Common Metals* 172, 943 (1991).
5. J. S. Noh, R. K. Agarwal and J. A. Schwarz, *Int. J. Hydrogen Energy*, 12, 693 (1987). US Patent 4,960,450 (1990).
6. J. S. Mattson and H. B. Mark, Jr., "Activated Carbons" Dekker, New York, 1971.
7. B. R. Puri, in "Chemistry and Physics of Carbon" (P. L. Walker, Jr., Ed.) Dekker, New York, 6, 191 (1970).
8. T. Wigmans, in "Carbon and Coal Gasification" (J. L. Figueiredo and J. A. Moulijn, Eds.) NATO ASI Series No. 105, Martinus Nijhoff Publ. Dordrecht, p. 559 (1986).
9. Walker, P. L., Jr., Austin, L. G., and Nandi, S. P., in "Chemistry and Physics of Carbon", (P. L. Walker, Jr., ed.) Vol. 2, p. 257, Marcel Dekker, New York (1966).
10. Koresh, J., and Soffer, A., *J. C. S. Faraday 1*, 76, 2457, 2472 (1980).
11. Koresh, J., and Soffer, A., *J. C. S. Faraday 1*, 77, 3005 (1981).
12. Kapoor, A., and Yang, R. T., *Chem. Eng. Sci.* 44, 1723 (1989).
13. Walker P. L., Jr., *Carbon* 28, 261 (1990).
14. Cabrera, A. L. Zehner J. E., Coe, C. G., Gaffney, T. R., Farris, T. S. and Armor, J. N., *Carbon* 31, 969 (1993).
15. Hynek, S, Fuller, W. and Bentley, J. *Int. J. Hydrogen Energy*, 22, 601 (1997)
16. R. F. Cracknell, K. E. Gubbins, M. Maddox and D. Nicholson, *Accounts of Chemical Research*, 28, 281 (1995)
17. C. Rhykerd, Z. Tan L. A. Pozzhar and K. E. Gubbins, *J. Chem. Soc. Faraday Trans*, 87 2011 (1991)
18. P. B. Balbuena, and K. E. Gubbins, *Langmuir*, 9 1801 (1993)
19. J. R. Anderson, "Structure of Metallic Catalysts" Academic Press, New York, 1975.
20. M. S. Dresselhaus, G. Dresselhaus, K. Suguhara, I. L. Spain, and H. A. Goldberg, "Graphite Fibers and Filaments", Springer-Verlag, Berlin, 1993.
21. M. S. Dresselhaus, and G. Dresselhaus, *Adv. Phys.* 30, 139 (1981).
22. R. T. K. Baker and N. M. Rodriguez, U.S. Patent 5,149,584.
23. M. S. Kim, N. M., Rodriguez and R. T. K. Baker, *J. Catal.* 131, 60 (1991).
24. N. M. Rodriguez, *J. Mater. Res.* 8, 3233 (1993).
25. N. M. Rodriguez, A. Chambers and R. T. K. Baker, *Langmuir* 11, 3862 (1995).
26. C. Park, A. Chambers, R. T. K. Baker and N. M. Rodriguez, *J. Phys. Chem.* in press.
27. M. Nielsen in "Phase Transitions in Surface Films" edited by J.G. Dash and J. Ruvalds. Plenum Press, NY 1980.

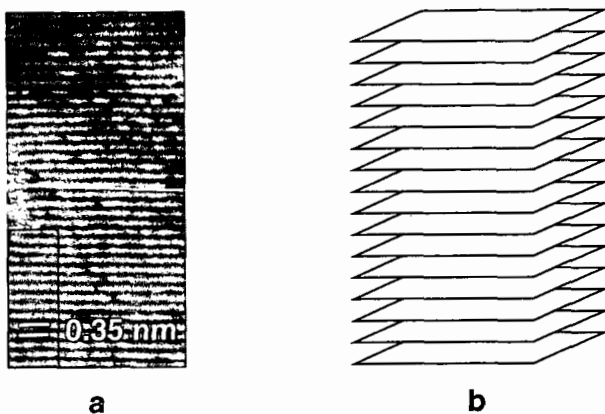


Figure 1. (a) Transmission electron micrograph showing the appearance of a graphite nanofiber produced from the interaction of an iron-based catalyst with carbon containing gases; (b) schematic representation of the arrangement of graphite platelets within GNF marked in a.

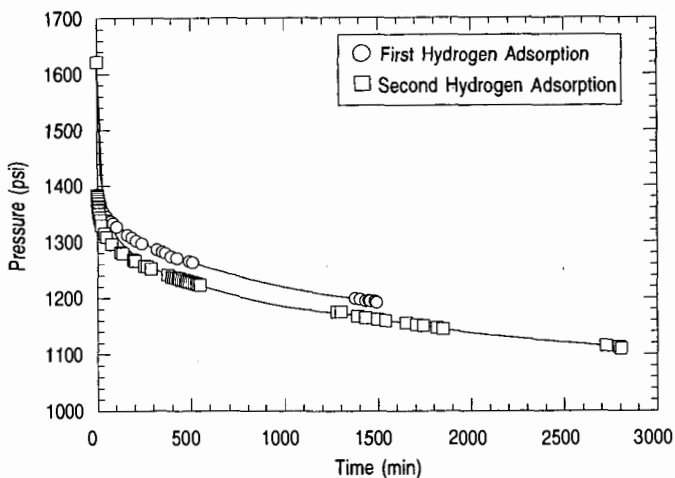


Figure 2. Change in hydrogen pressure as a function of time in the presence of 1.1285 g of GNF at room temperature.

AN OPTIMIZED ALTERNATIVE MOTOR FUEL FORMULATION: NATURAL GAS LIQUIDS, ETHANOL, AND A BIOMASS-DERIVED ETHER

Stephen F. Paul
Plasma Physics Laboratory
Princeton University
Princeton, New Jersey 08543

ABSTRACT

A multi-component, liquid, non-petroleum, alternative motor fuel for spark ignition engines has been developed. The fuel is composed of approximately equal volumes of: (1) medium-molecular weight alkanes, isoalkanes, and cycloalkanes (C₅ - C₈) which are extracted in the course of coalbed gas or natural gas production and/or processing, (2) anhydrous fermentation ethanol, and (3) 2-methylTHF, a biomass-derived heterocyclic ether. The ether serves as a co-solvent that reduces the volatility of the ethanol/hydrocarbon blend. The formulation can be adjusted to vary the fuel characteristics over a range similar to winter/summer and regular/premium gasoline grades: 87 - 94 octane; 0.74 - 0.78 specific gravity; and a 6.5 - 13.5 psi Reid vapor pressure. This fuel contains little or no sulfur, phosphorous, aromatics, olefins, or high-boiling-point hydrocarbons, but does contain 11 - 19% oxygen (by weight), with a corresponding reduction in heat content (100,000 - 106,000 BTU/gal). This fuel has been tested in 1996 and 1997 Ford Taurus ethanol-Flexible Fuel Vehicles which automatically adjust the air/fuel ratio over a wide range. Emissions testing (USEPA's FTP protocol) show the following differences in the tailpipe exhaust characteristics (compared to conventional gasoline): 40 - 50% less unburned hydrocarbons, 20% less CO, no significant change in NO_x, 4% less CO₂, 40% less ozone-forming potential, and 2 - 3 times less toxicity.

BACKGROUND

Natural gas liquids (NGL's) and coalbed gas liquids (CGL's) are underutilized alternatives to crude oil as hydrocarbon sources for spark ignition engine motor fuels. NGL's are recovered from natural gas wells as a gas-saturated liquid condensate.[1] The quantity of hydrocarbons with higher molecular weight is typically about 4 - 5%. Coalbed gases have long been recognized because of explosions that have occurring in the course of coal mining. In New Mexico and Europe, coalbed gas can contain significant amounts of heavier hydrocarbons, with C₂₊ fractions as high as 70%.[2] The liquids are classified by the Gas Processors Association [3] and the American Society for Testing and Materials (ASTM) according to carbon chain length as ethane, propane, n-butane, isobutane and "pentanes plus." Pentanes plus is further subdivided into iso-pentane and "natural gasoline". Pentanes plus are not generally desirable as gasoline is because they have low (65 - 70) octane and a 10 - 13 psi Reid Vapor Pressure (RVP) [4] which results in high evaporative losses and, in severe cases, engine vapor lock in warm weather.

Ethanol (EtOH) is a biomass-derived, octane-increasing motor fuel additive. While neat ethanol has a 2.3 psi RVP, when blended alone with gasoline, the resulting fuel has an RVP much higher than the ideal linear blending-RVP of gasoline ethanol mixtures.[5] This has been analyzed and explained as being a result of the strong dipole moment of ethanol.[6] EtOH's hydrogen bonding reduces its vapor pressure far below that expected from its molecular weight. But when mostly diluted in a non-polar substance such as gasoline, the attractive van der Waals force between the EtOH and the hydrocarbon dominates and is much weaker than the attraction due to hydrogen bonding. The maximum RVP is reached at 5-10% EtOH and is typically 1 psi above the base gasoline.

The situation is considerably more severe in NGL's. The high partial pressures of the low-carbon-number species in gasoline are the main contributors to the RVP. However, the deviation from ideal mixing is a function of the heavy hydrocarbons contained in the fuel.[7] The ideal vapor liquid equilibrium ratio is largely determined by the individual vapor pressure of the diluents and the vapor-phase fugacity coefficient. Non-ideal mixing effects alter the ideal vapor-liquid equilibrium and are parameterized in the activity coefficient. For EtOH, the activity coefficient is a stronger function of the composition of the heavy hydrocarbons than of carbon number. For a carbon number of 7, the activity coefficient for paraffins and naphthenes ranges from 25 - 35, for olefins it is ≈ 18 , and for aromatics, ≈ 11 . For pentanes, the primary constituent in pentanes-plus, it is ≈ 40 . Therefore the aromatic content, absent in NGL's, serves as a co-solvent for mixing EtOH in gasoline.

In the search for a non-toxic, renewable solubilizing agent to replace the aromatics, the solubility of the proposed solvent in both hydrocarbons and EtOH was considered. In general, hydrocarbons are more tolerant of ethers that contain non-polar groups. And ethers are quite tolerant of EtOH: the activity coefficients of EtOH in TAME, ETBE and MTBE are 10, 6.5 and 3.7 respectively. Because of its high density, low solubility in water, and low flashpoint, 2-methyl-tetrahydrofuran (MTHF) was selected as the primary candidate. It is produced from waste cellulosic biomass materials such as corn husks, corn cobs, straw, oat/rice hulls, sugar cane stocks, low-grade waste paper, paper mill waste sludge and wood wastes. It has been considered as a fuel additive to gasoline [8,9]. MTHF has been proposed as a low-cost, low-octane alternative oxygenate to EtOH in conventional gasoline [10]

METHODOLOGY

A fuel composition was prepared by blending 32.5% pentanes-plus, 35% 200 proof anhydrous EtOH, and 32.5% MTHF. The EtOH was pre-blended in the MTHF in order to avoid evaporative loss of the EtOH upon contact with the natural gasoline. The EtOH and MTHF were cooled to 40 °F prior to blending to further minimize evaporative losses. The pentanes-plus were cooled to 40 °F to minimize evaporative losses was poured into a cooled steel mixing tank. The blend of ethanol and MTHF was then added to the pentanes-plus while gently stirring for 5 seconds until a uniform, homogeneous blend was obtained.

The fuel characteristics were obtained in accordance with ASTM Standards.[6] To maintain the ability to test for exhaust emissions on both gasoline, E85 and/or this fuel without any manual engine adjustment, a 1996 Ford Taurus Flexible Fuel Vehicle (ethanol calibration) was used as the test vehicle. This engine includes a fuel sensor that, by measuring the dielectric constant of the fuel, enables it to calculate the concentration of ethanol. The vehicle was not modified between tests.

RESULTS

Hydrocarbon speciation of the NGL's (supplied as C₅⁺ from a natural gas processing plant) was measured using a gas chromatograph shows that the composition of the NGL's was $\approx 46\%$ pentanes, $\approx 33\%$ hexanes, $\approx 14\%$ heptanes, and $\approx 3\%$ octanes. The vapor pressure resulting from diluting EtOH in NGL's is shown in Figure 1. Unlike when blending with gasoline, the concentration of EtOH must exceed 50% to return the RVP down to 10.8 psi, the RVP the NGL's alone. The non-ideal mixing is very apparent in the curvature of the RVP plot. To achieve the 7 - 8 psi requirements of reformulated gasoline, 80- 85% EtOH would have to be blended. This is in distinct contrast to blending MTHF in NGL's, also shown in Figure 1. The RVP decreases in a nearly ideal fashion from the 10.8 psi RVP of the NGL's to the neat RVP of MTHF at 3.2 psi. Also, the MTHF blends with the EtOH, but there is a

stronger decline when the EtOH concentration exceeds 60%. While the solubility seems good, MTHF alone could not be a substitute for the aromatics, because the measured research octane number (RON) is only 86. The motor octane number (MON) is 72, 10 points below the minimum standard for regular fuel and the (R+M)/2 anti-knock index is 79, 9 points below the minimum standard. The low octane of the NGL's (67 measured in this case), means that substantial quantities of EtOH with a RON of 112 and a MON of 96 need be included.

After repeated experimentation, a blend of roughly equal parts of NGL's, EtOH, and MTHF was formulated as described in the methods section. The resulting fuel characteristics are shown in Table 1. The specific gravity, octane, RVP, and heat content are all within ranges detailed by ASTM specification for gasoline, D439-86. However, the distillation properties are quite different. The T₉₀ value indicates the amount of "heavy-end" components (polyaromatics, etc.) fuels. These components are considered to be a source of unburned hydrocarbons during the cold start phase of engine operation. The lower values for the EtOH/MTHF/NGL blends compared to gasoline (T₉₀ is \approx 350°F for gasoline) should reduce HC emissions.

After having been operated for 5,000 miles to age the vehicle's catalyst, the car was tested using the Federal Test Protocol (FTP), the transient driving cycle developed by the USEPA as specified in 40 CFR 86. The vehicle's engine block heater was not used to preheat the engine in any of these tests. The composite weighted results averaged over several (3-10) tests are shown in Table 2. For all the controlled pollutants, all the fuels emit 25-75% less than present federal standards (Tier I) allow at 50,000 miles.

Both the NGL/EtOH/MTHF blend and the CA RFG meet TLEV standards for NMHC. The CA RFG had the lowest NMHC emissions, and nearly met LEV standards, but in one of the three tests, .080 g/mi of NMHC was emitted. E85 emitted nearly 50% more NMHC than indolene, but all of the increase was during the cold-start phase. The low combustion temperature and high heat of vaporization of ethanol results in a longer warm-up period. Despite the 35% ethanol content of the NGL/EtOH/MTHF blend, it showed a 30% reduction in NMHC compared to indolene. reduction in adiabatic flame temperature. During the hot-stabilized portion (phase II) of the FTP, NMHC emissions from the NGL/EtOH/MTHF blend were 78% less than that of indolene.

Carbon monoxide emission was much more comparable among the fuels and was less than Tier I/TLEV/LEV standard of 3.4 g/mi. The NGL/EtOH/MTHF blend, Fed RFG and CA RFG emitted less than the 1.75 g/mi ULEV standard. The NGL/EtOH/MTHF blend emitted 7% less CO than indolene but the measurement error showed that this was not significant. In the stabilized portion (phase II) of the FTP, CO emissions from the summer blend were 49% less than that of indolene.

NO_x emissions for all fuels were less than half the Tier I/TLEV 0.4 g/mi standard and easily met the LEV/ULEV standards at 0.2 g/mile. The fuels containing ethanol had the higher NO_x emissions, though the increase was not proportional to the ethanol content. E85 exhibited an 7% increase in NO_x over indolene. The NGL/EtOH/MTHF blend showed a 30% increase and Federal RFG showed a 27% increase. During the stabilized portion of the FTP, NO_x emissions from the summer blend showed no change from indolene.

REFERENCES

- [1] N. P. Lieberman, Troubleshooting Natural Gas Processing. Tulsa: PenWell, 1987.
- [2] Dudley D. Rice, "Composition and Origins of Coalbed Gas", Hydrocarbons from Coal, Am. Assoc. of Petroleum Geologists Stud. in Geology #38, 1993, p. 159.
- [3] S.L. Montgomery, Editor, "Coalbed Methane: An Old Hazard Becomes a New Resource", Petroleum Frontiers, 3, (1986), Petroleum Information Corp. p. 8.
- [4] Annual Book of ASTM Standards, section 5, American Society for Testing and Materials. Easton, Maryland: ASTM, 1987.
- [5] "Industrial Uses of Agricultural Materials", USDA Economic Research Service, June 1993.
- [6] Ted R. Aulich, Xinming He, Ames A. Grisanti, and Curtis L. Knudson, "Gasoline Evaporation -- Ethanol and Nonethanol Blends", Journal of Air & Waste Management Association, 1994, 44:1004-1009.
- [7] D. Zudkevitch, A.K.S. Murthy, J. Gmehling, "Thermodynamics of reformulated automotive fuels", Hydrocarbon Processing, June 1995, p. 93.
- [8] Rudolph et al., Biomass, 16, 33-49 (1988).
- [9] Lucas et al., SAE Technical Paper Series, No. 932675 (1993).
- [10] S. Fitzpatrick, J Jarnefeld, "Biofine's Voyage from the Lab to the Plant . . .", Proceedings of the Seventh National Bioenergy Conference, SE Regional Biomass Energy Program, 1996, vol. 2, p 1083.

FIGURE 1.

Variation of RVP in 3 mixtures: EtOH in NGL's, MTHF in NGL's, EtOH in MTHF.

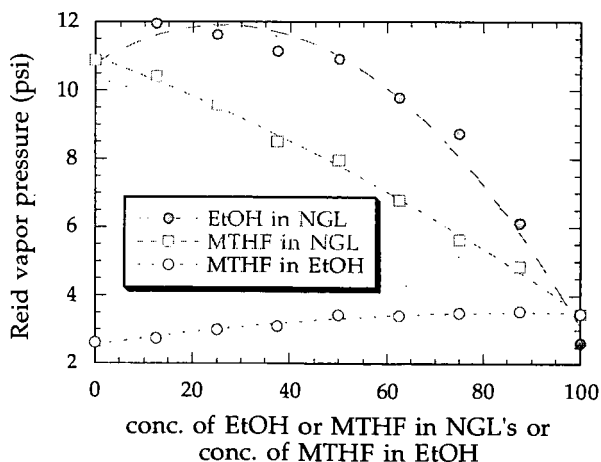


TABLE 1.
ASTM test results for NGL/EtOH/MTHF alternative fuel:

| TEST | METHOD | RESULT | UNITS |
|-----------------------|------------|---------------|--------------|
| API GRAVITY | ASTM D4052 | 52.1 | 60 DEGS F |
| COLOR | VISUAL | UNDYED | |
| DISTILLATION | ASTM D86 | | DEGS F |
| IBP | | 107.0 | |
| 10 PCT EVAPORATED | | 133.2 | |
| 50 PCT EVAPORATED | | 161.8 | |
| 90 PCT EVAPORATED | | 166.9 | |
| FBP | | 195.5 | |
| PCT RECOVERED | | 99.5 | WT. % |
| PCT RESIDUE | | 0.3 | WT. % |
| PCT LOSS | | 0.2 | WT. % |
| RVP, PSI | ASTM D5191 | 8.10 | |
| LEAD | ASTM D3237 | <0.01 | gm/gal |
| RESEARCH OCTANE NO. | ASTM D2699 | 96.8 | |
| MOTOR OCTANE NO. | ASTM D2700 | 82.6 | |
| R+M/2 | ASTM D4814 | 89.7 | |
| COPPER CORROSION | ASTM D130 | 1A | 3 HRS @ 1221 |
| GUM, (AFTER WASH) | ASTM D381 | 2.2 | mg/100 ml |
| SULFUR | ASTM D2622 | 3 | PPM |
| PHOSPHOROUS | ASTM D3231 | <0.004 | gm/gal |
| OXIDATION STABILITY | ASTM D525 | 165 | minutes |
| OXYGENATES -- ETHANOL | ASTM D4815 | 34.87 | PCT VOL |
| OXYGEN | ASTM D4815 | 12.48 | PCT WT |
| BENZENE | ASTM D3606 | 0.15 | PCT VOL |
| V/L 20 | CALCULATED | 135 | DEGS F |
| DOCTOR TEST | ASTM D4952 | POSITIVE | |
| APPEARANCE | VISUAL | BRIGHT/CLEAR | |
| AROMATICS | ASTM D1319 | 0.17/.41 | PCT VOL |
| OLEFINS | ASTM D1319 | 0.09 | PCT VOL |
| MERCAPTAN SULFUR | ASTM D3227 | .0010 | PCT WT |
| WATER TOLERANCE | ASTM D4814 | <-65°C | |
| HEAT CONTENT | ASTM D3338 | 18,663 BTU/lb | |

TABLE 2.

FTP weighted exhaust emissions for several fuels (all figures in grams per mile):

| | Tier I Fed Standards | Et/MTHF alt. fuel | indolene | E85 | Fed RFG | CA RFG Phase II |
|-------------------|-------------------------|----------------------|----------|-------|------------|--------------------|
| NMHC: | 0.25 | 0.085 | 0.122 | 0.142 | 0.136 | 0.071 |
| CO: | 3.40 | 1.66 | 1.78 | 1.82 | 1.70 | 1.47 |
| NO _x : | 0.40 | 0.161 | 0.124 | 0.132 | 0.157 | 0.097 |

notes:

- 1) indolene is EPA certified emissions testing gasoline (40 CFR 86)
- 2) RFG is reformulated gasoline
- 3) NMHC is non-methane hydrocarbons
- 4) CO is carbon monoxide
- 5) NO_x is oxides of nitrogen
- 6) Fed Winter RFG is blended from 92.5% indolene and 7.5% 200-proof ethanol. It is a premium grade (92 octane) winter fuel.
- 7) E85 is blended from 20% indolene and 80% 200-proof ethanol
- 8) CA RFG Phase II is a premium grade (93 octane) reformulated fuel
- 9) NGL/Et/MTHF is an 89 octane, 8.1 psi fuel alt. fuel with the following composition: 35% EtOH, 32.5% MTHF, 32.5% NGL's

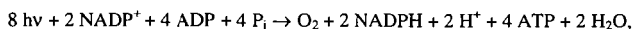
SOLAR HYDROGEN VIA A PHOTOSYNTHETIC Z-SCHEME ANALOGUE BASED ON SEMICONDUCTOR POWDERS

Clovis A. Linkous
Darlene K. Slattery
Florida Solar Energy Center
1679 Clearlake Road
Cocoa, FL 32922-5703

ABSTRACT

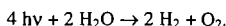
Mother Nature uses solar energy to oxidize water to O_2 and reduce protons onto $NADP^+$ via dual photosystems connected by a string of redox agents. By splitting the energetically challenging task of decomposing water between two separate photochemical reactions, more abundant and lower energy solar photons can be employed. This same approach can be utilized with semiconductor powders. Based upon their electronic band structure, semiconductors can be chosen that selectively oxidize or reduce water. One can then select O_2 -evolving and H_2 -evolving photocatalysts, disperse or immobilize them in separate containers, and use an appropriate reversible redox agent as an electron shuttle between them. We have had some success with this photosynthetic Z-scheme analogue using an alkaline iodate redox electrolyte and a variety of semiconductor compounds, such as TiO_2 and InP . Proof of concept has been demonstrated, but various materials problems underscore the need to identify other photocatalysts.

The scientific community has long marveled at Nature's ability to perform kinetically and/or thermodynamically challenging reactions such as O_2 reduction and N_2 fixation under ambient conditions. In particular, with the rise of mankind's consciousness toward environmental preservation and the need for a sustainable energy supply, we have sought ways to emulate Nature and develop our own approach to the light reaction of photosynthesis, where solar energy is stored by photo-oxidatively decomposing water to O_2 and synthesizing adenosine triphosphate, ATP, and reduced nicotinamide adenine dinucleotide phosphate, NADPH:



where $h\nu$ refers to light quanta and P_i is a phosphate oxyanion, HPO_4^{2-} .

In particular, we would like to skip the various phosphorylations and nicotinamide reductions and simply photo-decompose water to its constituent elements:



This energy-storing reaction would become the basis of the "Solar-Hydrogen Economy."

Even though the water-splitting reaction is mechanistically less ambitious than the overall photosynthetic reaction, the challenge is the same: how to use abundant, relatively low energy photons to drive a chemical system thermodynamically uphill.

Because the water decomposition process can be described in terms of a redox reaction or half cell reactions, it is convenient to look at the free energy relationships in terms of its voltage equivalent. The cell voltage corresponding the standard Gibbs free energy change for water decomposition is:

$$\Delta E^\circ = -\Delta G^\circ / nF = -(-56.6 \times 10^3 \text{ cal/mol})(4.184 \text{ J/cal}) / (2 \text{ equiv/mol})(96485 \text{ Coul/equiv}) \\ = 1.23 \text{ V}.$$

The various photosynthetic reactions can also be viewed in terms of their redox potentials. The general trend is shown in Figure 1a. Mother Nature has developed two photosystems; one for oxidative water splitting, one for reducing $NADP^+$. An electron transfer chain of redox reactions connects them. Note that the redox potential is shifted by an amount corresponding to the energy of the photon that was absorbed. The zigzag shifting of redox potential energy as an electron courses through the photosynthetic light reaction has engendered the appellation "Z-scheme" [1].

To enable water oxidation to occur, a ground state electron must be promoted from an energy level positive of +0.82 V at neutral pH (the standard state value calculated above assumes unit protonic activity, or approximately 1.0 M acid). To reduce the first acceptor state in the electron transfer chain (plastoquinone), one needs a redox potential of about 0.0 V. An excited state electron in chlorophyll *a* at 680 nm has an energy of 1.83 eV; therefore, in analogy to overpotentials in electrolysis, Nature is putting an extra eV of energy into the redox system to make sure there is a driving force on the reaction.

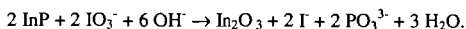
We have been attempting to put together our own water-splitting Z-scheme utilizing immobilized semiconductor powders, or photocatalysts, as our photosystem elements. We needed one material that would be O₂-evolving under illumination, and another that would be H₂-evolving. For this purpose we were able to draw from the wealth of photoelectrochemical work done over the last 25 years. Mainly because of the requirement to exhibit long term aqueous stability, most semiconductor materials are eliminated and only a few choices remain. For the water-oxidizing photocatalyst, there are a number of transition metal oxides that have been used as photoanodes, such as SnO₂, ZnO, WO₃, Fe₂O₃, and TiO₂. For the H₂-evolving photocatalyst, one can consider various photocathode materials; most of these have been metalloid phosphides and arsenides, such as GaP, InP, and GaAs. We chose TiO₂ and InP as the initial photosystem pairing.

To provide an electron transfer chain between our two photosystems, we needed to identify a "redox mediator", a reversible redox couple that would be highly soluble, optically transparent, allow facile charge transfer kinetics between the TiO₂ and InP dispersions. After testing many possible redox couples [2], it was decided to concentrate on the I⁻/IO₃⁻ and Br⁻/BrO₃⁻ systems in alkaline solution. In particular, the IO₃⁻ couple best facilitated an even split of the energy-storing requirement between the two photosystems.

In Figure 1b, the corresponding energy level diagram for the photocatalytic system is shown. The valence band edge of TiO₂ becomes the ground state electronic energy for the reaction center in Photosystem II. The photogenerated hole is easily capable of performing water oxidation. The conduction band is the excited state donor level that injects electrons into the electron transfer chain, which in our case is simply IO₃⁻ ion. Having been reduced to I⁻, the redox mediator migrates to the InP dispersion, or Photosystem I, where it is reoxidized by valence band holes in the InP photocatalyst. Photogenerated electrons in the conduction band of InP are energetically capable of reducing water to H₂.

We have studied each photocatalytic system separately and confirmed that the TiO₂/IO₃⁻ system evolved O₂ and only O₂, and that the InP/I⁻ system evolved H₂ and only H₂. Data for O₂-evolution from various TiO₂ particle dispersions are shown in Table I. The positive effect of adding a 1.0% by weight coating of noble metal co-catalyst is clearly evident. It is also clear that IO₃⁻ or some other electron acceptor must be present to achieve a reasonable photoreaction rate. While TiO₂ is satisfactory in terms of showing proof of concept, with a band gap of 3.0 eV, it is not an effective absorber of solar radiation. Narrower band gap materials need to be identified.

The InP, while showing initial H₂ evolution, would slow to virtually nothing after about an hour of photolysis. This was initially thought to be a form of photocorrosion, but after some control experiments, it became clear that the InP was being attacked by photogenerated IO₃⁻:



Thus alternatives to the H₂-evolving photocatalyst also need to be identified.

In both the natural photosynthetic and photocatalytic schemes, there needs to be some type of ordered, spatial arrangement of the photosystems and the electron transport chain to enable efficient charge and product separation. The photosynthetic organelle is the chloroplast. In higher plants, they appear as discs or flat ellipsoids 3-10 μm across. Within the chloroplast are many stacked arrays of flattened, sac-like membranes or thylakoids. Each stack, or granum, is about 500 nm in diameter. Both photosystems are embedded in the thylakoid membrane. They consist of bundles of several hundred chlorophyll molecules and associated species forming a 175 Å particle, as shown in Figure 2.

With a formal redox potential of -0.32 V (vs NHE) at pH 7.0, NADPH would be easily oxidized by O₂. However, this reaction is prevented because they are generated on opposite sides of the thylakoid membrane. The thylakoid membrane could be thought of as a semiconductor electrode, with a directed flow of charge carriers through it.

For the photocatalytic system, we have opted to disperse the two semiconductor powders in separate modules, or beds, as shown in Figure 3. A pump circulates a working fluid containing the redox mediator between them. The product gases are thus evolved at the macro scale in separate containers. This avoids the issue of how to safely separate the H_2 and O_2 co-evolved in a 2:1 ratio, well within the combustibility range.

Theoretical studies on the solar spectrum versus photovoltaic efficiency have shown that the optimum band gap for a single material is 1.3 eV. Efficiency can be improved upon by using multiple semiconductor materials in a tandem arrangement. By carefully lining up the band edges, so that the hole current in one layer feeds the electron current in the next, one can achieve a summation of individual voltages that can have a much higher efficiency. This comes from minimizing the energy lost in thermalizing a high energy charge carrier inside a wide energy band. In particular for water-splitting, the more efficient semiconductor materials, when used as a photoelectrode, cannot generate sufficient voltage to drive the electrolysis. The use of tandem electrodes, however, has made this possible. Work by Rocheleau on triple junction a-Si pin cells [3] and by Turner on GaAs/GaInP₂ cells [4] have demonstrated water decomposition using a single photoelectrode. Reported efficiencies have recently exceeded 12.8% [5].

The dual bed photocatalytic system can be "tandemized" as well by folding one bed underneath the other as shown in Figure 4. This would be feasible as long as: 1) the top layer photocatalyst has a wider band gap than the lower layer, so that light not absorbed in the first layer is transmitted underneath; and 2) the upper photocatalyst is finely dispersed, minimizing scattering losses. One may further be able to minimize mass transport problems by finely perforating the support membrane. The redox mediator would then travel through micro-channels instead of across the top face of the membrane in one direction and then back underneath. The resulting perforated, photocatalytic tandem membrane would then no longer require a circulating fluid, eliminating that parasitic loss.

It is interesting to note that Nature decided not to tandemize her photosynthetic apparatus, i.e., Photosystems I and II have nearly the same, instead of complementary, absorption spectra. Instead, the spectral gaps between the chlorophyll maxima at 650-700 and 430-470 nm are filled by secondary pigments, such as the carotenes, phycobilins, and xanthophylls. Perhaps the lesson here is that if solar power conversion efficiency percentages in the single digit range are acceptable, then concentrating on absorbing as much light as possible and then letting all the charge carriers thermalize to an energy band edge that can do useful chemistry is the preferred approach.

ACKNOWLEDGEMENT

The authors would like to thank the US Department of Energy, Office of Solar Thermal, Biomass Power, and Hydrogen Technologies, for their financial support.

REFERENCES

- 1- R. Hill and F. Bendall, *Nature* (London), 1960, Vol. 186, 136.
- 2- C.A. Linkous, D.K. Slatery, A.J.A. Ouellette, G.T. McKaige, and B.C.N Austin, "Solar Photocatalytic H_2 from Water Using a Dual Bed Photosystem," *Hydrogen Energy Progress XI*, proceedings of the 11th World Hydrogen Energy Conference, Stuttgart, Germany, June 23-28, 1996, Schön and Wetzel GmbH, Frankfurt am Main, 1996, p. 2545.
- 3- R. Rocheleau, E. Miller, A. Misra, and S. Song, *Hydrogen Energy Progress XI*, p. 2755.
- 4- J.A. Turner, D. Arent, M. Peterson, and S. Kocha, *Hydrogen Energy Progress XI*, p. 2749.
- 5- O. Khaselev and J.A. Turner, *Science*, April 7, 1998, Vol. 280, 425.

Table I. O_2 Evolution from TiO_2/IO_3^- Suspensions

250 mg photocatalyst
50 ml 1.0 N NaOH, 0.2 M KIO_3
1000 W Xe lamp irradiation
6 hour photolysis

| Photocatalyst: | TiO_2 | Pt- TiO_2 | Ir- TiO_2 | Ir- TiO_2 w/o IO_3^- |
|---------------------|---------|-------------|-------------|--------------------------|
| O_2 evolved (ml): | 0.58 | 1.3 | 2.5 | < 0.02 |

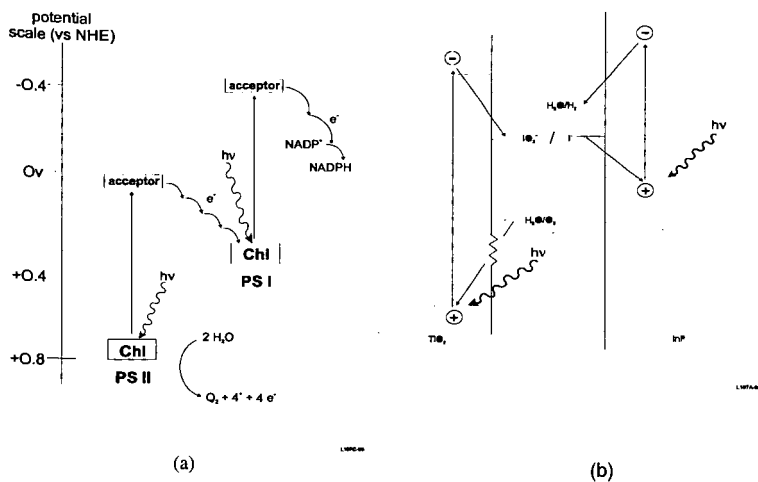


Figure 1. Energy level diagrams of: a) photosynthetic Z-scheme; and b) dual module water-splitting using semiconductor particulates.

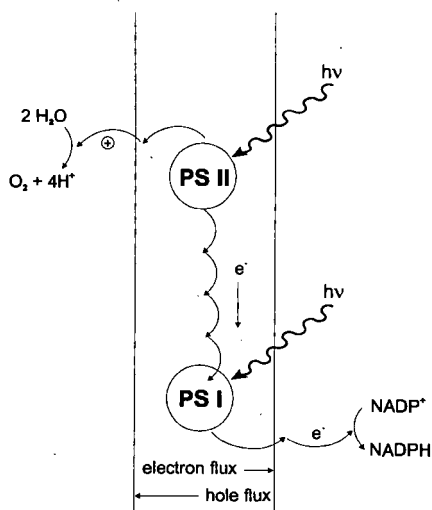
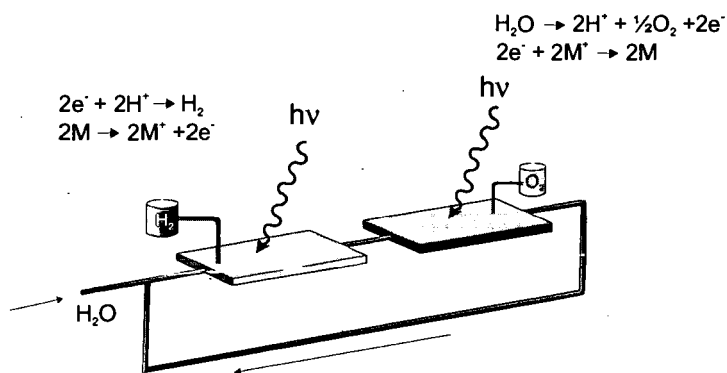


Figure 2. Schematic showing spatial arrangement of photosystems and charge flows in the thylakoid membrane of a chloroplast.



L108-98

Figure 3. Schematic of a dual bed photocatalytic water-splitting system.

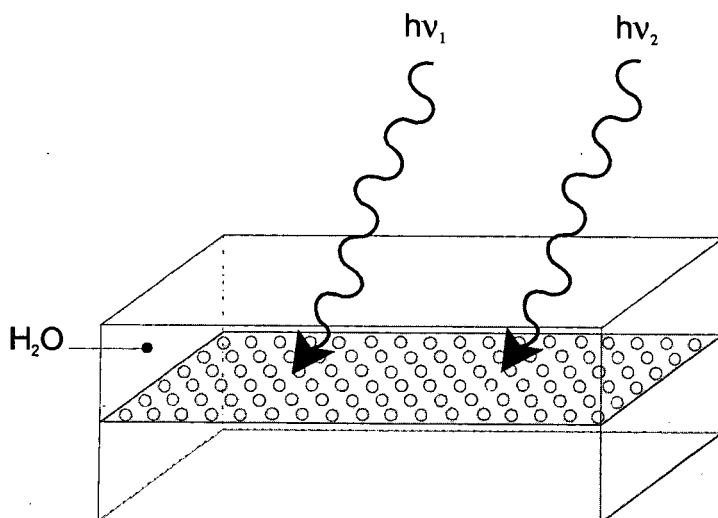


Figure 4. Schematic of a perforated, photocatalytic tandem membrane system.

A PRIVATE-FEDERAL COLLABORATIVE MODEL:
THE NATIONAL ALTERNATIVE FUELS LABORATORY PROGRAM

Ted Aulich, Tim Gerlach
University of North Dakota Energy & Environmental Research Center
Grand Forks, North Dakota 58202

KEYWORDS: ethanol, alternative fuels, aviation fuel

INTRODUCTION

The U.S. Department of Agriculture (USDA) -sponsored National Alternative Fuels Laboratory (NAFL) program at the University of North Dakota Energy & Environmental Research Center (EERC) was initiated to help build partnerships for demonstration and commercialization of alternative fuels. Approximately half of the NAFL annual budget is set aside for use in cost-share projects with nonfederal partners and advertised as the NAFL Request for Collaborative Proposals, which is published in ethanol industry newsletters and on the EERC Internet site. Successful proposals require 50% cost share and 90% of project labor performed at EERC. Descriptions of selected NAFL-initiated partnerships and projects are provided below.

AN ETHANOL-BASED ALTERNATIVE TO 100LL AVIATION FUEL

A team comprising EERC, South Dakota State University at Brookings (SDSU), Great Planes Fuel Development in Brookings, Lake Area Technical Institute at Watertown, South Dakota (LATI), the South Dakota Corn Marketing Board, and Texas Skyways, San Antonio, has developed and is pursuing commercialization of an economically competitive ethanol-based alternative to lead-containing aviation gasoline. Unlike essentially all commercial automobile fuel sold in the United States today, commercial 100-octane aviation fuel for piston engine aircraft (known as "avgas" or "100LL") still contains lead, which is a human health hazard. Replacing avgas with an ethanol-based aviation fuel will improve the environment (since the high octane rating of ethanol eliminates the need for lead) and reduce foreign oil dependency. Ethanol is also cheaper than avgas. Current ethanol and avgas prices are about \$1.50 and \$2.25 per gallon, respectively. An optimized blend of ethanol and a suitable petroleum-derived additive (to supply needed volatility and serve as a denaturant) can provide better engine performance and higher fuel efficiency than avgas by enabling the use of a higher engine compression ratio. An optimized ethanol blend will also enable better engine starting at lower temperatures than achievable with 98% (denatured) ethanol, because of an increase in Reid vapor pressure (Rvp) from about 2.3 pounds per square inch (psi) for 98% ethanol to about 7 psi for a blend of 80% to 85% ethanol with an appropriate additive.

Fuel formulations prepared using nondenatured ethanol and a high-octane petroleum blendstock from a major U.S. oil company were evaluated in the lab at EERC. Following optimization of a fuel comprising about 85% nondenatured ethanol and 15% petroleum blendstock-biodiesel mixture (biodiesel was added to provide lubrication), U.S. Bureau of Alcohol, Tobacco, and Firearms approval of the selected petroleum blendstock as an ethanol denaturant was requested and granted. GPFD successfully applied for Federal Aviation Administration (FAA) approval to flight-test two engine-airframe combinations with aviation-grade E85 (AGE85), and initiated on-ground engine testing and flight testing for FAA certification. As part of the certification process, EERC prepared a preliminary fuel specification for FAA review. Currently, GPFD is working with Texas Skyways to obtain FAA certification of three engine-airframe combinations for use with AGE85. In preliminary flight tests conducted with a Continental O-470-U/TS (that underwent minor carburetor modifications for use with AGE85 but no engine modifications), AGE85 and 100LL were shown to be essentially equal in performance, but the AGE85 provided significantly higher fuel energy utilization efficiency. Fuel utilization data acquired demonstrated that range is not simply a function of fuel energy content (about 88,200 and 120,000 Btu/gallon for AGE85 and 100LL, respectively), but also a function of how the energy is used. Because of its higher latent heat of vaporization than 100LL (and possibly, other factors), ethanol combustion produces less waste heat, which means that a greater portion of its energy goes toward moving a plane than compared to 100LL. This may be the

primary reason why the AGE85 range reduction is only about 10 to 15% versus 100LL, instead of the 27% that would be predicted based on the energy content difference between the two fuels and the assumption that the fuels will combust with equal thermodynamic efficiency. Fuel efficiency data for ethanol-based fuels versus petroleum fuels (with both aircraft and automobiles) need to be determined under lean-burn conditions that take advantage of ethanol's capability to provide engine-safe power and performance at higher air-to-fuel ratios than gasoline, especially under cruise conditions. Flight tests are ongoing, and oil company commitment is being sought to produce and distribute AGE85 or provide AGE85 petroleum blendstock for blending and distribution by another entity. Current effort is focused on companies with midwest oil production capability to enable use of regionally produced ethanol. Because of increasing U.S. EPA pressure that has resulted in the prohibition of avgas in pipelines and the need for shipment by truck, avgas producers are aware of the urgent need to develop unleaded avgas alternatives.

OFF-SITE REGENERATION OF ETHANOL DEHYDRATION MOLECULAR SIEVES

Molecular sieves (mol sieves) are used for dehydration at numerous ethanol production facilities and oil and gas refinery operations throughout the United States. In the ethanol industry, mol sieves adsorb water from 95% pure ethanol and yield 100% (200 proof) product, and sieve regeneration (dewatering) is performed on-site by applying a vacuum to the "bottles" in which the sieves are contained. In the event of a process upset or other unplanned occurrence, mol sieves can become contaminated and undergo a reduction in effectiveness, which may result in reduced product output. Remediation of reduced output requires either sieve replacement or off-site regeneration to remove the offending contamination. Off-site regeneration of mol sieves is common in the oil and gas industries and is normally achievable with thermal treatment under a specific atmosphere. Temperature and atmospheric requirements depend on type and extent of contamination.

Because of its demonstrated economic viability in the oil and gas industries, an EERC partnership with CRI International, a full-service catalyst management company, was initiated to pursue commercialization of off-site mol sieve regeneration for the ethanol industry. Normally, the price of off-site regeneration ranges from one half to two thirds the cost of new sieves. Factors affecting cost include treatment required (based on type of contamination, which can include carbohydrates and their polymerization products, sulfites, and lubricant entering the process stream due to a system upset), transportation, and amount of material requiring regeneration. Figure 1 compares the performance of contaminated mol sieves from a midwest ethanol plant to the performance of off-site regenerated sieves from the same plant. The figure demonstrates the technical feasibility of the process. Currently, EERC and CRI International are evaluating process economics with contaminated sieves from another producer.

FLEX-FUEL VEHICLE FUEL ECONOMY TESTING

Based on preliminary fuel economy data acquired during the above-described ethanol-based aviation fuel development effort, EERC initiated fuel economy testing with E85 automobiles. Initial results indicate highway and city driving mileage reductions of about 28%, which are consistent with industry-reported mileage and mileage calculated based on energy content per gallon versus gasoline and assuming gasoline thermodynamic efficiency. However, the E85 1997 flex-fuel Ford Taurus cars used for the tests are programmed to operate at stoichiometric fuel combustion conditions. While there are several reasons for avoiding "lean-of-stoichiometric" combustion of gasoline, including increased NO_x emissions and increased potential for valve damage, there are indications that leaner ethanol combustion may not produce the same negative effects (1-3). Current flex-fuel vehicle work is focused on adjusting fuel flow to achieve lean-of-stoichiometric combustion and monitoring emissions of NO_x , CO , CO_2 , O_2 , and total hydrocarbons in on-the-road tests with a vehicle-mounted infrared gas analyzer.

GASOLINE SURVEYING TO MONITOR COMMERCIAL FUEL COMPOSITION & PROPERTIES

To meet objectives of the 1990 Clean Air Act Amendments and help ensure against unsafe

levels of tropospheric carbon monoxide and ozone, many regions around the U.S. have implemented reformulated gasoline (RFG) or oxygenated gasoline (oxyfuel) programs. Programs that rely extensively on ethanol to meet fuel oxygen requirements are in a unique position to ensure and accelerate marketplace acceptance of ethanol as a high-octane blendstock for the U.S. gasoline pool. Success in these programs is crucial to the ethanol industry and requires that base gasolines used in ethanol blends meet health, environmental, and performance standards to ensure a positive relationship between ethanol and public health, air quality, and engine performance. Through the NAFL program, the EERC has formed partnerships with ethanol industry groups to perform gasoline surveys in which fuels are sampled (at the pump) and analyzed to provide data and insight on major supplier blending and marketing practices. Data from the surveys can be used to compare commercial fuel parameters to regulated parameters of the U.S. Environmental Protection Agency (EPA) RFG program, the California RFG program, other state gasoline programs, and the EPA Anti-Dumping Requirements for Conventional Gasoline. Table 1 lists EPA Phase 1 RFG typical properties, specifications for California Phase 2 RFG, and annual average parameters for "EPA Statutory Baseline" fuel.

To implement the anti-dumping requirements, EPA worked with gasoline refiners, blenders, and importers to develop individual "baseline fuel" specifications. Each refiner must meet individual baseline fuel requirements developed based on a set of fuel parameters, emissions, and volumes representing the quality and quantity of the refiner's 1990 gasoline. All individual baseline fuel specifications are confidential between EPA and refiners and are not available for public review. Anti-dumping compliance is based on annual average composition and characteristics for gasoline from each regulated refinery, refinery aggregate, importer, or blender. Each refiner reports annual gasoline data to EPA at the end of each production year, and EPA also periodically conducts audits of production, blending, storage, and loading facilities to help ensure that baseline fuel specifications are met. If a refiner does not have an established individual baseline fuel on file with EPA, this refiner is required to meet the specifications of the EPA Statutory Baseline. Demonstration of compliance using the statutory baseline is based on the annual fuel parameter values shown in Table 1. The statutory baseline fuel parameters were developed using 1990 fuel composition data compiled through a nationwide petroleum industry fuel survey. The data provided in the twice-annual industry gasoline surveys (which are guided by the American Petroleum Institute) are acquired by petroleum companies and supplied to the survey marketer compilation and reporting. All fuel composition data are reported without oil company identification, which prohibits use of the survey to associate a specific fuel with a specific refiner.

An EERC summer 1997 midwest region gasoline survey showed that 27 of 33 midgrade (89 octane) fuels sampled contained ethanol, including 15 of 21 fuels that were not required to contain oxygen, indicating the free-market use of ethanol to provide octane. The survey showed that although two of three major suppliers frequently chose to use ethanol as a viable blending component, one major supplier consistently avoided the use of ethanol except with fuels required to contain oxygen. Figure 2 compares EERC survey fuel data with BDM survey averages for the same region and EPA and California fuel specifications, and Figure 3 is a similar comparison using winter fuel data. The figures show that while both the EERC and BDM survey average fuel compositions meet EPA baseline specifications, one major supplier significantly exceeds (by almost double) the EPA statutory baseline value for olefins in both winter and summer. It is likely that this supplier has an individual baseline on file with EPA, and because this information is proprietary, it is impossible to determine compliance status with currently available information. Additionally, although EPA-specified sampling and analysis procedures were employed, compliance status determination would likely require a more extensive database than assembled for this survey. A key benefit of gasoline surveying is in helping to ensure that ethanol-blended gasolines are clean and perform well, which is crucial to ensuring ethanol's future as an automobile fuel.

ALTERNATIVE FUELS IMPLEMENTATION VIA RED RIVER VALLEY CLEAN CITIES

The Red River Valley Clean Cities (RRVCC) coalition was established to promote and implement regional alternative fuels use by building partnerships to erect alternative fuels

infrastructure, procure alternative fuel vehicles (AFVs), and demonstrate beneficial environmental, performance, and economic effects of alternative fuels. The NAFL-led coalition comprises government and industry stakeholders in Canada and the U.S. located in and between Grand Forks–East Grand Forks on the North Dakota–Minnesota border and Winnipeg, Manitoba, Canada. The route between Winnipeg and Grand Forks (Canada Highway 75 and U.S. I29) represents the northern end of the I29–I35 Midcontinent Trade Corridor. The coalition is fuel-neutral, as demonstrated by a stakeholder membership that includes regional ethanol and electricity interests and upper midwest propane and natural gas suppliers. Current RRVCC initiatives include working with the ethanol industry, grower organizations, state agencies, and gasoline retailers to establish commercial high-blend ethanol (E85) stations, working with the University of North Dakota to procure E85 and propane vehicles, establishing a group of natural gas interests, comprising natural gas and fueling equipment providers, state agencies and private fleets, and the U.S. Postal Service, which will construct compressed natural gas fueling sites in the region.

REFERENCES

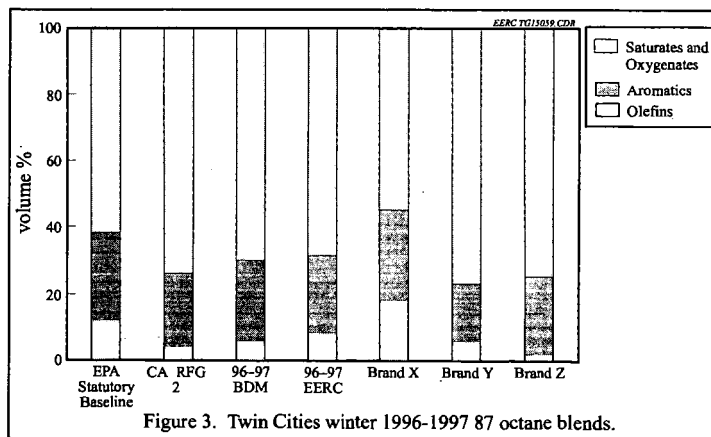
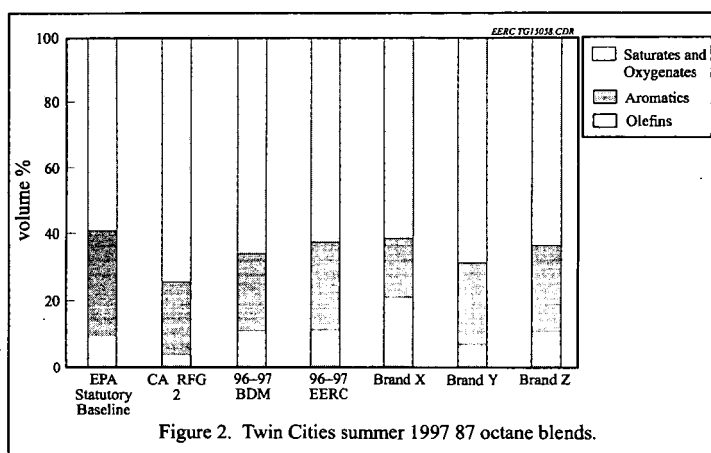
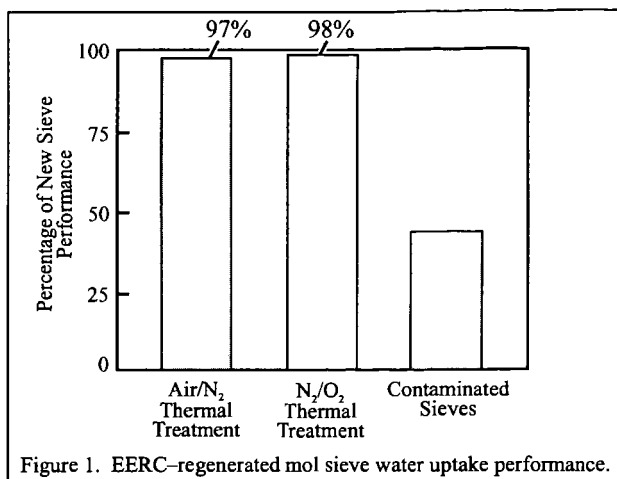
1. Bechtold, R. L., J.B. Pullman, Society of Automotive Engineers Paper No. 800260, 1980.
2. Bechtold, R. L., *Alternative Fuels Guidebook*, Society of Automotive Engineers, 1997.
3. Thomas, K., *The Future of Avgas*, *TBO Advisor*, January–February 1998.

Table 1. Regulatory Fuel Specifications.

| | EPA Phase 1 RFG Typical Properties | California Phase 2 RFG Specifications Average Limit | EPA Anti-Dumping Statutory Baseline Fuel Parameters Annual Average |
|-----------------|--|---|--|
| Rvp, psi | 7.2 – 15.0 | 7.0 ¹ | 8.7 |
| T50, °F | 202 | 200 | Not reported |
| T90, °F | 316 | 290 | Not reported |
| Aromatics, vol% | 23.4 | 22.0 | 28.6 |
| Olefins, vol% | 8.2 | 4.0 | 10.8 |
| Benzene, vol% | 1.0 | 0.8 | 1.6 |
| Sulfur, ppm | 302 | 30 | 338 |
| Oxygen, wt% | 2.0 | 1.8 – minimum ² 2.7 – maximum ² | Not required |

¹ Absolute maximum limit – no average limit allowed.

² Absolute limits for winter gasoline – summer values are 0.0 minimum, 2.7 maximum.



HYDROCARBON FUELS FOR FUTURE AUTOMOTIVE ENGINES

Ramon L. Espino and John L. Robbins
Exxon Corporate Research Laboratories
Route 22 East
Annandale, NJ 08801

In response to a need for transportation vehicles with less environmental impact, automakers around the world have been exploring a variety of novel advanced vehicle engine technologies. Fuel cells, devices that electrochemically oxidize fuels, have emerged as the focus of long range vehicle engine research: at least thirteen major auto makers now are exploring their use in light duty vehicle applications.

The Polymer Electrolyte Membrane (PEM) fuel cell has been the focus of most vehicle fuel cell research. It produces power at near ambient temperature, and thus offers advantages vs. other fuel cells that require preheating to 200°C or above before they can generate electric power. Rapid startup, with minimum power input, is a critical requirement for any vehicular application of fuel cells.

Figure 1 describes the operational principles of a PEM fuel cell. Hydrogen fuel dissociates at the anode catalyst to hydrogen ions and electrons. Hydrogen ions migrate across the electrolyte to the cathode side. At the cathode, oxygen from the air combines with electrons from the anode and hydrogen ions traversing the membrane to form water. The flow of electrons from the anode to the cathode, and the production of water generates electric power. Advanced fuel cell stacks, such as those produced by Ballard Power Systems, have achieved power density levels of 1 kW/liter. These figures exceed targets set by the US PNGV program for fuel cells aimed at light duty vehicle applications.

Fuel cells offer potential for step-out changes in vehicle emissions and efficiency. The H₂/air fuel cell produces no CO, NO_x, or particulate matter emissions. However, H₂ production may lead to emissions of one or more of these air pollutants, depending on how it is produced. Peak steady-state efficiencies of H₂ PEM fuel cells approach 60% when operated at the low end of their maximum load, while compression-ignition or spark-ignition engines achieve peak efficiencies (up to 45%) near the higher end of their peak load. Net efficiency credits for fuel cell vehicle systems will again depend on how the H₂ fuel is produced and distributed, as well as the way fuel cells or internal combustion engines are incorporated into a vehicle power train, e.g. as a stand-alone power source, or as an electric generator in a hybrid vehicle.

Net Efficiency Estimates

Higher energy efficiency in transportation is a major factor driving efforts to develop fuel cell vehicles. Here we use a method to compare net efficiencies of fuel and fuel cell vehicle systems that considers energy losses in the fuel cycle (fuel production, refining, distribution) and in operation of the vehicle. We compare systems for vehicles that store H₂ produced at a retail station from natural gas, methanol produced from natural gas, and gasoline produced from petroleum.

The first option considers hydrogen production at a retail-refueling site by steam reforming of natural gas. We chose natural gas steam reforming because it is currently the lowest cost method to produce hydrogen. Currently 97% of the world's hydrogen is produced by this process, but it is possible that long term, technology advances will reduce cost of H₂ from renewable resources to economically competitive levels (1,2). Natural gas is widely distributed in many developed countries, so fuel availability is not an issue (where it is not available, one could instead steam reform or partially oxidize fuels like gasoline, diesel, alcohols, etc).

Steam reforming is an endothermic process that generates H₂ and CO₂ from methane and water: $\text{CH}_4 + 2 \text{H}_2\text{O} + \text{heat} = \text{CO}_2 + 4 \text{H}_2$. The heat requirement is substantial, over 253 kJ/mole methane, or about 31% of methane's lower heating value. After the reforming step, there is a purification train to remove CO₂ and CO, followed by two-stage compressors and high pressure storage tanks. Overall thermal efficiency (heating value of H₂/heating value of methane fuel) of the process is 70-80%, depending on the level of plant heat integration and the final H₂ storage pressure (2). Assuming 90% efficiency in delivering natural gas wellhead to retail station, we obtain a net 63-72% efficiency for H₂ production.

The second fuel option considered is methanol produced from natural gas. Nearly all methanol is now produced from natural gas, usually near large, remote gas fields where distance from population centers makes pipeline distribution/sale of the gas impractical. This low-cost gas is instead converted to methanol near the production site, which is then shipped to the market by liquid tankers.

Methanol is produced from natural gas in a multi-step process. Gas is first processed to remove impurities such as H_2S , and then converted to synthesis gas (a mixture of H_2 , CO , and CO_2) by steam reforming (or partial oxidation) followed by water-gas shift reactions. This is fed to a methanol synthesis reactor where CO and CO_2 are catalytically hydrogenated to CH_3OH . The crude product is distilled and dehydrated to remove water, hydrocarbon, and alcohol impurities. The thermal efficiency of methanol production is typically 68-72% (3). Energy losses in transportation range from 1-2%, yielding a net fuel production efficiency of 67-71%.

The third option is a petroleum-based fuel (e.g. gasoline or diesel) stored and converted to an H_2 -rich gas by partial oxidation on-board the vehicle. Gasoline delivered at the pump in a retail station typically carries 85-90% of the heating value available from petroleum produced at the wellhead.

Table 1 lists compares net efficiencies of the three fuel options, considering energy efficiency of fuel production, fuel processing on-board the vehicle, and the fuel cell. The previous paragraphs outline assumptions used in estimating fuel production efficiencies. On-board fuel processing and fuel cell efficiencies estimates reflect ranges cited by others (4,5). Net efficiencies of all the options are significant improvements over current gasoline-fueled IC engines. On highway drive cycles (which are closest to the steady-state fuel cell system efficiencies cited above), these engines are 20 % efficient in delivering power to the wheels (6), yielding a net efficiency of 17-18% when gasoline production/delivery is included.

The data used to construct Table 1 contain some uncertainties. Fuel production efficiency figures are fairly solid, relying on many years of commercial experience in production of gasoline, methanol, and hydrogen in large scale. Fuel cell and fuel processor efficiencies are less certain. These rely on models and limited hardware data measured under steady-state operating conditions. Still, the exercise is valuable in that it shows that the fuel cell options have potential to significantly improve efficiency vs. current generation ICE vehicles. Overlapping ranges of the gasoline and compressed H_2 fuel option efficiencies illustrates the need to determine efficiencies and emissions of these systems in vehicles under realistic drive cycles.

Fuels from Natural Gas

The equivalent of over 800 billion barrels of oil currently lies dormant in natural gas reserves largely inaccessible by pipeline. These previously untapped resources along with underutilized light hydrocarbons associated with crude oil production could become energy sources for gas-to-liquids conversion technologies emerging from research and development efforts.

Chemical conversion of natural gas is a relatively newer route for preparing liquid hydrocarbons for transport to markets. Although current conversion processes have lower thermal efficiencies than LNG processing, under some circumstances this debit can be largely offset by higher value liquids which can range from ultrahigh quality refinery and petrochemical feed stocks to finished products. Moreover, these streams can be shipped and stored in conventional facilities obviating the need for dedicated cryogenic transportation equipment and tankage.

Natural gas can be converted to zero sulfur, zero aromatic hydrocarbons and also to methanol and methanol derivatives like dimethyl ether. The table below lists the potential of the various products for natural gas as fuels for advanced automotive power plants.

| | <u>Fuel Cell</u> | <u>Compressor Ignition Combustion</u> |
|-------------------------|------------------|---------------------------------------|
| Methanol | X | |
| Dimethylether | X | X |
| Fischer Tropsch Naphtha | X | |
| Fischer Tropsch Diesel | | X |

The process for producing methanol from natural gas was described earlier. Process schemes to convert natural gas to Fischer-Tropsch hydrocarbon products all start with the partial oxidation or

steam reforming of natural gas to a mixture of carbon monoxide and hydrogen. Various process schemes have been developed and demonstrated ranging from fluidized to packed bed reactors. All depend to varying degrees on the thermal combustion of the hydrocarbon and the reforming of the hydrocarbon with steam. The product is generally a synthesis gas with a ratio of hydrogen to carbon monoxide slightly above 2.0. This mixture is then converted at 25-40 atmospheres to a hydrocarbon mixture with a carbon distribution determined by a Schultz-Flory distribution. The product of the Fischer Tropsch reaction is in most cases further processed to adjust the product distribution according to market opportunities. The product options range from waxes, lubricant basestocks, specialty solvents, diesel fuel, naphthas and liquefied petroleum gas (7).

The transportation fuel market is by far the largest since worldwide consumption is on the order of 40 million barrels a day versus less than one million barrels for lubricant basestocks. The diesel product from Fischer Tropsch synthesis is particularly attractive since it has a very high cetane number, above 75, and essentially no sulfur or aromatics. The naphthas from Fischer Tropsch is not a very attractive gasoline component due to its low octane number (less than 50) however it is a very attractive fuel for the generation of hydrogen for fuel cell powered vehicles.

The Next Steps

At the present time there are many organizations, including Exxon, actively involved in evaluating the performance of a broad range of hydrocarbons and alcohols in fuel cell and internal combustion automotive power plants. The amount of data available is limited since research on these fuel/engine combinations are at the exploratory stage. In the next two years the results will begin to emerge and the assessment of their potential can begin under a sound footing of facts. The assessment process will not be easy since it will be necessary to balance complex factors like energy efficiency, emissions, vehicle and fuel cost and infrastructure costs. In the final analysis the public acceptance of the vehicle/fuel system will determine its market impact.

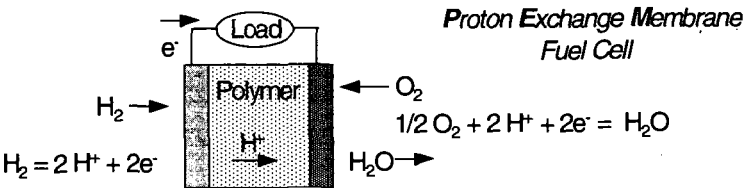
References

1. C. E. Borroni-Bird, *J. of Power Sources*, 61, 1966, 33-48.
2. K. DeJong and H. Van Wechem, *Intl. J. of H₂ Energy*, 20, 1995, 493-499.
3. Ullmann's Encyclopedia of Industrial Chemistry, 5th Edition (1990), Vol. A16, p.480.
4. A.D. Little Presentation to PNGV Peer Review Committee, October 17, 1996; also A.D. Little presentations in Proceedings of the 1995 Dept. of Energy Automotive Technology Development Contractors Coordination Meeting (Oct. 23, 1995).
5. S. Ahmed, R. Kumar, M. Krumpelt, R. Doshi, H. Geyer, and R. Ahluwalia, Dept. of Energy Fuel Cells for Transportation Exploratory R&D Review, Washington, DC, Sept. 1996.
6. PNGV Program Plan, revised edition published Nov. 29, 1995.
7. L. L. Ansell, R. F. Bauman, B. Eisenberg, and B. M. Everitt, Preprint: World Conference on Refining Technology and Reformulated Fuels, March 18-20, 1998, San Antonio, TX.

Table 1: Comparison of Net System Efficiencies

| <u>Efficiencies</u> | | | | |
|-------------------------|------------------------|-----------------------|------------------|-----------------------|
| <u>Fuel</u> | <u>Fuel Production</u> | <u>Fuel Processor</u> | <u>Fuel Cell</u> | <u>Net Efficiency</u> |
| Gasoline | 0.85-0.90 | 0.75-0.83 | 0.45-0.50 | 0.29-0.37 |
| Methanol | 0.67-0.71 | 0.78-0.85 | 0.50-0.55 | 0.26-0.33 |
| 5000 psi H ₂ | 0.63-0.72 | NA | 0.55-0.60 | 0.35-0.43 |

Figure 1: Operational Principles of an H₂ PEM Fuel Cell



ROLE OF PETROLEUM PRODUCTS TO MEET CANADA'S FUTURE TRANSPORTATION NEEDS

Arun K. Palit
Sunoco Inc., Suncor Energy
Canadian Petroleum Products Institute
1000 - 275 Slater Street
Ottawa, Canada K1P 5H9

ABSTRACT

Petroleum products will continue to play an important role in Canada's transportation industry and in other sectors of the economy today and for the foreseeable future. In recent years, environmental, health and security of supply concerns have been raised about the role of petroleum products in the Canadian economy. These public concerns and actions taken by the petroleum industry are reviewed. This paper discusses the currently announced major capital spending plans underway by the Canadian oil sands crude producers that will significantly increase the flow of Canadian "synthetic" crude to the USA. Properties of oil products produced from these synthetic crudes are examined. In the future, market forces and quality requirements will determine how these synthetic crudes will be upgraded for their environmentally acceptable use as transportation fuels.

INTRODUCTION:

In recent years, concerns have been raised about the role of petroleum products in the Canadian economy. Environmental, health and security of supply concerns have led to suggestions that Canada should reduce its dependency on oil products. The purpose of this presentation is to demonstrate that, while some of the concerns are legitimate, petroleum products will continue to play an important role in Canada's transportation industry and other sectors of economy to-day and for the foreseeable future.

The paper begins by acknowledging Canadian Petroleum Products Institute's (CPPI) recognition of the environmental and social concerns that the Canadian public has about oil products. The first part of this paper labeled "Main Public Concerns and Beliefs" is our understanding of what the public is concerned about and what it believes. We then seek to put these concerns in perspective by quantifying the magnitude of the issues and referencing benchmarks. The paper demonstrates that the petroleum industry continues to take action on many of the public's concerns. It informs the reader as to the very strong economic and social benefits and the secure nature of the Canadian oil products business. The paper then discusses the major capital spending plan underway by the Canadian oil-sands crude producers which will significantly increase the flow of Canadian "synthetic" crude to the USA. We compare the favourable properties of oil products produced from synthetic crudes to the less favourable properties and conclude by noting that market forces and future quality requirements will determine how these synthetic crudes will be upgraded for their environmentally acceptable use.

MAIN PUBLIC CONCERNS AND BELIEFS

A survey of recent public opinion polls and Canadian media identify several main concerns the public has with respect to petroleum usage.

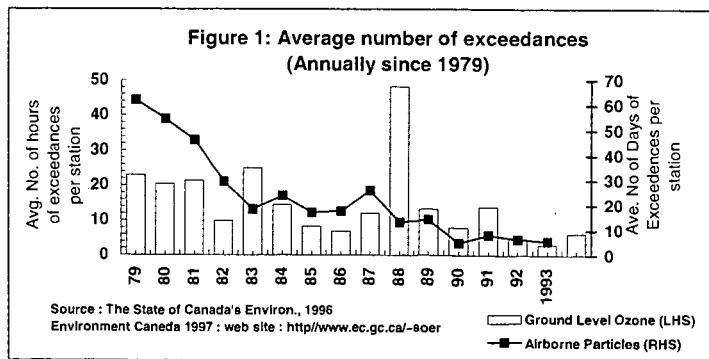
1. Pollution of air in our cities
2. Impact on personal health
3. High prices of oil products and consumer belief that prices are unfair
4. Oil spills and environmental damage
5. Global warming
6. Energy Security:
 - Do we have enough petroleum resources
 - What are the impacts from increasing demands
 - Are we using petroleum efficiently

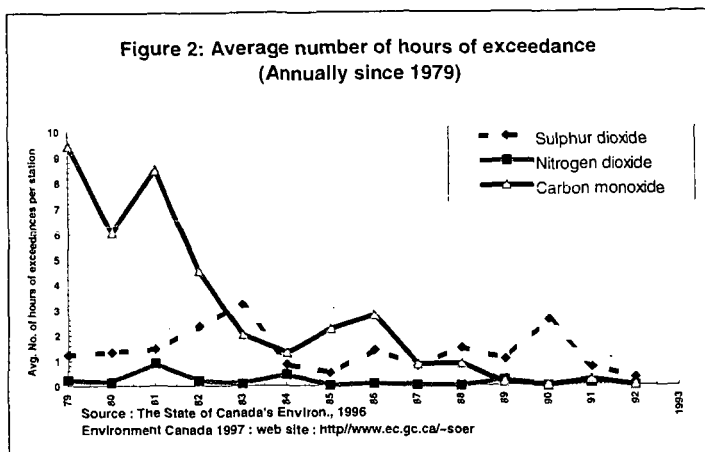
The public wants some actions now to address these concerns.

Clearly, oil products usage has an impact on urban air quality, and on air issues in general. Smog, a brown summer haze that intermittently forms over some of our cities, is comprised of ground level ozone (a combination of volatile organic compounds (VOC) and oxides of nitrogen (NOx) in the presence of sun light) and fine particulates. VOCs are emissions of light volatile hydrocarbons. The transportation sector (that is the industry plus the end users) is responsible for the majority of the VOCs and part of the NOx. The government has declared that over half of the Canadian population is periodically subjected to unacceptable ozone levels. Smog causes respiratory impact on humans, particularly the young and elderly as well as damaging forests and crops. Transportation sector also contributes to sulphur oxides (SOx) emission which in combination with NOx forms acid rain, that is associated with injury to marine life and vegetation. Heavy fuel oil burned in refineries and commercial heaters and boilers also adds to SOx emission. People are concerned that the air quality is bad and is getting worse due to urban growth. Similarly, oil products use can be linked to other human health issues. Carbon Monoxide (CO), a product of incomplete combustion of carbon based fuels, is a hazardous pollutant and causes oxygen deficiency in human lungs. Major portion of CO emissions are related to the transportation sector. Gasoline contributes to most of man-made benzene emissions through evaporative and exhaust emissions from engines. Benzene is a cancer causing substance. Fine air borne particulates of microscopic size (less than 2.5 microns) from the transportation sector is a complex mixture of soot, ash, metals, salts and acid. It has recently been associated with respiratory illness and premature deaths. People believe that oil products and their use are harmful to human health. Transportation cost, including petroleum products, is a major element of consumer spending, equaling food and greater than clothing. Gasoline price is an item of major debate. Most consumers do not understand why prices seem high, vary throughout Canada, are uniform all over a given market. People are concerned that there have been large international petroleum spills. Volume of transported oil is large, there have been some major international marine incidents and local spills continue to occur. People wonder whether the standards are too lax and will the industry ever improve its track record. Global warming is blamed for increased frequency of hurricanes, floods, fire, draught, loss of shoreline and such diseases as malaria. People believe that increasing emissions of greenhouse gases (GHG) are leading to global warming. In their mind they question the sustainability of fossil fuel burning, as over 75% of carbon dioxide, a leading greenhouse gas, comes from fossil fuel use. Finally, the public believes that we may be selfishly wasting petroleum, a precious non-renewable resource, thus depriving the future generations of its effective use. Overall, while oil products are central to modern life, public concerns about their use and effects are understandable and need to be addressed.

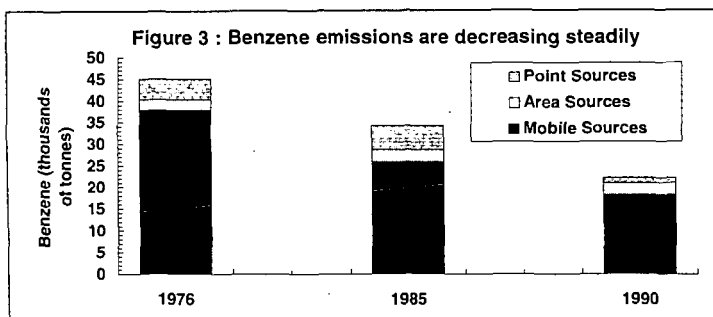
THE DIMENSIONS AND SCIENTIFIC ASPECTS OF THE PUBLIC CONCERNS

In fact, the Canadian air quality is very good and is getting better, but progress needs to continue. The figures below demonstrate that the average levels of pollutants measured in major cities throughout Canada are generally coming down (Figures 1, 2). Similarly, health issues related to oil product use will continue to diminish by sustained industry efforts to reduce toxic releases and reformulated oil products..

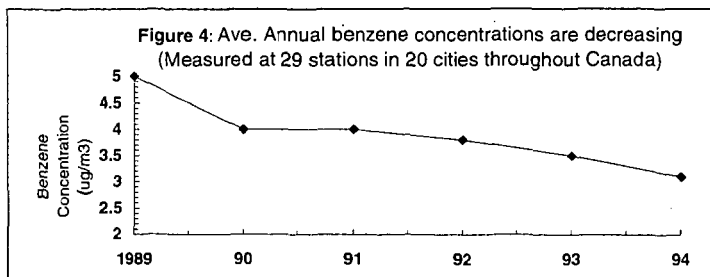




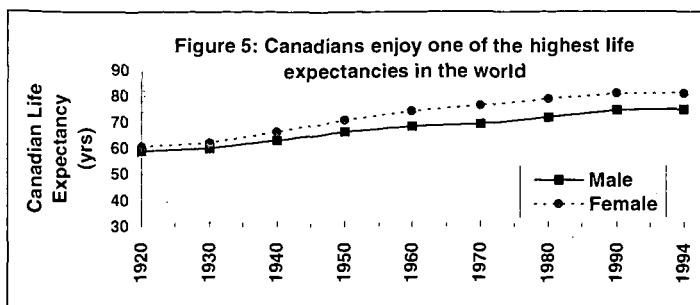
Canadians are fortunate to live in a beautiful land of great natural resources and to be among the healthiest people on earth (Figures 3,4,5). Gasoline is reasonably priced in Canada.



Source : BC DM Task Force on Cleaner Fuels, May 11, 1995

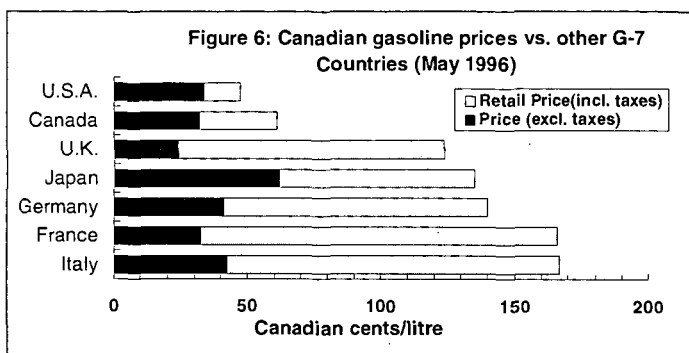


Source : Levels of Air Toxics in Canadian Cities : Benzene; Canada's National Environmental Indicator Series, 1996; URL : <http://www.ec.gc.ca/~soer>

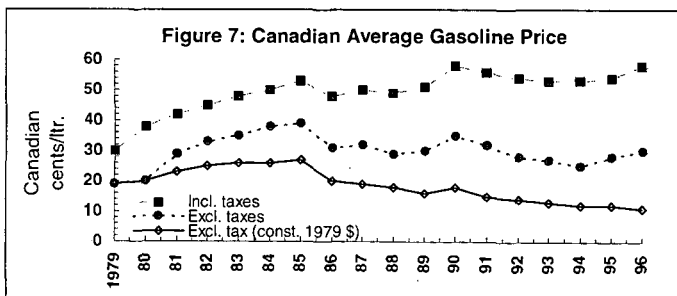


Source : Statistics Canada. Cat. 82-221-XDE

The Federal Competition Bureau has found through many investigations that our products are competitively priced. Canadian gasoline prices are lower than most G-7 countries. In fact, in real terms, gasoline prices have gone down (Figure 6, 7).



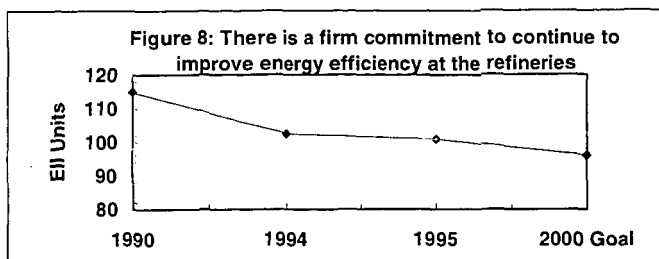
Source : Petroleum Communications Foundation, Gasoline Price Report, 05/28/96



Source : Sector Competitiveness Framework Study, 1994, Petroleum Communication Foundation, 05/28/96

To date, the size and the extent of Canadian spills cannot be compared with major ocean tanker disasters. The Canadian industry's goal is to achieve zero spills. Marine response continues to be a high priority for the industry. Three new response organizations became fully operational in 1995. Global climate change is an environmental issue with economic, social and trade dimensions. For sustainable development, these multi-dimensions need addressing in an integrated way considering Canada's unique national circumstances. Large, short term GHG reduction targets through limits on petroleum fuel use would significantly impair the Canadian economy. Climate change is a complex long term issue and the supporting science is still emerging. However, CPPI believes that reasonable steps can be taken meanwhile. Considering the impact that climate change actions would have on jobs, economic growth and deficit reduction, this long term issue needs flexible

long term goals as well as realistic short term targets. CPPI supports and is active on voluntary measures, improved energy efficiency (Figure 8) both in our operations and nationally through customer education.

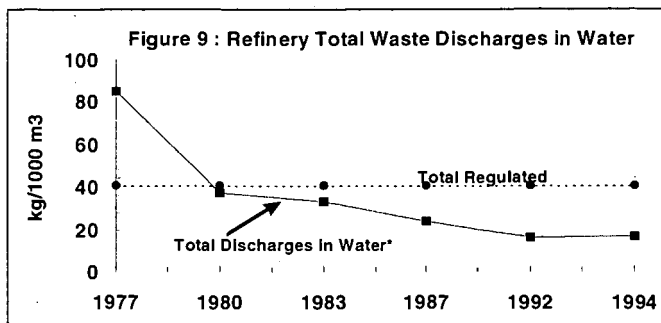


Source : CPPI 1995 Environmental and Safety Performance

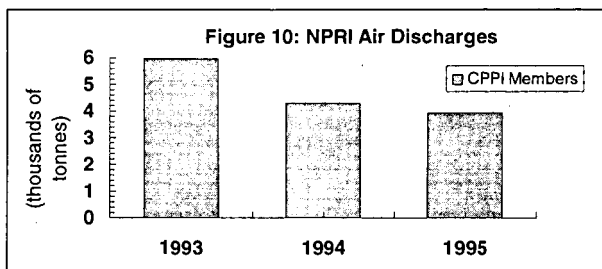
To achieve long term goals, CPPI supports R&D that allows emergence of new economically viable technology and reduces scientific and economic uncertainty as well as flexible policies which allow economic turnover of capital stocks towards least cost solution. Canada has abundant petroleum resources, proven hydrocarbon reserves which can be economically produced and the country is a net oil exporter. Canada has more oil in our oil sands than all the Mid-East combined. The industry is progressive, is a world leader in technological innovation and has increased investments and exploration activities which will extend the useful life of Canadian petroleum resources. In summary, the environmental issues and other public concerns surrounding oil products may not be as significant as one would initially suspect, but the industry need to continually improve its performance.

THE RECORD OF OIL PRODUCTS INDUSTRY IN RECOGNIZING AND RESPONDING TO ENVIRONMENTAL AND SOCIAL CONCERNS

Canadian oil products companies have continued to improve the environmental quality of products and operations to meet and better cleaner air goals. Some examples of the improvements are : gasoline reformulation to meet tough national standards to combat air pollution (1995), reduced gasoline volatility during the summer nationwide (1990), introduction of cleaner burning gasolines with deposit control additives (1985), gasoline vapour recovery implementation at terminals and other storage facilities (1991), national program for low sulphur diesel introduction (1994), fuel efficient lubricating oil introduction (1987) etc. Many changes are progressing in our manufacturing, oil product movement and retail operations. In refining facilities, fugitive emission control, enhanced sulphur recovery and flare minimization, toughest water effluent quality standards in the world and reduction of toxics are being achieved. In the area of oil and products movements we are trending towards double hull vessels to minimize spill impacts, pipeline leak detection systems, gasoline tank truck driver certification, and marine oil emergency plans are some areas to note. In retail operations we should list areas such as vapour recovery during gasoline delivery, replacement of underground tanks with new double walled fibreglass tanks, improved leak detection, ground water monitoring and contaminated soil remediation. We have significantly improved the environmental performance in areas such as refinery discharges to air and water. The bottom line is that the oil industry has recognized the importance of environmental issues and has taken real actions to improve performance of its products and operations (Figures 9,10).



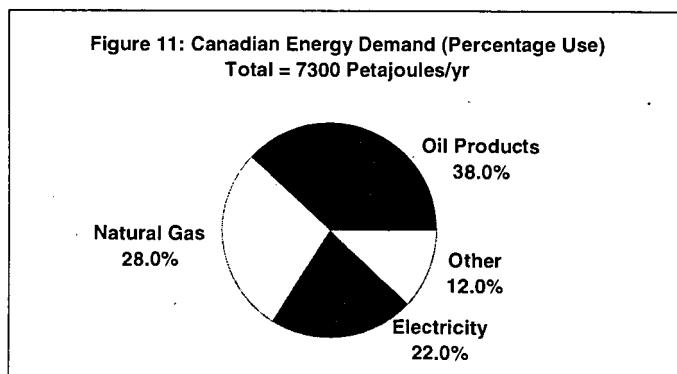
Source : CPPI, First Annual Performance Measures Report, April 24, 1996, P13



Source : CPPI Environmental and Safety Performance

THE IMPORTANCE OF THE PETROLEUM PRODUCTS INDUSTRY TO THE CANADIAN ECONOMY

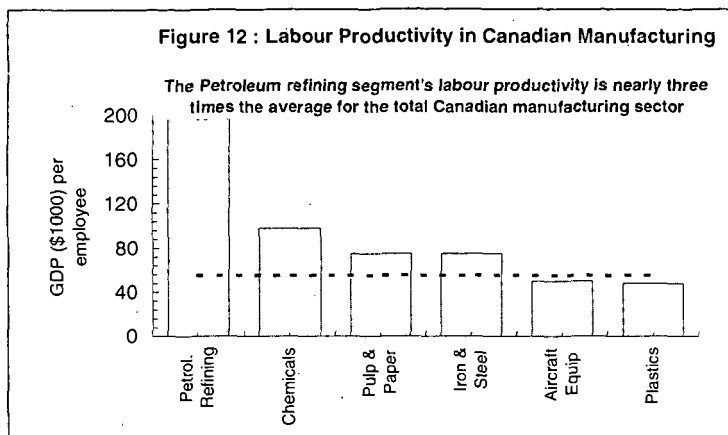
Oil products represent more than a third of Canada's current energy usage (Figure 11) and meet 98% of our transportation fuel needs. In fact, petroleum products are the competitive market place energy choices in most sectors of the Canadian economy. Given our vast size, climate and resource based economy, Canada is a high energy intense country.



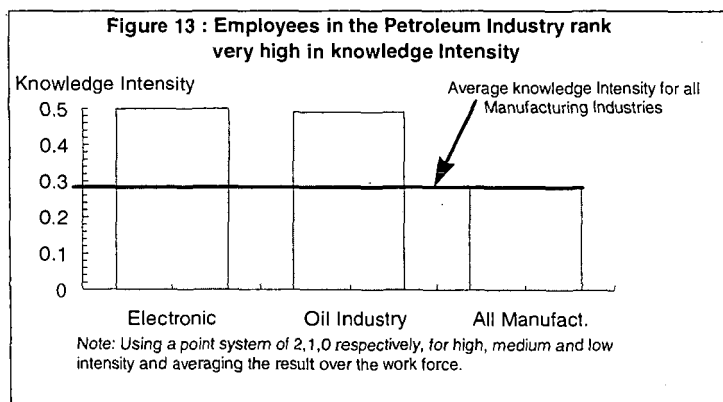
Source : Energy Efficiency trends in Canada : NRCan, April 1996, pp.85

However, Canada has the most diverse energy mix of the G7. The petroleum refining segment's labour productivity is nearly three times the average for the total Canadian manufacturing sector. In today's market, compared to other alternative fuels, oil products are the lowest priced transportation fuel on a pre tax basis. Taxes on the activities and products of the Canadian downstream industry are a major source of revenue to the

Canadian governments. Based on performance, reliability, safety and performance, Canadian consumers have made a substantial investment in vehicles and facilities designed to use oil products. The oil products industry is also a significant source of employment and highly skilled value adding jobs. Overall, the oil products industry is an important element of the Canadian economy, and is well positioned to meet Canada's energy needs (Figures 12, 13).



Source : Infometrics Limited, SCF Petroleum Products Part 1, 1996



Source : Sector Competitiveness Framework, Part I, 1996;
Statistics Canada Census Data 1986-91

CANADIAN OIL SANDS SYNTHETIC CRUDE INDUSTRY

In 1996, Canada produced over 150 million barrels of oil from Alberta's oil sands which is equivalent to about 20% of Canada's crude oil production. Alberta has over 300 billion barrels of recoverable reserves in the oil sands deposits, greater than all the Mid East combined estimated reserves. Several companies have announced mega-plans for increased production of crude and bitumen blends from Canadian oil sands (Table 1). Projected investments of CS 25 billion by 2020 is expected to triple Canadian oil sands crude and bitumen production. A significant portion of the existing oil sands production and the expanded production will be supplied to the USA. Synthetic crude end products qualities are different from conventional crudes. The favourable properties of oil products produced from synthetic crudes are compared to the less desirable properties (Table 2). Market forces and future quality requirements will determine how these synthetic crudes will be refined to supply the fuels for the year 2000 and beyond.

TABLE 1 : MAJOR EXPANSION PLANS FOR OIL SANDS & HEAVY OIL

| Company | Announced Capital (Billion \$C) | Comments |
|--|------------------------------------|---|
| Suncor | 2.2 | Expands Capacity from 105,000 bbl/d to 210,000 bbl/d |
| Shell | 1.0 | Bitumen Production capability : \$375 MM for a Heavy Oil pipeline to its refinery in Edmonton & additional capital for Upgrader |
| Mobil | 1.0 | Bitumen production within next five years |
| Syncrude | 3.0 | Expands capacity from 208,000 bbl/d to 312,000 bbl/d |
| Koch | 1.0 | 90,000 bbl/d of new bitumen facility by 2004 |
| Amoco, Pan Canadian, CS Resources, Gulf, Imperial Oil, Elan etc. | 2.5 | Various announced projects in Alberta |
| IPL Energy | 0.3 | Pipeline to carry Suncor's products |

TABLE 2 : SYNTHETIC CRUDE & PRODUCT QUALITIES DIFFER FROM CONVENTIONAL CRUDES

| Desirable Features | Less Desirable Features |
|--|---|
| <u>Whole Crude</u> | |
| <ul style="list-style-type: none"> ■ Low Sulphur 0.1 - 0.3 % ■ Low Bottoms ■ Very Low Corrosive Contaminants ■ High Gas Oils | <ul style="list-style-type: none"> ■ Diesel Cetane ~ 33 - 38 ■ Low Jet Smoke Point ■ High Diesel Aromatics ~ 45 % ■ High VGO Aromatics ~ 60 % |
| <u>Distillate Cut</u> | |
| <ul style="list-style-type: none"> ■ Low Sulphur ■ Low Pour Point < - 65 °F ■ Excellent Freeze Point & Cloud Point | |

ACKNOWLEDGEMENTS

The author wishes to acknowledge Ray Burton (Imperial Oil Ltd.), Gene Carignan (Petro-Canada), Gerry Ertel (Shell Canada Products Ltd.), Bruce Orr (Imperial Oil Ltd.) and the Canadian Petroleum Products Institute for their work on the original internal CPPI position paper which formed the basis of this article.

REQUIREMENTS FOR THE FUTURE AVIATION JET FUEL TO BE DEVELOPED BY MOLECULAR ENGINEERING OF LIQUID HYDROCARBON FRACTIONS

Jouni Enqvist, VTT Chemical Technology, P.O.Box 1402, 33101 Tampere, Finland and
Maarit Enqvist, J&M Group Ky, P.O.Box 61, 33960 Pirkkala, Finland

Abstract

Requirements for the molecular basis of the future aviation jet fuel will be discussed and the work going on in Finland for this goal will be reviewed. The most important environmental aspects are efficient combustion performance for suppressing formation of toxic compounds like nitrogen oxides and certain polycyclic aromatic hydrocarbons. The most harmful uncompleted combustion products are carbon containing nanoparticles that contain adsorbed nitrogen oxides and carcinogenic aromatic compounds. Therefore fuel combustion cleanliness is one of the most important goal in our investigations not only because of our health but also because of the cleanliness of critical fuel system components and the engine. These objectives together with the need of adding molecular specifications for the future fuel are discussed.

Introduction

The most important requirement for the future aviation jet fuel is to conserve the existing operational and handling safety of the present kerosene based fuels. Hydrogen and other gaseous or liquid low-boiling fuels require much more efforts to prevent fuel leakages and other safety arrangements in any accidental functional problems of the fuel system. Therefore, it is very likely that the jet fuel beyond the year 2000 will be a modified kerosene manufactured from crude oil, natural gas, coal or any carbon and hydrogen containing stock or waste material. This solution would be the most efficient for every day air traffic with jet engine air craft and also for the majority of the military air craft.

The necessary practical properties specified or otherwise important for commercial and military fuels like necessary chemical, physical and biological stability, clean combustion for the engine and environment, lubricity and corrosion prevention for the fuel system, conductivity to prevent electrical discharges, proper viscosity in different temperatures, proper temperature conductivity and cooling capacity for engine lubricant and other fuel cooled aircraft components and finally anti-icing property to prevent formation of ice crystals at low temperatures are presently obtained by formulating the kerosene fraction with several approved additives. In the future the above properties of the fuel will be most likely introduced to the kerosene in the fuel processing and therefore no or much less additives would be needed. This approach will simplify the fuel handling and logistics because specific fuel properties can be tailored in the refineries by molecular engineering of the kerosenes. There are several advantages of this approach because water separation will become unnecessary due to the controlled water solvating properties of the fuel and fuel compatibility with different types of engines, fuel system seals and any acceptable operating conditions.

The aim of this paper is to describe requirements for the future kerosene fuels on the basis the research work carried out several years in Finland and recently in a close cooperation with Finnish Air Force. The general approach has been to investigate and develop analytical methods for complete characterization of each of the hundreds of energy producing compounds of kerosenes as well as molecular structure and reaction mechanisms of natural and additive trace compounds that make kerosenes acceptable as the specified Jet A-1 or JP-8 fuels.

It is natural that new molecular specifications are needed in the future to achieve the perfect control of fuel performance in all conditions. Therefore, another goal of our research work is to develop chromatographic conditions for adequate separation of all jet fuel compounds that have significance on fuel behavior and specifications and, on the other hand, the development of retention index library for fuel compounds to make possible in the future an automated monitoring of molecular specifications of jet fuel compounds for principal energy producing molecules and for principal trace property molecules like stability, combustion, lubricity, anti-icing, conductivity etc. The complexity of kerosene fuels requires the use of hyphenated techniques like the two-stage retention index monitoring HRGC (RIM/RIM) method what we

have earlier used for monitoring benzene from gasoline. In development of RIM/RIM library mass spectrometric detection is necessary together with the high field NMR analysis of fuel fractions. The routine system would however be most likely based on HRGC/RIM/RIM with flame ionization detection (FID).¹⁻³

Experimental

Several Jet-A1 and JP-8 samples based on different kerosenes were analyzed using high resolution gas chromatography (HRGC), HRGC-mass spectrometry (MS) and high field nuclear magnetic resonance (NMR) spectrometry methods. Instruments used were Micromat HRGC 412 with two 15 m capillary columns (a cyanopropyl NB-1701 and a phenyl methyl silicone NB-30) and two flame ionization detectors (HNU Nordion) and Hewlett-Packard HP 5890 GC with HP 5970A Series Mass Selective Detector (MSD). Some samples were analyzed just as obtained from the refinery (Neste Oy), some of samples were of different age (Finnish Air Force) and one sample (Sabena Air Lines Depot) was allowed to stand up to two and half years before analysis. Some samples were also oxidized by bubbling air or oxygen through the fuel to follow the formation of oxidation products.⁴ NMR instrument used was Varian Unity 600 operating at 600 MHz for protons and at 150 MHz for carbon-13 measurements.

Results and Discussion

Jet fuel specifications were studied with the objective of elucidating chemical reaction mechanisms and physical interactions that determine the behavior of fuel as whole material and how individual major and trace compounds produce this bulk behavior for the fuel. Because some natural trace molecules and additives are extremely important in fuel performance careful library and patent search was carried out about these molecules and their functioning in combustion and fuel system was elucidated together with our own experimental work.

The most important result of this work is the critical evaluation of environmental aspects of jet fuel combustion. A conclusion was made on the basis of medical reasons. It is known that combustion exhaust of jet engine produces more or less small particles and gaseous contaminants from which nitrogen oxides and some polycyclic aromatic hydrocarbons are the most harmful. Amount and quality of these harmful exhausts depend on type and functioning of engine and amount of power taken from the engine at a moment of time and also on the chemical composition of the fuel.

While carbon dioxide has also been mentioned as a harmful exhaust it is not toxic and we consider it therefore as of the secondary importance. A sooting flame of jet engine produces visible particles of micron size or more but a non-sooting flame may also produce small nanometer scale particle that are not visible but may be even more harmful because of larger surface area which may be occupied by carcinogenic molecules. Therefore in the future the combustion should be perfect with any type of engines, with single or two-stage combustion zones, producing only carbon dioxide and water as the combustion products. This means that both the future engines and future fuels should be optimized and jointly developed. The fuel should be free of harmful trace elements and contain structural groups which enhance clean and efficient combustion without producing harmful deposits or other products.

Another important fuel property is its lubrication capability. Fuel is the only lubricant of fuel pumping system and the whole line of fuel system components up to the injector nozzle. It should therefore have an adequate corrosion inhibition and boundary lubrication behavior which works mainly through surface active alkyl phenols and carboxylic acids derivatives which are natural or additive trace molecules. We have studied commercial diesel fuels for boundary lubricants and use this data also for designing adequate lubricity for the future green jet fuel.⁵

Autooxidative, surface catalytic, pyrolytic and mechanochemical stability of fuel at high temperatures and the other necessary properties should on the basis of the above discussion be obtained by molecular tailoring of the fuel production process. With the present knowledge about catalysis these process modifications are realistic and cost effective so that production costs of the future green fuel will not be significantly higher compared to the present fuels.

To guide this work and also to make possible future fuel quality monitoring molecular specifications are needed and for this purpose we develop an automated sample preparation HRGC-RIM/RIM -system that can be used by oil companies, air line companies and military operators. Molecular procedure based on high field NMR and HRGC are being developed to

automatically determine combustion index, lubricity index, and fuel stability index from the analytical data. These figures are naturally calibrated with bulk property tests which data are used for refinement of fuel specification index calculations. This research and development work is going on in Finland and the first results will be a prototype green fuel according to the above guidelines and a prototype molecular level fuel analyzer.

References

1. Enqvist J. , "Kinetic study of complicated reactions by glass capillary gas chromatography.", Symposium on Chromatography, Kemian Päivät 77, Kemia-kemi 4 (1977) Nr 11 .
2. Hesso, A., Siivinen, K., Enqvist, J. and Kuronen, R., "Interphasing of capillary columns to a mass spectrometer; influence of vacuum on the separation efficiency.", Symposium on Separation and Fractionation Methods in Chemistry, Kemian Päivät 79, Kemia-Kemi 6 (1979) 12.
3. Enqvist, J. and Enqvist, M. "Comparison of two-stage retention index monitoring capillary gas chromatography and selected ion monitoring capillary gas chromatography - mass spectrometry as analytical tools", Journal of High Resolution Chromatography. Vol. 17 (1994) Nr: 3, pp. 141 - 144
4. Enqvist, J., Ranta, E. and Enqvist, M., "Characterization of Autooxidation Products of Aviation Jet Fuels by Gas Chromatography coupled with Mass Spectrometry. Preprints of the 215th ACS National Meeting , March 29 - April 2, 1998, Dallas, Texas.
5. Enqvist, J., Östman, P., Enqvist, M. and Wickström, J., "A High Resolution Gas Chromatography - Mass Spectrometric Selected Ion Monitoring Method for Determination of Boundary Lubricating Molecules in Cleanly Burning Diesel Fuels", ACS National Meeting at Boston, August 23-27, 1998. Symposium on Chemistry of Diesel Fuels, Division of Petroleum Chemistry.

A Perspective on Coal in the 21st Century

By

Craig Vogel
Manager, Technical Marketing
Cyprus Amax Coal Company

Abstract

Coal represents 95% of the United States fossil energy reserves and U.S. coal resources represent more energy than either world oil or natural gas reserves. Coal fired power plants currently produce 56% of U.S. electrical generation. Increasingly more stringent environmental standards for SO₂, NO_x, and mercury are putting pressure on future coal use. With current and evolving technologies, coal should be able to meet these new challenges and remain competitive with other generation options such as natural gas. There is, however, a major obstacle that severely threatens use of coal in the future. The issue of global climate change and corresponding requirements for CO₂ reductions present a major hurdle for the coal industry as we look towards the next century.

This paper presents a discussion of historical and projected electrical generation and fuel sources. It looks at technology options that will be cost effective and comply with increasingly more stringent environmental standards. Also, the issue of climate change and how coal could be affected by actions such as the Kyoto Protocol is presented.

Discussion

Coal currently is responsible for 56% of total electrical generation in the U.S.; natural gas, 13%; nuclear, 17%; hydro, 9%; renewables, 3%; oil, 2%. In EIA's 1998 forecast, coal is expected to grow at about 1% annually but will decrease its share of generation to 47% in 2015. Through retirements, nuclear's share decreases to 10%. Oil and hydro retain the same amount of generation but their contributions decrease to 1.5% and 7% respectively. Use of renewables increases slightly but its share remains around 3%.

While coal use increases, natural gas is forecast to be the big winner. The reason for this is partially due to the low capital costs of combined cycle gas plants and their attractive heat rates. The "wild card" is natural gas deliverability to utilities and delivered prices, which are assumed to increase only slightly from \$2.28/mmbtu in 1996 to \$2.74/mmbtu in 2015. Given natural gas' track record, these assumptions appear optimistic.

Comparing electricity prices for different regions we find that areas with the highest coal-fired generation have the lowest cost power. Interior regions relied on coal for 70% of generation in 1995 while coastal regions used 35% coal firing.

Lower cost coal fired generation has also resulted in increasing coal plant capacity factors.

The increasing concern over global climate change and carbon emissions reduction poses a significant threat for coal's future. Electric generation contributes about 36% of U.S. CO₂ emissions with transportation providing 33%. Both sectors are forecast to increase their emissions, however, due to the public's love affair with larger and less efficient vehicles, electrical generation may be called upon to bear a disproportionate amount of any required CO₂ reductions.

The Kyoto protocol requires the U.S. to reduce its carbon emissions to 7% below 1990 levels by 2008. This would require a 44% reduction from projected "business as usual" emissions in 2010.

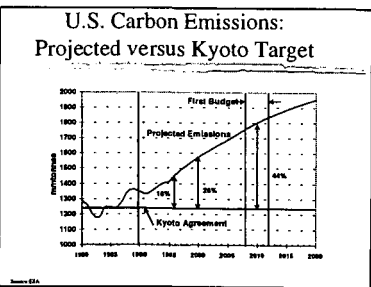
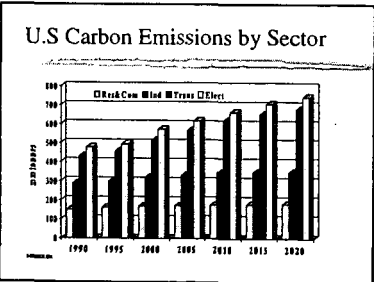
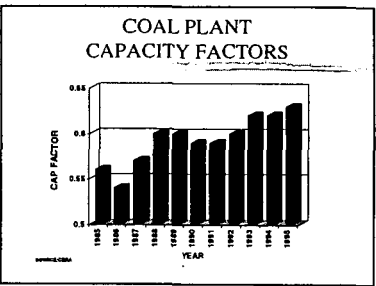
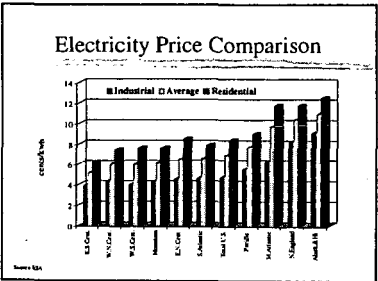
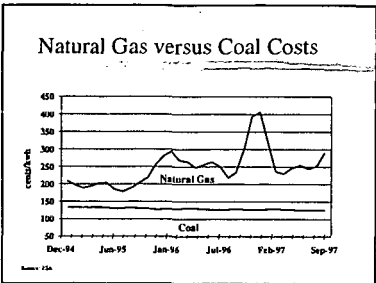
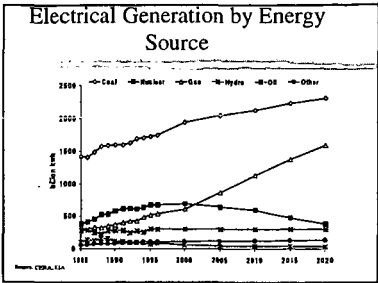
Historically, since 1970, the United States has had an average electrical growth rate of 3.14%. GDP has grown at a rate of 2.69% during this same period resulting in a ratio of electrical growth to GDP of about 1.2 to 1. U.S. total energy use grew at a rate of only 1.29%, about half that of electricity. This indicates that we are experiencing greater electrification. In 1995-96, the electrical growth to GDP ratio was 1.3 to 1. EIA's 1998 forecast assumes an increase in efficiency of more than 40% from today. This results in electrical growth to GDP ratio decreasing to 0.83 to 1 by 2000 and 0.73 to 1 by 2020.

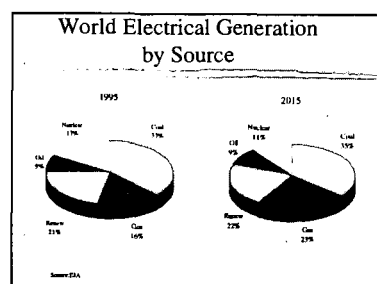
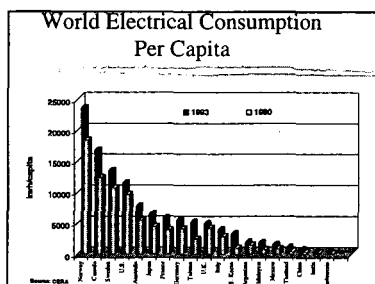
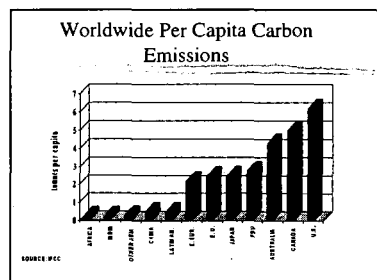
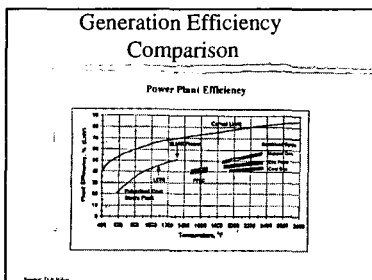
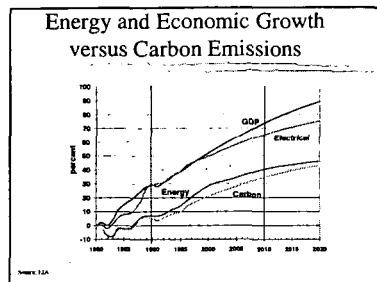
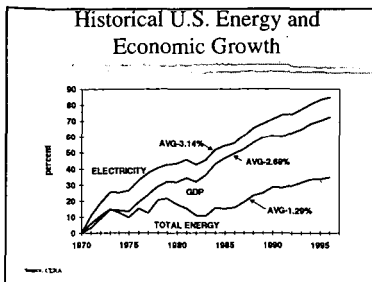
Since coal is carbon based, even with more efficient power plant designs such as the LEBS, with its 45% efficiency, coal emits twice as much CO₂ as a natural gas fired combined cycle gas turbine. Existing coal-fired plants can do little to improve efficiency to any great degree.

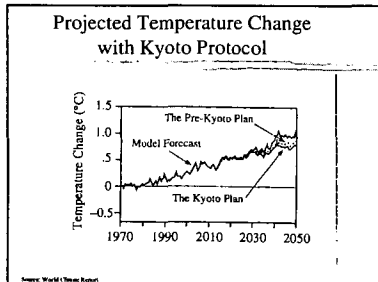
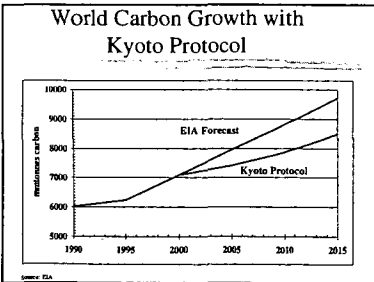
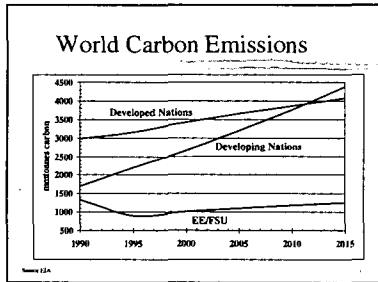
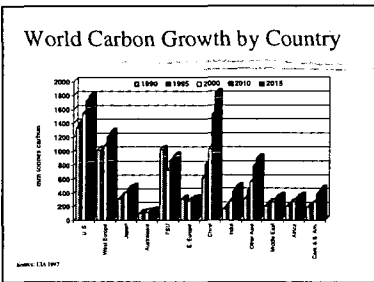
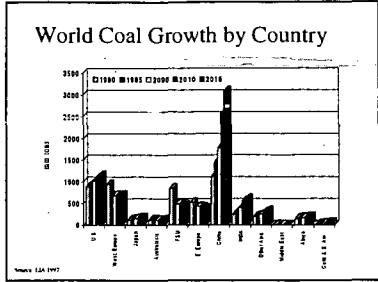
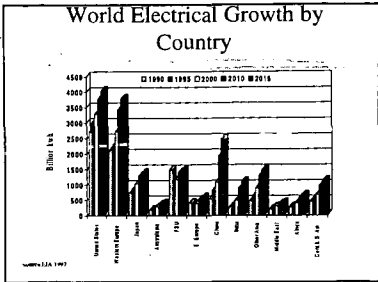
On a global basis, it is important that new technologies be continued to be developed and implemented for it is the developing nations that hold the key to future carbon emissions. While

the U.S. is clearly the largest emitter of carbon on both an absolute and per capita basis, projections show China to surpass the U.S. by 2015.

If the Kyoto Protocol were to be implemented, it would have little effect on global concentrations of carbon and projected global temperatures. It would have significant effects on the U.S. economy and would likely shift emissions from the U.S. to those countries not bound by the treaty. It would also prevent development of more efficient coal fired generation technologies that would help the third world nations as they grow their economies.







AUSTRALIAN FUELS, ENERGY, AND GREENHOUSE GAS EMISSIONS: IMPLICATIONS FOR THE 21ST CENTURY

B. C. Young, D. J. Allardice, and J. R. Hamilton
HRL Technology Pty Ltd, Mulgrave, Victoria, Australia 3170
ACS Paper, Boston, August 1998

INTRODUCTION

Australia with a population of only 18 million has abundant reserves of black and brown coal/lignite (hereafter referred to as brown coal), and substantial reserves of oil, natural gas, and uranium. Being a very large temperate-to-sub-tropical continent covering 7,682,300 km² (Australian Bureau of Statistics [ABS, 1997]), approximately equivalent in area to that of the continental U.S., Australia experiences abundant sunshine and significant windy regions. These natural characteristics along with the fossil fuels already mentioned, signifies the country as energy resource rich. As a consequence of its fossil fuel resources and its large reserves and diverse range of minerals, Australia has become both an export supplier of raw commodities, such as coal and iron ore, and of secondary processed materials, such as aluminium ingots and uranium yellowcake. These mining and mineral processing developments, along with the increased infrastructure and industrial, commercial, and domestic demands, and the large travel and transport distances, particularly over the last 25 years, have resulted in the country's greenhouse gas emissions being among the highest in the world on a per capita basis, (1.4 % of global greenhouse gas emissions [Skelton, 1997]).

This paper addresses fossil fuel resources and other energy sources in Australia, electricity generation and energy consumption, greenhouse gas emissions, and recent economic and structural changes in the electricity and gas industries. Issues to be briefly considered include new energy technologies, fuel alternatives, CO₂ reduction strategies, and future energy developments.

FOSSIL FUELS AND ENERGY SOURCES

By far the largest of Australia's fuel resources is coal, including bituminous, sub-bituminous, and brown coal, the resources of which are shown in Table 1. Australia is the world's largest exporter of black coal, exporting almost 146 million tonnes in 1997 (Australian Bureau of Agricultural and Resource Economics [ABARE, 1997]). It ranked as the fifth largest producer of hard coal in 1996 (World Coal Institute web page). In 1997 production was 6.7 % higher than that in 1996 at 207.5 million tonnes. The large black coal resources, mostly bituminous, are found in Queensland and New South Wales (NSW). Much smaller quantities of sub-bituminous coal exist in Western Australia, Queensland, and NSW. Brown coal is substantially located and mined in Victoria and lesser quantities in South Australia. This resource represents about 27 % of the Australia's total energy reserves.

Table 1 also shows the currently reported resources of gas, oil, and uranium. Australia is the second largest producer in the world of uranium (Uranium Institute, 1997) but it uses no uranium domestically for generating electricity. Self-sufficient in oil to the extent of 73 % at present, Australia is predicted to see a decline in self-sufficiency to about 61 % in the next five years, assuming no discovery of a major oil field [Private Communication, 1998]. Natural gas is produced in significant quantities on-shore, mainly in South Australia, Northern Territory, and Western Australia, as well as off-shore Victoria and Western Australia where the gas fields are much larger than on-shore. Significant quantities of liquefied natural gas are shipped in cryogenic form overseas but within Australia gas is the predominant fuel for domestic and industrial applications.

Australia's latitude enables it to receive monthly mean daily solar irradiation ranging from a minimum of 5.0 MJ/m² in Hobart and Launceston, Tasmania to a maximum of 31.0 MJ/m² at Geraldton, Western Australia, (Lee, Oppenheim and Williamson, 1995). Its solar potential is under utilised for energy generation but significant use is made of it for drying and heating purposes by the agricultural and chemical industries, e.g. for bagasse, salt, and by the domestic sector, e.g. for clothes drying, hot water systems. Australia is largely a dry continent, exhibiting substantial hot regions and variable but not extensive rainfall, from a minimum median annual rainfall of 100 mm at Lake Eyre in South Australia, to a maximum median annual rainfall of 4,048 mm at Tully in Queensland (ABS, 1997). These conditions along with extensive land clearing have led, in general, to sparse tree cover in areas beyond a relatively narrow strip around the eastern and southeastern seaboard and the island state of Tasmania.

Significant wind energy sources are located around the Australian mainland coast and southern islands, e.g. Tasmania, King Island, Lord Howe Island. Typically at selected points the wind speed will exceed 6 m/s at a height of 10 m, sufficient for a sustainable wind energy farm [Osborne, 1993].

Apart from solar and wind energy, other renewables available as energy sources in Australia are biomass and hydro. Particularly for Queensland, NSW, and Tasmania, there are significant quantities of bagasse from sugar cane production and other agricultural residues (e.g. cotton trash), forestry residues, saw mill waste, and municipal wastes (Spero, 1998). However, they are small in relation to the coal reserves and suffer from large volume to mass ratio, big distances between recovery points and end usage location, and consequently often greater cost and seasonal variability.

ELECTRICITY GENERATION AND ENERGY CONSUMPTION

Current electricity demand in Australia is around 160,000 GWh per year. Growth rate in electricity demand over the last decade has been 5 to 7 % per year [Schaap, 1998]. A lower growth rate is likely over the next decade, although the power demand in the manufacturing and commercial sectors is projected to be higher than that in the residential sector.

On a national basis the electricity generation supply mix is shown in Table 2. However, on a state by state basis there are significant variations, e.g. in Queensland and NSW 98 % and 93 % respectively of electricity generation is coal based; in Tasmania, virtually 100 % is based on hydro (Electricity Supply Association of Australia Limited, [ESAA, 1997]).

Brown coal, containing between 60 % and 70 % water, is Victoria's major fuel source for generating electricity, representing 97 % of the supply mix and producing 39,755 GWh in 1995/96 (ESAA, 1997). Victorian brown coal is also used to make briquettes in a cogeneration plant having a capacity of 1.2 million tonnes although recently operating at about half that throughput. The briquettes are used for steam raising, heating, and electricity generation by industry, hospitals, and residential homes (heating/cooking). A significant proportion of the production is exported to niche markets including Germany. The advantages of this solid fuel are low NO_x and SO₂ emissions on combustion, relatively low moisture (13-14 wt %) compared to the parent coal, very low mineral matter content (<2 wt %), ease of ignition and good combustion in a conveniently transportable solid form. Although the coal is reactive in the dried form, the briquettes can be safely stored and shipped in bulk to markets as far away as Europe.

Considering total energy consumption, it is noted that in 1995-96 the three dominant and virtually equal sectors are electricity generation, transport, and manufacturing at 26.9 %, 26.2 %, and 25.5 % share respectively. Far lower proportions of energy were consumed in the residential, mining and commercial sectors at 8.1 %, 5.1 % and 4.2 % respectively; the agriculture and other sectors were 1.5 % each. Over the next decade, the three major sectors are predicted to have similar shares of energy consumption but the mining sector will grow (to 6.5 %) and the residential decline (to 6.9 %) [Private Communication, 1998].

GREENHOUSE GAS EMISSIONS

Strategies for controlling and reducing greenhouse gas emissions are now receiving increased attention, especially in view of the recent Kyoto Greenhouse Summit in November 1997. In 1994, stationary energy (i.e., largely for power generation) produced 37 % of the total of CO₂-equivalent greenhouse gas emissions in Australia whereas the transport sector generated slightly less than a third of this amount (ESAA Greenhouse Challenge Workbook, August 1997). Given the commitments from Kyoto, and the Australian Federal Government Greenhouse Challenge Program, activities are in progress that are likely to change the type, mix, and use of fuels, as well as the implementation of new technology, as Australia enters the next century. The Australian Federal Government has also made a commitment to redefining strategies for land use clearing and forestry as well as defining objectives and offering incentives to enhance the use of renewables towards achieving a net reduction in Australia's release of CO₂, methane and other greenhouse gases. To stimulate the use of renewables, the Australian Government, for example, has set as a requirement an additional 2 % of electricity to be derived from renewable energy by 2010.

Already, efforts to increase efficiency of current plant equipment, and the installation of more efficient technology have begun as a means of reducing greenhouse gas emissions. For example, in Victoria, HRL Limited has anticipated the need for higher efficiency in future brown coal use (and low rank coal, in general) for electricity generation and has just completed a 3.5 year-development project, investigating the innovative technology of Integrated Drying Gasification

Combined Cycle (IDGCC) [Johnson et al, 1997]. The IDGCC concept essentially replaces a separate atmospheric pressure dryer before the gasifier and a high pressure gas cooler after the gasifier with a direct contact entrained flow dryer, which is a high-pressure pipe. Increased generation is achieved in the gas turbine cycle by the additional mass flow of the evaporated moisture passing through the turbine. The process is schematically shown in Figure 1. The project successfully demonstrated at a 10 MW scale a 20-30 % improvement in efficiency and a corresponding reduction in CO₂ emissions and cost over conventional thermal power generation using the same coal.

Other efforts to reduce greenhouse gas emissions have included the development and demonstration of photovoltaic receptor arrays and wind farms, albeit on a small scale at this stage. One Australian company, Pacific Solar, aims to construct its first facility for making 20 MW per year of photovoltaic modules in 1999 and be in operation by the last quarter of 2000. This first facility will produce, through a radically different manufacturing process, sufficient relatively low cost solar modules to meet the demands of 7000 homes per year, representing under 5 % on average of Australian homes built each year. The target installed cost is to be competitive with the current delivered price of conventional electricity in Australia (AUD 10-15 cents per kWh) [Lawley, 1998].

Wind farms are also on the agenda for achieving greenhouse gas reduction in Australia. States including Western Australia, N.S.W., Victoria and Tasmania have active programs, privately and publicly sponsored, to produce electricity from wind turbines. In Victoria, for example, a private company, Energy Equity Limited, has recently been granted approval to build Australia's largest renewable energy project excluding hydropower. Subject to resolving local objection, the company will install 35, 60-metre high wind turbines, about 400 metres apart, based on three sites near Portland, southwestern Victoria and generating 20 MW of power for domestic distribution [Watkins, 1998].

Electricity generation companies using coal as a fuel are taking steps to reduce CO₂ emissions apart from just increasing energy efficiency of existing plant. Plantations of fast growing trees have been established in the different regions adjacent to power stations and elsewhere. In Victoria, by the end of 1992, 1409 hectares of pine and eucalypt trees had been planted in proximity to the brown coal-fired electricity generation sites [State Electricity Commission of Victoria, 1992]. In addition, the various electricity generation companies and their consultants are watching developments in the sequestration of CO₂ such as via liquefaction and storage in deep caverns, and photosynthesis by specific algae. However, sequestration of CO₂ could cost AUD \$3-4 cents per kilowatt-hour, virtually doubling generation costs.

Adopting a "business as usual approach", the baseline Australian scenario for CO₂ emissions was projected to grow by 45 % between 1990 and 2010. In the Kyoto Protocol, Australia has been granted a national emissions budget of 108 % of the 1990 level. Given an estimated 20 % in population growth over next 20 years and an economic growth of 1.5 % per year, it has been concluded that absolute reductions would not have been possible and the special allowance was needed. Assuming CO₂ credits for reduction in land clearing and other changes in the forestry sector, it is possible that the energy sector emissions budget could approach 125 % of 1990 and still meet the Kyoto target for national greenhouse gas emissions for the period 2008-2012. Future developments in CO₂ emissions trading are also likely to offer the potential for offsetting expansion in the Australian energy sector (Key Economics, 1998).

ECONOMIC AND STRUCTURAL CHANGES IN ELECTRICITY AND GAS INDUSTRIES

The State of Victoria has led the way in the privatisation of the electricity industry in Australia. The four generating companies, privately owned by various consortia of international and national companies, are now operating in a deregulated market. Approximately AUD \$9,600 million has been paid for the 6000 MW of brown coal generating plants making premature closure an unrealistic option. The distribution companies are also under private control but not fully deregulated until 2001. Privatisation and deregulation of the gas industry is also progressing with sections of the former government-operated gas distribution entity being corporatised. Other Australian states are in various stages of privatisation of the electricity industry, with South Australia proceeding next.

The very substantial investments made in the Victorian electricity generating utilities are having major consequences. These include increased availability of generation plant (by 10-15 %), planned extension to operating life of the plant from 30 to 50 years typically, and new competitive constraints on the price of electricity "at the fence". The current effect of the latter is to drive the price dramatically downwards. In addition, a comprehensive review of personnel

levels, maintenance contracts, the implementation of new technology, environmental control and monitoring equipment, to name some issues, has led to radical changes concomitant with significant expenditure reductions. Economics is a major driver and long-term strategic planning needs are evaluated on a strict cost-benefit analysis. The new forces of economic and structural change will thus have a substantive and diverse impact on the development and practice of the electricity and gas industries as well as on the response of the consumers in the 21st Century. For future power requirements, gas is available particularly for peaking power, while advanced low rank coal technologies, having been demonstrated, will achieve substantial efficiency improvements in future brown coal plants.

CONCLUDING REMARKS

Coal is still Australia's dominant fuel resource for energy generation with reserves lasting about 550 years for brown coal and about 250 years for black coal, at present rates of usage, compared with reserves of oil and gas lasting approximately 40 and 60 years respectively. Coal fired power generation is forecast to be Australia's dominant stationary energy source well beyond the year 2000. Efforts are highly likely to be made to increase the use of alternative fuels, such as gas and biomass, and to implement new technologies along with alternative energy source options, such as photovoltaic arrays and wind power. However, their cost-effectiveness in relation to total plant investment will be closely scrutinised as the number of Australia's generation facilities are privatised. Also, fuel substitution on a large scale is a limited option due to cost, location, and availability factors but the creative use of biomass, say through reforestation, and a CO₂ emissions trading mechanism may provide alternative offsets to the greenhouse gas impact of energy expansion. Nonetheless, Australia in the 21st Century will probably see a greater mix of energy/fuel sources to meet the electrical, industrial, agricultural, and transport demands of the growing economy while concurrently endeavouring to limit the release of greenhouse gas emissions.

REFERENCES

- Australian Bureau of Agricultural and Resource Economics [ABARE, 1997]: Australian Commodities: Forecasts and Issues, 4 (4), 469-471, 1997.
- Australian Bureau of Statistics, [ABS, 1997]: Australian Year Book, 1997.
- Bureau of Resource Sciences (1997): "Australia's Identified Mineral Resources 1997"; "Oil and Gas Resources of Australia 1996"; Canberra, Australia.
- Electricity Supply Association of Australia Limited (ESAA, August 1997): Greenhouse Challenge Workbook.
- Electricity Supply Association of Australia Limited [ESAA 1997], Electricity Australia 1997, Fiftieth anniversary issue.
- Electricity Supply Association of Australia Limited [ESAA] web page.
- Johnson, T., Mouritz E., and Pleasance G.: "Development of the IDGCC Process for Cleaner and Cheaper Generation of Electricity from Low Rank Coal", Fifth Annual Technical Seminar "Clean Fossil Energy: APEC Choice for Today and Tomorrow" in the APEC Experts' Group on Clean Fossil Energy October 28-30, 1997, Reno, USA.
- Key Economics Pty Ltd: "Greenhouse Briefing: Australia After Kyoto", Report, March 1998, Kew, Victoria, Australia.
- Lawley, P.: "Photovoltaics: Future Directions", Proceedings of the 4th Renewable Energy Technologies & Remote Area Power Supplies Conference (ESAA), February 23-25, 1998, Hobart, Australia.
- Lee T., Oppenheim D., and Williamson, T. J., ERDC 249 Australian Solar Radiation Data Handbook - Main Report, Energy Research and Development Corporation [ERDC], April 1995.
- Osborne, J. (1993): Review of Renewable Energy Technologies for the Generation of Electricity in Victoria, June 1993.
- Private communication: ABARE Canberra, February 1998.

NATURAL GAS AND EFFICIENT TECHNOLOGIES A RESPONSE TO GLOBAL WARMING

Meyer Steinberg
Brookhaven National Laboratory
Upton, NY 11973

Key words - CO₂ mitigation, natural gas, efficient technologies

INTRODUCTION

Global Warming has become an environmental problem caused by the use of fossil energy. The emission of the radiative gas CO₂ from a particular country is intimately connected with the size of its population, its efficiency of utilization of fossil energy and the carbon content of the fuel. This paper deals with CO₂ mitigation technologies including the reuse of emitted CO₂ and indicates a direction for CO₂ emissions reduction for the U.S. economy.

The average CO₂ emissions for the three fossil fuels are as follows: Coal - 215 LbsCO₂/MMBTU (HHV = 11,000 BTU/Lb and C content of 76%); Oil - 160 Lbs CO₂/MMBTU (HHV = 6 MMBTU/Bbl) and Gas = 115 Lb CO₂/MMBTU (HHV = 1 M BTU/cu. ft.). Table 1 shows the U.S. fossil energy consumption and CO₂ emission, the total world consumption and emission and the principal energy supply service. In the U.S., most of the coal is used for generation of electrical power, in large central power stations. Oil is mainly used for production of transportation fuel (gasoline and diesel) with some limited electrical power production and gas is mainly used for industrial and domestic heating. However, there is also lately a growing consumption of natural gas for electrical power production.

Substituting Natural Gas for Coal for Electrical Power Production

If all the current electrical power production in the U.S. is generated by natural gas in combined cycle power plants, two benefits of CO₂ emission are achieved. First, the efficiency of electrical power production is increased from the current average coal-fired plant efficiency of 34% to over 55% for a modern natural gas fired turbine combined cycle plant and secondly the CO₂ emission per unit of energy from the fuel is reduced by 47% compared to the coal-fired plant. Applying this to the U.S. consumption, and assuming that natural gas usage remains the same a 22% reduction in the total CO₂ emission can be realized.

Substituting Natural Gas for Oil for Automotive Transportation

Compressed natural gas (CNG) vehicles are already on the market and if natural gas is substituted for oil in the transportation sector a 13% reduction in CO₂ emissions can be realized in the U.S. Thus, the substitution of natural gas for Coal and Oil in the electrical power and transportation sectors adds up to a 35% overall reduction in CO₂ emissions.

The Camol System for Preserving the Coal Industry for Electrical Power Production and Reducing Oil Consumption by Substituting Methanol in the Transportation Sector

The Camol System consists of generating hydrogen by the thermal decomposition of methane and reacting the hydrogen produced with CO₂ recovered from coal-fired central power stations to produce methanol as a liquid transportation fuel. Figure 1 illustrates the Carnol System which has the following advantages: 1. The Carnol System preserves the coal industry for electrical power production. 2. The Carnol System produces a liquid fuel for the transportation sector which fits in well with the current liquid fuel infrastructure. 3. The Carnol System reduces consumption of the dwindling domestic supplies of fuel oil in the U.S.

In the Camol System, the carbon from the coal is used twice, once for production of electricity and a second time for production of liquid fuel for fueling the transportation sector, in automobile vehicles. The reduction in CO₂ emissions results from two aspects. The elemental carbon produced from the thermal decomposition of the methane is not used as fuel. It is either sequestered or sold

*Based on the report by Meyer Steinberg, "Natural Gas and Efficient Technologies: A Response to Global Warming, BNL 65451, Brookhaven National Laboratory, Upton, NY 11973 (February 1998).

as a materials commodity. In this respect, thermal decomposition of methane (TDM) has an advantage over the conventional steam reforming of methane (SRM) for hydrogen production reduced. In the TDM process, carbon is produced as a solid which is much easier to sequester than CO₂ as a gas. Furthermore, the energy in the carbon sequestered is still available for possible future retrieval and use. The carbon can also be used as a materials commodity, for example, as a soil conditioner. Table 2 gives the estimate of CO₂ emissions using the Carnol System applied to the U.S. 1995 consumption and indicates a 45% overall CO₂ emissions reduction. The methanol in this case is used in conventional internal combustion engines (IC) which is 30% more efficient than gasoline driven IC engines. The natural gas requirement would have to increase to 62 Quad which is three times the current consumption of natural gas for heating purposes. The rise in natural gas requirement is because only about 58% of the natural gas energy is used for hydrogen for methanol. Methanol production and that carbon produced is sequestered unburned to the extent of 0.58 GT. This can be considerably reduced by going to fuel cell vehicles.

Carnol System with Methanol Fuel Cells for the Transportation Sector and Substituting Natural Gas with Combined Cycle Power for Coal Fired Central Station Power

In the not too distant future, fuel cells will be developed for automotive vehicles. This will improve the efficiency of automotive engines by at least 2.5 times compared to current gasoline driven internal combustion engines. Direct liquid methanol fuel cells are under development. If we use coal or oil for central power stations, there will be too much CO₂ generated for liquid fuel methanol by the Carnol Process for the transportation sector using fuel cells. Therefore, it is much more energy balanced if we use natural gas for power because it generates the least amount of CO₂ per unit of energy. In this scenario, the natural gas in a combined cycle plant displaces coal for power production and displaces oil for methanol by the Carnol Process for transportation. The results are shown in Table 3. Thus, by applying natural gas for electrical power production, liquid fuels production for fuel cell driven automotive engines and for heating purposes an overall CO₂ emissions reductions of over 60% can be achieved. This degree of CO₂ emission reduction could stabilize the CO₂ concentration and prevent the doubling of the CO₂ in the atmosphere expected by the middle of the next century if business is conducted as usual. The 0.32 GT of carbon required to be sequestered is about 3 times less than the amount of coal mined in the U.S. currently. If a market can be found for this elemental carbon, such as a soil conditioner, the cost of methanol production can be significantly decreased.

Natural Gas Supply and Utilization

The all natural gas energy system of Table 3 requires a three-fold annual consumption in natural gas. Recent reports indicate that the current estimated reserve of conventional natural gas is of the same order of magnitude as the current estimated oil reserves which might last only for another 80 years or so. However, unconventional resources, especially methane hydrates and coal bedded methane indicate an enormous resource which is estimated to be more than twice as large as all the fossil fuel resources currently estimated in the earth. If this is so, then we can begin to think of utilizing natural gas for reducing CO₂ emissions in all sectors of the economy. It appears that even today that deep mined coal in several parts of the world, especially in England, Germany, and the U.S., has become too expensive; and, as a result, many of these mines have been closed. Most economical coal used today comes from surface mined coal. Furthermore, the contaminants in coal, sulfur, nitrogen and ash in addition to the high CO₂ emission mitigate against its use. Rail transportation of coal also becomes a problem compared to pipeline delivery of natural gas. When natural gas becomes available, even at a somewhat higher cost, it can displace coal and even oil for power production and transportation. Long term supply of economical natural gas is the main concern for increased utilization of natural gas.

Economics of Natural Gas Displacing Coal and Oil

The current unit cost for fossil fuel in the U.S. is for coal \$1.00/MMBTU, oil \$3.00/MMBTU and for gas \$2.00/MMBTU. For the total consumption of 76 Quad in 1995, the primary fossil fuel energy bill was \$167 billion. Applying this to the all natural gas scenario of Table 3, we come up with a natural gas fuel bill for the required 49 quads of \$98 billion. So there is a resulting 41% savings in the current fossil fuel bill. The cost of natural gas could go up to \$3.50/MMBTU without the fuel bill exceeding the current energy bill. In order to achieve these results, capital investment in the replacement new technologies must be made. Only incremental replacement cost need be considered, since capital investment will be needed, in any case, to replace old equipment under

business as usual conditions. Table 4 indicates the incremental capital replacement cost to achieve the all natural gas economy based on the following data.

- a) Replacement of coal fired plants including scrubbers, etc., runs about \$2000/kw(€); for the more efficient natural gas combined cycle plants runs about \$1000/KW(€); thus, there is a \$1000/Kw(€) capital cost savings and when applied to an installed capacity of 400,000 MW(€), the savings amounts to \$400 billion.
- b) For replacing oil refineries with Carnol Methanol plants which require CO₂ removal and recovery from the natural gas power plants, it is estimated that the current unit cost is \$100,000 per daily ton of methanol. The total incremental cost to supply the total 14 quads of methanol for fuel cell vehicles is then \$220 Billion. No credit was taken for the replacement of oil refineries, over time, so that this incremental capital cost is probably high.
- c) New pipelines will have to be built to transport the natural gas and new methods of extracting natural gas eventually from deep sea wells containing methane hydrates. Assuming \$1 million per mile for these new gas supply facilities and a rough estimate of 200,000 miles needed gives a capital cost of roughly \$200 billion. It is also assumed that the liquid methanol pipeline and tanker distribution will be about equal to the current liquid gasoline distribution for the transportation sector.
- d) In terms of replacing the current existing more than 100 million gasoline driven IC engine vehicles with fuel cell vehicles, it eventually should not cost much more than the present average cost of \$15,000 to \$20,000 per vehicle. And, so the incremental cost should be negligible and may even show a savings because of the more efficient fuel cell vehicle than the IC engine vehicle.

Table 4 indicates that the incremental savings due to the new technologies in the one electrical power sector just about balances the incremental cost in the other three sectors. Thus, the new total incremental capital replacement cost is negligible compared to the capital cost requirement for continuing with the business as usual current power technology structures.

Conclusions

The ability of achieving a 60% reduction in the U.S. CO₂ emissions by natural gas fuel substitution with improved technologies is based on the following assumptions and developments:

1. that there are vast reserves of natural gas that can be recovered from both conventional and non-conventional natural gas resources especially from methane hydrates and coal bedded methane at costs which are not more than about double current gas productions cost.
2. that an efficient Carnol process for methanol production based on thermal decomposition of methane can be developed.
3. that an efficient direct methanol fuel cell vehicle can be developed.

The benefits in terms of mitigating global warming provides a strong incentive for working on and achieving the required development goals. The all natural gas economy with efficient technologies for CO₂ global warming mitigation avoids alternatives of (1) sequestering CO₂ in the ocean or underground, (2) switching to nuclear power, and (3) relying solely on solar and biomass energy.

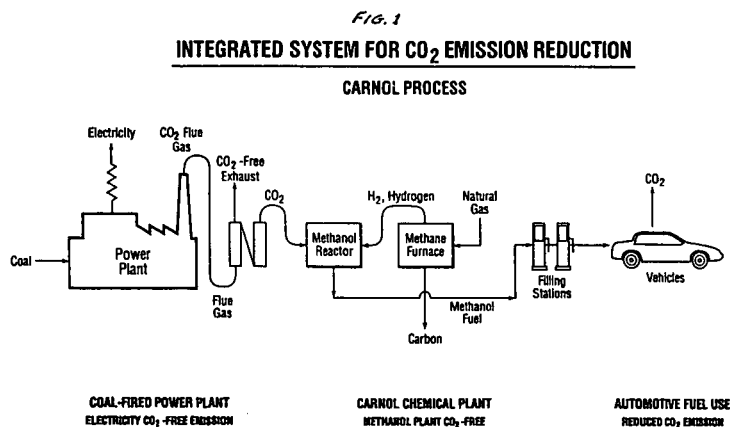


Table 1
Total Fossil Fuel Energy Consumption and CO₂ Emission for the U.S. in 1995^{a)}

| Fuel Type | Quantity | Energy Consumption Quads 10 ¹⁵ Q BTU | Principal Energy Service | CO ₂ Emission | |
|-------------|--------------------------|---|--------------------------|--------------------------|-----|
| | | | | GT(CO ₂) | % |
| Coal | 0.9x10 ⁹ tons | 20 | electricity | 2.15 | 35% |
| Oil | 5.8x10 ⁹ bbls | 35 | Auto transport | 2.80 | 45% |
| Gas | 21.0 TCF | 21 | heating | 1.21 | 20% |
| U.S. Total | | 76 | | 6.16 (1.68 GT(C)) | |
| World Total | | 330 | | 22.7 (6.2 GT(C)) | |

TCF = Trillion (10¹²) cubic feet
GT = Giga (10⁹) tons
Q = Quads (10¹⁵) BTU

Table 2
**Carnol Methanol Substitution for Oil in the Conventional Auto Transportation Sector
Produced from Natural Gas and CO₂ from Coal-fired Power Plants**

| Fuel Type | Natural Gas Consumed Quads | Energy Consumed Quads | Energy Service | CO ₂ Emissions GT(CO ₂) |
|--|-------------------------------|--------------------------|----------------|---|
| Coal ^{a)} | -- | 20 | Electricity | 0.22 |
| Methanol ^{b)} substitutes for gasoline | 41 | 24 | Auto Transport | 1.96 |
| Gas | 21 | 21 | Heating | 1.21 |
| Total | 62 | 65 | | 3.39 |
| Reduction from current CO ₂ emission | | | | 2.77 |
| % CO ₂ Emission Reduction from 1995 level | | | | 45.0% |
| Elemental carbon sequestered | | | | 0.58 GT (C) |

Table 3
**Natural Gas substituted for Coal Fired Power Production, Carnol Process for Methanol Production,
Substituting for Oil in Fuel Cell Vehicles for the Transportation Sector**

| Fuel Type | Natural Gas Consumption Quads | Energy Consumption Quads | Energy Service | CO ₂ Emission GT (CO ₂) |
|--|----------------------------------|-----------------------------|------------------------------|---|
| Natural gas for coal ^{a)} | 14 | 14 | Electricity | 0.08 |
| Methanol for oil | 24 | 14 | Auto Transport Fuel Cells | 1.12 |
| Gas | 21 | 21 | Heating | 1.21 |
| Total | 59 | 49 | | 2.41 |
| Reduction from Current CO ₂ Emissions | | | | 3.75 |
| % CO ₂ Emission Reduction from 1995 level | | | | 61% |
| Elemental carbon sequestered | | | | 0.34 GT (C) |

a) Natural gas for combined cycle power plant is 55% efficient and 90% of CO₂ emissions is recovered for Carnol plant.

Table 4
Capital Investment Required to Replace Present Power Structure

| Present Power Structure (and capacity) | Replacement Structure (and capacity) | Incremental Unit Capital Cost | Incremental Replacement Capital Cost \$10 ⁹ (\$ Billions) |
|---|---|--|--|
| Coal fired electrical ^{a)} power 400,000 MWe | Natural gas fired combined cycle electrical power | - \$1000/kw (savings) ^{a)} | - \$400 |
| Oil refineries ^{b)} 35 Quads | Carnol methanol plants 14 Quads | \$10 ⁹ /T/D Methanol ^{b)} | + \$200 |
| Wells and pipelines ^{c)} | additional pipeline and new methane hydrate wells | \$10 ⁹ /mile ^{c)} 200,000 miles of gas lines | + \$200 |
| Automotive IC vehicles 100 x 10 ⁶ | Fuel cell vehicles | 0 ^{c)} | - 0 |
| Net total incremental replacement cost | | | - 0 |

THERMOCHEMICAL CONVERSION RESEARCH & DEVELOPMENT ACTIVITIES IN CANADA

E.N.Hogan
Bioenergy Development Program
CANMET Energy Technology Centre
Natural Resources Canada
Ottawa, Ontario. K1A 0E4 Canada

ABSTRACT

An overview of the R & D activities and strategies of the Canadian Biomass Thermochemical Conversion Program, part of the CANMET Energy Technology Centre (CETC) will be presented. The paper will focus on the pyrolysis technology area and examine both the current status of research activities in Canada and the future research directions.

The major objective of this program is the development of cost competitive technologies that convert biomass into gaseous and liquid fuels and chemicals to be used for process heat, electricity, alternate refinery feedstocks and value added products. The program can be divided into the following main project areas: i) assessment of the potential of thermochemical conversion systems to process new biomass and/or waste feedstocks; ii) process development and optimization of thermochemical conversion processes; iii) evaluation of the potential of producing value added chemicals from pyrolysis products and determination of end use industrial applications for these; v) assessment of the commercial utilization of pyrolysis oils for heat and/or electricity production in boilers, diesel engines and gas turbines; and, vi) continued development and optimization of the production of high cetane diesel fuel from plant and vegetable oils.

INTRODUCTION

The objective of the biomass thermochemical conversion program is to develop cost competitive technologies that can thermochemically transform biomass materials into liquid, solid and gaseous fuels which can be converted to process heat, electricity, refinery feedstocks and value added products. Research efforts are focussing on processing, upgrading and utilization issues that will result in an optimal system for energy production. Work will also increasingly focus on the production of value added chemicals from the products of thermochemical conversion and will address the fractionation, isolation, recovery and application issues related to this. This paper will focus on the technology development and commercialization activities associated with pyrolysis technologies.

MAJOR PYROLYSIS RESEARCH AREAS

1. Assessment of the potential of pyrolysis to process new biomass and waste feedstocks, particularly those causing environmental disposal problems.
2. Process development and optimization of thermochemical conversion processes, including oil quality improvement and health and safety related issues.
3. Evaluation of the potential of producing value added chemicals from pyrolysis products and determination of end use industrial applications for these.
4. Assessment of the commercial utilization of pyrolysis oils for heat and/or electricity production in boilers, diesel engines and gas turbines.
5. Continued development and optimization of the production of cetane enhancers from plant and vegetable oils, including process optimization and scale up, co-product upgrading, laboratory engine and emission testing and field trials.

STATUS OF PYROLYSIS DEVELOPMENT

1. Assessment of the Potential of Pyrolysis and other Thermochemical Conversion Systems

In order to assist the fast pyrolysis technology in penetrating new industrial markets, various biomass feedstocks, particularly wastes presenting disposal problems, need to be assessed for

their potential concerning oil yields, product characteristics, etc. Waste biomass from a number of forest products companies have been successfully pyrolyzed by various groups involved in fast pyrolysis. Research projects with Ensyn Technologies and Pyrovac Institut to assess whether bark residues could be pyrolyzed have been completed, and the results indicate that industrial softwood and hardwood bark can be processed without operational difficulties. As a result of these tests, a number of forest companies are exploring the application of fast pyrolysis technology in the treatment of their bark wastes. Ensyn recently announced that a RTPTM plant will be built in the Prince George area of British Columbia with Northwood Pulp Timber Ltd. to convert bark residues to both a liquid bio-oil fuel and a natural resin to be used as a replacement for phenol or phenol formaldehyde in wood composite adhesive formulations. Pyrovac Institut is installing a plant in the St. Jonquiere region of Quebec to convert bark residues from forest operations in the area to bio-oil.

A research project is starting up with Kemestrie and Tembec's Chemicals Division to investigate fractionation methods that will result in the removal and recovery of extractives from bark rich residues. The work will identify marketable co-products that can be isolated from the extractives and address the use of the remaining biomass for subsequent fermentation or pyrolysis processing.

In evaluating further feedstock availability, agricultural crops and residues continue to represent a considerable potential. Feedstocks such as grasses and animal wastes are being examined by Ensyn Technologies and Resource Transforms Intl. to determine if pyrolysis could be part of an integrated biomass refining concept to produce a number of value added products, including energy, thereby increasing the overall commercial viability of biomass systems. Another problem associated with agricultural residues is the materials handling costs associated with bringing the biomass into a processing facility and an overall program priority is to examine systems, ie, collection, compaction, that will reduce the input feedstock costs.

Industrial biomass wastes represent another large source of biomass feedstocks that could provide economic opportunity, especially if the material has limited reuse, recycling or disposal options. An example of this is creosote treated railway ties. They continue to be used by railroads, combustion and landfilling are no longer considered as viable disposal methods and there is no alternate recycling program available. Stockpiling of these ties are costly and could pose a number of environmental concerns. As a result of this need to dispose of this ties, work is underway to evaluate wood treated with creosote to determine if they can be converted by pyrolysis to useful products. Ensyn Technologies and Resource Transforms Intl.(RTI) have also successfully processed a number of cellulosic packaging waste streams - corrugated, bleached and waxed cardboard to determine they can be converted to bio-oil with good liquid yields.

2. Process Development and Optimization of Thermochemical Conversion Processes

As thermochemical processes progress to commercialization, new technical problems that were not apparent previously concerning various aspects of the processes need to be addressed. Improved efficiencies of process components such as filtration methods or char separation systems are being proposed based on experience derived experimental pyrolysis runs. Current research projects are examining the technical viability of these methods as means of improving the efficiencies of the fast pyrolysis systems.

RTI Ltd. has recently developed a new fluidized bed pyrolyzer based on some concepts arising from a recently completed contract with CETC. Some principal features of this design include: blown through mode of char removal; bed temperatures between 360-490°C; residence times that can be greater than 2 seconds; indirect heating; deep fluidized bed with a height to width ratio greater than one; a mass ratio of recirculated non-oxidizing gas to biomass that is less than 2; biomass particles that are less than 3mm; and char that is thermally gasified in situ.

In another project related to health and safety issues, RTI Ltd. has performed a preliminary study on measuring the biodegradability of bio-oil using respirometry methods. The project results indicate that bio-oils are biodegradable in aquatic and soil environments; the biodegradability of bio-oil is substantially higher as compared to diesel fuel; and the neutralization of the bio-oil enhances their biodegradation in water. Additional studies using this respirometric approach will be required in order to develop an acceptable standard methodology.

3. Production of Value Added Chemicals from Pyrolysis

The production of co-product, value added chemicals, will improve the overall economics of biomass pyrolysis processes. This integrated recovery of fuels and chemicals from pyrolysis oils

is in the preliminary stages of development but will provide considerable impetus to the commercial implementation of pyrolysis processes if the existing technical and market barriers can be addressed.

Pyrolysis oil products in the early stages of development include: i) the development by Resource Transforms Intl. of a slow release fertilizer using pyrolysis oil as the binder/carrier; ii) the evaluation by Pyrovac Institut and Ensyn Technologies of the potential of using pyrolysis oil to produce a 'green resin' to replace phenol formaldehyde resins currently used in the production of waferboard, and; iii) the production of calcium salts by Dynamotive Corp. which when injected into coal fired burners may provide an effective means of reducing SOx and NOx emissions.

Various techniques are also being examined for the fractionation, isolation and recovery of pyrolysis oil components including pyrolytic lignin, levoglucosan and aldehydes. Lignin for example could be depolymerized to oxyaromatic monomers that could be upgraded to a variety of end products, ie, oxycyclic compounds, hydroxylated aromatics and Kemestrie Inc. is performing a feasibility study to evaluate this approach.

Another research focus in this area has been to examine the upgrading of the char produced from fast pyrolysis. A series of devolatilization and activation test runs and pelletizing/briquetting evaluations have been performed by pyrolysis industry groups to determine the potential commercial production of activated charcoal from the pyrolytic char and initial results look promising. In another char utilization project, the University of Saskatchewan is examining the characterization and steam gasification of high ash content pyrolysis chars. Preliminary work has found that the conversion (only of the combustible material, not counting the ash) ranges from 59% wt. For a Danish wheat straw sample to 93% for rice straw. The conversion appears to be a function of the source of the char (the type of feed material) and its history (residence time in the reactor and temperature) rather than the ash content of the char.

4. Assessment of Commercial Utilization of Pyrolysis Oils for Electricity and Heat Production

Boilers

A significant barrier to the commercialization of pyrolysis technology relates to the market acceptance of a novel fuel having different characteristics from traditional fossil derived fuels. Bio-oil has been fired in combustion boilers in a number of tests in Canada, the US and Europe. These tests have demonstrated that only minor boiler retrofitting is required, and combustion is clean and self-sustaining with no adverse change in emission levels. As a result, the use of pyrolysis oils in large industrial units (those greater than 1MWe) can now considered to be commercially viable. For example, at the Manitowoc Public Utilities, Wisconsin, USA, bio-oil was co-fired at a rate of about 11 million BTU/hr. in a coal-fired stoker boiler. This represented about 5% of the fuel input, or about 1Mwe of the 20 Mwe output of the was terminated when this bio-oil surplus supply was re-directed for internal boiler use at the Red Arrow Products facility where the bio-oil was produced. It should be noted that bio-oil has been commercially fired in a 20 MBTU/h West Waste Fuel Burner at the Red Arrow facility since 1989.

The remaining objective of this segment of the program is to work with burner manufacturers and end users to increase the applications of bio-oils in the area of small boiler and burners. As part of an international assessment of the feasibility of utilizing these oils as an energy source, the program will continue to provide technical support and oil samples to a number of industry and research groups, such as Neste Oy, Coen and VTT- Energy, who have projects underway in this area. Information from these groups on oil characteristics, combustion efficiencies, emissions, etc., will be made available to the pyrolysis community and accelerate the commercial acceptance of the technology.

Diesel Engines

The use of bio oils for power generation via diesel engines showed promise in preliminary tests performed in Finland. As a result, an industrial consortium from both Canada and Finland was formed to carry out a project to demonstrate the cost effective production of bio-oils from biomass feedstocks and to develop and warrantee a commercial diesel engine that would burn these bio oils in small to medium sized electrical generation systems. The consortium members from Finland included Wartsila Diesel, one of the world's largest suppliers of diesel engines for power applications; VAPO, a company involved in the sale of power and power generation equipment; and VTT-Energy, a government research agency involved in the development of bioenergy technologies. Ensyn Technologies and NRCan were the Canadian industrial member of this consortium. This project has been successfully completed and it is expected that diesel

engine manufacturers will be ready to provide performance warranties for bio-oil utilization in pyrolysis oil power production plants.

Gas Turbines

Orenda Aerospace has successfully completed a Phase I project to evaluate the concept of utilizing a biomass derived liquid fuel in a gas turbine, optimize the application of this concept and perform endurance testing of the gas turbine. Orenda was able to successfully operate the turbine over the full power range using 100% bio-oil. Performance tests were completed with detailed data acquisition at steady state operating points. Emission results were positive, with the bio-oil having lower levels of SO_2 and NO_x relative to diesel. As a result of the findings in this phase of the project, a Phase II project is planned to perform component and fuel system durability testing and a long term endurance test which will allow the turbine to be guaranteed for pyrolysis oil.

Microemulsions

Bio-oils have a number of technical problems including acidity, a calorific value half that of petroleum fuels, poor ignitability and high char and ash content. One of the ways to circumvent these problems would be to use the bio-oil as a diesel supplement by dispersing 10-30% of bio-oil in diesel. However, bio-oils are highly polar, retaining about 25% water and are immiscible with diesel. If a stable bio-oil in diesel microemulsion could be formed, it is likely that a conventional power generation systems could be run without major modifications. BDP has initiated a project in collaboration with the Processing and Environmental Catalysis Group, CETC which has shown that stable, combustible microemulsions can be produced from mixtures of bio-oil/diesel ranging from 5% - 40%. A 5 litre/hr. continuous unit has been built to demonstrate economic and technical viability at a larger scale and to produce larger samples for analysis and combustion tests. As a result of this work a follow project is being planned, which will include technical co-operation with VTT - Energy and the European Commission JOULE Programme under the Canada/EU Science & Technology Agreement. The objectives of this project are to optimize the microemulsion process and unit, including improved mixing and feeding systems, examining other surfactants, etc., testing pyrolysis oils derived from other biomass feedstocks, further combustion and emissions testing and the provision of samples to various groups for testing.

5. Development of Cetane Enhancer Technology

Arbokem Inc., in collaboration with BC Chemicals, was awarded the rights to this technology by the CANMET Energy Technology Centre(CETC) in 1991. As a result of successful pilot testing of the process and a positive independent study of the potential diesel market in North America, an industrial consortium was formed to commercialize the technology using tall oil derived from the pulping of softwoods as the input feedstock. The consortium successfully completed an research program to carry out scale up testing and production of a cetane fuel product (cetane numbers vary between 65 from tall oil feedstock to 90 for animal fats), laboratory vehicle emissions tests and field testing of the biodiesel fuel. The technology is now ready for commercialization and a number of implementation strategies are now being evaluated to determine which approach to take. In the interim, the IEA Alternative Motor Fuels has a project underway - "Annex XIII. Emissions Performance of Selected Biodiesel Fuels", and cetane fuel will be provided to these tests in order to further assess the emission characteristics of this fuel.

In the cetane enhancer process, conventional hydrotreating technology is used to convert tall oil and other biomass oils to a high cetane fuel through the addition of hydrogen. In addition to the middle distillate cetane enhancer fuel, heavy and light bio-naphtha fractions are produced as co-products. As part of a follow on project to improve the commercial opportunities of this process, a contract has recently been given to Kemestrie Inc to investigate the upgrading of these products. As part of their research on another project examining MSW gasification, Kemestrie developed a highly efficient catalyst that can generate hydrogen from the synthesis gas produced in biomass gasification processes. It was felt that this catalyst could produce similar results with the heavy bio-naphtha fraction from the cetane process. In recently completed tests, Kemestrie has shown that their catalyst can convert this fraction to hydrogen and that this hydrogen is of sufficient quality and quantity to more than provide all the infeed hydrogen required for the process(5 times the amount of hydrogen needed is produced), reducing the production costs of the cetane enhancer technology. It is estimated that the production of the hydrogen required from the heavy fraction could reduce treatment costs from approximately \$170/tonne to about \$150/tonne for a 25,000 tonne/year tall oil processing plant

Work is continuing to develop additional value added products from the light and remaining heavy bio-naphtha fractions.

International Activities

The Biomass Thermochemical Conversion R & D Program remains committed to maintaining good research links with the international biomass pyrolysis industry and research communities. In this regard it will continue to be active in Annexes of the International Energy Agency - Bioenergy Agreement and will join the Pyrolysis Network for Europe(PyNE) for its next triennium period.

TUNGSTATE-MODIFIED ZIRCONIA AS A HYDROISOMERIZATION CATALYST FOR HIGH MOLECULAR WEIGHT LINEAR PARAFFINS

Shuguang Zhang, Xin Xiao, John W. Tierney and Irving Wender*
Department of Chemical Engineering, 1249 Benedum Hall,
University of Pittsburgh, Pittsburgh, PA 15261

Keywords: tungstate-modified zirconia, hydroisomerization, linear alkanes

Introduction Isomerization of long-chain linear alkanes is desirable because isoparaffins, from C_{10} to C_{30} , are excellent solvents, have minimal odor, low reactivity and high stability. They are used in polyolefin manufacture, proprietary household products, food-related applications, pharmaceutical production and in many other ways. Oils rich in high molecular weight isoparaffins, rather than normal paraffins, are desired for use as motor oils, lubricants, diesel fuel and jet fuel due to their desirable low temperature properties.¹ Industry carries out oil dewaxing to lower the long-chain normal paraffin content in oils. Chevron has commercialized an all-catalytic wax isomerization process, called "isodewaxing", for the production of motor oils, lubricants and fuels.² This process converts linear alkanes to their isomers whose presence significantly improves the low temperature properties of the oils. Compared with widely used solvent dewaxing, catalytic dewaxing does not have environmental problems caused by fugitive emissions.³

In the Fischer-Tropsch (FT) synthesis, the yield of waxes can exceed 45 wt% of the total liquid products.⁴ Normal paraffins in the C_{20} - C_{30} range from this process require further processing to increase their commercial value. Isomers of these high molecular weight paraffins can be used as middle-distillate fuels and their low freezing points make them desirable for use as jet fuel.⁵ Upgrading waxes to lubricating oils is also possible.

Catalysts containing $AlCl_3$ or zeolites are traditionally used for isomerization. The former is corrosive and nonregenerable because of loss of chloride ions; the latter requires high operating temperatures (about 400°C) and favors cracking. SAPO-11 (a silicoaluminophosphate) is a relatively new molecular sieve; metal-promoted SAPO-11 is more selective than other zeolites for long-chain paraffin isomerization.^{6,7} However, it is generally used with high hydrogen to feed mole ratios (30/1) and high reaction temperatures.

Anion-modified metal oxides, such as sulfated zirconia (SO_4/ZrO_2) and tungstated zirconia (WO_3/ZrO_2), have been found to catalyze hydrocarbon conversions under mild conditions.⁸ These strong solid acids are environmentally benign and regenerable.⁹ Butane isomerization over sulfated zirconia has attracted considerable attention because isobutane is the precursor to methyl-*t*-butyl ether.¹⁰⁻¹³ Metal-promoted sulfated zirconia is effective for isomerization of short chain paraffins ($< C_7$) and for hydrocracking of long-chain paraffins including waxes and polyolefins.¹⁴⁻¹⁶ However, loss of activity due to coke formation and sulfur loss, especially under reducing conditions, are obstacles to certain practical uses of sulfated zirconia. Moreover, high isomerization selectivity is difficult to achieve over sulfated zirconia as the chain length increases, even at low conversions.¹⁵ Studies of tungstate-modified zirconia indicate that it is more stable than sulfated zirconia and is promising for hydroisomerization of high molecular weight linear paraffins.¹⁶⁻²⁰

It is known that there is an increasing ease of formation of carbenium ions on the interior carbons of linear molecules of long chains.²¹ Since isomerization of alkanes precedes cracking, catalysts with a certain optimal balance of metal and acid functions at suitable reaction conditions must be found to suppress cracking in order to achieve high isomerization selectivity for long-chain paraffins.^{7,22,23} Although these reactions proceed via carbenium ions, initiation of these species and subsequent reaction pathways on anion-modified zirconia catalysts are still unclear.^{24,25}

This study contributes to investigation of hydroisomerization of high molecular weight linear alkanes over metal-promoted tungstate-modified zirconia (metal/ WO_3/ZrO_2), using *n*-hexadecane as a model compound in a trickle bed reactor. Efforts are aimed at obtaining high hydroisomerization selectivity with high hydrocarbon conversion and at elucidating reaction pathways over this class of anion-modified metal oxide.

Experimental

Catalyst Preparation and Characterization The procedure for synthesis of metal/ WO_3/ZrO_2 consists of the following steps: (1) zirconium hydroxide precipitation by addition of ammonium

* Correspondence author

hydroxide to zirconium chloride; (2) anion-modification by addition of ammonium metatungstate solution; (3) impregnation of a metal (Pt, Pd, or Ni) salt; (4) calcination. Two preparation procedures (labeled I and II in Figure 1) were used. In I, there were two calcinations, one at 700°C for tungstate-modified zirconium hydroxide and the other at 500°C after metal salt impregnation; procedure II had only one calcination at 700°C after co-impregnation of zirconium hydroxide by the solution of tungsten and metal salts. The metal content and tungsten content in the catalysts were controlled by adjusting the concentration of salts. In this paper, the metal salt we used is $\text{H}_2\text{PtCl}_6 \cdot 6\text{H}_2\text{O}$. Figure 1 shows details of procedures I and II.

BET specific surface area (by nitrogen adsorption) and platinum distribution (by carbon monoxide adsorption) were measured using a Micromeritics ASAP 2010 instrument.

Reactor System and Operating Procedure Catalytic activity and selectivity tests were carried out in a continuous trickle bed stainless steel reactor with 0.305 inch i.d. Reaction temperature was controlled by a computer and system pressure by a back-pressure valve. $n\text{-C}_{16}$ (99 wt% from ICN Biomedical Inc.) was delivered from a feed tank into the reactor by a syringe pump at a constant rate of 6.6 ml/hr. Input rates of hydrogen and helium (make-up gas to keep gas flow rate constant when studying effects of pressure) were controlled by two mass flow meters, respectively. The catalyst was crushed to 40-60 mesh pellets and placed into the center of the reactor after mixing with an equal volume of quartz (50-70 mesh). Quartz was also used as packing at each end of the reactor. Variation in weight hour space velocity (WHSV) was obtained by changing the amount of catalyst. Before reaction, the catalyst was activated at 450°C with 20 ml/min of air for one hr. Liquid products were collected in an ice-water cooled vial for analysis using an HP-5980 GC.

Results and Discussion $n\text{-C}_{16}$ conversion is defined as the difference between $n\text{-C}_{16}$ weight percentage in the feed and that in the reaction products; $i\text{-C}_{16}$ selectivity is calculated by dividing $i\text{-C}_{16}$ percentage in the products with $n\text{-C}_{16}$ conversion; $i\text{-C}_{16}$ yield is the $i\text{-C}_{16}$ percentage. In order to obtain comparable $n\text{-C}_{16}$ conversion with different catalysts, we carried out the activity and selectivity tests at 300°C. Later, the possibility of operating reactions at lower temperatures, from 210 to 250°C, using our most active catalyst (6.5 wt% W) was investigated and the influence of reaction pressure was studied at 230°C.

Comparison of results from catalysts prepared by methods I and II These two $\text{Pt}/\text{WO}_3/\text{ZrO}_2$ catalysts, I and II, with the same composition (0.5 wt% platinum and 6.5 wt% tungsten) were tested under the same conditions but at varying WHSV: 300°C, 300 psig, $\text{H}_2/n\text{-C}_{16}$ (mole ratio)=2. Results are shown in Figure 2. $n\text{-C}_{16}$ conversion decreases and $i\text{-C}_{16}$ increases for both catalysts when WHSV increases, but the $n\text{-C}_{16}$ conversion with catalyst II declines more rapidly. At the same $n\text{-C}_{16}$ conversion, 90 wt%, for instance, the $i\text{-C}_{16}$ selectivity over catalyst I is about 20 wt% higher than that over catalyst II. A possible explanation is that the high temperature calcination (700°C) after platinum salt impregnation used in procedure II resulted in a low degree of platinum distribution and the metal function is weakened. These two catalysts have similar surface areas, about 67.5 m^2/g , but carbon monoxide chemisorption experiments show platinum distribution of catalyst I is 0.63, which is much better than that of II (0.14). It is known that metals, such as platinum, palladium or nickel, can provide hydride ions²⁶ and enhance acidity by hydrogen spillover in the presence of hydrogen²⁷. Lack of available hydride ions may result in long residence times for reaction intermediates and increase the opportunity for β -scission which produces cracked products.

Effect of tungsten content on catalyst reactivity Five $\text{Pt}/\text{WO}_3/\text{ZrO}_2$ catalysts with different tungsten contents but the same amount of platinum content (0.5 wt%) were prepared by method I. Properties are shown in Table 1. These catalysts were tested at the same temperature, pressure and hydrogen to $n\text{-C}_{16}$ ratio (Figure 2). Catalysts with 6.5 and 8 wt% tungsten have high hydroisomerization activities at relatively high conversion. Data from BET nitrogen adsorption measurement indicates the surface area of $\text{Pt}/\text{WO}_3/\text{ZrO}_2$ increases with increasing tungsten content. It has been postulated that tungsten oxide is reduced in the presence of hydrogen; the reduced species may play an important part in the reaction mechanism.²⁸ Surface density and particle size of tungsten oxide as well as acidity will be studied by TEM, XPS and TPD.

Effect of reaction temperature and pressure Influence of reaction temperature and pressure on conversion and isomerization selectivity was investigated using a $\text{Pt}(0.5 \text{ wt\%})/\text{WO}_3/\text{ZrO}_2$ (6.5 wt% W) catalyst prepared by procedure I. Data in Tables 2 and 3 indicates that $n\text{-C}_{16}$ conversion and $i\text{-C}_{16}$ selectivity are more sensitive to reaction temperature than to pressure. In the temperature range from 210 to 250°C, lowering the temperature resulted in low conversion but high selectivity. This catalyst is very active; 85.9 wt% $n\text{-C}_{16}$ conversion with 83.1 wt% $i\text{-C}_{16}$ selectivity was achieved at 230°C, $\text{WHSV} = 1 \text{ hr}^{-1}$. Comparable $n\text{-C}_{16}$ conversion (82.8 wt%) was

also obtained at higher temperature and larger WHSV (300°C, WHSV=24 hr⁻¹, line C in Figure 3), but the i-C₁₆ selectivity was only 74.3 wt%. This suggests that large i-C₁₆ yields will be obtained at relatively low temperature and small WHSV, rather than high temperature and large WHSV. The increase of pressure resulted in low conversion with high selectivity, indicating a negative reaction order of hydrogen. A similar effect of hydrogen on conversion was observed by Iglesias *et al.* in heptane isomerization using Pt/WO₃/ZrO₂.²⁶

Comparison of Pt(0.5 wt%)/SO₄/ZrO₂ and Pt(0.5 wt%)/WO₃/ZrO₂ At relatively low temperature (150°C), platinum-promoted sulfated zirconia (calcined at 630°C for 3 hr in air) was tested for n-hexadecane hydroisomerization. Its preparation procedure is described elsewhere.¹⁴ Results with Pt(0.5 wt%)/SO₄/ZrO₂ are compared with those obtained using Pt(0.5 wt%)/WO₃/ZrO₂ (6.5 wt% W) in Table 4. Pt(0.5 wt%)/SO₄/ZrO₂ is active at 150°C, but it favors cracking. Pt(0.5 wt%)/WO₃/ZrO₂ requires higher temperature, but has high isomerization selectivity even at high hexadecane conversion.

Acknowledgment We acknowledge the financial support of this work by the U.S. Department of Energy (Grant No. DE-FC22-93PC93053).

REFERENCES

1. Encyclopedia of Chemical Processing and Design, 15, Mcketta, M., Dekker, M., Inc. (1982).
2. Miller, S. J., Studies in Surface Science and Catalysis, Vol. 84 (1994), pp. 2319-2326.
3. Kim, I., Chem. Eng., Dec. 1995, pp. 71.
4. Encyclopedia of Chemical Technology, Fourth Edition, Vol. 12 (1996).
5. Coppola, E. N., M. S. thesis, University of Utah (1987).
6. Miller, S. J., preprints of Div. Petrochem., Am. Chem. Soc., 38 (1993), pp. 788-793.
7. Taylor, R. J., Pretty, R., Appl. Catal. A 119 (1994), pp. 121-138.
8. Hino, M. and Arata, K., J. Am. Chem. Soc., 101 (1979), pp. 39-40.
9. Yori, J. C., Luy, J. C. and Parera, J. M., Appl. Catal. 46 (1989), pp. 102-112.
10. Corma, A., Juan-Rajadell, M. I., Lopez-Nieto, J. M., Martinez, A., Martinez, C., Appl. Catal. A 111 (1994), pp. 175-189.
11. Yori, J. C., Parera, J. M., Appl. Catal. A 129 (1995), pp. 83-91.
12. Arata, K., Appl. Catal. A 146 (1996), pp. 3-32.
13. Liu, H., Lei, G. D., Sachtler, W. M. H., Appl. Catal. A 146 (1996), pp. 165-180.
14. Wen, M. Y., Wender, I., Tierney, J. W., Energy & Fuels, 4 (1990), pp. 372-379.
15. Keogh, R. A., Sparks, D., Hu, J., Wender, I., Tierney, J. W., Wang, W., and Davis, B. H., Energy & Fuels, 8 (1994), pp. 755-762.
16. Venkatesh, K. R., Hu, J., Wang, W., Holder, G. D., Tierney, J. W., and Wender, I., Energy & Fuels, 10 (1996), pp. 1163-1170.
17. Chang, C. D., Santiesteban, J. G., Stern, D. L., U.S. Patent 5,345,026 (1994).
18. Soled, S. L., Gates, W. E., Iglesia, E., U.S. Patent 5,422,327 (1995).
19. Larsen, G., Lotero, E., Raghavan, S., Prira, R. D., Querini, C. A., Appl. Catal. A 139 (1996), pp. 201-211.
20. Iglesia, E., Barton, D. G., Soled, S. L., Miseo, S., Baumgartner, J. E., Gates, W. E., Fuentes, G. A., and Meitzner, G. D., Stud. Surf. Sci. and Catal., Vol. 101 (1996), pp. 533-542.
21. Corma, A. and Wojciechowski, B. W., Catal. Rev.-Sci. Eng., 27(1) (1985), pp. 83.
22. Weitkamp, J., Jacobs, P. A. and Martens, J. A., Appl. Catal. 8(1983), pp. 123-141.
23. Girgis, M. J. and Tsao, Y. P., Ind. Eng. Chem. Res., 35 (1996), pp. 386-396.
24. Farcasiu, D., Ghenciu, A., and Li, J. Q., J. Catal., 158 (1996), pp. 116-127.
25. Parera, J. M., Appl. Catal. A 167 (1998), pp. 75-84.
26. Iglesia, E., Soled, S. L., and Karmer, G. M., J. Catal., 144 (1993), pp. 238-253.
27. Shishido, T., Hattori, H., Appl. Catal. A 146 (1996), pp. 157-164.
28. Larsen, G., Lotero, E., and Parra, R., Stud. Surf. Sci. and Catal., Vol. 101 (1996), pp. 543-551.

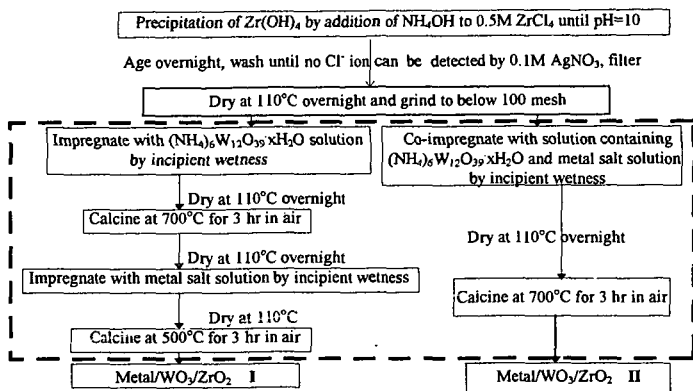


Figure 1 Two procedures for the preparation of Metal/ WO_3 / ZrO_2 catalysts

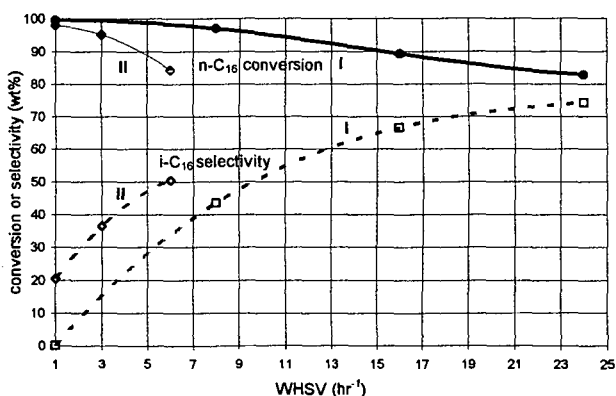


Figure 2 Comparison of conversion and selectivity for hydroisomerization of $n-C_{16}$ using $Pt(0.5wt\%)/WO_3/ZrO_2$ (6.5 wt% W) catalysts prepared by procedures I and II. [Reaction conditions: 300°C, 300 psig, $H_2/n-C_{16}$ (mole ratio)=2, 6th hr reaction results]

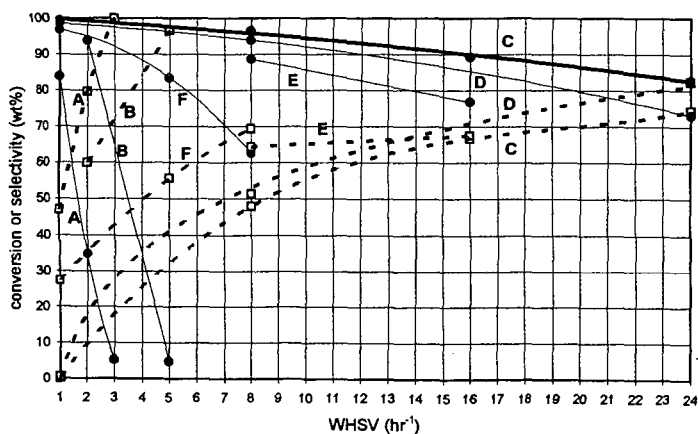


Figure 3 Effect of tungsten content in $Pt(0.5wt\%)/WO_3/ZrO_2$ on $n-C_{16}$ conversion (—) and $i-C_{16}$ selectivity (----) [catalysts prepared by procedure I; reaction conditions: 300°C, 300 psig, $H_2/n-C_{16}$ (mole ratio)=2, 6th hr results]

Table 1 Physical properties of Pt(0.5 wt%)/WO₃/ZrO₂ with different tungsten contents

| catalyst | A | B | C | D | E | F |
|--------------------------------|-------|-------|-------|-------|-------|-------|
| W wt% | 3 | 4.5 | 6.5 | 8 | 10 | 15 |
| surface area m ² /g | 42.46 | 56.4 | 67.49 | 74.87 | 90.01 | 99.10 |
| pore diameter Å | 125.1 | 111.8 | 96.8 | 88.2 | 87.3 | 72.5 |
| pore volume cm ³ /g | 0.14 | 0.16 | 0.16 | 0.16 | 0.20 | 0.18 |

Table 2 Effect of reaction temperature on n-C₁₆ conversion and i-C₁₆ selectivity over Pt(0.5 wt%)/WO₃/ZrO₂ (6.5 wt% W) by procedure I

| | | | | |
|------------------------------------|------|------|------|------|
| reaction temperature °C | 210 | 220 | 230 | 250 |
| n-C ₁₆ conversion, wt% | 33.5 | 53.8 | 85.9 | 98.3 |
| i-C ₁₆ selectivity, wt% | 99.1 | 96.6 | 83.1 | 0 |
| i-C ₁₆ yield, wt% | 33.2 | 52.0 | 71.4 | 0 |
| i-C ₁₆ distribution wt% | | | | |
| multibranched i-C ₁₆ | 5.4 | 10.7 | 26.6 | 0 |
| dimethyltetradecane | 31.3 | 36.6 | 42.8 | 0 |
| 7- and 8-methylpentadecane | 15.1 | 11.8 | 6.4 | 0 |
| 6-methylpentadecane | 13.0 | 10.8 | 5.8 | 0 |
| 5-methylpentadecane | 9.9 | 8.2 | 4.6 | 0 |
| 4-methylpentadecane | 8.7 | 7.3 | 4.0 | 0 |
| 3-methylpentadecane | 8.7 | 7.5 | 4.6 | 0 |
| 2-methylpentadecane | 6.3 | 5.9 | 4.0 | 0 |
| 3-ethyltetradecane | 1.5 | 1.2 | 0.8 | 0 |

Reaction conditions: 300 psig, H₂/n-C₁₆ (mole ratio)=2, WHSV= 1 hr⁻¹Table 3 Effect of reaction pressure on n-C₁₆ conversion and i-C₁₆ selectivity over Pt(0.5 wt%)/WO₃/ZrO₂ (6.5 wt% W) by procedure I

| | | | | |
|------------------------------------|------|------|------|------|
| reaction pressure | 300 | 400 | 500 | 600 |
| n-C ₁₆ conversion, wt% | 85.9 | 78.8 | 76.1 | 70.7 |
| i-C ₁₆ selectivity, wt% | 83.1 | 88.9 | 90.7 | 93 |
| i-C ₁₆ yield, wt% | 71.4 | 70.1 | 69.1 | 65.8 |
| i-C ₁₆ distribution wt% | | | | |
| multibranched i-C ₁₆ | 26.6 | 20.0 | 19.9 | 17.2 |
| dimethyltetradecane | 42.8 | 43.2 | 41.5 | 40.5 |
| 7- and 8-methylpentadecane | 6.4 | 8.0 | 8.8 | 9.3 |
| 6-methylpentadecane | 5.8 | 7.0 | 7.0 | 8.2 |
| 5-methylpentadecane | 4.6 | 5.7 | 6.0 | 6.6 |
| 4-methylpentadecane | 4.0 | 4.8 | 5.4 | 5.9 |
| 3-methylpentadecane | 4.6 | 5.3 | 5.6 | 6.1 |
| 2-methylpentadecane | 4.0 | 4.6 | 4.7 | 5.0 |
| 3-ethyltetradecane | 0.8 | 1.0 | 1.0 | 1.1 |

Reaction conditions: 230°C, H₂/n-C₁₆ (mole ratio)=2, WHSV= 1 hr⁻¹Table 4 Comparison of Pt(0.5 wt%)/SO₄/ZrO₂ (630°C) and Pt(0.5 wt%)/WO₃/ZrO₂ [6.5 wt% W (700, 500°C)]

| Catalyst | Pt(0.5 wt%)/SO ₄ /ZrO ₂ (630°C) | Pt(0.5 wt%)/WO ₃ /ZrO ₂ 6.5 wt% W (700, 500°C) |
|------------------------------------|--|---|
| Reaction conditions | 150°C, 300 psig, WHSV=1hr ⁻¹ | 230°C, 300 psig, WHSV=1hr ⁻¹ |
| n-C ₁₆ conversion, wt% | 76.7 | 85.9 |
| i-C ₁₆ selectivity, wt% | 19.8 | 83.1 |
| i-C ₁₆ yield, wt% | 15.2 | 71.4 |
| i-C ₁₆ distribution wt% | | |
| multibranched i-C ₁₆ | 21.2 | 26.6 |
| dimethyltetradecane | 44.3 | 42.8 |
| monomethylpentadecane | 33.6 | 29.4 |
| 3-ethyltetradecane | 0.6 | 0.8 |

THERMAL DECOMPOSITION CHARACTERISTIC OF VACUUM RESIDUE IN ATHABASCA TAR SAND BITUMEN

Masaaki Satou, Maki Mikuni and Hideshi Hattori
CARET, Hokkaido University, Sapporo 060-8628, Japan

Hiroshi Nagaishi and Tadashi Yoshida
Hokkaido National Industrial Research Institute, Sapporo 062-8517, Japan

Keywords: Tar sand bitumen, Thermal decomposition characteristic, Chemical structure

INTRODUCTION

To develop and establish the effective use of tar sand bitumen in the future, it is necessary to clarify the reaction characteristics related with the information of chemical structure. There were many studies on the chemical structure of tar sand bitumen¹⁻³⁾, and many kinetic reaction models were also proposed. However the study on the reaction characteristics concerned with the chemical structure is few^{4,5)}. The initial upgrading step in the conversion of bitumen to synthetic crude is the thermal decomposition of heavy macromolecule in bitumen, which would be the simplest reaction. This study aims at elucidating the thermal decomposition characteristic of vacuum residue in bitumen on the basis of conversion and chemical structure changes.

EXPERIMENTAL

Sample preparation

The used raw-bitumen is Athabasca tar sand bitumen (C: 82.6, H: 10.5, N: 0.5, O: 2.3, S (diff.): 4.1 wt%). Two kinds of sample series were prepared by a vacuum distillation based on ASTM D1160. One is the light fraction (boiling point range, 723K under) and vacuum residue. The other is the blended sample of vacuum residue with light fraction by various weight fractions.

Thermal decomposition reaction

Thermal decomposition reaction was conducted in a 60 cm³ autoclave with an electromagnetic stirrer. The autoclave was heated at 90 K/min by an infrared image furnace and cooled at 100 K/min by blowing air. Connecting the reactor with a 500 cm³ buffer vessel kept the pressure almost constant through each reaction. Five grams of sample were loaded in the reactor. The reaction temperature and pressure were 693 K and 10 MPa in N₂, respectively.

Product characterization

After each reaction, a product was recovered with dichloromethane. Produced gas yield was obtained from the data of TCD gas chromatograms.

Boiling point distribution of the product was measured by a thermogravimetric analysis (SD-TGA), which was in good agreement with the standard distillation method (ASTM D2892^{6,7)}. The distribution was plotted as a function of boiling point index that is not true one but fairly corresponds to it.

Samples for the ¹H-, ¹³C-NMR measurements were dissolved in deuteriochloroform. Both spectra were obtained with a α -500 type Fourier transform spectrometer (JEOL Ltd.). ¹³C-NMR spectra were obtained by using a pulse width of 11.5 μ s, total of 1000 transients and gated decoupling to ensure quantitative results. Tris(acetylacetonate)chromium(III)(Cr(acac)₃) was used as the relaxation reagent⁸⁾. From conventional ¹H-NMR spectra, aromatic-H_{ar}, H α , H β and H γ illustrated hydrogen distribution.

Elemental analyses were carried out with a CHNO analyzer. Molecular weight measurements were made with a KNAUER vapor pressure osmometer.

RESULTS AND DISCUSSION

Thermal decomposition characteristics of vacuum residue

Figure 1 shows the variation of product yields with reaction time for the vacuum residue. Yields of heavy and light components in a sample were calculated from SD-TGA data and a cut point between both components was 723 K. Loss was a volatile matter that was lost in product recovery from a autoclave, and might be low molecular hydrocarbons such as hexane and heptane. With the progress of the reaction, gas, loss and light component gradually increased.

To discuss the degree of decomposition of macromolecule in vacuum residue, a conversion was defined as the weight ratio of decrease of heavy component to initial one. Figure 2 shows the change in conversion and average molecular weight with the reaction time. At 0 min of nominal reaction time, no remarkable change of molecular weight was observed, but it was reduced to almost half up to 10 min. This suggests the decomposition of macromolecule in the vacuum residue. The molecular weight was finally almost constant, namely, about 400. While the conversion gradually increased with the progress of the reaction.

Chemical structural change during thermal decomposition reaction

Figure 3 shows the weight change of various carbon types by unit gram of vacuum residue with the reaction time. Carbon weight by unit gram was calculated based on the carbon distribution obtained from ^{13}C -NMR, elemental analysis data and product yield. Carbons are assigned six types from the chemical shifts in ^{13}C -NMR spectra^{9,12}, named as methyl carbons, methylene carbons, α -methylene carbons, unsubstituted aromatic carbons, bridgehead aromatic carbons and substituted aromatic carbons.

In Fig. 3, a remarkable weight decrease of α -methylene carbons was recognized in the initial stage of reaction. Methylene carbons and unsubstituted aromatic carbons had gradually weight decreasing and increasing tendency with the progress of the reaction, respectively. While, the values of weight of the other carbons were almost constant.

Carbons assigned α -methylene carbons included α -methylene carbons on an aliphatic methylene bridge and a side chain except for ethyl group, and methine carbons in a naphthenic ring¹². Methylene carbons included methylene carbons in a naphthenic ring and β or further position on a side chain from an aromatic ring, α -methylene carbons on an ethyl group, and methine carbons on a side chain.

In the initial stage of reaction, the decomposition of an aliphatic bridge including in a macromolecule, resulting in the reduction of molecular weight to half in Fig. 2, could explain the remarkable weight decrease of α -methylene carbons. At the same time, the dehydrogenation of naphthenic ring and the cleavage of an aliphatic chain would bring about mainly the weight increase of unsubstituted aromatic carbons and decrease of methylene carbons. With the progress of the reaction, these reactions would be prior.

To confirm the above consideration, numbers of aromatic and naphthenic rings in an average molecule were estimated¹³ as shown in Fig. 4. The naphthenic ring number changed in unique manner with the reaction time. Considerable decrease of naphthenic ring number up to 10 min was corresponding with the reduction of molecular weight to half resulting from the decomposition of a macromolecule. Furthermore, the naphthenic ring number increased at 30 min by a ring formation on a still remaining aliphatic chain. On the contrary, the aromatic ring number decreased in the initial stage of reaction, but was not the reduction to half. This also suggests the dehydrogenation of naphthenic ring. Subsequently aromatic ring number gradually increased after 30 min.

The conversion at 0 min of reaction time was not so high in spite of the reduction of molecular weight to half. The values of molecular weight and estimated total carbon number in an average molecule were about 540 and 38, respectively. According to our boiling point calculation¹⁴, the boiling point of this average molecule should be at least 790 K. At 60 min of reaction time, the boiling point of product would be 720 K as the total carbon number fell to about 30. Consequently, the conversion was still low in the initial stage of the reaction, and gradually increased with the progress of reaction.

Influence of light component on conversion of heavy one in a bitumen

To clarify the decomposition characteristics of heavy component in the presence of light one in bitumen, vacuum residues blended with light fraction in different ratios were prepared. If the thermal decomposition of heavy and light components occur independently each other, the conversion should not change regardless of light fraction content. In Fig. 5, the change in conversion at 60 min of reaction time with weight content of light fraction is shown. The conversion decreased with the increase of the weight content of light fraction. This suggests that the light component affects the conversion of heavy component to light one. In this section, interactions between the heavy and light components in a thermal decomposition would be clarified on the basis of chemical structure changes in a product.

Figures 6 and 7 show differences in the weight of aromatic and aliphatic carbon types by unit gram before and after reaction versus the weight ratio of light component to heavy one in a blended sample, respectively. The plots are scattered to some extent in both figures. A dashed line and open symbols were calculated on the assumption that the thermal decomposition of heavy and light components occurs independently each other, and a solid line is smoothing experimental values indicated by solid symbols. As a vacuum residue contains about 30 wt% of light component by SD-TGA, the minimum weight ratios in both figures are not zero but about 0.5. The differences in weight of aromatic and aliphatic carbons before and after reaction of 60 min became plus and minus values, respectively. If examined in detail, weight increase of unsubstituted aromatic carbons was remarkably kept down with the increase of light component content, and weight decrease of α -methylene carbons was also controlled by light component. The weight differences of other carbons were almost equal between calculated and observed ones in the presence of light component. These controls of weight change would be explained by some interpretations on the interaction between heavy and light components in the thermal decomposition. The condensed naphthenic ring formation and the polymerization of light component with heavy one would contribute the weight increase of α -methylene carbons. The control of dehydrogenation on a naphthenic ring would bring about the weight decrease of unsubstituted aromatic carbons.

Summarizing above discussion, the thermal decomposition characteristic of a blended sample was related with the chemical structure changes, though a detailed reaction scheme could not be illustrated at the present time.

CONCLUSIONS

A thermal decomposition characteristic of vacuum residue in bitumen is discussed from conversion and chemical structure changes.

In the initial stage of reaction, cleavage of aliphatic bridge occurs, resulting in the decrease in average molecular weight. With the progress of the reaction, the dehydrogenation at naphthenic rings and release of low molecular weight hydrocarbon from side chain take place, therefore a remarkable change of average molecular weight was not observed, but the conversion is gradually increasing.

In the thermal decomposition of residue with the light fraction, the conversion decreased with the increase in weight ratio of light fraction in blended samples. Polymerization of the light component with the heavy one would be suggested.

ACKNOWLEDGMENTS

The authors gratefully acknowledge Prof. M.R.Gray and Syncrude Canada Ltd. for supply of the tar sand bitumen sample.

REFERENCES

- 1) T.Suzuki, M.Itoh, Y.Takegami and Y.Watanabe, *Fuel*, 61, 402(1982)
- 2) F.Khorasheh, M.R.Gray and I.G.D.Lana, *Fuel*, 66, 505(1987)
- 3) M.R.Gray, J.H.K.Choi, N.O.Egiebor, R.P.Kirchen and E.C.Sanford, *Fuel Sci. Tech. Int'l.*, 7, 599(1989)
- 4) M.R.Gray, *Ind. Eng. Chem. Res.*, 29, 505(1990)
- 5) M.R.Gray, P.Jokuty, H.Yeniova, L.Nazarewycz, S.E.Wanke, U.Achia, A.Krzywicki, E.C.Sanford and O.K.Y.Sy, *Can. J. Chem. Eng.*, 69, 833(1991)
- 6) Y.Hasegawa, T.Yoshida, H.Narita and Y.Maekawa, *J. Fuel Soc. Japan*, 66, 855(1987)
- 7) H.Nagaishi, M.Sasaki, T.Kotanigawa and Y.Maekawa, *J. Japan Inst. Energy*, 72, 964(1993)
- 8) T.Yoshida, Y.Maekawa, H.Uchino and S.Yokoyama, *Bull. Chem. Soc. Jpn.*, 52, 3676(1979)
- 9) T.Yohida, Y.Narita, R.Yoshida, S.Ueda, N.Kanda and Y.Maekawa, *Fuel*, 61, 824(1982)
- 10) J-M. Derreppe, C.Moreaux, P.Landais and M.Monthieux, *Fuel*, 66, 594(1987)
- 11) L.Michon, D.Martin, J-P.Planche and B.Hanquet, *Fuel*, 76, 9(1997)
- 12) K.Hayamizu and O.Yamamoto, "¹³C NMR Spectra of Polycyclic Aromatic Compounds", Japan Industrial Technology Association, Tokyo, 1982
- 13) K.H.Altgelt and M.M.Boduszynski, "Composition and Analysis of Heavy Petroleum Fractions", Marcel Dekker, New York, 1994, pp. 335
- 14) M.Satou, S.Yokoyama and Y.Sanada, *Fuel*, 71, 565(1992)

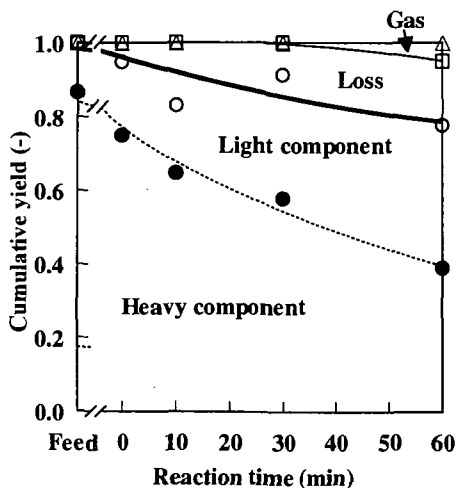


Fig. 1 Change in cumulative yield of product with reaction time

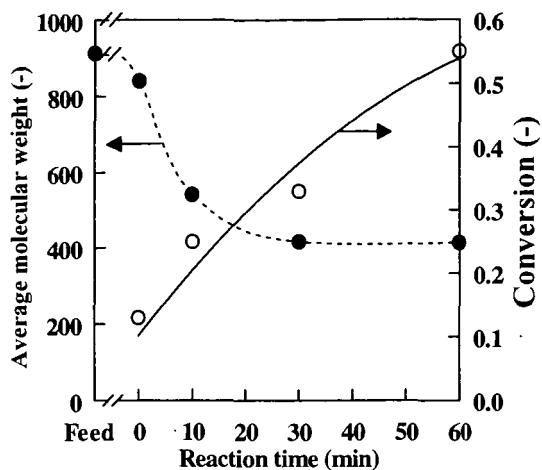


Fig. 2 Change in average molecular weight and conversion with reaction time

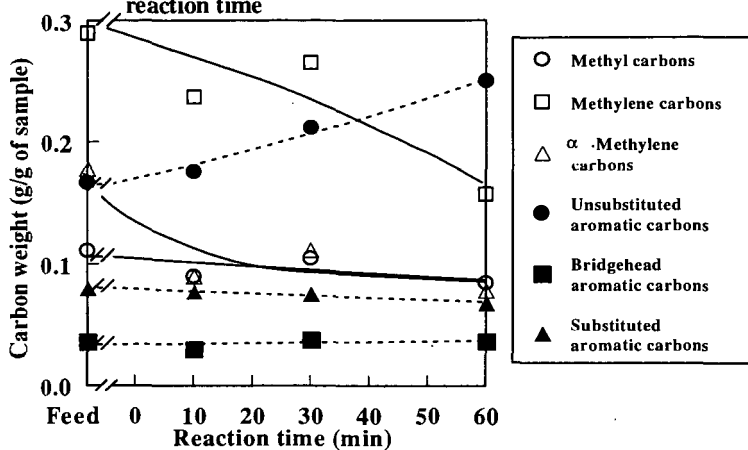


Fig. 3 Change in carbon weight by unit weight of sample with reaction time

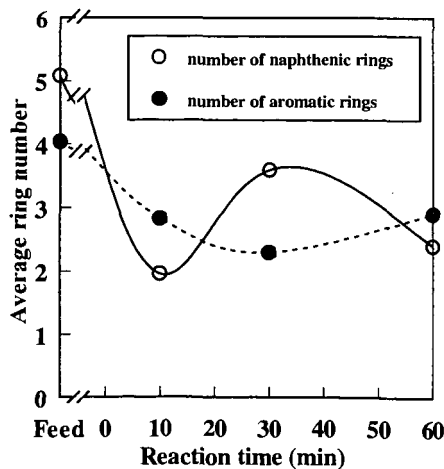


Fig. 4 Change in aromatic and naphthenic ring with reaction time

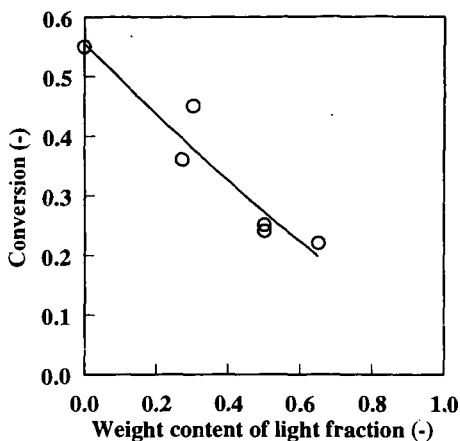


Fig. 5 Change in conversion for blended sample with weight content of light fraction

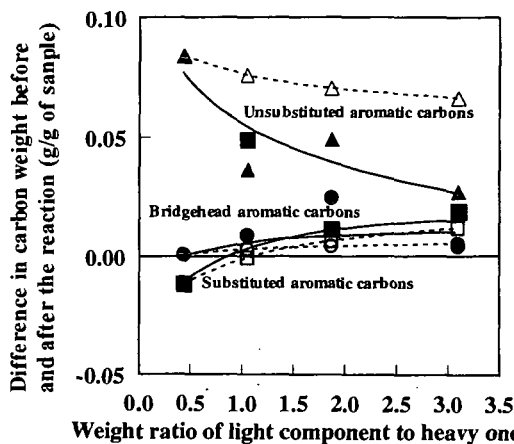


Fig. 6 Change in weight difference of aromatic carbons with weight ratio of light component to heavy one

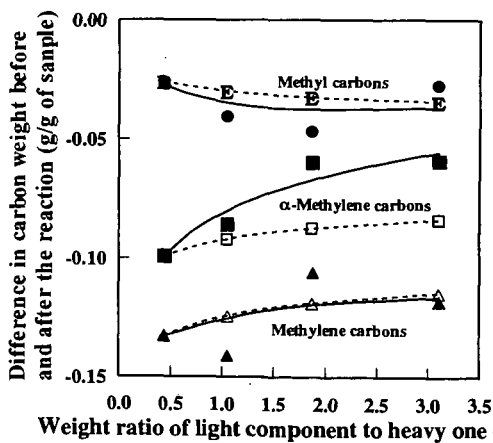


Fig. 7 Change in weight difference of aliphatic carbons with weight ratio of light component to heavy one

ADDITIVE FOR VISBREAKING: AVB-95

J.A. Carrillo Guarin and F. Pantoja
ECOPETROL-ICP
Piedecuesta, Santander
A.A. 4185 Bucaramanga, Colombia

Key Words: visbreaking, additives

SUMMARY

The primary goal for visbreaking is reducing the viscosity of heavy feedstocks by means of a mild thermal breakdown so it may be possible to produce fuel oils, as well as to prepare the feed for subsequent catalytic breakdown. The major operating costs of this process are strongly dependent on two factors: diluent consumption needed in the fuel oil formulation, and plant's coking rate resulting from the severity of the treatment. Some additives available on the market are specifically designed to exert a counteraction against the coking tendency of the heavy feedstocks inside the furnace tubes; and they, to a greater or lesser degree, accomplish this task. These commercial additives performance was evaluated and compared to that of an additive package, based on several mechanism of action, recently developed by Instituto Colombiano del Petróleo (ICP). As a result of the pilot plant experiments and field trials, it was found that the new additive considerably reduces the quantity of diluent necessary for fuel oil preparation; and moreover, the run time is increased with less plant maintenance requirements.

INTRODUCTION

The visbreaking process is a mild thermal cracking process wherein vacuum residues and asphalt are processed in order to prepare the feedstock for FCC and to reduce the viscosity of these feeds to produce fuel oil (1-3).

Among the reactions taking place in the visbreaking process we have:

- Side-chains from resins and aromatics are broken leading to further decrease in the average molecular weight, and consequently reducing their peptizing capability.
- Free radicals are reacted to form asphaltenes.
- The asphaltenes are subjected to dealkylation and dehydrogenation reactions whose products are more difficult to peptize, causing the colloidal system destabilization and asphalt precipitation.
- The saturated components (paraffins) are split into shorter, non-polar compounds which facilitate asphaltene precipitation.

These undesired reactions are responsible for the main drawbacks and limitations in the run time and severity applied in visbreaking operations. This is why we rely on additives (4-7) to avoid the aforementioned problems.

MATERIALS AND METHODS

Three commercial additives already tried at an industrial scale were chosen for evaluation on a visbreaking pilot unit built by the ICP (Figure 1). Besides, the heavy residues used in the experiments came from Ecopetrol's refinery in Barrancabermeja, and had the physicochemical characteristics sketched in Table 1. The operating conditions set up were 870°F (465°C), and 25 minutes residence time.

The working mechanism for these latter additives is based on the formation of a protective film over the tubes metallic walls at the prevailing operating conditions, but they do not act upon the system stability. At the beginning of the run the surface temperature is around 870°F (465°C) and becomes slowly increased with time as the coke layer starts to deposit, forming an insulating barrier. The evaluation at pilot scale showed that, coincidentally, the additive having the best performance was the one being used at the Ecopetrol's plants at that time. It was also observed that said commercial additives were not effective as operating temperatures were over 884°F (473°C), maybe due to product decomposition.

This clear disadvantage of available commercial additives led us to think about developing new additives working under mechanisms, different from that of film-forming, such as: hydrogen transfer, metal passivators, and free radicals scavengers. As a result

we obtained a package of additives having a higher protective efficiency against coking than commercial products, as it is seen in Figure 3.

RESULTS

With the available additive used by the Cartagena Refinery, acceptable gas, nafta and gas-oil performance was obtained, which was increased by the application of the AVB-95 additive. These differences are shown in table 2.

Benefits from the application of AVB-95

Although performance of the commercial additive being used in the Cartagena refinery was considered satisfactory from the standpoints of gas, naphta, and gas-oil yields; a remarkable increase in these variables output was seen once the AVB-95 was applied. The additional benefits are clearly depicted in Figure 4.

1. Profit due to VBN (viscosity blending number) increase

Depending on the severity and the additive dosage, an increase in VBN from 1.0 to 2.5 points is easily reached. It should be carefully considered that a single point increase in VBN for a plant that processes vacuum residues means total savings of about KUS \$800 per year.

2. Savings with maintenance

Due to a more porous and softer coke formation caused by the additive action, maintenance work on the furnace and the fractional towers is made easier, and cost noticeably reduced. These savings equal to KUS\$220 per year.

In the Cartagena refinery the average coke film thickness within the furnace tubes was reduced in almost 1.5 cm. The coke deposition rate in the fractional towers was also lowered and its smooth consistency allowed an easier removal.

3. Increase in the service factor

For run #37 at the Cartagena refinery, an increase in the service factor of 76% was registered due to a greater operating time equivalent time to 9 days a year. The benefit was then around KUS \$583 per year.

4. Versatility in operation

Through the use of this additive it may be possible to obtain a reaction product having a lower asphaltene content and greater distillate production, which at the same time permits operating at the same severity levels for longer run times. These latter condition bear an increase in conversion without risking the stability of the fuel oil or coking the furnace.

5. Product performance

The Cartagena refinery plant used a commercial additive and for this reason the action of additive AVB-95 is not compared with an actual target, but additional benefits are readily achieved over the commercial additive (See Table 2).

Through the addition of the new additive we were able to increase the conversion by 1.52%, specially in nafta production, by 0.71%, but also in gas-oil, by 0.81%.

The analysis of saturate, aromatic, resin and asphaltene content (SARA) of the visbreaking tars shows a broad change in the distribution of each family as a result of the free radicals caping action and the increase of hydrogen concentration in the system foreseen by the anti-coking agent AVB-95.

The average changes in composition for the visbroken resids are:

Saturates: increased by 1.21%

Aromatics: increased by 10.0%

Resins: decreased by 8.9%

Asphaltenes: decreased by 3.0%

This new chemical distribution improves the VBN in the visbreaking tar, allowing the operating plant a severity similar to previous runs, increasing run time due to a lower quantity of asphaltenes in the system, hence producing less coke. As a secondary

effect there is an increase in the conversion of nafta and gas-oils, operating at the same severity.

CONCLUSIONS

With the use of AVB-95 there are the followings benefits:

- Increase in the ΔVBN of the tars.
- Less coke production in the fumace and run time increases.
- Easy removal of the coke.
- More conversion.

REFERENCES

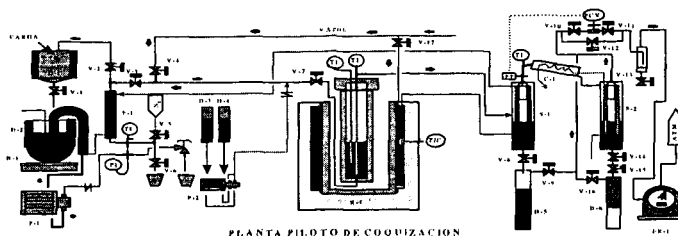
1. José A. Celestinos Y., René Hernández Pérez. Processes compared for upping Maya distillate yield. Technology, Oil & Gas Journal, April 26, 1982, 111-115.
2. A. Del Bianco, N. Panariti, M. Anelli, P.L. Beltrame and P. Carniti. Thermal cracking of petroleum residues. Fuel, 1993, Vol 72, January, 75-80.
3. Indra D. Singh, Vilma Kothiyal, Mahendra P. Kapoor, Veda Ramaswamy and Mahesh K. S. Aloopwan. Structural changes during visbreaking of light Arabian mix short residue: comparison of feed and product asphaltenes. Fuel 1993, Vol 72, Number 6, 751-754.
4. Michel Thomas, Bernard Fixari, Pierre Le Perchec, Yves Princic and Louis Lena. Visbreaking of Safaniya vacuum residue in the presence of additives. Fuel, 1989, vol 68, March, 318-322.
5. A. Del Bianco, N. Panariti, B. Prandini, P.L. Beltrame and P. Carniti. Thermal cracking of petroleum residues. Hydrogen-donor solvent addition. Fuel, 1993, Vol 72, January, 81-86.
6. P. Le Perchec, M. Thomas and B. Fixari. Fraction characterization of safaniya vacuum residue from visbeaking in the presence of sulfides and H-donor additives. Symposium on correlations between resid characterization and processability. American chemical society. Dallas meeting, April 1989, 422-427.
7. A.S. Bakshi, Y. H. Lutz. Adding hydrogen donor to visbreaking improves distillate yields. Oil and Gas Journal, July 13, 1987, 84-87.

Table 1. Characterization of visbreaking loads

| Property | Vacuum residue | Demex residue |
|-----------------------------|----------------|---------------|
| Density, 15,6 °C | 0.989 | 1.08 |
| Sulfur, %w | 2.26 | 2.32 |
| Conradson Carbon, %w | 18.98 | 31.5 |
| Penetration, 25 °C, 1/10 mm | 2.8 | 0 |
| Softening point, °C | 57 | 91 |
| Ni, ppm | 119 | 195.1 |
| V, ppm | 343 | 403.7 |
| | 2.3 | -2.1 |

Table 2. Performance with additives

| Additive | Commercial | AVB-95 |
|------------|--------------|--------------|
| Load, BPD | 20.000 | 17.000 |
| Fraction | Output, % wt | Output, % wt |
| Gases | 3.90 | 3.68 |
| Naphta | 5.45 | 6.16 |
| Gasoil | 34.36 | 35.17 |
| Residues | 59.00 | 57.60 |
| Conversion | 39.80 | 41.32 |



PLANTA PILOTO DE COQUIZACION

D-1: celula de carga, D-1: embudo de carga, D-2: tambor de carga, D-3: tambor de aditivos, D-4: tambor de aditivos, D-5: tambor de lodos, D-6: tambor de naftas, S-1: Separador de naftas y gases, S-2: separador de gases, E-1 y E-2 Interchambios, C-1: condensador, FR-1: medidor de gases, P-1: bomba de carga, P-2: bomba de aditivos, H-1: horno de vacuoreducción.

Figure 2. Evaluation of commercial additives

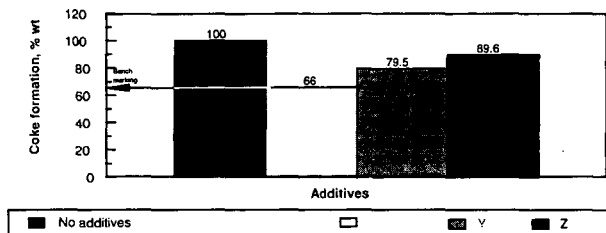


Figure 3. Evaluation of additives developed by the ICP

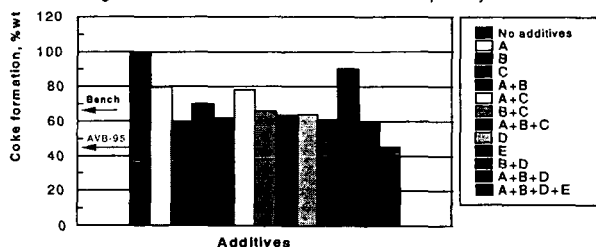
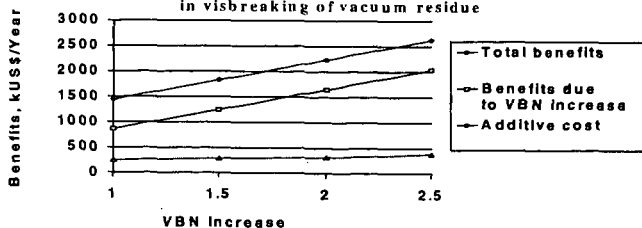


Figura 4. Benefits from the use of the AVB-95 additive in visbreaking of vacuum residue



COMPARISON OF OIL-SANDS-DERIVED AND CONVENTIONAL-CRUDE-OIL-DERIVED DIESEL FUELS AT DIFFERENT ENGINE OPERATING CONDITIONS

Xiaobin Li and Ömer L. Gülder
Combustion Research Group
Institute for Chemical Process and Environmental Technology
National Research Council Canada
Building M-9, Montreal Road, NRC
Ottawa, Ontario, Canada K1A 0R6

KEYWORDS: Diesel Fuels, Exhaust Emissions, Oil Sands

INTRODUCTION

In Canada, 21% of annual petroleum crude processed is oil-sands-derived crude oil. This figure is expected to increase as the conventional crude oil resources are depleted. In the diesel boiling range, the oil-sands-derived crude oil is low in sulfur but higher in aromatics (although low in multi-ring aromatics) compared to conventional crude oil. The oil-sands-derived crude also contains more cycloparaffins. Diesel fuels produced from oil-sands-derived crude tend to have relatively poor cetane quality but good low temperature properties. The specific emission behavior of oil-sands-derived diesel fuels is not well documented.

The general approach in fuel property studies is to blend fuels such that a single fuel property can be varied in a large range while maintaining the other fuel properties within a narrow span. This task is always challenging and sometimes impossible. Consequently, most of the studies to investigate the influence of fuel properties on diesel emissions are biased by the specific fuel matrix design and by the inter-correlation between the fuel properties. One way of alleviating this problem is a careful fuel matrix design consisting of a large number of fuels.

One of the disadvantages of running the U.S. EPA heavy-duty transient emission tests is that it is not possible to differentiate the contributions of different operating conditions to exhaust emissions. Some of the engine operating conditions are more sensitive to fuel properties than some others. In this study, the AVL 8-mode steady state simulation of the EPA transient test procedure was used. The composite emissions obtained from steady-state tests simulate the EPA transient results. The emission test results are therefore comparable to the results obtained with EPA transient test. At the same time, the engine test results from different engine modes offer detailed information so that the influence of each fuel property on oxides of nitrogen (NO_x) and particulate matter (PM) formation at different engine operating conditions can be investigated.

The focus of this study was to investigate the emission behavior of oil-sands-derived diesel fuels and compare it with diesel fuels derived from conventional crude oil. The effects of total aromatic content and fuel density were also investigated. We used two fuel matrices consisting a total of 19 diesel fuels.

EXPERIMENTAL

The engine used in this study is a single-cylinder research version (Ricardo Proteus) of a Volvo TD123 heavy-duty truck engine. The engine is a direct injection type and has a displacement volume of 2 liters. The research engine incorporates many features of contemporary medium- to heavy-duty diesel engines. It is tuned to meet the U.S. EPA 1994 emission standards. Detailed information on the test engine can be found in [1, 2]. The test procedure used in this study is the AVL eight-mode steady-state simulation of the U.S. EPA transient test procedure [3]. The engine speed and load at each of the eight modes are listed in Table I. To check the repeatability of the emission measurements, a low sulfur fuel obtained locally (Table III, fuel Ref2) was run in the engine periodically. The results showed that the standard deviations of NO_x and PM emission measurements were 0.9% and 4.3% of their means, respectively. No engine performance shift was

observed and the experimental data obtained with all test fuels were not adjusted for engine shift or experimental system error.

Among the 19 test fuels, 12 were blended using refinery streams. Six of these 12 fuels were originated from oil sands and the other six were derived from conventional crudes. A total of 22 components obtained from seven refineries were used in this fuel matrix. The parameters controlled in this fuel matrix were:

- ◆ total aromatics (10, 20 and 30% by mass)
- ◆ sulfur content (<500 ppm by weight)
- ◆ cetane number (42 to 46)
- ◆ viscosity, cloud point and distillation properties (within the typical range of current commercial diesel fuels in Canada).

The major properties of these test fuels are listed in Table II.

Seven other fuels obtained from various sources were run in the engine so that the regression models generated using the 12 blended fuels can be examined. The major properties of these fuels are listed in Table III.

RESULTS AND DISCUSSION

Composite Emissions

Using correction factors generated in the earlier stages of this research program[5], the composite NO_x and PM emission results were corrected to 150 ppm sulfur content and 44 cetane number. The effect of a small change in injection timing caused by the differences in fuel properties was also corrected. The NO_x and PM emission results are shown in Figure 1 and Figure 2 versus total aromatic content and fuel density.

The oil-sands-derived fuels yield NO_x emissions similar to the conventional-crude-oil-derived fuel blends. A good correlation between the composite NO_x emissions and fuel aromatic content and density was observed. The higher the total aromatic content and the density, the higher the composite NO_x emissions. NO_x emissions do not correlate with T90 or viscosity.

Comparing the two fuel groups, oil-sands-derived fuels generated higher composite PM emissions at the same aromatic level. This difference can be attributed mostly to the density difference between the two fuel groups in the test fuel matrix – the oil-sands-derived fuels having higher densities than the conventional-crude-oil-derived fuels at the same aromatic level. A modest correlation between composite PM emissions and fuel density was observed. A higher density leads to higher PM emissions. A slight increasing trend was also observed in PM emissions when total aromatic content was increased. There was no correlation between PM emissions and T90 or viscosity.

Regression analyses were performed to examine the correlation between the engine exhaust emissions and various fuel properties. The fuel properties considered in the regression analyses are: density, viscosity, T90, T50, T10, total aromatic content, and poly-aromatic content (di+-aromatics). The regression analysis results are shown in Table IV. Fuel density and total aromatic content were found to be the significant variables for NO_x emissions. These two properties account for 92.8% of the total changes in NO_x emissions ($R^2 = 0.928$). Both factors are highly significant, although total aromatic content is more so:

Density is the sole significant variable for PM emissions, accounting for 53.2% of the changes. The total aromatic content was not a significant variable. Considering the low R^2 value, the model can not be viewed as conclusive.

The proposed models were used to predict the NO_x and PM emissions of the 7 test fuels that had not been included in generating the correlations. The NO_x emission model was able to predict the NO_x emission results of six test fuels. The only exception was fuel Ref3 that has properties far away from those represented by the 12 test fuels. This indicates that total aromatic content and density are likely to be two important factors

affecting NO_x emissions. The PM model predictions for 6 of the 7 fuels were reasonable. The exception was fuel F. The model prediction was substantially lower than the actual measured PM emission result. Since fuel F had a substantially higher tri-+aromatic content, the result seems to suggest that multi-ring aromatics might be a factor influencing PM emissions.

Exhaust Emissions at Different Engine Operating Conditions

The eight-mode steady-state test procedure enables us to examine the impact of fuel properties at different engine operating conditions. The effects of cetane number and cetane improvers were significant at low load conditions such as modes 1, 2 and 5. An increase in cetane number from 44 to 64 reduced NO_x emissions by as much as 25% [2][4]. At the same time, PM emissions at low load conditions tended to increase when cetane number was increased. The effects of cetane number on NO_x and PM emissions were not significant at medium to high load conditions. Therefore, the cetane number corrections were performed on NO_x and PM emissions at modes 1, 2 and 5 only using the individual correction formula obtained from engine tests for each corresponding mode.

The sulfur correction formulas were found to be different for different modes. In general, the effect of sulfur appeared to be the largest at the low idle condition, mode 1. Individual correction formulas were used for corresponding modes.

The effects of injection timing on NO_x emissions could be described using second order polynomials for all the modes [5]. This effect was greater at low speed and low load conditions (such as modes 1 and 2). The effects of injection timing on PM emissions were best described using linear relationships. The engine injection timing affected PM emissions more at high load conditions (such as modes 4 and 8).

The corrected brake specific NO_x and PM emissions at each mode were calculated. The results at low idle and the heavy load conditions are plotted in Figure 1 and Figure 2 in comparison with the composite emissions. For NO_x emissions, the oil-sands-derived fuels behaved the same as the conventional-crude-oil-derived fuels at all eight modes. At medium to high load conditions (modes 3,4,6,7 and 8), the NO_x emissions increased with total aromatic content and fuel density. At light load conditions (modes 1,2 and 5), NO_x emissions were not affected by fuel properties.

The PM emissions at individual modes had relatively larger scattering than the composite PM emissions. Consequently, the oil-sands-derived fuels did not show clear difference from conventional-crude-oil-derived fuels in terms of PM emissions at individual modes. The total aromatic content and fuel density impacted on PM emissions differently at different modes. The effects of fuel properties on PM emissions appeared greater at low load conditions (modes 1 and 5); an increase in PM emissions was observed when total aromatic content and fuel density were increased. However, at heavy load conditions (such as modes 4 and 8), the effects of fuel properties on PM emissions were not significant.

The fuel density generally affects the fuelling rate when conducting transient tests. If all the test fuels are run using the same power curve that is generated from a reference fuel, the fuel with a higher density will run at a higher fuelling rate on mass basis. This fuelling discrepancy can bias emission comparison between fuels. In this study, steady-state tests were conducted, and the power outputs of all the fuels were kept the same. This minimized the fuelling discrepancy between the test fuels. The specific fuel consumption changed less than 1% and was not a function of density.

The effect of fuel density on NO_x emissions is likely to be a physical one. A higher fuel density leads to a higher injection rate on a mass basis and therefore shorter injection duration. This effect becomes more significant at heavy load condition due to longer injection duration. Between the heaviest and the lightest fuels, a 4% difference was observed in the mean cylinder pressure that was averaged from the start of mixing controlled burning to the end of fuel injection. This indicates that a higher injection rate

caused more fuel to be injected into the high temperature region, leading to higher NO_x emissions.

The effect of total aromatic content on NO_x emissions could be a chemical one. At high load conditions, major portion of the fuel was burned at fuel-rich locations where the chemical composition of the fuel is likely to have an impact on the local gas temperature. The fuel with a higher total aromatic content can be expected to generate a higher temperature in these fuel-rich regions because the adiabatic temperatures of the hydrocarbons with ring structures tend to be higher.

CONCLUSIONS

In this work, we compared the emission behaviors of fuels derived from oil sands and from conventional crude oil at different engine operating conditions. We also investigated the effects of total aromatic content and density of diesel fuels on NO_x and PM emissions. Our results lead to the following conclusions:

- Oil-sands-derived diesel fuels behave similarly as conventional-crude-oil derived diesel fuels in terms of NO_x emissions at all engine operating conditions.
- Oil-sands-derived diesel fuels exhibit higher composite PM emissions than their conventional-crude-oil-derived counterparts at the same total aromatic content. This can be attributed to the higher densities of the oil-sands-derived fuels. However, this trend was not clear at each individual engine operating mode.
- Different fuel properties influence NO_x and PM emissions at different engine operating conditions. Fuel density and total aromatic content influence NO_x emissions at medium to heavy load conditions, whereas the effects of fuel density and total aromatic content on PM emissions appear to be greater at low load conditions. It is therefore important to investigate the interaction between fuel properties and engine operating conditions.

ACKNOWLEDGEMENTS

We thank Mr. W. L. Chippior for his assistance in obtaining engine experimental data. Funding of the study has been provided by National Research Council Canada, Program for Energy Research and Development, Shell Canada Ltd., Syncrude Canada Ltd. and Imperial Oil Ltd. The majority of the test fuels were blended by Shell. The fuel properties were analyzed by NRC, Syncrude, Shell and National Centre for Upgrading Technology. We acknowledge Ken Mitchell, Jean Cooley, Keith Richardson, Maya Veljkovic and Craig Fairbridge for their valuable comments.

REFERENCES

- [1] Li, X., Chippior, W. L. and Gülder, Ö. L., "Effects of Fuel Properties on Exhaust Emissions of a Single Cylinder DI Diesel Engine", 1996 SAE Transactions, Paper No. 962116, 1996.
- [2] Li, X., Chippior, W. L. and Gülder, Ö. L., "Effects of Cetane Enhancing Additives and Ignition Quality on Diesel Engine Emissions", 1997 SAE Transactions, Paper No. 972968, 1997.
- [3] Cartellieri, W. P. and Herzog, P. L., "Swirl Supported or Quiescent Combustion for 1990's Heavy-Duty DI Diesel Engines - An Analysis", SAE Paper No. 880342, 1988.
- [4] Li, X. and Gülder, Ö. L., "Effects of Fuel Cetane Number, Density and Aromatic Content on Diesel Engine NO_x Emissions at Different Operating Conditions", Fourth International Symposium on Diagnostics and Modeling of Combustion in Internal Combustion Engines, July 20-23, Kyoto, Japan, 1998.
- [5] Li, X., Chippior, W. L. and Gülder, Ö. L., "Canadian Diesel Fuel Composition and Emissions - I", NRC Report No. 37645, 1997.

TABLE I AVL 8-MODE STEADY-STATE SIMULATION OF EPA TRANSIENT TEST PROCEDURE

| Mode | Speed (rpm) | Load (%) | Weighting Factor |
|------|-------------|----------|------------------|
| 1 | 600 | 0 | 35.01 |
| 2 | 743 | 25 | 6.34 |
| 3 | 873 | 63 | 2.91 |
| 4 | 1016 | 84 | 3.34 |
| 5 | 1900 | 18 | 8.40 |
| 6 | 1835 | 40 | 10.45 |
| 7 | 1835 | 69 | 10.21 |
| 8 | 1757 | 95 | 7.34 |

TABLE II PROPERTIES OF BLENDED TEST FUELS

| FUEL ID | Oil-sands-derived | | | | | | Conventional-crude-oil-derived | | | | | |
|---------------|-------------------|-------|-------|-------|-------|-------|--------------------------------|-------|-------|-------|-------|-------|
| | S10A | S10B | S20A | S20B | S30A | S30B | C10A | C10B | C20A | C20B | C30A | C30B |
| Density | 827.2 | 834.2 | 833.6 | 838.4 | 840.8 | 838.4 | 804.9 | 817.1 | 821.4 | 823.1 | 835.4 | 828.1 |
| Viscosity | 1.65 | 2.14 | 1.7 | 1.92 | 1.81 | 1.73 | 1.62 | 2.01 | 1.97 | 1.66 | 2.18 | 1.70 |
| Cloud Point C | -44 | -27 | -26 | -25 | -28 | -33 | <-70 | -27 | 3 | -39 | -10 | -37 |
| IBP, C | 155.0 | 158.5 | 156.5 | 156.5 | 170.5 | 170.5 | 189.5 | 201.5 | 187.0 | 173.5 | 178.5 | 175.5 |
| T10, C | 175.5 | 183.0 | 181.0 | 179.0 | 185.0 | 186.5 | 200.0 | 207.5 | 191.0 | 194.0 | 198.5 | 198.5 |
| T50, C | 217.5 | 244.0 | 224.0 | 232.0 | 222.5 | 224.5 | 212.5 | 221.5 | 223.0 | 219.5 | 244.0 | 231.0 |
| T90, C | 286.0 | 317.0 | 284.5 | 323.5 | 324.0 | 301.5 | 242.0 | 285.5 | 335.0 | 272.0 | 317.0 | 268.0 |
| EP, C | 313.5 | 344.5 | 310.5 | 348.5 | 347.5 | 334.5 | 284.5 | 320.5 | 379.0 | 315.0 | 352.0 | 301.0 |
| Cetane Index | 41.0 | 46.8 | 40.9 | 41.8 | 37.9 | 39.5 | 47.4 | 46.1 | 45.0 | 43.2 | 46.5 | 45.1 |
| Cetane No. | 41.0 | 43.4 | 40.2 | 42.9 | 42.3 | 42.0 | 40.4 | 41.6 | 46.5 | 41.9 | 43.9 | 44.2 |
| Sulphur, ppm | 13.2 | 2.4 | 28.8 | 31.1 | 84.7 | 3.0 | 8.1 | 131 | 31.4 | 134.0 | 270.0 | 202.0 |
| Hy. Cont. m% | 13.75 | 13.73 | 13.49 | 13.42 | 13.08 | 13.16 | 14.18 | 14.13 | 13.72 | 13.68 | 13.28 | 13.40 |
| Nitrogen, ppm | 27.9 | 0.3 | 56.4 | 1.5 | 24.8 | 2.5 | 1.0 | 17.5 | 4.7 | 19.7 | 41.2 | 21.8 |
| Total arom. % | 12.4 | 12.9 | 20.2 | 23.5 | 30.0 | 31.4 | 10.8 | 11.0 | 20.7 | 20.2 | 30.0 | 29.8 |
| 1-Ring | 10.9 | 9.5 | 17.9 | 2.02 | 25.2 | 27.4 | 9.6 | 7.8 | 16.0 | 16.8 | 22.1 | 25.1 |
| 2-Ring | 1.5 | 2.9 | 2.2 | 2.7 | 4.3 | 3.6 | 1.1 | 2.9 | 4.3 | 3.2 | 7.1 | 4.4 |
| 3+-Ring | 0.0 | 0.5 | 0.1 | 0.5 | 0.6 | 0.3 | 0.1 | 0.3 | 0.3 | 0.3 | 0.8 | 0.3 |

TABLE III PROPERTIES OF OTHER FUELS

| FUEL ID | Ref1 | Ref2 | Ref3 | A | C | E | F |
|---------------|---------|---------|---------|-------|-------|-------|-------|
| Source | Conven. | Conven. | Conven. | Both | Both | Both | Both |
| Density | 836.2 | 835.0 | 842.0 | 829.7 | 841.0 | 836.8 | 857.3 |
| Viscosity | 2.135 | 2.207 | 4.03 | 1.752 | 1.723 | 1.439 | 2.464 |
| Cloud Point C | -22 | -19 | -6 | | | | |
| IBP, C | 178.5 | 172.9 | 175.5 | 166 | 170 | 170 | 170 |
| T10, C | 205.6 | 198.9 | 244.8 | 183 | 185 | 183 | 189 |
| T50, C | 245.5 | 255.9 | 297.8 | 220 | 224 | 209 | 245 |
| T90, C | 306.1 | 311.4 | 333.8 | 284 | 284 | 251 | 344 |
| EP, C | 343.3 | 336.7 | 352.6 | 317 | 313 | 282 | 378 |
| Cetane Index | 46.6 | 49.7 | 55.5 | 40.7 | 38.0 | 34.2 | 39.5 |
| Cetane No. | 43.9 | 46.2 | 55.4 | 45.8 | 43.5 | 40.3 | 43.1 |
| Sulphur, ppm | 287.0 | 351.0 | 9.2 | 466 | 460 | 374 | 299 |
| Hy. Cont. m% | 13.38 | 13.37 | 13.95 | 13.78 | 13.28 | 13.29 | 13.19 |
| Nitrogen, ppm | 54.1 | 42.9 | 2.5 | | | | |
| Total arom. % | 27.3 | 27.5 | 4.8 | 10.8 | 24.5 | 25.2 | 23.5 |
| 1-Ring | 21.8 | 19.9 | 4.0 | 6.5 | 17.8 | 20.4 | 11.4 |
| 2-Ring | 4.9 | 6.7 | 0.7 | 3.6 | 6.2 | 4.7 | 8.6 |
| 3+-Ring | 0.5 | 1.0 | 0.1 | 0.7 | 0.5 | 0.1 | 3.6 |

TABLE IV REGRESSION ANALYSIS OF CORRECTED COMPOSITE EMISSIONS

| Emission | Variables | Std. Error | Std. Coefficient | F-Value | Probability | R ² |
|-----------------|-------------|------------|------------------|---------|-------------|----------------|
| NO _x | Density | 0.0012 | 0.4559 | 14.31 | 0.0043 | 0.928 |
| | Total Arom. | 0.0016 | 0.5964 | 24.48 | 0.0008 | |
| PM | Density | 0.0004 | 0.7293 | 11.36 | 0.0071 | 0.532 |

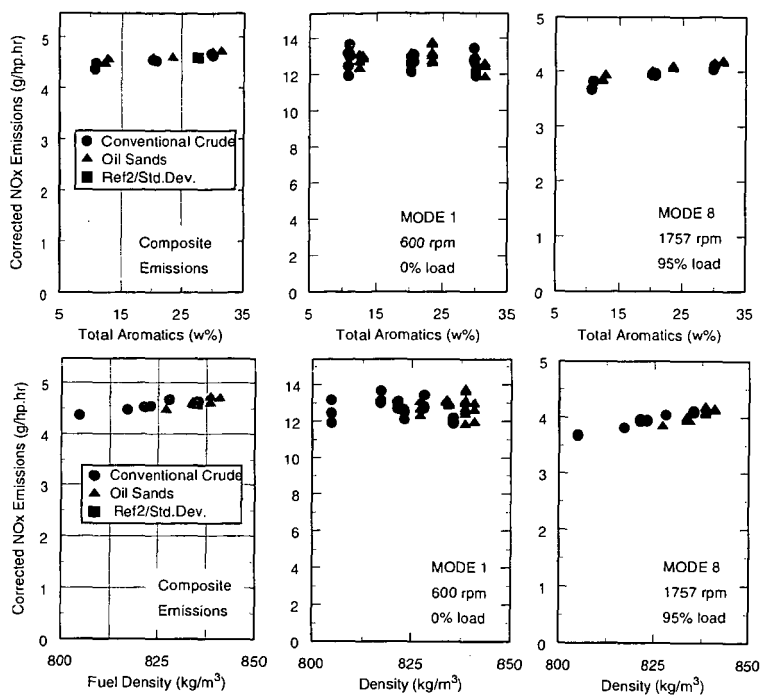


Figure 1 Corrected NO_x Emissions versus Total Aromatic Content and Fuel Density

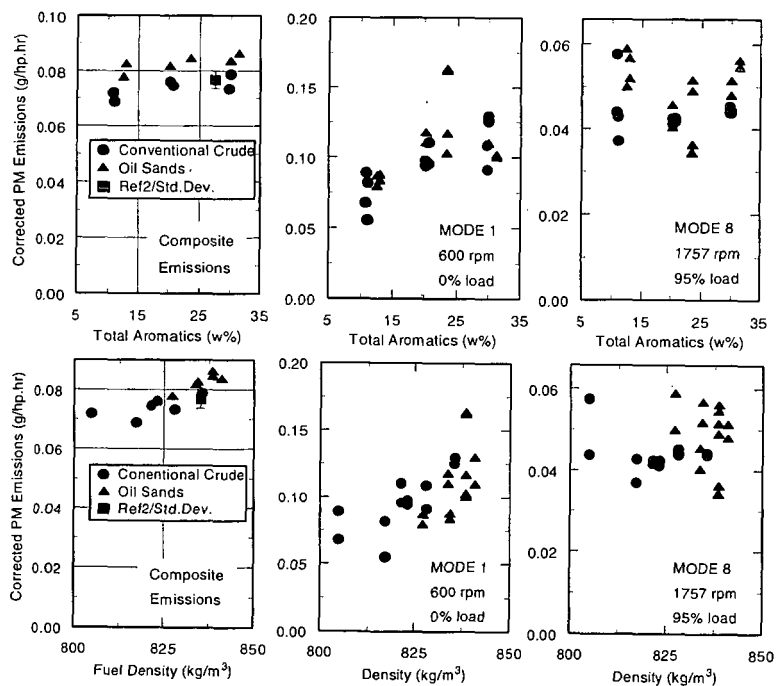


Figure 2 Corrected PM Emissions versus Total Aromatic Content and Fuel Density

THE SHENHUA DIRECT LIQUEFACTION PLANT

Alfred G. Comolli, Theo L.K. Lee, Gabriel A. Popper, Robert H. Stalzer,
And Peizheng Zhou (Project Manager)
Hydrocarbon Technologies, Inc. (HTI)
1501 New York Avenue
Lawrenceville, NJ 08648

INTRODUCTION

On September 22, 1997, Hydrocarbon Technologies Inc. (HTI) signed an agreement with Shenhua Clean Coal Technology Development Company, Ltd. (SCCT) and China Coal Research Institute (CCRI) on the feasibility study for a Direct Coal Liquefaction plant in China, one major project in China's ninth five-year plan. China is the world's largest hard coal producer and possesses huge reserves in trillions of tons of all types of coal and, although China also ranks as about the eighth largest worldwide producer of oil, it is now a net importer. This is due to its expanding economy and 1 billion plus population. Consequently, the cost-effective use of coal for transportation fuels in an environmentally-friendly manner is justified for China.

The project is to build a mine-mouth liquefaction plant using coals produced in the Shenhua coalfield in Northern Shaanxi Province and Inner Mongolia near Baotou City. Shenhua coalfield, previously known as Shenmu coalfield, is the largest developing coalfield in China and the eighth largest deposit of coal in the world, with coal mines owned and operated by Shenhua Group Corporation, Ltd., the parent company of SCCT. China's State Planning Commission has selected Shenhua coal as a candidate for liquefaction on the basis of its abundant reserves, good quality, reasonable cost, and a strategic location. See *Figure 1*, Map of China.

According to the Agreement, the study includes two phases of work. Phase I is a preliminary feasibility study that involves a bench-scale continuous flow unit (CFU) test at HTI and a preliminary economic evaluation based on the test results and local economic data for the plant. Phase II will be a Process Development Unit (PDU)-scale testing and a more in-depth technoeconomic analysis. Following Phase II, the detailed engineering design, procurement, and construction would commence on the \$1.5 billion China grassroots plant complex.

PROCESS

The HTI COAL™ Process consists primarily of two backmixed reactor stages utilizing a proprietary dispersed superfine, iron catalyst (GelCat™) and fixed bed in-line hydrotreating. Operations are in the resid extinction mode, whereby unconverted residuum is recycled or used for hydrogen production, and a 750°F minus refined product is produced. A low/high reactor temperature staging that promotes hydrogenation and improves solvent quality is practiced. The process operates under a pressure of 17 MPa.

A slurry of pulverized coal in recycled, heavy coal-derived oil is premixed and pumped through a preheater along with hydrogen and catalyst into the first stage reactor. The effluent from the first stage undergoes separation to remove gases and light ends with the heavier liquid stream flowing to the higher temperature second stage. Effluent from the second stage, joined with overhead from the interstage separator, flows to the fixed bed in-line hydrotreater for enhanced upgrading to very clean fuels. The effluent from the hydrotreater is the major liquefaction product, mostly diesel, naphtha, and a jet fuel fraction. Bottoms product from the second-stage separator is flashed, and the overheads are pumped to the in-line hydrotreater for upgrading. The atmospheric bottoms stream containing solids is used as recycle with a portion going to a vacuum still and to solvent solids separation, with the resulting bottoms going to partial oxidation and the overheads to recycle. A condensed flow diagram is shown in *Figure 2*.

PROGRAM

The overall program consists of two stages. Stage 1 comprises the agreement to conduct a feasibility study and technical assessment of the HTI technology applied to Shenhua coal. Stage 2 is the financing, design, and construction phase of the project. Further detail is provided in *Figure 3*, Pioneer Plant Project Task and Schedule.

Phase I of Stage 1 has been successfully completed and reported to China. Results as discussed further were very encouraging; higher than predicted yields of clean distillate fuels were produced projecting improved economics.

Planning for Phase II is now underway with coal being readied for shipment to HTI from the new mine-mouth plant site. A 5 ton/day 30-day Process Development Unit run is scheduled for July of this year to provide scale-up data and products for evaluation and to prove the concept.

Ford Motor Company has included data from HTI's Direct Liquefaction into a Fuel Life Cycle Analysis for China, and an engineering relationship is being established with ABB Lummus Global, Inc. of New Jersey. The US Department of Energy is providing support and guidance for the project work at HTI. China is providing technical assistance, coal preparation, and the end use evaluation. China has also indicated a willingness to the containment and control of CO₂ and other emissions. A project schedule is shown in *Figure 3*.

DEVELOPMENTS

Samples of two major Shenhua Coal seams were selected and shipped to HTI for Continuous Flow Unit (50 Kg/day) CFU testing using HTI's COAL™ Process. See *Figure 2*. Data from this run was then used to conduct a pre-feasibility study using Chinese economic data. The coal analysis, as shown in *Table 1*, classifies the coal as a low ash, high volatile bituminous coal.

A CFU run of 26 days was conducted to maximize distillate yield, quality, and selectivity. Test conditions for the two coal samples were selected based on batch experimental results previously obtained by CCRI and HTI. Variables studied were catalyst concentration,, space velocity, and reaction temperatures.

Coal conversions for the entire run varied from 90 to 93 percent on moisture, ash free basis (maf) with an average of 91 percent for both coals. The C₄-524°C distillate and 524°C resid yields were higher than projected by batch experiments. Distillate yields varied between 52 to 68 percent maf, and 824°C⁺ residuum yields varied between 7 to 22 percent maf. The Shenhua #2 seam coal gave lower distillate yields at 54 to 63W percent maf. Distillate selectivity, naphtha (IBP-177°C), middle distillate (177 to 343°C), and heavy distillate (343-524°C) varied with higher catalyst loading and recycle ratio. At the highest yield condition, there was 15 percent naphtha, 55 percent middle distillate, and 30 percent heavy distillate. *Figure 4* illustrates the varying selectivity at each run condition. For China, the mid-distillate for diesel fuel is preferred.

Hydrogen efficiency, distillate/hydrogen ratio, varied between 7.3 to 8.8 while consumption averaged 6.5 wt% maf. C₁-C₃ gas selectivity, gas/distillate ratio, varied between 0.18 to 0.22 with the lowest occurring at the highest distillate rates.

The total distillate product was subjected to a true boiling point distillation, and the fractions were characterized. The sulfur content of the medium naphtha (82-204°C) was 11 ppm, and the light naphtha (IBP-82°C) had a content less than 1.0 ppm. Since gasoline is made from these two coals, the sulfur levels far below specs for the US and China for the year 2000 (309 ppm and 1500 ppm, respectively). Also, the aromatic content at 3.11 percent and the olefin content at 1.4 percent are well under target for the US where aromatic is 22.0 percent and olefin is 4.0 percent, respectively. The light distillate cut (204-228°C) had a sulfur content of 475 ppm versus the China limit of 2000 ppm, while the freeze points are much lower than required.

Based on the overall distillate fraction properties, the gasoline (IBP-204°C) and diesel fuel (204-343°C) fractions most likely do not need to be further hydrotreated. Also, they can be a component in the refinery gasoline and diesel pools where the gasoline octane number and the diesel fuel cetane number can be met by blending with other refinery product streams.

The preliminary feasibility study envisions construction of a 12,000 metric ton per day coal liquefaction complex, complete and stand-alone with facilities for coal preparation, coal mixing, and liquefaction, hydrogen manufacture, and product upgrading to finished product gasoline and diesel fuels. Also included are by-product recovery, effluent handling and treatment, and utility generation except for power.

A coal liquefaction flow and block diagram are shown in *Figure 5* and *Figure 6*. As depicted in *Figure 6*, coal is received at the site from the coal mine, and is crushed, dried, and ground to size in the coal preparation plant. A portion of the coal is used in manufacturing hydrogen by partial oxidation, while the majority of coal is fed to the liquefaction plant. In the liquefaction facility, coal is reacted with hydrogen in the presence of a catalyst, to produce liquids, gases, and unconverted coal plus residual oil. Liquid products from coal liquefaction consist of a C₃ to 204°C naphtha fraction, a light distillate boiling in the 204 to 343°C range, and a heavy distillate boiling in the 343 to 524°C range. Naphtha is hydrotreated and then catalytically reformed to a

finished gasoline product. Light distillate is sent directly to diesel fuel product, and heavy distillate is mildly hydrotreated and sent to a fluid catalytic cracker (FCC) for conversion into gasoline and diesel fuel products.

Unconverted coal and residual oil, boiling above 524°C, are sent to the partial oxidation (POX) plant, along with some of the coal previously mentioned. The bulk of the hydrogen requirement of the complex is produced in this unit.

Gaseous and aqueous products from liquefaction and from product upgrading are handled separately and conventionally.

The 12,000 metric ton/day Pioneer Plant is based on three train two-reactor systems using 33.3 percent equity with long term (10 years) debt at 10.53 percent interest, 20-year plant life, and China raw material and product prices and tax structures. The model calculates the financial net present value (FNPV), defined as the sum of the annual cash flows discounted yearly at 12 percent, compounded over the life of the project. Factors were applied to US Gulf Coast Construction prices for labor and construction costs in China, and a 15 percent contingency was added for the total constructed units including fee. Salvage value was taken as zero.

The total plant cost was estimated to be 12,576 MM RMB, or US \$1.52 billion, with annual revenues and operating costs of 6,599 MM RMB (US \$796 million) per year and 5,297 RMB (US \$639 million), respectively. The net cash flow before taxes was estimated to be 1,302 MM RMB (US \$157 million) per year.

Rates of return and FNPV, before and after China taxes, are:

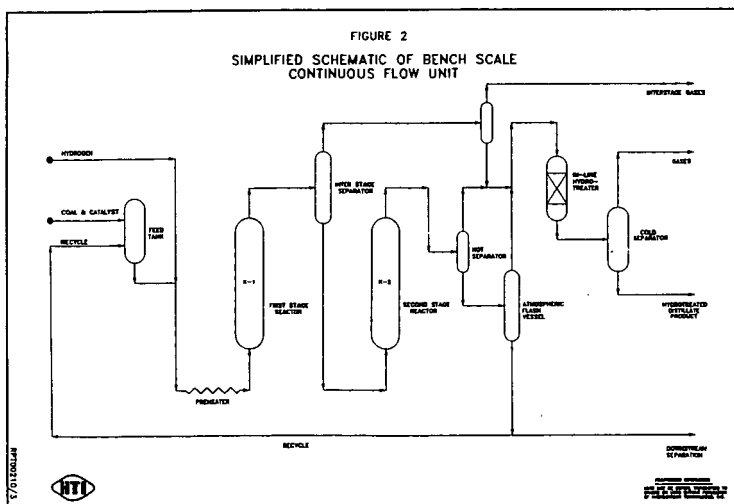
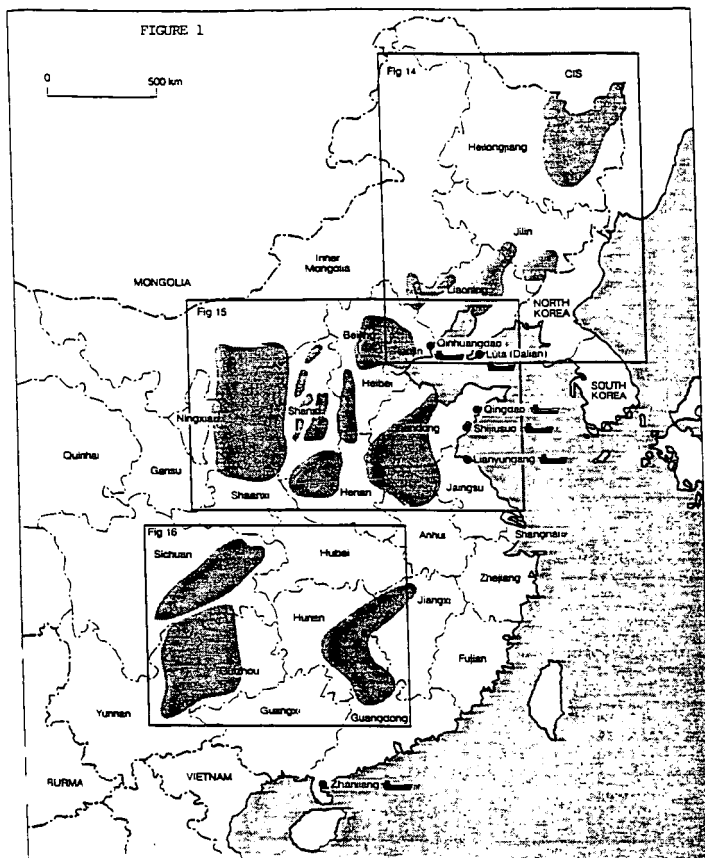
| | <i>Before Tax</i> | <i>After Tax</i> |
|--------------------|-------------------|------------------|
| Rate of Return, % | 23.3 | 18.5 |
| FNPV @ 12%, MM RMB | 4,524 | 2,282 |

CONCLUSIONS

Specific conclusions of the study are:

- With HTI's advanced liquefaction technology, GelCat™ catalyst, and at proven reactor operating conditions, both Shenhua #2 and Shenhua #3 coals can be processed in excess of 92 percent coal conversion to produce C₄-524°C distillate yields in the range of 63 – 68 W% maf coal. This could be processed with liquid product qualities comparable to those obtained with US coals.
- The products from coal liquefaction should meet or exceed SINOPEC Standards for gasoline and diesel fuel products, using commercially-proven refinery techniques for product upgrading.
- A site has been chosen for a commercial coal liquefaction venture near Baotou City, Inner Mongolia, close to the coal mine and conveniently located for access to railway and highway transportation of the raw materials and products.
- Using liquefaction yields demonstrated with Shenhua #3 coal, a conceptual process design for a commercial standalone grassroots facility has been completed for a coal feed rate of 12,000 MT/D. The facility would produce 3,073 MT/D of gasoline and 18 MT/D ammonia and 53 MT/D sulfur.
- The economics of a commercial coal liquefaction plant are promising, showing an 18.5 percent discounted-cash-flow rate of return, with 33.3 percent equity financing and a 10-year debt carrying an interest rate of 10.5 percent.
- Economics are improved by decreasing the investment cost and the coal price, extending the operating life, by being exempt of state and local taxes, and by increasing the selling price of the gasoline and diesel fuel products.
- Use of natural gas to make hydrogen is less preferable than use of coal, at the prices expected in China.
- Proper management of air, water, and solid waste qualities will permit existing and anticipated environmental standards to be met and exceeded.

Acknowledgments: CCRI, China Coal Research Institute, Shenhua Coal Company, United States Department of Energy, and Hydrocarbon Technologies, Inc. (HTI)



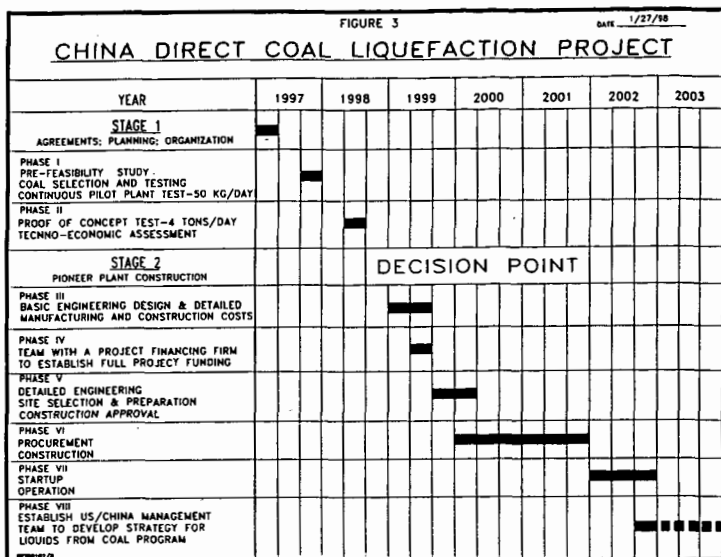
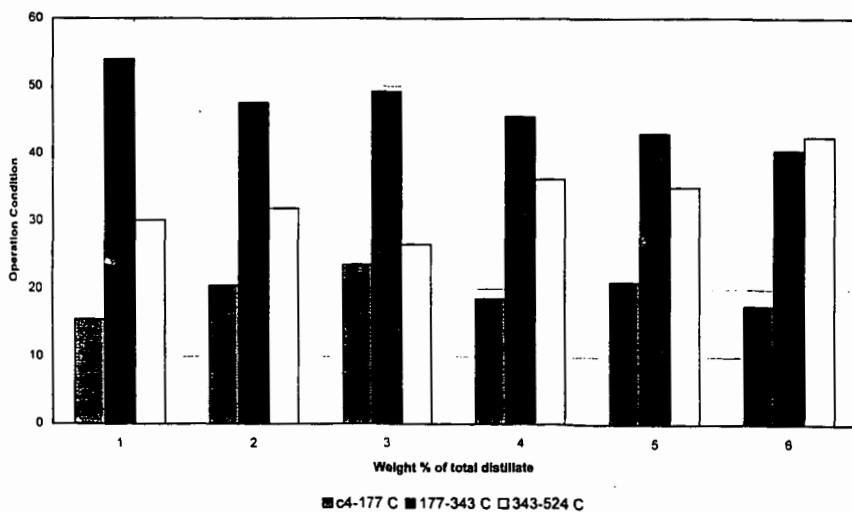
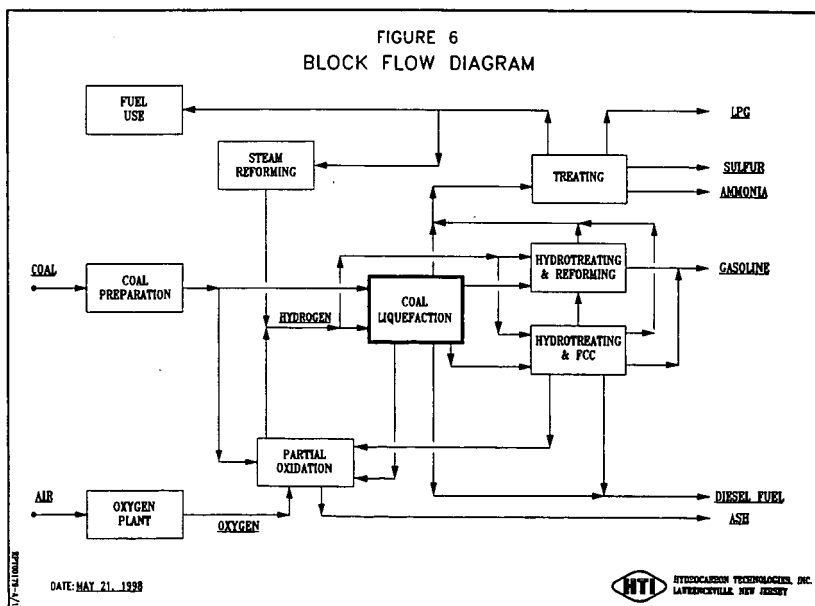
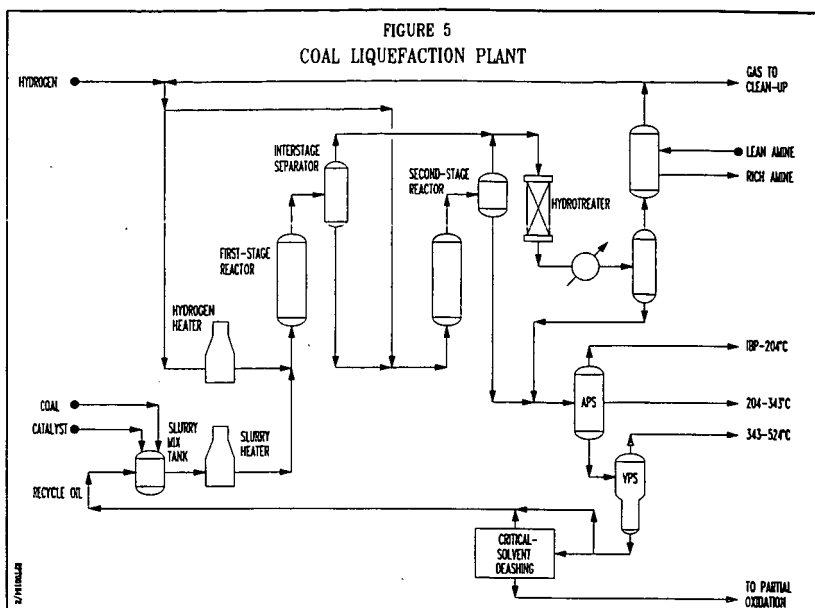


TABLE 1
ANALYSIS OF SHENHUA COALS

| Seam Number | Proximate Analysis | | | Ultimate Analysis | | | | | | |
|-------------|--------------------|-----------------|------|-------------------|----------|----------|--------|--------|------|------------------|
| | Fixed Carbon | Volatile Matter | Ash | Carbon | Hydrogen | Nitrogen | Sulfur | Oxygen | Ash | H/C Atomic Ratio |
| 2 | 57.95 | 35.84 | 6.21 | 75.87 | 4.24 | 0.98 | 0.42 | 12.28 | 6.21 | 0.67 |
| 3 | 61.79 | 36.47 | 4.25 | 79.47 | 4.13 | 1.05 | 0.42 | 10.68 | 4.25 | 0.62 |

Figure 4: Distillate Selectivity





ESTER FUELS VIA NON-AQUEOUS ENZYME-CATALYZED REACTIONS OF FATTY ACIDS

E.S. Olson, H. K. Singh, and M. Yagelowich
Universal Fuel Development Associates, Inc.
223 Circle Hills Drive, Grand Forks, ND 58201

ABSTRACT

The use of nonaqueous enzyme slurries for the production of fatty ester fuels from coal-derived alcohols and fatty acids was investigated. Phenolic tars from coal gasification wastes were fractionated and treated with ethylene oxide to convert them to an alcohol, and the intermediate alcohols were esterified with the fatty acids in a nonaqueous lipase system. Lipases in a variety of organic solvents were investigated for acylation of coal-derived alcohols. The two step process transformed the black poorly soluble phenolics to clean paraffin-soluble esters. Diesel testing demonstrated that the phenoxyethyl esters could be substituted for diesel fuels.

INTRODUCTION

The production of diesel fuels from vegetable oils by conversion of the triglyceride to a less viscous ester has been extensively investigated. Most of the focus has been on methyl and ethyl esters, because of the ease of preparation and the low cost of methanol. Coal-derived alcohols may represent another inexpensive alcohol source for forming the ester diesel fuel. Phenolic materials are produced in large amounts during coal conversion processing to coke, liquids, or synthesis gas. Coal gasification produces a crude phenol/cresol stream from extraction of the condensate water. At the Great Plains Gasification plant operated by Dakota Gasification Company, the Phenosolvan extraction process recovers about 97 million pounds per year of the crude phenolics (1). The phenolics can be esterified with acid chlorides and anhydrides, but not with the less inexpensive esters or acids.

Alcohols can be produced from coal liquefaction and gasification byproduct phenolics by reaction of the phenolic hydroxyl groups with epoxides to give phenoxyalkanols. The hydroxyethylated and hydroxypropylated phenolics undergo esterification reactions at the alcohol group with esters and acids that do not occur readily with the original phenolic group.

Non-aqueous enzyme systems can greatly facilitate many organic reactions, especially those that result in formation of esters and amides. We previously reported the application of non-aqueous enzyme slurries to the production of fatty ester fuels from coal-derived alcohols (2,3). Most of our earlier work utilized triglyceride substrates as the acyl source for transesterification or interesterification reactions of these alcohols. But some inexpensive fatty acids are available from sources such as tall soaps and wastes from vegetable oil processing.

In order to develop an economical process for production of alternative ester fuels, a study of lipase-catalyzed reactions of fatty acids was carried out in nonaqueous solvents. The goal of this work was to exploit the advantage that enzymes in nonaqueous solvents can offer by driving the equilibrium toward the ester products. This paper will discuss the conversion of phenolic materials from coal gasification byproduct streams to a diesel fuel by using enzyme-catalyzed esterification reactions.

EXPERIMENTAL

Hydroxyethylated phenolics

The hydroxyethylation of the Great Plains crude phenols with ethylene oxide or other reagents was previously discussed (2,3). The composition of the hydroxyethylated intermediate was determined to be as follows: 2-phenoxyethanol, 45%; 2-(2'-methylphenoxy)ethanol, 10%; 2-(3- and 4-methylphenoxy)ethanol, 23%; other alkylphenoxyethanols 22%.

Acylation of hydroxyethylated phenolics

Hydroxyethylated Great Plain phenols (0.300 g) were reacted with 0.600 g of oleic acid in a slurry containing 100 mg Amano PS-30 lipase in 15 ml of solvent at 65°C. The reaction was allowed to proceed for 20 hrs. The product mixture was centrifuged to separate the enzyme, and the reaction mixture was analyzed by GC.

RESULTS AND DISCUSSION

The crude phenolic stream from the Great Plains Gasification Plant was reacted with ethylene oxide to give a hydroxyethylated intermediate (2). The lipase-catalyzed esterification reaction of the hydroxyethylated phenolics with equimolar amounts of oleic acid (free acid form) was found to give a high yield of the oleate ester in hexane solvent. With the Amano PS-30 lipase, a conversion of 83% to oleate ester was achieved for both the phenoxyethanol and the methylphenoxyethanol components of the intermediate. The corresponding transesterification conversions obtained using triglyceride substrates (tripalmitin, canola oil) were 90-95% (3), but these transesterification reactions used an excess of the triglyceride to drive the reaction. The reaction of oleic acid was repeated on a large batch to verify the high yield of ester product. The same yield of ester was obtained.

The reaction of 2-phenoxyethanol (the major component of the hydroxyethylated phenolic mixture) with oleic acid was further investigated with Amano PS lipase and with porcine pancreatic lipase in various solvents to determine the role of the organic solvent in the reaction. Yields of the phenoxyethyl ester product from oleic acid utilizing Amano PS lipase as a slurry phase in various organic solvents are reported in Table 1. The high yield of ester in the nonpolar hydrocarbon solvents may be attributed to formation of reverse micelles of unreacted fatty acid that can trap the water byproduct so that the reverse reaction (hydrolysis) does not occur at a fast rate. The reverse micelles do not form in the polar solvents, and the water is miscible and able to participate in the hydrolysis (reverse) reaction. Thus, the esterification reaction can be effectively driven to high conversion only in a nonpolar solvent. An excess of the fatty acid could probably give even higher yields by driving the equilibrium to the right, but this was not investigated, since an excess of fatty acid is not desirable in the fuel product. An extra step might then be required for removal of unreacted fatty acid.

The high conversion found for toluene as the solvent contrast significantly with the results obtained earlier for the transesterification with triglyceride. In these earlier studies with canola oil, use of toluene as the solvent resulted in poor conversions to the ester. The low transesterification reactivity in toluene has not been adequately explained. Hexane is a good solvent for both esterification and transesterification, however.

An additional tactic for shifting the equilibrium and thereby increasing the conversion to ester is the removal of product water from the reaction by the addition of molecular sieves. Several attempts were made to increase the ester yields for the reaction of phenoxyethanol and hydroxyethylated Great Plains phenols by adding molecular sieves to the bacterial lipase slurry. These experiments gave low yields of ester, unfortunately. The molecular sieve may have efficiently absorbed the water byproduct and then effectively catalyzed the hydrolysis reaction, overcoming the enzyme-catalyzed esterification. Also the molecular sieve may have removed the essential water associated with the enzyme protein, resulting in conformation changes that deactivated the enzyme.

The lipase-catalyzed reaction of the potassium salt (soap) of oleic acid was also investigated, since soaps are the form of tall acid byproduct obtained directly from the Kraft process. The reaction was carried out in chloroform. It was hoped that the metal ion would be carried along in the micellar form. The reaction gave no ester product, however. Possibly the carboxylate form of the acid was not acceptable at the lipase active site.

The direct esterification reaction of oleic acid with 2-phenoxyethanol was also investigated with porcine pancreatic lipase but poor yields (1-6%) of ester were obtained with this enzyme even in the nonpolar solvents. In contrast, good yields were obtained in earlier studies of transesterification with this lipase. The reason for the inactivity of the pancreatic enzyme in esterification reactions has not been determined. The esterification results with the Amano AK lipase obtained from a different *Pseudomonas* strain paralleled the lower rates found for this enzyme in other catalytic reactions.

Another set of experiments was carried out to determine the extent to which the lipases are deactivated by the gasification byproduct derivatives. The samples contain small amounts of soluble black materials that are not easily removed by distillation, adsorption, or solvent extraction. These are possibly condensation products of dihydroxybenzenes and indoles or other nitrogen heterocyclics. Accumulation of these impurities at the enzyme sites might be responsible for considerable shortening the lifetime of an enzyme catalyst bed. Earlier

experience with coals, humates, and low-severity liquefaction products from several coals showed that the lipases are substantially inhibited by many coal-derived materials (1).

The series of reactions carried out with recovered enzymes demonstrated that significant deactivation of the enzyme occurred. In a series of four reactions, the activity decreased by 20% in each successive reaction. The enzymes recovered from the fourth reaction were washed with acetone to determine whether substances that deactivated the enzyme could be removed by a more polar solvent or were instead bound reversibly. Reaction of the acetone-washed enzymes in the same system as above resulted in no ester formation initially. However, it was known from previous work that acetone removes essential water from the bacterial lipases, converting them to an inactive form. Thus, a small amount of water was added back to the enzymes which were then used for oleic acid esterification. The ester yield from the rehydrated or regenerated lipase was 25%, demonstrating partial restoration of the activity.

In previous studies with triglycerides, enzyme deactivation of the lipase was observed, but only to 3 to 10% of the original activity. Thus, there may be some kind of synergistic inhibitory effect involving the free fatty acid forms and the inhibitors present in the hydroxyethylated GP phenol intermediate.

Ester fuel prepared by acylation of hydroxyethylated GP phenols with canola oil exhibited a viscosity of 32.8 centipoise. This is substantially higher than that of sunflower methyl ester or #2 diesel oil. A 1:1 mixture of the ester product with #2 diesel gave acceptable viscosity (12.2 centipoise). Diesel tests with the mixture showed ignition delays (1.97 ms) that were slightly longer than the #2 diesel (1.84), but pressure curves were virtually identical.

CONCLUSIONS

Lipase-catalyzed reactions of inexpensive fatty acids with coal-derived alcohols in hydrocarbon solvents gave high yields of ester products. The high conversion of the acid form is very interesting, since it means that the very poorest grades of vegetable oils and the byproducts from their refining can be used in the preparation of esters. These oils contain high concentrations of the fatty acids. Raw tall oil from the Kraft pulping process also contains high concentrations of fatty acids. Much of the tall soap has no market and is mostly burned on site for heating the black liquor for recovering sulfide. Tall fatty acids are mainly oleic and linoleic acid.

The enzyme-deactivation results demonstrate that the impure hydroxyethylated phenolic streams cannot be effectively utilized without purification to remove the inhibitory compounds prior to the enzymatic reactions. Thus, the use of cleaner alcohols (from fermentation or Fischer-Tropsch) offer a better possibility for lipase-catalyzed fatty acid esterification. Alternatively, acid-catalyzed reactions in nonpolar solvents might give high enough yields of paraffin-soluble esters for use in diesel engines.

ACKNOWLEDGEMENTS

The support of the U.S. Department of Energy SBIR Contract # DE-AC02-88ER80614 is gratefully acknowledged.

REFERENCES

1. Sinor, J.E. *Production of Jet Fuels from Coal Derived Liquids Vol. 1*. 1987. Air Force Wright Aeronautical Lab Technical Report AFWAL-TR-87-2042, Vol.1. J.E. Sinor Consultants Inc.
2. Olson, E.S.; Singh, H.K.; Yagelowich, M.L.; Diehl, J.W.; Heintz, M.J.; Sharma, R.K.; Stanley, D.C. *Fuel*, **1993**, 73, 1687.
3. Olson, E.S.; Singh, H.K.; Yagelowich, M.L. *Proceedings: First Biomass Conference of the Americas*, Vol. II, August 30, 1993, Burlington, VT, 837.
4. Kirchner, G.; Schollar, M.P.; Klibanov, A.M. *J. Amer. Chem. Soc.* **1985**, 107, 7072.

Table 1. Yields of 2-phenoxyethyl oleate from Amano PS 30 lipase-catalyzed reaction of oleic acid with 2-phenoxyethanol (55°C for 24 hrs).

| Test | Solvent | % Yield |
|------|---------|---------|
| 1 | Hexane | 86 |
| 2 | Toluene | 86 |
| 3 | Acetone | 24 |
| 4 | THF | 0 |

TOXICOLOGY OF SYNTHETIC FUELS - A MINI REVIEW

Raymond Poon and Ih Chu
Bureau of Chemical Hazards,
Health Canada, Ottawa, Canada

Recent analytical and toxicological studies on synthetic fuels have confirmed previous observations that higher boiling fractions and blends are more toxic. It has also been reported that toxic effects of synfuels are related to the polycyclic aromatic hydrocarbon (PAH) content, including nitrogen containing and polar PAHs. Although carcinogenicity and mutagenicity are the main health concern of higher boiling synthetic fuels, the systemic toxicity (effects on liver, blood, bone marrow, thymus and thyroid) should not be overlooked. The marked thymic atrophy and perturbation of immune cells of PAH treated animals suggest that these fractions are immuno-suppressive. The lower-boiling fractions possess relatively weak carcinogenicity, mutagenicity and systemic toxicity, but their dermal irritant effects are still of concern in occupational settings. In the fractions and blends studied, the benzo(a)pyrene level is an indicator of their PAH content and hence toxicity. However, it is also clear that different composition of PAH mixtures in the high boiling fractions produce interactive effects that results in complex toxic and biochemical manifestations. The purpose of this article is to review recent mammalian toxicity data of various synfuels, and to shed some light on their potential human health hazards.

CARCINOGENICITY AND MUTAGENICITY

Early epidemiological studies showed that workers involving in the production of coal gas had a significantly higher rate of bladder and lung cancer (Doll et al., 1972), and those in the production of shale oils had a higher incidence of skin and scrotum cancer (Costello, 1979; Purde and Etlin, 1980). Reviews conducted by the International Agency for Research on Cancer concluded that shale oils were human carcinogen (IARC 1985), and exposure to "older" coal-gasification processes was carcinogenic to humans (IARC 1984). Workers in coal liquefaction plants were also reported to have a higher incidence of skin cancer (Shepard, 1981). A large body of evidence indicated that coal-derived synthetic fuels (Reilly and Renne, 1988; McKee et al., 1995; for review see Chu et al., 1994) and shale oils (Holland et al., 1981) were carcinogenic in animal studies and mutagenic in bacterial bioassays. In general, the middle and high boiling streams were more tumorigenic. More recent studies on coal coprocessing products and bitumen derived products also indicated that the middle and high-boiling fractions were more mutagenic (Table 1) (Otson and Peake, 1993).

SUBCHRONIC TOXICITY

Although carcinogenicity and mutagenicity are the main health concern of high-boiling synthetic fuels, their subchronic toxicity data are also required for health risk assessment. Table 2 summarizes the data from animal studies that provide no-observed-adverse-effect levels (NOAELs) for the fuels tested. It can be seen that the major target organs are liver, blood, bone marrow, thymus and thyroid. The effects on hematological disorders, and on the liver, consisting principally of hepatomegaly and microsomal enzyme induction were reported (Chu et al., 1988, 1992, 1994; Poon et al., 1994, 1996). The higher boiling fractions were more toxic and had NOAELs of less than 8 mg/kg/day. In contrast, petroleum derived unleaded gasoline and Fuel Oil no. 1 were less toxic, with NOAELs of greater than 250 mg/kg/day (Table 2).

EFFECTS ON THE SKIN

While the lowest boiling distillates showed the weakest tumor induction and systemic effects, they were shown to be a strong skin irritant. For example, shale-oil derived distillates, jet fuels (Holland et al., 1981; ATSDR, 1995), and the light gas oil fraction of bitumen upgrading products (Poon et al., 1994) produced severe skin lesions in rats. Feuston (1994) suggested that the skin irritation was associated with 2-ring aromatics, which were found to be most abundant in the low-boiling fractions. Chemical-induced skin phototoxicity appears to be a major concern for high-boiling distillates and bottom fractions. McKee and Maibach (1985) reported that EDS liquids with boiling points above 200°C produced skin phototoxic effects in guinea pigs. In a survey of workers at a pilot coal liquefaction plant, Driscoll et al., (1995) noted that self-reported photosensitivity reactions were strongly associated with dermal exposure to the solvents containing bottom fractions of coal liquids. Paint that contained bitumen was considered to be the cause of an outbreak of skin phototoxicity and ocular symptoms in workers in a dockyard (Davies, 1996). Coal tar and its products have been known to cause photosensitive skin reactions (Gould et al., 1995). PAHs in coal tar and bitumens, such as acridine, pyrene, and phenanthrene were reported to be potent phototoxins (Gendimenico and Kochevar, 1984; Davies, 1996). These compounds are also present in the high-boiling fractions

(Table 1).

EFFECTS ON IMMUNE FUNCTIONS

Studies with laboratory animals showed that high-boiling coal liquefaction products (Springer et al., 1986), high-boiling coal co-processing products, and medium- and high-boiling bitumen upgrading products (Chu et al., 1992; Poon et al., 1994) produced thymic atrophy. Because the thymus is an essential organ for the normal development of immunological functions in early life, these observations suggest that treatment with higher-boiling fuels may compromise the immune system. In contrast to a paucity of immunotoxicity data on synthetic fuels, these effects of PAHs were well documented (reviewed in Ward et al., 1985; Davila et al., 1997). In addition to benzo(a)pyrene, other PAHs such as phenanthrene and fluoranthene, which are widely present in synthetic fuels, were also found to have immunosuppressive effects (Davila et al., 1996; Yamaguchi et al., 1996; Tsien et al., 1997). Recent surveys of coke-oven workers exposed to PAHs revealed significant changes in their immune functions (Szczeklik et al., 1994; Winker et al., 1996).

COMPLEX MIXTURES

It is generally accepted that the toxicities of higher boiling synthetic fuels are predominantly related to their high PAH level, and the benzo[a]pyrene content is often used as an indicator of the total PAHs in synfuels (Table 3). However, it would be an oversimplification to solely rely on the benzo[a]pyrene level as the predictor of toxicity because different fuels have different PAH compositions, and various chemicals in the mixtures may exert individual and interactive effects. For example, individual PAHs were reported to exert an interactive effect on the mutagenicity of the other hydrocarbon components coexisted in the mixtures (Hermann, 1981). Neutral PAHs were associated with skin carcinogenicity while nitroaromatic and other polar aromatic compounds appeared to be potent mutagen (Otson and Peake, 1993; McKee et al., 1995). Hydrotreatment is known to substantially reduce the carcinogenicity, mutagenicity and acute toxicity of various synthetic fuels (Holland et al., 1981; McKee and Lewis 1987). However, detail studies on the effect of hydrotreatment on the PAH composition are still lacking.

SUMMARY

Prolonged exposure to synthetic fuels produces a broad range of systemic effects which include carcinogenicity, growth suppression, biochemical changes, anemia and other hematological disorders. Bone marrow, liver, kidney, thymus and skin are target organs affected by treatment. The effects are more severe with heavy distillates, and distillates containing N-PAHs are more biologically active. Although there is limited information on the occupational effects of synthetic fuels, experience in the health effects of workers in petroleum industry and coke-oven operations can serve as a guide in the implementation of industrial hygiene programs for synthetic fuel operations. These include engineering controls, personal monitoring, hygiene practices and medical surveillance.

REFERENCES

- ATSDR. Agency for Toxic Substances and Disease Registry. Toxicological Profile for "Jet Fuels (JP4 and JP7)". 1995, U.S. Department of Health and Human Services. Atlanta, Georgia.
- Beck, L.S., Hepler, D.I., and Hansen, K.L., 1983, The acute toxicology of selected petroleum hydrocarbons. In: MacFarland H.N., Holdsworth, L.E., MacGregor J.A., et al., eds. Proceedings on the 1st Symposium on the toxicology of petroleum hydrocarbons. Washington, DC: American Petroleum Institute. May 1982. 1-12.
- Chu, I., Villeneuve, D.C., Cote, M., Secours, V., Otson, R., and Valli, V.E., J. Toxicol. Environ. Health. 25:509-525, 1988.
- Chu, I., Suzuki, C.A.M., Villeneuve, D.C., and Valli, V.E., Fundam. Appl. Toxicol. 19:246-257, 1992.
- Chu, I., Villeneuve, D.C., and Rousseaux, C.G., J. Appl. Toxicol. 14: 241-256, 1994.
- Costello, J., Environ. Health Perspect. 30:205-208, 1979.
- Cruzan, G., Low, L.K., Cox, G.E., Meeks, J.R., Mackerer, C.R., Craig, P.H., Singer, E.J., and Mehlman, M.A., Toxicol. Ind. Health. 2:429-444, 1986.

- Davies, M.G., *Cont. Dermatitis*. 35:188-189, 1996.
- Davila, D.R., Romero, D.L., and Burchiel, S.W., *Toxicol. Appl. Pharmacol.* 139: 333-341, 1996.
- Davila, D.R., Mounho, B.J., And Burchiel, S.W., *Toxicol Ecotoxicol. News/Review*. 4:5-9, 1997.
- Doll, R., Vessey, M.P., Beasley, R.W.R., Buckley, A.R., Fear, E.C., Fisher, R.E.W., Gammon, E.J., Gunn, W., Hughes, G.O., Lee, K., and Norman-Smith, B., *Br. J. Med.* 29:394-406, 1972.
- Driscoll, T., Mandryk, J., Corvalan, C., Nurminen, M., Hull, B., Rogers, A., Yeung, P., Hollo, C., Ruck, E., and Leigh, J. *Occup. Med.* 45:239-246, 1995.
- Feuston, M.H., Low, L.K., Hamilton, C.E., and Mackerer, C.R., *Fund. Appl. Toxicol.* 22:622-630, 1994.
- Gendimenico, G.J., and Kochevar, I.E., *Toxicol. Appl. Pharmacol.* 76: 374-382, 1984.
- Gould, J.W., Mercurio, M.G., and Elmets, C.A., *J. Am Acad. Dermatol.* 33:551-573, 1995.
- Griest, W.H., Guerin, M.R., Yeatts, L.B., and Clark, B.R. 1981. Sample management and chemical characterization of the PARAHO/SOHIO/U.S. Navy crude and refined shale oil suite. In: Griest W.H., Guerin, M.R., and Coffin, D.L. eds. *Health Effects Investigation of Oil Shale Development*. Ann Arbor Science, Ann Arbor, Michigan. 1981. P. 27-44.
- Hermann, M., *Mut. Res.* 90:399-409, 1981.
- Holland, J.M., Gibson, L.C., Whittaker, M.J., and Stephens, T.J. 1981. Chronic dermal toxicity of Paraho shale oil and distillates. In: Griest, W.H., Guerin, M.R., Coffin, D.L. (Eds): *Health Effects Investigation of Oil Shale Development*. Ann Arbor Science, Ann Arbor, Michigan, pp 97-116.
- IARC 1984. International Agency for Research on Cancer Monograph no. 34. Polynuclear Aromatic Compounds, Part 3, Industrial exposures. World Health Organization. Lyon, France.
- IARC 1985. International Agency for Research on Cancer Monograph no. 35. Polynuclear Aromatic Compounds, Part 4, Bitumens, Coal-tars and Derived Products, Shale-oils and Soots. World Health Organization. Lyon, France.
- McKee R.H., and Maibach, H.I., *Cont. Dermatitis*. 13:72-79, 1985.
- McKee, R.H., and Lewis, S.C., *Can. J. Physiol. Pharmacol.* 65:1793-1797, 1987.
- McKee, R.H., Traul, K.A., and Przygoda, R.T., *J. Appl. Toxicol.* 15: 159-165, 1995.
- NTP. 1986. National toxicological program technical report series no. 310: Toxicology and carcinogenesis studies of marine diesel fuels and JP-5 navy fuel in B6C3F1 mice (dermal studies). Research Triangle Park, NC: National Toxicology Program/National Institute of Health. NIH publication no. 86-2566.
- Otson, R., and Peake, E. 1993. Characterization of bitumen upgrading and coprocessing products. In: P. Garrigues and M. Lamotte (eds.), *Polycyclic Aromatic Compounds. Synthesis, Properties, Analytical Measurements, Occurrence and Biological Effects*. PAH XIII, Gordon and Breach, Langhorn, PA.
- Peake, E. 1990. Characterization of coal coprocessing products. The toxicology of heavy distillates. A final report to the Health Protection Branch, Department of National Health and Welfare, Ottawa, Canada.
- Poon, R., Chu, I., Villeneuve, D.C., and Valli, V.E., *Fundam. Appl. Toxicol.* 23:237-250, 1994.
- Poon, R., Chu, I., Davis, H., Yagminas, A.P. and Valli, V.E., *Toxicology*. 109:129-146, 1996.
- Purde, M., and Etlin, S. 1980. Cancer cases among workers in the Estonian oil shale processing industry. In: Rom, W.N. and Archer, V.E.(eds.) *Health Implications of New Energy Technologies*, Ann Arbor Science, Ann Arbor, Michigan, pp. 527-528.
- Rao, T.K., Allen, B.E., Ramsey, D.W., Epler, J.L., Rubin, B., Guerin, M.R., and Clark, B.R., *Mutat.*

Res. 84:29-39, 1981.

Reilly, C.A., and Renne, R.A. 1988. Toxicological effects of coal-based synfuels. In: Gray, R.H., Drucker, H., Massey, M.J. (eds.). *Toxicology of Coal Conversion Processing*. John Wiley & Sons, New York, p.57-245.

Shepard, H., J. Soc. Occup. Med. 31:9-15, 1981.

Szczeklik, A., Szczeklik, J., Galuszka, Z., Musial, J., Kolarzyk, E., and Targosz, D., *Environ. Health Perspect.* 102:302-304, 1994.

Springer, D.L., Miller, R.A., Weimer, W.C., Ragan, H.A., Buschbom, R.L., and Mahlum, D.D., *Toxicol. Appl. Pharmacol.* 82:112-131, 1986.

Tomkins, B.A., Kubota, H., Griest, W.H., Caton, J.E., Clark, B.R., and Guerin, M.R., *Anal. Chem.* 52:1331-1334, 1980.

Tomkins, B.A., Reagan, R.R., Caton, J.E., and Griest, W.H., *Anal. Chem.* 53:1213-1217, 1981.

Tsien, A., Diaz-Sanchez, D., Ma, J., and Saxon, A., *Toxicol. Appl. Pharmacol.* 142:256-263, 1997.

Ward, E.C., Murray, M.J., and Dean, J.H. 1985. Immunotoxicity of nonhalogenated polycyclic aromatic hydrocarbons. In: *immunotoxicology and immunopharmacology* (J.H. Dean, M. I. Luster, A.E. Munson and H. Amos, Eds.). pp. 291-300. Raven Press, New York.

Winker, N., Tuschl, H., Kovac, R., and Weber, E., *J. Appl. Toxicol.* 17:23-29, 1996.

Yamaguchi, K., Near, R., Shneider, A., Cui, H., Ju, S-T., and Sherr, D.H., *Toxicol. Appl. Pharmacol.* 139:144-152, 1996.

Table 1. Mutagenicity (Salmonella test) of synthetic fuels.

| Material tested | Without S-9 | With S-9 | Reference |
|--|-------------|----------|-----------------------|
| <u>Coal Liquefaction Products</u> | | | |
| Hydrotreated naphtha (<200°C) | NT | - | McKee et al., 1995 |
| EDS ¹ process, RS-I (200-427°C) | NT | + | McKee et al., 1995 |
| EDS process, RS-II (200-427°C) | NT | + | McKee et al., 1995 |
| Pittsburgh Energy Technology Center | NT | + | Ran et al., 1995 |
| COED pyrolysis process | NT | + | Rao et al., 1995 |
| <u>Coal Coprocessing Products</u> | | | |
| CANMET LGO (< 243°C) | - | - | Otson and Peake, 1993 |
| CANMET HGO I (243-409°C) | - | + | Otson and Peake, 1993 |
| CANMET HGO II (387-521°C) | + | + | Otson and Peake, 1993 |
| <u>Bitumen Upgrading Products</u> | | | |
| CANMET LGO (200-315°C) | - | - | Otson and Peake, 1993 |
| CANMET HGO I (315-415°C) | - | + | Otson and Peake, 1993 |
| CANMET HGO II (415-525°C) | + | + | Otson and Peake, 1993 |

¹Abbreviations: EDS, a direct liquefaction process that utilizes an "in stream" catalytic hydrotreatment process; RS, recycle solvent; COED, Char-oil Energy Development liquid; CANMET, Canadian Centre for Mineral and Energy Technology; LGO, light gas oil; HGO, Heavy gas oil; NT (Not tested)

Table 2. Systemic toxicity of synthetic fuels via percutaneous administration.

| Synthetic fuel | Animal/Length of Exposure | Target organ | NOAEL ^a (mg/kg/day) | Reference |
|-----------------------------------|---------------------------|--|--------------------------------|---------------------|
| <u>Gasoline (unleaded)</u> | Rabbits/2 weeks | Liver, blood, skin | 590 | Beck et al., 1983 |
| <u>Fuel oil No. 1</u> | Mice/13 weeks | Blood | 250 | NTP 1986 |
| <u>Clarified slurry oil</u> | Rats/13 weeks | Liver, thymus, bone marrow | <8 | Cruzan et al., 1986 |
| <u>Coal liquefaction products</u> | | | | |
| CANMET HGO-I (154-378°C) | Rats/13 weeks | Liver, blood, bone marrow | <50 | Chu et al., 1988 |
| <u>Coal coprocessing products</u> | | | | |
| CANMET HGO-II (387-521°C) | Rats/13 weeks | Liver, blood, thymus, thyroid, bone marrow | <8 | Chu et al., 1992 |
| <u>Bitumen upgrading products</u> | | | | |
| CANMET LGO (200-315°C) | Rats/4 weeks | Bone marrow, skin | 25 | Poon et al., 1994 |
| CANMET HGO-I (315-415°C) | Rats/4 weeks | Liver, blood, bone marrow, thymus | <25 | |
| CANMET HGO-II (415-525°C) | Rats/4 weeks | Liver, blood, bone marrow, thymus | <25 | |
| CANMET HGO-II (415-525°C) | Rats/13 weeks | Liver, blood, bone marrow, thymus, thyroid | <8 | Poon et al., 1996 |

^a NOAEL = no-observed-adverse-effect-level

Table 3. Benzo(a)pyrene content in petroleum and synthetic fuels.

| Synthetic fuel | Benzo(a)pyrene (µg/g) | Reference |
|---------------------------------------|-----------------------|-----------------------------------|
| <u>Jet Fuel JP5 (from shale oil)</u> | ND ¹ | Griest et al., 1981 |
| <u>Petroleum (crude)</u> | 2.8-3.7 | IARC 1985 |
| <u>Shale oil (SRM 1580 certified)</u> | 3.3-192 | IARC 1985 |
| <u>Coal liquefaction products</u> | | |
| Coal derived fuel oil | 82 | Tomkins et al., 1980 |
| NBS Coal liquid oil | 179 | Tomkins et al., 1981 |
| Coal-II heavy distillate, 288-454°C | 550 | Springer et al., 1986 |
| <u>Coal coprocessing products</u> | | |
| HGO I, 315-435°C | 211 | Otson and Peake, 1993; Peak, 1990 |
| <u>Bitumen upgrading products</u> | | |
| LGO, 200-315°C | 6.5 | Otson and Peake, 1993; Peak, 1990 |
| HGO I, 315-415°C | 23 | |
| HGO II, 415-525°C | 590 | |

¹ ND - non-detectable

UPGRADING HEAVY OIL/BITUMEN EMULSIONS VIA IN SITU HYDROGEN GENERATION

Flora T.T. Ng
Department of Chemical Engineering
University of Waterloo
Waterloo, Ontario
Canada, N2L 3G1
email: ftng@cape.uwaterloo.ca

Keywords: upgrading, heavy oil/bitumen emulsions, in situ hydrogen

Abstract

Canada has large reserves of heavy oils and tarsand bitumen. These heavy oils are recovered as emulsions via steam injection techniques. Current technologies for emulsion treatment and upgrading require multistage processing. Recently, we have developed a novel process for upgrading heavy oil emulsions in a single stage process where emulsion breaking and upgrading occurred in the same reactor. This process is based on the activation of water in an emulsion via the water gas shift reaction to generate hydrogen for in situ upgrading. This paper is focussed on the catalytic desulphurization in an emulsion using dispersed catalysts. The activity of in situ hydrogen will be compared with that of molecular hydrogen. Synthesis gas was found to be effective for upgrading emulsions. The emulsion upgrading technology could also be used to process emulsions derived from hot water extraction of tarsands bitumen.

Introduction

Canada has large reserves of high sulphur heavy oils and oil sand bitumen. As conventional oil reserves continue to decrease, it will become necessary to utilize more of the high sulphur heavy oil and oil sand bitumen in the future. Technologies for the recovery of heavy oils include steam flooding, cyclic steam injection or fire flooding of reservoirs while hot water was used to extract bitumen from tarsands. These methods of recovery of heavy oil and bitumen produce emulsions. In order to utilize the heavy oils and bitumen, the emulsions have to be broken and separated into water and oil phases in emulsion treatment plants. Subsequently, the bitumen or heavy oils are upgraded where sulphur removal and hydrocracking occurred before being utilized in conventional refineries. In summary, current technologies for emulsion treatment and upgrading require multistage processing and are costly. Thus alternative technologies for processing heavy oil/bitumen emulsions would be attractive.

We have developed in our laboratory a novel single stage process for upgrading emulsions via activation of water in the emulsion through the water gas shift reaction (WGSR) to provide hydrogen in situ for catalytic desulphurization and hydrocracking (1). This process could potentially reduce the environmental impact derived from the discharge of emulsions into tailings ponds. It is clear that in order to further develop the heavy oil/bitumen resources, new processes should be economically viable, flexible while assuring the quality of the environment. Our novel emulsion upgrading process could potentially achieve the above goals. It is envisaged that a single stage emulsion upgrading will minimize waste streams, lower the cost for hydrogen production and potentially break very stable emulsions which cause environmental hazards as in tailings pond.

In addition to our patents on emulsion upgrading, there are other patents related to the use of CO and synthesis gas for upgrading emulsions or heavy oils, including down hole upgrading (2). Aquathermolysis which utilizes water at 280 °C for hydrolysis of hydrocarbons in heavy oil, resulting in viscosity reduction and sulphur removal has been reported (3). There are also reports of the aqueous high temperature chemistry of hydrocarbons and heterocycles (4) with a view to elucidate the chemistry involved in the steam stimulation of heavy oil reservoirs (~ 200-300 °C).

Experimental

All experiments were performed either in a 300 mL or a 1000 mL stainless steel batch autoclave (Autoclave Engineers). The synthetic emulsions were prepared by using toluene, water and an emulsifier (BASF P105). Dispersed catalysts such as molybdic acid, phosphomolybdic acid, ammonium molybdate and ammonium tetrathiomolybdate were used. Model compounds such as benzothiophene (BTH) , dibenzothiophene were used to obtain kinetics of desulphurization (HDS) in an emulsion. HDS of a diesel fraction from Cold Lake bitumen was also studied.

The experiments were carried out over a temperature range of 320- 380 °C. The reactor was heated up at a rate of 2 °C per minute as recommended by Autoclave Engineers. The initial loading pressure of CO, synthesis gas (a 1:1 mol ratio of CO: H₂) or H₂ was between 300- 600 psig. For some of the experiments , samples of gas or liquid were taken for analysis. At the end of the reaction , the reactor was allowed to cool down overnight to room temperature. Gas, liquid and solids were then collected and analyzed. The gaseous product was collected in a gas bag and analyzed using gas chromatography (Perkin Elmer Model 8500) equipped with a thermal conductivity detector. The inlet system composed of a 1.5 m Hayesep C column in series with a 2 m molecular sieve column. Liquid analysis was carried out in the same GC using a 30 m DB-1701 fused silica capillary column and a flame ionization detector. X-ray fluorescence (Oxford Model Lab X-1000) was used to determine the sulphur content of the diesel fraction. X-ray diffraction, X-ray photoelectron spectroscopy and thermoanalysis techniques were used to characterize the spent catalysts.

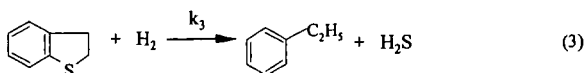
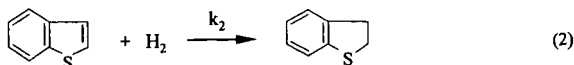
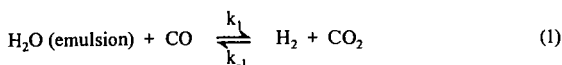
Results and Discussion

Our initial research was based on the desulphurization of a synthetic emulsion (toluene/water) containing benzothiophene, a model compound for sulphur species in heavy oil. Simulated emulsions were used to provide a better understanding of the chemical and physical processes involved in upgrading heavy oil emulsions. Such information serves to provide a basis for the interpretation of data from experiments involving heavy oil emulsions.

Under the reaction conditions of 320 -380 °C and 300 -600 psig initial loading pressure of CO, the dispersed Mo catalysts were found to be effective catalysts for the HDS of BTH in an emulsion. The emulsion was found to be broken completely into 2 separate oil and water phases, with some black solids identified to be some form of MoS_x accumulated at the bottom of the reactor. Essentially complete sulphur removal could be achieved. Gas samples taken during the reaction showed that CO decreases as a function of time, while that CO₂ and H₂ increases as a function of time. In the absence of sulphur compounds ,the amount of CO₂ and H₂ were found to be equimolar as expected according to the stoichiometry of the water gas shift reaction shown in equation 1 (Fig 1). However, in the presence of sulphur compounds, the amount of H₂ was found to be less than CO₂ which was attributed to the consumption of H₂ during the reaction (Fig. 2).

A kinetic study was carried out for the production of hydrogen from the water gas shift reaction. In the absence of benzothiophene, the reaction followed a reversible pseudo first order kinetics. In the presence of benzothiophene, an irreversible first order reaction was observed (5). Similar behaviour was observed for molybdic acid and phosphomolybdic acid. The rate constants obtained for both catalysts were very similar suggesting that probably the same catalytic species was involved in the reaction (Table 1). It is interesting to note that the rate constant obtained in the presence of benzothiophene is higher than in the absence of benzothiophene. This could be attributed at least partly to the formation of a MoS_x species when benzothiophene was present and it has been reported that MoS_x is more active for the water gas shift reaction than Mo oxides (6). Indeed we found that the WGSR reaction proceeded at a faster rate when ammonium tetrathiomolybdate was used. Variation of the initial CO loading pressure from 300 - 600 psig also indicated a first order dependence on CO.

The kinetics of the HDS of BTH was obtained by analysis of liquid samples taken from the reactor. GC analysis indicated that dibenzothiophene was the intermediate of the reaction and that ethylbenzene was the final product (Fig 3). Therefore the reaction pathway for the desulphurization of benzothiophene could be represented by equations 1-3.



Mechanisms for the desulphurization of benzothiophene have been reviewed by a number of researchers (7). Two reaction schemes have been proposed. One involves the initial hydrogenation of benzothiophene to dihydrobenzothiophene, followed by sulphur removal to give ethylbenzene and H_2S . The second scheme is the direct desulphurization via C-S bond cleavage resulting in H_2S and styrene which is then hydrogenated to give ethylbenzene. Since dihydrobenzothiophene was detected as an intermediate in our reaction, the predominant pathway for desulphurization is hydrogenation of benzothiophene to give dihydrobenzothiophene which then undergoes hydrogenolysis to give ethylbenzene.

The desulphurization of benzothiophene in an emulsion with externally supplied molecular hydrogen was carried out. The reactivity of in situ hydrogen was found to be about 7 times that of supplied molecular hydrogen. This may be attributed to the fact that the in situ hydrogen may be more like atomic hydrogen and hence has a higher reactivity than molecular hydrogen. A higher reactivity of in situ hydrogen for HDS reactions has also been reported (8).

Results of HDS of dibenzothiophene in an emulsion indicated the rate constant for water gas shift reaction is essentially the same as that obtained with benzothiophene (10). The rate constant for sulphur removal is about a factor of 5 smaller than that of benzothiophene. This result is in accordance with the data by Ma et al (10). The activity of in situ hydrogen was found to be higher than that of molecular hydrogen. Product analysis revealed that the major pathway for desulphurization is via the hydrogenation of the aromatic ring to give tetrahydrodibenzothiophene. Since hydrogenation rather than hydrogenolysis apparently is the main pathway for the desulphurization of benzothiophene and dibenzothiophene, it may account for the higher activity of in situ hydrogen compared with molecular hydrogen.

Recently we examined the desulphurization of a diesel fraction from Cold Lake (11). Water was added to the diesel to simulate an emulsion. The reaction was carried out under the same reaction conditions as the model compounds benzothiophene and dibenzothiophene. The rate constant for the water gas shift reaction was found to be similar to that obtained in the presence of model compounds. However, the rate constant for desulphurization with in situ hydrogen was found to be similar to that of molecular hydrogen. It has been reported that diesel contains a mixture of sulphur compounds including substituted dibenzothiophenes which are very resistant to desulphurization. The difference between the reactivity of in situ hydrogen and molecular hydrogen towards model compounds and diesel may be due to the presence of highly substituted dibenzothiophene type compounds. Due to the steric hindrances of the substituted alkyl groups, the in situ hydrogen that was produced from the water gas shift reaction will decompose to give molecular hydrogen before it could be utilized for the desulphurization process.

Similar rate constants for desulphurization were observed when synthesis gas (1:1 mol ratio of $CO:H_2$) was used for the upgrading of diesel. This is an important result since this implies that CO is not an inhibitor for HDS. Since the cost of hydrogen for upgrading is high, the use of a cheaper source of hydrogen for upgrading will be attractive for the process economics.

Conclusions

Dispersed molybdenum catalysts are effective for catalyzing the water gas shift reaction to generate hydrogen in situ for the desulphurization and upgrading of heavy oil/bitumen emulsions. The in situ hydrogen was found to be more active for the desulphurization of model compounds such as benzothiophene and dibenzothiophene. However, the reactivity of in situ hydrogen and molecular hydrogen was found to be about the same for the desulphurization of diesel. Synthesis gas could be utilized for the upgrading of heavy oil/bitumen emulsions.

Acknowledgement

Financial support from the Natural Sciences and Engineering Research Council of Canada (Strategic Grant Research Program, Industrially Oriented Research Program) and the Imperial Oil Research Grant Program are gratefully acknowledged.

References

1. Ng, F.T.T. and Tsakiri, S.K., US Patent, 5,055,175,199, 1991; Canadian Patent, 1317150, 1993; Ng, F.T.T. and Tsakiri, S.K., Fuel, **71**, 1309 (1992); *ibid*, **72**, 211 (1993)
2. Weissman, J.G., Kessler, R.V., Sawicki, R.A., Belgrave, J.D.M., Laureshen, C.J., Mehta, S.A., Moore, R.G. and Ursenbach, M.G., Energy and Fuels, **10**, 883, (1996).
3. Clarke, P.D., Clarke, R.A., Hyne, J.B., and Lesage, AOSTRA J. Res., **6**, 29 (1990)

4. Katritzky, A.R. Lapucha, A.R., Luxem, F.J. Greenhill and Siskin, M., *Energy and Fuels*, **4**, 572 (1990).
5. Milad, I.K., Hajek, P., Rintjema, R. J. and Ng, F.T.T. , unpublished data.
6. Hou, P., Mecker, D., Wise, H., *J. Catal.*, **80**, 280 (1983).
7. Daly, F.T., *J. Catal.*, **51**, 221 (1978).
8. Kumer, M., Akgerman A., and Anthony R.G., *Ind. Eng. Chem. Process Dev.*, **23**, 88 (1984) :
- Hook, B.D. and Akgerman, A., *ibid*, **25**, 278 (1986).
9. Liu, C., Guruparanathan, S., Ganeshalingham, S. and Ng, F.T.T., unpublished data.
10. Ma, X., Sakanishi, K., Isoda, T. and Mochida, I., *Ind. Eng. Chem. Res.* **34**, 748, (1995)
11. Siewe, C.N., and Ng, F.T.T., *Energy and Fuels*, (1998) , in press.

Table I. Rate Constants for WGS and HDS of BTH at 340 °C
(4775 ppm Mo, 600 psig CO loading pressure, 49 mL toluene,
9.8 mL BTH, 21 mL water, stirring speed = 500 rpm)

| Catalyst | Pseudo First Order Rate Constant ^a | | |
|----------|---|------------------------------------|------------------------------------|
| | $k_1' \times 10^4 (\text{s}^{-1})$ | $k_2' \times 10^4 (\text{s}^{-1})$ | $k_3' \times 10^4 (\text{s}^{-1})$ |
| MA | 2.3 1.4 ^b | 2.0 | 4.1 |
| PMA | 2.2 1.1 ^b | 2.3 | 3.8 |

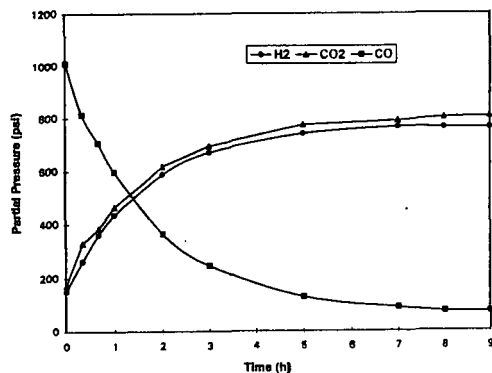
^a $k_1' = k_1[\text{H}_2\text{O}]$, $k_2' = k_2[\text{H}_2]$, $k_3' = k_3[\text{H}_2]$

^b WGS runs, no BTH added

MA = molybdc acid

PMA = phosphomolybdc acid

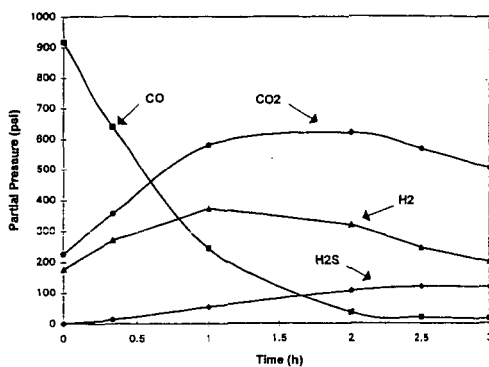
Figure 1. Product Distribution with time for the WGS



REACTION PROFILE FOR WGS @ 380 °C.

($P_{\text{CO}_0} = 600$ psig ; 70 ml H_2O /196 ml TOLUENE;
1.78 g MoO_3 ; 1300 rpm).

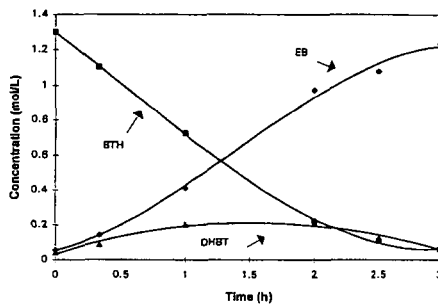
Figure 2. Product distribution of the WGSR with time in the presence of BTH



REACTION PROFILE FOR WGSR @ 380 °C.

($P_{CO_0} = 600$ psig ; $BTH_0 = 267$ mmol; 70 ml $H_2O/163$ ml TOLUENE; 1.78 g MoO_3 ; 1300 rpm).

Figure 3. Product distribution for the HDS of BTH with *in situ* H_2



REACTION PROFILE FOR HDS @ 380 °C.

($P_{CO_0} = 600$ psig ; $BTH_0 = 267$ mmol; 70 ml $H_2O/163$ ml TOLUENE; 1.78 g MoO_3 ; 1300 rpm).

Viscosity Reduction in Extra Heavy Crude Oils

Mark W. Badger and Harold H. Schobert
The Laboratory for Hydrocarbon Process Chemistry
The Energy Institute, 209 Academic Projects Building
The Pennsylvania State University
University Park, Pennsylvania, 16802-2303

Introduction

The next few years will see a change in the sources of crude oil in the global market. Advances in exploration and production technologies in the petroleum industry are creating new major sources in areas that were previously off limits for reasons of geography, politics and technology. Some of the new areas at exploitation will have a major significance on the US markets, namely, Latin America, especially Venezuela, and Canadian heavy oil and synthetic crude oil projects (1).

Latin American sources are expected to increase production to around 4.2 million bbl/day by 2005. Of this 1 million bbl/day is expected to be extra-heavy Orinoco oil from Venezuela. It has been projected that imports to the US from Latin America will increase by around 2.7 million bbl/day during the same period. As well as this, a big increase in crude oil production will come heavy crude oil reserves in Western Canada. These reserves are intended to be produced a diluted heavy crudes and as synthetic oils, with varying degrees of upgrading. It is expected that by 2005 another 700,00 bbl/day will be coming from Canadian heavy oil fields. Most of this will end up in the US Mid-West Market. This supply will replace the US supplies at lighter crude.

With such increases of heavy crude oil sources making there way into the US market in the near future now seems a good time to exploit new avenues of research into the reduction at their viscosity. Some of these crude oils can have viscosities in excess of 15,000 centistokes at 100°F (2). In order for these crude oils to be transported via pipeline from the source, the viscosity must be lower than 150 centistokes at 100°F. The crude oils being very viscous on extraction have to go through some processing e.g. gas plasticization, thermal cracking or blending with lighter distillate fractions, to enable them to be transported by pipeline.

Taking blending for an example, typically the crude oils are blended with a kerosene distillate fraction. This process has its disadvantages. In some cases up to 30 wt.% of kerosene must be added to sufficiently reduce the viscosity, this uses up a great quantity of a valuable commercial product. Also the added kerosene must be processed again through the refinery along with heavy crude oil.

It is widely assumed that the asphaltene molecules in oils agglomerate to form micelle-like clusters. Interactions between these clusters contribute towards the viscosity of the oils. By breaking these agglomerates apart viscosity will be reduced. The kerosene used to cut the oils and reduce viscosity only does so by being an effective diluent. It does not break down the agglomerates by any significant amount. The following work is from a scoping study, the objective of which was to see whether the viscosity of extra heavy crude oils could be reduced by the addition of other chemical compounds and/or distillate fractions, which may break down the asphaltene agglomerates, and thus achieve greater viscosity reductions, when compared with kerosene. The intention is to then augment the better of these additive compounds with kerosene, thus initiating viscosity reduction for less volume of diluent.

In this period of initial investigation several dispersants with differing physical and chemical properties have been assessed for their effect on viscosity reduction. Figure 1 shows the chemical structure and the polarity of the compounds, in Debye units (DU). The compounds were chosen for their ring type structures. The presence of π electrons in the ring may play a role in the interaction between the compounds added and the π electrons in the polyaromatic systems of the asphaltene agglomerates. The compounds were kept to one ring to keep the size of the molecules small and allow for a greater diffusion through the crude oil matrix, and penetration into the asphaltene agglomerates.

Experimental

All of the compounds used in this study were purchased from the Aldrich Chemical company, except for the xylenes mix which came from Marathon Oil's Texas City refinery. The sample characteristics of the extra heavy crude oil are shown in Table 1.

The experiments were performed using 70ml tubing bomb reactors, into which was placed a known weight of extra heavy crude oil. To this 2.4, 4.8 or 8.3 wt.% of additive compound was added, the reactor was sealed and purged with nitrogen gas. The reactors were placed into a heated sandbath and shaken for 2 hours at 200 °C. The resulting mixtures were then removed from the reactors and stored in sealed containers under nitrogen.

The viscosity measurements were carried out using a Brookfield DV-III programmable viscometer, fitted with Thermosel system for viscosity measurements at elevated temperatures. The viscosities were measured at 140 °F. The measurements were taken when the sample was at equilibrium. That is at the point when increases in the shear rate (related to spindle rotation) resulted in no or little (<1%) change in the viscosity measured. In other words the mixture exhibited signs of a Newtonian fluid.

Table 1. Sample characteristics of the extra heavy crude oil used in this study.

| SAMPLE CHARACTERISTICS | |
|--------------------------|---------------|
| Carbon | 76.6% |
| Hydrogen | 10.5% |
| Nitrogen | 0.7% |
| Sulfur | - |
| Average Molecular Weight | 548 |
| Liquid Density (g/ml) | 1.013 |
| API Gravity | 8 |
| Boiling Point/Wt% | >200 °C/99.8% |
| Viscosity (cP@140 °F) | 7800 |

Results and Discussion

Figure 2 shows the raw viscosity/dispersant data to date. In the plot it can be seen that the additive compounds used have a diverse effect on viscosity. The major general trend to note is that with the increasing polarity of the dispersant there is an increase in the measured viscosity. The higher the polarity of an additive compound the stronger the dipole-dipole interactions are between them (3,4). Therefore they can break down the asphaltene agglomerates, but still have an attractive binding force throughout the mixture which in turn binds the molecules together and hence increases viscosity. The viscosity reduction however may not just be related to the break down of the asphaltene agglomerates. A more simple answer may be related to Eyring's theory of liquid viscosity (5). Although we have not looked in depth into using Eyring's theory, a relationship between dilution effects and viscosity can be deduced from it. More accurate calculations must be conducted including the relative densities, heats of vaporization, molar volumes and molecular weight of the as received compounds and the mixtures. However these calculations do not take into account the full effect of the dipole interactions, which are significant.

These are not the only factors worth noting. Solubility of the dispersant in the heavy crude will play a major role in viscosity reduction. If partial solubility or phase separation is occurring, then a lower than expected viscosity measurement will be recorded. This is because when phase separation occurs then the more fluid phase, i.e. the additive compound, may tend to concentrate around the spindle of the viscometer, and thus lower apparent viscosity. This would then explain why the viscosity measurements seems to be low for acetophenone and cyclohexanone (see Figure 3). We know that the crude oil sample is soluble in toluene, xylenes and the N-methyl pyrrolidinone. The curve in the line is too low where the cyclohexanone and acetophenone are. It is not likely that viscosity would level off when using miscible additive compounds with polarities between 1 and 3 DU. Therefore, partial solubility must be the cause for the lower measurements. However, solubility experiments should be conducted to prove this hypothesis.

Assuming that the heavy crude oils are soluble in the dispersants, then molecular size of the additive compound may have an important role in viscosity reduction. Smaller molecules or molecules with the correct physical and chemical characteristics to fit into the gaps between the asphaltene agglomerates can reduce the viscosity to a greater extent. This is caused by deeper penetration, which induces greater break up of the asphaltene agglomerates.

One of the goals of this work is to determine whether an additive compound could be added to the kerosene diluent and enhance viscosity reduction. This theory assumes that the additive can break down the asphaltene agglomerates. For this to take effect only a small quantity of additive compound may be needed. For example, if 1 wt.% is sufficient to initiate the breakdown of the asphaltene agglomerates, then less kerosene would be needed to cut the viscosity to a level required for pipeline transportation.

Figure 4 shows a plot of log log viscosity against weight percent of additive compound in the crude oil. From this we took the y axis intercept for each additive compound and plotted it against its polarity. The resulting plot (Figure 5) was produced. From this we can assume that at low concentrations of additive compound in the crude oil, a compound with a polarity of around 0.6-0.7 Debye units and the right structural and chemical characteristics could lower viscosity more than other additive compounds, due to its greater dispersive qualities. This conclusion however needs verification through a detailed study of additive compounds with polarities in this area, as well as studies using mixtures of kerosene and additive compounds.

It can be seen from the data in Figure 2 that when toluene or xylenes mix is used then the measured viscosities are up to 50% lower than the equivalent weight percent for kerosene. In areas of heavy oil extraction where a supply of these lighter distillates is available, then using toluene or a xylenes mix from the BTX fraction may be a viable alternative to kerosene. Also a lower volume of distillate would be used. An extra advantage is that toluene and xylenes have a low enough boiling point that they could be removed, at nearly a 100% yield, from the crude oil prior to processing. By setting up a recycle stream costs of the operation would be lowered considerably. Plus if the feed for the recycle stream needs to be topped up, toluene and xylenes are made from the heavy crude oils during the refining process.

Conclusions

In this period of initial investigation it has been shown that the viscosity of extra heavy crude oils can be reduced to a greater extent using some additive compounds, when compared to using the conventional diluent kerosene. Interesting interactions, related to polarity, have been observed between the additive compounds and the crude oil matrix. There may be some scope to initiate a computer simulation of these interactions, as well as studying the mechanism through which asphaltene agglomerates are broken apart. Further work must include the study of additive compounds with polarities between 0.5 and 2.5 Debye units. Also reduction in the quantity of additive compound to 1 wt.% and lower must be studied, to evaluate whether there is still a linear relationship to the viscosity reduction at low concentrations.

References

1. Hermes, R.A., *Oil and Gas Journal* **26**, 3, 16, (Jan. 19th 1998)
2. Butler, R.M., in "Thermal Recovery of Oil and Bitumen" Prentice-Hall, New Jersey. 1991.
3. Temperley, H.N.V, Trevena, D.H., in "Liquids and Their Properties - A Molecular and Macroscopic Treatise with Applications" Wiley, New York. 1978.
4. Reichardt, C., in "Solvent Effects in Organic Chemistry" Verlag Chemie-Weinheim, New York. 1979.
5. Glasstone, S., Laidler, K.J., Eyring, H., in "The Theory of Rate Processes - The Kinetics of Chemical Reactions, Viscosity, Diffusion and Electrochemical Phenomena" McGraw-Hill, New York. 1941.
6. Riddick, J.A., Bunger, W.B., in "Techniques of Chemistry. Volume II - Organic Solvents" Third Edition. Wiley-Interscience, New York.

Acknowledgments

The authors would like to thank the Marathon Oil Company for its financial support of this project. Also to Dr. Mark Plummer (Marathon Oil) and Professor Paul Painter (Penn State University) for their help, and Mihai Marasteanu, Steve Krumm and Craig Brickley of the Pennsylvania Transport Institute, at Penn State University, for their help with the viscometry measurements.

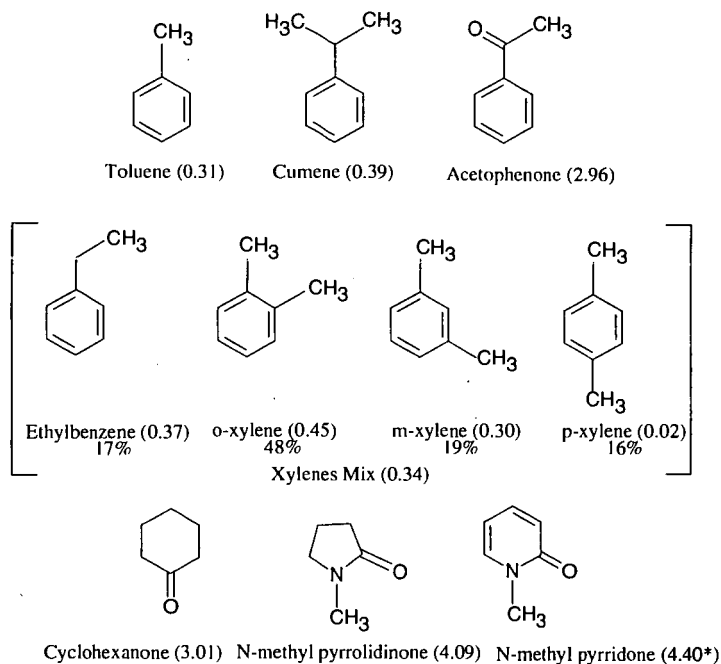


Figure 1. Chemical structures and polarities (in Debye units) of the additives used.

* This value was calculated. The rest were taken from known data (6).

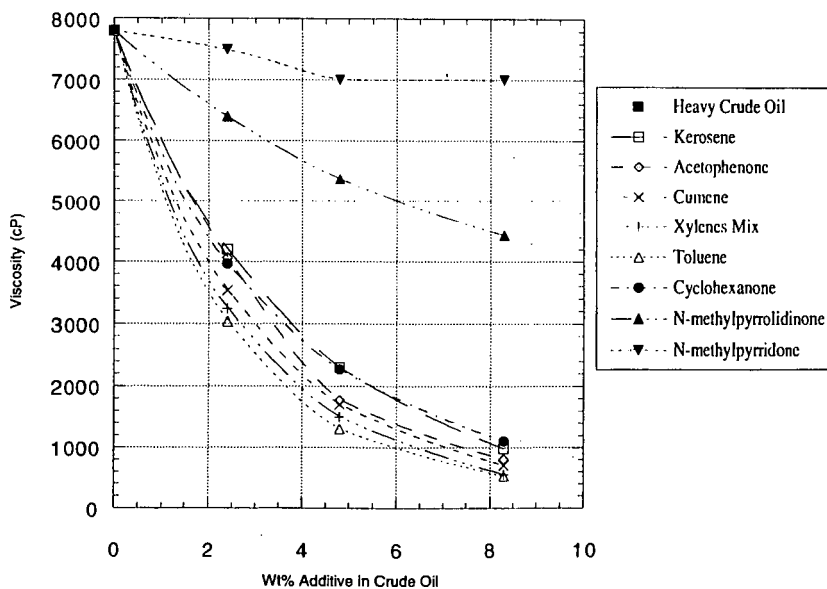


Figure 2. Plot of viscosity against wt.% of additive compound in the crude oil.

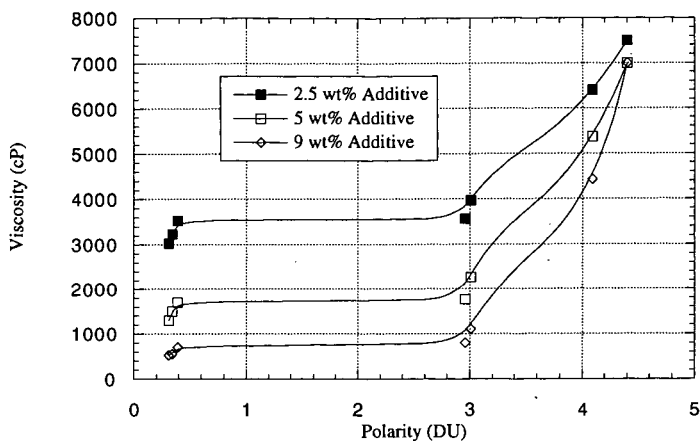


Figure 3. Plot of polarity of additives against measured viscosity

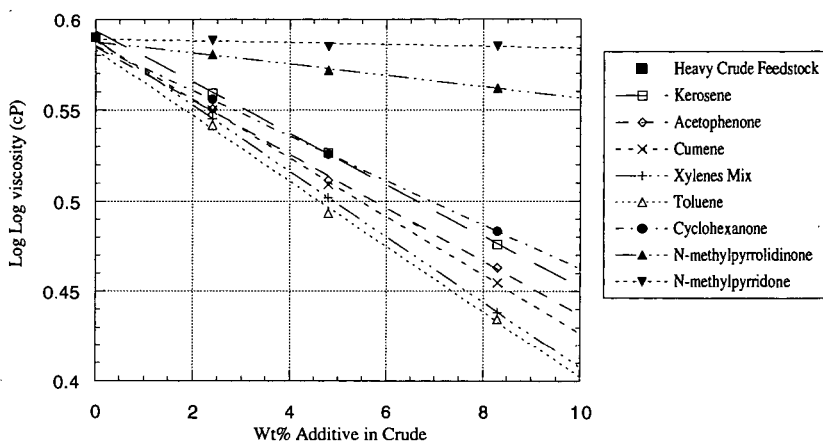


Figure 4. Log log viscosity vs. wt.% of additive in crude oil

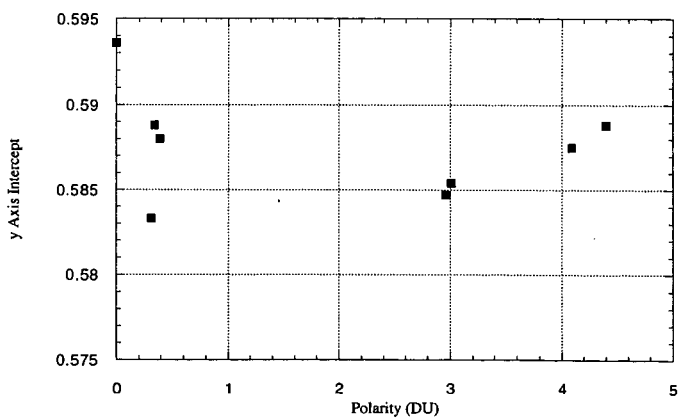


Figure 5. Plot of polarity of additive compounds against y axis intercepts from Figure 4.

RESID CONVERSIONS WITH CATALYSTS DERIVED FROM PHOSPHOMOLYBDATES

Belma Demirel, Ann Thomas and Edwin N. Givens

University of Kentucky Center for Applied Energy Research, 2540 Research Park Drive,
Lexington, KY 40511-8410

ABSTRACT

Hydroconversion of coal and petroleum derived heavy resids have been studied using both dispersed and impregnated Mo catalysts derived from phosphomolybdic acid (PMA). The dispersed catalysts were generated *in situ* by introducing the PMA supported on coal. During reaction the support essentially disappears producing a highly dispersed Mo catalyst, which is as active as the catalysts produced from common organic-soluble Mo precursors. The activity of PMA impregnated high-surface area aluminas has been compared with commercially available Mo catalysts. The resid conversion activities of catalysts prepared from both Ni and Co phosphomolybdates have also been determined. The activities of the alumina supported salts will be compared with the corresponding commercially-available alumina-supported bimetallic catalysts.

INTRODUCTION

Resid is defined as the fraction of petroleum, bitumen or coal liquids that does not distill under vacuum at atmospheric equivalent boiling points over 500°C. Resids are typically coked, hydroprocessed or used in manufacturing asphalts [1-5]. Coprocessing of coals with petroleum resid has been the subject of a number of studies in recent years with the intention of integrating coal into conventional petroleum refining operations [2, 3, 6-10]. Studies have suggested that combining coal liquefaction and heavy residue upgrading is economically feasible. It has been claimed that the presence of coal will reduce the deposition of coke and metals on the catalyst. In addition, heavy resids will also act as hydrogen transfer agents for coal conversion [2-4, 11-12].

In the near future, the resid content is expected to increase as price increases. Therefore, it becomes necessary to upgrade these fractions into distillable fractions. Hydrogenation is required in order to convert resids into more valuable products. Molybdenum based catalysts are generated *in-situ* from inorganic or organometallic compounds as precursors [13]. The metal precursors typically decompose thermally transforming into highly dispersed metal sulfides [14]. Although the exact form of the catalyst is not known, it appears to be some form of molybdenum sulfide, although apparently not MoS₂. Lopez et al. reported that the atomic ratio of molybdenum was less than two in the active catalysts isolated from processing heavy petroleum fractions with ammonium molybdate and thiomolybdate precursors [15]. Polyoxomolybdates have been known to create active, well-dispersed catalysts for converting both coal and resids. Bearden and Aldridge [16, 17] and Gatsis and Plaines [18] have reported hydroconversion processes for converting oil, coal or mixtures utilizing a catalyst prepared by first forming an aqueous solution of PMA and phosphoric acid. Our studies showed that phosphomolybdic acid (PMA) is readily transformed in the reaction media to produce an active form of catalyst for liquefaction of Wyodak coal [5, 19].

We have further expanded our work on PMA derived catalysts to investigate various methods of dispersing the molybdenum in the reaction mixture. The use of coal as a carrier is intriguing since it is inexpensive and largely converts to liquid product during the reaction thereby eliminating the necessity of recovering and disposing of a solid byproduct. Unfortunately, coal does not possess the unique activating effect that alumina imparts to molybdenum catalysts. This work reported here compares the activities of precursors when dispersed on coal and supported on Al₂O₃. The objective of this work is to convert both coal and petroleum derived resids to distillates boiling below 525°C using PMA and Ni and Co phosphomolybdate precursors.

EXPERIMENTAL

Wyodak coal from the Black Thunder Mine in Wright, Wyoming was supplied by Hydrocarbon Technologies, Inc. Proximate and ultimate analysis of the coal are given in Table I. The solvents combined a 343-524°C distillate (Wilsonville Run 258 period B) and 524°C⁺ deashed resid (Wilsonville Run 258 period A) that were obtained from the Advanced Coal Liquefaction R&D

Facility at Wilsonville, Alabama. Alumina was obtained from AKZO (AO-60; surface area, 180 m²/g). Phosphomolybdic acid (PMA) was supplied by Aldrich Chemicals Inc. Co₃(PMo₁₂O₄₀)₂ (CoPM), Ni₃(PMo₁₂O₄₀)₂ (NiPM) and K₃PMo₁₂O₄₀ (KPM) were synthesized in our laboratory.

The Ni, Co and K salts of PMA were impregnated onto either coal or Al₂O₃ by adding aqueous solutions that contained the appropriate concentration of the individual metal salts to provide a final loading of 15 mg or 1000 mg of Mo per kg feed. During addition, the powdered coal or the Al₂O₃ support was continually stirred to assure even dispersion. The potassium salt was soluble only after adding a few drops of KOH to the water.

Activity tests were carried out in a 50-cc micro autoclave at 440°C and 1350 psig (cold) for 30 minutes. The reactor was equipped with a thermocouple, and connected to a pressure transducer for monitoring temperature and pressure during the reaction. Experiments were repeated at least once to confirm the reproducibility. In a typical experiment, 2.5 g of 524°C distillate, 4.0 g of deashed resid and 0.35 g of metal impregnated coal (on dry basis) or Al₂O₃. The reactor was loaded, pressurized with H₂S/H₂ (3 wt% H₂S in H₂), submerged in a fluidized sand bath and agitated continuously at the rate of 400 cycles per minute at the specified temperature. After quenching, solid and liquid products were removed from the reactor using tetrahydrofuran (THF). The filtered solids were extracted in a Soxhlet extractor overnight. The THF insoluble fraction was dried in a vacuum oven and weighed. The soluble fraction was distilled under vacuum (modified ASTM D-1160-87) to an atmospheric equivalent end point of 524°C. Resid conversion was calculated as follows:

$$\text{Resid Conv} = \left(1 - \frac{524^\circ\text{C}^* \text{Resid}_{\text{out}}}{524^\circ\text{C}^* \text{Resid}_{\text{feed}} (\text{madf})} \right) \times 100$$

where madf is moisture, ash and distillate free. Mayan resid was processed with precursors dispersed or supported on coal or Al₂O₃. Larger scale simulations were performed in a 300-cc autoclave.

RESULTS AND DISCUSSION

PMA is a unique Mo precursor since it is relatively stable even in the presence of hydrogen to temperatures in excess of 300 °C. The stability of PMA has been associated with the Keggin structure in which the 12 Mo atoms surround the central phosphorus atom. The catalytic activity of PMA in a number of oxidation reactions has been associated with the Keggin structure. Although H₂S causes limited sulfidation at somewhat lower temperatures, the limited introduction of sulfur in the structure suggests that some ionic features may still be intact at relatively high temperatures, though certainly not at liquefaction temperatures. Yong et al. recognized that, in some cases, associated cations impart additional thermal stability on the Keggin structure [22]. For this reason, the thermal and catalytic activity of three metallic salts of PMA were investigated, namely the Co, Ni and K, and compared with the activity of PMA.

The thermal stability of the three salts in He is shown in Figure 1. The endotherm associated with dehydration of these materials is quite different for these salts. The K salt appears to dehydrate most rapidly, even more rapidly than PMA. Dehydration of the Ni and Co salts occurs over a much wider temperature range. An endothermic spike appears for these two salts at 330-400 °C which is lower than for PMA. This has been ascribed to the loss of constitutional water and collapse of the Keggin structure. Such a spike is not observed in the K structure until 500 °C suggesting that the Keggin ion may be stable at this temperature. In H₂ (see Figure 2), the initial loss of water from KPM occurs over a more narrow temperature range than for PMA. The material formed at 150 °C is quite stable. By contrast, the Ni salt and, to a lesser extent, the Co salt appear to continually lose weight over the whole region suggesting that dehydration is quickly followed by further changes in the ionic structure. After dehydration, the K salt is unusually stable at temperatures beyond 450 °C suggesting that the Mo may have remained in the +6 oxidation state. When H₂S is added along with H₂ (Figure 3), the PMA and Ni salt show a major loss in weight at approximately 300 °C, probably indicating breakdown of the Keggin ion. The K salt showed initially a weight gain suggesting incorporation of sulfur into the structure. However, at 350 °C, a very significant loss in weight occurs in an exothermic reaction. This suggests formation of a significant amount of water, destruction of the Keggin structure and reduction of Mo, probably to the +4 state, although this has not been confirmed. Clearly, the H₂S leads to a significant change in the stability of the K salt.

Resid conversions in the absence of a catalyst (Table 2) after 30 min was 10.9%. When coal equivalent to the amount used as a carrier for the metal catalyst was added to the reaction mixture, conversion increased by 1%. Although the thermal conversions are still incomplete, they are essentially unaffected by the presence of the coal. The addition of PMA at the 1000 ppm for the 30 min runs increased resid conversion by about 2%, whereas at the 15 ppm level there was no change

(Table 3). Increasing the run time to 90 minutes gave a significant increase in the level of conversion, also for the thermal reaction. Since the 15 ppm metal addition probably had no effect, the 21-22% conversion observed for both PMA and CoPM at this level is probably indicative of the thermal reaction. Increasing the metal concentration to 1000 ppm gave a sizable increase in conversion. Both PMA and the CoPM gave 31% conversion of resid to distillate. Although this work is in progress, it will be used to guide processing runs to be performed in a continuous batch configuration. The results from the conversion of petroleum resids and larger scale simulations will be discussed.

CONCLUSION

Thermal stability tests of PMA and bimetallic phosphomolybdates showed that these materials are mostly stable up to 400-450°C in the presence of He or H₂. The H₂S leads to a significant change in the stability, but transforms these materials into an active form of catalyst. Catalytic activity tests of PMA and bimetallic phosphomolybdates also showed that they have significant effect on resid conversion.

REFERENCES

- [1] Nelson, W. L., *Petroleum Refinery Engineering*, McGraw-Hill, NY, 1958.
- [2] Curtis, C. W., Guin, J. A., Pass, M. C. and Tsai, K-J., *Prepr. Pap.- Amer. Chem. Soc., Div. Fuel Chem.* **1984**, 29 (5), 155.
- [3] Curtis, C. W., Guin, J. A., Pass, M. C. and Tsai, K-J., *Fuel Sci. Technol. Int.* **1987**, 5, 245
- [4] Moschopedis, S. E. and Hepler, L. G., *Fuel Sci. Technol. Int.* **1987**, 5, 1.
- [5] Demirel, B. and Givens, E. N., *Energy and Fuels* (in print).
- [6] Curtis, C. W., Tsai, K-J. and Guin, J. A., *Ind. Eng. Chem. Res.* **1987**, 26, 12.
- [7] Curtis, C. W., Tsai, K-J. and Guin, J. A., *Fuel Process. Technol.* **1987**, 16, 71
- [8] Curtis, C. W. and Cassell, F. N., *Energy and Fuels* **1988**, 2, 1.
- [9] Flynn, T., Kemp, W., Steedman, W., Bartle, K. D., Burke, M., Taylor, N. and Wallace, S., *Fuel Process. Technol.* **1989**, 23, 197.
- [10] Steedman, W., Flynn, T., Kemp, W., Bartle, K. D., Taylor, N. and Wallace, S., *Int. J. Energy Research* **1994**, 18, 299.
- [11] Huber, D. A., Lee, Q., Thomas, R. L., Frye, K. and Rudins, G., *Prepr. Pap.- Amer. Chem. Soc., Div. Fuel Chem.* **1986**, 31 (4), 227.
- [12] Gray, M. R., *Upgrading Petroleum Residues and Heavy Oils*, Marcel Dekker, Inc., N.Y., 1994.
- [13] Del Bianco, A., et al., *Appl. Cat. (A)* **1993**, 94, 1.
- [14] Kim, H. et al., *Prepr. Pap.- Amer. Chem. Soc., Div. Fuel Chem.* **1989**, 34, 1431.
- [15] Lopez, J. McKinney, J. D. and Pasek, E. A., U.S. Patent 4557821, Dec. 10, 1985.
- [16] Bearden, R. and Aldridge, C. L., U. S. Patent 4,637,870, Jan. 20 1987.
- [17] Aldridge, C. L. and Bearden, R., U. S. Patent 4196072, Apr. 1, 1980
- [18] Gatsis, J. G. and Plaines, D., U. S. Patent 3331769, July 18, 1967.
- [19] Demirel, B. and Givens, E. N., *Catalysis Today* (in print)
- [20] Del Bianco, A., Panariti, N., Anelli, M., Beltrame, P. L. and Carniti, P., *Fuel* **1993**, 72, 75.
- [21] Marchionna, M., Lami, M. and Ancillotti, F., *Fuel Process. Technol.* **1994**, 40, 1.
- [22] Yong, W. J., Quan, X. X. and Zheng, J. T., *Thermochimica Acta* **1987**, 111, 325.

ACKNOWLEDGEMENT

The authors gratefully acknowledge financial support provided by the U.S. Department of Energy Federal Energy Technology Center under contract number DE-AC22-91PC91040.

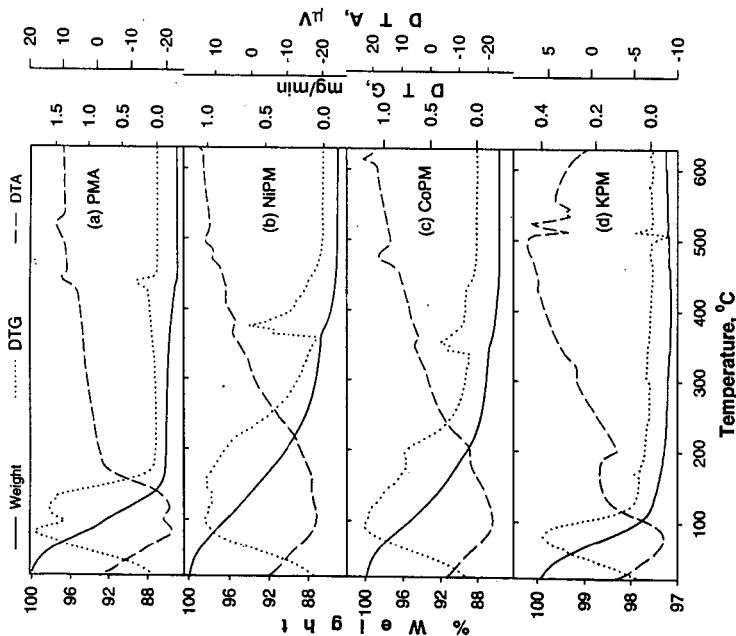


Figure 1. TG spectra of PMA and bimetallic phosphomolybdates in He.

Table 1. Analysis of Wyodak Black Thunder Coal.

| Proximate Analysis | | w% | Ultimate Analysis | w%(dry) | Sulfur Analysis | w% |
|--|-----------------|-------|----------------------------|---------|-----------------|------|
| Moisture Ash Volatile matter Fixed carbon | Moisture | 8.89 | Carbon | 70.62 | Total | 1.94 |
| | Ash | 5.76 | Hydrogen | 5.03 | Pyritic | 0.80 |
| | Volatile matter | 39.88 | Nitrogen | 1.13 | Sulfate | 0.80 |
| | Fixed carbon | 45.47 | Sulfur | 0.52 | Organic | 0.34 |
| | | | Oxygen (diff) | 16.38 | | |
| | | | Ash | 6.32 | | |
| | | | Ash, SO ₂ -free | 5.47 | | |

Table 3. Conversion of coal resid using PMA and CoPM.

| Precursor | Resid Conversion, wt% | | | |
|--------------------|-----------------------|------|------|------|
| | PMA | | CoPM | |
| Reaction time, min | 30 | 90 | 30 | 90 |
| 15 ppm Mo/g feed | 11.9 | 22.2 | 12 | 21.1 |
| 1000 ppm Mo/g feed | 14.3 | 31.2 | — | 31.4 |

Table 2. Conversion of coal resid without catalyst.

| Reaction time, min | Resid conversion, wt% | |
|------------------------|-----------------------|----|
| | 30 | 90 |
| no catalyst, with coal | 10.9 | — |
| no catalyst, no coal | 11.9 | — |

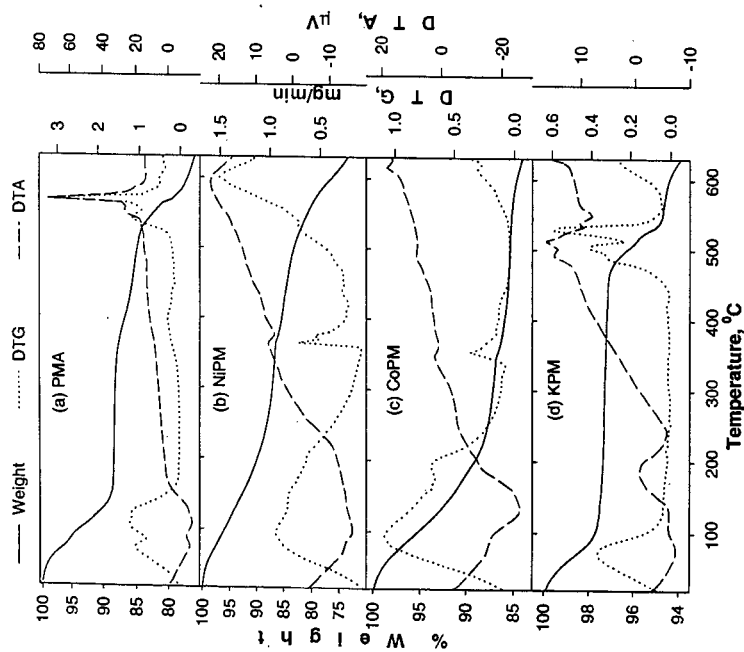


Figure 2. TG spectra of PMA and bimetallic phosphomolybdates in H_2 .

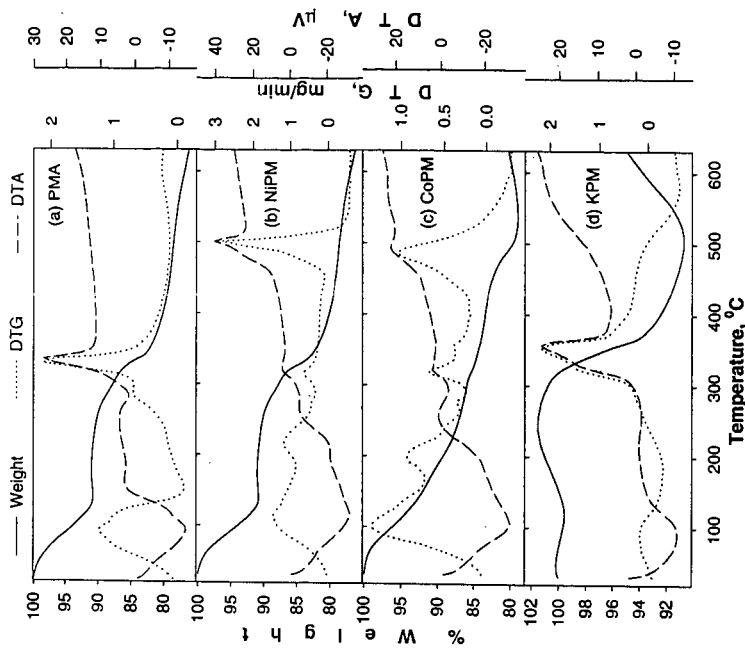


Figure 3. TG spectra of PMA and bimetallic phosphomolybdates in $H_2/S/H_2$.

Upgrading a High Asphaltene Content Petroleum Residue by Hydrogenation with a NiMo-supported Catalyst

Ming-Gang Yang and Semih Eser

*Fuel Science Program
and
The Energy Institute
209 Academic Projects Building
The Pennsylvania State University
University Park, PA 16802*

INTRODUCTION

Upgrading petroleum heavy fractions has been increasingly important in petroleum refining for both economic benefit and environmental protection. Many technologies and strategies are now available for upgrading heavy residua. These processes can be divided into two broad categories: carbon rejection and hydrogen addition¹. Carbon rejection processes redistribute hydrogen among the various components, resulting in fractions with increased or decreased H/C atomic. On the other hand, hydrogen addition processes involve external addition of hydrogen and result in an overall increase in H/C ratio of the products compared to that of the starting feedstocks. Hydroprocessing with NiMo (or CoMo)-supported catalysts has been widely used in commercial units because of high yields of liquid products and heteroatom removal^{2,4}. Various heavy fractions have been used as feedstock for hydroprocessing. Process conditions depend on two major factors: feedstock properties and product specifications.

Catalyst deactivation in hydroprocessing is considered an important part of the process cost. Many deactivation processes, such as blocking of active sites by adsorption of asphaltenes, coke formation on the catalyst surface, pore blockage caused by metal accumulation, were researched^{5,6}. Asphaltenes are considered to be responsible to the initial deactivation of the catalysts in heavy oil hydroprocessing^{7,8}, because of their adsorption on cobalt (or nickel) and molybdenum oxides and sulfides. At relatively high temperatures, asphaltenes are transformed to coke which deposits on the catalyst surface and causes deactivation of the catalysts. Therefore, the removal of asphaltenes is important for inhibiting catalyst deactivation and improving the downstream operating severity in a refinery.

Hydrogen-carbon atomic ratio (H/C) of feedstock is one of important factors determining the operation conditions. High H/C ratio means the feedstock has high hydrogen saturation and can be processed at relatively severe operation conditions. The change in H/C atomic ratio during the upgrading process can be used to measure the hydrogenation activity of a catalyst.

The present work explores the effects of a NiMo-supported catalyst and reaction conditions on upgrading a petroleum heavy residue, a ROSE pitch, which has high asphaltene and sulfur contents. Specifically, asphaltene conversion, sulfur removal, change in H/C atomic ratio, coke formation, and distillate production were investigated.

EXPERIMENTAL

The properties of the ROSE pitch used in the present work are listed in Table 1. The asphaltene and sulfur contents of the pitch are 29, and 6.0 wt%, respectively, and its H/C atomic ratio is 1.27. A simulated distillation analysis showed that the vacuum residue fraction (b.p.>525 °C) comprises more than 95 wt% of the pitch. A commercial catalyst, NiMo/SiO₂-Al₂O₃, was used for hydrogenation experiments. The catalyst was sulfided in a batch reactor with CS₂ (anhydrous, > 99 %) as sulfur agent in *n*-dodecane (anhydrous, > 99 %) in two temperature stages: 200 °C for 2 h, and, then, 350 °C for 3 h before it was used in the experiments.

Reactions were carried out in 316 stainless steel batch reactors (25 mL) heated in a fluidized-sand bath. After adding the pitch and the catalyst, the headspace gas in the reactor was replaced three times with hydrogen before the reactor was charged with hydrogen to the desired cold pressure. Then, the reactor was plunged into a preheated sand bath. The experiments were carried out in the following range of conditions: 375 to 425 °C, initial H₂ pressure of 600-1250 psig, catalyst concentration of 10 - 20 wt%, and time periods of 30 - 90 min. The reactor contents reached the desired reaction temperature within 3 minutes. At the end of the reaction, the reactor was quenched in cold water. Liquid products (THF soluble) and solids (catalyst and deposited coke, THF insoluble) mixtures were washed with THF (Tetrahydrofuran, purity > 99.9 %). After separation of the solids from the mixture, the liquid products were recovered by evaporation of THF.

Asphaltene contents of the pitch and the liquid products were measured by treating the samples (0.2 ± 0.02 g) with *n*-hexane (20 mL) in an ultrasonic bath for 5 minutes, followed by settling for another 10 minutes before vacuum filtration through a previously weighed GF/A filter paper. The filtration residue was washed with excess hexane (about 30 mL). The solid residue and vial (as some residue remains adhered to the vial surface) were dried in a vacuum oven and weighed to determine the asphaltene content of the sample. The H/C atomic ratio and sulfur content of the feedstock or liquid products were measured by CHN-600 elemental analyzer and LECO sulfur analyzer, respectively. The coke on the catalyst was defined as the difference in weight between the solid products (THF insoluble materials and catalyst) and the fresh catalyst. The fractional distribution of liquid products with respect to boiling point ranges was determined by Simulated Distillation gas chromatography (Hewlett Packard Series II 5890) with a high-temperature Megabore column P/N SD-002 HTC and a flame ionization detector.

RESULTS AND DISCUSSION

In order to investigate the effect of the catalyst on asphaltene conversion, the experiments were carried out either with or without the catalyst, but in the presence of hydrogen at the same initial pressure for both reaction systems. As shown in Figure 1, in the absence of the catalyst, both at 400 and 425 °C, the asphaltene conversion showed negative values, indicating an increase in asphaltene content after thermal reactions. In the same reaction system, the H/C ratio also decreased from 1.27 for the feedstock to 1.20 for the liquid products. The coke formation increased from 2 wt% of the feedstock at 400 °C to 10 wt% at 425 °C, as shown in Figure 2.

When the catalyst was present in the reaction system, both the asphaltene conversion and the H/C atomic ratio of the products increased. An asphaltene conversion of 44 and 46 wt % was achieved at 400 and 425 °C with the liquid product H/C of 1.35 and 1.37 at the corresponding reaction temperatures, respectively. These results are attributed to hydrogenation activity of the catalyst. The catalyst also showed high hydrodesulfurization (HDS) activity and suppressed coke formation (Figure 2). At 425 °C, more than 65 wt% sulfur was removed from the liquid products with only 1.5 wt% of the feedstock transformed to coke, compared to approximately 10 wt% coke obtained without the catalyst.

Figure 3 shows the change in asphaltene conversion and H/C ratio with increasing the temperature from 375 to 425 °C for 45 minute reaction. A significant increase in both parameters was observed upon increasing the temperature from 375 to 400 °C, with slight changes upon further increase in temperature from 400 to 425 °C. It appears that the thermal reactions, e.g., cracking and polymerization, become significant enough above 400 °C to offset the increase in hydrogenation activity of the catalyst. With the increasing reaction temperature from 375 to 425 °C, sulfur conversion increased proportionally from 13.5 to 45.7 wt %, and coke formation increased from 0.58 to 1.3 wt %, as shown in Figure 4.

Figure 5 shows the effect of hydrogen pressure on asphaltene conversion and H/C ratio at 425 °C for 90 min with a catalyst concentration 20 wt %. Both parameters increased almost linearly with the increasing cold hydrogen pressure from 600 to 1250 psig. An asphaltene conversion of 92 wt% and a H/C ratio of 1.51 were achieved at the highest pressure used in the experiments. High hydrogen pressure also promoted sulfur removal, as shown in Figure 6, but it did not affect the coke formation to any significant extent in the range of 600-1250 psig initial H₂ pressure.

Increasing the reaction time from 30 to 45 min increased the asphaltene conversion from 31 to 46 wt% at 425 °C, 1000 psig initial H₂ pressure and 10 wt % catalyst concentration. Further increase in reaction time to 90 min did not cause any significant change in asphaltene conversion or in the H/C ratio of the liquid products. These observations can also be explained by the competing catalytic and thermal reactions, as discussed before for high temperature experiments.

Figures 7 shows the simulated distillation curves of the liquid products as a function of reaction temperature at 1000 psig initial hydrogen pressure, 45 min and 10 wt % catalyst. The distillation curve for the starting residue is also shown in Figure 7 for comparison. With the increasing reaction temperature, the curve shifts to lower temperatures, indicating the production of lower boiling-point material. The conversion of 525 °C⁺ fraction was 5.2, 12.2 and 35.5 wt% at 375, 400 and 425 °C, respectively. The conversion increased nearly three times when the reaction temperature increased from 400 to 425 °C. Increasing the reaction time to 90 min at 425 °C (not shown in the figure) gave approximately 50 wt% conversion of the 525 °C⁺ fraction. This means that thermal reactions essentially controlled the cracking at higher reaction temperatures.

CONCLUSIONS

Hydrogenation of a ROSE pitch produced liquids with low asphaltene and sulfur content and high H/C atomic ratio because of the high hydrogenation activity the NiMo-supported catalyst used in this work. At both low and high reaction temperatures, the hydrogenation activity of the catalyst was predominantly responsible for the asphaltene conversion and increase in the H/C atomic ratio. High extents of sulfur removal and suppression of coke formation were also possible because of the high hydrogenation activity of the commercial catalyst.

ACKNOWLEDGMENTS

This work was supported by funds from USX Foundation at the Laboratory for Hydrocarbon Process Chemistry at Penn State University. We thank Dr. Mark Plummer and Mr. Rolf Schroeder of Marathon Oil Company for many helpful discussions. We thank Dr. Mark Badger of PSU for his help with experimental work during the initial phase of this study. The catalyst sample was provided by Criterion.

REFERENCES

1. Dickenson, R. L.; Biasca, F. E.; Schulman, B. L.; Johnson, H. E. *Hydrocarbon Processing* **1997**, *76*, 57.
2. Sonnemans, J. W. M. In *Catalysts in Petroleum Refining and Petrochemical Industries 1995*; Stud. Surf. Sci. Catal., Elsevier Sci. B. V. **1996**, Vol. 100, p 99-115.
3. Yang, M.-G.; Nakamura, I.; Fujimoto, K. *J. of The Japan Petroleum Institute* **1997**, *40*, 172.
4. Yang, M.-G.; Nakamura, I.; Fujimoto, K. *Catal. Today* **1998**, in press.
5. Oballa, M. C.; Wong, C.; Krzywicki, A. In *Catalytic Hydroprocessing of Petroleum and Distillates*, Marcel Dekker, New York, **1994**, p 33-54.
6. Richardson, S. M.; Nagaishi, H.; Gray, M. R. *Ind. Eng. Chem. Res.* **1996**, *35*, 3940.
7. Bartholomew, C. H. In *Catalytic Hydroprocessing of Petroleum and Distillates*, Marcel Dekker, New York, **1994**, p 1-13.
8. Trimm, D. L. In *Catalysts in Petroleum Refining and Petrochemical Industries 1995*; Stud. Surf. Sci. Catal., Elsevier Sci. B. V. **1996**, Vol. 100, p 65-76.

Table 1. Properties of ROSE Pitch Feedstock

| | |
|------------------------------|------|
| Simulated distillation, wt % | |
| naphtha (IBP - 171 °C) | 0.0 |
| kerosene (171 - 232 °C) | 0.0 |
| gas oil (232 - 370 °C) | 0.7 |
| VGO (370 - 525 °C) | 3.7 |
| residue (525 °C+) | 95.6 |
| Asphaltene, wt % | 29 |
| Elemental analysis, wt % | |
| C | 82.4 |
| H | 8.7 |
| N | 0.61 |
| S | 6.0 |
| H/C atomic ratio | 1.27 |

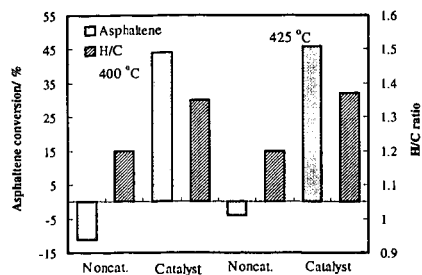


Figure 1. Comparison of thermal and catalytic reactions in asphaltene conversion and H/C atomic ratio change. 1000 psig H_2 pressure; 90 min; 10 wt % catalyst.

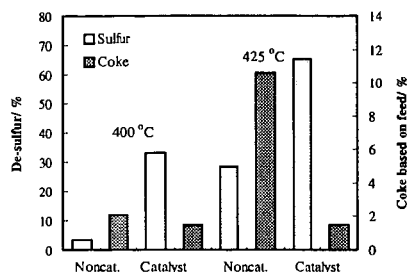


Figure 2. Comparison of thermal and catalytic reactions in sulfur conversion and coke deposits. 1000 psig H_2 pressure; 90 min; 10 wt % catalyst.

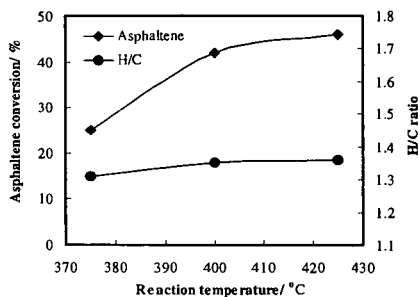


Figure 3. The effect of reaction temperature on asphaltene conversion and H/C atomic ratio increase. 1000 psig H_2 pressure; 45 min; 10 wt % catalyst.

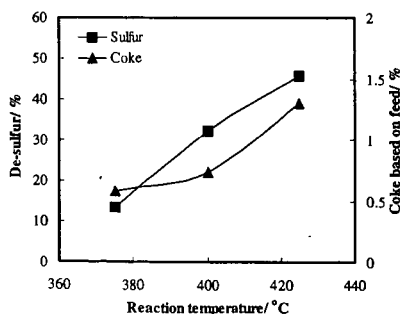


Figure 4. The effect of reaction temperature on sulfur conversion and coke deposits. 1000 psig H_2 pressure; 45 min; 10 wt % catalyst.

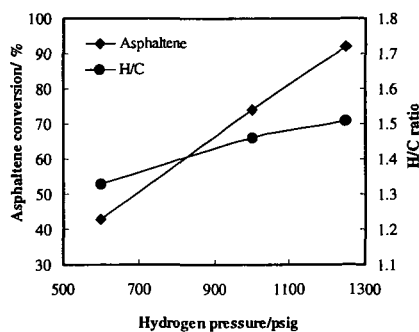


Figure 5. The effect of initial H_2 pressure on asphaltene conversion and H/C atomic ratio increase. 425 °C; 90 min; 20 wt % catalyst.

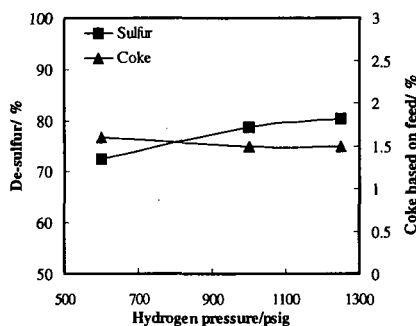


Figure 6. The effect of initial H_2 pressure on sulfur conversion and coke deposits. 425 °C; 90 min; 20 wt % catalyst.

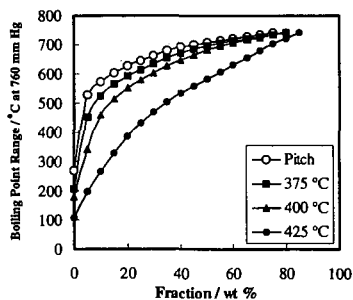


Figure 7. Distillation curves of feedstock and products at different reaction temperature. 1000 psig H_2 pressure; 45 min; 10 wt % catalyst.

THE USE OF METHANE AS SOURCE OF HIGHER HYDROCARBONS AND HYDROGEN FOR UPGRADING HEAVY OILS AND BITUMEN

Parviz Rahimi, Craig Fairbridge, National Centre for Upgrading Technology, 1 Oil Patch Drive, Suite A202, Devon, Alberta, Canada, T9G 1A8

Dennis Tanner, Department of Chemistry, University of Alberta, Edmonton, Alberta, T2G 2G2

Key words: Helium-methane plasma, helium-hydrogen plasma, hydrogen addition, methyl radicals, higher hydrocarbon from methane

ABSTRACT

Both the production of synthetic crude from the oil sands in Alberta and the upgrading of heavy oils to lighter products require hydrogen. The production of hydrogen by the steam reforming of methane is not only expensive but also contributes significantly to the production of greenhouse gases. Therefore, in bitumen and heavy oil upgrading, there is a major incentive to use methane directly. This paper describes the reactions of hydrogen and of methane plasma with olefin and aromatic model compounds and presents possible reaction mechanisms.

INTRODUCTION

Because of economic and environmental impacts, the direct use of methane or natural gas which contains 90 mole % methane in place of hydrogen has attracted considerable attention in recent years. It has been shown that different ranks of coal under coal liquefaction conditions and presence of methane produce more volatile products than under nitrogen.¹⁻³ Using model compounds such as benzene, naphthalene, toluene, bibenzyl and phenol, it has been demonstrated that a moderate degree of methylation can be achieved under certain conditions.⁴⁻⁶ Recently, Pang et al.⁷ concluded that, in the reaction of methane with petroleum and coal model compounds and the presence of catalyst, methylation yields are low because of the thermodynamics of the reaction is unfavorable. Ovalles et al.⁸⁻⁹ reported the use of methane as a source of hydrogen for the upgrading of heavy oils. These authors reported a significant decrease in the viscosity of the crude and conversion of 540° C⁺ with methane. Ilton and Maron have also demonstrated that the activity of methane can be enhanced in the presence of certain catalysts and their enhancement results in a high conversion of methane into higher hydrocarbons.¹⁰

Using microwave discharge, Mazur et al.¹¹ reported that atomic hydrogen can be generated from hydrogen gas and this atomic hydrogen can be reacted with olefins to form saturated and dimeric products. Tanner et al.¹² subsequently showed that the addition of hydrogen to olefins can be regiospecific.

The available data in the literature regarding the use of methane as a source of hydrogen indicate that methane is not useful for upgrading heavy hydrocarbons to lighter products because the use of methane results in low or no conversion. Other efficient methods for methane activation must be discovered in order to be able to use more or all of the available hydrogen in this molecule.

For the data reported in this paper, the use of methane as a source of hydrogen and higher hydrocarbons was investigated using microwave discharge. The objective was to follow the fate of methyl radicals and hydrogen atoms formed from methane under microwave discharge and reacted with model compounds containing double bonds. Furthermore, to shed light on the mechanism of dealkylation or cleavage of strong C-C bonds, the reaction of hydrogen atoms generated from hydrogen/helium plasma was investigated using toluene.

EXPERIMENTAL

General method for CH₃ radicals and H atoms reaction

Experimental details for H atom reactions with model compounds can be found elsewhere.¹² Similar Pyrex reactor and experimental conditions were used for the reaction of CH₄ with the model compounds. Briefly, the reactions with substrates (model compounds) were carried out in a Pyrex reactor neat or in acetone solution at -78°C. Helium-hydrogen or helium-methane was

introduced into the reactor system at the desired flow rate. The pressure of the reactor was maintained at 3-4 Torr. H_2 -He or H_2 - CH_4 plasma was generated in the microwave cavity. Hydrogen atoms or methyl radicals were swept into the stirred solution. The reaction products were analysed and identified using GC/FTIR and GC/MS and quantified using a Varian Vista 6000, equipped with FID detector and a glass capillary column (PONA, 30 mx0.25mm, HP).

RESULTS AND DISCUSSION

Reaction of CH_4 with model compounds

In a previous study, the results of hydrogen radical addition to model compounds indicated that these molecules can be saturated at very low temperatures.¹² In the present study, the reaction of methane as a source of hydrogen with 1-octene and cyclohexane was investigated. The product distributions from He/ CH_4 plasma are shown in Table 1 and Table 2. For comparison, the products from the reaction of He/ H_2 plasma with these model compounds are also shown in these tables. No attempts were made to optimize the product yields. The results show that the products in the reaction of He/ CH_4 plasma with both olefins are identical to those of the reaction of H_2 /He plasma with the olefins. However, in the reaction with CH_4 , a number of higher alkanes which were assumed to be resulting from the polymerization of methane could be identified (not quantified) in the reaction mixtures. Formation of higher hydrocarbons in these experiments was not quantified but their production signifies the possibility of the formation of higher hydrocarbons from methane. Although there was no evidence of the reaction of methyl radicals with the olefinic substrates, methyl radicals could be trapped by a spin trap such as tert-butylphenylnitron. This material was added to the reaction mixture before the plasma was activated; upon treatment with methane plasma the stable EPR spectra of the methyl radical spin adduct was observed.

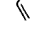







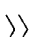

The product distribution in the reaction of He/ CH_4 plasma with toluene at -78°C is shown in Table 3. Beside hydrogenation products, addition of, methyl radicals to toluene produced substituted toluene and combination reactions of benzyl and methyl radicals produced ethyl benzene. Formation of benzene in this reaction mixture has mechanistic significance since it indicates that hydrogen atoms had displaced methyl radical via ipso attack.

The mechanistic investigation of hydrogen addition to substituted aromatics was further continued by the reaction of H_2 /He plasma with model compounds such as bibenzyl, 9-dodecylanthracene, dodecylbenzene, dibenzothiophene and 2-naphthalene thiol, but this investigation will be the subject of a later publication.

REFERENCES

1. Yang, K., Batts, B.D., Wilson, M.A., Gorbaty, M. L., Maa, P.S., Attalla, M.I., Long, M.A., and He, S.J.X., *Fuel*, 76, 1105 (1997).
2. Sundaram, M. S. and Steinberg, M., US Patent No. 4,687,570, 1987.
3. Egiebor, N.O. and Gray, M.R., *Fuel*, 69, 1276 (1990).
4. Wilson, M.A., Attalla, M.I., Yang, K., He, S.J.X., Long, M.A., Batts, B.D., Smith, J.W., Voigtmann, M.F. and Smith, D.R., *Synthetic Fuels from Coal and Natural Gas*, NERDPP End of Grant Report Project No. 1613, Canberra, Australia, 1993.
5. Scott, D.w., Bulletin 666, US Bureau of Mines, 1974.
6. He, S. X. J., Long, M.A., Wilson, M.A., Gorbaty, M. L., and Maa, P.S., *Energy and Fuels*, 9, 616 (1995).
7. Yang, K., Wilson, M.A., Quezada, R.A., Prochazka, J.L., Long, M.A., He, S.J.X., Gorbaty, M. L., and Maa, P.S., *Fuel*, 76, 1091 (1997).
8. Ovalles, C., Hamana, A., Rojas, I., and Bolivar, R., *Proceedings of Eastern Oil Shet Symposium*, 161, 1993.
9. Ovalles, C., Arias, E.S., Hamana, A., Badell, C.B., and Gonzalez, G., *Fuel Chemistry preprints*, 39, 973 (1994).
10. Iton, L.E. and Maron, V.A., US Patent No. 5,068,485, 1991.
11. Berri, A., Berman, E., Vishkautsan, R., and Mazur, Y., *J. Am. Chem. Soc.*, 108, 6413 (1986).
12. Tanner, D.D and Zhang, L. J. *Am. Chem. Soc.*, 116, 6683 (1994).

Table 1. A comparison of the product distribution of the addition of atomic hydrogen (generated by microwave discharge of methane or H_2^a) to 1-octene at $-78^\circ C$.

| Reaction % | CH ₄ Flow Rate ML/min (min) |  |  |  |  |  |  |  |  |  |  |
|-------------------|--|---|---|---|---|---|---|---|---|---|---|
| 4.26 | 1 (30) | 20.2 | 32.6 | 20.2 | 9.90 | 2.60 | 13.3 | 1.20 | | | |
| 3.58 | 2 (35) | 23.5 | 31.7 | 22.1 | 7.30 | 0.90 | 12.9 | 1.60 | | | |
| 3.36 | 3 (30) | 9.8 | 24.1 | 40.9 | 11.20 | 3.10 | 9.8 | 1.00 | | | |
| 7.88 | 4 (30) | 25.2 | 34.9 | 14.7 | 7.30 | 2.30 | 14.2 | 1.00 | | | |
| 2.00 | 4 (30) | 17.4 | 29.0 | 29.4 | 9.50 | 2.10 | 11.8 | 0.70 | | | |
| 4.06 ^d | 4 (30) | 22.9 | 34.9 | 14.8 | 9.20 | 2.90 | 14.3 | 0.90 | | | |
| | | | | | | | | | | | |
| | H ₂ Flow Rate ML/min (min) | | | | | | | | | | |
| 3.09 | 4 (11) | 16.4 | 27.7 | 29.8 | 10.9 | 2.54 | 11.7 | 0.92 | | | |
| 8.05 | 4 (11) ^d | 22.8 | 34.9 | 14.2 | 11.0 | 2.33 | 14.5 | 0.85 | | | |

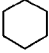
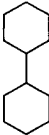
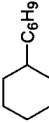
^a See Ref. 12.

^b Products formed by the disproportionation reactions.

^c Products formed by the addition of hydrogen atom to a secondary alkyl radical.

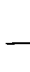
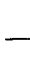
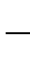
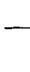
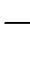




^d 1 M solution in acetone.

Table 2. A comparison of the product distribution of the addition of atomic hydrogen (generated by microwave discharge of methane or H₂) to cyclohexene at ~-78°C.

| Reaction % | CH ₄ or H ₂ Flow Rate (mL/min) | Time (min) |  |  |  |
|------------------|--|------------|---|---|---|
| 0.90 | 4 | 15 | 79.6 | 15.8 | 4.7 |
| 0.80 | 6 | 30 | 73.6 | 17.3 | 9.0 |
| 0.80 | 1 | 30 | 55.3 | 29.4 | 15.3 |
| 1.4 ^a | 4 | 20 | 91.8 | 5.9 | 2.3 |
| 2.1 ^a | 4 | 30 | 86.0 | 11.3 | 2.7 |

^a Reaction with H₂.

Table 3. The Reaction of a CH₄ Plasma with Toluene (~78°C).

| CH ₄ (mole) Passed into The System | Reaction Time (min) | C ₂ H ₆ |  |  |  |  |  |  |  |  |  | Dimer | % CH ₄ Consumed |
|---|---------------------------|-------------------------------|---|---|---|--|---|---|---|---|---|-------|-------------------------------|
| 0.008 | 65 | NQ | 98.2 | 0.04 | 1.07 | 0.08 | 0.08 | 0.06 | 0.18 | 0.29 | 26 | | |
| 0.007 | 40 | | 99.2 | 0.02 | 0.20 | 0.05 | 0.05 | 0.06 | 0.44 | 16.1 | | | |
| 0.016 | 90 | | 98.7 | 0.02 | 0.32 | 0.13 | 0.06 | 0.07 | 0.50 | 8.8 | | | |
| 0.0018 | 10 | | 99.4 | 0.03 | 0.10 | 0.04 | 0.05 | 0.05 | 0.13 | 37.9 | | | |

NQ - not quantitated.

HYDROCRACKING OF LIAOHE VACUUM RESIDUE WITH BIMETALLIC OIL-SOLUBLE CATALYSTS

Ruihua Shen, Chenguang Liu and Guohe Que
Department of Chemical Engineering, University of Petroleum
Dongying, Shandong, 257062, P. R. China

ABSTRACT

Hydrocracking of Liaohe vacuum residue was investigated in an autoclave promoted by oil-soluble molybdenum dithiocarboxylate, nickel and iron naphthenates as well as their mixtures. The reaction was conducted at temperature of 430°C, residence time of 1 hour, catalyst concentration of 200ppm(based on metal in feed), and initial hydrogen pressure of 7.0MPa. It was found experimentally that high residue conversion, and low coke(toluene insoluble) and light gas yields were achieved in the presence of the mixed catalysts, indicating the mixed catalysts to be more active than the single one for the hydrocracking of vacuum residue. It was also discovered that the synergism was obviously present for the bimetallic catalysts when the weight ratio of molybdenum to nickel or iron was 3 to 2. X-ray diffraction(XRD) analyses of the toluene insolubles indicated that the active species of catalysts were non-stoichiometric metal sulfides, and no joint sulfides occurred in the presence of bimetallic catalysts. Microscopy and transmission electron microscopy(TEM) analyses further revealed that the dispersion of catalysts was improved in the presence of the second metal.

KEY WORDS: Hydrocracking, Bimetallic Oil-soluble Catalyst, Vacuum Residue

INTRODUCTION

The use of homogeneous oil-soluble metal compounds to enhance the liquid yield and to reduce coke formation has been explored extensively in the hydrocracking of heavy feedstocks. These compounds are based on transition metals, such as Mo, W, Co, Ni, V, and Fe[1]. It is well known and of great industrial importance that the addition of a second transition metal such as Co or Ni to a binary sulfide such as MoS_2 or WS_2 can give rise to an enhancement of HDS activity. In this paper we investigated the application of bimetallic oil-soluble catalysts and evaluated the relative activities of these homogeneous catalysts for liquid phase catalytic hydrocracking of Liaohe vacuum residue.

It is generally accepted that Mo-based catalysts give the best performances in terms of coke inhibition and product upgrading. On the other hand, Fe-based materials are often used in slurry processes because of their lower cost even though they show very low activity toward hydrogenation reactions.

The degree of dispersion of the catalyst strongly affects its activity. Although high levels of catalyst dispersion can be achieved by introducing some techniques[2,3,4], adding oil-soluble catalyst precursors seems the best way to promote a good dispersion. A systematic investigation showed that catalyst performances are almost independent of the organic group bonded to the metal as long as the organic group has provided oil solubility as well as the thermal lability to the precursor[5].

It is clear that the most promising new catalysts might stem from research on promoted or multicomponent systems. The objective of the present investigation was to develop bimetallic oil-soluble catalysts and to evaluate the relative activities of these homogeneous catalysts. The aim was to determine whether sufficiently small quantities of these catalysts could be used so that they would not need to be recovered after hydrocracking. The objective was to accelerate the rate of the hydrogenation reactions to permit them to keep pace with thermal cracking of the asphaltene and thus yield more stable distillates.

EXPERIMENTAL

The hydrogenation reactions were performed on a vacuum residue (500+) of Liaohe crude with bimetallic oil-soluble compounds as catalyst precursors. The vacuum residue feedstock used throughout the experiments was Liaohe Tuozili vacuum residue supplied by the Liaohe Petrochemical Refinery. The properties of this feedstock were reported in Table 1. These catalysts were mixtures of molybdenum dithiocarboxylate (MoDTC) and nickel or iron naphthenate (NiNaph or FeNaph) which was prepared from the commercially-available precursors. The weight ratio of the two metals varied from 1:4 to 4:1.

The hydrocracking experiments were all conducted with 35g Liaohe vacuum residue in a 100mL magnetically-stirred autoclave equipped with a thermocouple well. The weight of metal catalyst was calculated to give 200 ppm of metal based on the vacuum residue feed. The catalyst was weighed and added directly to the residue in the autoclave without vehicle or solvent. Then little elemental sulfur was added to promote the generation of the active form of the catalyst. Next, the autoclave was sealed, purged of air, and the hydrogen pressure brought up to 7.0MPa. The autoclave temperature was brought up to 300°C at a heating rate of 13°C min⁻¹ and held at that temperature for half an hour to sulphidize the catalyst. Then the temperature was brought up to the reaction temperature of 430°C and holds for an hour.

After reaction the final autoclave pressure was measured and the autoclave was then cooled to room temperature. The gases in the autoclave were slowly vented to the fumehood and the autoclave was opened to permit the removal of the hydrocracked liquid product. The liquid products of the reactions were directly pumped into a weighed sample bottle and distilled using a modified ASTM D1160 procedure. Three distillate fractions were collected over three atmospheric boiling point ranges: initial boiling point (IBP) to 200°C, 200-350°C, 350-500°C and a residue of 500+°C.

Duplicate autoclave experiments were performed for the characterization the percentage yields of the coke (toluene-insoluble). The coke was then characterized in terms of elemental analysis, x-ray diffraction (XRD) analysis and transmission electron microscopy (TEM) analysis.

RESULTS AND DISCUSSION

Influence of Catalysts on Yield and Product Distribution

In order to obtain a preliminary indication of the effect of the bimetallic catalysts, we carried out several experiments with one oil-soluble catalyst. All experiments with one or two oil-soluble catalysts and the results were shown in Table 2 and Table 3. Runs 1, 7 and 13 were processes with one oil-soluble catalyst Mo, Ni and Fe. Others were processes with two catalysts of different metal ratios. The yields of coke and hydrocarbon gas reflect the activity of the catalyst. In general the changes in the two criteria associated with the changes of the organic portion of the catalyst were relatively minor. So from these two criteria it appears that the metals gave the following order of activity: Mo symbol 62 < "Symbol" < 12 > Ni symbol 62 < "Symbol" < 12 > Fe.

When the mixture of two oil-soluble catalysts was used, the yields of coke and light gas were lower than either the nickel naphthenate or iron naphthenate was employed alone under the same hydrocracking operating conditions. The conversion of the residue (the yield of the distillates 500°C-) were higher than the molybdenum dithiocarboxylate was employed alone. Especially when the weight ratio of molybdenum to nickel or iron was 3 to 2, the yields of coke and gas were the lowest. A comparison on the basis of the percentage yield of coke of the performance of the bimetallic oil-soluble catalysts suggests that the activity of the catalysts of this ratio was approximately the equivalent to that of the molybdenum dithiocarboxylate and superior to that of nickel or iron naphthenate.

Characterization of Catalysts

Solids (coke + catalyst) obtained from hydroconversion were characterized by several

techniques. At first, the x-ray diffraction data showed no evidence for the formation of a Ni-Mo (or Fe-Mo) sulfide. The two metals give rise to separate non-stoichiometric sulfides that may act as supplementary catalytic materials. Two metals bonded together, however, could produce a significantly modified Mo structure. When the ratio of the two metals was 3 to 2, the synergism was obvious.

From transmission electron microscopy (TEM) analysis, it appears that catalyst particles appears as irregular clusters of lamellas with a mean thickness of about 2-7nm (Figure 1). The size of the particles and irregular clusters in the presence of the bimetallic catalyst was smaller than that of the single-metal catalyst. This showed the dispersion of the promoted system was improved.

The microscopy analysis of the hydrocracked liquid phase verified previous conclusion (Figure 2). The very fine materials maybe catalyst particles absorbed with hydrocracked distillates. The mean size of the fine materials of the promoted system was much lower than that of the single-metal system. This indicated that the presence of the second metal improved the dispersion of the catalysts.

CONCLUSIONS

The results of this work demonstrate that the nature of the catalyst metal in the oil-soluble catalyst played a very significant role in governing the yields of coke and gaseous as well as liquid products. On improving the amount of hydrogen transfer under hydrocracking conditions by the using of mixtures of two oil-soluble catalysts, the coke yield decreased greatly. The bimetallic oil-soluble catalysts were superior in terms of residue conversion, as well as yield of coke and light gas, as compared to the use of single-metal catalysts. The synergism was especially obvious when the weight ratio of molybdenum to nickel or iron was 3 to 2.

X-ray analysis showed that, under the hydrocracking conditions, there is no evidence for the formation of a Ni-Mo (or Fe-Mo) sulfide. The synergism must stem from other causes. One reason maybe the improvement of the dispersion of the catalysts that was verified by TEM and microscopy analysis.

Promoted or multicomponent catalysts have excellent potential. If the concentration of the expensive metals can be decreased to an extremely low level, there is no necessary to recover the metals. However, further work is required to confirm these observations in a scaled-up operation. Additionally, it will be more advantageous to use the less expensive metal such as cobalt or nickel instead of the molybdenum for hydrocracking.

ACKNOWLEDGMENTS

We thank Biao Wang and Huaiping Wang for the XRD analyses and interpretation and Ziping Ai for the TEM analyses and interpretation as well as Ping Wen for the microscopy analyses.

REFERENCES

1. Del Bianco, A.; Panariti, N.; Di Carlo, S.; Elmouchnino, J.; Fixari, B.; Le Perche, P., *Appl. Catal.* 1993, 94, 1.
2. Hager, G.T.; Bi, X.X.; Derbyshire, F.J.; Eklund, P.C.; Stencel, J.M., *Am. Chem. Soc. Div. Fuel Chem., Preprints*, 1991, 36(4), 1900.
3. Rouleau, L.; Baccard, R.; Breysse, M.; Dufour, J., *Appl. Catal.* 1991, 104, 137-149.
4. Ikura, M.; Stanculescu, M.; Kelly, J.E., U.S. Patent 5,283,217, 1994.
5. Chen, H.H.; Montgomery, D.S.; Strausz, O.P., *AOSTRA J. Res.*, 1989, 5(1), 33.

Table 1.
Liaohe 500°C Vacuum Residue Feed

| | | | |
|----------------------|--------|--------|------|
| Density(20°C) | 0.9976 | C,% | 86.9 |
| Viscosity(100°C),cSt | 3380 | H,% | 11.0 |
| CCR,% | 19.0 | S,% | 0.4 |
| SARA analysis,% | | N,% | 1.1 |
| saturate | 17.4 | Ni,ppm | 123 |
| aromatic | 30.3 | V,ppm | 2.9 |
| resin | 50.2 | Fe,ppm | 38 |
| Asphaltene(n-C7) | 2.1 | Ca,ppm | 96 |

Table 2.
Effect of the Mo/Ni Catalysts on Products and Distribution

| Run No. Ni/(Mo+Ni) | 1 0.0 | 2 0.2 | 3 0.4 | 4 0.5 | 5 0.6 | 6 0.8 | 7 1.0 |
|-----------------------|----------|----------|----------|----------|----------|----------|----------|
| %Gas | 5.4 | 5.6 | 4.8 | 5.4 | 6.0 | 6.7 | 6.5 |
| %Coke | 1.7 | 1.8 | 1.5 | 1.7 | 1.7 | 1.9 | 2.9 |
| IBP-200°C(%) | 5.3 | 3.0 | 3.4 | 3.4 | 4.4 | 3.1 | 6.6 |
| 200-350°C(%) | 17.3 | 15.3 | 16.0 | 17.5 | 16.1 | 17.0 | 18.8 |
| 350-500°C(%) | 28.5 | 27.0 | 26.9 | 27.4 | 28.3 | 28.7 | 26.1 |
| 500°C+(%) | 41.8 | 47.3 | 47.4 | 44.6 | 43.5 | 42.6 | 39.1 |
| Coke Quality | | | | | | | |
| H/C (at) | 0.64 | 0.64 | 0.66 | 0.67 | 0.68 | 0.67 | 0.65 |
| %N | 3.5 | 3.3 | 3.2 | 3.5 | 3.5 | 3.4 | 3.5 |

Table 3.
Effect of the Mo/Fe Catalysts on Products and Distribution

| Run No. Fe/(Mo+Fe) | 1 0.0 | 8 0.2 | 9 0.4 | 10 0.5 | 11 0.6 | 12 0.8 | 13 1.0 |
|-----------------------|----------|----------|----------|-----------|-----------|-----------|-----------|
| %Gas | 5.4 | 5.6 | 5.8 | 6.2 | 7.0 | 7.1 | 10.0 |
| %Coke | 1.7 | 2.0 | 1.7 | 2.9 | 3.0 | 3.3 | 7.1 |
| IBP-200°C(%) | 5.3 | 5.1 | 5.6 | 5.9 | 6.1 | 7.1 | 7.3 |
| 200-350°C(%) | 17.3 | 17.1 | 18.4 | 18.6 | 20.3 | 21.9 | 23.7 |
| 350-500°C(%) | 28.5 | 28.8 | 26.7 | 28.1 | 27.2 | 25.4 | 28.4 |
| 500°C+(%) | 41.8 | 41.4 | 41.8 | 38.3 | 36.4 | 35.2 | 23.5 |
| Coke Quality | | | | | | | |
| H/C (at) | 0.64 | 0.66 | 0.64 | 0.65 | 0.68 | 0.67 | 0.65 |
| %N | 3.5 | 3.5 | 3.3 | 3.5 | 3.3 | 3.2 | 3.5 |

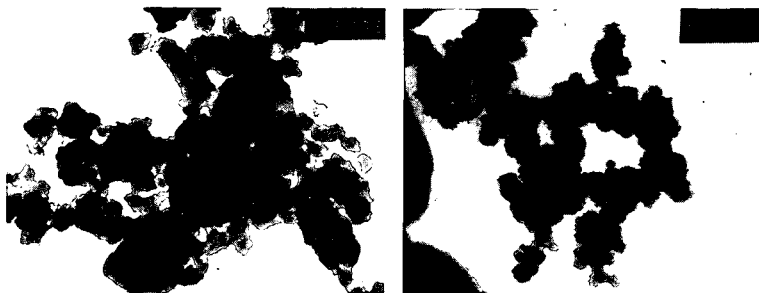


Figure 1. TEM micrograph of the solid obtained from Mo/Fe system (Mo:Fe=3:2, Magnification is $\times 19,000$ and $\times 100,000$ for left and right, respectively.)

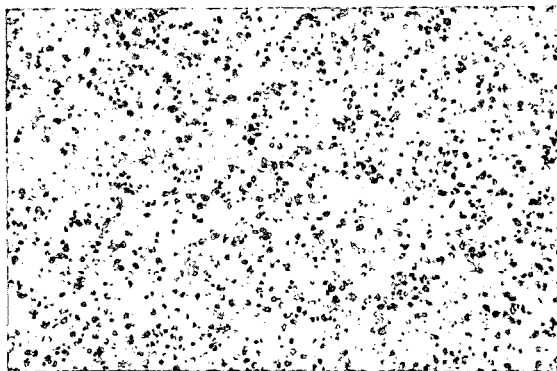


Figure 2. Micrograph of the hydrocracked liquid with Mo/Fe catalyst(Mo:Fe=3:2)

CATALYTIC HYDROCRACKING OF PETROLEUM VACUUM RESIDUE BY USING A COMBINATION OF MOLYBDENUM-BASED OIL-SOLUBLE AND IRON-BASED WATER-SOLUBLE CATALYSTS

Zong-Xian Wang, Hong-Yu Zhang, Ai-Jun Guo and Guo-He Que
National Heavy Oil Processing Laboratory, University of Petroleum (East China)
Dongying, Shandong 257062, P. R. China

ABSTRACT

Synergism was investigated of molybdenum-based oil-soluble catalyst and iron-based water-soluble catalyst in catalytic hydrocracking system of Liaohe vacuum residue. A combined use of water-soluble catalysts and active oil-soluble catalyst could enhance conversion and effectively inhibit coke formation, without much expense of relatively expensive oil-soluble catalysts. This can be explained by following reasons: (1) At early stage of hydrocracking, some kinds of polyaromatics can be partially hydrogenated to hydroaromatics, which can act as hydrogen donors and can be a complement to the active hydrogen molecules directly activated by catalysts in the subsequent hydrocracking. (2) The cheap water-soluble catalyst can not only activate molecular hydrogen to inhibit coke formation, but also make the sacrifice of the sites of coke deposition, thus save partially the active Mo-based catalyst from deactivation by coke deposition.

Key words: synergism, oil-soluble and water-soluble catalysts, hydrocracking, vacuum residue

INTRODUCTION

The catalytic hydrocracking processes of heavy oils or bitumen concerning the use of dispersed catalysts (oil-soluble, water-soluble or fine particles of catalysts) have been extensively reported [1]. Nearly all these processes are operated at relatively high temperature, well above 430°C, and aim at high conversion to light products and low coke formation. The catalysts or additives used in these processes have little catalytic activity towards the cracking reactions; the conversion to lighter products is almost entirely a thermal process [2]. But these catalysts are more or less effective in inhibiting coke formation, some of which are even really effective [1-3], such as Mo-based oil-soluble catalysts used in M-coke process [4].

The chemical nature, the catalytic activity and the cost of these catalysts are the key factors for the optimization and development of efficient catalytic hydroconversion processes [2]. Some catalysts are active, but much expensive, such as Molybdenum, Nickel, and Vanadium-based oil-soluble catalysts. On considering their high price, a once-through scheme of hydrocracking process can be considered only in employing low catalyst concentrations (< 200ppm, base on metals); but if the catalyst concentration is too low under given hydrogen partial pressure, the large amount of coke formation may result. It is worth noting that higher H₂ partial pressure and higher concentrations of low active and not expensive catalysts, such as Fe-based oil soluble, water-soluble catalysts and powdered catalysts, can counter-balance the activity of Mo-based oil-soluble catalyst as used in trace concentration.

Generally, for the same metal, its oil-soluble salts can be distributed more well in heavy oil than its water-soluble salts and therefore, are usually more active than its water-soluble salts [1]; but may be more expensive than its water-soluble salts. Some oil-soluble catalysts are relatively expensive, but quite active, such as Molybdenum-based oil-soluble catalysts. Some water-soluble catalysts are relatively very cheap, but not quite active, such as iron-based water-soluble salts. To optimize the use of these catalysts, it is possible to use a mixture of these catalysts. If the concentration of a more expensive component can be reduced, the use of the second component could reduce catalyst cost. However, up to date, few studies have been carried out to investigate the synergism of the use of active oil-soluble catalysts and very cheap water-soluble catalysts (quite different solubility systems). In the presentation, a Molybdenum-based oil-soluble catalyst and an iron-based water-soluble catalyst are in combination used in hydrocracking of Liaohe vacuum residue to investigate the synergism of these two kinds of catalysts.

1. EXPERIMENTAL

1.1 Sample

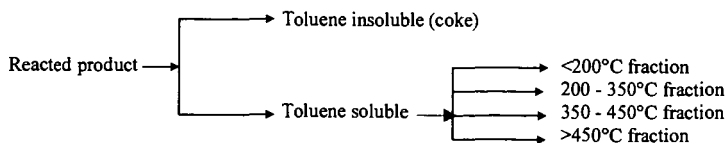
Liaohe vacuum residue(>500°C) was collected from Liaohe Petrochemical Plant in March 1996. Carlo Erba 1160 elemental analyzer was used for C, H, N analysis; atomic absorption method was used to determine Ni, V, Fe and Ca contents. Average molecular weight was measured by using VPO method (benzene as solvent, 45°C) with Knauer molecular weight analyzer. The general properties of Liaohe vacuum residue are listed in Table 1. For comparison, the general properties of Gudao vacuum residue (the feed to VRDS unit at Qilu Oil Company) was also tabulated here.

Table 1 Properties of Liaohe vacuum residue (VR)

| Property | Liaohe VR | Gudao VR |
|--|-----------|----------|
| Density(20°), g./cm ³ | 0.9976 | 0.9998 |
| Viscosity(100°)/mm ² .s ⁻¹ | 3375 | 1710 |
| Pour point, °C | 42 | 41 |
| Flash point, °C | 312 | 327 |
| Carbon residue, % | 19.0 | 15.6 |
| Elemental composition | | |
| C, % | 87.0 | 85.4 |
| H, % | 11.4 | 11.4 |
| S, % | 0.43 | 2.52 |
| N, % | 1.08 | 0.80 |
| H/C(Atomic ratio) | 1.50 | 1.60 |
| Total Metal/PPM | 258.6 | 131.6 |
| Ni, ppm | 122.6 | 48.0 |
| V, ppm | 2.9 | 2.2 |
| Fe, ppm | 37.5 | 13.8 |
| Ca, ppm | 95.6 | 33.8 |
| Ash, % | 0.06 | 0.03 |
| SARA fractions: | | |
| Saturates, % | 17.4 | 14.5 |
| Aromatics, % | 30.3 | 34.8 |
| Resins, % | 50.2 | 47.2 |
| nC7-Asphaltene, % | 2.1 | 3.5 |
| Structural Parameters | | |
| F _A | 0.27 | 0.18 |
| F _N | 0.26 | 0.33 |
| R _A /R _N | 0.93 | 0.47 |

1.2 Catalytic hydrocracking of Liaohe vacuum residue

The experiments were carried in a 100ml FDW-01 autoclave reactor with an up-and-down stirrer at 120 times of reciprocation per minute. Initial pressure was 7.0MPa H₂ for catalytic hydrocracking. Catalyst used in the hydrocracking reaction was Molybdenum-based oil soluble and iron-based water-soluble catalyst (ca.50~1000 ppm based on metal concentration in feed). The former was compatible with the vacuum residue and gave rise to the homogeneous system with the vacuum residue, and the later was emulsified into the vacuum residue to form emulsion system. After sulphurization by elemental sulfur at 320°C for 30minute (S/Metal atomic ratio=3/1), these catalyst precursors were in situ reacted to real active catalysts. Then, the temperature was raised to 430°C for hydrocracking reaction. After 1-hour reaction time, the reactor was quenched (cooled) to room temperature, the reactor gas was vented, and toluene slurry was prepared from the reactor contents. Any solids adhering to the reactor walls or internals was carefully scraped off. The slurry was then centrifuged and the toluene insoluble (TI or coke) were separated and washed (extracted) with boiling toluene by using quantitative filter paper. The solids were dried and weighed. The toluene soluble was distilled into several fractions. The distillation scheme is as follows.



2. RESULTS AND DISCUSSION

2.1 The activity of catalysts

In order to make a comparison of catalytic activity between the Mo-based oil-soluble catalyst and the Fe-based water-soluble catalyst used in Liaohe vacuum residue hydroconversion processes, the same concentrations of these two kinds of catalysts were separately used in the hydrocracking tests, the results are listed in table 2. Both of the catalysts could suppress coke formation and cracking reactions in comparison with thermal cracking system without adding catalysts. The Mo-base oil soluble catalyst accounted for lower total conversion yield than the Fe-based water-soluble catalyst did; but the former gave rise to higher conversion per unit coke than the latter did. The conversion per unit coke was 53.1% for the Mo-based oil-soluble catalyst, 11.9% for Fe-based water-soluble catalyst and 8.8% for pure thermal cracking without added catalyst. In consideration of the over-cracking and condensation reactions during Liaohe vacuum residue

hydrocracking, the following formula was proposed for evaluation of the catalytic activity of catalysts: $R = (GL \times \text{Coke}) / CP$. Here, R is named coke and over-cracking suppressing index; GL is gas and light fraction yield, strictly the <200°C fraction yield; CP is the conversion per unit coke. Under the given reaction conditions, the R-value is 0.22 for the Mo-based catalyst, 10.7 for the Fe-based catalyst and 25.0 for thermal cracking without catalysts.

Table 2 Hydroconversion of Liaohe vacuum residue by using different catalysts at 430°C, 7.0MPa initial H₂ pressure, 1hr

| Cat., ppm | Conv. wt % | conv. per unit coke, wt % | 200°C-, wt % | 200-350°C, wt % | 350-480°C, wt % | Coke, wt % |
|-----------|------------|---------------------------|--------------|-----------------|-----------------|------------|
| Mo, 470 | 49.4 | 54.9 | 13.4 | 11.1 | 24.0 | 0.9 |
| Fe, 470 | 64.4 | 11.9 | 23.5 | 16.5 | 19.0 | 5.4 |
| No cat. | 69.2 | 8.8 | 27.9 | 12.5 | 20.9 | 7.9 |

Note: cat. ~ Catalyst; conv. ~ conversion; wt % ~ weight percent.

2.2 Catalytic hydrocracking of Liaohe vacuum residue by using the Mo-based oil-soluble and Fe-based water-soluble catalysts

As indicated in table 3, the combined use of Mo-based oil-soluble catalyst and the Fe-based water-soluble catalyst could really give rise to a synergetic effect on coke inhibition. With promotion of 400ppm Fe-based water-soluble catalyst, the relatively expensive Mo-based catalyst could be reduced from 470ppm to only 70 ppm without much loss of total catalytic activity. Under the given reaction conditions, the concentration of the more expensive component can be reduced to under 100ppm, the use of the second component (Fe-based water-soluble catalyst) could reduce total catalyst cost and hence avoid the catalyst recovery [1]. It seems that the synergism of these two kinds of catalysts can not be clearly understood simply by their complementary function; this will be further discussed in section 2.3.

Table 3 Synergetic effect of Mo-based oil-soluble and Fe-based water-soluble catalysts on hydroconversion of Liaohe vacuum residue (430°C, 7.0MPa H₂, 1 hr)

| Cat., ppm | | Conv. wt % | conv. per unit coke, wt % | 200°C-, wt % | 200-350°C, wt % | 350-480°C, wt % | Coke, wt % | R |
|-----------|-----|------------|---------------------------|--------------|-----------------|-----------------|------------|------|
| Mo | Fe | | | | | | | |
| 470 | 0.0 | 49.4 | 54.9 | 13.4 | 11.0 | 24.0 | 0.9 | 0.22 |
| 70 | 400 | 48.7 | 48.7 | 15.5 | 10.0 | 22.1 | 1.0 | 0.32 |
| 25 | 445 | 56.4 | 25.6 | 18.4 | 13.0 | 22.8 | 2.2 | 1.58 |
| 0.0 | 470 | 64.4 | 11.9 | 23.5 | 16.5 | 19.0 | 5.4 | 10.7 |

Table 4 Synergetic effect of Mo-based oil-soluble and Fe-based water-soluble Catalysts on Hydroconversion of Liaohe vacuum residue

| Cat., ppm | | Conv. wt % | conv. per unit coke, wt % | 200°C-, wt % | 200-350°C, wt % | 350-480°C, wt % | Coke, wt % | R |
|-----------|-----|------------|---------------------------|--------------|-----------------|-----------------|------------|------|
| Fe | Mo | | | | | | | |
| 0.0 | 70 | 50.0 | 35.7 | 13.4 | 8.9 | 26.3 | 1.4 | 0.53 |
| 100 | 70 | 52.8 | 33.0 | 17.7 | 10.4 | 23.1 | 1.6 | 0.85 |
| 200 | 70 | 55.9 | 32.9 | 18.4 | 11.4 | 24.4 | 1.7 | 0.95 |
| 400 | 70 | 48.7 | 48.7 | 15.5 | 10.0 | 22.2 | 1.0 | 0.32 |
| 600 | 70 | 47.0 | 52.2 | 14.4 | 9.9 | 21.8 | 0.9 | 0.25 |
| 800 | 70 | 52.0 | 74.3 | 15.2 | 10.5 | 25.6 | 0.7 | 0.14 |
| 1000 | 70 | 45.7 | 76.2 | 13.2 | 9.9 | 22.0 | 0.6 | 0.10 |
| 1000 | 0.0 | 56.4 | 17.8 | 16.6 | 12.9 | 23.7 | 3.2 | 2.98 |

With the Mo-based catalyst being kept in concentration of 70ppm and the Fe-based catalyst being increasingly added from 0ppm to 1000ppm, the coke suppressing ability is at first getting down, and then becoming higher and higher from 400 ppm to 1000ppm of Fe-based catalyst in use. The results were listed in table 4. When Fe-based catalyst added in the hydrocracking system was above 600ppm (total 670ppm Mo and Fe), the performance of the Mo-Fe catalysts in coke inhibition and over-cracking suppression was better than that of pure Mo-based catalyst used in 470ppm; this could be interpreted by their R values.

2.3 The synergism of active oil-soluble catalyst and water-soluble catalyst in the catalytic hydroconversion of Liaohe vacuum residue

At early stage of catalytic hydrocracking of vacuum residue, the oil soluble and water-soluble catalyst precursors are sulphidized, by indigenous sulfur or pre-added sulfur, to dispersed fine molybdenum sulfide and iron sulfide particles, which are real active catalysts. During the stage, the catalytic hydrocracking system was of following characters:

- High activity of the catalysts
- high hydrogen partial pressure
- Low cracking reactions and low free radical concentration

The former two characters could give rise to high concentration of active hydrogen surrounding catalyst fine particles. Therefore, little coke would be formed through polyaromatic radical combination or condensation because active radicals would be timely scavenged or hydrogenated by active hydrogen before their combination. However, condensed phase of asphaltene might be formed because of the adsorption of catalyst fine particles to asphaltene molecules. The latter character along with former two would lead to an excess of active hydrogen beside the active hydrogen used to scavenge polyaromatic free radicals. The excessive active hydrogen would hydrogenate some active polyaromatics to hydroaromatic species, which could act as hydrogen donors in subsequent reactions. This kind of hydrogen donors might be more active in coke suppression than directly activated hydrogen by catalysts because there would exist a higher compatibility and an easier hydrogen transfer between the hydrogen donors and coke precursors.

In fact, there may be large differences between catalysts in the abilities to generate these kinds of hydroaromatics---secondary hydrogen donors. Some catalysts may be not active enough to hydrogenate polyaromatics to hydroaromatics. With Mo-based additives, the reaction system can not only inhibit coke formation through shutting coke precursor radicals by catalytic active hydrogen but also develop a reservoir of active hydrogen---hydroaromatics. However, the less active Fe-based catalyst could not create so active hydrogen. But the less active catalyst could be a promoter of Mo-based catalyst to effectively inhibit coke formation during severe cracking stage. Meanwhile, if used alone, a large amount of less active additives would be needed to reach effective coke inhibition. Besides, some synergism may come from in situ formed combined Mo-Fe bimetal catalysts as the supported catalysts (such as Mo/Ni/Al₂O₃) do. But, in the authors' opinion, even there exists the kind of synergism; it may not be the main synergetic effect in the slurry-phase hydrocracking system.

3. CONCLUSION

The synergetic effect of active Mo-based oil-soluble catalyst and Fe-based water-soluble catalyst is concluded here:

- Active Mo-based catalyst is used for:
 - (1) Inhibiting coke formation of the species with high coke formation tendency especially at the early stage.
 - (2) Creating the secondary hydrogen donors---hydroaromatics that may be quite active in coke suppression.
 - (3) Playing a great role in coke inhibition during the whole hydrocracking process.
- Less active Fe-based catalyst for:
 - (1) Making the sacrifice of the sites of coke deposition, thus partially saving the active Mo-based catalyst from deactivation by coke deposition.
 - (2) Playing significant role in coke suppression during the severe cracking stage when used in relatively large amount.

Therefor, the synergism of Mo-based oil-soluble catalyst and Fe-based water-soluble catalyst in catalytic hydrocracking of Liaohe vacuum residue is not only simple complementary effect, but also comprehensive promotion effect.

REFERENCES

- (1) Del Bianco, A., Panariti, N., Di Carlo, S., Elmouchino, J., Fixari, B. and Le Perchec, P., *Applied Catalysis, A: General*, **94**, 1-16(1993)
- (2) Del Bianco, A., Panariti, N., Marchionna, M. *Am. Chem. Soc., Preprints, Div. Petrol.* **40**(4),743-746(1995)
- (3) Le Perchec, P., Fixari, B., Vrinta, M., Morel, F., *Am. Chem. Soc., Preprints, Div. Petrol.* **40**(4)747-751(1995)
- (4) Bearden, R. and Aldridge, C. L., *Energ. Progress*, **1**(1-4), 44(1981)

THIRD-BODY ENHANCED METHANE CONVERSION IN A DIELECTRIC-BARRIER DISCHARGE REACTOR

Terence A. Caldwell, Pattama Poonphatanaricha, Sumaeth Chavadej, Richard G. Mallinson, and Lance L. Lobban, School of Chemical Engineering and Materials Science, University of Oklahoma, Norman, OK 73019

ABSTRACT

A great deal of recent research in fuel chemistry has been focused on the utilization of the vast global natural gas reserves. A dielectric barrier discharge has proven to be an effective method of activating methane, the primary component of natural gas, which leads to the formation of higher hydrocarbons with hydrogen as a byproduct. Carbon chain building begins with the combination of activated C_1 species to form C_2 . C_2 can react with C_1 to form C_3 or react with another C_2 to form C_4 . C_3 may also react with C_1 to form C_4 species. Hydrogen is produced when a carbon-carbon bond forms. The reverse "chain scission" reactions also occur. Olefin production becomes more likely when H_2 concentrations are reduced. Other species, such as helium, hydrogen, and light paraffins have been added to the methane feed stream to determine if they have any synergistic effects on methane conversion or if they alter product selectivity.

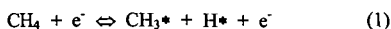
INTRODUCTION

Recent projections indicate that the majority of global oil reserves will be depleted within the next century. Therefore, it has become necessary to study new methods of obtaining the required fuels for the world's vehicles and energy suppliers and to find alternate sources of feedstocks for the petrochemical industry. One plentiful resource that has shown a great deal of promise in relieving the world's dependence upon rapidly diminishing oil reserves is natural gas. Natural gas, which is composed primarily of methane, exists in large quantities trapped within the Earth's crust. Large natural gas reservoirs are found in many different parts of the world, many of which are in very remote locations.

Presently, natural gas is used primarily as an environmentally friendly combustion fuel in industrial processes. Since methane is composed of carbon and hydrogen only, its potential as a building block to form synthetic, impurity-free fuels and chemical feedstocks is significant. Most of the proven technologies for methane conversion are processes that include the initial reaction of methane with high pressure steam to form a mixture of carbon monoxide (CO) and hydrogen (H_2) known as synthesis gas. The synthesis gas can then be converted to methanol using a nickel catalyst or to higher hydrocarbons using an iron or cobalt catalyst via Fischer-Tropsch synthesis. Unfortunately, the methods that require the initial formation of synthesis gas from methane are multi-step processes that have high capital costs that limit their application.

In recent years, extensive research has been conducted on the conversion of methane using single step processes. Some of these methods include the direct partial oxidation of methane to methanol and the oxidative coupling of methane to C_2 hydrocarbons. Each of these processes uses oxygen to activate the methane molecule at elevated temperatures and/or pressures to form the desired products. Unfortunately, these conditions not only result in higher utility and capital costs, the high temperatures tend to favor the oxidation of the desired intermediate species to undesired species such as carbon monoxide, carbon dioxide, and water.

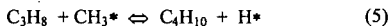
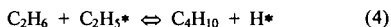
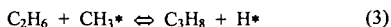
The dielectric-barrier discharge, commonly referred to as a *silent electric discharge*, has proven to be an effective method of activating methane. The silent electric discharge occurs in the gas gap between a pair of electrodes that have the same geometry, that is, between two flat-plate electrodes or in the annulus between two concentric cylindrical electrodes. A dielectric barrier that is often made of glass covers at least one of the electrode surfaces. The dielectric controls the charge transfer within the reactor and promotes a uniform charge distribution. A high voltage alternating current is used to provide the electrical potential across the electrodes. When the potential across the gas gap exceeds the minimum breakdown voltage of the system, a large number of micro-discharges are formed. These discharges are spread uniformly over the electrode surface and in the reaction volume. The discharges produce high energy electrons that interact with the methane molecules and transform the methane into a reactive species.



The resulting reactions lead to the formation of higher hydrocarbons, primarily alkanes, with hydrogen as a byproduct. The carbon chain building begins with the coupling of activated C_1 species to form a C_2 species.



The C₂ species can then react with C₁ species to form C₃ or react with another C₂ species to form C₄. C₃ may also react with C₁ to form a C₄ species. Hydrogen (H₂) is produced when a carbon-carbon bond forms.



The high energy electrons within the reaction zone also cause the reverse "chain scission" reactions to occur. The listed equations are meant to illustrate possible chain building reactions and do not represent a complete and accurate mechanism.

The silent electric discharge reactor (SEDR) is capable of converting over 50% of the methane feed to higher hydrocarbons. Presently, this high conversion requires significant power and lengthy residence times. Since methane is a relatively stable molecule compared to the other species within the reaction environment, the rate limiting step for the chain building process appears to be the activation of the methane molecule. The activation of methane must become more efficient before a process based upon the SEDR can be cost effective.

In an attempt to enhance the activation of the methane molecule, other species have been added to the methane feed stream. Mallinson et al. (1987) and Bhatnager et al. (1995) conducted extensive research using oxygen in the methane feed stream. Oxygen is more easily activated in the electric discharge environment than methane. Therefore, a larger fraction of activated oxygen species would be present than activated methane species under the same discharge conditions. It was hoped that the activated oxygen would interact with methane causing it to activate and react more readily. Their work showed that the presence of oxygen did indeed increase the rate of methane conversion in a SEDR. However, the presence of oxygen also promoted the continued oxidation of the desired intermediate species, primarily methanol, to less valuable products like carbon monoxide, carbon dioxide, and water.

Other species, such as helium, hydrogen, and light paraffins have been added the methane feed stream to determine their effect on methane conversion and product selectivity. These other species were selected because they are either chemically inert or are already present in the product stream when pure methane is run as the feed.

EXPERIMENTAL

A schematic of the silent electric discharge reactor is shown in Figure 1. The reactor system consisted of two metal electrodes made from flat aluminum plates. A dielectric barrier made of glass covered one electrode surface. The dielectric had a thickness of 0.090 in. A Teflon spacer 0.070 in. thick was situated between the dielectric and the opposite electrode. The spacer provided a channel for the inlet gases to flow axially through the reaction zone. The spacer also provided an airtight seal. The total volume of the reaction zone was about 150 cm³.

The back side of one electrode was in contact with cooling water that was maintained at a temperature between 10 and 20 °C. Thermocouples were placed at the inlet and outlet of the cooling water jacket to measure the heat given off by the reaction. No significant temperature change was ever measured in the cooling water. This means that the reactor generated little heat during operation.

Two different power supply systems were used for these experiments. The first system was powered by wall current with a voltage of 220 V and a frequency of 50 Hz that was connected to a step-down variable transformer. The transformer allowed the voltage to be varied from 0 to 110 V while the frequency remained at 50 Hz. The output line of the variable transformer was connected to a secondary high voltage AC (HVAC) transformer. The HVAC stepped up the voltage by a factor of 125. This allowed voltages as high as 15 kV to be generated. The output lines of the HVAC were then connected to the aluminum plate electrodes to generate the high potential required for electric breakdown.

The second power supply used a wall current with a voltage of 120 V and a frequency of 60 Hz. The wall current was used to supply power to an Elgar Model 501SL AC power supply that was able to generate potentials up to 250 V. Connected to the power supply was a BK Precision 5 MHz Function Generator. This instrument generated a sinusoidal waveform and allowed the frequency to be varied over the range used, from 50 to over 300 Hz. Also connected to the output line of the power supply was a Microvix MK 1.2 Energy Analyzer that was used to measure the voltage, current, power, power factor, and frequency generated by the power supply. The output of the power supply was connected to a Franceformer Gaseous Tube Transformer that has a voltage multiplying factor of 125. The high voltage cables from the transformer were then connected to the electrodes of the reactor system.

The volumetric flow rates of the feed and product gases were measured by using soap bubble flowmeters. The analysis of the gas stream was done using a Perkin-Elmer "Autosystem" Gas Chromatograph or a Carle 400 Series AGC. The latter also had the capability of measuring hydrogen. The resulting chromatogram peak areas were converted to mole fractions by correlating the individual gas concentrations to their component peak responses. The correlations were derived from calibrations using known gas compositions.

The pressure within the reactor system was assumed to be approximately atmospheric ($1 \text{ atm} \pm 0.05 \text{ atm}$). Each experiment was conducted at ambient temperature ($25^\circ\text{C} \pm 5^\circ\text{C}$). Any increase in the reactor temperature due to the electric discharge and any exothermic reactions was assumed to be negligible.

RESULTS

Previous experiments with the SEDR were conducted using a feed of pure methane at a flow rate of 20 ml/min. A typical plot of the methane conversion and product selectivity versus applied voltage is shown in Figure 2. The frequency of the alternating current for these initial experiments was 50 Hz. The methane conversion increases significantly as the applied voltage increases. However, the selectivities of the products remain essentially the same.

For the remaining experiments, the applied voltage was set at 4.5 kV and the frequency was adjusted to 100 Hz. The methane conversion was maximized at 100 Hz for this reactor configuration. The molar flow rates for the major chemical species produced from the conversion of pure methane are shown in Figure 3. Since the concentrations of the product species are much lower than that of the feed species, the product flow rates are displayed on an inset graph with a different scale for clarity. The major products for this reaction are ethane and hydrogen. For each carbon-carbon bond formed, a hydrogen molecule is produced. The propane concentration is about a third less than that of ethane while the butane production is about half that of propane. Only a trace of C_2 or higher olefins are produced using pure methane.

Figure 4 shows the molar flow rates of the species produced from the reaction of pure ethane in a SEDR. The overall conversion of ethane is greater than the conversion of pure methane. Ethylene formation is significantly higher than that seen for the pure methane reaction. Also, the concentrations of the higher paraffins, propane and butane, are greater as well. Chain scission to form methane is also significant.

The next test involved adding an ethane fraction to the methane feed stream. The methane to ethane feed ratio was maintained at 4:1. The resulting molar flow rates are displayed in Figure 5. The total conversion of methane was larger than was the case for pure methane. The production of C_2 olefins is much greater than that for pure methane as well. Also, the production rate of propane and butane nearly tripled.

Figure 6 shows the molar flow rates associated with the reaction of ethane and hydrogen at a 1:1 feed ratio. The overall hydrogen to carbon ratio is the same as that for the pure methane case. Like the pure methane experiment, olefin production was very low. However, the chain scission reaction did not completely dominate as one might expect. A significant fraction of methane was formed, but a greater fraction of higher paraffins was formed as well, particularly butane.

DISCUSSION

The product selectivities shown in Figure 2 for the pure methane experiments suggest the following predominant reaction pathway for this feed condition: an activated C_1 species reacts with another C_1 species to form ethane and hydrogen. The ethane may crack to reform methane, or it can react with a C_1 species to form propane or with another C_2 species to form butane. Since olefin production is very low, it is apparent that dehydrogenation reactions are not favored. Also, the reaction of activated species to form unsaturated products is not significant. The high methane to ethane ratios in the exit gas stream suggests that the activation and reaction of methane is the rate limiting step or that the cracking reactions of the C_2+ species dominate.

The data in Figure 4 for the pure ethane experiment shows that although the chain scission reactions are significant, they do not overwhelm the chain building steps. A significant fraction of C_3+ species were formed along with methane. Also, the lower hydrogen to carbon ratio in the feed stream resulted in the formation of a large fraction of unsaturated hydrocarbons through dehydrogenation.

Ethane was added to the pure methane feed to determine its effect on the activation of the methane molecule. The resulting methane conversion was significantly higher than that for the pure methane case. It appears that the active species derived from ethane assist in the activation of methane resulting in enhanced methane conversion to higher hydrocarbons. Again, the lower hydrogen to carbon ratio in the feed stream results in a larger fraction of unsaturated species.

To test the effect of the hydrogen to carbon feed ratio on product selectivity, a feed consisting of an equimolar mixture of ethane and hydrogen was reacted. The ethane conversion

in this experiment was significantly higher than for the pure ethane experiment. Also, dehydrogenation was suppressed by the high hydrogen concentration. Judging from the relatively high ethane conversions for each of these experiments, it appears that ethane is activated and reacts much more readily than methane. These tests indicate that the low activation rate of the methane molecules limits the production of more valuable species for the pure methane feeds.

Several researchers have attempted to enhance the conversion of methane to higher hydrocarbons by adding a chemically inert species to the feed stream. The hope was to find a third-body that would lower the activation energy of the methane molecule without disrupting the conversion pathway to more valuable products. Thanyachotpaiboon et al. (1998) studied the synergistic effect of helium on methane conversion in a SEDR. A helium to methane feed ratio of 1:1 resulted in a significant increase in the methane conversion. If helium did not interact with the methane in the discharge environment, one might expect the helium to serve only as a diluent and cause a decrease in the overall methane conversion due to the decreased partial pressure of methane. These results suggest that some of the helium is "activated" within the discharge environment and aids the activation of methane molecules through a third-body energy transfer. Unfortunately, on an industrial scale, adding helium to the methane feed stream, removing it from the product gases, and recycling it back to the feed may prove to be costly. Therefore, experiments on methane conversion enhancement were conducted using chemical species that are already present in the pure methane reaction process.

Some preliminary experiments have been conducted using propane and butane in the methane feed stream. In these cases, it appears that chain scission begins to dominate the reaction. The product concentrations are similar to those produced from ethane enhanced methane conversion.

CONCLUSIONS

The silent electric discharge reaction has proven to be a relatively effective means of activating methane molecules allowing them to react to form more valuable products. However, the activation rate is presently too low to make this process economically feasible on a large scale. Therefore, attempts have been made to enhance the conversion of methane by adding other species to the methane feed stream. Oxygen, helium, hydrogen, and light paraffins have all aided the conversion of methane with varying degrees of success. With the exception of helium, these species also change the selectivities of the reaction products. These changes may prove beneficial depending on the nature of the application. For example, the formation of liquid oxygenates by using oxygen may be favored in areas where the transportation of liquids through pipelines is possible. Olefin formation by limiting the amount of hydrogen in the feed may be encouraged in industrialized areas where poly α -olefin production takes place.

ACKNOWLEDGEMENTS

The authors would like to express their appreciation to the National Research Council of Thailand, the National Science Foundation for sponsoring a Graduate Research Traineeship in Environmentally Friendly Natural Gas Technologies, and the United States Department of Energy (Contract DE-FG21-94MC31170).

REFERENCES

- Bhatnager, R. and R.G. Mallinson, "The Partial Oxidation of Methane Under the Influence of an AC Electric Discharge," *Methane and Alkane Conversion Chemistry*, M.M. Bhasin and D.N. Slocum (eds.), Plenum Publishing, New York, 249 (1995)
- Mallinson, R.G., C.M. Slipceovich, and S. Rusek, "Methane Partial Oxidation in Alternating Electric Fields," American Chemical Society National Meeting, New Orleans, LA, August, 1987, Preprints: American Chemical Society Fuel Chemistry Division, Vol. 32, No. 3, 266 (1987)
- Thanyachotpaiboon, K., T.A. Caldwell, L.L. Lobban, S. Chavadej, and R.G. Mallinson, "Conversion of Methane to Higher Hydrocarbons in AC Non-Equilibrium Plasmas," submitted to *AIChE Journal* (1998)

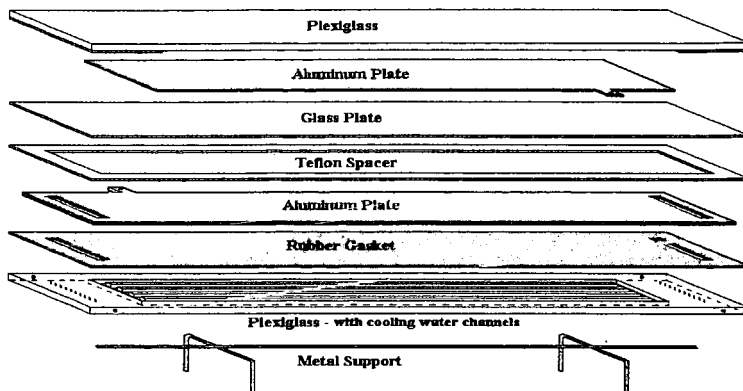


FIGURE 1: A DIAGRAM OF THE SILENT ELECTRIC DISCHARGE REACTOR.

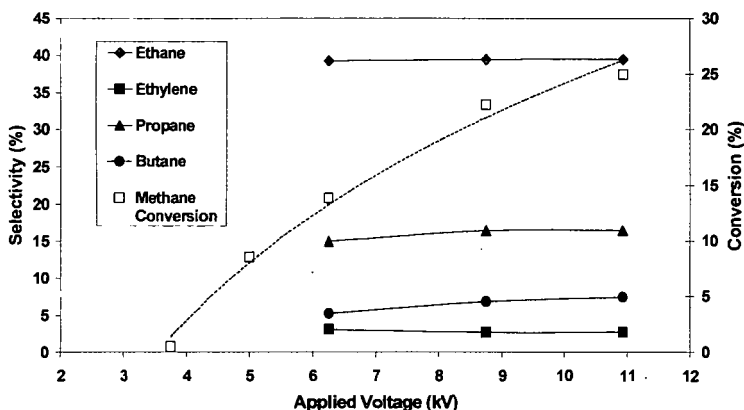


FIGURE 2: DISTRIBUTION OF PRODUCT SELECTIVITIES AS A FUNCTION OF THE APPLIED VOLTAGE. FREQUENCY = 50 HZ

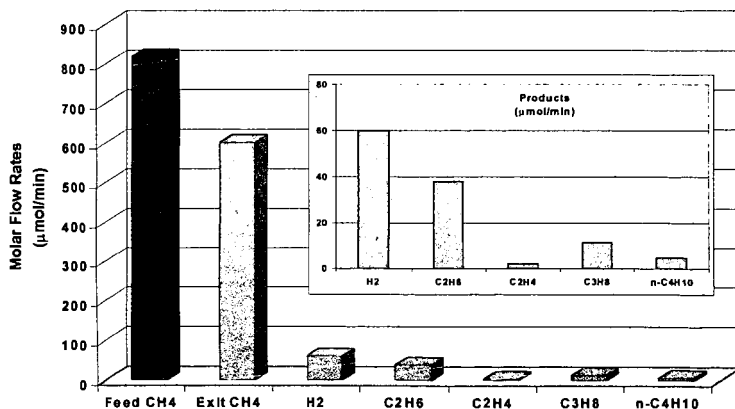


FIGURE 3: MOLAR FLOWRATES OF THE CHEMICAL SPECIES PRODUCED DURING THE REACTION OF PURE METHANE IN A SEDR. 4.5 KV 100 HZ

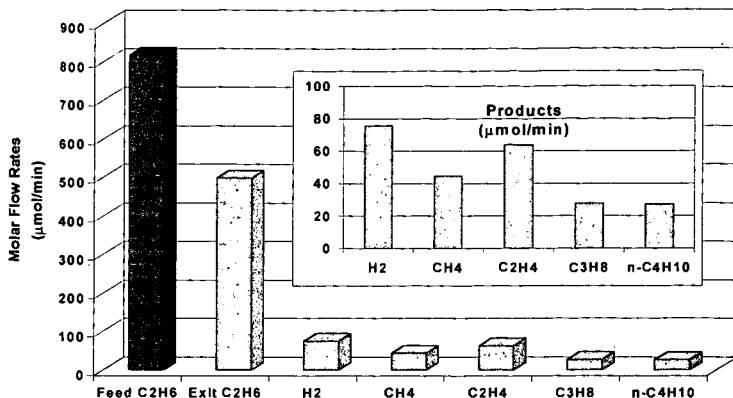


FIGURE 4: MOLAR FLOWRATES OF THE CHEMICAL SPECIES PRODUCED DURING THE REACTION OF PURE ETHANE IN A SEDR. 4.5 KV 100 HZ

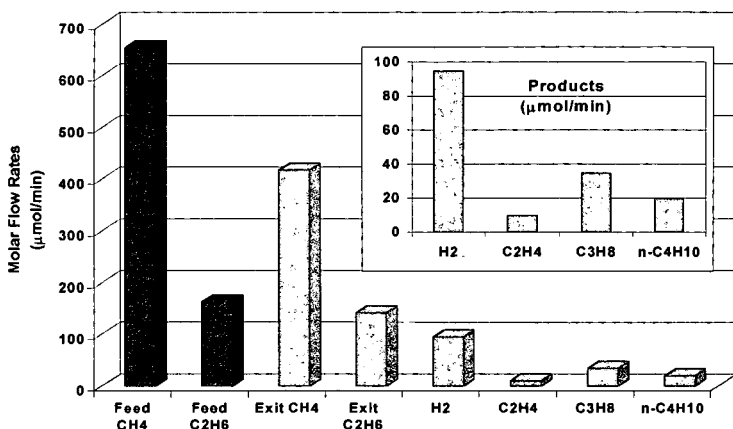


FIGURE 5: MOLAR FLOWRATES OF THE CHEMICAL SPECIES PRODUCED DURING THE REACTION OF A 4:1 MOLAR RATIO OF METHANE TO ETHANE IN A SEDR. 4.5 KV 100 HZ

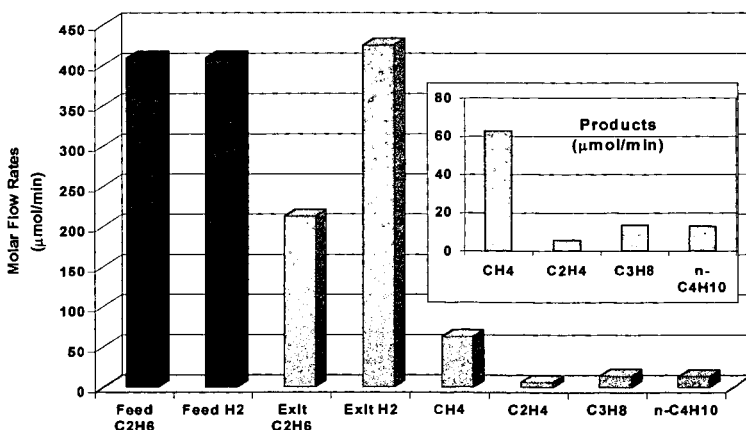


FIGURE 6: MOLAR FLOWRATES OF THE CHEMICAL SPECIES PRODUCED DURING THE REACTION OF AN EQUIMOLAR MIXTURE OF ETHANE AND HYDROGEN IN A SEDR. 4.5 KV 100 HZ

DISPERSION AND ACTIVITY OF INORGANIC CATALYST PRECURSOR IN HEAVY OIL

Richard A. McFarlane, Alberta Research Council, 250 Karl Clark Road, Edmonton, Alberta T6N 1E4, CANADA

Randall W.T. Hawkins, National Centre for Upgrading Technology, 1 Oil Patch Drive, Suite A202, Devon, Alberta T9G 1A8, CANADA

Ted Cyr, Alberta Department of Energy, 14th Floor Petroleum Plaza North, 9945- 108 Street, Edmonton, Alberta T5K 2G6, CANADA

Keywords: molybdenum sulphide, dispersion, heavy oil

ABSTRACT

Compared to supported catalysts, highly dispersed catalyst particles suspended in heavy oil are less susceptible to deactivation during heavy oil upgrading. Oil soluble catalyst precursors produce highly dispersed catalyst particles but can be expensive even when used at low concentrations. The dispersion of an aqueous catalyst precursor using an atomizing nozzle suspended in Cold Lake heavy oil has been carried out in the laboratory and the activity of the resulting catalyst was verified in semi-batch autoclave tests. The activation of the catalyst could be achieved simply by heating the heavy oil and catalyst precursor to reaction temperature. Although the catalyst particles are larger than those produced by oil soluble precursors their activities appear to be as good. The catalyst particles were shown to maintain their activity when recycled in sequential batch tests. Some details of the catalyst preparation, testing and properties are presented.

INTRODUCTION

Hydrocracking catalysts for upgrading heavy oil and bitumen are typically composed of metal sulphides dispersed on a porous oxide support in the form of extrudates. These types of catalysts suffer loss of activity due to the deposition of coke and metals, such as nickel and vanadium present in the heavy oil. Eventually, the fixed bed reactors employing these catalysts must be shut down and the catalyst replaced at a significant expense. Process technologies, such as moving bed and ebullated bed catalysts, which avoid shutdown by continuous addition of fresh catalyst are available but they can be expensive in capital and operating costs. Other processes have included the continuous addition of small amounts (< 5wt%) of finely dispersed catalysts and oil soluble catalyst precursors such as molybdenum naphthenate [1] to the heavy oil. The use of highly dispersed catalysts to upgrade heavy feeds has been recently reviewed by Del Bianco *et al.* [2]. The active catalysts are generally considered to be in a colloidal state and range in size from sub-micron to several microns. Typically, the concentration of catalyst on metal basis is 50 - 1000ppm but even at these concentrations they can be expensive to use. The ability to recycle the catalyst is important for the economics of the process especially if the metal catalyst is used in high concentrations (>100ppm).

Molybdenum is the basic constituent of the most active catalysts. The major source of molybdenum is the mineral molybdenite (crystalline molybdenum sulphide) which is roasted to produce molybdenum oxide, purified by dissolution in aqueous ammonia to produce ammonium heptamolybdate and separated by fraction crystallization. Thus, ammonium heptamolybdate is one of the cheapest sources of molybdenum. An active dispersed catalyst precursor produced from this material in a simple process could have low cost compared to oil soluble catalyst precursors.

EXPERIMENTAL

Catalyst Dispersion: An atomizing nozzle was used to sparge an aqueous solution of ammonium heptamolybdate into the heavy oil held in a stirred heated tank. The temperature and pressure of the aqueous solution and hydrocarbon were maintained such that the water was immediately vapourized during the injection. A nitrogen purge tube was inserted at the top of the tank to minimize air oxidation and to aid in removal of water vapour and ammonia liberated during the process. The degree of dispersion was

controlled by adjustments in the solution concentration and, the pressure and flow rate of the atomizing nozzle.

By varying the concentration of Mo in the aqueous solutions while maintaining similar injection conditions, it is possible to produce products with suspended particulates having the same total surface area but different mass percent concentrations. Thus, two feeds were produced with different Mo concentration but with the same calculated total surface area for ammonium heptamolybdate particles and by extension MoS_2 surface areas.

Materials: The feedstock (F-0) used was Cold Lake heavy oil (Table 1). The catalyst precursor was ammonium heptamolybdate, $(\text{NH}_4)_6\text{Mo}_7\text{O}_{24}\cdot 4\text{H}_2\text{O}$. This salt was dissolved in de-ionized distilled water to the desired concentration and then injected into the heavy oil. Two feeds, F-1 and F-2, were produced having Mo concentrations of 212 and 611ppm, respectively. The oil soluble catalyst used was molybdenum naphthenate obtained as a 6wt.% Mo solution in oil. The required amount was added to the heavy oil after dilution in 21g of a diluent (BP: 200-343°C).

Activity Testing: The feedstocks containing the dispersed catalysts were processed in a 2L semi-batch autoclave that was purged with N_2 , charged with approximately 750g of the feedstock and pressurized to 1000psig with H_2 at room temperature. In order to ensure sulphiding of the catalyst before hydrocracking conditions were reached, the autoclave system was modified to allow the injection of dimethyldisulphide (DMDS) at high pressure. The autoclave was heated to 350°C at which point the pressure was about 2000psig. The flow of H_2 commenced at 2L/min., was maintained for 30 minutes then stopped. DMDS was introduced from the bottom of the reactor and the system held at 350°C for 30 minutes without H_2 flow. Following this period, H_2 flow was restarted and increased to 6.0slpm as the temperature increased to 450°C. These final conditions were maintained for a fixed period and then the reaction was quenched in less than 5 minutes. A comparison test was also performed using molybdenum naphthenate as the catalyst precursor. Tests were also performed without this activation procedure and without addition of DMDS by heating straight to 450°C.

Vapour flow from the autoclave was passed through a series of three condensers, two held at 0°C and the third at -78°C. Dry gas (C_1 - C_3) passing through these condensers was accumulated in a tank. C_4 - C_5 product liquid was taken as the volatiles lost at atmospheric pressure and room temperature from the three condensers after let-down to sample collection bottles.

Asphaltene were determined by precipitation using n-pentane in a ratio of 40:1 with the oil. The 525°C+ pitch contents were determined by crude simulated distillation ASTM D5307.

RESULTS AND DISCUSSION

The results of autoclave tests are summarized in Table 2. The first three tests were carried out under identical conditions using the prepared feedstocks (Test-1 and -2) and the as-received heavy oil containing the oil soluble organometallic precursor (Test-3). In terms of coke and liquid yields, the catalyst formed from water-soluble precursor provided comparable performance to that from the oil soluble precursor. Slightly higher asphaltene and CCR conversions were obtained with the water soluble catalyst precursor.

Test -1 and -3 show that nearly identical product distributions can be obtained using similar Mo concentrations prepared from either water or oil soluble precursors. The small differences lie in the C_4 - C_5 and C_{6+} liquid yields. Asphaltene conversion was 10% higher in Test-1 using the water-soluble precursor compared to Test-3 with the oil soluble precursor. Thus, if the dispersion can be made high enough water-soluble catalyst precursors can be used in place of more expensive organometallic precursors.

The flexibility of the injection process to achieve a range of dispersions is illustrated by Test-1 and -2. In this case, the feedstocks F-1 and F-2 were prepared so that the calculated total surface area of the precursor per gram of oil was identical but the Mo

concentrations were different. Identical precursor and catalyst surface areas should exhibit the same activity. While the apparent catalyst activities were similar in Test-1 and -2, a slightly higher activity was exhibited in Test-2 which also had the higher Mo concentration. However, if feedstock F-2 was diluted with additional oil so as to make the Mo concentration similar to that of F-1, the lower activity per mass of Mo is evident in Test-4 where coke yield is higher while liquid yield and, CCR and asphaltene conversions, are lower than in Test-1.

As detailed in the experimental section, dimethyldisulphide (DMDS) was added to the feedstock in Tests 1-4 and a complex temperature program was used to ensure conversion of the catalyst precursor to the active MoS_2 phase. In Test-5, no DMDS was added and the feedstock was heated room temperature straight to 450°C . The results from Test-5 are almost identical to those from Test-2 and indicate that a complex sulphiding process is not required for proper catalyst activation.

Test-6 and -7a illustrate the performance of the catalyst at longer residence time and higher $525^\circ\text{C}+$ pitch conversion. Compared to Test-2, higher pitch conversions in Test-6 and -7a resulted in greater amounts of dry gas, naphtha and gas oil but solids increased from 0.5 to a maximum 0.8wt.% of feed. Liquid yield was reduced slightly at the highest conversion. In Test-6, the pitch conversion determined was 94.3%. This high value for pitch conversion is probably misleading and reflects the limitation of the crude simulated distillation. Based on the conversion in Table 2, the asphaltene content was 6.7wt.% whilst the $525^\circ\text{C}+$ pitch content was only 3.8wt.% and this is not reasonable. The true pitch conversion is probably between 78% and 90%.

Test-7a and -7b illustrate the performance of the catalyst in a simulated recycle operation. Following a run identical to that in Test-7a, the bottoms from this test were left in the autoclave and an additional amount of fresh oil equal to mass of liquid collected in the product condensers was added to the autoclave. The autoclave was then operated at the same conditions as before. The results for Test-7b presented in Table 2 represent the combined products from conversion of 290.33g of bottoms from Test-7a and 483.6g of fresh feed. As shown in Table 2, the amount of solids did not increase from Test-7a to Test-7b. Dry gas yield increased because of additional conversion of the recycled bottoms. This result suggests that this catalyst could be used effectively in a bottoms recycle process. This conclusion would have to be verified in a continuous true-recycle test.

The MoS_2 catalyst was found to be concentrated along with V and Ni in the product coke. The ash contents of the cokes listed in Table 2 varied from about 14wt.% to 33wt.% for runs using 212 and 611ppm Mo catalyst, respectively. Optical microscopy under cross-polarized light indicated that the coke in all cases except for Test-3 consisted of angular and rounded particles that possess a porous and isotropic matrix. The matrix was embedded with a varying amount of anisotropic mesospheres mostly 2 - 10 microns in diameter but occasionally larger. In the case of Test-3, the porous matrix showed an anisotropic (mosaic) texture and the mesospheres were larger, consisting of spheres approximately 30 microns in diameter.

Figure 1 shows the XRD spectrum of the coke produced in Test-2. The peak near $14^\circ 2\theta$ corresponds to scattering perpendicular to the (002) plane in hexagonal MoS_2 . Other MoS_2 peaks include 33.0° , 39.5° and 58.5° attributable to scattering from the (100), (103) and (110) planes [3]. The two sharp peaks at 31.7° and 45.5° are due to sodium chloride that was present in the as received oil. Using the Debye-Scherrer equation, the width of the peak near $14^\circ 2\theta$ can be used to calculate the average stacking height of the hexagonal layers. In this case it corresponds to an average layer height of 35\AA , i.e., 5.6 MoS_6 stacked layers. Daage and Chiannelli [4] have shown that the stacking height is related to catalyst hydrogenation activity and selectivity for hydrogenation compared to hydrodesulphurization. Scanning electron microscopy (SEM) showed that the MoS_2 crystallites are needle shaped and unencumbered with coke. The minor axis ranged from approx. 0.5 - 1.5 microns while the major axis varied from 5 to over 30 microns. The larger dimensions obtained by SEM compared to XRD indicate that the stacked layers

that make up the crystallite were highly folded and disordered. This was confirmed with the aid of transmission electron microscopy (TEM) and selected area diffraction. The needle-like crystals were observed to be composed of a collection of rods that are less than 100nm in diameter. The composition and structure of the particles were confirmed by analysis using energy dispersive x-ray (EDX) analysis and selected area diffraction. The diffraction patterns indicated that the MoS_2 was polycrystalline but had some preferred orientation.

CONCLUSIONS

It has been show that a water soluble catalyst precursor, ammonium heptamolybdate, can produce highly dispersed and active MoS_2 catalyst. The activity of these catalyst approaches that achieved by oil soluble catalysts which are reported to be highly dispersed even though the catalyst particles were larger than those from the oil soluble catalyst. TEM confirmed that these large catalyst particles (5-30 microns) were made up of smaller particles (0.1 microns). The catalyst maintained its activity in a simulated recycle test. The lower cost of the water soluble catalyst, its larger aggregate size and its activity relative to the oil soluble catalyst make it a potential candidate for upgrading processes which use highly dispersed catalyst and employ bottoms recycle.

ACKNOWLEDGEMENTS

This work was sponsored and wholly supported by the Alberta Department of Energy and the Alberta Research Council for which the authors are grateful.

REFERENCES

1. R. Bearden and C.L. Aldrige, Energy Prog. 1984, Vol. 1, 44.
2. A. Del Bianco, N. Panariti, S. Di Carlo, J. Elmouchnino, B. Fixari and P. Le Perchec, Appl. Catal. A, 94, 1 (1993).
3. N. Rueda, R. Bacaud and M. Vrinat, J. Catal. 1997, Vol.169, 404.
4. M. Daage and R.R. Chianelli, J. Catal. 1994, Vol. 149, 414.

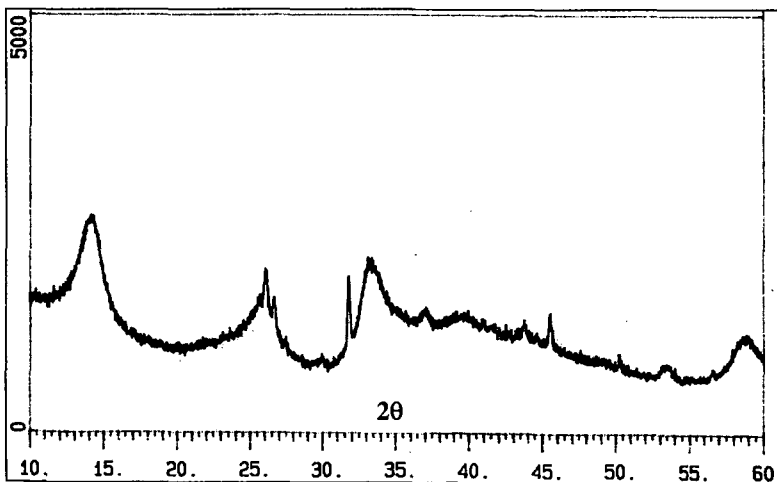


Figure 1. XRD of MoS_2 in coke from Test-2.

Table 1. Properties of Cold Lake heavy oil.

| | |
|-------------------------|-------|
| Carbon (wt.%) | 82.8 |
| Hydrogen (wt.%) | 10.4 |
| Nitrogen (wt.%) | 0.40 |
| Sulphur (wt.%) | 4.60 |
| Asphaltenes (wt.%) | 16.9 |
| CCR (wt.%) | 12.6 |
| H ₂ O (wt.%) | 1.54 |
| Nickel (ppm) | 66 |
| Vanadium (ppm) | 178 |
| °API Gravity | 10.7 |
| Viscosity @ 38°C (cP) | 8,675 |
| IBP – 200°C (wt.%) | 0 |
| 200 – 343°C (wt.%) | 10.7 |
| 343 – 525°C (wt.%) | 35.5 |
| 525°C+ (wt.%) | 53.8 |

Table 2. Results of autoclave activity tests.

| Test | 1 | 2 | 3 ^a | 4 | 5 | 6 | 7a | 7b |
|---|------|------|----------------|------|------|-------------------|------|-------------------|
| Feedstock | F-1 | F-2 | F-0 | F-2 | F-2 | F-2 | F-2 | F-2 ^c |
| Mo Concentration (ppm) | 212 | 611 | 200 | 200 | 611 | 611 | 611 | 611 |
| Residence Time (min.) | 45 | 45 | 45 | 45 | 45 | 90 | 70 | 70 |
| C ₆₊ Liquids (wt. % feed) | 87.5 | 90.4 | 89.3 | 86.7 | 89.5 | 86.5 | 88.2 | 89.8 |
| C ₄ –C ₅ Liquid (wt. % feed) | 5.6 | 4.6 | 4.4 | 4.5 | 4.3 | 3.8 | 4.0 | 1.6 |
| Dry Gas (wt. % feed) ^b | 4.6 | 4.2 | 4.7 | 5.3 | 3.7 | 5.9 | 4.8 | 6.7 |
| H ₂ S (wt.% feed) ^b | 2.4 | 2.3 | 2.1 | 2.2 | 1.9 | 2.3 | 2.0 | 1.9 |
| Solids (wt. % feed) | 0.7 | 0.5 | 0.9 | 2.1 | 0.6 | 0.8 | 0.5 | 0.5 |
| Ash (wt.% of solids) | 14.4 | 33.1 | 21.7 | 11.2 | 29.8 | 23.3 | 35.8 | 38.4 |
| Simulated Distillation of C₆₊ Liquids | | | | | | | | |
| IBP – 200°C (wt.%) | 21.4 | 17.5 | 20.0 | 21.0 | 18.8 | 33.0 | 22.5 | 20.0 |
| 200 – 343°C (wt.%) | 34.0 | 34.2 | 35.6 | 33.1 | 33.7 | 38.8 | 37.1 | 36.2 |
| 343 – 525°C (wt.%) | 26.7 | 28.4 | 26.0 | 20.5 | 27.4 | 24.3 | 25.9 | 28.3 |
| 525°C+ (wt.%) | 17.9 | 19.9 | 18.3 | 25.4 | 20.1 | 3.8 | 14.5 | 15.6 |
| Conversions (%) | | | | | | | | |
| Asphaltenes | 65.7 | 72.3 | 56.3 | 41.3 | 67.5 | 66.7 | 71.0 | 45.9 ^d |
| CCR | 58.8 | 63.4 | 52.5 | 53.0 | 61.8 | 56.6 | 75.4 | 54.3 ^d |
| 525°C+ | 73.5 | 69.3 | 69.6 | 60.3 | 69.3 | 94.3 ^e | 78.2 | 60.8 ^d |

a. Product yield corrected for 21.7g of added diluent (BP: 200-343°C)

b. Values for Tests 1 to 4 include CH₄ and H₂S products from 10.0g of dimethyldisulphide.

c. Includes a calculated 290.3g of reactor bottoms (containing coke and catalyst) from Test-7a and 483.6g of virgin oil.

d. Conversions based on composite composition of virgin oil and reactor bottoms used in Test-7b.

e. Determined by crude simulated distillation ASTM D5307. See text.

Activities of Molybdenum Based Dispersed Catalyst Precursors

X. Zhan, M. Dieterle, B. Demirel, E.N. Givens

Center for Applied Energy Research
University of Kentucky
2540 Research Park Dr.
Lexington, KY 40511-8410

Keyword: Molybdenum Catalyst, Coal Liquefaction

ABSTRACT

This paper discusses the activation of several Mo-based precursors for coal liquefaction, including various molybdate salts (ammonium, potassium, and nickel), phosphmolybdic acid, and an oil soluble Mo complex (Molyvan L). Except for nickel molybdate which was essentially inactive, the activities of the other precursors towards coal and resid conversions were basically the same. Presulfiding promoted the activity of ammonium molybdate but had almost no effect on the other precursors. The low activity of nickel molybdate is attributed to its stability under liquefaction conditions.

INTRODUCTION

Numerous molybdenum based compounds are readily converted to active dispersed catalysts for coal liquefaction and resid hydroprocessing. These include both inorganic and organic Mo based compounds. The oil soluble Mo precursors are usually dissolved in the reaction system and readily form highly dispersed catalysts. Alternatively, water soluble precursors are impregnated onto the feed coal. During reaction they decompose *in situ* to form an active phases.

Previous liquefaction work in this laboratory has shown that recycled Mo catalyst always gave higher coal and resid conversions than freshly added catalysts.¹ This conclusion was based upon recycled catalyst contained in ashy resid obtained from Wilsonville pilot plant when Wyodak coal was processed with Molyvan L catalyst. The higher activity of recycled Mo catalyst led to the speculation that activation was time dependent and the Mo based catalyst precursors had to experience a few cycles in a continuous process before it could be fully activated. Our recent studies have also indicated that, when sulfur-free ammonium heptamolybdate was used as precursor, complete transformation to active catalyst *in situ* did not occur.² However, coals impregnated with thiomolybdates were slightly more active than the oxomolybdates in the absence of added sulfur. We also found that presulfiding oxomolybdate impregnated coal quite significantly increased conversion.

Coal liquefaction using dispersed Mo based bimetallic catalysts has also been widely studied in laboratory-scale batch reactors. The promotional effects of Fe and Ni on Mo catalysts have been reported by a number of researchers using a variety of coals.^{3,4,5,6} Synergism was typically explained by the complementary effect of the metals or the formation of a new phase which was responsible for the high activity. However, recent pilot scale test have indicated that introducing Ni and Fe to a molybdenum impregnated coal does not influence conversion.⁷

Although inorganic molybdates have been widely used as catalyst precursors, most of the works has concentrated on ammonium based compounds because of their easy decomposition under liquefaction conditions. The objective of this study is to examine the effectiveness of other non-ammonium based molybdate precursors. Also, since some of these compounds contain more than one type of metal in the molecule, another objective is to examine if there is any advantage to using a compound containing two active metals.

EXPERIMENTAL

Materials Elemental analysis of the Black Thunder Wyodak coal are presented in Table 1. The as-received coal was impregnated with an aqueous solution containing various

concentrations of catalyst precursors at the level of 0.5 g solution/g coal. The concentration of the aqueous solution was varied so that desired Mo loadings on coal could be achieved. In all cases, the coal paste was dried at 125 Torr and 100 °C for two days to completely remove water. Solvent used in this study comprised mixtures of heavy distillate and deashed resid from Run 262e made at the Advanced Coal Liquefaction R&D Facilities at Wilsonville, AL. The properties of these materials, which were produced when the plant was operated with the same coal, are also summarized in Table 1. The following materials were used as received: Molyvan L (8.1% Mo, 6.4% P, R.T. Vanderbilt Co.), ammonium heptamolybdate (AHM, Aldrich), phosphomolybdic acid (PMA, Aldrich), potassium molybdate (KM, Alfa), nickel molybdate (NiM, Aldrich), and tetrahydrofuran (THF, Aldrich). In all experiments, catalyst loadings were reported as mg Mo per kg dry coal.

Catalyst Pretreatment In some experiments, the catalyst impregnated coal was treated with H₂ containing 8 vol% H₂S prior to reaction. In a typical run, the reactor was loaded with coal slurry and placed horizontally in a furnace after purging with H₂ to remove air. The pretreatment was conducted at 300 psig and a gas flowrate of 200 ml/min (STP). The furnace was heated to 120 °C and held for 30 min after which it was successively heated to 250 and 360 °C while holding for 30 minutes at each temperature. After pretreating at 360 °C, the reactor was cooled, vented and subjected to regular reaction procedures described in the following section.

Coal Liquefaction Reaction Procedures All of the experiments were conducted in a 65 ml microreactor which was agitated at 400 rpm in a fluidized sand bath (Techne, SBL-2D) maintained at 440 °C with an Omega CN4600 temperature controller. In every run, 3 g dry coal, 1.8 g heavy distillate, and 3.6 g deashed resid were added to the reactor which was then pressurized to 1000 psig at room temperature with H₂ containing 3 vol% H₂S. After 30 minutes reaction time, the reactor was removed and quenched in ice water. The liquid and solid products were scraped from the reactor using THF and subjected to Soxhlet extraction for 18 hours. The THF soluble material was distilled at 1 Torr and an atmospheric equivalent cut point of 566 °C according to ASTM method D-1160. This cut point corresponds to that used in the pilot plant where the solvent was generated. All experiments were replicated at least twice to assure the reproducibility.

THF coal conversion and resid conversion were defined below as a measure of catalyst activity on an maf coal basis.

$$\text{Coal Conv.} = 100 \times \left(1 - \frac{[IOM]_{\text{product}}}{\text{Coal}(\text{maf})} \right) \quad (1)$$

$$\text{Resid Conv.} = 100 \times \left(\frac{[\text{Coal}(\text{maf}) + \text{Resid}]_{\text{feed}} - [IOM + \text{Resid}]_{\text{product}}}{\text{Coal}(\text{maf})} \right) \quad (2)$$

RESULTS AND DISCUSSION

The liquefaction experiments using these catalyst precursors were performed at Mo loadings of 100 ppm and 300 ppm with/without H₂S/H₂ pretreatment. Figure 1 shows that at the Mo loading of 300 ppm without pretreatment, there is essentially no difference toward both coal and resid conversions for Molyvan L, AHM, PMA, and KM. The mean THF coal conversion of these four Mo precursors was 90.1±0.6% and mean resid conversion was 81.1±1.0%. For the Mo catalyst loading of 100 ppm as shown in Figures 2-3, the mean THF and resid conversions were 85.5±0.3% and 74.4±1.2%, respectively. The similar activities of these catalyst precursors, both the oil-soluble organic complex and water-soluble inorganic salts, may imply the formation of a similar active phase under liquefaction conditions. Considering the research work in this laboratory in the past years and those in open literatures, it is suggested that the formation of dispersed molybdenum catalyst is relatively independent of the starting material, as long as they decompose.

When the metal impregnated coal slurry was pretreated with H₂S/H₂, however, the

activities of these precursors varied. At Mo loading of 100 ppm with pretreatment, coal conversions with AHM and KM increased slightly while that with PMA decreased. For resid conversion, AHM gave about 9% increase but PMA decreased by 4%, in line with its performance for THF coal conversion. The behavior of PMA in this study is consistent with the observation when this material was presulfided separately and then impregnated on coal.⁸ Overall, it appears that pretreatment with H₂S improves the activity of AHM for resid conversion, does not affect the activity of KM, and slightly reduces the activity of PMA for both coal and resid conversions.

The major difference between KM, AHM and PMA is the presence of an ammonium group in AHM. As already noted, the catalyst precursors can not be fully activated *in situ* during a 30 minutes batch liquefaction run. Only a fraction of the precursors are converted to an active phase. Thus, the differences in activities between precursors may not be distinguishable. When these precursors are subjected to pretreatment, AHM is converted to an active phase through loss of the ammonium group. Thus, AHM exhibited higher activity than the other two precursors. Of course, over a longer period of exposure, such as that in a continuous process with catalyst recycle, most of the precursor would have converted to an active phase. As a result, these precursors show similar activities, although their activation kinetics may be different. The pilot plant test results indicated essentially no activity difference between AHM and PMA precursors.⁷

An interesting observation was that NiM improved coal conversion by less than 5% and resid conversion by less than 3% at all conditions tested. The low activity of NiM can be attributed to its stability under liquefaction conditions. TG analysis of NiM showed that this material is very stable in He at temperatures up to 600 °C. In H₂S/H₂/He containing 5 vol% H₂S, there was a 1.5% weight gain at 450 °C indicating insignificant addition of sulfur, which is necessary to create an active catalyst phase. Unlike other Mo-based precursors, NiM is not readily converted to nickel and molybdenum sulfides that are active toward coal liquefaction. Therefore, NiM showed almost no advantage over thermal runs. In contrast, AHM and PMA have both been reported to form active phases^{8,9} and showed high activities for both coal and resid conversions.

CONCLUSIONS

The inorganic and organic molybdenum compounds tested in this study showed essentially the same activities towards coal liquefaction and resid conversion. The nature of catalyst precursors is different and their activation mechanism may vary. In batch reactors which are typical of short reaction time, these precursors may exhibit different activities. It is expected, however, that in a continuous process with Mo catalyst recycle, the catalyst activity will be independent on precursor type as long as they decompose under liquefaction conditions. The low activity of nickel molybdate is probably due to its stability under liquefaction conditions.

ACKNOWLEDGMENTS

This research project was supported by the U.S. Depart of Energy under contract number of DE-AC22-91PC91040.

REFERENCES

1. Rantell, T., Anderson, R., and Givens, E.N., *Prepr.-Am. Chem. So., Div. Fuel Chem.*, 1996, 41(3), 993-997
2. Zhan, X., Dieterle, M., Lucas, A., Van Woert, H.C., and Givens, E.N., *Prepr.-Am. Chem. So., Div. Fuel Chem.*, 1998, 43(2), 320-324
3. Garg, D., and Givens, E.N., *Prepr.-Am. Chem. So., Div. Fuel Chem.*, 1983, 28(5), 200-209
4. Hulston, C.K.J., Redlich, P.J., Jackson, W.R., Larkins, F.P., and Marshall, M., *Fuel*, 1996, 75(12), 1387-1392
5. Derbyshire, F., Davis, A., Schobert, H., and Stansberry, P., *Prepr.-Am. Chem. So., Div. Fuel Chem.*, 1990, 35(1), 51-60

6. Zhan, X, Shabel, M., Cash, R., and Givens, E.N., *Prepr.-Am. Chem. So., Div. Petro. Chem.*, 1997, 42(3), 639-642
7. Givens, E.N. et al. "Bench-scale Testing of Advanced Concepts for Direct Coal Liquefaction: Evaluation of Dispersed Mo Catalysts." Paper presented to the Pittsburgh Energy Technology Coal Liquefaction and Solids Fuel Contractor's Review Conference, Pittsburgh, PA, Sept. 3-4, 1997.
8. Belma, D., and Givens, E.N. *Prepr.-Am. Chem. So., Div. Fuel Chem.*, 1998, 43(2), 325-329
9. Lopez, J., and Pasek, E.A., "Process for Preparing Heavy Oil Hydroprocessing Slurry Catalyst", *US Patent 4,710,486*, 1987.

| Table 1. Properties of Wyodak Coal and Feed Solvent | | | |
|---|-------------------|------------------|---------------|
| | Coal | Solvent | |
| | Ultimate Analysis | Heavy Distillate | Deashed Resid |
| <566°C | - | 96.9 | 14.7 |
| Composition (wt%) | | | |
| Carbon | 70.62 | 88.86 | 89.79 |
| Hydrogen | 5.03 | 9.91 | 7.26 |
| Nitrogen | 1.13 | 0.44 | 0.86 |
| Sulfur | 0.52 | <0.03 | 0.03 |
| Oxygen (diff) | 16.38 | 0.79 | 1.33 |
| Ash | 6.32 | | 0.73 |
| Ash, SO ₃ -free | 5.46 | | |

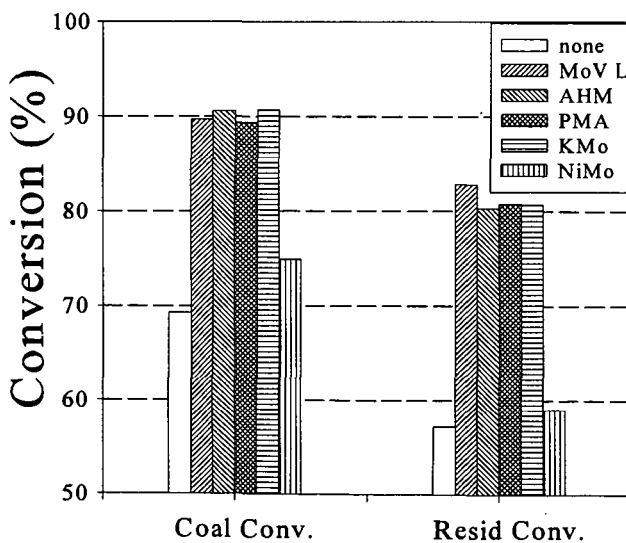


Figure 1 Effect of Various Mo Based Catalyst Precursors on THF Coal and Resid Conversions with Mo Loading of 300 ppm.

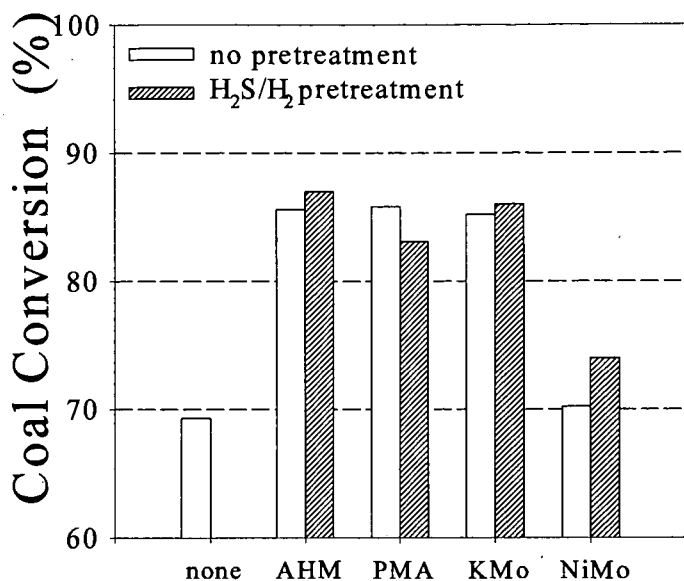


Figure 2 Effect of H₂S/H₂ Pretreatment on THF Coal Conversion with Mo Loading of 100 ppm

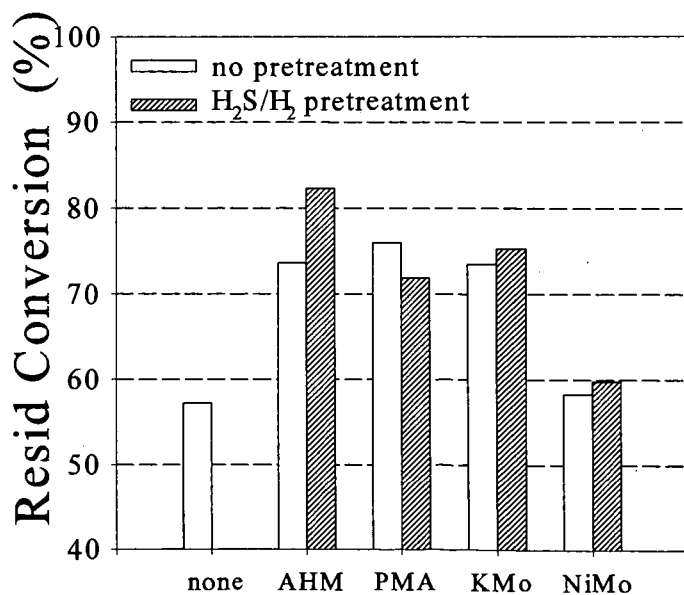


Figure 3 Effect of H₂S/H₂ Pretreatment on Resid Conversion with Mo Loading of 100 ppm

BIOPROCESSING OF CRUDE OILS AND DESULFURIZATION USING ELECTRO-SPRAY REACTORS

Eric N. Kaufman^{*} and Abhijeet P. Borole
Bioprocessing Research and Development Center
Chemical Technology Division, Oak Ridge National Laboratory^{*}
Oak Ridge, Tennessee, USA 37831-6226

"The submitted manuscript has been authored by a contractor of the U.S. Government under contract DE-AC05-96OR22464. Accordingly, the U.S. Government retains a nonexclusive, royalty-free license to publish or reproduce the published form of this contribution, or allow others to do so, for U.S. Government purposes."

ABSTRACT

Biological removal of organic sulfur from petroleum feedstocks offers an attractive alternative to conventional thermochemical treatment due to the mild operating conditions afforded by the biocatalyst. Electro-spray bioreactors were investigated for use in desulfurization due to their reported operational cost savings relative to mechanically agitated reactors and their capability of forming emulsions $<5\ \mu\text{m}$. Here, the rates dibenzothiophene (DBT) oxidation to 2-hydroxybiphenyl (2-HBP) in hexadecane, by *Rhodococcus* sp. IGTS8 are compared in the two reactor systems. Desulfurization rates ranged from 1.0 and 5.0 mg 2-HBP/(dry g cells-h), independent of the reactor employed. The batch stirred reactor was capable of forming a very fine emulsion in the presence of the biocatalyst IGTS8, similar to that formed in the electro-spray reactors, presumably due to the fact that the biocatalyst produces its own surfactant. While electro-spray reactors did not prove to be advantageous for the IGTS8 desulfurization system, it may prove advantageous for systems which do not produce surface-active bioagents in addition to being mass transport limited.

KEY WORDS: oil desulfurization, *Rhodococcus*, electrostatic spraying, dibenzothiophene, biodesulfurization

INTRODUCTION

Biological refining of fossil fuel feedstocks offers an attractive alternative to conventional thermochemical treatment due to the mild operating conditions and greater reaction specificity afforded by the nature of biocatalysis. Efforts in microbial screening and development have identified microorganisms capable of petroleum desulfurization (see for example [1-12]), denitrification [6], demetalization [6], cracking [6, 13] and dewaxing. Further investigation and manipulation of enzymatic pathways responsible for these reactions [4, 14-17] has led to processes which are approaching commercial application, particularly in the area of biological desulfurization [7, 18]. Biological desulfurization of petroleum may occur either oxidatively (see for example [3, 5, 8, 9, 12, 17, 19-21]), or reductively [2, 22-24]. In the oxidative approach, organic sulfur is converted to sulfate and may be removed in process water. This route is attractive due to the fact that it would not require further processing of the sulfur and may be amenable for use at the well head where process water may then be reinjected. In the reductive desulfurization scheme, organic sulfur is converted into hydrogen sulfide which may then be catalytically converted into elemental sulfur, an approach of utility at the refinery. A sampling of desulfurization rates achieved with oxidative and reductive microorganisms have been summarized in [25]. Regardless of the mode of biodesulfurization, key factors affecting the economic viability of such processes are biocatalyst activity and cost, differential in product selling price, sale or disposal of co-products or wastes from the treatment process, and the capital and operating costs of unit operations in the treatment scheme.

The selection of the petroleum feedstock in biodesulfurization will play a large role in the overall economic viability of the process. Biodesulfurization may be utilized as a pretreatment to crude oil before entering pipelines, may be applied as an alternative to hydrotreating the crude at the refinery, or may be applied in the polishing of refinery products such as diesel or gasoline. The particular application will determine the extent of desulfurization necessary and hence the treatment cost per barrel. At the wellhead, a biodesulfurization unit may be used to treat marginally sour crudes (0.6 - 0.7% S) converting them to sweet crudes ($<0.5\%$ S) and claiming the price differential in sweet versus sour crude in segregated pipeline systems (currently, the premium for sweet crude is $\sim \$1/\text{Bbl}$). For this application, the extent of desired desulfurization is quite low and this may serve as an attractive initial niche for biodesulfurization. When utilized for refinery applications, the biodesulfurization process must compete

^{*}Research supported by the Office of Oil and Gas Processing, U.S. Department of Energy under contract DE-AC05-96OR22464 with Lockheed Martin Energy Research Corp.

with conventional hydrotreating. Here the economic viability of biorefining will be based upon its competitiveness relative to the catalyst replacement, hydrogen, and octane penalty costs associated with hydrotreating.

While significant activity is progressing in the engineering and chemical modification of enzymes so that they may function in purely organic solutions [26-28], inherent to all of the current bioprocessing of fossil feedstocks schemes is the need to contact a biocatalyst containing aqueous phase with an immiscible or partially miscible organic substrate. Factors such as liquid / liquid and gas / liquid mass transport, amenability for continuous operation and high throughput, capital and operating costs, as well as ability for biocatalyst recovery and emulsion breaking are significant issues in the selection of a reactor for aqueous / organic contacting. Traditionally, impeller-based stirred reactors are utilized for such mixing due to their ease of operation and wide acceptance in the chemical and biological processing industries. Such mechanically stirred reactors contact the aqueous and organic phases by imparting energy to the entire bulk solution, i.e. the impeller must move the contents of the reactor. Energy input in the stirred reactor is a function of the phase ratio, oil viscosity, density, reactor size, impeller speed, etc. [29]. Typically, impeller based reactors are capable of achieving water or oil droplet sizes of 100 -300 μm in diameter when surfactants are not present [25] and require on the order of 1-6 W/L to do so based upon empirical correlation's [29]. It is estimated that if impeller based systems were capable of producing 5 μm droplets, it would require ~25 kW/L [30] if surfactants are not present. Furthermore, no capacity exists for biocatalyst separation or emulsion breakage within the reactor.

Alternative processing schemes [18] propose the use of "motionless mixers", in which the two phases are pumped over a reversing helical coil which creates turbulent eddies. While this method reduces the number of moving parts in the reactor, it does not reduce power requirements since costs are transferred from the impeller to the pumps required to move the liquids past the coil. Liquid velocities greater than 4 m/s are required to form emulsions (~10 μm) and one can not form emulsions in coil tubes greater than 3 mm in diameter [31]. For tubes greater than 10 cm in diameter one can not form droplets smaller than 1 mm. Like the stirred reactor, no capacity exists for emulsion breaking within the motionless mixer.

Recent advances in the area of contactors for solvent extraction have lead to the development of electrically driven emulsion phase contactors (EPCTM) for efficient contact of immiscible phases [32-37]. In this concept, the differing electrical conductivity between the aqueous and organic phases causes electrical forces to be focused at the liquid / liquid interface, creating tremendous shear force (see for example [38]). This shear causes the conductive phase to be dispersed (5 μm droplet size - [30]) into the non-conductive phase, but does so with decreased energy requirements relative to mechanical agitators due to the fact that energy is imparted only at the liquid / liquid interface and not the entire bulk solution. Electrostatic crude oil desalters have been operated for several years [39]. More recently, devices based upon the EPCTM have been used commercially to water wash methyl tert-butyl ether feedstocks (with greater than 10-fold reduction in stage height [40]) and for organic extraction from aqueous analytical samples [41]. Energy consumption on a volumetric basis has been measured to be 2.4 W/L for a 30% tributyl phosphate / 70% dodecane / distilled water system, four orders of magnitude less than mechanical systems creating as fine an emulsion [30, 36].

The configuration of the EPCTM developed at the Oak Ridge National Laboratory is shown in Figure 1 where the contactor serves to disperse a liquid with a greater density than the continuous phase. The reactor employs two different types of electrode regions in order to increase liquid throughput. The first, termed the "nozzle region", provides a high capacity droplet dispersion by providing an electric field with a significant vertical component. This vertical field creates the dispersion at the nozzle entrance and accelerates it into the continuous phase. A second region termed the "operating channel" employs parallel plates carrying a modulated dc offset with high voltage spikes. This signal creates an oscillating horizontal electrical field which controls the residence time of the dispersed phase and serves to continuously coalesce and redisperse the droplets as they progress in a serpentine manner through the reactor. At the base of the reactor, an electrical field exists between the electrified central plate and the grounded aqueous phase, which accelerates the aqueous droplets to the organic / aqueous interface. In this manner, droplet coalescence and hence separation on the interface is enhanced. The EPCTM creates droplets of water containing biocatalyst ~5 μm in diameter within an organic phase, and does so with a power requirement of 3 W/L [25].

With the success the EPCTM has exhibited in the area of solvent extraction, it was proposed that it could be an efficient reactor system for aqueous / oil contacting in biorefining [42]. In our previous work [25], we characterized the emulsion quality and power requirements of the EPCTM, and demonstrated that there was no detrimental effect on the cells due to the electric fields. Here, we compare the performance of the EPCTM to that of a batch stirred reactor (BSR), investigate the required level of biocatalyst activity before the surface area afforded by the EPCTM becomes a factor in reactor performance, and characterize the emulsion formed by both reactors in the presence of bacteria.

MATERIALS AND METHODS

Biocatalyst and solvent systems

The oxidation of dibenzothiophene (DBT) in hexadecane was studied to investigate reactor design and performance in an easily tractable chemical system. *Rhodococcus sp.* wild strain IGTS8 (ATCC 53968) was provided by Energy BioSystems Corp. and served as the biocatalyst. The sequence of DBT oxidation by IGTS8 is shown in Figure 2, (Kilbane, 1989) and detailed enzymatic steps in the pathway are discussed in [17]. Cells were supplied as a frozen paste and had a cell dry weight of 0.28 g/g of original frozen material. The aqueous phase in all experiments consisted of 0.156M, pH 7.5 potassium phosphate buffer. DBT (Aldrich, D3,220-2), dissolved in n-hexadecane (Aldrich, H670-3), served as the organic phase, with typical initial DBT concentrations being 0.6 wt.%.

Analytical

Liquid samples collected from the reactors were centrifuged at 14,000 RPM for 5 minutes to separate the aqueous phase and cell debris. DBT and 2-hydroxybiphenyl (2-HBP) concentrations in n-hexadecane were measured by gas chromatography using a Hewlett Packard 5890 gas chromatograph equipped with a flame ionization detector. A 1 μ L sample was injected onto a 15 m DB-1 column (J&W Scientific, catalog number 125-1012) which was used with a helium carrier flow of 10 mL/min. The temperature program was 150°C for 1 min followed by an initial ramp rate of 5°C/min up to 200°C and a final ramp rate of 25°C/min to a final temperature of 280°C. The column was calibrated with DBT and 2-HBP (Aldrich, #24,021-4) standards. The injector was operated at 250°C and the detector was operated at 300°C. In the experiments reported here, DBT and 2-HBP concentrations in the aqueous phase were below our levels of detection. Hence only concentrations in the organic phase are reported.

Batch stirred reactor experiments

Experiments conducted in batch stirred reactors (BSR) typically utilized 50 g of frozen *Rhodococcus sp.* wild type strain IGTS8 (ATCC 53968) cell paste which were brought up to 750 mL with 0.156M (pH 7.5) phosphate buffer (1X cell density) and added to 250 mL of 0.6wt% DBT in n-hexadecane. The reactor vessel was a 1-L VirTis Omni-Culture fermentor (model 178657, Gardiner, NY), utilizing a 6-bladed Rushton-type impeller with 2 baffles. The impeller was mounted on the shaft 0.5 inches from the aerator and 2 inches from the bottom of the vessel. The reactor was kept at 30°C, agitated at 800 RPM, and aerated with either room air or pure oxygen at a rates of either 0.2 or 1.0 SLPM. Specific aeration procedures are noted in the text. To collect samples, agitation and aeration were ceased for 5 min to allow the aqueous and organic phases to separate. A 1.5 mL sample from the top of the organic phase was then taken for analysis.

Mass transport experiments were conducted in the BSR to determine if the desulfurization process was liquid-liquid (l-l) or gas-liquid (g-l) mass transfer limited. The mass transport experiments were conducted as above except that aeration was performed using 1/4 " stainless steel tubing rather than the aerator supplied by the manufacturer. Unlike the previous experiments, the mass transport experiments were organic continuous as 250 mL of aqueous phase was dispersed into 750 mL of hexadecane containing 0.6wt% DBT. Five batch stirred reactors were run simultaneously with different quantities of *Rhodococcus sp.* wild type strain IGTS8 (ATCC 53968) cell paste added to each reactor. Using a 250 mL basis for the aqueous phase, the quantities of frozen biocatalyst added to the 0.156 M (pH 7.5) phosphate buffer in each reactor were 8.3, 16.7, 83.3, 166.7, and 250 g respectively. The cell density corresponding to 16.7 g frozen biocatalyst in 250 mL aqueous phase was considered as 1X cell concentration. Thus, the cell density was varied from 0.5X to 15X in this experiment. To collect samples, agitation and aeration were ceased for 5 min to allow the aqueous and organic phases to separate. A 1.5 mL sample was taken from the top of the organic phase in each reactor every hour for 10 h, and again at 24 h into the experiment.

Gas - liquid mass transport experiments were conducted using air and oxygen at 0.2 and 1.0 slpm. In order to determine whether or not an oxygen mass transport limitation was a factor in the experiments using different cell densities, two batch stirred reactors were run at 800 RPM, 30°C, containing 750 mL hexadecane with 0.6 wt.% DBT, 166.7 g biocatalyst (10X cell density) in 250 mL of phosphate buffer. The aeration rate was 1.0 slpm of room air for the control condition, and 1.0 slpm pure oxygen in the experimental condition. Samples were collected every hour for 8 h using the procedure described above.

EPC™ experiments

The design and operation of the EPCTM utilized in these experiments are adaptations of those described by Scott *et al.* [36]. A schematic of EPCTM operation is shown in Figure 3. The Teflon body of the EPCTM measured 10 cm x 10 cm x 61 cm. The front and rear plates were made of clear Lexan, allowing for visual inspection of reactor operation. A thin sheet of Teflon was placed between the body and the front and rear plates to prevent wetting and current leakage to the Lexan. Three stainless steel electrodes, placed parallel to each other, measured 30 cm x 6 cm. The center electrode was charged, while the two outer electrodes were grounded. This adaptation to the original EPCTM design was found to minimize biomass fouling of the reactor. The center electrode was connected to the high-voltage electric supply through a supporting steel rod to avoid disturbance of electrostatic-spraying in the nozzle region. High-voltage (up to 40 kV) was generated using a pulsed DC power supply and automobile ignition parts. A power supply (Hewlett Packard 6653A, Avondale, PA) and two sweep/function generators (BK Precision 3030, Chicago, IL) were used to produce the signal which was then passed through an ignition coil (Mallory Promaster 29901, Carson City, NV) to step up the signal. In order to prevent discharge of the electrodes through the circuit, a high-voltage diode (Collmer Semiconductor CS4107X30, Dallas, TX) was placed between the coil and the EPCTM. From the diode, the positively charged terminal was connected to the rings surrounding the capillary tubes, and the negative lead was attached to the center electrode. The charged rings created an initial dispersion of biocatalyst as the aqueous phase emerged from the capillary tubes. The parallel electrodes lower in the reactor enhanced droplet dispersion as the more dense aqueous phase descended to the bottom of the reactor.

In EPCTM experiments, the organic liquid served as the continuous phase into which an aqueous biocatalyst was dispersed. The organic phase consisted of 2,400 mL n-hexadecane containing 0.6 wt.% dibenzothiophene. The temperature of the organic phase was controlled at 30°C by pumping the liquid from the top of the EPCTM, through a stainless steel coil submerged in a heated bath, and then returning the hexadecane to the bottom of the EPCTM. Typically, biocatalyst (26.7 g of frozen cell paste was brought to a volume of 100 mL with potassium phosphate buffer) was recirculated through the reactor at 5.0 mL/min using a peristaltic pump. The cell density with respect to the amount of aqueous phase used in these EPCTM experiments corresponded to a 4X concentration. A higher cell density was used in the EPCTM as compared to the BSR experiments due to the lower aqueous:organic phase ratio in the EPCTM and to enable DBT conversion significant enough to be observed by the analytical procedure employed. Aqueous phase containing the biocatalyst was sprayed into the reactor at the nozzle region, was continuously coalesced and redispersed in the operating region, and coalesced at the base of the EPCTM. To better aerate, sample, and control the aqueous phase, it was circulated from the reactor base to an external reservoir at a rate of 5.0 mL/min. The external container allowed for temperature control, pH and O₂ measurement, agitation, and aeration of the biocatalyst. The liquid was then returned to the top of the reactor through two 1.6-mm-OD, 1-mm-ID capillary tubes (U-140, Upchurch Scientific, Oak Harbor, WA) where it was again sprayed into the hexadecane. A water bath controlled the temperature of the jacketed aqueous reservoir at 30°C. The pH was monitored throughout the experiment, and remained in the pH range of 7.0 to 7.5. Agitation of the aqueous reservoir from a magnetic stirrer and room air aeration through a diffuser at 20 mL/min permitted more favorable conditions for the biocatalyst than did the long residence time at the bottom of the EPCTM, a location which lacked both aeration and agitation. In order to help alleviate possible oxygen deficiency inside the reactor, another diffuser was introduced 3 cm from the bottom of the EPCTM at airflow rate of 36 mL/min. Samples from the EPCTM were drawn hourly for twelve hours through a 2m x 3.175mm Teflon tube placed 10cm through the top of the reactor against a sidewall. Using a 30mL glass-bodied syringe, the tubing was flushed with liquid from the EPCTM three times before a 1.5mL sample was drawn. Samples were centrifuged as described above. Due to the small amount of 2-HBP production in the EPCTM, and hence greater associated error in GC analysis, samples were run in triplicate.

In experiments to determine possible mass transport limitations in the EPCTM, 66.7 g of frozen cell paste was brought to 100 mL with potassium phosphate buffer (10X cell density) and used as the aqueous phase. In order to evaluate if oxygen mass transfer was a limiting factor, the aqueous reservoir used for recirculating the aqueous phase was sparged with pure oxygen at a flow rate of 50 mL/min. This experiment was also conducted at a 10X cell density.

RESULTS AND DISCUSSION

2-HBP production in the EPCTM and BSR

Desulfurization activity of the *Rhodococcus sp.* in both reactors was typically between 1 and 5 mg 2-HBP produced per dry g of biocatalyst per hour. Rates of 2-HBP production in the two reactor systems were within experimental variance and no appreciable difference in desulfurization rates were seen between the two reactors. Note that in the experiments reported here, the only available carbon and energy source for the biocatalyst other than what may be carried over in the frozen cell paste, was

hexadecane and DBT. Other studies (outlined in [25]) have utilized additional external carbon and energy sources and have reported higher activities with *Rhodococcus* sp. Due to the high surface area reported in the EPCTM [25], higher rates were expected in the EPCTM, however, similar performance was observed in both reactors. Experiments were conducted with higher cell densities to determine at what point the BSR becomes mass transfer limited and the high surface area afforded by the EPCTM would become beneficial.

Mass transport limitations

Results of the DBT desulfurization experiments conducted at varying cell densities in BSR's are given in Figure 4. The rate of desulfurization, when normalized with respect to cell mass, was found to decrease with increasing cell density indicating that mass transfer resistance was the controlling process in desulfurization. A statistical analysis of the data was conducted using the analysis of variance (ANOVA) test and the t-test (Table 1). Based on a 95% confidence interval, a significant difference in the rates of HBP production was observed between 5X and 10X cell density BSR's. This suggests that the desulfurization process becomes mass transfer limited at a cell density of 10X. The mass transfer limitation may be due to gas-liquid or liquid-liquid mass transport resistance.

The results of experiments conducted in the BSR at 10X cell density to evaluate possible gas-liquid mass transfer limitations are given in Figure 5. Increasing the rate of air supply or increasing the oxygen tension in the reactor through the use of pure oxygen rather than air was not seen to affect HBP production. It was determined that oxygen mass transfer was not the limiting factor in the desulfurization of DBT even at 10X cell density. This suggests that the system may be limited by liquid-liquid mass transfer. Since the EPCTM reportedly provides larger liquid-liquid interfacial area, the BSR was compared with the EPCTM for desulfurization activity at equal cell density.

EPCTM vs BSR at 10X cell density

Comparison of the EPCTM and BSR at 10X cell density is given in Figure 6. As shown, no difference was observed in the desulfurization rates between the two reactors. Thus, either the system is not truly mass transport limited or the EPCTM does not provide a larger surface area for reaction under the present conditions.

Emulsion characterization

To determine whether the EPCTM offers larger surface area than BSR, samples were collected from the reactors and observed under a microscope using a 100x oil emersion objective. Due to the opaqueness rendered by high cell densities employed, observations could not be made *in situ* during reactor operation. Samples collected during the run were immediately mounted on a slide and observed under a microscope. In addition to sampling conducted during a run, samples were also collected at the end of a run from a cuff layer formed after gravity settling of the aqueous and organic phases. The cuff layer (which was previously characterized as being 92.7% hexadecane) was observed to contain a major portion of the biocatalyst. In addition, a significant amount of the biocatalyst was extracted and existed in the organic phase. Microscopic examination of samples from the cuff layer of the BSR showed a very fine emulsion with droplet sizes ranging from 1 to 10 μm . A similar cuff layer was also formed during EPCTM experiments. Average droplet size for EPCTM and BSR samples collected at 4 hours during normal operation were $2.54 \pm 2.40 \mu\text{m}$ and $3.08 \pm 1.78 \mu\text{m}$, respectively ($n > 300$). Figure 7 shows a micrograph of the emulsion obtained in an EPC. Thus, a very fine emulsion is formed in the EPCTM as well as the BSR, and it appears that it is for this reason that an augmentation in desulfurization rate is not seen in the EPCTM relative to the BSR. Formation of such an emulsion in the BSR may be presumed due to production of biosurfactants by the biocatalyst IGTS8. Other *Rhodococcus* sp. have been previously reported to produce glycolipids in the presence of hexadecane as well as some crude oils [43]. Earlier characterization of droplet size in a BSR [25] was performed either with no biocatalyst present, or with an extremely small amount to allow *in situ* observation of the droplets in the reactor. Our previous work revealed a decrease in droplet size from 210 to 118 μm when adding just 5 g of cells in 750 mL aqueous phase. Thus, the emulsion characterization reported here (with 67 g of cells in 250 mL aqueous phase) is in no way contradictory to our previous reports. Preliminary experiments varying the concentration of DBT ten-fold did not affect the rate of desulfurization, indicating that the aqueous side liquid mass transfer may be controlling.

CONCLUSIONS

The performance of EPCTM was similar to BSR for desulfurization of a model system containing DBT in hexadecane treated with biocatalyst *Rhodococcus rhodochrous* IGTS8. The system was not limited by

gas-liquid oxygen mass transfer at high cell densities (10X). The equal desulfurization rates in two reactors were due to almost equal interfacial area and the high degree of cell extraction into the organic phase. Higher interfacial area than normally expected in mechanically stirred reactors were realized in BSR, presumably due to formation of surfactants by the biocatalyst present. While EPC™ did not prove to be advantageous for the IGTS8 desulfurization system in terms of rates of desulfurization, it may prove advantageous for electro-static emulsion breaking, in reducing power requirements for mixing, and for creating large amounts of surface area for systems that do not produce surface active bioagents.

ACKNOWLEDGMENTS

This work was supported by the Office of Oil & Gas Processing, U.S. Department of Energy under contract DE-AC05-96OR22464 with Lockheed Martin Energy Research Corp. The authors acknowledge the material contributions of Energy BioSystems Corp., and the technical assistance of Drs. Punjai Selvaraj and Costas Tsouris at the Oak Ridge National Laboratory.

REFERENCES

1. Constanti, M., Giralt, J. and Bordons, A., "Desulfurization of dibenzothiophene by bacteria," *World Journal of Microbiology and Biotechnology*, **10**, 510-516 (1994).
2. Finnerty, W.R., "Organic sulfur desulfurization in non-aqueous media," *Fuel*, **72**, 1631-1634 (1993).
3. Kayser, K.J., Bielaga-Jones, B.A., Jackowski, K., Odusan, O. and Kilbane, J.J., "Utilization of organosulfur compounds by axenic and mixed cultures of *Rhodococcus rhodochrous* IGTS8," *Journal of General Microbiology*, **139**, 3123-3129 (1993).
4. Kim, T.S., Kim, H.Y. and Kim, B.H., "Petroleum desulfurization by desulfovibrio desulfuricans m6 using electrochemically supplied reducing equivalent," *Biotechnology Letters*, **12**, 757-760 (1990).
5. Lee, M.K., J.D., S. and Grossman, M.J., "Sulfur-specific microbial desulfurization of sterically hindered analogs of dibenzothiophene," *Applied and Environmental Microbiology*, **61**, 4362-4366 (1995).
6. Lin, M.S., Premuzic, E.T., Yablon, J.H. and Zhou, W.M., "Biochemical processing of heavy oils and residuum," *Applied Biochemistry and Biotechnology*, **57/58**, 659-664 (1996).
7. Monticello, D.J., "Biocatalytic desulfurization," *Hydrocarbon Processing*, **February 1994**, 39-45 (1994).
8. Ohshiro, T., Hine, Y. and Izumi, Y., "Enzymatic desulfurization of dibenzothiophene by a cell free system of *Rhodococcus erythropolis* D-1," *FEMS Microbiology Letters*, **118**, 341-344 (1994).
9. Ohshiro, T., Hirata, T. and Izumi, "Microbial desulfurization of dibenzothiophene in the presence of hydrocarbon," *Appl. Microbiol. Biotechnol.*, **44**, 249-252 (1995).
10. Shennan, J.L., "Microbial attack on sulfur-containing hydrocarbons: Implications for the desulfurization of oils and coals," *J. Chem. Tech. Biotechnol.*, **67**, 109-123 (1996).
11. Sorokin, D.Y., "Biological oxidation of sulfur atoms in C1-sulfur and other organosulfur compounds," *Microbiology (NY)*, **62**, 575-581 (1993).
12. Wang, P. and Krawiec, S., "Desulfurization of dibenzothiophene to 2-hydroxybiphenyl by some newly isolated bacterial strains," *Arch. Microbiol.*, **161**, 266-271 (1994).
13. Premuzic, E.T., Lin, M.S., Jin, J.Z., Manowitz, B. and Racaniello, L., *Biochemical Alteration of Crude Oils in Microbial Enhanced Oil Recovery*, in *Biohydrometallurgical Technologies*, Torma, A.E., Apel, M.L. and Briarley, C.L., Editors. 1993, The Minerals, Metals, and Materials Society. p. 401-413.
14. Denome, S.A., Oldfield, C., Nash, L.J. and Young, K.D., "Characterization of the desulfurization genes from *Rhodococcus* sp. strain IGTS8," *Journal of Bacteriology*, **176**, 6707-6716 (1994).
15. Ohshiro, T., Kanbayashi, Y., Hine, Y. and Izumi, Y., "Involvement of Flavin coenzyme in dibenzothiophene degrading enzyme system from *Rhodococcus erythropolis* D-1," *Biosci. Biotech. Biochem.*, **59**, 1349-1351 (1995).
16. Vazquez-Duhal, R., Westlake, D.W.S. and Fedorak, P.M., "Cytochrome *c* as a biocatalyst for the oxidation of thiophenes and organosulfides," *Enzyme Microb. Technol.*, **15**, 494-499 (1993).
17. Gray, K.A., Pogrebinsky, O.S., Mrachko, G.T., Xi, L., Monticello, D.J. and Squires, C., "Molecular mechanisms of biocatalytic desulfurization of fossil fuels," *Nature Biotechnology*, **14**, 1705-1709 (1996).
18. Dounias, G.A. and Stavropoulos, K.D., *Economic Feasibility of Biochemically Upgrading Heavy Crudes*, . 1995, Brookhaven National Laboratory.
19. Kilbane, J.J. and Bielaga, B.A., "Toward sulfur-free fuels," *CHEMTECH*, **december**, 747-751 (1990).
20. Olson, E.S., Stanley, D.C. and Gallagher, J.R., "Characterization of intermediates in the microbial desulfurization of dibenzothiophene," *Energy and Fuels*, **7**, 159-164 (1993).
21. Omori, T., Saiki, Y., Kasuga, K. and Kodama, T., "Desulfurization of alkyl and aromatic sulfides and sulfonates by dibenzothiophene desulfurizing *Rhodococcus* sp. strain SY1," *Biosci. Biotech. Biochem.*, **59**, 1195-1198 (1995).
22. Kim, H.Y., Kim, T.S. and Kim, B.H., "Degradation of organic sulfur compounds and the reduction of dibenzothiophene to biphenyl and hydrogen sulfide," *Biotechnology Letters*, **12**, 761-764 (1990).
23. Lizama, H.M., Wilkins, L.A. and Scott, T.C., "Dibenzothiophene sulfur can serve as the sole electron acceptor during growth by sulfate reducing bacteria," *Biotechnology Letters*, **17**, 113-116 (1995).
24. Kim, B.H., Kim, H.Y., Kim, T.S. and Park, D.H., "Selectivity of desulfurization activity of *Desulfovibrio desulfuricans* M6 on different petroleum products," *Fuel Processing Technology*, **43**, 87-94 (1995).

25. Kaufman, E.N., Harkins, J.B., Rodriguez, M., Selvaraj, P.T., Tsouris, C. and E., M.S., "Development of an electro-spray bioreactor for crude oil processing," *Fuel Processing Technology*, **52**, in press (1997).
26. Almarsson, O. and Klibanov, A.M., "Remarkable activation of enzymes in nonaqueous media by denaturing organic solvents," *Biotechnology and Bioengineering*, **49**, 87-92 (1996).
27. Scott, C.D., Scott, T.C., Blanch, H.W., Klibanov, A.M. and Russel, A.J., *Bioprocessing in Nonaqueous Media Critical Needs and Opportunities*, . 1995, Oak Ridge National Laboratory.
28. Woodward, C.A. and Kaufman, E.N., "Enzymatic catalysis in organic solvents: polyethylene glycol modified hydrogenase retains its sulphydrogenase activity in toluene," *Biotechnology and Bioengineering*, **52**, 423-428 (1996).
29. Perry, R.H., Green, D.W. and Maloney, J.O., *Perry's Chemical Engineering Handbook*, . 1984, McGraw-Hill: New York. p. 2336.
30. Scott, T.C. and Sisson, W.G., "Droplet size characteristics and energy input requirements of emulsions formed using high intensity pulsed electric fields," *Separation Science and Technology*, **23**, 1541-1550 (1988).
31. Chemineer, *Kenics Static Mixers KTEK Series*, . 1988: North Andover, MA. p. 32.
32. Byers, C.H. and Ammi, A., "Understand the potential of electro-separations," *Chemical Engineering Progress*, **91**, 63 (1995).
33. Kowalski, W. and Ziolkowski, Z., "Increase in rate of mass transfer in extraction columns by means of an electric field," *Int. Chem. Eng.*, **21**, 323 (1981).
34. Martin, L., Vignet, P., Fombarlet, C. and Lancelot, F., "Electrical field contactor for solvent extraction," *Sep. Sci. Technol.*, **18**, 1455 (1983).
35. Scott, T.C. and Wham, R.M., "An electrically driven multistage countercurrent solvent extraction device: the emulsion phase contactor," *Ind. Eng. Chem. Res.*, **28**, 94 (1989).
36. Scott, T.C., DePaoli, D.W. and Sisson, W.G., "Further development of the electrically driven emulsion phase contactor," *Ind. Eng. Chem. Res.*, **33**, 1237-1244 (1994).
37. Thorton, J.D., "The application of electrical energy to chemical and physical rate processes," *Rev. Pure and Appl. Chem.*, **18**, 197 (1968).
38. Ptasiński, K.J. and Kerkhof, P.J., "Electric field driven separations: phenomena and applications," *Sep. Sci. Technol.*, **27**, 995 (1992).
39. Warren, K.W. and Prestidge, F.L., "Crude oil desalting by counterflow electrostatic mixing," in proceedings of the National Petroleum Refiners Association Annual Meeting, San Antonio, TX, (1988).
40. Schwartz, E., Rock, K., Byeseda, J. and Pehler, R., "An improved process for MTBE unit feed pretreatment," in proceedings of the First Separations Division Topical Conference on Separations technologies: New developments and Opportunities, (1992).
41. Wood, T.S., Cernohlavek, L.G., Grant, D.T., Kelly, K.P., Lochhaas, P.D., Maynard, A.E., Ragsdale, D.N., Schrier, L.C., Stalling, D.L., Strumpf, D.M. and Tsang, A.Y., "Rapid, automated liquid / liquid extraction of contaminants from aqueous samples containing suspended solids," in proceedings of the First Separations Division Topical Conference on Separations technologies: New developments and Opportunities, (1992).
42. Lizama, H.M., Scott, T.C. and Scott, C.D., *Apparatus and Method for the Desulfurization of Petroleum by Bacteria*, . 1995, United States Patent Number 5,458,752.
43. Finnerty, W.R. and Singer, M.E., "A microbial biosurfactant-physiology, biochemistry and applications," *Developments in Industrial Microbiology*, **25**, 31-46 (1984).

Table 1. Results of analysis of variance (ANOVA) and t-Test (assuming unequal variance) comparing desulfurization rates over a range of cell densities. The second column gives p values for an analysis of variance over the complete range of data. The 3rd through 6th column gives p values for t-Tests comparing two experiments at a time. Numbers in parentheses indicate the cell densities compared. The p values comparing the data at 5X and 10X cell densities are all below 0.05, showing a significant difference between the two sets. This suggests that the desulfurization process may be mass-transfer limited at 10X cell density with statistical certainty.

| Time, hr | ANOVA (p) | p (0.5 & 1) | p (1 & 5) | p (5 & 10) | p (0.5 & 5) |
|----------|-----------|-------------|-----------|------------|-------------|
| 1hr | 3.62E-10 | 0.2170 | 0.7420 | 0.0010 | 0.0739 |
| 2hr | 4.53E-02 | 0.2150 | 0.0953 | 0.0177 | 0.1820 |
| 3hr | 2.60E-03 | 0.0787 | 0.3380 | 0.0066 | 0.0600 |
| 4hr | 5.40E-03 | 0.4706 | 0.3340 | 0.0006 | 0.0950 |
| 5hr | 5.30E-03 | 0.3250 | 0.4600 | 0.0146 | 0.2190 |
| 6hr | 3.89E-05 | 0.7440 | 0.3580 | 0.0370 | 0.1310 |
| 7hr | 3.00E-03 | 0.0750 | 0.0384 | 0.0025 | 0.0390 |
| 8hr | 2.00E-04 | 0.0328 | 0.0510 | 0.0190 | 0.0180 |
| 9hr | 6.00E-05 | 0.0951 | 0.1984 | 0.0031 | 0.0110 |
| 10hr | 1.18E-02 | 0.5820 | 0.1458 | 0.0066 | 0.1920 |
| 24hr | 9.00E-07 | 0.1343 | 0.0301 | 0.0005 | 0.0110 |

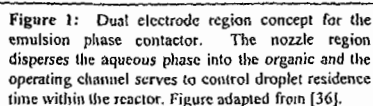


Figure 2: Biochemical pathway showing the sequence of DBT oxidation by IGTS8.

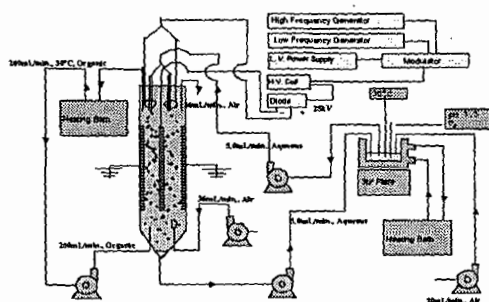


Figure 3: Schematic of the emulsion phase contactor and ancillary equipment.

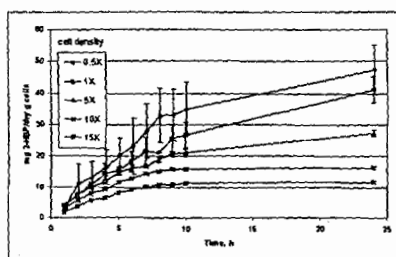


Figure 4: Effect of cell density on 2-HBP production rate. The 0.5X – 15X refers to cell density and 1X corresponds to 16.7 g cell paste in 250 mL aqueous phase. As observed from this plot, mass transfer may be a limiting factor in the DBT desulfurization process.

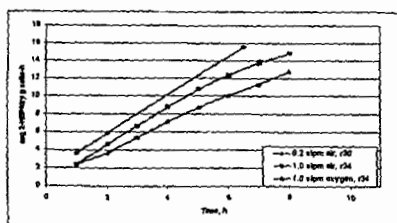


Figure 5: Effect of aeration rate and oxygen tension on 2-HBP production in batch stirred reactor. The experiment was conducted by dispersing 250 mL aqueous phase containing 166.7 g cell paste (10X cell density) in 750 mL hexadecane containing 0.6 wt% DBT.

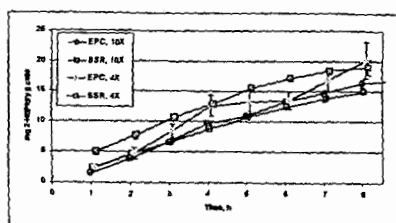
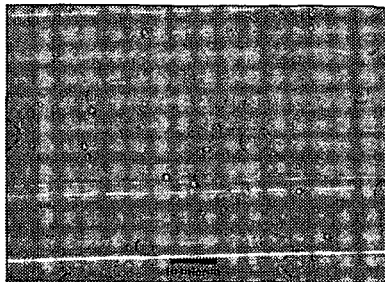


Figure 6: Comparison of 2-HBP production rate in EPCTM and BSR. The BSR experiment was conducted by contacting 250 mL aqueous phase containing 166.7 g cell paste (10X cell density) in 750 mL hexadecane containing 0.6 wt. DBT. In the EPCTM experiment, 107 mL aqueous phase containing 66.7 g cell paste (10X) was contacted with 2400 mL organic phase.

Figure 7: Micrograph of an EPC™ sample collected at 4 hours after beginning of reactor operation. The sample was collected from the central region between the electrodes using a Teflon tubing connected to a syringe and observed under a microscope as described earlier. The average droplet size was measured to be $2.54 \pm 2.40 \mu\text{m}$ ($n=300$).



Biocatalytic Ring Cleavage of Aromatic Hydrocarbons and Heterocycles Commonly Present in Petroleum Distillates.

Q. Wu*, P.M. Fedorak, M.A. Pickard, M.R. Gray, and J.M. Foght
Univ. of Alberta, Edmonton, Alberta CANADA.

Keywords: Biotransformation, fused-ring aromatics, distillates

ABSTRACT

A potential alternative to conventional fuel upgrading techniques is to use bacteria under near-ambient conditions to catalyze aromatic ring cleavage in the first step of a two-stage upgrading process. The resulting biocatalytic products would be chemically hydrogenated under mild conditions in the second stage to produce the desired alkylbenzenes. Experiments testing biocatalytic ring cleavage of aromatic hydrocarbons are described in this study.

Pseudomonas fluorescens LP6a was chosen as the biocatalyst because of its broad-specificity aromatic hydrocarbon-degrading enzymes which confer the ability to oxidize a wide range of polycyclic aromatic hydrocarbons and heterocycles commonly present in petroleum middle distillates. Pre-grown, induced whole cell biocatalysts in aqueous suspension produced the predicted polar intermediates from aromatic substrates without altering the aliphatic carrier and without carbon loss from the aromatic substrate. Quantitative studies with ^{14}C -labeled aromatic substrates incorporated into synthetic and authentic distillates were carried out to reveal potential process-limiting factors. Parallel studies were performed using gas chromatography with a flame ionization detector to quantify aromatic ring cleavage in authentic distillates.

INTRODUCTION

Chemical hydrogenation processes are currently used to upgrade middle distillates produced by thermochemical cracking of heavy oils and bitumen. These distillates have a high content of low fuel value di- and tricyclic aromatics, which are reduced by expensive high temperature-high pressure hydrogenation to compounds such as alkylbenzenes. The catalysts involved are frequently deactivated by sulfur- and nitrogen-containing compounds in the feedstocks. These expenses make it desirable to explore an alternative to conventional upgrading techniques. An attractive alternative is to use bacteria to enzymatically cleave the fused-ring aromatics under near-ambient conditions, followed by mild chemical hydrogenation to produce the desired alkyl aromatics.

Biocatalytic technology has been used widely in crude oil biodegradation and is being assessed for biodesulfurization. It can be cost effective, competitive or compatible with current technology. It is well known that one ring of the di- and tricyclic aromatics can be opened selectively by bacterial enzymes. Although the oxygenated ring cleavage products are themselves undesirable, they may be converted to alkylaromatics under milder hydrogenation conditions than the parent feedstocks, resulting in cost savings.

Besides yielding the desired ring fission products, two primary requirements of the biological process are essential. First, the biocatalytic activity must be restricted to aromatic compounds and must be effective over the wide range of di- and tricyclic aromatic hydrocarbons, heterocycles and alkyl-substituted homologues common to middle distillates. Second, there should be no carbon loss from the aromatic substrates as a consequence of microbial oxidation; that is, the process has to be blocked at certain stage to prevent complete oxidation. Other advantages such as the ability of the cells to catalyze ring cleavage in a resting state and to be pre-grown quickly to high density in an active state would greatly benefit the process.

The research project described here deals with the biocatalytic stage for ring cleavage of aromatics in the middle distillates. *Pseudomonas fluorescens* LP6a was previously reported to possess several of the properties listed above and thus was chosen for this study. For example, LP6a mutant 21-41 has been shown to accumulate the expected ring cleavage products from a variety of pure aromatic compounds commonly present in petroleum distillates (Foght et al. 1997). In the experiments reported here, ^{14}C -labeled phenanthrene was incorporated into synthetic and authentic distillates to detect biotransformation of the substrate into water-soluble ring cleavage products. Parallel studies were performed using gas chromatography (GC) with a flame

ionization detector (FID) to quantify aromatic ring cleavage in authentic distillates. These results are leading towards optimization of biocatalytic ring cleavage for bio-upgrading of petroleum distillates.

METHODS AND MATERIALS

Preparation of biocatalyst

Transposon mutants of *P. fluorescens* LP6a were generated by conjugation using a suitable Tn5 donor plasmid with subsequent screening for desired phenotypic changes (Foght and Westlake, 1996). Cultures of *P. fluorescens* LP6a mutants were incubated to high density in Tryptic Soy Broth (Difco; typically 200 mL) containing kanamycin (to maintain the transposon) at 30°C with agitation for 24 h. Enzymatic activity was specifically induced with salicylic acid (Yen and Serdar, 1988), and the cells were harvested by centrifugation and resuspension in 3 mM potassium phosphate buffer (pH 7). The protein content of biocatalyst suspensions was determined using the biocinchoninic acid assay (Pierce, Rockford IL).

Substrates and middle distillates

Seventeen aromatic compounds including naphthalene and its methyl-, ethyl- and dimethyl-substituted homologues, phenanthrene and dibenzothiophene (DBT) have been tested for ring cleavage with the chosen mutant 21-41 (Foght et al. 1997). Selected aromatic model compounds were dissolved in the aliphatic carriers *n*-hexadecane or heptamethylnonane (HMN; Efroymson and Alexander 1991) to provide a two-phase system referred to as a "synthetic distillate," or presented directly in authentic distillates. A brief description of the distillates used in this study is summarized in Table 1. The substrate solution was then added to the suspension of induced biocatalyst and incubated for 24 h to effect biotransformation of the substrates. Parallel sterile controls were also prepared.

Table 1. Brief description of authentic distillates used in this study

| SOURCE | TYPE | Boiling point range | S content * (mol% of cut) |
|----------|-------------------|---------------------|---------------------------|
| 3HPP0015 | Middle distillate | 177-343°C | 0.118 |
| 3HPP0016 | Middle distillate | 177-343°C | 0.319 |
| 3HPP0017 | Middle distillate | 177-343°C | 0.407 |
| 3HPP0018 | Middle distillate | 177-343°C | 0.359 |
| E #1 | Distillate cut | 177-343°C | NA |
| LCGO | Gas oil | NA | NA |

* the 3HPP series was subjected to various hydrogenation conditions; elemental analyses were performed, with only the sulfur content reported here.

NA = not available

Radioactive and chemical analysis

To determine the biotransformation of the aromatic compounds quantitatively, ¹⁴C-labeled phenanthrene (Amersham) was incorporated into synthetic and authentic distillates and incubated with the biocatalyst as described above. A two-step extraction procedure was used to extract and recover the radioactivity. First, unaltered non-polar substrates and distillates were recovered by extraction with pentane in the presence of the cells at neutral pH. Second, after the cells had been removed by centrifugation and the supernatant acidified to pH < 2, ethyl acetate was used to recover the polar ring fission products. Radioactivity was measured by liquid scintillation (Beckman model LS 3801) and the ratio of radiolabel recovered from the polar phase to that of total added was calculated as the percent converted to polar metabolites ("biotransformation percentage").

Similar extraction procedures were applied to the incubated cultures in quantitative GC experiments. Phenanthrene was usually used as the model substrate and biphenyl and benzothiophene were added as the internal standards to determine the relative residual mass of the model substrate in the pentane extracts. The biotransformation percentage was determined by comparing the relative residual mass of the model substrate incubated with the biocatalyst with that of the model compound in a parallel sterile control.

A silica gel column fractionation technique (Fedorak and Westlake 1981) was used to characterize the composition of the authentic distillates. The saturates and aromatics fractions were studied in detail to determine their susceptibility to microbial transformation by the biocatalyst compared with the whole distillate. Routine GC analysis of fractions and distillates was performed on a Hewlett-Packard model 5890 GC system equipped with a FID and a sulfur-selective flame photometric ionization detector. Chromatography conditions have been described previously (Foght and Westlake 1996).

RESULTS AND DISCUSSION

Radiometric determination of substrate biotransformation

Radiolabeled phenanthrene was incorporated into an aliphatic carrier or an authentic distillate to serve as a surrogate substrate for biotransformation. The radioactivity of the corresponding extracts was measured by liquid scintillation and the total recovery of the radiolabel and the conversion percentage were calculated. In this way, conversion of a specific compound can be monitored in the context of a complex mixture of substrates. Results are shown in Table 2.

Table 2. Transformation of [9-¹⁴C]-phenanthrene presented in a hydrocarbon carrier: synthetic or authentic distillates or fractions of authentic distillates. Percent biotransformation is the fraction of added radiolabel recovered from the polar phase. Total recovery is expressed as a percentage of the radiolabel added.

| Presentation of ¹⁴ C-phenanthrene in: | Radioactivity | |
|---|------------------|------------|
| | % biotransformed | % recovery |
| Heptamethylnonane (HMN) | 80 | 100 |
| Mixture of HMN and the aromatics fraction of 3HPP0015 (2:1 V/V) | 76 | 90 |
| Aromatics fraction of 3HPP0015 | 68 | 91 |
| Saturates fraction of 3HPP0015 | 72 | 91 |
| Whole authentic distillate 3HPP0015 | 16 | 99 |
| Whole authentic distillate 3HPP0016 | 58 | 102 |

The total recovery of the radiolabel was ≥90% for all experiments. Biotransformation of phenanthrene in HMN and the individual distillate fractions was relatively high, but biotransformation was substantially lower for whole 3HPP0015 than for whole 3HPP0016; the reason for this observation is unknown at present.

Gas chromatographic quantitation of biotransformation

In general, biotransformation levels of >80% can be obtained either for pure phenanthrene or phenanthrene presented in a synthetic distillate, and quantitation by GC is relatively easy because of the simplicity of the samples. However, quantitative GC analysis in the presence of the authentic distillates is difficult, with the results being semi-quantitative due to the complexity of the substrates.

A silica gel column fractionation technique was used to gravimetrically determine the composition of selected distillates (Table 3). Some fractions then were used as carriers for presentation of radiolabeled or unlabeled phenanthrene to investigate whether specific fractions or the whole distillate were inhibitory to biotransformation. Biotransformation was analyzed radiometrically or by GC as reported in Table 4.

It can be seen from Table 4 that distillate saturates fractions did not inhibit biotransformation of phenanthrene. The saturates fractions were not oxidized by the biocatalyst, as determined by GC analysis (data not shown). However, certain aromatics fractions, especially the aromatics fraction of LCGO, had an inhibitory effect on phenanthrene bioconversion. The aromatics in the authentic distillates may compete with the analyte substrate (phenanthrene) for enzyme activity, or may inhibit the conversion of phenanthrene through toxicity to the biocatalyst directly or via their metabolites. Alternatively, inhibition may be a reflection of poor mass transfer during the biotransformation process.

Table 3. Fraction composition of selected distillates, prepared by silica gel column fractionation; mean \pm 1 standard deviation, n=2

| Distillate | Distillate composition (weight % of fraction) | | | |
|------------|---|----------------|---------------|---------------|
| | Saturates | Aromatics | Polar | Asphaltenes |
| 3HPP0015 | 55.4 \pm 4.7 | 26.2 \pm 2.2 | 0.80 \pm 0 | 0.5 \pm 0.4 |
| 3HPP0016 | 41.2 \pm 2.6 | 41.2 \pm 4.8 | 2.2 \pm 0.6 | ND |
| 3HPP0018 | 59.7 \pm 0.4 | 33.3 \pm 0.1 | 1.2 \pm 0.3 | ND |
| E #1 | 59.0 \pm 2.9 | 27.2 \pm 1.6 | 6.2 \pm 0.6 | ND |
| LCGO | 36.4 \pm 3.7 | 55.5 \pm 3.5 | 5.4 \pm 0.2 | ND |

ND = not determined

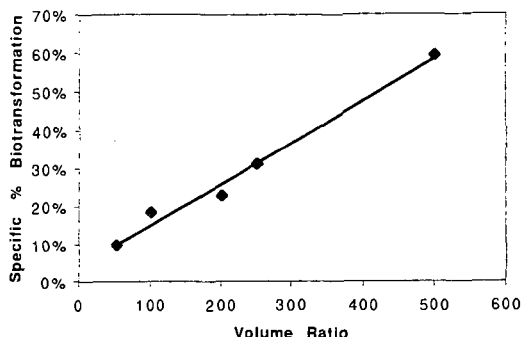
Table 4. Summary of biotransformation of phenanthrene presented in different carriers and incubated under standard conditions. Fractions were obtained by silica gel column chromatography of the authentic distillates listed in Table 3. The biotransformation percentage was determined either radiometrically or by quantitative GC, compared with parallel sterile controls.

| Distillate | Presentation of phenanthrene in: | % Biotransformation | Analytical method |
|------------|----------------------------------|---------------------|-------------------|
| 3HPP0015 | Saturates fraction | 72 | Radiometric |
| | Aromatics fraction | 76 | Radiometric |
| | Whole distillate | 36 | GC-FID |
| 3HPP0016 | Whole distillate | 60 | GC-FID |
| E #1 | Saturates fraction | 74 | GC-FID |
| | Aromatics fraction | 64 | GC-FID |
| | Whole distillate | 62 | GC-FID |
| LCGO | Saturates fraction | 94 | GC-FID |
| | Aromatics fraction | 43 | Radiometric |
| | Whole distillate | 53 | GC-FID |

To distinguish among these possibilities, experiments were designed to elucidate limiting factor(s), using phenanthrene presented in the aromatics fraction of LCGO, an inhibitory carrier. In the first experiment, replicate samples of biocatalyst were suspended in different volumes of phosphate buffer to yield cell suspensions covering a 10-fold range of biomass density (measured as mg protein per ml suspension). To these suspensions, a constant volume of carrier containing 8.9 mg of phenanthrene was added, so that the only variable among tests was the biomass density. Biotransformation of the phenanthrene was calculated in either absolute units (percentage of phenanthrene biotransformed) or specific units, obtained by dividing the absolute units by the biomass density. Results are shown in Figure 1.

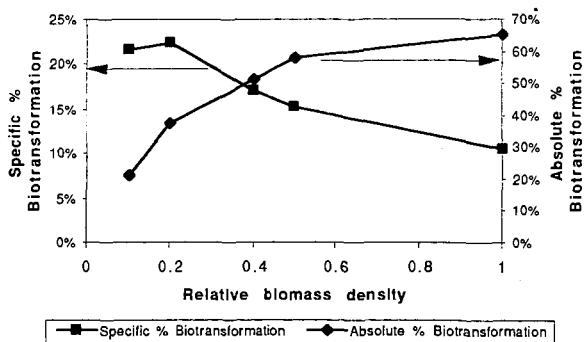
If the inhibitory effect of the carrier was due to competition for enzyme activity between phenanthrene and alternate substrates in the carrier, a constant specific % biotransformation would have resulted (i.e. a horizontal line) because the ratio of phenanthrene to the carrier was constant in the flasks and the same total biomass was present in all flasks. The results in Figure 1 are best explained if toxicity is the predominant inhibitory factor, because increasing biotransformation was observed as the volume ratio of cell suspension to carrier increased. That is, with increasing biocatalyst suspension volumes, the concentration of toxic compounds would decrease regardless of whether these toxic compounds were the parent aromatics or their metabolites.

Figure 1. Specific biotransformation (% biotransformation of phenanthrene per mg biomass protein per ml biocatalyst suspension) as a function of the volume ratio of biocatalyst suspension to carrier. Phenanthrene was presented in the aromatics fraction of LCGO and measured by quantitative GC-FID.



In the second set of experiments, the biomass density was varied over a 10-fold range by resuspending different amounts of biocatalyst in a constant volume of phosphate buffer, keeping the phenanthrene concentration and carrier volume constant. That is, the volume ratio of cell suspension to carrier was kept constant with only the biomass density varying. Phenanthrene bioconversion is presented in Figure 2 both as the absolute % biotransformation in a flask and as the specific % biotransformation, calculated per mg biomass protein. These values were plotted against the relative biomass density, with 1.0 being the cell density of an overnight culture and 0.1 being one-tenth this cell density.

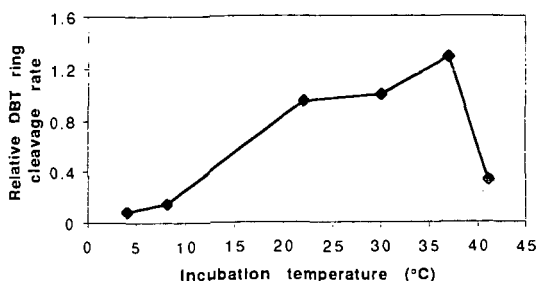
Figure 2. Absolute % biotransformation of phenanthrene and specific % biotransformation of phenanthrene as a function of the relative biomass density, with 1.0 being the biomass density of an overnight culture. Phenanthrene was presented in the aromatics fraction of LCGO and measured by quantitative GC-FID.



The absolute % biotransformation increased as the biomass density increased. This is as predicted, because the total amount of phenanthrene converted to polar metabolites should be greater if more cells are present. This biotransformation begins to plateau at about 60% when the relative biomass is approximately 1.0. In contrast, the "efficiency" of biocatalyst activity, calculated as specific % biotransformation, decreased above a relative biomass density of 0.2. That is, as the cell density increased, the biotransformation activity per mg biomass protein decreased. This may be due to mass transfer effects as the substrate has less access to individual cells due to "crowding" of the biocatalyst in suspension, or due to limitation of oxygen diffusion in the suspension, or it may be due to increased accumulation of toxic metabolites by the increased mass of cells. We cannot discriminate among these possibilities at present, although

mass transfer seems unlikely to be a significant factor at the relatively low cell densities used in these experiments, and it seems unlikely that oxygen is limited under the fairly vigorous aeration conditions provided in the flasks (200 rpm agitation).

Figure 3. Relative rates of DBT ring cleavage at increasing incubation temperatures, normalized to enzyme activity at 30°C.



The effect of incubation temperature on biocatalysis was determined at six temperatures by incubating replicate batches of biocatalyst with DBT, a heterocyclic aromatic substrate. Rates of DBT ring cleavage were calculated spectrophotometrically (Foght et al. 1997) as Absorbance Units at 475 nm (the maximum absorption wavelength for the DBT ring cleavage product) produced per min incubation. Rates were normalized to the rate at 30°C as the indicator of relative enzyme activity, as shown in Figure 3. The ring cleavage rate increased with temperature, reaching maximum activity around 37°C, typical for a mesophilic bacterium like *P. fluorescens* LP6a.

CONCLUSIONS

- *P. fluorescens* LP6a biocatalyzes ring cleavage of the substrate phenanthrene when presented in several water-immiscible carriers including heptamethylnonane, various whole authentic distillates, and the saturates and aromatics fractions of those authentic distillates.
- Greater than 80% of the substrate can be biotransformed by the biocatalyst into polar ring cleavage products within a 24-h contact period.
- Ring cleavage activity is influenced by toxicity of some component(s) of the authentic distillates or their metabolites, particularly in the aromatics fraction. This knowledge may lead to general rules of distillate susceptibility to ring cleavage biocatalysis.
- Ring cleavage activity is influenced by temperature, with an optimum of ca. 37°C

ACKNOWLEDGMENTS

Grateful acknowledgment is made of funding from Texaco Group, Inc., Imperial Oil Resources Ltd., the National Centre for Upgrading Technology (Canada), and the Natural Sciences and Engineering Research Council of Canada (Collaborative Research & Development Program).

REFERENCES

- FOGHT, J. M., WU, Q., FEDORAK, P., PICKARD, M. and GRAY, M., *Proceedings of BIOMINET/NCUT Symposium at the 48th Annual Technical Meeting of the Petroleum Society*, June 9, 1997
- FOGHT, J. M. and D. W. S. WESTLAKE, *Biodegradation* Vol. 7, pp. 353-366, 1996.
- YEN, K. M. and C. M. SERDAR, *Critical Reviews in Microbiology* Vol. 15, pp. 247-268, 1988.
- EFROYMSON, R. A. and M. ALEXANDER, *Applied and Environmental Microbiology* Vol. 57, pp. 1441-1447, 1991.
- FEDORAK, P. M. and D. W. S. WESTLAKE, *Canadian Journal of Microbiology* Vol. 27, pp. 432-443, 1981.

USE OF A DISPERSED IRON CATALYST FOR UPGRADING EXTRA-HEAVY CRUDE OIL USING METHANE AS SOURCE OF HYDROGEN.

Cesar Ovalles, Eduardo Filgueiras, Alfredo Morales, PDVSA-INTEVEP, Apdo. 76343, Caracas 1070A, Venezuela.

Carlos E. Scott, Centro de Catálisis, Petróleo y Petroquímica. Facultad de Ciencias, Universidad Central de Venezuela, Apdo. 47102, Caracas 1040A, Venezuela.

Fernando Gonzalez-Gimenez, B. Pierre Embaid, Depto. de Física, Ciencias, UCV, Apdo. 47586, Caracas 1041A, Venezuela.

Key Words: Extra-heavy Crude Oil, Upgrading, dispersed iron catalyst

INTRODUCTION

The use of natural gas (methane) as hydrogen source for the upgrading of extra-heavy crude oil [1-6] and coal [7-15] has been the subject of numerous studies during the last few years. In this particular, the reaction of Hamaca crude oil ($^{\circ}\text{API} = 8.3$) under thermal conditions (380°C , 11.0 MPa of CH_4 for 4 hours residence time) and in the presence of water as additive, led to a decrease of two orders of magnitude in the viscosity of the upgraded product (from 500 to 1.99 Pa s at 30°C), conversion of the $>540^{\circ}\text{C}$ fraction of 60%, and 11.3% of reduction of sulfur with respect to the original crude [1-3]. By ^1H - and ^2D -NMR analysis, the most probable pathway is a free-radical mechanism, which involves incorporation of methane via production of methyl radicals [3].

Using an alumina supported molybdenum-nickel catalyst and at similar conversion of the $>540^{\circ}\text{C}$ fraction, a relatively higher percentage of desulfurization (28%) and lower percentage of asphaltenes (9.3%) was obtained than those found in thermal reaction (11% and 11.8%, respectively) [1, 4]. These results indicate that methane can be catalytically activated and used for upgrading of extra-heavy crude oil. Furthermore, using a dispersed molybdenum catalyst, derived from $\text{MoO}_2(\text{acac})_2$ (where acac = acetyl-acetonate) and by carbon isotope ratio mass spectrometry analysis, labeled methane ($^{13}\text{CH}_4$) was found to incorporate into the crude oil (estimated value 0.01% w/w) giving conclusive evidence on the involvement of CH_4 in the extra-heavy crude oil upgrading process [5-6].

In this work, we studied the use of an iron dispersed catalyst, derived from $\text{Fe}_3(\text{CO})_{12}$ for extra-heavy crude oil upgrading using methane as source of hydrogen. The iron catalyst was isolated from the coke produced from the upgrading reaction and was analyzed by XPS, EDAX, and Mössbauer Spectroscopy. Also, the characterization of the products by ^1H -RMN were carried out in order to understand the methane activation processes that are occurring during the crude oil upgrading reactions.

EXPERIMENTAL

The crude oil employed in this work came from the Hamaca oil field in the Orinoco Belt and its analysis is as follows: API Gravity at $15.6^{\circ}\text{C} = 8.7$, Water (% w/w) = <1 , H/C wt. Ratio = 0.115, Sulphur (% w/w) = 3.40, Nickel (ppm) = 91.9, Vanadium (ppm) = 412, Asphaltenes (% w/w) = 12.5, % of Residue (500°C) = 57%, Viscosity at 30°C (Pa s) = 500. The upgrading reactions were carried out batchwise in a stainless-steel 300 ml Parr reactor with 250 ppm of Fe at a temperature of 410 - 420°C , a pressure of 11 MPa of CH_4 and a residence time of one hour as described elsewhere [5-6].

The percentages of volatile material were determined by the method reported by Ceballos and coworkers using a Hewlett-Packard gas-chromatograph, model 5880 [16]. The percentage of conversion of the residue $>500^{\circ}\text{C}$ was defined elsewhere [3,5-6]. X-ray Photoelectron Spectroscopic (XPS) experiments were carried out in using a Leybold-Heraeus Surface Analysis System which was operated with an aluminium anode (1486.6 eV). Pass energy was set at a constant value of 50 eV and the data acquisition and manipulation were performed using a 486 IBM compatible computer. The instrument sensitivity factors used for scaling the photoelectron peak areas were calculated using the method reported by Leon and Carrazza [17]. The Mössbauer spectroscopy was carried out at room temperature, with a constant acceleration spectrometer, in the triangular symmetric mode for the velocity. The source was a ^{57}Co in palladium.

RESULTS AND DISCUSSION

The reaction of Hamaca extra-heavy crude oil (Table 1) at 11 MPa of methane and 410°C for 1 h (Table 1, control run) led to a reduction of two order of magnitude in the viscosity (from 500 to 2 Pa s), 10% of reduction in sulfur content and 41% conversion of the >500°C fraction in the upgraded product with respect to the original crude. Analogous reaction carried out in the presence of $\text{Fe}_3(\text{CO})_{12}$ as dispersed catalyst (Table 1, run 1) yielded a product with further reduction in the viscosity (1.3 Pa s), higher reduction in sulfur content (14%) and similar value of conversion of the heavy fraction (40%). Additionally in the presence of the catalyst, a slightly reduction of coke formation (from 7.7 to 6.9%) was observed in comparison with the control experiment. These results indicate that the presence of the iron catalyst is necessary in order to enhance the upgrading of extra-heavy crude oil in the presence of methane.

A reaction carried out in an inert argon atmosphere (Table 1, run 2) yielded a product with higher viscosity (2.7 Pa s), less reduction of sulfur content (8%) and lower conversion of the >500°C fraction (36%) with respect to the methane containing experiment (Table 1, run 1). These results indicate that methane is involved, as a source of hydrogen, in the upgrading reaction and that it can be activated by the metal catalyst.

An experiment (Table 2, run 3) conducted under hydrogen atmosphere afforded an upgraded product with slightly better properties (1.2 Pa s, 22% HDS, 40% conversion of >500°C fraction and 5% coke) than those obtained under methane (run 1) and argon (run 2) atmospheres. Thus, the order of reactivity is $\text{H}_2 > \text{CH}_4 > \text{N}_2$ as found by Ovalles *et al.* [3] and Sundaran [7] for thermally activated processes. Also, similar order of reactivity was reported by Egiebor and Gray in their iron catalyzed coal liquefaction experiments [9] and Ovalles *et al.* for Mo-Ni/ Al_2O_3 catalyzed extra-heavy crude oil upgrading [4, 6].

From the methane upgrading reaction using $\text{Fe}_3(\text{CO})_{12}$ as dispersed catalyst, the coke formed was characterized by EDAX, XPS and electron microscopy. X-ray diffraction and XPS analyses (after 1 h etching with Ar^+ ions) showed the presence of iron and sulfur.

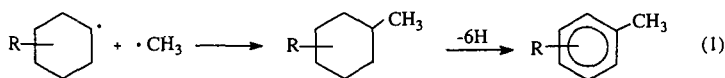
Furthermore, the binding energy for the Fe 2p_{3/2} was found (Table 2) at 707.4 eV and can be assigned to Fe^{+2} according to the data reported in the literature [18]. Additionally, a sulfur species detected in the S2p region at 161.3 eV, which can be assigned to S^{-2} [19].

The ratio of the atomic percentages of Fe^{+2} (0.54) and S^{-2} (1.31) is 0.53, which is lower than that (1.1-1.4) reported by Reucroft and coworkers [19]. To determine which type of Fe compound was present, a Mössbauer study was undertaken. The recorded spectrum is shown in Fig. 1A with the continuous line representing the result of a computer adjustment, which included, apart IS (Isomer Shift), FWHM and QS (quadrupole splitting), a hyperfine field distribution whose histogram is also shown in Fig. 1B. Due to the small concentration of iron, the spectrum has a rather poor statistics, however the histogram obtained indicates the unambiguous presence of an Fe and V mixed sulfide, when compared with the spectra obtained in the systematic study of those sulfides [20-22]. According to the previous results, the composition of the present mixed sulfide should be near: $(\text{Fe}_{0.6}\text{V}_{0.4})_z\text{S}$, where z is in the range of 0.8-0.9.

The formation of the Fe-V mixed sulfide is certainly achieved *in situ*, by decomposition of the iron carbonyl ($\text{Fe}_3(\text{CO})_{12}$) and subsequently the reaction of sulfur and vanadium coming from the feedstock [23]. A very similar mechanism, which demonstrated the appearance of those mixed-sulfides as the active phases, has been put in evidence in HDM reactions [24-25] undertaken with clay catalysts (the precursor is Fe_2O_3) acting on a Pao-X1 heavy crude from the Orinoco belt.

In order to gain mechanistic information, H-NMR analyses were carried out to the upgraded crude oil and the results are shown in Table 3. For $\text{Fe}_3(\text{CO})_{12}$ soluble catalyst, an increase (17.2%) in the amount of α -hydrogen bonded to aromatic rings was observed in comparison with those observed for the control run (14.7%) and for the crude oil (15.5%). Similar catalytic runs carried out under argon and hydrogen atmospheres and $\text{Fe}_3(\text{CO})_{12}$ led to lower amount of α -hydrogen bonded to aromatic rings (16 and 15 % for Ar- and H_2 -containing experiments, respectively) than that found in the CH_4 -containing experiment (17%).

Furthermore, an intense aromatization occurred for all the upgrading reactions as shown by the increase in the percentages of aromatic protons from 5.1% in the original crude to approximately 10% for runs 1-3. These results can be rationalized by incorporation of the methyl groups (or, in general, CH_x species where $x = 1, 2$, or 3) to the crude oil molecules, as shown in eq. 1 [6].



Where R = hydrocarbon (aliphatic or aromatic)

Naphtenic radicals shown in eq. 1 can be generated by either thermal or catalytic breaking of C-H bond under the reaction temperature (410°C). Egiebor and Gray found methyl and dimethyl products by GC analysis of the donor solvent (tetralin), which was attributed to direct alkylation by reaction with methane in their iron catalyzed coal liquefaction experiments [9]. Also, similar results were obtained previously for extra-heavy crude oil upgrading under thermal [3] and catalytic conditions [6]. The incorporation of CH₄ species, coming from methane, into the crude oil molecules was confirmed by isotopic carbon distribution measurements (¹³C/¹²C) using ¹³CH₄ as a source of hydrogen [6].

REFERENCES

- 1) Ovalles, C.; Hamana, A., Bolivar, R. and Morales, A., U. S. Patent 5,269,909 1993.
- 2) Ovalles, C.; Arias E. S., Hamana, A.; Badell, C. B. and Gonzalez, G., *ACS Fuel Chem. Preprints* 1994, 39: 973.
- 3) Ovalles, C.; Hamana, A., Rojas, I. and Bolivar, R., *Fuel* 1995, 74, 1162.
- 4) Ovalles, C.; Hamana, A., Bolivar, R. and Morales, A. Proceeding X Conference of UNITAR, Houston, Texas, Feb. 1995.
- 5) Morales, A., Salazar, A., Ovalles, C. and Filgueiras, E., Proceedings 11th International Congress. Catalysis-40th Anniversary. Studies in Surface and Catalysis, J. W. Hightower, E. Iglesia and A. T. Bell (Eds.), 101, 1215 (1996).
- 6) Ovalles, C., Filgueiras, E., Morales, A., Rojas, I., de Jesus, J. C. and Berrios, I., to be published in *Energy & Fuels*.
- 7) Sundaram, M. U.S. Patent 4,687,570 (1987). b) Sundaram, M. and Steinberg, M. *ACS Fuel Chem. Preprints*, 1986, 28: 77.
- 8) Steinberg, M., *Int. J. Hydrogen Energy* 1986, 11: 715.
- 9) Egiebor, N. O., Gray, M. R., *Fuel* 1990, 69: 1276.
- 10) Qin, Z. and Maier, W. F. *Energy & Fuels* 1994, 8, 1033.
- 11) Maier, W. F. and Franke, R. *Fuel* 1994, 73, 5.
- 12) Steinberg, M. and Fallon, P. T. *Hydrocarbon Process* 1982, Nov, 92.
- 13) Calkins, W. H. and Bonifaz, C. *Fuel* 1984, 63, 1716.
- 14) Brackman-Danheux, C.; Cypres, R.; Fontana, A. and van Hoegaerden, M. *Fuel* 1995, 74, 17.
- 15) Yang, K., Batts, B. D., Wilson, M. A., Gorbaty, M. L., Maa, P. S., Long, M. A., He, S. X., Atalla, M. I., *Fuel* 1997, 76, 1105.
- 16) Ceballo, C. D., Bellet, A., Aranguren, S., Herrera, M., *Rev. Tec. INTEVEP*, 1987, 7, 81.
- 17) Leon, V., Carrazza, J., *Rev. Tec. INTEVEP* 1989, 9, 81.
- 18) Kim, J. Y., Reucroft, P. J., Taghiei, M., Pradhan, V. R., Wender, I., *Energy & Fuels* 1994, 8, 886.
- 19) a) Des Marais, D. J., Hayes, J.M., *Anal. Chem.*, 1976, 48, 1651. b) Gillet, S., Rubini, P., Delpuech, J-J, Escalier, J-C, Valentin, P. *Fuel* 1981, 60, 221.
- 20) Embaid, B. F., Gonzalez-Jimenez, F., Scott, C. E., *Hyperfine Interactions* 1994, 83, 385.
- 21) Scott, C. E., Embaid, B. P., Luis, M. A., Gonzalez-Jimenez, F., Gengembre, L., Hubaut, R., Grimblot, J., *Bull.Soc.Chim.Belg.*, 1995, 104, 331.
- 22) Scott, C.E., Embaid, B.P., Gonzalez-Jimenez, F., Hubaut, R., Grimblot, J., *J. Catalysis*, 1997, 166, 333.
- 23) Derbyshire, F. *CHEMTECH* 1990, 20, 439 and references therein. b) Weller, S. W. *Energy & Fuels* 1994, 8, 415 and references therein.
- 24) Gonzalez-Jimenez, F., Constant, H., Iraldi, R., Jaimes, E., Rosa-Brussin, M., *Hyperfine Interactions*, 1986, 28, 927.
- 25) Gonzalez-Jimenez, F., Bazin, D., Dexpert, H., Villain, F., Constant, H. Rosa-Brussin, M., *Physica B*, 1989, 158, 215.

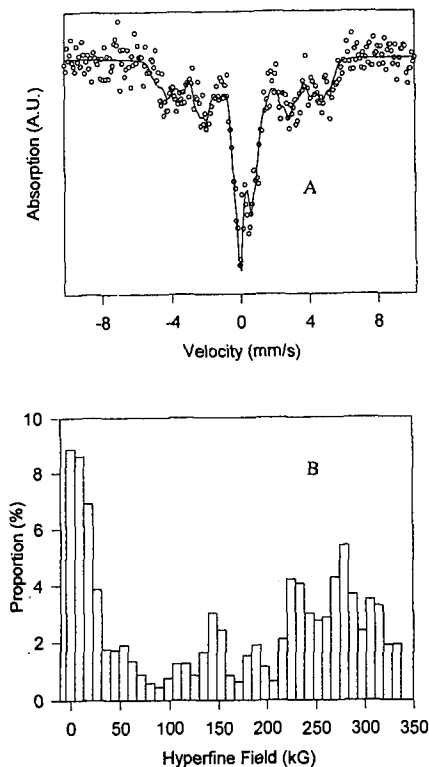


Fig. 1. A) Mössbauer spectrum with the continuous line representing the result of a computer adjustment including, IS (Isomer Shift), FWHM and QS (quadrupole splitting).

Table 1. Upgrading of Extra-Heavy Crude Oil using $\text{Fe}_3(\text{CO})_{12}$ as Organometallic Precursor^a

| Run | Gas used | HDS ^b (wt%) | % Conv. >500°C ^c | Viscosity (Pa s) ^d | Coke (wt%) | Gases (wt%) | Liquids (wt%) |
|----------------------|-----------------|------------------------|-----------------------------|-------------------------------|------------|-------------|---------------|
| Hamaca crude oil | - | (3.40% S) | - | (500) | - | - | - |
| Control ^e | CH ₄ | 10.0 | 41 | 1.99 | 7.7 | 4.6 | 87.7 |
| 1 | CH ₄ | 14 | 40.5 | 1.34 | 6.9 | 4.6 | 88.5 |
| 2 | Argon | 8 | 35.8 | 2.77 | 6.0 | 3.1 | 90.9 |
| 3 | H ₂ | 22 | 39.7 | 1.20 | 5.0 | 4.5 | 90.5 |

^aThe reactions were carried out in a 300-ml batch reactor at 410°C, 250 ppm of Fe, 11 MPa of final pressure for a 1-h period. The results are the average of at least two different reactions. ^bPercentage of desulfurization with respect to the starting crude oil. ^cPercentage of conversion of the residue >500°C as defined in ref. 3, 5-6. ^dViscosity measured at 30°C. ^eControl experiment, i. e. no catalyst was used.

Table 2. Results of the XPS analysis of the coke isolated from upgraded Hamaca crude oil using $\text{Fe}_3(\text{CO})_{12}$ as catalyst precursor after 1 h etching with Ar^+ ions^a

| Element | Binding energy (eV) | Atomic % ^b | Assignment ^c | Reference |
|---------|---------------------|-----------------------|----------------------------|-----------|
| Fe2p3/2 | 707.4 | 0.54 | Fe^{+2} as in FeS | 18-19 |
| S 2p | 161.3 | 1.31 | S^{-2} as in FeS | 20 |
| C 1s | 284.6 | 97.24 | Adventitious carbon | 18-20 |
| O 1s | 532.8 | 0.91 | Organic Oxygen | 18-20 |

^aThe reactions were carried out as described in Table 1. The coke was isolated by filtration after diluting the upgraded crude oil in toluene. ^bAtomic percentage on the surface. ^cMost probable assignment according to the published literature.

Table 3. Protons distributions for upgraded Hamaca crude oil measured by ^1H -NMR using $\text{Fe}_3(\text{CO})_{12}$ as catalyst precursor^a.

| Run | Gas used | H_{arom}^b | $\text{H}_{\text{aliph}}^c$ | H_{α}^d | H_{β}^e | H_{γ}^f |
|----------------------|---------------|----------------------------|-----------------------------|-----------------------|----------------------|-----------------------|
| Hamaca crude oil | - | 5.1 | 94.9 | 14.7 | 56.2 | 24.0 |
| Control ^g | CH_4 | 9.0 | 91.0 | 15.5 | 52.0 | 23.5 |
| 1 | CH_4 | 8.4 | 91.6 | 17.2 | 51.2 | 23.0 |
| 2 | Argon | 8.9 | 91.1 | 16.2 | 51.3 | 23.3 |
| 3 | H_2 | 8.7 | 91.3 | 15.2 | 51.5 | 24.6 |

^aThe reactions were carried out as described in Table 1. ^b H_{arom} = Hydrogen bonded to aromatic carbons. ^c H_{aliph} = Hydrogen bonded to aliphatic carbons. ^d H_{α} = Hydrogen bonded to aliphatic carbons in α position to an aromatic ring. ^e H_{β} = Hydrogen bonded to aliphatic carbons in β position to an aromatic ring. ^f H_{γ} = Hydrogen bonded to aliphatic carbons in γ or more position to an aromatic ring. ^gControl experiment, i. e. no catalyst was used.

UPGRADING OF ALBERTA HEAVY OILS BY SUPERACID-CATALYZED HYDROCRACKING

Otto P. Strausz, Thomas W. Mojelsky, John D. Payzant, Department of Chemistry, University of Alberta, Edmonton, AB Canada T6G 2G2;

George A. Olah and G.K. Surya Prakash, Hydrocarbon Research Institute, University of Southern California, Los Angeles, CA 90089-11661.

Keywords: bitumen, asphaltene, hydrocracking, superacid

INTRODUCTION

An alternative to conventional catalytic hydrocracking of tar sand bitumens would be a superacid-catalyzed hydrocracking. Olah *et al.*¹ have shown the superacid HBF₄ to be an excellent catalyst at low temperatures (105–170°C) and hydrogen pressure (500 psi) for the depolymerization/liqefaction of coal. Superacids prepared from anhydrous HF and metal halides (e.g. TaF₅)² and Lewis acids³ have also been used for the catalytic hydrocracking of petroleum. However, HBF₄, with activity function⁴ $H_0 \sim -16$, offers the unique advantage, in addition to being non-reducible (hence would not oxidize products), of being a gas and readily falling apart to HF and BF₃, thus permitting the corrosive superacid components to be easily removed from the liqefaction/reaction mixture.

In Olah¹ *et al.*'s papers on the superacid treatment of coal, no product analysis data were reported. A study, however, was published on model compounds thought to represent the molecular bridging groups holding coal "monomers" together. Dibenzyl, diphenylmethane and biphenyl (along with their ether and sulfide analogs) were used. Under superacid conditions near quantitative conversions to products such as benzene, toluene, anthracene, p-xylene (phenol, benzenethiol) were obtained in high yields.

The aim of the present exploratory study was to assess the feasibility of employing HBF₄ for the depolymerization/hydrogenation of tar sand bitumens and asphaltenes. The characteristic features of this process can be summarized as follows:

- it involves ionic mechanisms, in contrast to the free radical mechanisms in thermocatalytic cracking and therefore may produce different, possibly more valuable, products than those obtained from the latter reactions;
- the temperature and hydrogen pressure required are much lower than in conventional hydrocracking;
- a gaseous catalyst is free of all the problems associated with solid catalysts (poisoning, core plugging, recovery);
- both HF and BF₃ can be readily separated from the product oil by distillation and recycled;
- neither HF nor BF₃ would cause any oxidative degradation of products; and
- the process is free of fluorine incorporation into products.

EXPERIMENTAL

Hydrocracking was done on 2.0–5.5 g samples of Athabasca or Cold Lake bitumen or asphaltene. Mixtures of the sample with 0–30 mL dry methylcyclohexane were placed in a 250-mL Parr autoclave under a dry nitrogen atmosphere. The autoclave was cooled to –78°C (in a dry ice-acetone bath) and 50-mL anhydrous HF was added. The vessel was closed tightly, warmed to room temperature and 500 psi BF₃ was introduced, followed by 500 psi H₂. Then the autoclave was heated to the desired reaction temperature and maintained at that temperature for 2–24 h. At the conclusion of the reaction, the autoclave was cooled to room temperature, depressurized, opened and the contents quenched with 500-mL ice water. The organic layer was separated and washed several times with a 10% sodium bicarbonate solution to remove traces of acid. The acid-free organic layer was then analyzed by conventional class separation and in some cases by capillary GC-MS, FTIR and ¹H and ¹³C NMR spectroscopy.

RESULTS AND DISCUSSION

The HBF₄-catalyzed hydrocracking of Athabasca bitumen (5.5 g) was carried out in a 24-h reaction at 170°C using, as in all subsequent experiments, 50-mL HF and 500 psi pressure each, BF₃ and H₂. The reaction yielded 33.0% *n*-pentane solubles, 14.7% CH₂Cl₂ solubles ("asphaltene") and 1.8% CH₂Cl₂ insolubles, indicating the formation of 50.5% volatiles (which were not recovered). This experiment demonstrated the high efficiency of the HBF₄ + H₂ superacid system in causing deep-rooted chemical alterations in the bitumen. The extent of the alterations can be appreciated by keeping in mind that in thermocatalytic hydrocracking at 170°C practically no reaction would occur and the yield of volatiles would be only a few percent.

In previous studies on coal liqefaction Olah *et al.*¹ used methylcyclohexane (MCH) as a solvent and hydrogen transfer agent thought to facilitate the process. For this reason, in a series of experiments the effect of added MCH on the hydrocracking of Athabasca bitumen and asphaltene was next examined. The percentage recoveries of bitumen, maltene and asphaltene from the reactions are presented in Figure 1 and Table 1. The data show that under the reaction conditions indicated in Table 1, increasing the volume of added MCH increases the yield of recovered products: bitumen, maltene and asphaltene. The only exception is the asphaltene from

the hydrocracking of asphaltene with 30-mL MCH. Total product yields above ~20-mL MCH exceed the amount of the initial feedstock from both bitumen and asphaltene and rapidly rise with further amounts of MCH. Thus, it is clear that the excess amount of products must be coming from the reactions of added MCH. Since neat MCH does not appear to react under similar reaction conditions, it must be concluded that the intermediates in the HBF_4 -catalyzed hydrocracking of bitumen or asphaltene serve as initiators of the decomposition of MCH. At less than 5 mL, MCH does not appear to decompose or affect the hydrocracking of the bitumen or asphaltene feedstocks, except perhaps by the suppression of the small amount (1.8%) of coke which forms in long reactions. Five-mL MCH in short runs (≤ 2 h) and 30-mL MCH in long runs (24 h) suppressed formation of coke. Product yields with 5-mL MCH are about the same as without MCH.

Table 1. Superacid Treatment of Athabasca (Suncor Coker Feed) Bitumen and Asphaltene. Effect of the Quantity of Added MCH.

| MCH (mL) | Asphaltene | | Maltene | |
|------------|-------------|------------------------|-------------|------------------------|
| | % recovered | % of starting material | % recovered | % of starting material |
| Bitumen | | | | |
| 5 | 18.5 | 8.1 | 81.5 | 35.7 |
| 15 | 13.1 | 9.4 | 86.9 | 62.3 |
| 30 | 5.8 | 11.7 | 94.2 | 191.6 |
| Asphaltene | | | | |
| 5 | 57.1 | 44.6 | 42.9 | 33.5 |
| 15 | 54.6 | 49.2 | 45.3 | 40.8 |
| 30 | 19.1 | 38.4 | 80.9 | 161.6 |

^a 500 psi H_2 , 500 psi BF_3 , 50-mL HF, 1 h, 190°C, reactor volume 250 mL, sample size 2.5–3.1 g. ^b The asphaltene content of the bitumen was 15.5%.

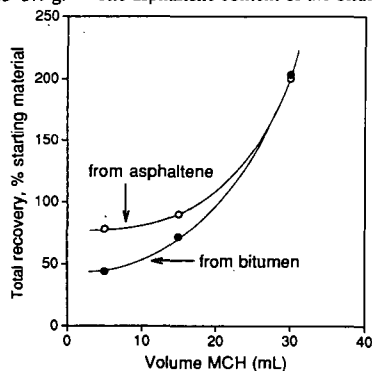


Figure 1. Product (bitumen) yields as a function of added MCH

The low yield of recovered products, Figure 1, in the reactions with 5-mL added MCH represents high conversions to volatiles, 56% from bitumen and 22% from asphaltene. At the same temperature, 190°C and 1-h reaction time, practically no decomposition takes place. With asphaltene, along with the volatiles, 30% conversion to *n*-pentane solubles also occurred. The results obtained from experiments with added MCH further validate the result obtained in the neat bitumen hydrocracking reaction.

Before progressing further, it is noted here that in the early stages of the investigations considerable difficulties were experienced with the lack of reproducibility. Moreover, it was noted that the maltene product—especially from the asphaltene reactions with added MCH—was highly reactive and upon exposure to air it reacted with oxygen, transforming the colorless mobile liquid oil to a translucent gum. This observation suggested that conjugated alkenes may have been produced, providing a possible explanation for the lack of reproducibility. Next, it was found that the fresh maltene product from the hydrocracking of Cold Lake bitumen contained no oxygen, but after two days' exposure to air the oxygen content was 5.8%.

Comparison of the IR spectra of air-protected and air-exposed samples, Figures 2 and 3, revealed the absence and presence of intense carboxylic (1705 and 3440 cm^{-1}) and possibly alcoholic (1080 cm^{-1}) group absorptions and the presence and absence of conjugated triene absorptions (1500–1700 cm^{-1}). It was also found that the double bonds could be readily brominated. Oxidation with *m*-chloroperbenzoic acid converted the "saturate" fraction to some polar material in >98% yield, suggesting the absence of any paraffinic hydrocarbons.

Furthermore, the GC of the "saturate" fraction featured two broad humps superimposed by a large number of peaks corresponding to individual compounds. Four of six selected major

peaks from GC-MS could be assigned to isomers of a $C_{16}H_{24}$, and the remain two to some $C_{17}H_{26}$ hydrocarbons. These structures possess five $C=C$ double bond equivalents. Next, in order to determine the number of double bonds in these structures, the "saturate" fraction was subjected to PtO_2 -catalyzed hydrogenation which led to chemical changes. It is known that tetra-substituted double bonds are not affected under these conditions.

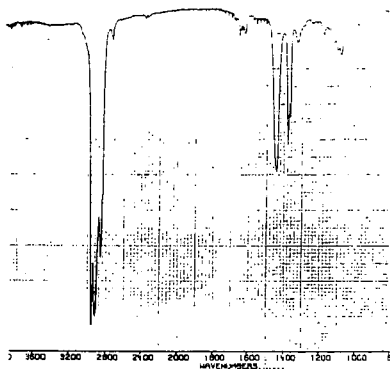


Figure 2. Infrared spectrum of the "saturate" fraction of Cold Lake superacid-treated asphaltene, stored under nitrogen.

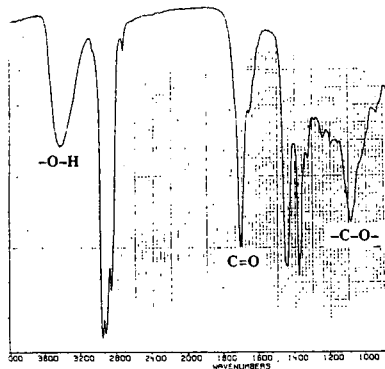
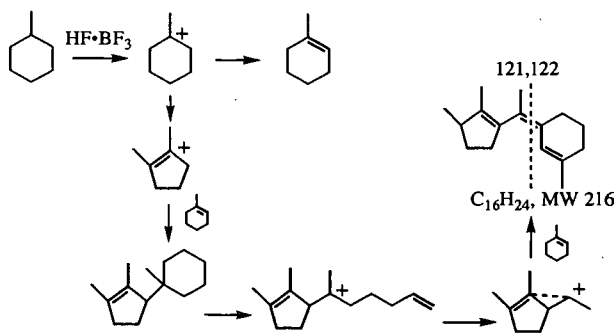


Figure 3. Infrared spectrum of the "saturate" fraction of Cold Lake superacid-treated asphaltene, exposed to air.

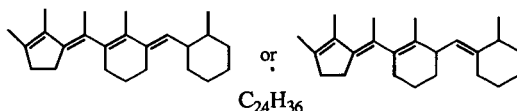
The 1H NMR spectrum of the "saturates" consisted almost entirely of aliphatic hydrogens with a small contribution from alkene hydrogens. The ^{13}C NMR spectrum showed significant signals in the 125–135 ppm range which are due to alkene carbons and from the attached proton test it appeared that the carbons resonating in the 125–135 ppm range had no attached hydrogens. This suggests that, in agreement with the 1H NMR spectrum, the resonances correspond to tetra-substituted alkenes.

In an attempt to obtain further structural information, the "saturate" fraction was subjected to ionic hydrogenation ($(Et)_3SiH$, CF_3CO_2H , $BF_3 \cdot Et_2O$, $0^\circ C$, 1 h) which, after alumina chromatography, gave ~35% yield of hydrogenated product. GC-MS analysis of this material showed that the $C_{16}H_{24}$ and $C_{17}H_{26}$ compounds in ionic hydrogenation were converted to $C_{16}H_{30}$ and $C_{17}H_{32}$ compounds, both of which contain two saturated rings. Therefore, the original $C_{16}H_{24}$ and $C_{17}H_{26}$ compounds each contained three carbon-carbon double bonds which must have been conjugated in order to account for the high reactivity of these molecules, as manifested by their spontaneous rapid reaction with atmospheric oxygen. Moreover, from the NMR spectra it is clear that the alkene carbons are quaternary. Therefore, we are forced to conclude that under the experimental conditions of the superacid-catalyzed hydrogenation employed, the MCH solvent undergoes ionic rearrangement, degradation and oligomerization. Speculative structures and mechanisms for the formation of the bicyclic conjugated quaternary tri-olefins are shown in Scheme 1.



Scheme 1. Superacid-catalyzed solvent polymerization

Most of the peaks in the GC-MS of the "saturate" fraction correspond to molecules with structures analogous to the $C_{16}H_{24}$ and $C_{17}H_{26}$ compounds. Thus, for example, in the chemical ionization GC-MS of the "saturate" fraction three major selected peaks corresponded to isomeric $C_{24}H_{36}$ compounds which would fit the tricyclic conjugated tetra-alkene structure



Thus, the C_{24} compounds appear to be the homologs of the C_{16} and C_{17} compounds having one more MCH ring, with or without an extra carbon atom.

The results from studies on the HBf_4 -catalyzed hydrocracking in the presence of MCH point to the general reactivity of the HBf_4 superacid system indicating that acyclic and cyclic hydrocarbons can be attacked. Indeed, the typical gas chromatograms of the saturates from the native bitumens displaying the series of biological markers are altered beyond recognition after the hydrocracking process (suggesting the destruction of cheilanthanes, hopanes, isoprenoids, etc.). Also, the monoaromatic subfraction after hydrocracking appears to be rich in 1-phenyl, 2,2-dimethyl- n -alkanes, whereas in the native asphaltene the aromatic-attached alkyl groups are n -alkyl, and branched alkyls are hardly present. The appearance of these products is consistent with the known tendency of superacids to catalyze the break-up of alkyl chains and bring about their isomerization to t -butyl structures. Superacids also catalyze the transalkylation of aromatic compounds which, together with the above isomerization reactions, could account for the generation of the branched alkyl products.

SUMMARY AND CONCLUSIONS

- It has been established that the superacid HBf_4 is a highly effective catalyst for the hydrocracking of bitumens and asphaltenes even under very mild conditions (170–190°C, 1 h or less);
- The reactions involved proceed with ionic mechanisms as opposed to the free radical mechanisms in thermal hydrocracking, resulting in deep-rooted alterations of the chemical composition of the bitumen, evidenced by the high (56%) conversion of the bitumen to volatiles, the drastic changes in the gas chromatograms of the various compound classes of the bitumen and the appearance of many prominent branched alkylbenzene peaks, etc.
- In asphaltene, parallel to depolymerization some secondary polymerization leading to the formation of asphaltene-like materials takes place upon prolonged reaction times. Therefore, establishing the optimal reaction time is essential to obtain the most favorable conversions.
- Methylcyclohexane exhibits high reactivity with respect to the $HF \cdot BF_3$ superacid under the conditions of the bitumen or asphaltene hydrocracking process—typifying the general reactivity of cycloalkanes—resulting in the oligomerization of methylcyclohexane to produce conjugated alkenes; this reaction also reflects some of the possible ways by which the superacid may react with the bitumen or asphaltene since both these materials are known to contain cycloalkane units.
- Fluorine incorporation into the bitumen does not take place and no evidence could be found for catalyst consumption.
- BF_3 is a gas and HF a low-boiling liquid (b.p. 20°); both are highly water-soluble and therefore should be readily separable from the hydrocracked bitumen and recycled for further use. Thus, taking the above results in conjunction with the ready recoverability of the catalyst, it can be concluded that $HF \cdot BF_3$ superacid catalysis has considerable potential for commercial application in the bitumen upgrading industry.

ACKNOWLEDGEMENTS

We thank the Alberta Oil Sands Technology and Research Authority for financial assistance.

REFERENCES

1. Olah, G.A.; Bruce, M.R.; Edelson, E.H.; Husain, A. *Fuel* **1984**, *63*, 1130–1137; Olah, G.A.; Husain, A., *Fuel* **1984**, *63*, 1427–1431; Olah, G.A.; Bruce, M.R.; Edelson, E.H.; Husain, A. *Fuel* **1984**, *63*, 1432–1435; Olah, G.A. US Pat. 4,394,247 (1983).
2. Siskin, M.; Wristers, J.P.; Purcelli, J.J., *US Patent* 3,901,790 (1975).
3. Ignasiak, T.; Bimer, J.; Samman, N.; Montgomery, D.S.; Strausz, O.P. In *Chemistry of Asphaltenes*, Advances in Chemistry Series 195, Bunger, J.W.; Li, N.C., Eds, American Chemical Society: Washington, D.C., 1981, pp 183–201.
4. Olah, G.A.; Prakash, G.K.S., *Superacids*, J. Wiley & Sons: New York, 1985.

STUDY ON HYDROGEN DONATION ABILITY OF RESIDUE HYDROCRACKING SYSTEM CATALYZED BY OIL-SOLUBLE AND WATER-SOLUBLE CATALYSTS

Zong-Xian Wang, Hong-Yu Zhang, Ai-Jun Guo, and Guo-He Que,
National Heavy Oil Processing Laboratory, University of Petroleum (East China),
Dongying, Shandong 257062, P. R. China

Molybdenum-based oil-soluble and iron-based water-soluble catalyst precursors were separately used in catalytic hydrocracking systems of Liaohe vacuum residue in order to investigate the hydrogen donation ability of mild hydrocracking products. The catalytic hydrocracking tests were conducted in an 100ml autoclave, at 430°C, 30min, 7.0MPa initial hydrogen and 50°C, 500ppm catalysts (based on metal in feed). Anthracene (ANT) was used as a hydrogen acceptor to react, under conditions of 405°C, 2MPa N₂ and 30 minutes, with the atmospheric residue (AR) of hydrocracking products to determine the hydrogen donation ability of the AR. Thus, the hydroaromatic species in the AR might donate active hydrogen to anthracene, which make anthracene change to dihydroanthracene (DHA). GC technique was used to quantify the DHA formation, which was indirectly indicative of the hydrogenation activity of different hydrocracking catalysts. The results showed that Fe-based water-soluble catalysts have little ability to hydrogenate the polycyclic aromatics to hydroaromatics, the hydrogen donors, though they could inhibit coke formation when used in relatively large amount. However, Mo-based oil-soluble catalyst has higher hydrogenation activity, and even could promote hydroaromatics generation. These secondary hydrogen donors could act as a reservoir of active hydrogen and a complement to the active hydrogen molecules activated directly by catalysts in the subsequent hydrocracking stage.

Key words: hydrogen donation, catalytic hydrocracking, vacuum residue

INTRODUCTION

Dispersed metal catalysts used in slurry phase hydrocracking of residue are commonly prepared either by the addition of finely divided inorganic powders to the residue, or by the addition of water- or oil-soluble metal salts to the heavy oils [1-8]. For the same metal, its oil-soluble salts seems more active than its water-soluble salts and its inorganic powders, as its oil-soluble salts can be homogeneously mixed into the heavy oil and can form superfine active catalyst particles after sulfidation [1,5]. For different metals, Mo, Ni, Co, Fe are most commonly used [1-8], of which Mo seems the most active in residue hydrocracking and Fe may be the lowest in their salt prices.

All these catalysts can suppress coke formation during residue hydrocracking by hydrogenating unstable polynuclear aromatic free radicals that are generated thermally [1,3]. Some may be quite active even in very low concentrations (100-200ppm, based on metal to residue), such as oil-soluble Mo-based catalysts [1,5]; some others can counterbalance the total catalytic activity only as in a large amount (1000-5000ppm), such as Fe-based water-soluble or powdered catalysts [1,6,7]. Hence, it seems that there is a little difference in coke suppression mechanism between these two relatively extreme catalysts. The present study uses anthracene (ANT) as a chemical probe to characterize the hydrogen donation ability of residue hydrocracking systems catalyzed respectively by Mo-based oil-soluble and Fe-based water-soluble catalysts. The hydroaromatic species in residue can donate hydrogen to anthracene and make the anthracene mainly change to dihydroanthracene (DHA) [9-12]. The hydrogen donation ability is indicative of inter- or intra-molecular hydrogen transfer between the donors and coke precursors free radicals. The higher is the hydrogen donation, the higher the coke suppression ability.

EXPERIMENTAL

Sample

Liaohe vacuum residue(>500°C) was collected from Liaohe Petrochemical Plant in March 1996. Carlo Erba 1160 elemental analyzer was used for C, H, N analysis; atomic absorption method was used to determine Ni, V, Fe and Ca contents. Average molecular weight was measured by using VPO method (benzene as solvent, 45°C) with Knauer molecular weight analyzer. The general properties of Liaohe vacuum residue are listed in Table 1.

Catalytic hydrocracking of Liaohe vacuum residue

The experiments were carried in a 100ml FDW-01 autoclave reactor with an up-and-down stirrer at 120 times of reciprocation per minute. Initial pressure was 7.0MPa H₂ for catalytic hydrocracking.

Catalyst used in the hydrocracking reaction was Molybdenum-based oil soluble and iron-based water-soluble catalyst (ca.50~1000 ppm based on metal concentration in feed). The former was compatible with the vacuum residue and gave rise to the homogeneous system with the vacuum residue, and the later was emulsified into the vacuum residue to form emulsion system. After sulfidation by elemental sulfur at 320°C for 30 minutes (S/Metal atomic ratio=3/1), these catalyst precursors were in situ reacted to real active catalysts. Then, the temperature was raised to 430°C and kept at the temperature just for 30 minutes for hydrocracking reaction. After that, the reactor was quenched (cooled) to room temperature, the reactor gas was vented, and toluene slurry was prepared from the reactor contents. Any solids adhering to the reactor walls or internals was carefully scraped off. The slurry was then centrifuged and the toluene insoluble (TI or coke) were separated and washed (extracted) with boiling toluene by using quantitative filter paper. The solids were dried and weighed. The toluene soluble was distilled into several fractions. The results were listed in table 2.

Measurement of hydrogen donation abilities of Liaohu vacuum residue hydrocracking products

Anthracene (ANT) was used as a hydrogen acceptor to react, in a 50 cm³ stainless steel tubular reactor with a 30 cm³ quartz inner tubular microreactor, with >350°C fraction of the hydrocracking products under 405°C and 2MPa N₂ atmosphere. The feed charge is a mixture of 1-gram oil sample and 2 gram anthracene. Thus, the secondary hydroaromatics in >350°C fraction of hydrocracking products can donate active hydrogen to anthracene, which make anthracene change to 9,10-dihydroanthracene (DHA)[9-12]. The reaction products were analyzed by gas chromatography using a Varian3400 chromatograph equipped with a 30m×2.65um HP-5 (crosslinked 5% Ph Me silicon) column and a FID detector and naphthalene and DHA as the internal standards. The contents of DHA generated in the thermal reaction system were listed in table 3. The quantity of molar hydrogen accepted from one gram of charged oil sample could be calculated by following equation:

$$MN=Y_{DHA} \times W_{mix} / (M_{DHA} \times W_{oil})$$

Here, MN is the moles of hydrogen accepted from 1 gram of oil sample, Y_{DHA} the yield of DHA in the thermal reaction system, W_{mix} the weight of charged mixture of oil and ANT, M_{DHA} the molecular weight of DHN and W_{oil} the weight of charged oil sample. The MN values for different oil samples were also tabulated in table3.

RESULTS AND DISCUSSION

Distribution of hydrocracking products

It seems that the coke formation has a tendency to increase with the Mo-based catalysts at the early stage of Liaohu vacuum residue hydrocracking as indicated in table 2. This coke may largely consist of condensed-asphaltene. Under the induction of polar catalyst particles, the structure of asphaltene micellae may become loose, and asphaltene may be adsorbed by MoS₂ particles (with relatively higher polarity) and may condense on the particles, leading to the formation of toluene insoluble materials, a physically condensed state of asphaltene of higher polarity, not a real chemical coke. The more the MoS₂ catalysts, the stronger the induction to polar asphaltene may be, the more the initial coke will form, but the less the ratio of the coke to MoS₂; and, relatively, the total catalyst activity is still high. The product distribution indicates that with increasing Mo-based catalyst, conversion to VGO seems to increase and the conversion to lighter product decreases, showing an increase in hydrogenation ability.

Hydrogen donation ability of Liaohu vacuum residue and its hydrocracking products

This work aimed at determining the hydrogen donation abilities of Liaohu vacuum residue and its hydrocracking products, VGO(350 - 480°C) and hydrocracked vacuum residues (HVR), processed under different conditions. As table 3 indicated, the Liaohu Atmospheric residue has higher hydrogen-donating ability than its vacuum residue. The hydrogen-donating abilities of thermal cracked products of Liaohu vacuum residue are less than those of its catalytic hydrocracking products, showing that the catalysts could, at least, suppress the cracking of hydrogen-donating species in the residue reaction system. In comparison, Mo-based oil-soluble catalyst could give rise to higher hydrogen-donating abilities of its catalyzed hydrocracking products than Fe-based water-soluble catalyst. It seems that the hydrogen activated by Fe-based catalyst was not enough high to hydrogenate polycyclic aromatics to hydroaromatics, leading to only a little difference in hydrogen-donating abilities between its catalyzed products and thermal cracking products. The Mo-based catalysts might catalyze hydrogenation of some active polycyclic aromatics to hydroaromatics beside its high coke suppression ability by directly catalyzing hydrogenation of

polycyclic aromatic free radicals. The hydroaromatics generated in situ could act as hydrogen donors in subsequent reactions. The active hydrogen transfer from the hydrogen donors to polycyclic aromatic free radicals may be easier than the active hydrogen directly activated by the catalysts because the hydroaromatics are more compatible with the free aromatic radicals than the catalysts.

With the increase of Mo-based catalyst, the hydrogen-donating abilities of its catalyzed hydrocracking products increase. As Mo was over 160ppm, the hydrocracked vacuum residues were very near to Liaohe vacuum residue in hydrogen-donating ability. On the basis of one gram of Liaohe vacuum residue, the total hydrogen donations of its catalytically hydrocracked AR were 4.56×10^{-4} , 5.02×10^{-4} , 6.25×10^{-4} , 6.42×10^{-4} , 7.01×10^{-4} , 7.12×10^{-4} , and 7.14×10^{-4} moles for no catalyst, 470ppm Fe, 74ppm, 86ppm, 168ppm, 316ppm and 619ppm Mo respectively. In comparison to 470ppm Fe, 86ppm Mo could make the AR a net gain of 1.40×10^{-4} moles of hydrogen donation. Except for direct free radical hydrogenation ability of Mo catalyst, the net gain of hydrogen donation ability might play a great role in coke suppression during further hydrocracking process. For example, prolonging hydrocracking time from 30minutes to 1hour could make the coke formation to increase from 1.6% to 5.7% as 470ppm Fe catalyst was used, and make the coke formation to increase from 0.2% to only 1.3% when 86ppm Mo-based catalyst was used.

CONCLUSION

Anthracene was used as a chemical probe to determine the hydrogen donation ability of Liaohe vacuum residue and its mild catalytic hydrocracking products. In comparison to pure thermal cracking, the catalysis of Fe-based water-soluble catalysts was little in promoting the formation or in suppressing the cracking of the hydroaromatics--the secondary hydrogen donors, though Fe catalysts could inhibit coke formation when used in relatively large amount [1]. However, Mo-based oil-soluble catalyst has higher hydrogenation activity, and even could promote hydroaromatics generation in comparison to Fe-based catalyst. These secondary hydrogen donors could act as a reservoir of active hydrogen and a complement to the active hydrogen molecules activated directly by catalysts in the subsequent hydrocracking stage.

ACKNOWLEDGEMENT

The authors thank Miss F. Gao and Mr. R-F. Liu for helpful experimental work, and Miss J-X Xing for GC analysis.

REFERENCES

- (1) Del Bianco, A., Panariti, N., Di Carlo, S., Elmouchnino, J., Fixari, B. and Le Perchec, P., *Applied Catalysis, A: General*, **94**, 1-16(1993)
- (2) Del Bianco, A., Panariti, N., Marchionna, M. *Am. Chem. Soc., Preprints, Div. Petrol.* **40**(4)743-746(1995)
- (3) Le Perchec, P., Fixari, B., Vrinta, M., Morel, F., *Am. Chem. Soc., Preprints, Div. Petrol.* **40**(4)747-751(1995)
- (4) Bearden, R. and Aldridge, C. L., *Energ. Progress*, **1**(1-4), 44(1981)
- (5) Strausz, O.P., Lown, E.M., Mojesky, T.W., *Am. Chem. Soc., Preprints, Div. Petrol.* **40**(4)741-742(1995)
- (6) Liu, C., Zhou, J., Que, G., Liang, W., Zhu, Y., *Fuel*, **73**, 1545-1550(1994)
- (7) Smith, K.J., Duangchan, A., Hall, A.G., *Am. Chem. Soc., Preprints, Div. Petrol.* **42**(3)479-483(1997)
- (8) Del Bianco, A., Panariti, N., Marchionna, M., *Am. Chem. Soc., Preprints, Div. Petrol.* **42**(3)484-488(1997)
- (9) Yokono, T., Marsh, H., Yokono, M., *Fuel*, **60**, 607-611(1981)
- (10) Yokono, T., Obara, T., Iyama, S., Sanada, Y., *Carbon*, **22**(6)623-624(1984)
- (11) Wang, S.L., Curtis, C.W., *Energy & Fuels*, **8**, 446-454(1994)
- (12) Pajak, J., Krebs, V., Mareche, J.F., Furdin, G., *Fuel Processing Technology*, **48**, 73-81(1996)

Table 1 General properties of Liaohe vacuum residue (VR)

| | | | |
|--|--------|-------------------|-------|
| Density(20°), g./cm ³ | 0.9976 | SARA fractions: | |
| Viscosity(100°)/mm ² .s ⁻¹ | 3375 | Saturates, % | 17.4 |
| Pour point, °C | 42 | Aromatics, % | 30.3 |
| Flash point, °C | 312 | Resins, % | 50.2 |
| Carbon residue, % | 19.0 | nC7-Asphaltene, % | 2.1 |
| Elemental composition | | Total Metal/PPM | 258.6 |
| C, % | 87.0 | Ni, ppm | 122.6 |
| H, % | 11.4 | V, ppm | 2.9 |
| S, % | 0.43 | Fe, ppm | 37.5 |
| N, % | 1.08 | Ca, ppm | 95.6 |
| H/C(Atomic ratio) | 1.50 | Ash, % | 0.06 |

Table 2 Effect of catalysts on Liaohe vacuum residue hydroconversion
(430°C, 7MPa initial hydrogen pressure, reaction time 30 min.)

| Catalyst, ppm | <350°C, % | 350-480°C, % (VGO) | >480°C, % (HVR) | Coke, % |
|---------------|-----------|--------------------|-----------------|---------|
| none | 23.0 | 22.5 | 52.7 | 1.8 |
| Fe, 470 | 21.5 | 20.1 | 56.8 | 1.6 |
| Mo, 74 | 14.0 | 18.0 | 68.0 | 0.2 |
| Mo, 86 | 14.3 | 17.0 | 68.5 | 0.2 |
| Mo, 168 | 13.4 | 17.3 | 69.1 | 0.2 |
| Mo, 316 | 13.1 | 18.4 | 68.2 | 0.3 |
| Mo, 619 | 12.9 | 20.0 | 66.6 | 0.5 |

Table 3. Hydrogen transfer in thermal reaction system
of initial hydrocracking products of Liaohe residue

| Oil Sample/ANT (m/m) | DHA generated in thermal reaction system | MN × 10 ⁴ |
|---|--|----------------------|
| LHVR, (0.2170:1) | 1.32% | 8.22 |
| LHAR, (0.1970:1) | 1.26% | 8.49 |
| VGO(H ₂), (0.5042:1) | 1.99% | 6.60 |
| VGO(H ₂ ,Fe470), (0.4879:1) | 2.13% | 7.22 |
| VGO(H ₂ ,Mo74), (0.5032:1) | 2.39% | 7.93 |
| VGO(H ₂ ,Mo86), (0.5058:1) | 2.42% | 8.00 |
| VGO (H ₂ ,Mo168), (0.5143:1) | 2.59% | 8.47 |
| VGO (H ₂ ,Mo316), (0.5042:1) | 2.75% | 9.12 |
| VGO (H ₂ ,Mo619), (0.4938:1) | 2.72% | 9.14 |
| HVR (H ₂), (0.5073:1) | 1.79% | 5.91 |
| HVR (H ₂ ,Fe470), (0.5083:1) | 1.91% | 6.30 |
| HVR (H ₂ ,Mo74), (0.5120:1) | 2.16% | 7.09 |
| HVR (H ₂ ,Mo86), (0.4742:1) | 2.14% | 7.39 |
| HVR (H ₂ ,Mo168), (0.5001:1) | 2.41% | 8.03 |
| HVR (H ₂ ,Mo316), (0.4934:1) | 2.37% | 7.97 |
| HVR (H ₂ ,Mo619), (0.4945:1) | 2.42% | 8.12 |

VGO--350-450°C fraction; HVR--hydrocracked vacuum residue.

LHVR--Liaohe vacuum residue; LHAR--Liaohe atmospheric residue.

Amorphous Microporous Mixed Oxides, New Selective Catalysts with Chemo- and Shape-Selective Properties

Wilhelm F. Maier
Max-Planck-Institut für Kohlenforschung
D-45470 Mülheim an der Ruhr, Germany

The increasing economical and ecological demands on chemical processes have led to a growing need for more selective heterogeneous catalysts. Selectivity based on hindered diffusion of molecules of different polarity or size in micropores, the so called shape selectivity, is key to the success of zeolites [1]. However, fundamental limitations with respect to chemical composition and pore architecture restrict general applications of these catalysts. Amorphous microporous mixed oxides (AMM) are promising new materials, whose catalytic properties can be controlled during a one-step preparation procedure of the sol-gel-type. By acid catalyzed copolycondensation of an alkoxide of Si, Zr, Al or Ti with a soluble derivative of a catalytically active element, such as Mn, Mo, V, Ti, Sn, In, Cu, Fe, Cr, atomically distributed active centers in the oxide matrix can be obtained. In the absence of any template, the reaction conditions followed by drying and calzining provides a highly porous mixed oxide with a narrow pore size distribution around 0.6-0.9 nm. The surface polarity of such an oxide can be controlled by the addition of alkoxides containing a nonhydrolyzable alkylgroup, such a methyltriethoxysilane, to the copolycondensation reaction. The basic reaction for silica based AMM-8materials is shown below:



| | | | |
|------------------------------|------------------------------|-------------------------------|--|
| <i>catalytic centers</i> | <i>polarity modifier</i> | <i>microporous matrix</i> | <i>Amorphous Microporous Mixed oxide (AMM)</i> |
|------------------------------|------------------------------|-------------------------------|--|

The materials are denoted as AMM-M_xM', where M' stands for the base oxide and x for the atom% of the additional oxide M. After proper calzination, these materials remain amorphous and have a porosity of 10-35%. A typical pore size distribution and a high resolution TEM-micrograph (AMM-Ti₃Si = 3 % titania in 97 % silica) are shown in Figure 1.

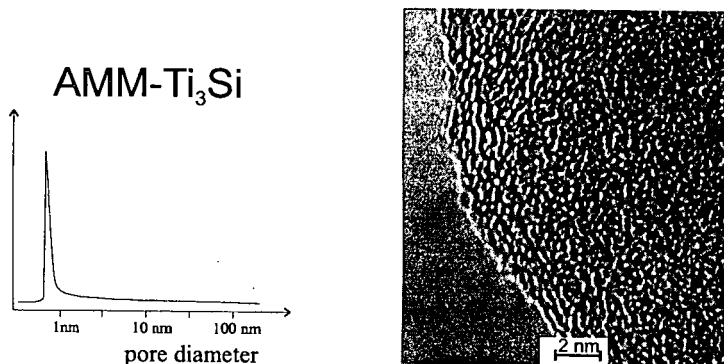


Fig. 1: Pore size distribution (Horvat-Kawazoe-method) and TEM-micrograph of a typical AMM-catalyst.

Rheological studies show a simultaneous increase in elasticity and viscosity under these sol-gel conditions indicative of a linear chain growth in the polycondensation process [2]. The porosity of these amorphous materials has been shown to be stable up to 800 °C. Diffuse reflectance IR, XANES [3] and diffuse reflectance UV [4] provide evidence for homogeneity and atomic isolation of the Ti-centers in AMM-Ti_xSi at Ti-concentrations < 5%. PFG-NMR studies on hydrophobic and hydrophilic AMM-Si-materials with small molecules show diffusion rates comparable to those observed in Y-zeolites. It was found, that the diffusion of unpolar molecules like hydrocarbons is not affected by the surface polarity, while the diffusion of polar molecules like water and butanol is strongly hindered in hydrophilic AMM-Si, while both molecules are not observable in the hydrophobic AMM-Me₂Si₂Si [5].

In general, AMM-materials can be described as catalysts prepared to contain isolated catalytically active centers in the shape selective environment of micropores. The lack of inherent limitations with respect to chemical composition and pore size makes AMM-materials versatile catalyst for many uses. AMM-materials have already shown promising properties as selective heterogeneous catalysts in a variety of applications:

Hydrocracking: Decane hydrocracking is an established test reaction for the precise assignment of pore structure and pore architecture of zeolites [6]. After impregnation with 0.5 % Pt, AMM-Ti₃Si, AMM-Ti₁₇Si and AMM-V₁₀Si have been exposed to the decane hydrocracking test under standard conditions. The product distribution positioned the Ti-containing AMMs in the range of large pore zeolites, while the AMM-V₁₀Si is positioned in the zeolite free range between the medium-pore 10-ring zeolites and the large pore 12-ring zeolites. The test furthermore identifies the AMM-materials as having a tubular pore system lacking larger cavities and pore intersections [7]. These results showed for the first time shape selective properties of amorphous materials. Therefore shape selective properties are not associated with crystallinity, but only with a small pore size and a narrow pores size distribution.

Redox-catalysis with organic hydroperoxides: With TBHP as oxidizing agent AMM-Ti₃Si catalyzes the selective epoxidation of alkenes. With linear and cyclic olefins, the rate of epoxidation decreases rapidly with increasing number of carbon atoms [7]. A similar decrease in the rate of epoxidation of alkenes with TS-1 has been ascribed to molecular shape selectivity [8]. AMM-V_xSi and AMM-Ti_xSi can selectively oxidize olefins and saturated hydrocarbons [9]. Like other crystalline and amorphous Ti-silicates the catalysts are deactivated during epoxidation reactions by product inhibition, caused by pore- or surface blocking with the alcohol formed from the hydroperoxide. The catalysts are not active with hydrogen peroxide as oxidant.

Redox-catalysis with hydrogen peroxide: Due to unconnected surface coordination sites highly porous oxides are rich in surface hydroxyl groups and thus highly hydrophilic. By copolycondensation of increasing amounts of Me-Si(OEt)₃ with Si(OEt)₄ and 1% (iPrO)₄Ti a series of AMM-materials with increasing hydrophobicity was prepared. The most hydrophobic materials (AMM-Ti₁₆Me₄Si₄Si) show several interesting properties. The catalysts do not deactivate during epoxidation reactions and they can be reused. They can be used with hydrogen peroxide as oxidant. In fact, with H₂O₂ these hydrophobic amorphous microporous Ti-Si-oxides show comparable activities as Ti-containing zeolites for a wide range of selective oxidation reactions, such as ammoxidation, oxidation of alcohols, and oxidations of saturated hydrocarbons [11].

Acid catalyzed etherification and esterification reactions: Solid acid catalysts are of increasing importance as potential replacement of homogeneous acid catalysts in the production of fine and bulk chemicals. AMM-Sn_xSi with low Sn-content have been found to be very active and selective mild acid catalysts. The catalysts are Lewis-acidic, no evidence for Brønsted acidity was obtained by IR-studies. The catalysts showed excellent catalytic activities for esterification reactions of pentaerythritol with stearic acid and for the formation of t-butylethers [12].

Oxidative dimerization of propene with air: Oxidative coupling of propene with air in the gas phase under selective formation of 1,5-hexadiene has been reported with diene selectivities peaking at 60 % at propene conversions far below 10 %. With AMM-In₂Si at 560 °C under continuous gas phase flow conditions propene (23 % conversion) is selectively converted with air to 1,5-hexadiene (selectivity 84 %). The unusual selectivity is attributed to the presence of isolated In-centers (confirmed by EXAFS-studies) in the shape selective environment of the

micropores [13]. With AMM-Cu₆Si at 370 °C acrolein is formed with a remarkable selectivity of 93 % at a propene conversion of 10 % [14].

Selective Oxidation of toluene to benzaldehyde with air: In a gas phase flow reaction at continuous reaction conditions AMM-Mn₃Si selectively oxidizes toluene to benzaldehyde with air (normal pressure, 450 °C, toluene conversion 5 %, selectivity 83 %). EXAFS investigations identify the Mn as isolated centers of oxidation state II [15].

Selective aromatic alkylation: The isopropylation of naphthalene and biphenyl have been investigated with various AMM-catalysts. The AMM-Al₃Si materials show the most promising activity. After deactivation of external acid sites, AMM-Al₃Si exhibits highly selective alkylation behaviour. In the gas phase at continuous flow conditions at 250 °C 4,4'-diisopropylbiphenyl is formed directly from biphenyl with a selectivity of 61 % at a biphenyl conversion of over 7 %. At identical reaction conditions a H-Mordenite reaches 73 % selectivity. Isopropylation of naphthalene at unoptimized conditions at a conversion of 46 % produces only mono and diisopropylnaphthalene (ratio 2:1), the latter consists to 44.5 % of the 2,7- and to 50 % of the 2,6-isomer. This shows that AMM-catalysts can be modified to become selective dialkylation catalysts comparable to the best zeolites [16].

Microporous catalyst membranes: Another promising area is the application of catalytic membranes as a means to improve the selectivity of heterogeneously catalyzed reactions. The combination of permselectivity with catalysis opens a new field of reaction engineering and reactor design [17]. Due to the preparation process, which passes through a sol, thin AMM-catalyst films can be prepared by dip-coating [18]. With the use of proper support membranes, thin catalyst membranes have been prepared, characterized and applied in various heterogeneously catalyzed reactions. Poison resistant catalysis has been achieved in the hydrogenation of fatty esters by dosing the hydrogen through a microporous AMM-Pt₃Ti membrane catalyst. Addition of well known poison molecules like tetrahydroacridine or quinoline in equimolar amounts have no effect on the rate of hydrogenation, since the poison molecules are too large to penetrate the micropores of the membrane containing the catalytically active sites [19]. A higher turnover frequency (TOF) in the membrane relative to the batch reactor was noted. In a more detailed study of the rate of hydrogenation of 1-octene in the batch reactor relative to the membrane reactor, this higher TOF could be confirmed. It was shown, that comparable TOFs in the membrane reactor and in the batch reactor are obtained, when the hydrogen is dosed through the liquid sitting on top of the catalyst membrane, while the TOF increases by a factor of 10 when hydrogen is dosed through the catalyst membrane to the alkene containing solution. By competition experiments it is shown, that the normally occurring competitive adsorption of alkene and hydrogen on the Pt-sites does not seem to occur, when hydrogen is dosed through the membrane [20]. In another investigation a new way to prevent secondary reactions has been demonstrated. The basic scheme is to pass a solution of two reactants through a catalytically active microporous membrane. When the pores are so narrow, that molecular passing of reactants is hindered or inhibited during the diffusion through the pores (single file diffusion), secondary reactions cannot take place as long as the concentration of the limiting reactant does not allow a second reaction to occur. The action of the micropores is to provide a defined reaction zone and to completely prevent backmixing of the products formed with the reactants. With AMM-Pt₃Ti-membranes at proper reaction conditions 1,3-hexadiene can be hydrogenated selectively to monoenes at conversions of up to 40 %. At 20 % conversion 2-hexyne is selectively hydrogenated to cis-2-hexene. In both reactions no n-hexane formation is detectable. However, when the hydrogen pressure is increased (increases the hydrogen concentration in the solution and the pores) n-hexane formation occurs. The same AMM-Pt₃Ti-catalysts is completely unselective in the batch reactor at identical reaction conditions [21]. The prevention of back-mixing by microporous catalyst membranes is a new means to avoid secondary reactions.

Clearly, amorphous microporous mixed oxides are a promising class of selective heterogeneous catalysts, ready and waiting for technical applications.

References:

- [1] Zeolites and Related Materials: State of the Art 1994, (eds.: J. Weitkamp, H.G. Karge, H. Pfeifer, W. Hölderich), Elsevier, Amsterdam 1994; W. Hölderich, M. Hesse, F. Nümann, Angew. Chem. Int. Ed. 1988, 27, 226.
- [2] Tilgner, I.-C., Fischer, P., Bohnen, F.M., Rehage, H., Maier, W.F., Microporous Materials, 5 (1995) 77.
- [3] S. Klein, S. Thorimbert, W.F. Maier, J. Catal., 163 (1996) 477.
- [4] S. Klein, W.F. Maier, B.M. Weckhuysen, J.A. Martens, P.A. Jacobs, J. Catal., 163 (1996) 489.
- [5] C. Krause, S. Klein, J. Kärger, W.F. Maier, Advanced Mat. 8 (1996) 912.
- [6] J.A. Martens, P.A. Jacobs, S. Cartledge, Zeolites 1989, 9 423.
- [7] W.F. Maier, S. Klein, J. Martens, J. Heilmann, R. Parton, K. Vercuyse, P.A. Jacobs, Angew. Chem. Int. Ed. 35 (1996) 180.
- [8] A. Corma, P. Esteve, A. Martinez, S. Valencia, J. Catal. 1995, 152, 18.
- [9] S. Klein, J. Martens, R. Parton, K. Vercuyse, P.A. Jacobs, W.F. Maier, Catal. Lett., 38 (1996) 209.
- [10] S. Klein, W.F. Maier, Angew. Chem., 108 (1996) 2376; Int. Ed. 35 (1996) 2330.
- [12] S. Storck, W.F. Maier, W. Ben-Mustafa, H. Bretinger, I.M.M. Salvado, J.M. Ferreira, D. Guhl, J.A. Martens, W. Souverijns, J. Catal., 172 (1997) 414.
- [13] S. Bukeikanova, H. Orzesek, U. Kolb, K. Kühlein, W.F. Maier, Catal. Lett. 50 (1998) 93.
- [14] H. Orzesek, PhD-Thesis, University of Essen, Germany, 1998.
- [15] F. Konietzki, U. Kolb, U. Dingerdissen, W.F. Maier, J. Catal. in print.
- [16] S. Neunerdt, PhD-Thesis, University of Essen, Germany, 1998.
- [17] H.P. Hsieh, Catal. Rev. Sci. Eng. 33 (1997) 1.
- [18] Maier, W.F.; Tilgner, I.-C.; Wiedorn, M.; Ko, H.-C.; Ziehfried, A.; Sell, R. Advanced Materials, 10 (1993) 730.
- [19] Maier, W.F.; Ko, H.C. Catal. Today, 25 (1995) 429.
- [20] I.-C. Tilgner, C. Lange, H.-W. Schmidt, W. F. Maier, CIT, 69 (1997) 1776.
- [21] C. Lange, B. Tesche, S. Stork, W. F. Maier, J. Catal. 175 (1998) 280.

THERMAL UPGRADING OF PETROLEUM RESIDS USING POLAR H-DONOR SOLVENTS

Richard Dutta¹, Shona Martin², Mark Plummer³ and Harold H. Schobert¹

¹The Energy Institute, Penn State University, University Pk., PA 16802

²Dept. of Pure and Applied Chemistry, Univ. of Strathclyde, Glasgow G1 1XL, Scotland, UK

³Marathon Oil Co. PO Box 269, Littleton, CO 80180-0269

KEYWORDS: Petroleum resids, hydrogen donor solvents, tetrahydroquinoline

INTRODUCTION

As a novel approach to upgrading petroleum resids it was proposed that experiments should be carried out utilizing polar H-donor solvents (e.g. tetrahydroquinoline (THQ) and indoline) in an effort to increase H/C ratio, increase desulfurization and demetallation, and improve the boiling point distribution to 90% boiling below 1000°F.

The objectives of this project were as follows: 1) To identify potential hydrogen-donating solvents for upgrading petroleum resids. 2) To screen these solvents and compare their effectiveness in improving the boiling point distribution and elemental composition of the resids. 3) Once the initial screening has been done, to fully test one or two of the best solvents in larger batch reactors, to fully analyze the effectiveness of the solvent. 4) To undertake model compound and solvent reactions and modeling to understand the H-transfer efficiency, docking interactions etc.

This paper will discuss the major findings for these objectives and make conclusions as to the potential use of H-donors in upgrading heavy petroleum resids.

EXPERIMENTAL

All reactions were carried out in 25ml microautoclaves and a 300ml batch reactor (Marathon Oil Co.). Petroleum resids were obtained from Marathon Oil and potential solvents were obtained from various chemical companies. In each reaction, a measured amount of resid/pyrene was weighed into the reactor along with a carefully weighed amount of solvent in various wt/wt (or mol/mol) proportions. The reactor was purged twice with nitrogen and pressurized to either 200psi with nitrogen (inert atmosphere) or 500-1500psi hydrogen. The reactor was then lowered into a fluidized sand bath set at a pre-defined temperature (375-450°C) for a pre-determined reaction time (60-180 minutes). After the reaction time had expired, the reactor was removed from the sand bath and immediately quenched in cold water. The reaction products were extracted with THF and hexane to determine conversion of the asphaltene fraction of the resid. The products were analyzed by gas chromatography to determine conversion of the solvent, and simulated-distillation (SIMDIST) to determine the boiling point distribution. Elemental analysis was carried out to determine C, H, and S.

RESULTS AND DISCUSSION

Thermal Cracking of vacuum resid (VR1) using Donor/Non-donor Solvent

In order to stop retrogressive reactions that occur during thermal cracking of resids, several experimental approaches can be undertaken: 1) Use molecular hydrogen to try and cap the reactive radicals which are recombining, 2) Use molecular hydrogen and a catalyst to improve conversion levels, 3) Utilize solvents that can be a source of hydrogen for radical capping and hydrogenation of aromatic rings. In order to assess these approaches, a study into vacuum residue (VR1) upgrading using various donor/non-donor solvents, hydrogen vs. inert atmosphere, and the impact of a catalyst on the reaction, was undertaken. The major results are shown in Figure 1, which gives conversion of asphaltene data and boiling point (by simulated distillation) data (<400°C and <550°C). Use of non-donor solvents (naphthalene, toluene, quinoline) in the reaction leads to retrogressive reactions, similar to those seen when no solvent is used. Tetralin (low polarity H-donor) does give up some hydrogen to cap the reactive radicals but the asphaltene fraction is not converted as much as when THQ (highly polar H-donor) is used. Hydrogen atmosphere does increase conversion of asphaltenes, but the use of a catalyst precursor, ammonium tetrathiomolybdate (ATTM), does not significantly improve the results. Quinoline (polar non-donor) is effective only when ATTM and hydrogen are present. This is due to the hydrogenation of quinoline to THQ which then acts as a donor. This idea of hydrogen shuttling between gas phase hydrogen, quinoline, THQ and the resid molecules will be discussed in detail later in the paper. Figure 1 also shows the effect of increasing THQ concentration of the solvent system on conversion and boiling point distribution. When 100% toluene is used, retrogressive reactions are occurring, leading to a negative conversion of 36%. As THQ is added to the solvent, conversion increases. With 100% THQ, asphaltene conversion increases to +30%.

One of the interesting features of Figure 1 is that there appears to be a relationship between asphaltene conversion and conversion of the resid to <400°C and <550°C material. This can be seen more clearly in Figure 2, where these two parameters are plotted against each other. It can be seen that as the heavier asphaltene molecules are converted to hexane soluble material, the amount of cracking to lower boiling products, decreases. There are some exceptions, which are pointed out in Figure 2 as catalytic reactions. The results suggest that there may be two mechanisms that need to be separately addressed when considering upgrading resids. Firstly, thermal cracking of side chains from the multicyclic compounds that make up a large proportion of these resids and cracking of smaller molecules to produce the distillable material, and secondly, hydrogenation and subsequent cracking of large polycyclic macromolecules that make up the asphaltene structure. To convert asphaltene requires hydrogen, which also reduces cracking of smaller compounds due to reactive radical capping. In a real process, it would be necessary to reach a compromise in conversion of asphaltenes and production of distillates. This would depend on the final product requirement. For example, in the case of resids, it may be important to produce a product that can be fed into the FCC for further treatment.

Thermal cracking of ROSE pitch using THQ

After the initial screening studies using VR1, it was decided to switch the initiative of the research to ROSE pitch. This was partly due to the fact that ROSE pitch is more difficult to upgrade and whatever we could achieve with this material we could probably repeat with the vacuum resid. ROSE pitch also contains a larger proportion of asphaltenes which have to be converted in order for the process to work efficiently.

The experimental approach was to determine the effect of temperature and hydrogen pressure on conversion of asphaltenes and cracking of the pitch to distillable products. Table I shows boiling point data, asphaltene conversion, solvent conversion and H/C ratio for ROSE pitch products under various reaction conditions. Asphaltene conversion is at a maximum at 425°C (33%). At 450°C, conversion drops to 24%. This is due to coking reactions occurring at this elevated temperature. From the boiling point data, it can be seen that as reaction temperature increases the amount of distillable products increases. At a reaction temperature of 450°C, 64% of the reaction products boil below 1000°F. However, an optimum temperature of 425°C was chosen for ROSE pitch based on asphaltene conversion and also at 450°C, there is evidence that THQ degrades via ring-opening, which would render the solvent useless for recycle. The results show that increasing hydrogen pressure does not have a great effect on cracking of the pitch to distillable. There is a significant difference in conversion of asphaltenes with increasing hydrogen pressure, and variation in solvent composition. This backs up the idea that we are dealing with two distinct reactions and mechanisms. Asphaltene conversion needs hydrogen to saturate the aromatic rings before they can be cracked. Cracking of side chains is more of a purely thermal process which is not as sensitive to increase in hydrogen pressure, but is sensitive to hydrogen donation ability of donors.

The initial H/C value of ROSE pitch is 1.27. At 375°C, H/C increases to 1.46. As reaction temperature increases to 400-425°C, there is the onset of major thermal cracking, which gives a further increase in H/C to 1.54. At 450°C, the increase in thermal cracking, is counterbalanced by a decrease in aromatic ring hydrogenation (thermodynamically limited). Also, there is probably major hydrocarbon gas production (methane, ethane) at 450°C, which decreases the H/C ratio of the products. When molecular hydrogen is used in the reaction system, H/C ratio increases to 1.62 (thermodynamics more favorable for hydrogenation of rings).

It has been postulated before that when considering the upgrading of resids, two distinct reactions have to be accounted for. Firstly, the behavior of the heavy asphaltene fraction, and second, the cracking of the lower molecular weight compounds. To explore this idea, the ROSE pitch was separated into hexane-soluble (oil) and insoluble fractions (asphaltene) and reacted separately. The products were analyzed by elemental composition and SIMDIST. The data are shown in Table I. By upgrading the ROSE pitch without the asphaltene fraction, it is possible to achieve a product which has a high H/C (1.70). We now know that we are achieving good products from the hexane-soluble fraction of ROSE pitch, but the question remains, what are we doing to the asphaltene molecules. At 425°C, 1000psi hydrogen, and 120 minutes reaction time, only 8% of the asphaltene fraction is converted to <800°F material, compared to 19% conversion from the oil fraction. 34% asphaltene conversion to <1000°F material is achieved under the same conditions compared to 36% oil conversion to <1000°F. This data is somewhat misleading, because a close look at the chromatograms obtained through SIMDIST, shows a different product distribution. Asphaltene molecules are converted to primarily 'pre-asphaltenes' shown by a hump in the chromatogram. The oil fraction is converted primarily to lower boiling compounds, e.g., alkanes.

Product evaluation of solvent donor experiments in stirred-tank reactor

Figure 3 shows how the <1000°F component concentration and contaminant removal varies with hydrogen consumption (measured by hydrogen donation from the solvent). Extrapolation shows that a hydrogen consumption of 4000-4400 scf/bbl of pitch will be required to obtain products of commercial interest, that is, products exhibiting <1000°F contents of 80-90 wt%.

During the upgrading of ROSE pitch with THQ at 425°C and 1000psi hydrogen, 38% of the sulfur was removed as hydrogen sulfide. This gives a final sulfur wt% of 3.7 (feed=6.0%). Of this 3.7 wt%, 8.8, 5.7, 40.7, and 44.6% of the unconverted sulfur was retained in the <460°F, 460-484°F, 484-1000°F, and >1000°F respectively. Calculation gives a product boiling less than 1000°F having a sulfur concentration of 2.1wt%. Therefore, the lighter products would still have to be further treated to remove the sulfur to acceptable levels.

Figure 4 show the boiling point distribution of upgraded ROSE pitch at 425°C for various reaction times. At 425°C, conversion of pitch was essentially completed after 97 minutes. The stop in conversion is probably due to the equilibrium conversion of THQ to quinoline, i.e., hydrogen transfer stops once THQ and quinoline have reached equilibrium conversion. Once all the available hydrogen is used, retrogressive reactions will set in, leading to coke formation. It may be possible to increase conversion at 425°C, if hydrogen availability is increased. This could be achieved by increasing the solvent to resid ratio or increasing the hydrogen pressure. If successful, hydrogen consumption may exceed 4000 scf/bbl, which could give a <1000°F component concentration approaching 90%. This should also lead to a greater removal of contaminants.

Hydrogen transfer from various solvents to pyrene

To determine the hydrogen transfer ability of various polar solvents, pyrene was used as a model reactant. Table 2 shows the pyrene/solvent conversion data for these compounds (dihydropyrene is the only major pyrene hydrogenation product under these conditions). It can be seen that in terms of pyrene conversion, THQ and indoline are the best H-donors. However, in terms of hydrogen-transfer efficiency (solvent conversion compared with pyrene conversion), THQ is the better candidate. This prompted a closer look at H-transfer from THQ to pyrene.

Figure 5 shows how pyrene and THQ conversion, and H-transfer efficiency vary with hydrogen pressure. At low pressure (0-500 psi), H-transfer is 50% efficient. There could be

different explanations for this value. Thermodynamics (equilibrium conversion) could limit the hydrogenation of pyrene. Another reason for achieving only 50% efficiency can be explained if the docking reaction between THQ and pyrene is looked at more closely. Two of the hydrogens will be donated from THQ to pyrene to produce dihydropyrene. As they are transferred, THQ will become unstable and will have to release the remaining two hydrogens to produce the stable molecule, quinoline. However, they will probably not be able to transfer to pyrene because of steric constraints (only one pyrene molecule can dock with THQ at a time). Therefore, the hydrogen will be released from THQ as molecular hydrogen.

As pressure increases to 1000 and 1500psi, efficiency increases past 100% and approaches 130% at 1500psi. This means that gas phase hydrogen is being utilized in the hydrogenation of pyrene. Quinoline produced by the dehydrogenation of THQ is being hydrogenated by the gas-phase hydrogen back to THQ. This H-shuttling mechanism can explain the >100% efficiency.

Figure 6 shows how pyrene conversion and THQ conversion varies with reactant ratio at 425°C, 120 minutes reaction time and inert atmosphere. The figure shows that increasing the solvent ratio to 20:1 increases the conversion of pyrene with respect to THQ. At 425°C, pyrene hydrogenation is thermodynamically limited to a maximum conversion of 36% under these conditions (20:1 molar ratio). At 2:1 molar ratio, the reaction is limited by the availability of transferable hydrogen, which limits conversion to 24%. The thermodynamic limitation can be overcome by dropping the temperature to 400°C, but this will have an effect on the kinetics of the transfer of hydrogen from THQ to pyrene. Experimentation has shown that it takes 120 minutes more reaction time at 400°C to reach the same conversion level seen at 425°C. It will be necessary to make a trade-off between reaction temperature, reaction time and the solvent/resid ratio. This will depend on how good the final product needs to be, and the economics of the process.

CONCLUSIONS

This study has shown that polar H-donors such as THQ and indoline are good solvents for upgrading petroleum resids. Model compounds studies using pyrene have shown that THQ is a better donor in terms of amount of conversion of the solvent with respect to the model compound. This will be an important aspect of future research as any process involving H-donors will have to consider the recycle of the solvent, i.e., rehydrogenation. THQ also acts as a H-shuttler between the gas phase and the reactant.

It was found from research undertaken using a large batch reactor, that a hydrogen consumption level of 4400 scf/bbl will be required to get a 90% conversion of the resid to <1000°F boiling material. This will also increase heteroatom removal but further hydrogenation will have to be done on the product to get the sulfur levels to less than 1%.

Studies undertaken in smaller microautoclaves have shown that an increase in H/C ratio of 25% is possible (1.62 is maximum obtained using THQ and 1000psi hydrogen pressure). From the SIMDIST data, asphaltene conversion data, and elemental analysis, a potential trade-off between cracking and hydrogenation of both the heavy asphaltene molecules and the lighter boiling material is envisioned. Because this system is non-catalytic, it will not be possible to get high cracking and high hydrogenation levels. The final process should be determined based on the required final product, e.g., does the product only need to be good enough for feeding to the FCC?

ACKNOWLEDGEMENTS

This work was supported by a grant from USX foundation. Thanks to Rolf Schroeder for many useful discussions and the research staff at Marathon Oil Technology Center, Denver, for running batch reactions and product analysis.

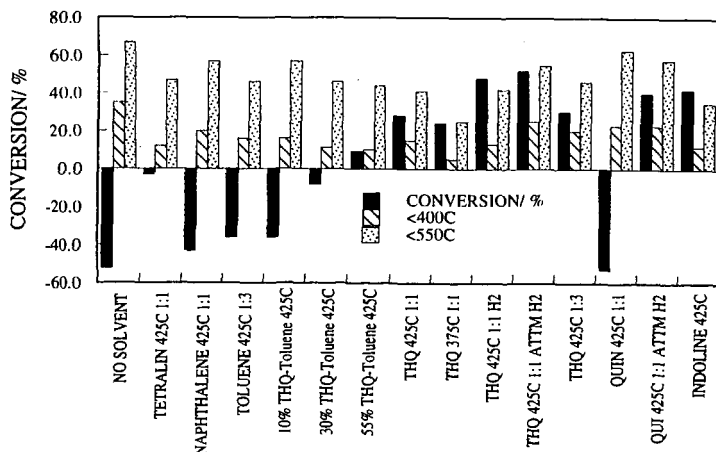


Figure 1. Effect of various solvents and reaction conditions on upgrading vacuum residue: 1 hour reaction time

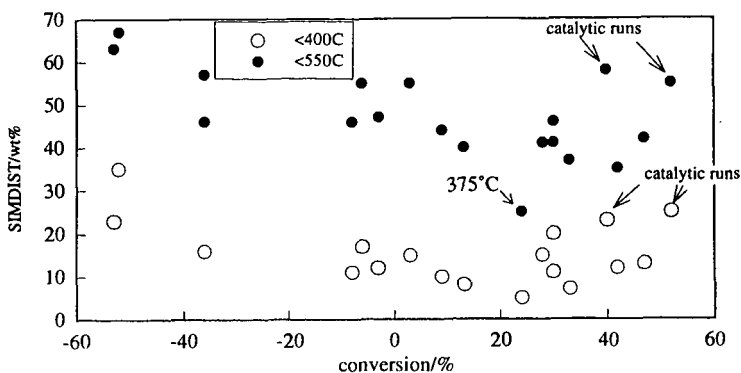


Figure 2. Vacuum resid conversion of asphaltene vs. SIMDIST results: various reaction conditions

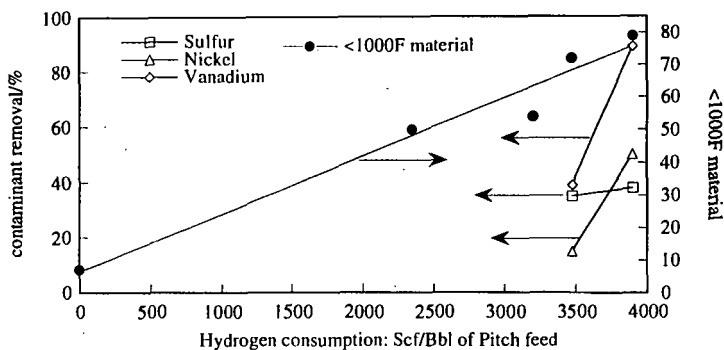


Figure 3. Conversion of ROSE pitch to <1000°F material and removal of contaminants vs. H-consumption: THQ and indoline

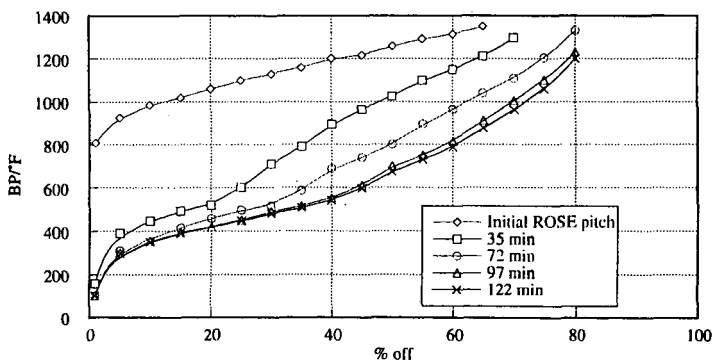


Figure 4. Boiling point distribution for products from THQ hydrogen donation to ROSE pitch: effect of donation time at 425°C, 2:1 solv/resid, 1000psi H₂

Table 1. Effect of temperature, hydrogen pressure and reaction time on conversion of ROSE pitch and THQ, and H/C ratio of products.

| Feedstock | Temperature/ °C | H ₂ Pressure/ psi | time/ min | <800°F % | <1000°F % | Asphaltene Conv./% | THQ Conv./% | H/C |
|----------------------------|--------------------|------------------------------------|--------------|-------------|--------------|-----------------------|----------------|------|
| ROSE pitch | - | - | - | 2 | 9 | - | - | 1.27 |
| ROSE pitch | 375 | 0 | 60 | 7 | 18 | 12 | - | 1.46 |
| ROSE pitch | 400 | 0 | 60 | 9 | 23 | 17 | - | 1.54 |
| ROSE pitch | 425 | 0 | 60 | 18 | 38 | 33 | - | 1.51 |
| ROSE pitch | 450 | 0 | 60 | 40 | 64 | 24 | - | 1.55 |
| ROSE pitch | 425 | 500 | 120 | 32 | 55 | 32 | 53 | 1.55 |
| ROSE pitch | 425 | 1000 | 120 | 32 | 55 | 36 | 33 | 1.62 |
| ROSE pitch | 425 | 1500 | 120 | 29 | 50 | 40 | 36 | - |
| ROSE pitch (oil) | - | - | - | 5 | 8 | - | - | 1.33 |
| ROSE Pitch (asphaltene) | - | - | - | 0 | 2 | - | - | 1.09 |
| ROSE pitch (oil) | 425 | 1000 | 120 | 24 | 44 | - | - | 1.70 |
| ROSE pitch (asphaltene) | 425 | 1000 | 120 | 8 | 36 | - | - | 1.40 |

Table 2. Effect of various donor/non donor solvents on pyrene conversion : 425°C, 1000 psi hydrogen pressure

| Model Compound | Solvent | mol/mol | Time/ min. | pyrene conversion/% | solvent conversion/% |
|-------------------|---------------------|---------|---------------|------------------------|-------------------------|
| pyrene | acridine | 2 | 60 | 8.5 | 83 |
| pyrene | acridine | 2 | 120 | 13.7 | 95 |
| pyrene | pyrrolidine | 2 | 120 | 13.1 | - |
| pyrene | tetrahydrocarbazole | 2 | 120 | 16.3 | 18 |
| pyrene | indoline | 2 | 60 | 47 | 48 |
| pyrene | indoline | 2 | 120 | 47 | 78 |
| pyrene | toluene | 2 | 120 | 7.4 | - |
| pyrene | THQ | 2 | 60 | 32 | 12 |
| pyrene | THQ | 2 | 120 | 32 | 14 |
| pyrene | octahydroacridine | 2 | 60 | 17 | 2 |
| pyrene | octahydroacridine | 2 | 120 | 22 | 12 |

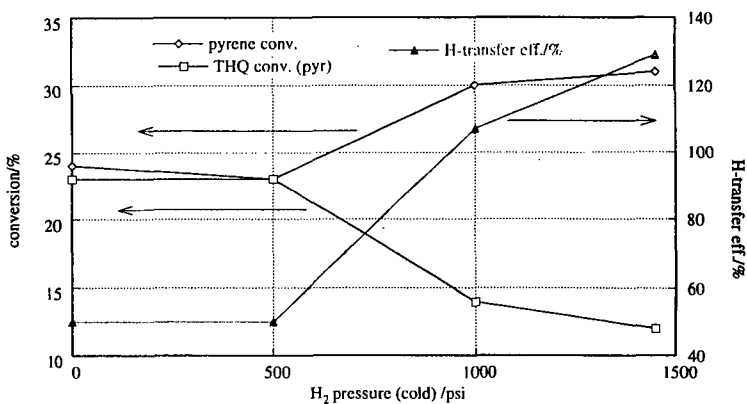


Figure 5. Pyrene/THQ conversion and H-transfer efficiency vs. H₂ pressure: 425°C, 120min

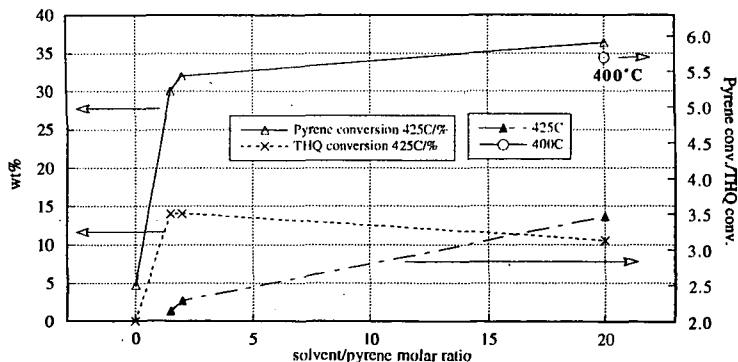


Figure 6. Pyrene and THQ conversion vs. reactant ratio : 425°C, 120 minutes, 1000psi H₂

THIOPHENE HYDRODESULFURIZATION OVER COBALT OXIDE LOADED SMECTITE CLAY MINERALS

Eiji Iwamatsu^{1)*}, Syed A. Ali¹⁾, Mohammad E. Biswas¹⁾, Shakeel Ahmed¹⁾
Halim Hamid¹⁾, Yuzo Sanada¹⁾ and Toshikazu Yoneda²⁾

1) Research Institute, King Fahd University of Petroleum & Minerals,
Dhahran 31261, Saudi Arabia
2) Petroleum Energy Center, Japan

* Corresponding author: Tel & Fax +966-3-860-3847, E-mail iwamatsu@kfupm.edu.sa

Key words: hydrodesulfurization, cobalt, clay

ABSTRACT

Co oxide loaded smectite clay minerals catalysts showed high hydrodesulfurization (HDS) activity of thiophene used as a model compound. Among these catalysts, HDS activity of Co oxide loaded porous saponite was higher than CoMo/Al₂O₃ which is known to be a highly active catalyst for HDS. Further, HDS activity was increased by the calcination up to 600°C before Co oxide loading. MgO content was decreased and CoO content was increased with increasing calcination temperature up to 600°C before Co oxide loading. These catalysts were characterized by means of XRD and XPS. The correlation between the characteristics of catalysts and their activities were discussed. It can be concluded that (1) there are two types of Co oxide species : between the clay layers due to ion exchange with Na⁺ : and at the edge of the clay layer due to ion exchange with Mg, and (2) the latter type is highly active for thiophene HDS reaction.

INTRODUCTION

Generally, HDS catalyst applied in industry are derives from oxides of an element of Group VIB (Mo or W) and Group VIII (Co or Ni) supported on Al₂O₃. Catalytic activity is supposed to be connected with the presence of Group VIB elements while Group VIII elements are believed to act as promoters. However, it has been reported recently that only one metal, such as Co or Ni, oxide loaded on some supports shows higher HDS activity than CoMo/Al₂O₃ catalysts. Duchet et al. has reported the high HDS activity of carbon-supported Co sulfide¹⁾. In another report, Klopogge et al. prepared Ni sulfide supported on Al oxide pillared montmorillonite catalysts with a high thiophene HDS activity²⁾. Further, Sychev et al. has reported that sulfided Cr oxide pillared montmorillonite, showed high activity for thiophene HDS and the consecutive hydrogenation of butenes³⁾. In the above references, montmorillonite is a well known clay used as catalyst support. However, other smectite clay minerals (saponite, hectorite, stevensite and so on) have not been used as a support of HDS catalyst in spite of their similar feature. Therefore, in this study, Co oxide loaded smectite clays were prepared and HDS activity was evaluated. Moreover, the active sites of Co oxide loaded porous saponite, which showed the highest HDS activity, was also discussed.

EXPERIMENTAL

Smectite clay minerals were supplied by Kunimine Kogyo Co. Ltd. Co oxide was loaded on various clay minerals by means of ion exchange. Ion exchange method is as follows. Co nitrate solution (Co(NO₃)₂·6H₂O 29.0 g and distilled water 500 ml) was aged at 80 °C for 2 h. Then 10 g of clay was added to the solution and stirred at 80 °C for 1.5 h. After that, the solution was filtered. The residue thus obtained was washed with water and ethanol, and dried at 120 °C for 12 h and calcined at 400 °C for 12 h.

Hydrodesulfurization experiments were carried out in a pulse flow reactor. Prior to the activity test, the catalyst (0.1 g) was sulfided at 400 °C by using a mixed gas of 5 % H₂S in H₂ (60 ml/min., 2 kg/cm²) for 2 h. Then, the temperature and the gas flow rate were changed to the reaction condition (H₂ 60 ml/min., 2 kg/cm²). Thiophene (0.3 µl) was injected and its conversion was measured by an on-line gas chromatograph, after the pulse reaction results had been stabilized.

RESULTS AND DISCUSSION

Table 1 shows thiophene HDS activity of Co oxide loaded smectite catalysts. As shown in this table, the smectite-supported catalysts showed higher activity than the Al₂O₃-supported catalyst (Co/Al₂O₃). Further, Co oxide loaded porous saponite showed the highest

thiophene conversion in the Co oxide loaded other smectite series and its activity was higher than that of CoMo/Al₂O₃ which is known to be highly active catalyst for HDS reaction. Then, the modification of porous saponite was carried out in order to improve the activity, further. In this experiment, the precalcination at various temperatures up to 700 °C in the air for 24 h before Co oxide loading was carried out. Table 2 shows the results. As shown in this table, thiophene HDS activity was increased with increasing precalcination temperature up to 600 °C. It is noted that the HDS performance is remarkable as low as 225 °C.

Table 3 shows properties of Co oxide loaded porous saponite catalysts. As shown in this table, the amount of MgO was decreased and that of CoO was increased with increasing precalcination temperature up to 600 °C. Therefore, it is supposed that the ion exchange of Na with Co takes place at first, then, ion exchange of Mg with Co takes place. It seems that the increase of Co oxide amount loaded on porous saponite by precalcination up to 600 °C is one of the reasons for HDS activity improvement. Phase transition from saponite to enstatite between 600 and 700 °C was observed by means of XRD. The drastic change of specific surface area by the precalcination at 700 °C may be due to this phase transition. It seems that the decrease of thiophene HDS activity at 700 °C is caused by the decrease of CoO amount due to this phase transition which was observed by the substantial reduction in specific surface area and XRD.

Table 1. HDS activity of Co-smectite catalysts

| Support | Loaded metal as oxide (wt%) | Thiophene conversion (%) | | |
|--------------------------------|-----------------------------|--------------------------|-------|-------|
| | | 300°C | 350°C | 400°C |
| Montmorillonite | 3.1 | 25.7 | 50.7 | 69.6 |
| Saponite | 5.0 | 73.1 | 78.5 | 86.2 |
| Porous saponite | 7.7 | 92.7 | 96.0 | 97.9 |
| Hectorite | 7.8 | 67.0 | 80.0 | 88.5 |
| Stevensite | 8.6 | 57.5 | 71.9 | 81.1 |
| Al ₂ O ₃ | 4.0 | 7.4 | 14.7 | 22.0 |
| - | 100 ^{a)} | 7.2 | 11.5 | 17.2 |
| Al ₂ O ₃ | Co 4wt% + Mo 15wt% | 85.0 | 97.0 | 98.3 |

a) CoO was used as catalyst

Table 2. HDS activity of Co-porous saponite catalysts

| Sample | Precalcination Temperature (°C) | CoO (wt.%) | Thiophene conversion (%) | | | |
|--------------------|---------------------------------|------------|--------------------------|------|------|-------|
| | | | 225 | 250 | 275 | 300°C |
| Porous saponite* | - | - | 0.0 | 0.0 | 0.0 | 0.0 |
| Co-porous saponite | - | 7.7 | 28.2 | 73.5 | 81.8 | 92.7 |
| | 200 | 7.9 | 36.9 | 79.7 | 83.0 | 92.0 |
| | 300 | 8.6 | 33.5 | 85.5 | 90.7 | 94.6 |
| | 400 | 10.5 | 47.4 | 90.3 | 91.4 | 94.1 |
| | 500 | 13.5 | 56.4 | 92.2 | 92.8 | 95.1 |
| | 600 | 18.0 | 69.6 | 92.5 | 93.0 | 94.4 |
| | 700 | 9.3 | 10.7 | 25.1 | 40.0 | 52.1 |

* as received

Table 3. Properties of Co-porous saponite catalysts

| Support | Precalcination Temperature (°C) | Composition (wt.%) | | | | | Surface Area (m ² /g) |
|--------------------|---------------------------------|--------------------|------|--------------------------------|-------------------|------|----------------------------------|
| | | SiO ₂ | MgO | Al ₂ O ₃ | Na ₂ O | CoO | |
| Porous saponite* | - | 49.2 | 29.2 | 4.5 | 3.0 | - | 514 |
| Co-porous saponite | - | 50.5 | 27.3 | 4.7 | 0.04 | 7.7 | 510 |
| | 200 | 46.9 | 24.9 | 4.5 | 0.05 | 7.9 | 415 |
| | 300 | 47.5 | 24.6 | 4.5 | 0.05 | 8.6 | 467 |
| | 400 | 46.9 | 22.9 | 4.5 | 0.05 | 10.5 | 402 |
| | 500 | 48.2 | 21.6 | 4.5 | 0.11 | 13.5 | 378 |
| | 600 | 44.9 | 16.9 | 4.3 | 0.08 | 18.0 | 342 |
| | 700 | 50.7 | 27.4 | 4.7 | 0.75 | 9.3 | 121 |

* as received

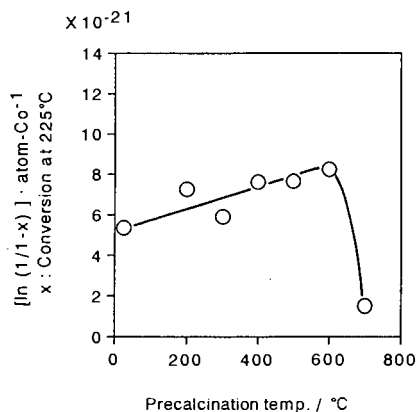


Fig. 1 $[\ln(1/(1-x))] \cdot \text{atom-Co}^{-1}$ as a function of precalcination temperature of porous saponite

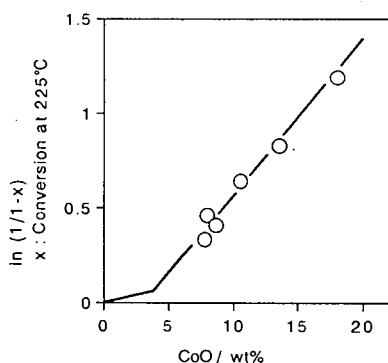


Fig. 2 $\ln(1/(1-x))$ as a function of CoO content over porous saponite

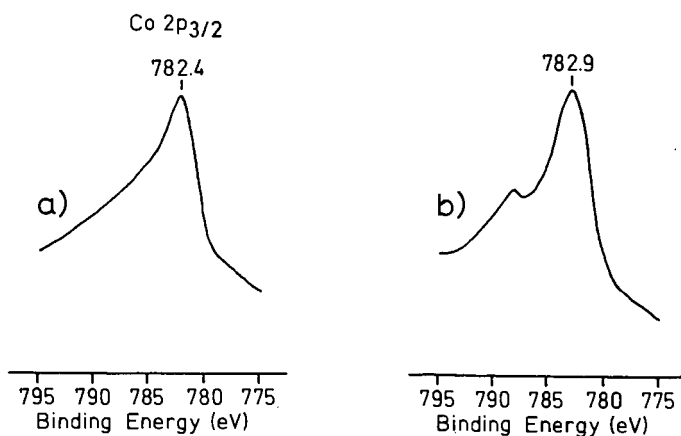


Fig. 3 XPS spectra of Co-porous saponite
a) Co-porous saponite (non calcined before Co oxide loading)
b) Co-porous saponite (calcined at 600°C before Co oxide loading)

On the basis of the assumption that thiophene HDS is first-order reaction, the relation between $[\ln(1/1-x)] \cdot \text{atom-Co}^{-1}$ and precalcination temperature of Co oxide loaded porous saponite was investigated. The HDS activity at 225 °C was used as x , because of the low conversion values. Fig.1 shows the results. The vertical axis means the activity index per Co atom. This value was increased with increasing precalcination temperature up to 600 °C. Therefore, it seems that the increase of activity with increasing precalcination temperature is not due to the increase of the equivalent Co species.

Assuming that ion exchange of Na with Co takes place at first, then, ion exchange of Mg with Co takes place, as mentioned before, the amount of CoO just after the ion exchange of all Na with Co was 3.9 wt% in case of Co oxide loaded porous saponite. Hence, good relation between the activity and CoO amount was obtained by using this point (3.9 wt%) as an inflection point (Fig.2). The slope after this inflection point was larger than before 3.9 wt%. Therefore, it seems that Co species which is exchanged with Mg is more active than that which is exchanged with Na.

Fig.3 shows XPS spectra of Co oxide loaded porous saponite. XPS spectra pattern of Co oxide loaded porous saponite, which was non-calcined before Co oxide loading, was similar with Co_3O_4 type, and that of Co oxide loaded porous saponite, which was precalcined at 600 °C before Co oxide loading was similar with CoO type^{4,5}. Therefore, Co species exchanged with Na, which were located between the clay layers, seem to be mainly Co_3O_4 type. On the other hand, Co species exchanged with Mg, inside the clay layer, seem to be mainly CoO type. It seems that the part of Mg which exist at the edge of the clay is easier to exchange with Co than with Mg located inside the bulk. Consequently, this CoO type species at the edge of the clay seems to show higher HDS activity than Co_3O_4 type species between the clay layers.

CONCLUSIONS

Co oxide loaded smectite catalysts showed high HDS activity of thiophene. Among these catalysts, HDS activity of Co oxide loaded porous saponite was higher than $\text{CoMo}/\text{Al}_2\text{O}_3$ which is known to be a highly active catalyst for HDS. Further, HDS activity is increased by the calcination before cobalt oxide loading. MgO content was decreased and CoO content was increased with increasing calcination temperature before Co oxide loading. It can be concluded that (1) there are two types of Co oxide species : between the clay layers due to ion exchange with Na : and at the edge of the clay layer due to ion exchange with Mg, and (2) the latter type is highly active for thiophene HDS reaction.

ACKNOWLEDGEMENTS

The authors wish to acknowledge the support of Petroleum Energy Center, Japan, with the subsidy of the Ministry of International Trade and Industry Japan, and the Research Institute of the King Fahd University of Petroleum and Minerals, for this work under KFUPM/RI Project No.21151.

REFERENCES

1. J. C. Duchet, E. M. van Oers, V. H. J. de Beer and R. Prins, *J. Catal.*, **80**, 386 (1983).
2. J. T. Klopogge, W. J. J. Welters, E. Booy, V. H. J. de Beer, R. A. van Santen, J. W. Geus and J. B. H. Jansen, *Appl. Catal.*, **97**, 77 (1993).
3. M. Sychev, V. H. J. de Beer, R. A. van Santen, R. Prihod o and V. Goncharuk, *Stud. Surf. Sci. Catal.*, **84**, 267 (1994).
4. R. L. Chin and D. M. Hercules, *J. Phys. Chem.*, **86**, 3079 (1982).
5. Y. Okamoto, T. Imanaka and S. Teranishi, *J. Catal.*, **65**, 448 (1980).

DEEP HYDRODESULFURIZATION OF GASOILS - MECHANISM OF ALKYLDIBENZOTHIOPHENES TRANSFORMATION ON BIFUNCTIONAL CATALYSTS

G. PEROT, P. MICHAUD and J.L. LEMBERTON, Laboratoire de Catalyse en Chimie Organique, UMR 6503, UFR Sciences, 40 avenue du Recteur Pineau, 86022 Poitiers Cedex, France, email : Guy.perot@cri.univ-poitiers.fr

Keywords: hydrodesulfurization, dibenzothiophene, 4,6-dimethyldibenzothiophene, nickel-molybdenum sulfides, bifunctional catalysts

INTRODUCTION

In order to decrease the pollution by diesel engines, the authorized maximum sulfur content in fuels has been severely lowered in certain countries. However, total hydrodesulfurization of gasoils is very difficult to reach with the catalysts used at present in the industrial units, probably because of the presence of hydrodesulfurization resistant molecules, such as 4,6-dimethyldibenzothiophene (1,2). Indeed, while dibenzothiophene is easy to decompose, this is not the case for 4,6-dimethyldibenzothiophene. Most of the other dialkyldibenzothiophenes are as reactive as dibenzothiophene, some of them being even more reactive (3-5). Consequently, one possibility of improving the reactivity of 4,6-dimethyldibenzothiophene is to transform it into a more reactive molecule, for example through isomerization (6,7). This reaction can be performed using acid catalysts (8,9).

In the present work we compare the transformation of dibenzothiophene and of 4,6-dimethyldibenzothiophene on catalysts such as a sulfided commercial NiMo on alumina catalyst, a physical mixture of this catalyst with silica-alumina, and on a NiMo on alumina catalyst containing Y-zeolite.

EXPERIMENTAL

The hydrodesulfurization of dibenzothiophene (DBT) and of 4,6-dimethyldibenzothiophene (46DMDBT) was carried out in a flow reactor at 340°C under a 4 MPa total pressure. Decalin was used as a solvent to which dimethyldisulfide was added to generate H₂S. The partial pressures were: DBT or 46DMDBT = 0.01 MPa, decalin = 0.89 MPa, H₂ = 3.0 MPa, H₂S = 0.05 MPa.

The reference hydrotreating catalyst was a commercial NiMo/alumina containing 3 wt.% NiO and 14 wt.% MoO₃. The silica-alumina was a Ketjen K14 sample, containing 14 wt.% alumina. The NiMo-Y zeolite catalyst was supplied by the « Institut Français du Pétrole » (Rueil-Malmaison, France). It contained 5 wt.% Y zeolite mixed with NiMo on alumina (NiO + MoO₃ = 16.8%). All the catalysts were first sulfided *in situ* by a mixture of 5 vol.% dimethyldisulfide in n-heptane, under the same hydrogen partial pressure and total pressure as those used for the reaction. The H₂S partial pressure was 0.125 MPa and that of n-heptane 0.75 MPa. The sulfiding feed was injected at a starting temperature of 150°C, raised to 350°C at a 5°C.min⁻¹ rate. After 14 hours, the temperature was lowered to 340°C, and the reaction mixture was substituted for the sulfiding feed.

The reactor effluents were condensed, and liquid samples were periodically collected and analyzed by gas-liquid chromatography (Varian 3400) on a 50-m DB17 capillary column (J&W Scientific). Unknown products were identified by GC-MS (Finnigan INCOS 500). The HDS conversions of the reactants were determined by using an external standard (1-methylnaphthalene).

4,6-Dimethyldibenzothiophene was synthesized (10) - and kindly supplied - by the « Institut de Recherche sur la Catalyse » (Villeurbanne, France). The other products were purchased from Aldrich.

RESULTS AND DISCUSSION

Transformation of dibenzothiophene and 4,6-dimethyldibenzothiophene over the sulfided NiMo on alumina catalyst.

The sulfided NiMo on alumina catalyst has a very stable activity for the conversion of DBT and of 46DMDBT. Figure 1 shows the total activity of the NiMo catalyst for the conversion of the two molecules. We can see that DBT, under our experimental conditions, is almost 5 times more reactive than 46DMDBT.

The DBT reaction products are biphenyl, tetrahydrodibenzothiophene, cyclohexylbenzene, and dicyclohexyl. If one considers the distribution of these products as a function of contact time, it is clear that biphenyl and tetrahydrodibenzothiophene are the only primary reaction products. In agreement with previous work (11,12), further experiments showed that, under our experimental conditions, biphenyl did not transform into cyclohexylbenzene, which means that cyclohexylbenzene is produced only from tetrahydrodibenzothiophene. Consequently, it can be concluded that the

transformation of DBT occurs through two parallel reactions : direct desulfurization (DDS) yielding biphenyl, and desulfurization after hydrogenation (HYD), yielding first tetrahydridibenzothiophene, then cyclohexylbenzene. We can estimate that the DDS reaction occurs faster than the HYD reaction (by a factor of 4 in this case), in agreement with the literature (13-15).

The 46DMDBT reaction products are similar to the DBT products, except for the methyl groups. The reaction scheme is the same as in the case of DBT, but the product distribution differs significantly from the one observed in the case of DBT. Figure 1 shows that the HYD reaction (yielding 4,6-dimethyltetrahydridibenzothiophene and 3-(3'-methylcyclohexyl)-toluene) is 5 times faster than the DDS reaction (yielding 3,3'-dimethylbiphenyl), which is the contrary of what was observed with DBT. The HYD reaction occurs at similar rates for both molecules, whereas the DDS reaction of DBT is faster by a factor of 25 than the DDS reaction of 46DMDBT. Consequently, we can conclude that it is owing to a very slow DDS reaction that 46DMDBT, when compared to DBT, transforms with difficulty (5, 16).

Transformation of dibenzothiophene and 4,6-dimethyldibenzothiophene on silica-alumina.

Long contact times were needed to observe the transformation of DBT and 46DMDBT on pure silica-alumina. In both cases, a very high conversion was obtained initially, but this conversion decreased very rapidly during the first 4 hours, then slower to reach approximately a zero value after 15 hours. Surprisingly, even at high conversion, none of the reaction products obtained with the NiMo on alumina catalyst was detectable by chromatographic analysis. In fact, the reactant transforms into products impossible to distinguish from those resulting from the decalin isomerization and cracking which also occur under the operating conditions.

Transformation of dibenzothiophene and 4,6-dimethyldibenzothiophene on bifunctional (acid + sulfide) catalysts.

The transformations of DBT and 46DMDBT were carried out either on a (1:5) physical mixture of NiMo on alumina with silica-alumina, or on the NiMo-Y zeolite catalyst. Both catalysts exhibited a slow 2-hour-deactivation period with 46DMDBT (the activity decreased by a factor 1.5), and were fairly stable with DBT.

Figure 2 compares the activities of all the catalysts calculated per kg of the sulfide component alone. The presence of an acid component had no effect in the case of DBT conversion, but increased the 46DMDBT reactivity by a factor of 2-2.5, which has already been observed by other authors (6,7). Moreover, two new products were formed from 46DMDBT : the first one was identified by GC-MS as an isomer of 46DMDBT, we suppose it to be 3,6-dimethyldibenzothiophene (36DMDBT) according to the chromatographic analyses reported in the literature (7); the second one, identified by GC-MS as an isomer of dimethylbiphenyl, is most likely 3,4'-dimethylbiphenyl (7). However, we observed that the amounts of DBT and 46DMDBT which were consumed were not balanced by the amounts of the hydrodesulfurization reaction products. In the case of DBT, smaller amounts of cyclohexylbenzene were detected with the bifunctional catalysts than with the pure sulfide catalyst. In the case of 46DMDBT, no 3-(3'-methylcyclohexyl)-toluene was detected. Because of the presence of the acid component, the missing compounds were converted into products which, owing to chromatographic interactions with the solvent reaction products, could not be detected.

To be able to observe the lacking reaction products, the transformations of DBT and of 46DMDBT were carried out on the NiMo-Y zeolite catalyst substituting cyclohexane for decalin as a solvent. Under these conditions, methylcyclohexane and toluene could be detected, and the amounts of consumed reactants were well-balanced by the amounts of the products formed. Figure 3 shows that 3,6-dimethyldibenzothiophene, 3,3'-dimethylbiphenyl and 4,6-dimethyltetrahydridibenzothiophene are obviously primary reaction products, whereas 3,4'-dimethylbiphenyl, methylcyclohexane and toluene are secondary products. This allows us to propose a reaction scheme for the transformation of 46DMDBT on a bifunctional catalyst (scheme 1). In this scheme, the two reactions identified in the case of the pure sulfide catalyst can be found, the direct desulfurization (DDS) yielding 3,3'-dimethylbiphenyl, and the hydrogenation (HYD) yielding the methylcyclohexyltoluenes. The presence of an acid component induces the appearance of another reaction (ISOM). This acid-catalyzed reaction allows 46DMDBT to transform into 36DMDBT which in turn transforms, mainly through direct desulfurization, into 3,4'-dimethylbiphenyl (no 3,6-dimethyltetrahydridibenzothiophene was found in the 4,6DMDBT reaction products). No methylcyclohexyltoluenes could be detected in the presence of an acid component, as reported by Landau et al. (6), but the presence of toluene and methylcyclohexane suggests that the methylcyclohexyltoluenes transformed through hydrocracking, as is commonly observed with bifunctional catalysts (18). Moreover, Figure 3 shows that there is more toluene than methylcyclohexane at high 46DMDBT conversions. We must suppose that 3,3'-dimethylbiphenyl or

3,4'-dimethylbiphenyl transform into toluene, as proposed by Lecrenay and Mochida (19). This reaction can occur through a mechanism which is derived from the reverse of the mechanism proposed by Gates, Katzer and Schuit (20) for the transformation of benzene into biphenyl. Owing to the existence of the ISOM reaction (scheme 1), the DDS reaction rate is higher than the HYD reaction rate, and thus produces an excess in toluene.

CONCLUSION

As expected, our results indicate that, owing to a very significant deactivation, the use of a purely acid catalyst is of no interest. However, a « bifunctional » catalyst, such as a sulfided NiMo on alumina plus an acidic function (silica-alumina or Y zeolite) is reasonably stable compared to the pure acid catalyst. The combination of an acid component with a hydrogenating component changes the deactivation process, which is well-known in hydrocracking reactions on bifunctional catalysts. However, the initial decrease in activity of these catalysts observed during 46DMDBT transformation suggests that part of the active sites deactivate. If this deactivation could be avoided, it is clear that the gain in activity resulting from the addition of the acid component could be even greater.

The reactivity of 46DMDBT is higher, at least by a factor 2, on the stabilized bifunctional catalysts than on the pure sulfided catalyst, whereas there is no effect of the acid component on the reactivity of DBT. The increase in 46DMDBT reactivity is linked to the formation of an isomer, most likely 36DMDBT. This is in agreement with the conclusion that alkyl groups in the 4 and 6 positions in DBT inhibit the DDS reaction more significantly than alkyl groups in other positions. In the case of DBT, the isomerization reaction is of course impossible, and it is quite normal to have no effect of an added acid component on the DBT transformation rate.

ACKNOWLEDGEMENT

This work was carried out within the framework of a contract entitled « Hydrodésulfuration des gazoles ». It was supported by CNRS-Ecotech, Elf, IFP, Total and Procatalyse. The authors are particularly grateful to V. Lamure-Meille, C. Traversa and E. Schulz who contributed to this work by preparing 4,6-dimethyldibenzothiophene (10).

LITERATURE CITED

- (1) Ma X., Sakanishi K. and Mochida I., *Ind. Eng. Chem. Res.*, **33**, 218 (1994).
- (2) Kabe T., Ishihara A. and Tajima H., *Ind. Eng. Chem. Res.*, **31**, 1577 (1992).
- (3) Kilanowski D.R., Teeuwen H., De Beer V.H.J., Gates B.C., Schuit G.C.A. and Kwart H., *J. Catal.*, **55**, 129 (1978).
- (4) Houalla M., Broderick D.H., Sapre A.V., Nag N.K., De Beer V.H.J., Gates B.C. and Kwart H., *J. Catal.*, **61**, 523 (1980).
- (5) Meille V., Schulz E., Lemaire M. and Vrinat M., *J. Catal.*, **170**, 29 (1997).
- (6) Landau M.V., Berger D. and Herskowitz M., *J. Catal.*, **158**, 236 (1996).
- (7) Isoda T., Nagao S., Korai Y. and Mochida I., *Am. Chem. Soc. Prepr. Div. Petrol. Chem.*, **41**, 559 (1996); **41**, 563 (1996).
- (8) Ward J.W. and Hansford R.C., *J. Catal.*, **13**, 154 (1969).
- (9) Guisnet M. and Gnep N.S., in : *Zeolites : Science and Technology*, NATO ASI Series, eds. Ribeiro F.R., Rodriguez A.E., Rollmann L.D. and Naccache C., (Martinus Nijhoff Publishers, The Hague/Boston/Lancaster, 1984) p. 571.
- (10) Meille V., Schulz E., Lemaire M., Faure R. and Vrinat M., *Tetrahedron*, **52**, 3953 (1996).
- (11) Nagai N., Sato T. and Aiba A., *J. Catal.*, **97**, 52 (1986).
- (12) Rollmann L.D., *J. Catal.*, **46**, 243 (1977).
- (13) Singhal G.H., Espino R.L., Sobel J.E. and Huff G.A., *J. Catal.*, **67**, 457 (1981).
- (14) Houalla M., Nag N.K., Sapre A.V., Broderick D.H. and Gates B.C., *AIChE J.*, **24**, 1015 (1978).
- (15) Nag N.K., *Appl. Catal.*, **10**, 53 (1984).
- (16) Kabe T., Ishihara A. and Zhang Q., *Appl. Catal. A : Gen.*, **97**, L1 (1993).
- (17) Prater C.D. and Lago R.M., *Adv. Catal.*, **8**, 293 (1956).
- (18) Lecrenay E. and Mochida I., in : *Hydrotreatment and Hydrocracking of Oil Fractions*, Studies in Surface Science and Catalysis, Vol. 106, eds. Froment G.F., Delmon B. and Grange P., (Elsevier, Amsterdam/Lausanne/New York/Oxford/Shannon/Tokyo, 1997) p. 333.
- (19) Gates B.C., Katzer J.R. and Schuit G.C.A., in : *Chemistry of Catalytic Processes*, Chemical Engineering Series, eds. Carberry J.J., Fair J.R., Peters M.S., Schowalter W.R. and Wei J. (Mc Graw-Hill Book Company, New-York, 1979) p. 17.

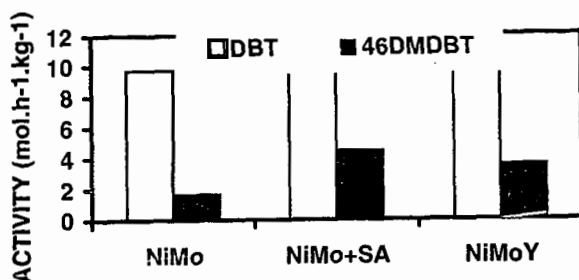


Figure 1. Activities of the sulfided NiMo on alumina catalyst for the transformation of dibenzothiophene (DBT) and 4,6-dimethyldibenzothiophene (46DMDBT). DDS = direct desulfurization reaction, HYD = hydrogenation reaction.

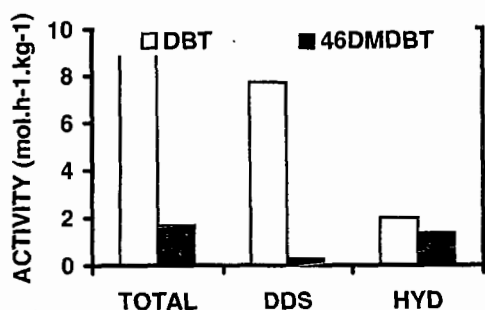


Figure 2. Activities of the sulfide functions of the catalysts for the transformation of dibenzothiophene (DBT) and 4,6-dimethyl dibenzothiophene (46DMDBT), NiMo = pure NiMo on alumina; NiMo + SA = NiMo on alumina mixed with silica-alumina; NiMoY = bifunctional NiMo - Y zeolite catalyst.

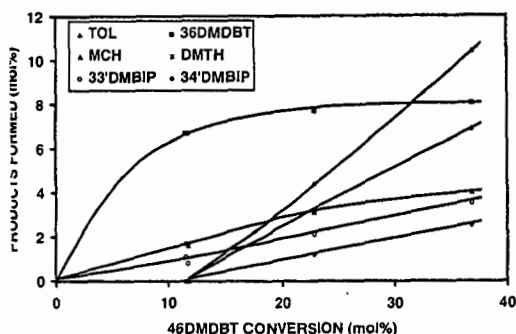
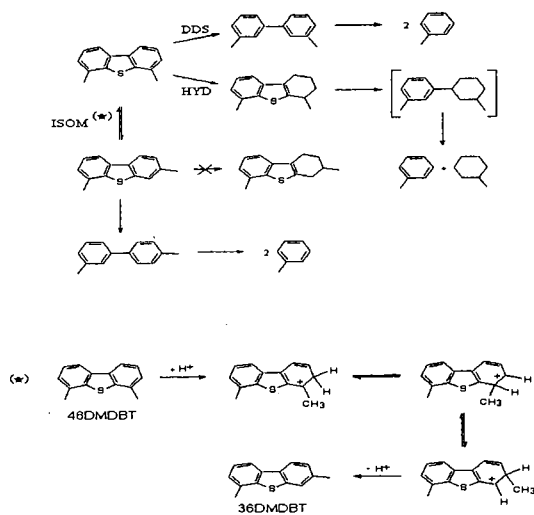
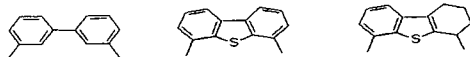


Figure 3. Hydrodesulfurization of 4,6-dimethyldibenzothiophene on sulfided NiMo on alumina - Y zeolite catalyst. TOL = toluene, 36DMDBT = 3,6-dimethyldibenzothiophene, MCH = methylcyclohexane, DMTH = 4,6-dimethyltetrahydrodibenzothiophene, 33'DMBiP = 3,3'-

dimethylbiphenyl, 34'DMBiP = 3,4'-dimethylbiphenyl



Scheme 1. Transformation of 4,6-dimethylbenzothiophene on sulfided NiMo on alumina - Y zeolite catalyst.

TRANSITION METAL TETRACHLOROALUMINATE CATALYSTS FOR PROBE REACTIONS SIMULATING PETROLEUM RESIDS UPGRADING

Masahide Sasaki, Chunshan Song and Mark A. Plummer^{*}
Fuel Science Program & Laboratory for Hydrocarbon Process Chemistry
Pennsylvania State University, 209 Acad. Proj. Bldg.
Univ. Park, PA 16802

Petroleum Technology Center, Marathon Oil Company, Littleton, CO 80160
Keywords: Transition Metal Tetrachloroaluminate, Acidity, Bond Cleavage

INTRODUCTION

In current commercial practice for catalytic upgrading of heavy oil and resids, there are two approaches. One is hydrocracking to obtain light and middle distillates, and the other is hydrotreating followed by FCC to produce gasoline components. While commercial hydroprocessing uses metal sulfide catalysts, an alternative approach would be to convert resids into lower-molecular-weight hydrocarbons with Lewis acidic catalysts. The present work deals with petroleum resid upgrading using Lewis acidic dual-functional salts as catalysts, which contain transition metal halides(1,2). Dual-function here refers to cracking via acid-catalyzed C-C bond cleavage for molecular weight reduction, and hydrogenation of reactive intermediates (from bond cleavage) and polyaromatics for production of stable molecules of low molecular weight. Plummer(3) suggested that sodium and hydrogen tetrachloroaluminates (NaAlCl_4 and HAlCl_4) was effective as catalyst for molecular weight reduction of resids. The NaAlCl_4 was the major molecular weight reduction and synthesis component, and HAlCl_4 added a hydrogenation function. Historically, such catalysts have been used in synthesis-type reactions such as isomerization, alkylation and polymerization(4,5).

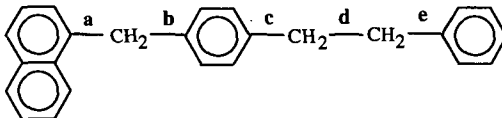
The present work examines the potential of transition metal tetrachloroaluminates as resid upgrading catalysts. This is a fundamental applied research using model compounds as probe molecules. The MCl_x in the alkali metal or transition metal tetrachloroaluminate $\text{MCl}_x\text{-(AlCl}_3)_x$ includes three kinds of alkali metal chlorides, LiCl , NaCl and KCl , and six transition metal chlorides, VCl_3 , CoCl_2 , NiCl_2 , ZnCl_2 , MoCl_3 . We selected four compounds as models, including 4-(1-naphthylmethyl) bibenzyl (NMBB), eicosane (n-C_{20}), dibenzothiophene and pyrene. Batch tests with model compounds were carried out at 425 °C for 20 min in autoclave under hydrogen pressure. The catalytic performance was evaluated in the reaction of model compounds with respect to bond cleavage reaction of C-C bond, hydrogenation, methylation and ring opening of aromatics.

EXPERIMENTAL

Catalyst Precursor and Compound

Three kinds of alkali metal chlorides, LiCl , NaCl and KCl , and six transition metal chlorides, VCl_3 , CoCl_2 , NiCl_2 , ZnCl_2 , MoCl_3 and PdCl_2 , were used for preparing the $\text{MCl}_x\text{-(AlCl}_3)_x$ catalysts. Ammonium tetrathiomolybdate (ATTM) also was used as catalyst precursor.

4-(1-naphthylmethyl)bibenzyl (NMBB), eicosane (n-C_{20}), dibenzothiophene and pyrene were used as a model compound. The structure of NMBB is



An intriguing feature of the NMBB structure is the presence of five different $\text{C}_a\text{-C}_b$ or $\text{C}_a\text{-C}_c$ bonds. Following the system established by earlier workers, these bonds are denoted as a through e in the structure shown above. (Some authors refer to this compound as naphthylbibenzylmethane and use the abbreviation NBBM; the system of labeling the bonds remains the same.) ATTM and these model compounds were used without further purification.

Catalyst Preparation

Before catalyst preparation, the precursors were dried at 210 °C for 6 h in vacuum. Catalysts were prepared by using a quartz tube insert, which was placed in a vertical microautoclave reactor with a capacity of 25 mL. Precursor loading amount depends on its valence number, x, for example, $\text{CoCl}_2\text{-(AlCl}_3)_x$ was $\text{CoCl}_2/\text{AlCl}_3=0.5$. The reactor was heated at 400 °C for 20 min, including heat-up time for about 6 min, under nitrogen pressure (300 psig-cold). The combination of LiCl , NaCl , KCl and ZnCl_2 with AlCl_3 were melt at 400 °C, which indicated these catalysts made molten salt. Other combinations did not become molten salts even at 400 °C. However, strong interactions between MCl_x and AlCl_3 may occur even if the combination $\text{MCl}_x\text{-(AlCl}_3)_x$ is not in molten state at the reaction temperature.

Model Compound Reaction

A horizontal microautoclave reactor with a capacity of 25 mL was loaded with the reactant and 10 mol% of catalyst based on molar number of reactant. The amounts of reactants were as follows; NMBB: 0.78 mmol; eicosane : 1.8 mmol; DBT : 2.0 mmol; pyrene: 2.0 mmol. After loading reactant and catalyst, the reactor was sealed and purged three times with hydrogen, then pressurized with 800 psig- H_2 at room temperature. A preheated fluidized sand bath was used as a heating source, and the reactor was vertically agitated to provide mixing (about 240 strokes / min). Most of the reactions were carried out at 425 °C for 20 min including heat-up time for about 6 min. After the reaction the reactor was quenched in a cold water bath. Gaseous products were collected into a sample bag. The solid and liquid products were washed out with about 20 mL CH_2Cl_2 , then

filtered to separate to solid and liquid products. The solid material was dried at 50 °C for 6 h in vacuum. The CH_2Cl_2 insoluble product was defined as coke.

Analysis

Gaseous products were analyzed by GC-FID using a Parkin Elmer AutoSystem GC for C_1 to C_6 hydrocarbon gases.

Liquid products were identified by GC-MS using a Hewlett-Packard 5890 II GC coupled with a HP 5971 A mass-selective detector operating at electron impact mode (EI, 70 eV). The column used for GC-MS was a J&W DB-17 column; 30 m x 0.25 mm, coated with 50 % phenyl - 50 % methylpolysiloxane with a coating film thickness of 0.25 μm . For quantification, a Perkin Elmer 8500 GC with flame ionization detector and the same type of DB-17 column used. Both GC and GC-MS were programmed from 80 to 280 °C at a heating rate of 6 °C/min, and an initial holding time of 0 min and a final holding time of 2 min (or 22 min for NMBB as a reactant). The response factors for all the reactant and 8 of the products were determined using pure compounds(6,7).

RESULTS AND DISCUSSION

NMBB conversion over $\text{MCl}_x\text{-(AlCl}_3)_x$ catalyst

Table 1 shows the results of non-catalytic and catalytic runs of NMBB at 425 °C for 20 min. Complete conversion of NMBB was achieved with significant coke formation with CoCl_2 , NiCl_2 , ZnCl_2 , and PdCl_2 containing catalyst. For coke formation, the yield with the fourth row in periodic table metal containing catalysts were much higher than that with the fifth row ones. It was with MoCl_3 containing catalyst that there was no coke formation.

For liquid products distribution, the main products in liquid were naphthalene, methyl-naphthalene, bibenzyl and methylbibenzyl. Using transition metal $\text{MCl}_x\text{-(AlCl}_3)_x$ enhanced hydrogenation activity (yield of tetralin), especially NiCl_2 , ZnCl_2 , and PdCl_2 . Table 1 also gave the results of ATTM as a catalyst precursor, which produces MoS_2 in situ. For the reaction with ATTM, there was no dimethylated products in liquid, for example DiMe-naphthalene and DiMe-bibenzyl. It means that methylation activity of molybdenum sulfide catalyst is much lower than that of $\text{MCl}_x\text{-(AlCl}_3)_x$ catalysts. However, molybdenum sulfide catalyst showed much higher hydrogenation activity (yield of tetralin).

Computer-aided reaction pathway analysis(8) indicated that bond cleavage in catalytic reaction of NMBB may occur favorably in bond **a** (between naphthyl and methylene) with Mo sulfide catalyst, in bond **b** (between the two methylene carbon in bibenzyl part) with Lewis acidic Mo chloride catalyst, and bond **d** (between naphthyltolyl and methylene) in noncatalytic thermal reaction. These results suggested that the main cracking products for catalytic reaction can be represented by Me-bibenzyl and bibenzyl. Therefore, we introduced the molar ratio Me-bibenzyl / bibenzyl as an index of bond cleavage of NMBB, as summarized in Table 2. For thermal cracking of NMBB, the yields of these compounds were very low, because bond cleavage reaction mainly occurred at **d**. In this case, the main cracking products were naphthyltolymethane and toluene. For catalytic reaction with $\text{MCl}_x\text{-(AlCl}_3)_x$, a/b values for transition metals were lower than those with alkali metal, but in all cases, a/b values were less than 1. It means bond cleavage reaction at **b** position was significant for $\text{MCl}_x\text{-(AlCl}_3)_x$ catalyst. On the other hand, a/b value with ATTM is much higher than the others (over 1). This higher value indicated that bond cleavage reaction mainly occurred at **a** position. These experimental data of bond cleavage reaction are consistent with the results of computational analysis.

In addition, we also determined the ratio of $i\text{-C}_4$ / $n\text{-C}_4$ as an index, which is a relative measure of the acidity of the catalysts. Figure 1 shows the relation between a/b value and $i\text{-C}_4/n\text{-C}_4$ ratio. From this figure, the selectivity of bond cleavage (a/b) decrease with increasing $i\text{-C}_4/n\text{-C}_4$ ratio. This result suggests that the selectivity of bond cleavage of NMBB depends on catalyst acidity for $\text{MCl}_x\text{-(AlCl}_3)_x$ catalysts.

Table 2 also specified the result with Na tetrachloroaluminate catalyst at 400 °C. There was no remarkable difference in conversion between reaction at 400 °C and that at 425 °C, conversion value was 91.5 and 91.7 wt%, respectively. At 400 °C, the degree of bond cleavage reaction at **a** position was almost same as that at **b** position(selectivity: 1.12). On the other hand, bond cleavage reaction at **b** was dominant reaction at 425 °C(selectivity: 0.48). These results indicated that bond cleavage reaction of NMBB with binary catalyst is sensitive to reaction temperature. On the other hand, it should be noted that demethylation reaction and some hydrocracking reaction also occurred, as can be seen from the $\text{C}_7\text{-C}_8$ products shown in Table 1.

Eicosane conversion over $\text{MCl}_x\text{-(AlCl}_3)_x$ catalyst

Table 3 shows the results of non-catalytic and catalytic runs of eicosane ($n\text{-C}_{20}$) at 425 °C for 20 min. Using transition metal in $\text{MCl}_x\text{-(AlCl}_3)_x$ [$\text{MCl}_x = \text{VCl}_3$, CoCl_2 , NiCl_2 , ZnCl_2 , PdCl_2] caused great enhancement in long-chain paraffin hydrocracking. In these cases, C_7 and C_8 hydrocarbons were main products. Complete conversion of eicosane was achieved without any coke formation with NiCl_2 , ZnCl_2 , and PdCl_2 . $\text{MoCl}_3\text{-(AlCl}_3)_3$ catalyst was not very active for eicosane hydrocracking among the transition metal-containing catalysts.

On the other hand, alkali metal-based $\text{MCl}_x\text{-(AlCl}_3)_x$ [$\text{MCl}_x = \text{LiCl}$, NaCl , KCl] catalysts were not as effective as transition metal-containing ones. The order of conversion was : $\text{LiCl} > \text{NaCl} > \text{KCl}$.

Table 4 shows a selected group distribution of liquid products. Here the liquid products are divided into two groups for convenience, one is C_9 to C_{11} and the other is C_{12} to C_{19} . The value of $A/(A+B)$ (the fifth column) indicates the degree of hydrocracking of eicosane molecule. In all cases, the values of transition metal are higher than that of alkali metal, which means transition metal catalyst has higher hydrocracking activity for eicosane molecule. In addition, this value is closely related to total conversion.

Table 1 NMBB Conversion at 425 °C for 20 min.

| Exp. # | 393 | 336 | 340 | 344 | 348 | 352 | 374 | 360 | 364 | 368 | 420 |
|--|------|------|------|------|------------------|-------------------|-------------------|-------------------|-------------------|-------------------|------|
| MCIX-(AlCl ₃) _x | None | LiCl | NaCl | KCl | VCl ₃ | CoCl ₂ | NiCl ₂ | ZnCl ₂ | MoCl ₃ | PdCl ₂ | ATTM |
| Conv. (wt%) | 17.1 | 82.8 | 64.3 | 36.2 | 81.0 | 100.0 | 100.0 | 100.0 | 72.9 | 100.0 | 96.8 |
| Gas yield (wt%) | 6.1 | 0.0 | 2.2 | 0.0 | 2.4 | 1.5 | 12.4 | 10.5 | 3.4 | 13.5 | 2.8 |
| Liquid yield (wt%) | 5.8 | 48.8 | 45.1 | 13.1 | 54.2 | 62.6 | 52.3 | 48.1 | 43.8 | 52.0 | 77.7 |
| Coke yield (wt%) | 0.0 | 7.3 | 2.9 | 0.0 | 8.9 | 15.1 | 20.0 | 20.3 | 0.0 | 10.3 | 0.0 |
| Liquid products (mol%) | | | | | | | | | | | |
| toluene | 2.4 | 5.1 | 4.3 | 1.2 | 4.3 | 6.5 | 4.5 | 6.4 | 2.9 | 6.5 | 1.4 |
| p-, m-xylene | 0.6 | 2.9 | 2.7 | 0.4 | 3.2 | 5.0 | 5.5 | 8.1 | 1.9 | 9.7 | 6.9 |
| o-xylene | 1.1 | 0.3 | 0.2 | | 0.3 | 0.5 | 0.5 | 0.6 | 0.2 | 0.7 | |
| 1,3,5-trimethylbenzene | | 0.4 | 0.3 | | 0.5 | 0.9 | 1.1 | 1.6 | 0.2 | 2.0 | 0.9 |
| 1,2,4-trimethylbenzene | | | | | 0.1 | 0.1 | 0.2 | 0.3 | | 0.3 | |
| 1,2,3-trimethylbenzene | | | | | | 0.2 | 0.2 | 0.3 | | 0.4 | |
| tetralin | 0.7 | 2.0 | 0.7 | | 1.8 | 2.3 | 7.6 | 13.7 | 0.8 | 20.6 | 34.4 |
| Me-istralin* | | 0.5 | | | 0.4 | 0.6 | 2.0 | 3.3 | | 4.7 | 3.2 |
| naphthalene | 1.0 | 41.0 | 44.5 | 19.0 | 45.7 | 46.4 | 32.3 | 20.7 | 47.7 | 11.3 | 37.3 |
| 1-Me-naphthalene | | 3.6 | 3.9 | 0.7 | 4.8 | 4.2 | 3.3 | 2.3 | 3.7 | 2.1 | 4.0 |
| 2-Me-naphthalene | | 7.0 | 4.9 | | 6.4 | 8.0 | 5.8 | 4.0 | 4.8 | 3.5 | 0.6 |
| 1,2-DiMe-naphthalene | | 0.1 | | | | 0.2 | | 0.2 | | 0.3 | |
| 1,3-DiMe-naphthalene | | 0.5 | | | 0.3 | 0.4 | 0.2 | 0.2 | | 0.2 | |
| 1,4-DiMe-naphthalene | | 0.3 | 0.2 | | 0.2 | 0.4 | 0.3 | 0.2 | 0.1 | 0.2 | |
| 1,5-DiMe-naphthalene | | 0.6 | 0.4 | | 0.5 | 0.8 | 0.6 | 0.5 | 0.3 | 0.6 | |
| 1,6-DiMe-naphthalene | | 0.3 | | | | 0.1 | | 0.2 | | 0.2 | |
| 2,6-DiMe-naphthalene | | | | | 0.4 | 0.4 | | | | 0.5 | |
| 2,7-DiMe-naphthalene | | | | | | 0.4 | 0.1 | 0.6 | | | |
| bibenzyl | 0.2 | 36.0 | 29.0 | 4.7 | 36.1 | 43.9 | 40.5 | 34.0 | 25.7 | 36.2 | 12.5 |
| 4Me-bibenzyl | 1.6 | 5.9 | 12.6 | 3.0 | 14.9 | 11.7 | 7.4 | 2.7 | 13.0 | 3.1 | 54.8 |
| Me-bibenzyl | | 3.5 | 1.3 | | 2.7 | 4.3 | 4.2 | 3.5 | 1.2 | 4.2 | 0.7 |
| DiMe-bibenzyl* | | | | | 0.4 | 1.1 | 0.5 | 0.5 | | 1.5 | |
| 1-benzyl-naphthalene | 0.5 | | | 0.2 | | | | | | | |
| naphthyltolylmethane | 2.3 | | | 1.1 | | | | | | | |
| 4H-NMBB | 0.3 | 0.0 | | | | | | | | | |
| NMBB isomer | | 1.9 | 6.9 | 38.0 | 5.0 | | | | 6.1 | | |
| NMBB | 82.9 | 15.3 | 28.8 | 25.8 | 16.8 | | | | 21.0 | | 3.2 |
| Gaseous Products (mol%) | | | | | | | | | | | |
| CH ₄ | 35.9 | 0.0 | 13.8 | 0.0 | 6.1 | 5.0 | 15.0 | 22.9 | 14.4 | | 8.0 |
| C ₂ H ₆ | 3.1 | 0.0 | 2.8 | 0.0 | 3.3 | 2.4 | 14.5 | 18.3 | 1.8 | | 2.7 |
| C ₃ H ₈ | 14.3 | 0.0 | 1.5 | 0.0 | 5.8 | 3.8 | 22.5 | 20.9 | 1.8 | | 1.7 |
| iso-C ₄ H ₁₀ | 0.0 | 0.0 | 2.2 | 0.0 | 2.0 | 1.3 | 18.1 | 18.3 | 3.1 | | 1.5 |
| n-C ₄ H ₁₀ | 1.3 | 0.0 | 0.5 | 0.0 | 0.8 | 0.4 | 5.8 | 2.0 | 1.0 | | 1.5 |
| i-C ₄ / n-C ₄ | 0.0 | | 3.8 | | 2.8 | 2.9 | 5.9 | 9.1 | 2.9 | | 1.0 |

* including isomers

Table 2 Selectivity bond cleavage of binary catalyst system at 425 °C for 20 min.

| Exp # | Catalyst | Cleavage at (a), Me-Bibenzyl | Cleavage at (b), Bibenzyl | Selectivity | i-C ₄ / n-C ₄ |
|-------|--|------------------------------|---------------------------|-------------|-------------------------------------|
| | MCIX-(AlCl ₃) _x | (mmol)(1) | (mol %)(2) | (a)/(b) | |
| 393 | None | 0.012 | 1.6 | 0.004 | 0.5 |
| 336 | LiCl | 0.073 | 9.3 | 0.282 | 36.0 |
| 340 | NaCl | 0.109 | 13.9 | 0.228 | 29.0 |
| 313* | NaCl | 0.128 | 16.3 | 0.114 | 14.6 |
| 344 | KCl | 0.024 | 3.0 | 0.037 | 4.7 |
| 348 | VCl ₃ | 0.138 | 17.6 | 0.284 | 36.1 |
| 352 | CoCl ₂ | 0.127 | 16.1 | 0.346 | 43.9 |
| 374 | NiCl ₂ | 0.092 | 11.6 | 0.320 | 40.5 |
| 360 | ZnCl ₂ | 0.048 | 6.2 | 0.267 | 34.0 |
| 364 | MoCl ₃ | 0.111 | 14.2 | 0.201 | 25.7 |
| 368 | PdCl ₂ | 0.057 | 7.2 | 0.284 | 36.2 |
| 425 | ATTM | 0.456 | 55.5 | 0.098 | 12.5 |

(1): 4Me-Bibenzyl + isomer

(2): Based on feed molar number of NMBB

*: Reaction temperature 400 °C

n/a : not available

Table 3 Eicosane Conversion at 425 °C for 20 min.

| Exp. # | 392 | 333 | 337 | 341 | 345 | 349 | 371 | 357 | 361 | 365 |
|---|------|------|------|------|------------------|-------------------|-------------------|-------------------|-------------------|-------------------|
| MClx-(AlCl ₃) _x | None | LiCl | NaCl | KCl | VCl ₃ | CoCl ₂ | NiCl ₂ | ZnCl ₂ | MoCl ₃ | PdCl ₂ |
| Conv. (wt%) | 21.8 | 36.0 | 26.9 | 23.0 | 88.7 | 83.2 | 100.0 | 100.0 | 37.2 | 100.0 |
| Gas yield (wt%) | 7.7 | 15.7 | 4.7 | 3.6 | 59.0 | 47.9 | 85.4 | 71.6 | 22.6 | 81.5 |
| Liquid yield (wt%) | 7.8 | 7.1 | 5.9 | 8.8 | 2.9 | 2.6 | 0.8 | 2.1 | 5.2 | 1.2 |
| Coke yield (wt%) | 0.0 | 0.0 | 0.0 | 0.0 | 4.9 | 6.0 | 0.0 | 0.0 | 0.0 | 0.0 |
| Liquid products (mol%) | | | | | | | | | | |
| n-nonane | 1.0 | 2.4 | 0.7 | 4.5 | 1.9 | 0.5 | 0.6 | 3.7 | 0.8 | 0.5 |
| C9H ₁₈ | 0.7 | | | 0.2 | | 0.2 | | | 0.6 | |
| C9H ₁₈ or C9H ₂₀ isomer | | 0.1 | 1.4 | 0.5 | 0.4 | 0.6 | | | 1.7 | |
| n-decane | 0.9 | 0.5 | 1.2 | 1.1 | 0.7 | 0.3 | 0.7 | 0.2 | 0.9 | 0.8 |
| C10H ₂₀ | 0.7 | | 0.1 | 0.1 | | 0.1 | | | 0.1 | |
| C10H ₂₀ or C10H ₂₂ isomer | 0.3 | 0.2 | 0.2 | 0.9 | 0.6 | 0.7 | 0.0 | 0.5 | 0.9 | 0.7 |
| n-undecane | 0.9 | 0.5 | 1.2 | 1.1 | 0.3 | 0.2 | 0.2 | 0.1 | 0.8 | 0.0 |
| C11H ₂₂ | 0.6 | | | 0.1 | | | | | 0.2 | |
| C11H ₂₂ or C11H ₂₄ isomer | | 0.2 | 0.3 | 0.4 | 0.8 | 0.9 | 0.1 | | 0.3 | 0.4 |
| C12H ₂₄ | 0.6 | | 0.1 | 0.1 | 0.1 | 0.1 | | 0.0 | 0.0 | |
| C12H ₂₄ or C12H ₂₆ isomer | | | | 0.4 | 0.3 | 0.4 | | | 0.1 | |
| n-tridecane | 0.8 | 0.5 | 1.0 | 1.0 | 0.2 | 0.2 | | | 0.7 | |
| C13H ₂₆ | 0.5 | | 0.1 | 0.1 | | | | | | |
| C13H ₂₆ or C13H ₂₈ isomer | | | | 0.4 | | 0.0 | | | | |
| n-tetradecane | 0.8 | 5.6 | 0.9 | 1.0 | 0.1 | 0.4 | | | 0.6 | |
| C14H ₂₈ | 0.5 | | | 0.1 | | | | | | |
| C14H ₂₈ or C14H ₃₀ isomer | | | | 0.2 | | | | | | |
| n-pentadecane | 0.7 | 0.4 | 0.9 | 0.9 | 0.1 | 0.1 | | | 0.6 | |
| C15H ₃₀ | 0.4 | | | 0.1 | | | | | | |
| C15H ₃₀ or C15H ₃₂ isomer | | | | 0.1 | | | | | | |
| n-hexadecane | 0.7 | 0.4 | 0.7 | 0.8 | 0.1 | 0.1 | | | 0.5 | |
| C16H ₃₂ | 0.4 | | | 0.1 | | | | | | |
| C16H ₃₂ or C16H ₃₄ isomer | | | | 0.1 | | | | | | |
| n-heptadecane | 0.6 | 0.4 | 0.7 | 0.8 | 0.1 | 0.1 | | | 0.5 | |
| C17H ₃₄ | 0.3 | | | | | | | | | |
| C17H ₃₄ or C17H ₃₆ isomer | | | | 0.1 | | | | | | |
| n-octadecane | 0.2 | 0.1 | 0.1 | 0.1 | | | | | 0.1 | |
| C18H ₃₆ | 0.3 | | | | | | | | | |
| C18H ₃₆ or C18H ₃₈ isomer | | | | 0.1 | | | | | | |
| n-nonadecane | 0.1 | | | | | | | | | |
| C19H ₃₈ | 0.1 | | | | | | | | | |
| C19H ₃₈ or C19H ₄₀ isomer | | | | | | | | | 0.0 | |
| n-eicosane | 78.3 | 64.0 | 73.1 | 77.0 | 11.3 | 16.8 | | | 62.8 | |
| Gaseous Products (mol%) | | | | | | | | | | |
| CH ₄ | 3.3 | 5.0 | 2.9 | 2.0 | 27.3 | 16.7 | 17.4 | 26.4 | 6.1 | 19.9 |
| C ₂ H ₆ | 12.0 | 6.4 | 10.2 | 8.1 | 19.9 | 13.6 | 18.5 | 20.4 | 11.1 | 28.4 |
| C ₃ H ₈ | 12.9 | 29.9 | 10.4 | 7.4 | 140.3 | 99.3 | 148.0 | 170.4 | 37.2 | 180.2 |
| iso-C ₄ H ₁₀ | | 42.6 | 1.2 | 1.2 | 123.8 | 112.7 | 161.8 | 160.6 | 46.4 | 157.0 |
| n-C ₄ H ₁₀ | 7.0 | 2.1 | 1.6 | 1.7 | 31.3 | 25.7 | 34.0 | 31.7 | 13.2 | 39.4 |
| i-C ₄ / n-C ₄ | 0.0 | 20.7 | 0.7 | 0.4 | 4.0 | 4.4 | 4.1 | 5.1 | 3.5 | 4.0 |

Table 4 Degree of Hydrocracking of eicosane with MClx-(AlCl₃)_x Catalysts

| Exp.# | MClx-(AlCl ₃) _x | A: C ₉ -C ₁₁ (mmol) | B: C ₁₂ -C ₁₉ (mmol) | A/(A+B) | i-C ₄ / n-C ₄ | Conv.(wt%) |
|-------|--|---|--|---------|-------------------------------------|------------|
| 392 | None | 0.1016 | 0.1162 | 0.466 | 0.00 | 21.8 |
| 333 | LiCl | 0.0706 | 0.1314 | 0.350 | 20.65 | 36.0 |
| 337 | NaCl | 0.0964 | 0.0790 | 0.550 | 0.72 | 26.9 |
| 341 | KCl | 0.1693 | 0.1035 | 0.621 | 0.41 | 23.0 |
| 345 | VCl ₃ | 0.0918 | 0.0082 | 0.918 | 3.96 | 88.7 |
| 349 | CoCl ₂ | 0.0696 | 0.0159 | 0.814 | 4.39 | 83.2 |
| 371 | NiCl ₂ | 0.0289 | 0.0000 | 1.000 | 4.11 | 100.0 |
| 357 | ZnCl ₂ | 0.0804 | 0.0000 | 1.000 | 5.07 | 100.0 |
| 361 | MoCl ₃ | 0.1124 | 0.0528 | 0.680 | 3.52 | 37.2 |
| 365 | PdCl ₂ | 0.0427 | 0.0000 | 1.000 | 3.99 | 100.0 |

* With transition metal catalyst, more cracking occurs, giving A / (A+B) ratio of close to or equal to 1.0.

DBT conversion over $\text{MCl}_x(\text{AlCl}_3)_x$ catalyst

The results of DBT reaction with $\text{MCl}_x(\text{AlCl}_3)_x$ catalyst are summarized in Table 5. It was observed that transition metal-based catalysts gave higher conversion compared with alkali metal-based ones. From the liquid products distribution, MoCl_3 containing catalyst afforded higher biphenyl yield compared with others. This result suggests that Mo containing catalyst has high hydrodesulfurization activity and selectivity. In addition there was no coke formation with Mo containing catalyst. Other transition metal catalyst showed good methylation activity of DBT molecule and significant coke formation. On the contrary, alkali metal-containing catalysts showed much less activity for DBT conversion. Their order of activity (DBT conversion) was $\text{LiCl} > \text{NaCl} > \text{KCl}$, which is the same as that observed for eicosane conversion.

Pyrene conversion over $\text{MCl}_x(\text{AlCl}_3)_x$ catalyst

Table 6 shows the results of pyrene reaction with $\text{MCl}_x(\text{AlCl}_3)_x$ catalyst. Hydrogenation and ring opening and subsequent dealkylation were more remarkable with $\text{VCl}_3(\text{AlCl}_3)_3$, $\text{NiCl}_2(\text{AlCl}_3)_2$ and $\text{ZnCl}_2(\text{AlCl}_3)_2$. The yield of C_2H_6 appears to be the most important dealkylation product. MoCl_3 containing catalyst showed high hydrogenation activity (higher yield of hydrogenated pyrene) and selectivity, and there was no coke formation. Other transition metal containing catalysts resulted in significant amount of coke formation. The alkali metal containing catalysts displayed an order of activity ($\text{LiCl} > \text{NaCl} > \text{KCl}$) which is consistent with those observed in other reactions.

CONCLUSION

From the results of model compounds reactions, transition metal containing catalysts showed higher activity in most cases, especially with eicosane and DBT as reactants. The selectivity of bond cleavage of NMBB molecule appears to be related to $i\text{-C}_4 / n\text{-C}_4$ ratio which is a relative measure of the acidity of the catalysts. In addition, this selectivity was sensitive to reaction temperature. $\text{MoCl}_3(\text{AlCl}_3)_3$ catalyst has a specific character for model compound reaction compared with other transition metal containing catalysts, for example, higher activity and selectivity of desulfurization of DBT and higher activity of hydrogenation of pyrene. The most important feature with $\text{MoCl}_3(\text{AlCl}_3)_3$ is no coke formation in all cases. In the present paper there was no remarkable difference than can be attributed to the molten state of the catalyst, such as that between molten $\text{ZnCl}_2(\text{AlCl}_3)_2$, and a mixture of $\text{MCl}_x(\text{AlCl}_3)_x$ catalyst that do not become molten salt at the reaction temperature. The activity of alkali metal tetrachloroaluminate catalysts was found to decrease in the order of $\text{LiCl} > \text{NaCl} > \text{KCl}$ in all the reactions examined.

ACKNOWLEDGMENT

The authors wish to thank Marathon Oil Company for supporting this work. We also thank Prof. Harold H. Schobert for technical support and helpful discussions.

LITERATURE CITED

- (1) Song, C., Nomura, M. and Ono, T., PREPRINTS, Am. Chem. Soc., Div. Fuel Chem., 36, 586 (1991)
- (2) Song, C., Nomura, M. and Miyake, M., Fuel, 65, 922 (1986)
- (3) Plummer, M. A., Fuel Process. Technol., 11, 313 (1985)
- (4) Lien, A.P., D'Ouville, E.L., Evering, B. L., and Crubb, H. M., Ind. Eng. Chem., 44, 351 (1952)
- (5) Alul, H.R. and McEwan, G.J., J. Org. Chem., 37, 4157 (1972)
- (6) Schmidt, E., Song, C. and Schobert, H.H., Energy & Fuels, 10, 597 (1996)
- (7) Cooke, W. S., Schmidt, E., Song, C. and Schobert, H.H., Energy & Fuels, 10, 591 (1996)
- (8) Song, C., Ma, X., Schmidt, E., Yoneyama, Y. and Schobert, H. H., PREPRINTS, Am. Chem. Soc., Div. Petrol. Chem., 42, 674 (1997)

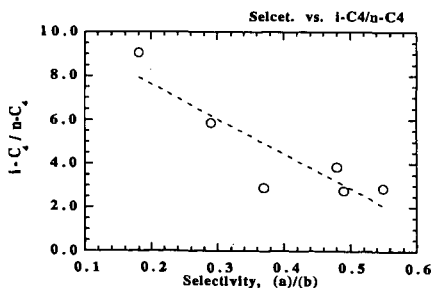


Figure 1 Relation between $i\text{-C}_4 / n\text{-C}_4$ ratio and selectivity of bond cleavage

Table 5 DBT Conversion at 425 °C for 20 min.

| Exp. # | 334 | 337 | 341 | 346 | 350 | 372 | 358 | 362 | 366 |
|-------------------------------------|------|------|------|------------------|-------------------|-------------------|-------------------|-------------------|-------------------|
| MClx-(AlCl ₃)x | LiCl | NaCl | KCl | VCl ₃ | CoCl ₂ | NiCl ₂ | ZnCl ₂ | MoCl ₃ | PdCl ₂ |
| Conv. (wt%) | 23.8 | 15.4 | 10.2 | 79.5 | 46.5 | 82.0 | 76.2 | 83.5 | 87.6 |
| Gas yield (wt%) | 0.0 | 1.3 | 0.0 | 13.8 | 7.0 | 12.8 | 13.8 | 25.0 | 22.5 |
| Liquid yield (wt%) | 3.6 | 2.0 | 1.2 | 9.3 | 10.4 | 14.3 | 11.0 | 33.1 | 18.4 |
| Coke yield (wt%) | 0.0 | 0.0 | 0.0 | 25.9 | 3.6 | 26.4 | 36.8 | 0.0 | 3.9 |
| Liquid products (mol%) | | | | | | | | | |
| toluene | 0.0 | 0.3 | | 0.9 | 0.3 | 0.8 | 1.0 | 0.6 | 3.6 |
| p-, m-xylene | 0.1 | | | 1.0 | 0.3 | 1.0 | 0.7 | 0.8 | 3.0 |
| o-xylene | 0.5 | 0.1 | | 0.1 | | 0.1 | 0.1 | 0.1 | 0.6 |
| 1,3,5-trimethylbenzene | | | | 0.2 | | 0.2 | 0.1 | | 0.7 |
| 1,2,4-trimethylbenzene | 0.7 | | | | | | | | |
| 1,2,3-trimethylbenzene | | | | | | | | | |
| biphenyl | 1.7 | 1.5 | 1.0 | 1.1 | 1.5 | 1.3 | 1.7 | 29.8 | 1.4 |
| 2-Me-biphenyl | | | | | | 0.1 | 0.1 | | 0.1 |
| 3-Me-biphenyl | | | | 0.2 | 0.1 | 0.3 | 0.3 | 0.3 | 0.3 |
| 4-Me-biphenyl | | | | 0.1 | 0.1 | 0.2 | 0.1 | 0.2 | 0.2 |
| 4H-DBT* | 1.3 | 0.6 | 0.3 | 0.8 | 2.2 | 1.0 | 1.4 | 1.8 | 1.8 |
| Me-DBT* | 0.1 | | | 3.5 | 3.6 | 5.1 | 3.6 | | 3.4 |
| DiMe-DBT* | | | | 1.5 | 1.7 | 3.2 | 1.8 | | 2.6 |
| DBT | 76.2 | 84.6 | 89.8 | 20.5 | 53.5 | 18.0 | 23.8 | 16.5 | 12.4 |
| Gaseous Products (mol%) | | | | | | | | | |
| CH ₄ | 0.0 | 0.7 | 0.0 | 5.2 | 1.9 | 2.5 | 5.3 | 12.6 | 3.5 |
| C ₂ H ₆ | 0.0 | 0.6 | 0.0 | 5.9 | 1.5 | 3.3 | 4.4 | 9.5 | 5.6 |
| C ₃ H ₈ | 0.0 | 0.4 | 0.0 | 18.3 | 7.0 | 8.3 | 18.2 | 25.9 | 21.1 |
| iso-C ₄ H ₁₀ | 0.0 | 0.9 | 0.0 | 17.5 | 10.8 | 12.1 | 19.2 | 27.0 | 25.8 |
| n-C ₄ H ₁₀ | 0.0 | 0.3 | 0.0 | 4.2 | 1.1 | 3.4 | 4.7 | 4.2 | 7.2 |
| i-C ₄ / n-C ₄ | | 3.3 | | 4.2 | 10.0 | 3.0 | 4.1 | 6.4 | 3.6 |

* including isomers

Table 6 Pyrene Conversion at 425 °C for 20 min.

| Exp. # | 335 | 339 | 343 | 347 | 351 | 373 | 359 | 363 | 367 |
|-------------------------------------|------|------|------|------------------|-------------------|-------------------|-------------------|-------------------|-------------------|
| MClx-(AlCl ₃)x | LiCl | NaCl | KCl | VCl ₃ | CoCl ₂ | NiCl ₂ | ZnCl ₂ | MoCl ₃ | PdCl ₂ |
| Conv. (wt%) | 73.5 | 69.3 | 9.0 | 85.7 | 69.5 | 86.7 | 93.9 | 44.4 | 89.7 |
| Gas yield (wt%) | 0.0 | 0.0 | 0.0 | 2.8 | 0.2 | 3.4 | 2.2 | 4.8 | 7.2 |
| Liquid yield (wt%) | 19.6 | 18.6 | 6.5 | 15.0 | 17.3 | 12.6 | 9.4 | 17.9 | 12.4 |
| Coke yield (wt%) | 31.6 | 19.9 | 0.0 | 50.4 | 33.2 | 53.6 | 64.9 | 0.0 | 49.1 |
| Liquid products (mol%) | | | | | | | | | |
| toluene | 0.2 | 0.2 | | 0.1 | 0.1 | 0.2 | 0.1 | 0.1 | 0.1 |
| p-, m-xylene | 0.2 | 0.1 | | 0.2 | 0.2 | 0.2 | 0.2 | 0.1 | 0.2 |
| o-xylene | 0.1 | 0.1 | | | 0.0 | 0.1 | | | |
| 2H-fluorene | 0.7 | 0.5 | | 0.7 | 0.4 | 0.9 | 0.9 | | 1.1 |
| 2H-Me-fluorene | 0.2 | 0.1 | | 0.1 | 0.1 | 0.2 | 0.2 | 0.1 | 0.2 |
| 4H-pyrene* | 2.2 | 2.5 | 0.2 | 1.7 | 1.7 | 0.9 | 0.6 | 2.1 | 0.8 |
| 6H-pyrene* | 1.9 | 2.2 | 0.2 | 1.5 | 1.2 | 0.8 | 0.5 | 1.5 | 0.8 |
| 2H-pyrene* | 8.3 | 9.1 | 5.3 | 5.0 | 8.1 | 3.9 | 1.9 | 13.2 | 3.1 |
| Me-pyrene* | 1.1 | 0.7 | | 1.0 | 1.2 | 1.2 | 1.1 | 0.1 | 2.0 |
| DiMe-pyrene* | 3.3 | 1.8 | | 2.9 | 3.1 | 2.9 | 2.3 | 0.3 | 2.1 |
| pyrene | 25.6 | 30.6 | 91.0 | 14.3 | 30.5 | 13.3 | 6.1 | 55.6 | 10.3 |
| Gaseous Products (mol%) | | | | | | | | | |
| CH ₄ | 0.0 | 0.0 | 0.0 | 3.1 | 0.3 | 3.3 | 3.6 | 2.9 | 7.3 |
| C ₂ H ₆ | 0.0 | 0.0 | 0.0 | 9.4 | 0.9 | 9.8 | 8.8 | 3.6 | 19.9 |
| C ₃ H ₈ | 0.0 | 0.0 | 0.0 | 2.0 | 0.2 | 2.4 | 1.7 | 1.5 | 4.7 |
| iso-C ₄ H ₁₀ | 0.0 | 0.0 | 0.0 | 0.7 | 0.1 | 1.2 | 0.3 | 2.8 | 2.0 |
| n-C ₄ H ₁₀ | 0.0 | 0.0 | 0.0 | 0.3 | 0.1 | 0.7 | 0.2 | 1.0 | 1.6 |
| i-C ₄ / n-C ₄ | | | | 2.1 | 2.0 | 4.3 | 1.5 | 3.0 | 1.2 |

* including isomers

NEW DEVELOPMENTS IN DEEP HYDROCONVERSION OF HEAVY OIL RESIDUES WITH DISPERSED CATALYSTS: THE EFFICIENCY OF HYDROGEN DONORS ADDITION IN HYDROCRACKING OF LIAOHE VACUUM RESIDUE WITH DISPERSED CATALYSTS.

Shi Bin ,Li PeiPei, Que GuoHe

Department of Chemical Engineering, University of Petroleum
Dong Ying, Shan Dong 257062, P.R.China

Introduction

Among other future challenges, refineries must cope with heavy feed stocks of lower quality, i.e., with higher viscosity, Conradson Carbon, heteroatom content and metal content. Furthermore, to satisfy market demand for light petroleum cuts, improved treatment of the "bottom of the barrel" is needed. To achieve deep conversion of heavy residues into distillates, it is necessary to develop new hydrocracking processes because of their applicability. Among these hydrocracking processes, "slurry-bed" hydrocracking seems to be a promising process to converse poor-quality petroleum residues into distillates. During reaction time, inhibition of excessive coke yield is critical in high conversion of heavy poor-quality feed stocks in order to keep the reaction units smoothly operating. According to literature and patents[1], the dispersed catalysts in reaction system could be an important inhibitor of coking.

It is well known that hydrogen donor solvents have been employed into coal hydroliquefaction [2-4] and some processes of oil residues such as hydrogen-donor visbreaking (HDV)[5-6] . However, they have never been used with the combination of dispersed catalysts in heavy petroleum residue upgrading. Hydrogen donors exhibit hydrogen-donating properties and inhibit coke formation [5-9]. Thus the donor could reduce coke yield, which was added into hydroconversion system of heavy oil residue with dispersed catalysts.

Experimental

The heavy oil chosen was Liaohe vacuum residue. Its main characteristics are C%,86.9%,H%,11.0%,N%,1.08%,S%,0.43%,Ni,123ppm,V,2.9ppm,Fe,38ppm,Ca,96,density,0.9976,CCR,19.0.

The oil-soluble metal compounds tested were molybdenum-dithiocarboxylate (MoDTC), FeNaphthenate (Fenaph), NiNaphthelate (Ninaph), CoNaphthelate (Conaph). Runs were conducted batch-wise in an 100cm³ stainless steel autoclave pressured with H₂(7.0 or 5.0Mpa cold) . About 30g feed and the catalyst precursor and Tetralin(5 or 10wt% to feed) were introduced. Element sulfur(0.1000g)was added into the autoclave to keep the catalysts totally sulfurized. The run temperature were attained in 40 mins by heating stove and efficient stirring ensured dispersion of the oil-soluble metal compounds. After run completion, gases were vented off and a solid fraction was seperated from the liquid effluent by centrifugation in toluene. The fractions(150-350°C, 350-450°C) were distilled after toluene was recovered. Naphthalene and Tetralin in 150-350°C fraction were analyzed for donating yield by GC. Conversion of the feed into distillates were calculated by the difference between the weight of the residue feed and of coke and reacted resid.

Results

The inhibition for coking of the catalysts is known for us and take an important role in achieving deep conversion of residues[1].The four oil-soluble catalysts tested were all effective for hydrocracking of Liaohe VR . The catalytic activities of base metals were in order of :Mo>Co>Ni>Fe(see Table 1). RN of Mo was 3.51 and of Fe was 8.63 .This means that MoDTC provide the smallest coke yield in the four metals tested when achieving the same conversion. After combined with 10%wt tetralin, the coking yields were considerably decreased at the same conversion, and more VGO yields were achieved comparing with non-addition of tetralin, and

hydrocracking conversion could hardly be affected. In this case, the order of inhibiting coke still was Mo>Co>Ni>Fe, all of the RN became smaller, but Mo combined with tetralin was more outstanding for reducing coke yields and RN (see Fig.1—4 and Table 1). Only Mo combined with tetralin could remain higher activity for inhibiting coking during the most reaction time.

Literature and patents[1] show that most of the "slurry-bed" hydrocracking processes employed disposable catalysts under high hydrogen pressure (up to 20Mpa). It is necessary to reduce the amounts of used catalysts in order to decrease the cost of catalysts at the same time the reactors maintain smooth operation. However, excessively coking would generate if insufficient coke inhibitors such as active catalysts existed in the reaction system. But combined with small amounts of tetralin, little amounts of catalysts play the same part in decreasing coke yields. Table 2 show that 60ppm Mo combined with 10%wt tetralin could decrease coke yields from 3.54% to 0.98%wt, on the other hand, 500ppm Mo alone give 1.45%wt. 30ppm Mo combined with 10%wt tetralin provide smaller coke yields than 100ppm Mo alone.

To take advantage of hydrogen donor, it is necessary to combine with reasonable amount of dispersed catalysts. The disposed catalysts will be saved and the expense of operation will be decreased.

Conclusion

It was found that hydrogen donor has efficient inhibition of the coke production. Dispersed catalysts combined with hydrogen donors would be a way to upgrade heavy petroleum residues. More active catalysts with the addition of donors could yield less coke. The amounts of employed catalysts could be reduced and high hydroconversion would be achieved at non-excessive coke formation by way of this method.

Literature cited

- (1)Del Bianco,A. et al, Chemtech, 11,35-42,1995.
- (2)Furlong,L.E. et al Chem. Eng. Prog. 72.(8).1976.
- (3)Er.V.J.Kuhlmann. et al Fuel.64.1552-1557
- (4)Isao. Mochida. et al. Advances in Catalysis. Vol(40).39-85.1994.
- (5)Fisher,I.P, et al. Oil Gas J.(22).111.1982.
- (6)Baskshi, et al. Oil Gas J.(13).84.1987.
- (7)U.S Patent 4615 791,1986.
- (8)U.S Patent 4814 065,1989.
- (9)Del Bianco, et al. Fuel (72).81-85.1993.

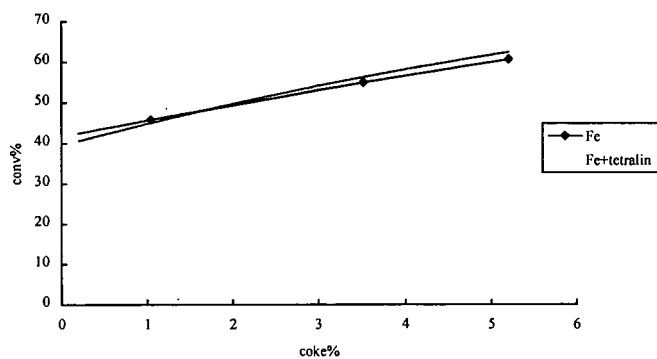


Figure 1. Comparison between Fenaph and Fenaph+Tetralin residue hydrocracking.

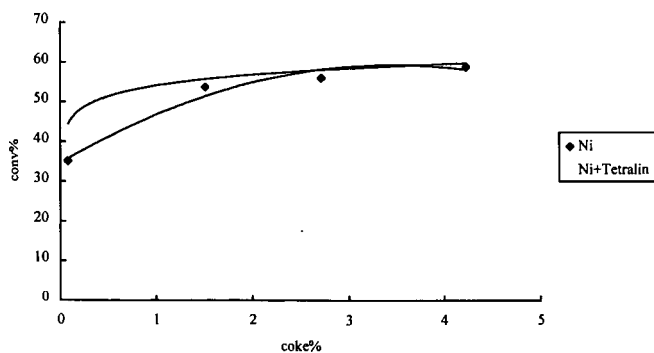


Figure 2. Comparison between Ninaph and Ninaph+Tetralin residue hydrocracking.

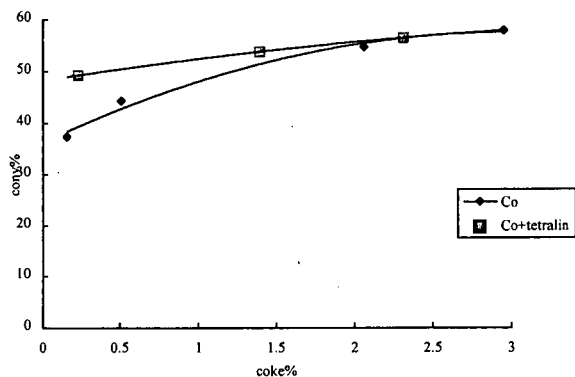


Figure3.Comparison between Conaph and Conaph+Tetralin residue hydrocracking.

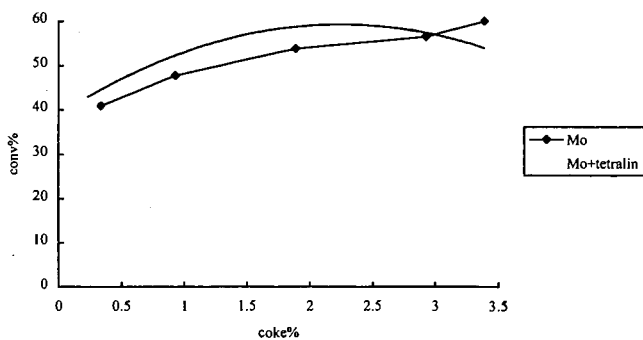


Figure 4 Comparison between MoDTC and MoDTC+Tetralin residue hydrocracking.
(all experimental conditions of the four figures are 430°C,7.00Mpa,200ppmmetal ,10.00%Tetralin)

Table 1 Hydroconversion of LHVR in the presence of Mo,Co,Ni,Fe and 10.00wt%Tetralin
(at 430oC,60 mins ,200ppm base metal and 7.0Mpa,cold)

| | product yields ,wt% | | | | conv. of resids. wt% | &RN |
|--------|---------------------|-----------|--------|------|----------------------------|------|
| | <350°C | 350-450°C | >450°C | coke | | |
| MoDTC | 31.12 | 22.71 | 47.37 | 1.89 | 53.83 | 3.51 |
| | 25.14 | 27.29 | 47.57 | 0.71 | 52.43 | 1.35 |
| Ninaph | 34.13 | 21.50 | 44.37 | 2.72 | 55.63 | 4.89 |
| | 30.90 | 23.90 | 45.20 | 1.89 | 54.80 | 3.45 |
| Conaph | 30.96 | 24.00 | 45.04 | 2.06 | 54.96 | 3.75 |
| | 27.65 | 26.15 | 46.20 | 1.39 | 53.80 | 2.58 |
| Fenaph | 37.78 | 22.60 | 39.62 | 5.21 | 60.38 | 8.63 |
| | 33.98 | 24.61 | 41.42 | 4.06 | 58.58 | 6.93 |

footnotes:1. &RN=(coke %/conv.of resids %*100) 2. is 200ppm metal+10.00wt%tetralin.

Table 2 Hydroconversion of LHVR in the presence of MoDTC and Tetralin
(at 430°C , 60mins and 7.0Mpa H₂ at cold)

| | 0%tetralin | | 5.00%tetralin | | 10.00%tetralin | |
|--------|-------------|-------------|---------------|-------------|----------------|-------------|
| | coke wt% | conv wt% | coke wt% | conv wt% | coke wt% | conv wt% |
| MoDTC | | | | | | |
| 30ppm | 4.45 | 58.80 | 2.95 | 56.30 | 2.25 | 54.76 |
| 60ppm | 3.54 | 56.90 | 2.71 | 55.79 | 0.98 | 53.81 |
| 100ppm | 2.89 | 54.65 | 1.11 | 53.49 | 0.74 | 52.98 |
| 200ppm | 1.89 | 53.83 | 0.94 | 52.85 | 0.71 | 52.43 |
| 500ppm | 1.45 | 50.90 | 1.05 | 49.54 | 0.75 | 48.42. |

footnote: conv% =(feed-coke-reacted resids)%wt

**THE REDUCTION OF NITROGEN- AND SULFUR-CONTAINING
HETEROAROMATIC COMPOUNDS IN A BIPHASIC MEDIUM USING A GROUP
VIII HYDROSOLUBLE ORGANOMETALLIC COMPLEX**

Pérez, D. E.^a, Andriollo, A.^a, López-Linares, F.^a, Galiasso, R. E.^a, Revete, J. A.^a, Sánchez-Delgado, R.^b, and Fuentes, A.^b

a. PDVSA-INTEVEP, Process Department, Apdo. 76343, Caracas 1070A, Venezuela. Fax (582) 908-7415.
b. IVIC, Centro de Química, Apdo. 21827, Caracas 1020A, Venezuela.

Keywords: Heteroaromatic, Biphasic, Organometallic.

ABSTRACT

Two-phase hydrogenation of heteroaromatic compounds such as quinoline (Q) and benzothiophene (BT) were performed using as catalytic precursor a mixture of ruthenium trichloride and an excess of the water-soluble ligand *m*-sulfonatophenildiphenylphosphine, in its sodium salt form (TPPMS). The products obtained from the hydrogenation were 1,2,3,4-tetrahydroquinoline (THQ) and dihydrobenzothiophene (DHBt), respectively.

The initial rate of hydrogenation for benzothiophene is enhanced in the presence of quinoline. Other organic nitrogen bases such as aniline, acridine, tetrahydroquinoline, piperidine and triethylamine were also important as promoters in the hydrogenation of benzothiophene. Understanding novel upgrading processes in fuels is the quest for this investigation.

1. INTRODUCTION:

Sulfur and nitrogen-containing aromatics are major contaminants in petroleum derived fuels (e.g., Naphtha, Diesel, etc.). Thiophene (Th), benzothiophene (BT) and derivatives are the most abundant sulfur aromatics in fuel. Quinoline (Q) and other related species represent the main nitrogen-containing aromatics [1]. New legislation represent a threat to these highly refractory compounds because they have to be reduced severely to comply with quality product standards. Degradation of these compounds is carried out via hydrotreating like HDS and HDN; however, limitations in heteroaromatic reduction severely affect upgrading [2].

Industrial HDS and HDN are generally carried out together with many other reactions such as aromatic saturation, olefin hydrogenation, hydrocracking, etc. [1]. Some of these side-reactions are desirable (e.g. regioselective aromatic saturation) because it permits a rational transformation of other undesirable products (polyaromatics). The ability to understand and eventually control hydrotreating reactions may lead to highly selective ways of either removing contaminants for continuing downstream processes or improving the quality of the hydrocarbon itself (e.g. transformations of two-rings fused aromatics into alkyl monoaromatics, helping octane and avoiding smoke in fuel combustion).

To understand the actual mechanistic details in hydrotreating, one could study the selective hydrogenation or hydrogenolysis of heteroaromatic compounds in a homogeneous medium [2]. It will be interesting to investigate whether the rupture of the C-S and C-N bonds (hydrogenolysis) occurred prior or subsequent to the hydrogenation of the heterocyclic rings on solid catalysts. While this information is unknown, it is believed that is much easier to remove sulfur and nitrogen once the aromatic rings have been reduced via hydrogenation [2]. Selective hydrogenation could shed light on novel upgrading in hydrotreating.

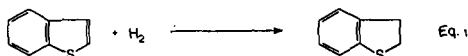
A way to go is the use of transition metal complexes, because they may be characterized by spectroscopic techniques that are much easier to comprehend and handle [2]. Several late transition metal complexes are known to catalyze the regioselective homogeneous hydrogenation of BT and that of Q, and the mechanisms of such reactions have been investigated in detail [3, 4]. Nevertheless, separation problems commonly encountered in homogeneous processes make this approach unattractive for application in petroleum-derived fuels [5,6]. To overcome this problem, the selective hydrogenation step could be done using liquid biphasic catalysis [7]. In this case, the catalytic active species is immobilized in one of the two liquid phases (e.g., water), with the reactants and products maintained in the other (Naphtha); thus allowing a continuous flow process design and better understanding of the different steps involved [8].

2. EXPERIMENTAL:

All manipulations were carried out using standard Schlenk technique, under dry argon or nitrogen. Solvents were purified by conventional procedures. Catalytic runs were performed in an autoclave (PARR, 300 ml, SS-316) with internal stirring and temperature controller. The hydrogenation conditions were 130°C, 69 bar, 613 rpm, S/C, 50:1. Products were analyzed via GC and GC-MS against authentic samples, when available. TPPMS was prepared following published procedure [9].

3. RESULTS AND DISCUSSION:

3.1 Hydrogenation of BT



When a water solution of ruthenium trichloride hydrated and excess TPPMS was placed in a reactor together with a decaline solution of BT, under hydrogenation reaction conditions, the catalytic transformation of BT to DHBT was observed soon after the first hour of reaction (Eq. 1). Two experiments were carried out to establish the responsibility of ruthenium in the catalysis:

- (i) Addition of elemental mercury to the reaction mixture did not affect the catalysis [10].
- (ii) A thermally decomposed aqueous solution containing RuCl_3 and TPPMS yielded a Ru metal suspension which was found to be inactive toward BT hydrogenation under the same reaction conditions.

The initial turnover rate for the conversion of BT to DHBT was $2.9 \text{ mol (mol Ru)}^{-1}\text{h}^{-1}$. For comparison, the homogeneous hydrogenation of BT using $\text{RuCl}_2(\text{PPh}_3)_3$ and $\text{RuHCl}(\text{CO})(\text{PPh}_3)_3$ as the catalyst precursors proceeded with initial turnover frequencies of 6.1 and $2.2 \text{ mol (mol Ru)}^{-1}\text{h}^{-1}$, respectively, under more stringent conditions (170°C, 110 bar H_2) [3a].

As expected for a reaction at an interface, the stirring rate has a strong influence on the rate of hydrogenation, which went from 30% conversion to 70% conversion, after 18 h, on going from 200 rpm to 600 rpm under the conditions described above [11]. The catalytic solutions were recycled up to four times under strictly anaerobic conditions and used to hydrogenate fresh BT in decaline, without any apparent loss of activity. In contrast, a solution exposed to air after the first hydrogenation run was completely inactive for further hydrogenation.

When the biphasic hydrogenation of BT is carried out in the presence of a nitrogen base (1:1 molar ratio with respect to TPPMS), the initial turnover rate is enhanced. Fig. 1 shows typical reaction profiles in the presence of bases such as quinoline (Q) and aniline (An) in comparison with a non base promoted (NB) reaction. From the linear part of the curves, maximum turnover frequencies can be estimated at 10.2 and $10.4 \text{ mol (mol Ru)}^{-1}\text{h}^{-1}$ for Q and An, respectively. The basicity of aniline (pK_b 9.3) resembles that of Q (pK_b 9.1). This may be a good reason for the apparent behavior. However, Q plays also a role as phase transfer and emulsion stabilization agent.

Other nitrogen bases such as acridine (Ac, pK_b 8.4), piperidine (Pp, pK_b 2.9) and triethylamine (Tea, pK_b 2.9) can also enhance the rates of BT hydrogenation to the various degrees presented in Fig. 2. The base neutralizes the HCl that is formed in the heterolytic cleavage of H_2 during formation of the catalyst precursor [3e].

3.2 Hydrogenation of Q



Quinoline acts as a co-catalyst in the hydrogenation of BT and it is also hydrogenated to THQ (Eq. 2). Under the same reaction conditions, the hydrogenation of Q is faster than that of BT. The initial turnover rate for this reaction was 78 mol (mol Ru)⁻¹h⁻¹, compared with 2.9 mol (mol Ru)⁻¹h⁻¹ for BT (27 times less active). Organic bases do not influence the initial rate. However, increasing hydrogen pressure has a positive influence in the hydrogenation. In fact, most of the studies on the biphasic hydrogenation of Q were carried out at 35 bars in order to determine more accurately the initial turnover rate (35 mol (mol Ru)⁻¹h⁻¹).

3.3 Catalytic species in aqueous solutions

In the absence of the base, RuCl₃·3H₂O reacts with excess TPPMS in water or methanol to yield [RuCl₂(TPPMS)₂]₂, which in turn reacts with hydrogen to produce the hydride [RuHCl(TPPMS)₂]₂. The latter complex is broken, for instance by cinnamaldehyde leading to an active catalyst for the regioselective hydrogenation of the carbonyl (C=O) bond of CA [12]. In agreement with this, the major Ru-containing products isolated from the aqueous phases after BT hydrogenation in presence of Q or An were characterized by ¹H and ³¹P{¹H} NMR spectroscopy as the complexes RuHCl(TPPMS)₂L₂ (L = THQ, 1 and An, 2).

Complexes 1 and 2 were independently synthesized by reaction of [RuHCl(TPPMS)₂]₂ with an excess of THQ or An in water, and characterized by NMR and FAB/MS [13].

A fresh sample of 1 was used in the hydrogenation of Q (35 bars, 135°C, 3 h) given the profile observed in Fig. 4 (P1). The water solution was carefully worked up under anaerobic conditions and the brown solid obtained was characterized by NMR, after the catalysis (signals were identical to the fresh catalyst). The complex was redissolved in water and reused in the catalysis of a fresh decaline solution of Q, given the profile P2. This work is a clear indication of the recycle capacity of the complex; which must have a structural relationship with the catalytic active species formed when ruthenium halide reacts with excess TPPMS in the presence of an organic base.

Since both complexes 1 and 2 are coordinately saturated, they are probably not the ones directly involved in the catalysis, but a stabilized form of the actual catalyst, which could conceivably be the corresponding 16-electron species "RuHCl(TPPMS)₂L". Further mechanistic studies are in progress and will be reported elsewhere.

4. CONCLUSIONS:

The regioselective hydrogenation of BT and Q was achieved using a biphasic (water/decaline) catalytic system comprised by ruthenium trichloride and excess *meta*-sulfonatophenyldiphenylphosphine (TPPMS). The hydrogenation of BT is influenced by the addition of organic nitrogen bases as co-catalysts; the order of hydrogenation being: An ≈ Q > Ac > THQ > Pp > Tea. Species of the type HRuCl(TPPMS)₂L₂ (L = An, THQ) have been isolated from the aqueous solutions after the hydrogenation. These species were also obtained using preparative procedures and characterized by NMR and FAB/MS. The tensoactivity of the TPPMS ligand and the phase transfer character of the base are important in the transformation of BT under biphasic conditions. Novel upgrading process of petroleum fuel is the main quest of the work presented.

REFERENCES:

- [1] (a) C. J. Thompson, in: *Organic Sulfur Chemistry*, Eds. R. Kh. Friedlina, A. E. Skovora, p201 (Pergamon, New York, 1981); (b) B. C. Gates, J. R. Katzer and G. C. A. Schuit, *Chemistry of Catalytic Processes* (McGraw-Hill, New York, 1979); (c) A. N. Startsev, *Catal. Rev. -Sci. Eng.*, 37 (1995) 353; (d) P. T. Vasudevan and J. L. G. Fierro, *Catal. Rev. -Sci. Eng.*, 38 (1996) 161; (e) H. Topsøe; B. S. Clausen and F. E. Masoth, *Hydrotreating Catalysis-Science and Technology*, in: *Catalysis, Science and Technology*, Ed. M. Boudart, Vol. 11 (Springer-Verlag, Berlin, 1996).

- [2] (a) R. J. Angelici, *Acc. Chem. Res.*, 21(1988) 387; (b) R. J. Angelici, *Coord. Chem. Rev.*, 105(1990) 61; (c) R. A. Sánchez-Delgado, *J. Mol. Catal.*, 86 (1994) 287; (d) R. J. Angelici, *Bull. Soc. Chim. Belg.*, 104 (1995) 265; (e) T. B. Rauchfuss, *Prog. Inorg. Chem.*, 39 (1991) 259; (f) C. Bianchini and A. Meli, in: *Applied Homogeneous Catalysis with transition metal Compounds*, Eds. B. Cornils and W. A. Herrmann, Vol. 2, p 969 (VCH, Weinheim, 1996); (g) Bianchini, C.; Herrera, V.; Jimenez, M. V.; Meli, A.; Sánchez-Delgado, R. and Vizza, F.; *J. Am. Chem. Soc.*, 117 (1995) 8567; (h) Bianchini, C. and Meli, A., *J. Chem. Soc., Dalton Trans.*, (1996) 801.
- [3] (a) R. A. Sánchez-Delgado and E. Gonzalez, *Polyhedron*, 8 (1989) 1431; (b) R. A. Sánchez-Delgado, V. Herrera, L. Rincón, A. Andriollo and G. Martín, *Organometallics*, 13 (1994) 553; (c) V. Herrera, A. Fuentes, M. Rosales, R. A. Sánchez-Delgado, C. Bianchini, A. Meli and F. Vizza, *Organometallics* (in press).
- [4] (a) R. H. Fish, J. L. Tan and A. D. Thormodsen, *J. Org. Chem.*, 49 (1984) 4500; (b) R. H. Fish, J. L. Tan and A. D. Thormodsen, *Organometallics*, 4 (1985) 1743; (c) R. H. Fish, E. Buralat and S. J. Smith, *organometallics*, 4 (1991) 54; (d) E. Baralt, S. J. Smith, I. Hurwitz, I. T. Horváth and R. H. Fish, *J. Am. Chem. Soc.*, 104 (1992) 5187; (e) R. H. Fish, in *Aspects of Homogeneous Catalysis*, R. Ugo (Ed.), Vol. 7, P 65 (Kluwer; Dordrecht, 1990).
- [5] G. W. Parshall and S. D. Ittel, *Homogeneous Catalysis* (John Wiley & Sons, New York, 1992).
- [6] B. Cornils and W. A. Herrmann, in: *Applied Homogeneous Catalysis with Transition Metal Complexes*, eds. B. Cornils and W. A. Herrmann, Vol. 2, p 576 (VCH, Weinheim, 1996).
- [7] Y. Dror and J. Manasen, *J. Mol. Catal.*, 2 (1977) 219.
- [8] (a) D. E. Pérez, A. Andriollo, R. A. Sánchez-Delgado, N. Valencia, F. López-Linares and R. Galiasso, *U. S. Pat. Appl.* 08/657.960 (June 4, 1996); (b) Bianchini, C.; Meli, A.; Patinec, V.; Serna, V. and Vizza, F.; *J. Am. Chem. Soc.*, 119 (1997) 4945.
- [9] S. Ahrland, J. Chatt, N. R. Davies, and A. A. Williams, *J. Chem. Soc.*, 88 (1958), 276.
- [10] (a) Lin, Y. and Finke, R. G., *Inorg. Chem.*, 33 (1994) 4891; (b) R. Crabtree and D. R. Anton, *Organometallics*, 2 (1983) 855.
- [11] D. E. Pérez, A. Andriollo, J. Carrasquel, J. Mariño, F. A. López-Linares, I. Rojas and N. Valencia, *J. Mol. Catal.*, 116 (1997) 157.
- [12] R. A. Sánchez-Delgado, M. Medina, F. López-Linares and A. Fuentes, *J. Mol. Catal. A: Chem.*, 116 (1997) 167.
- [13] Data for complex 1: ^1H NMR (CD_3OD), THQ: 5.62 (t, $J = 5.7$ Hz, H_2), 4.38 (t, $J = 6.6$ Hz, H_3), 5.14 (t, $J = 5.7$ Hz, H_4), 8.30 (s, H_5), 8.33 (s, H_6), 8.51 (s, H_7), 8.55 (s, $\text{H}_{8,9}$), -10.30 (t, $J_{\text{H-P}} = 36$ Hz, Ru-H), 8.11 - 7.10 (M, ppm). $^{31}\text{P}\{^1\text{H}\}$ NMR system δ_A 60.38; δ_M 57.57 ($J_{\text{P-P}} = 35$ Hz). Data for complex 2: ^1H NMR (CD_3OD), 8.37 (m, aniline), 5.43 (t, $J = 6$ Hz, NH_2), -10.18 (t, $J_{\text{H-P}} = 37$ Hz, Ru-H), 8.11-7.10 (m, TPPMS). $^{31}\text{P}\{^1\text{H}\}$ NMR: 57.9 (s). FAB-MS (m-nitrobenzyl alcohol) (Z/e): 1122 $[\text{RuHCl}(\text{TPPMS})_2(\text{An})] + \text{H}$; 996 $[\text{RuHCl}(\text{TPPMS})_2(\text{An})] + \text{H}$; 941 $[\text{RuHCl}(\text{TPPMS})_2] + \text{H}$; 902 $[\text{Ru}(\text{TPPMS})_2] + \text{H}$; 880 $[\text{Ru}(\text{TPPMS})_2\text{Na}] + \text{H}$; 400 $[\text{TPPMS-Na } 2\text{H}_2\text{O}]$.

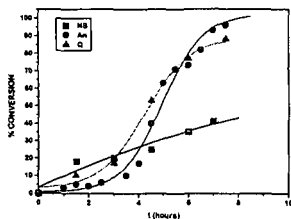


Fig. 1 Profile for the biphasic hydrogenation of BT. NB, No base added, An, aniline and Q, quinoline.

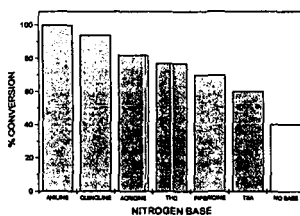
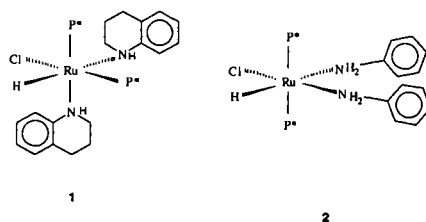


Fig. 2 Influence of basicity in the biphasic hydrogenation of BT with RuCl_3 and TPPMS.



$P^* = \text{TPPMS} = (\text{C}_6\text{H}_5)_2\text{P}(m\text{-C}_6\text{H}_4\text{SC}_3\text{Na})$

Fig. 3. Structures of aqueous organometallic species characterized during the reaction of RuCl_3 , excess TPPMS and THQ or An.

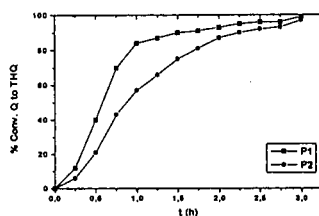


Fig. 4. Profiles for the biphasic hydrogenation of Q using the same catalyst, but two fresh solutions of Q in decaline.

OVERVIEW OF HYDROGEN STORAGE TECHNOLOGIES

Brian D. James

Directed Technologies, Inc., 4001 North Fairfax Drive Suite 775, Arlington VA, 22203

Hydrogen is becoming increasingly acknowledged as the energy carrier of choice for the twenty first century. Clean and inexhaustible, substitution of hydrogen for petroleum for use as an automotive fuel would largely eliminate smog in inner cities and health concerns related to air born particulates, and would reduce dependence on foreign oil reserves. Coupled with the high efficiency of Proton Exchange Membrane (PEM) fuel cells as an automotive power plant, simultaneous significant increases in vehicle fuel economy can be made. Indeed, the recent flurry of strategic alliances in the automotive fuel cell world (Ford/Daimler-Benz/Ballard/dbb, General Motors/Toyota) attests to the seriousness with which the automotive industry views fuel cell propulsion, and since fuel cells fundamentally depend on hydrogen fuel, attests to the increasing importance and prominence of hydrogen production, storage, and distribution for the future.

Clearly the hydrogen star is rising. What is less certain is whether the hydrogen bulk supplier community will be able to accommodate the increased consumer demand for hydrogen in the near, mid and far term time frames. The use of liquid hydrocarbons (gasoline, methanol, DME) in onboard reformer fuel cell vehicles is under active development as an interim step to a full hydrogen economy. Such onboard chemical reformation plants capable of converting widely available fuels (gasoline) into a hydrogen rich reformat stream for use by the fuel cell have the major advantage of not requiring major fuel infrastructure alternations. However, creating a load following, highly efficient, compact, low cost reformer is technically challenging and necessarily compromises vehicle system performance compared to a pure hydrogen system. For this reason, onboard hydrocarbon reformation is viewed as an interim link between today's gasoline internal combustion engine automobiles and tomorrows pure hydrogen fuel cell vehicles.

Whether for vehicular onboard storage or stationary bulk storage, the storage of hydrogen has been problematic due to hydrogen's low volumetric density and resulting high cost. This presentation will outline current hydrogen storage techniques for both vehicular and stationary storage and will discuss future hydrogen research trends.

The following methods of hydrogen storage are of interest:

- Liquid hydrogen (LH2)- Liquid hydrogen storage is currently the bulk hydrogen storage medium of choice and has a very impressive safety record. The hydrogen is typically liquefied at the production site in large quantities (10-30 tons per day) and then trucked cross-country in 11,000 gal LH2 tankers with no boil-off losses. Unfortunately, the energy requirements of liquefaction are high, typically 30% of the hydrogen's heating value, leading to relatively high hydrogen cost as compared to gaseous hydrogen. LH2 will likely remain the main technique of bulk, stationary hydrogen storage for the foreseeable future.

Vehicular LH2 systems have the highest H2 mass fractions and one of the lowest system volumes, along with near zero development risk, good fast fill capability, and acceptable safety characteristics. They would appear to be an excellent choice except for two adverse factors: dormancy and infrastructure impact. Dormancy concerns arise due to boil-off losses that will inevitably concern the average car owner, although daily use or proper planning for route or fleet applications can remove most if not all dormancy concerns. Infrastructure impacts are three fold: first, the liquefaction process is costly, second, small scale LH2 production is impractical, and third, low volume distribution/dispensing of LH2 is expensive. Consequently, LH2 systems will not easily support a transition from anemic start-up to a robust H2 economy. Overall, LH2 storage is a most appropriate for a mature H2 economy where the inherent difficulties (and high cost) of large scale remote LH2 production and very small scale LH2 dispensing are least encountered.

- Compressed Gaseous Hydrogen (GH2)- Vehicular compressed hydrogen systems consisting of 34.5 MPa (5,000 psi) gaseous hydrogen in metal or plastic lined, carbon fiber wound pressure vessels offer simplicity of design and use, high H2 fraction,

rapid refueling capability, excellent dormancy characteristics, minimal infrastructure impact, high safety due to the inherent strength of the pressure vessel, and little to no development risk. The disadvantages are system volume and use of high pressure. Integrating the moderate-to-large system volume will clearly challenge the automotive designer, but such a tank volume can be packaged into a "clean sheet" vehicle. In our opinion, the many advantageous features of compressed gas storage outweigh its larger volume. Compressed gas storage is supportable by small-scale H₂ production facilities (on-site natural gas reforming plants, partial oxidation burners, and electrolysis stations) as well larger scale LH₂ production facilities. Thus a plausible H₂ infrastructure transition pathway exists. For these reasons, room temperature compressed gas storage is viewed as the most appropriate fuel storage system for PEM fuel cell vehicles.

For stationary hydrogen storage, GH₂ also offers the advantages of simplicity and stable storage (no boil-off losses) but at a considerably greater volume than LH₂. Even accounting for compression costs, high pressure gaseous hydrogen is cheaper than LH₂. However, except of pipeline transmission, GH₂ lacks the bulk transportability of LH₂. Consequently, GH₂ will mostly be employed for storage of limited hydrogen quantities, for long term storage, or when the cost of liquefaction is prohibitive. Remaining issues for GH₂ include its safety perception, and the current high cost of the pressure vessels and hydrogen compressors.

- **Metal Hydrides-** Metal hydrides can be subdivided into two categories: low dissociation temperature hydrides and high dissociation temperature hydrides. The low temperature hydrides suffer from low H₂ fraction (~2%). The high temperature hydrides require a heat source to generate the high temperature of dissociation (~300°C). Both systems offer fairly dense H₂ storage and good safety characteristics. Indeed it is the bad characteristics of dissociation (high temperature, high energy input) that create the good safety characteristics (no or slow H₂ release in a crash). Overall for vehicular hydrogen storage, metal hydrides are either very much too heavy or their operating requirements are poorly matched to PEM vehicle systems. Without a dramatic breakthrough achieving high weight fraction, low temperature, low dissociation energy, and fast charge time, metal hydrides will not be an effective storage medium for PEM fuel cell vehicles. For stationary storage, the high weight of metal hydride system is not an adverse factor. Consequently, their attributes of high volumetric storage density and stability make them quite attractive. Improving resistance to gaseous contaminants and increasing system cycle life remain as obstacles to overcome.
- **Carbon Adsorption-** Gaseous hydrogen can be adsorbed onto the surface of carbon to attain storage volumetric densities greater than liquid hydrogen. Adhesion capacity is greatly increased by low temperature (particularly cryogenic temperatures) and by high pressure. Indeed significant fractions of the hydrogen contained in carbon adsorbent systems is actually held in gaseous form within the interstitial volume of the carbon adsorbent. Carbon nanofibers are a special type of carbon adsorbent systems which may exploit a fundamentally different mechanism of hydrogen storage and thereby achieve dramatically improved storage capability. However, development and evaluation of nanofibers is at an early stage of development and system characterization is speculative.
- **Microspheres-** Microsphere hydrogen storage systems consists of hollow glass spheres that are "charged" with hydrogen (300°C-500°C, 27-62 MPa for an hour), and discharged by heating (200°C-250°C) and reducing pressure. The microspheres can be pumped or poured from one tank to another, making them viable for vehicular hydrogen storage. Overall, system characterization is immature. Microsphere shelf life remains a concern.

In summary, multiple techniques of hydrogen storage are viable for both vehicular storage and bulk stationary storage. However, no one storage mechanism is ideal. As demand for hydrogen grows, industry must respond by supplying (and storing) hydrogen in ways suitable for the new class of consumers and must educate the public in its safe use.

ANALYTICAL AND EXPERIMENTAL EVALUATION OF PRESSURE VESSELS FOR CRYOGENIC HYDROGEN STORAGE

S. M. Aceves and G.D. Berry
Lawrence Livermore National Laboratory
7000 East Ave., L-641
Livermore, CA 94551, USA
saceves@llnl.gov

ABSTRACT

Insulated pressure vessels are cryogenic-capable pressure vessels that can be fueled with liquid hydrogen (LH_2) or ambient-temperature compressed hydrogen (CH_2). Insulated pressure vessels offer the advantages of liquid hydrogen tanks (low weight and volume), with reduced disadvantages (lower energy requirement for hydrogen liquefaction and reduced evaporative losses).

This paper shows an evaluation of the applicability of the insulated pressure vessels for light-duty vehicles. The paper shows an evaluation of evaporative losses and insulation requirements and a description of the current analysis and experimental plans for testing insulated pressure vessels. The results show significant advantages to the use of insulated pressure vessels for light-duty vehicles.

INTRODUCTION

Probably the most significant hurdle for hydrogen vehicles is storing sufficient hydrogen onboard. Hydrogen storage choices can determine the refueling time, cost, and infrastructure requirements, as well as indirectly influence energy efficiency, vehicle fuel economy, performance, and utility. There are at least three viable technologies for storing hydrogen fuel on cars. These are: compressed hydrogen gas (CH_2), metal hydride adsorption, and cryogenic liquid hydrogen (LH_2), but each has significant disadvantages.

Storage of 5 kg of hydrogen (equivalent to 19 liters; 5 gallons of gasoline) is considered necessary for a general-purpose vehicle, since it provides a 320 km (200 mile) range in a 17 km/liter (40 mpg) conventional car; or a 640 km (400 mile) range in a 34 km/liter (80 mpg) hybrid vehicle or fuel cell vehicle. Storing this hydrogen as CH_2 requires a volume so big that it is difficult to package in light-duty vehicles (Pentastar Electronics 1997), and it certainly cannot be used in freight trucks. The external volume for a pressure vessel storing 5 kg of hydrogen at 24.8 MPa (3600 psi) is 320 liters (85 gal). Hydrides are heavy (300 kg for 5 kg of hydrogen [Michel 1996]), resulting in a substantial reduction in vehicle fuel economy and performance.

Low-pressure LH_2 storage is light and compact, and has received significant attention due to its advantages for packaging (Braess 1996). Significant recent developments have resulted in improved safety (Pehr 1996) and fueling infrastructure (Hettinger 1996). Disadvantages of low-pressure LH_2 storage are: the substantial amount of electricity required for liquefying the hydrogen (Peschka 1992); the evaporation losses that occur during fueling low-pressure LH_2 tanks (Wetzel 1996); and the evaporation losses that occur during long periods of inactivity, due to heat transfer from the environment.

An alternative is to store hydrogen in an insulated pressure vessel that has the capacity to operate at LH_2 temperature (20 K), and at high pressure (24.8 MPa; 3600 psi). This vessel has the flexibility of accepting LH_2 or CH_2 as a fuel. Filling the vessel with ambient-temperature CH_2 reduces the amount of hydrogen stored (and therefore the vehicle range) to about a third of its value with LH_2 .

The fueling flexibility of the insulated pressure vessels results in significant advantages. Insulated pressure vessels have similar or better packaging characteristics than a liquid hydrogen tank (low weight and volume), with reduced energy consumption for liquefaction. Energy requirements for hydrogen liquefaction are lower than for liquid hydrogen tanks because a car with an insulated pressure vessel can use, but does not require, cryogenic hydrogen fuel. A hybrid or fuel cell vehicle (34 km/l, 80 mpg) could be refueled with ambient-temperature CH_2 at 24.8 MPa (3600 psi) and still achieve a 200 km range, suitable for the majority of trips. The additional energy, costs, and technological effort for cryogenic refueling need only be undertaken (and paid for) when the additional range is required for longer trips. With an insulated pressure vessel, vehicles can refuel most of the time with ambient-temperature hydrogen, using less energy, and most likely at lower ultimate cost than LH_2 , but with the capability of having 3 times the range of room temperature storage systems.

Insulated pressure vessels also have much reduced evaporative losses compared to LH_2 tanks. These results are based on a thermodynamic analysis of the vessels, and are the subject of the next section of this paper.

From an engineering and economic perspective, insulated pressure vessels strike a versatile balance between the cost and bulk of ambient-temperature CH_2 storage, and the energy efficiency, thermal insulation and evaporative losses of LH_2 storage.

THERMODYNAMIC ANALYSIS

The first law of thermodynamics written for a pressure vessel is (VanWylen 1978):

$$M \frac{du}{dt} + M_v \frac{d(c_{p,v}T)}{dt} = Q - \left(\frac{p}{\rho} \right) \dot{m} \quad (1)$$

The two terms in the left-hand side of Equation (1) are the rates of change of the internal energies of the hydrogen and the vessel. Heat transfer into the vessel (Q in the equation) is positive and tends to increase the temperature of the vessel. However, the last term in the right hand side of Equation (1) represents a cooling effect on the vessel, when mass is extracted ($\dot{m} > 0$). Considering that the density of hydrogen is very low, this term is often significant. The last term in Equation (1) is commonly known as the flow work, since it is the work that the hydrogen stored in the vessel has to do to push out the hydrogen being extracted.

Equation (1) is solved for a low-pressure LH₂ storage and for the insulated pressure vessel. The equation is solved iteratively with a computer program which includes subroutines for calculating hydrogen properties. The required property values are obtained from McCarty (McCarty 1975). The specific heat of the vessel materials, $c_{p,v}$, is obtained as a function of temperature from correlations given in the literature (Scott 1967).

VESSEL CHARACTERISTICS

This paper considers three vessels, described as follows:

1. A conventional, low-pressure LH₂ tank with a multilayer vacuum superinsulation (MLVSI) and 0.5 MPa maximum operating pressure.
2. An insulated pressure vessel (24.8 MPa maximum operating pressure) with MLVSI fueled with LH₂.
3. An insulated pressure vessel with microsphere insulation (aluminized microspheres within a vacuum) fueled with LH₂.

Vessel properties are listed in Table 1.

RESULTS

Figure 1 shows hydrogen losses during operation. The figure assumes that the vessels are filled to full capacity (5 kg), and then the vehicles are driven a fixed distance every day. The figure shows total cumulative evaporative hydrogen losses out of a full tank as a function of the daily driving distance. The figure includes information for 17 km/l and 34 km/l cars respectively in the lower and upper x-axes. The figure shows that a low-pressure LH₂ tank loses hydrogen even when driven 50 km per day in a 17 km/l car (100 km in a 34 km/l car). Losses from a low-pressure LH₂ tank grow rapidly as the daily driving distance drops. Insulated pressure vessels lose hydrogen only for very short daily driving distances. Even a microsphere-insulated vessel does not lose any hydrogen when driven 10 km/day or more (20 km/day in the 34 km/l car). Since most people drive considerably more than this distance, no losses are expected under normal operating conditions.

Figure 2 shows losses for a parked vehicle. The figure shows cumulative hydrogen losses as a function of the number of days that the vehicle remains idle. The most unfavorable condition is assumed: the vehicles are parked immediately after fueling. The low-pressure LH₂ tank has 2 days of dormancy (2 days without fuel loss) before any hydrogen has to be vented. After this, losses increase quickly, and practically all of the hydrogen is lost after 15 days. This may represent a significant inconvenience to a driver, who may be unable to operate the vehicle after a long period of parking. Insulated pressure vessels have a much longer dormancy (up to 16 days). Total losses for the insulated pressure vessel with MLVSI is only 1 kg after 1 month of parking. In addition to this, insulated pressure vessels retain about a third of their total capacity even when they reach thermal equilibrium with the environment after a very long idle time, due to their high pressure capacity, therefore guaranteeing that the vehicle never runs out of fuel during a long idle period.

EXPERIMENTAL TESTING AND STRESS ANALYSIS OF INSULATED PRESSURE VESSELS

The analysis presented in this paper has assumed that insulated pressure vessels can be built to withstand the thermal stresses introduced when an initially warm vessel is filled with LH₂. It is desirable to use commercially-available aluminum-lined, fiber-wrapped pressure vessels to avoid the cost of custom-made vessels, even though commercially-available pressure vessels are not designed for low-temperature operation. While the applicability of these vessels for LH₂ storage in vehicles has not been demonstrated, an experiment has been carried out (Morris 1986) in which carbon fiber-aluminum and kevlar-aluminum vessels were cycled over a limited number of cycles (17) at LH₂ temperature. The vessels were burst-tested after cycling. The results of the experiment showed that there was no performance loss (no reduction in safety factor) due to cycling. This experiment indicates that it may be possible to use commercially-available fiber-wrapped aluminum vessels for operation at LH₂ temperature and high pressure. However, additional cyclic testing is necessary, because a vehicle requires many more than 17 fueling cycles.

To accomplish the required testing, an experimental setup has been built inside a high-pressure cell. A schematic is shown in Figure 3. The plan consists of running the vessels through 1000 high-pressure cycles and 100 low-temperature cycles. The cycles are alternated, running 10 pressure cycles followed by a temperature cycle, and repeating this sequence 100 times. Liquid nitrogen will be used for low-temperature cycling, and gaseous helium for high-pressure cycling. This test is expected to replicate what would happen to these vessels during operation in a hydrogen-fueled car.

Cyclic testing of the pressure vessels is being complemented with a finite element analysis, which will help to determine the causes of any potential damage to the vessel during low-temperature operation. Finite element analysis is currently under progress. A mesh has been built, and a thermal analysis of the pressure vessel has been conducted. Validation of the finite element analysis will be done by applying strain gages and temperature sensors to the vessel. Cycled vessels will then be analyzed with non-destructive evaluation techniques, and finally they will be burst-tested, to evaluate any reduction in safety factor due to cycling.

Additional work in progress includes the design of an insulation. This is shown in Figure 4, which indicates that an outer jacket will be built around the vessel. This is necessary for keeping a vacuum space, required for obtaining a good thermal insulation with multilayer insulation (MLVSI). As a part of the insulation design, a pressure vessel outgassing experiment is currently being conducted. This is necessary, because an excessive outgassing rate from the pressure vessel material (fiber and epoxy) may result in a loss of vacuum, considerably reducing the performance of the insulation. The insulation design includes access for instrumentation for pressure, temperature, level and strain, as well as safety devices to avoid a catastrophic failure in case the hydrogen leaks into the vacuum space.

The instrumented and insulated vessel will be cycled with liquid hydrogen to test the instrumentation and insulation performance. Testing will be conducted outdoors at a high-explosives facility to avoid the risk of an explosion that may occur as a result of hydrogen venting.

CONCLUSIONS

This paper shows that insulated pressure vessels have good packaging characteristics and thermal performance compared to LH₂ tanks, and also a potential for reduced need for liquid hydrogen. For these reasons, they are considered to be a good alternative for hydrogen storage. The most important results can be summarized as follows:

1. Insulated pressure vessels do not lose any hydrogen for daily driving distances of more than 10 km/day for a 17 km/l energy equivalent fuel economy. Since almost all cars are driven for longer distances, most cars would never lose any hydrogen.
2. Losses during long periods of parking are small. Due to their high pressure capacity, these vessels retain about a third of its full charge even after a very long period of inactivity, so that the owner would not risk running out of fuel.
3. Previous testing has determined the potential of low-temperature operation of commercially-available aluminum-lined wrapped vessels for a limited number of cycles. Further testing will extend the number of cycles to the values required for a light-duty vehicle. Additional analysis and testing will help in determining the safety and applicability of insulated pressure vessels for hydrogen storage in light-duty vehicles.

NOMENCLATURE

| | |
|-----------|--|
| $c_{p,v}$ | specific heat of the vessel enclosed within the insulation |
| \dot{m} | mass flow rate of hydrogen extracted from the vessel |
| M | total mass of hydrogen stored in the vessel |
| M_v | mass of the vessel enclosed within the insulation |
| p | pressure |
| Q | heat transfer rate from the environment into the vessel |
| t | time |
| T | temperature |
| u | specific internal energy of hydrogen |
| ρ | density of the hydrogen leaving the vessel |

ACKNOWLEDGMENTS

Work performed under the auspices of the U.S. Department of Energy by Lawrence Livermore National Laboratory under Contract W-7405-ENG-48.

REFERENCES

- Braess, H.H., and Strobl, W., 1996, "Hydrogen as a Fuel for Road Transport of the Future: Possibilities and Prerequisites," Proceedings of the 11th World Hydrogen Energy Conference, Stuttgart, Germany.
- Hettinger, W. Michel, F., Ott, P., and Theissen, F., 1996, "Refueling Equipment for Liquid Hydrogen Vehicles," Proceedings of the 11th World Hydrogen Energy Conference, Stuttgart, Germany, pp. 1135-1143.

McCarty, R.D., 1975, "Hydrogen: Its Technology and Implications, Hydrogen Properties, Volume III," CRC Press, Cleveland, Ohio.

Michel, F., Fieseler, H., Meyer, G., and Theissen, F., 1996, "Onboard Equipment for Liquid Hydrogen Vehicles," Proceedings of the 11th World Hydrogen Energy Conference, Stuttgart, Germany, pp. 1063-1077.

Morris, E.E., Segimoto, M., and Lynn, V., 1986, "Lighter Weight Fiber/Metal Pressure Vessels Using Carbon Overwrap," AIAA-86-1504, Proceedings of the AIAA/ASME/SAE/ASEE 22nd Joint Propulsion Conference, June 16-18, Huntsville, Alabama.

Pehr, K., 1996, "Experimental Examinations on the Worst Case Behavior of LH₂/LNG Tanks for Passenger Cars," Proceedings of the 11th World Hydrogen Energy Conference, Stuttgart, Germany.

Pentastar Electronics, 1997, "Direct-Hydrogen-Fueled Proton-Exchange-Membrane Fuel Cell System for Transportation Applications, Conceptual Design Report," Report DOE/CE/50390-9, prepared for U.S. Department of Energy, Office of Transportation Technologies, under contract DE-AC02-94CE50390.

Peschka, W., 1992, "Liquid Hydrogen, Fuel of the Future," Springer-Verlag, Vienna, Austria.

Scott, R.B., 1967, "Cryogenic Engineering," D. Van Nostrand Company, Inc. Princeton, NJ.

Van Wylen, G.J., and Sonntag, R.E., 1978, "Fundamentals of Classical Thermodynamics," John Wiley and Sons, New York, NY.

Wetzel, F.J., 1996, "Handling of Liquid Hydrogen at Filling Stations," Proceedings of the 11th World Hydrogen Energy Conference, Stuttgart, Germany, pp. 1123-1134.

Table I. Characteristics of the Hydrogen Vessels Being Analyzed.

| | liquid Tank 1 | insulated pressure vessels | |
|--|--------------------|----------------------------|-------------|
| | | Vessel 2 | Vessel 3 |
| Mass of hydrogen stored, kg | 5 | 5 | 5 |
| Total weight, kg | 21 | 30 | 30 |
| Internal volume, liters | 85 | 95 | 95 |
| External volume, liters | 112 | 144 | 144 |
| Internal diameter, m | 0.39 | 0.42 | 0.42 |
| Internal surface area, m ² | 0.98 | 1.1 | 1.1 |
| Aluminum mass within insulation, kg | 9 | 10 | 10 |
| Carbon mass within insulation, kg | 0 | 10 | 10 |
| Design pressure, MPa (psi) | 0.5 (70) | 24.8 (3600) | 24.8 (3600) |
| Performance factor ¹ , m (10 ⁶ in) | - | 33000 (1.3) | 33000 (1.3) |
| Safety factor | - | 2.25 | 2.25 |
| Insulating material | MLVSI ² | MLVSI ² | microsphere |
| Thermal conductivity of insulator, W/mK | 0.0001 | 0.0001 | 0.0004 |
| Insulation thickness, m | 0.02 | 0.02 | 0.02 |
| Heat transfer through accessories, W | 0.5 | 0.5 | 0.5 |

¹ defined as burst pressure*volume/weight.

² MLVSI = multilayer vacuum superinsulation

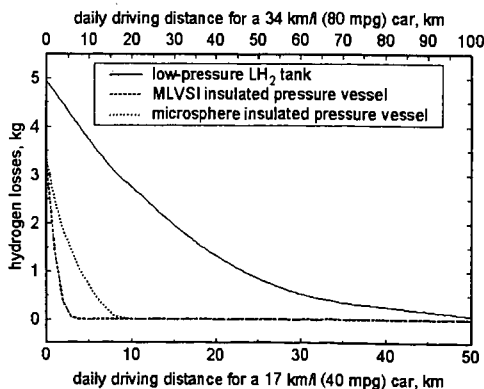


Figure 1. Cumulative hydrogen losses in kg as a function of daily driving distance, for vehicles with 17 km/liter (40 mpg); or 34 km/l (80 mpg) fuel economy, for the three vessels being analyzed in this paper.

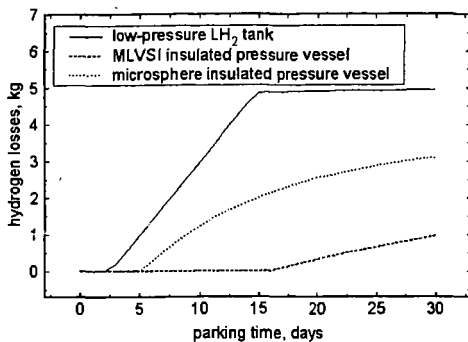


Figure 2. Cumulative hydrogen losses in kg as a function of the number of days that the vehicle remains idle, for the three vessels being analyzed in this paper, assuming that the vessels are initially full.

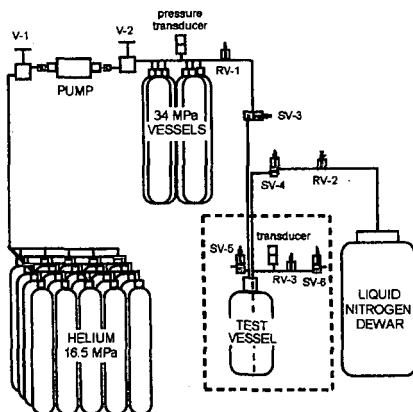


Figure 3. Schematic of the experimental setup for temperature and pressure cycling of a pressure vessel.

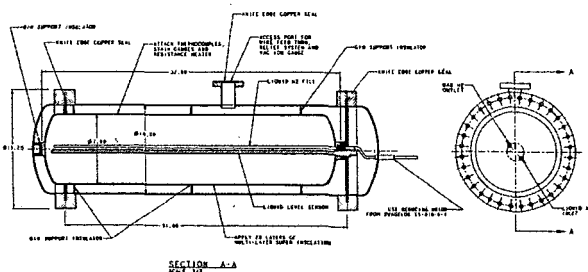


Figure 4. Insulation design for pressure vessel. The figure shows a vacuum space, for obtaining high thermal performance from the multilayer insulation, and instrumentation for pressure, temperature, level and strain.

The Use of Adsorbed Natural Gas Technology for Large Scale Storage.

R.W. Judd, D.T.M. Gladding, R.C. Hodrien, D. R. Bates, J.P. Ingram, M. Allen
BG Technology, Gas Research and Technology Centre, Ashby Road, Loughborough, LE11 3GR, UK

Abstract

Considerable understanding of ANG technology has been gained from work aimed at implementing this method of storage in natural gas vehicles (NGVs). For vehicle applications, maximum gas storage density becomes the ultimate requirement to produce vehicles with an acceptable mileage range. Bulk storage applications require a number of different issues to be addressed relative to vehicle onboard storage, particularly with regard to configuration and physical properties of the adsorbent. A complex compromise of cost versus performance is required which leads to a very different technology configuration than would be expected for vehicles.

1 Introduction

Adsorbed natural gas (ANG) provides a method of storing gas at a substantially higher concentration than can be achieved with simple compression. Although not attaining the density typically found with methods such as LNG, it is potentially much simpler, not requiring the use of refrigeration methods or significant ancillary equipment. Although adsorption on carbon materials developed to date produces its greatest *absolute* enhancement at pressures around 35 bar, higher *relative* gains are obtained in the 3-10 bar range more appropriate to local storage and distribution systems.

Considerable experience of ANG technology has been gained from work on natural gas vehicles (1). For vehicle applications, maximum gas storage density becomes the ultimate requirement, in order to produce vehicles with an acceptable mileage range. To this end, a great deal of research effort has been expended to try and produce active carbons capable of storing up to 190 volumes of gas per volume of storage space (v/v) at pressures of approximately 35 bar. This research has led to the production of some extremely highly engineered carbon materials.

Bulk storage applications require a number of significantly different issues to be addressed in comparison to onboard vehicle storage, particularly configuration, cost and nature of the adsorbent. For bulk storage applications, the viability of the method is critically dependent on the cost of the adsorbing material. Thus although considerable gains can be made in storage capacity by choosing a high performance carbon, the price tends to increase disproportionately to the advantage gained. In addition, high performance carbons tend to have high densities. High density carbons will occupy a smaller volume in the storage vessel; as carbons are priced by weight, there is a proportional rise in cost with increasing density. A compromise in cost/performance is therefore required which leads to a very different choice of carbon for large scale carbon compared to small scale vehicle applications.

This paper will give an overview of work at BG Technology which looks at the feasibility of applying ANG to large scale storage of natural gas

2 The Technical Challenges

Adsorption isotherms in physical chemistry are generally expressed as concentration of adsorbed phase per unit mass of adsorbent. For ANG applications we are concerned with the storage per unit volume. As a result, the density of the adsorbent becomes increasingly important. The storage capacity under these circumstances is usually expressed in terms of volume per volume stored (v/v). This expresses the enhancement in capacity of a particular volume of storage medium relative to an empty container at standard temperature and pressure.

2.1 Carbon development and the adsorption process

Activated carbon is made from cheap natural products such as coconut shells or peach stones. They are subjected to either chemical impregnation followed by heating, or are first pyrolysed to carbon and then subjected to steam treatment. As such they have an extremely high surface area (up to 2500m²/g) and pore sizes as low as 2 nanometres. A typical carbon will be a mixture of small micropores, larger macropores, mesopores from which the gas can escape, and void space. The distribution of these governs the storage capacity of the carbon and is dependent on the preparation

process. The carbon itself can be produced as powder, granules or formed into monoliths or briquettes. Highly activated carbons, and shaped and densified materials have the highest storage capacities, but the increased number of steps required in preparation can push costs per kg very high. Theoretical enhancements of the order of 270 v/v are possible, but practically, the best seen so far are around 150 v/v. Doubling capacity from 75 to 150 v/v at 35 bar can potentially lead to a 20 fold increase in the cost per kg of the carbon. Such monolithic carbons are ideal for vehicle applications where maximum storage capacity is critical and the cost of the carbon is a relatively small part of the overall process. However, as already stated, the excessive cost mitigates against their use for bulk storage. For large scale storage applications, the carbon used is more likely to be in the 80-100 v/v range.

2.2 Deliverability

Any discussion of adsorbed natural gas should make clear that it is not simply the storage capacity of the system which is being considered. *More important is the quantity of gas which can be delivered on desorption.* The storage capacity of an ANG system is always greater than the delivered capacity, usually by around 15%, but sometimes by as much as 30%. The nature of adsorption on microporous systems leads to a large extent of capacity being filled at atmospheric pressure. The amount of gas remaining on the carbon under atmospheric conditions is around 10 times that which would be present in an empty vessel. This gas cannot be discharged from the vessel without reduction in pressure, or displacing it with a more strongly adsorbing gas. The amount of gas which remains in the system is highly dependent on the carbon used. Highly microporous carbons have very steep initial slopes to their uptakes, and therefore retain a larger proportion of the gas on delivery. Careful choice of carbon is necessary to minimize the quantity of retained gas, particularly if use is to be made of ANG in relatively low pressure systems.

2.3 Heat management

The extent of uptake on an adsorbent reduces with increasing temperature, so warming of the system is likely to lead to reduced uptake. Adsorption is of course a process which evolves heat. Due to the highly thermal insulating nature of the carbon material, in a large storage vessel the degree of equilibration of the system with its surroundings is likely to be limited during a typical 8 hour fill. Although filling a completely gas free ANG vessel can produce enough heat to increase temperatures by up to 100°C in a perfectly insulated vessel, it should be borne in mind that in practice this is not the case. At the start of the fill cycle at 0 barg or 1 bara, there is already a layer of adsorbed gas on the carbon, as discussed in the previous section. Adsorption at these initial sites tends to produce the highest heat of adsorption. As anything up to 30% of the total capacity of the bed is present in this non-delivered gas, the total amount of heat released during a typical fill is considerably reduced.

It should also be borne in mind that the total amount of gas stored within a carbon or other adsorbent under pressure is not simply the amount adsorbed in the micropores. This ignores the contribution made by the natural gas in the voids and larger pores where it is stored at the gas phase density of the adopted storage pressure. For a promising carbon, up to 25% of the stored methane can be present as pressurised gas in the voids and therefore contributes no heat of adsorption. Temperature rises of 40-50°C are in fact more likely during a typical fill.

A similar analysis can be used to consider the cooling effect of desorption, where temperatures can drop extensively. The main problem this can cause is in the ease of delivery of the gas at the lowest temperatures, where the rate of desorption will slow.

The experimental programme currently underway indicates that the average carbon temperature is likely to oscillate between -10°C and 40°C, with wall temperatures only varying between 12-25°C. Prevailing environmental conditions during fill and discharge phases are likely to benefit temperature effects during the diurnal phases, as the external temperature is likely to be warmest during delivery of gas when heat is required, and coolest during the fill, when heat is evolved.

2.4 Gas composition

The composition of natural gas varies widely and it always contains gases other than fuel gases, for example, odorant, higher hydrocarbons, CO₂ and N₂. Whereas the adsorption capacity for methane in ANG systems remains constant throughout many adsorption and desorption cycles, such cyclic operation using real natural gas would result in a gradual deterioration of capacity (2,3). This

problems caused by heat transfer during diurnal cycles, and also to issues relating to use of natural gas rather than pure methane. The experimental programme should also allow the tailoring of carbon properties to the requirements of diurnal storage applications, and also allow determination of the ideal internal configuration of the vessel. This latter issue relates particularly to extra methods which may have to be used to cope with problems of heat management.

A development programme was implemented which included parallel experimental work and development of a numerical model.

3.2 The experimental rig

The experimental facility (fig 2) is based around a 500dm³ carbon steel pressure vessel, which has been equipped with 24 positioned thermocouples, internal and external, and 2 internal pressure transducers. The vessel has full bore flanged covers top and bottom and has been designed to allow it to be rotated through 90° to allow measurements to be taken in both upright and horizontal configurations. It is rated up to 40 bar and over a 180°C to -30°C pressure range. Flow into and out of the vessel is controlled using 200dm³/min flow controllers. Temperature, flow and pressure data are continuously logged during experimental runs using a National Instruments 'Labview' based system.

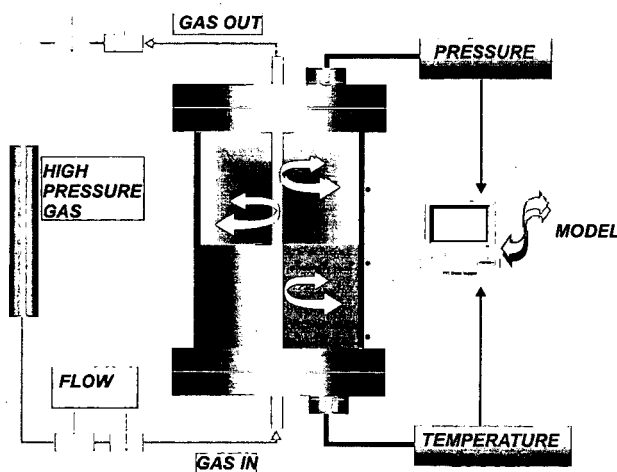


Fig 2. Schematic of experimental rig for cyclic diurnal simulation

3.3 The numerical model

The cylindrical rig has been modelled in its axial and radial dimensions form using a finite difference (explicit scheme) program written in Fortran 90. The model comprises a steel outer shell and a steel inner tube, together with the carbon bed. A single element is assumed to be at equilibrium at a single temperature and the carbon bed pressure is therefore uniform. Conduction is modelled in two dimensions but mass flow (and consequently its associated convective heat transfer) is only allowed in the radial direction. Loading of methane onto the carbon bed, desorption from the bed and the static situation (with no net gain or loss of gas) can be simulated, together with combinations of these phases as is the case in practice. The fit of a simulated run to an experiment involving loading and desorption with a static period in-between is shown in Figure 3.

3.4 Illustrative results

Fig 3 show a subset of data from a simulated diurnal cycle in the 500dm³ vessel, using a commercial carbon material. Only temperature and pressure data are shown here for simplicity. The thermocouples from which these data were obtained were situated in the bulk of the carbon. Close agreement is obtained between experimental and simulated data. Other sets of thermocouples,

deterioration is the result of accumulation of the impurity gases on the adsorbent used because of the preferential adsorption of the heavier hydrocarbon gases.

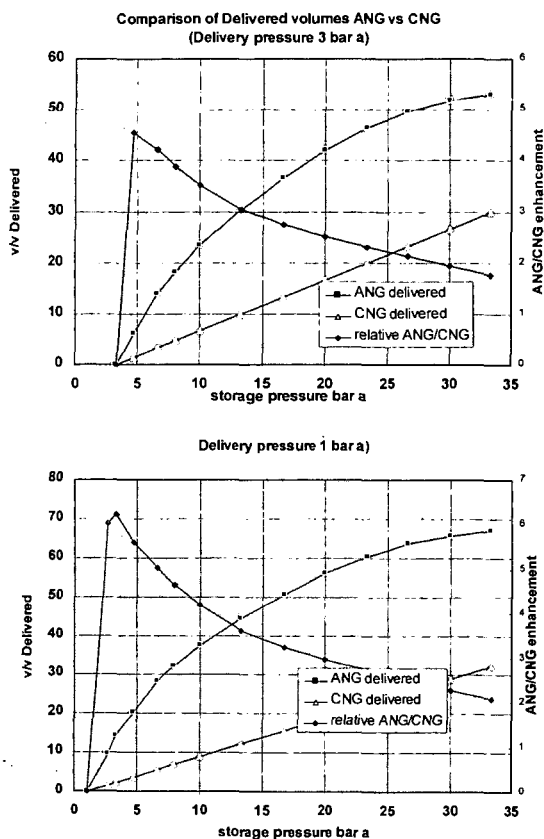


Fig 1. Delivered gas curves for a commercial carbon for different base pressures.

This problem has been addressed in NGV work by the use of some form of preadsorption system to remove the heavier hydrocarbon gases prior to adsorption in the main storage tank. All hydrocarbons adsorb more strongly on carbon than methane, as do the odorants added to natural gas (4,5). One component of natural gas which may require special treatment is water, which although only present at ppm levels in distributed natural gas, tends to adsorb strongly. Experimental work currently under way aims to determine the necessary physical and operating characteristics of a preadsorbing system to protect the main carbon bed.

3 Work in the BG Technology Programme

3.1 Philosophy of work programme

Work is currently underway to estimate the merits of ANG technology for large scale and diurnal storage applications. Techno-economic analyses appeared to indicate that there was a good probability that cost targets for technology use could be met. An experimental programme was initiated to provide predictive data for scale up. These data relate particularly to the extent of any

placed at the vessel core, vessel inner and outer walls and vessel inlet and outlet show corresponding agreement with modelled data. Uptakes of gas were also measured and modelled as a function of time, again with close agreement, but are not illustrated here. The major outcome of this work is the illustration that a real diurnal storage case can be effectively modelled, and current work is extrapolating these data to large scale cases for a variety of practical scenarios.

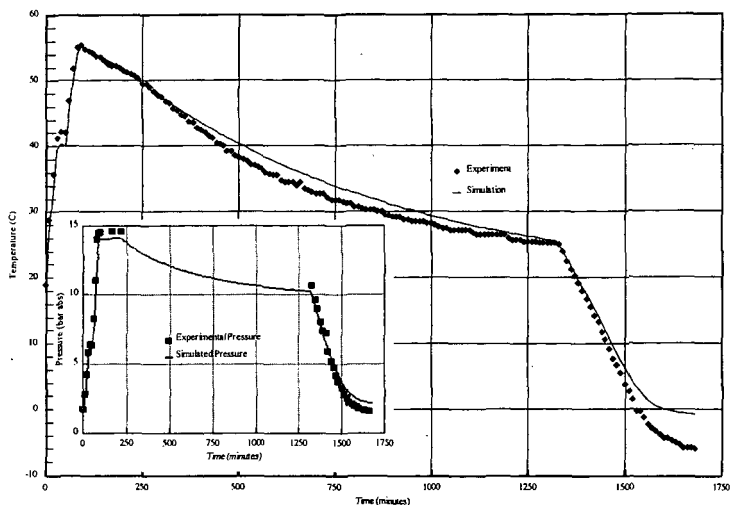


Fig 3. Illustrative data from experimental run and model.

4 Conclusions

The ANG storage method can provide enhancements over pressurisation of the order of 2-10 times depending on storage pressure. Relative gains over pressurisation are greatest at lower pressures, although the absolute amount of gas stored increases with pressure. Delivered rather than stored gas needs to be optimised in order to gain maximum benefit from the technique. The economics of the process depend critically on the choice of carbon adsorbent. Lower density carbons with low cost and high performance are preferred. A compromise between these factors will be required to obtain the most favourable implementation. Adsorbent lifetimes should not be a problem, as long as care is taken to prevent adsorption on the main bed of components which could irreversibly adsorb and degrade performance.

5 References

- 1 C. Komodromos, S. Pearson and A. Grint. The Potential of Adsorbed Natural Gas for Advanced on Board Storage in Natural Gas Fuelled Vehicles. IGRC, Florida, 1992.
- 2 R.W. Judd, C. Komodromos and D.W.J. Jack. Adsorbed Natural Gas: The Potential For Bulk Storage. Internal BG report.
- 3 A. Golvoloy and E.J Blais, SAE Conference Proc., Pittsburgh p 47 (1983).
- 4 A.L Chafee, H.J Loeh, and A.G Pandolfi Methane Adsorption on High Surface Area Carbons. CSIRO, Report FT/IR 031R (1989).
- 5 J.A. Ritter and R.T. Yang, Ind. Eng. Chem. Res. 26 1679 (1987).

6 Acknowledgements

The authors would like to thank BG plc for permission to publish this paper, and also Dr R.E. Critoph of Warwick University for extensive input into the production of the numerical model.

CARBON MOLECULAR SIEVES DERIVED FROM POLYMERS FOR NATURAL GAS STORAGE

C. H. Chang* and A. Stella**, AlliedSignal Inc.
*Des Plaines, IL 60017 & **Morristown, NJ 07962

ABSTRACT

In the last several years, advances have been made in the development of adsorbents for the storage of natural gas. At AlliedSignal, we have focused on the polymer-derived carbon molecular sieves for the control of micropore size, micropore volume, bulk density, and packing efficiency to enhance storage capacity. A deliverable storage efficiency of 150 volumes of methane per volume of adsorbent has been achieved at a storage pressure of 500 psig. This presentation will discuss the synthesis of the materials and the preparation and characterization of the advanced carbon molecular sieves. Structural parameters and storage capacities of these carbon molecular sieves will be compared with other carbonaceous materials. In addition, theoretical studies on determining optimum pore sizes for methane storage and molecular simulations of isotherms and isosteric heats will be presented for comparison with our carbon molecular sieves.

1. INTRODUCTION

Storage of natural gas with an adsorbent has been considered a promising technology for the on-board storage of natural gas for vehicular applications^{1,2}. Among adsorbents investigated, carbon materials are most effective in the storage of natural gas at low pressures (e.g. 300-500 psig)³. Critical issues in the commercialization of the adsorbed natural gas storage technology include the storage capability of the adsorbent and the ease and cost of its manufacture.

The objective of the present study is to develop a high capacity carbon adsorbent which can be commercially produced at a reasonable cost. In the course of the study, molecular modeling and simulation efforts, similar to those reported by Matranga, Stella, Myers and Glandt⁴, were conducted to help in the design and optimization of the pore structure of the carbon adsorbent for the storage of natural gas.

2. EXPERIMENTAL AND RESULTS

2.1 Adsorption Theory and Development of Carbon Molecular Sieves

The adsorbents developed in this study are all variants of activated carbon molecular sieves developed by AlliedSignal Inc. The development involved first understanding the theoretical basis for adsorption followed by experimentation to achieve material properties suggested from the theoretical results.

Molecular modeling and simulation were used in the optimization process for these sorbents. An understanding of the potential energy functions between methane and the carbon surface was applied to pore size control. Calculation of the second virial coefficients for adsorption, B_{1S} , as a function of graphitic carbon slit width, was performed by numerical integration of the gas-solid potential over the pore volume⁵. The maximum second virial coefficient lends insight into the optimal slit width for methane adsorption. Slits that are too large have too small a B_{1S} , due to a lack of cooperative interaction between the adsorbate and both walls of the slit. This means that the attractive forces are too small due to the large dimensional width of the pore. At too small a pore width, the repulsive forces become too large for effective adsorption. The calculation showed an optimal slit pore width of 11.4 Å for methane adsorption.

Using the information from the second virial coefficient study, carbon sorbents were prepared from a proprietary polymer through a multi-step process. The carbon molecular sieve (CMS) materials were synthesized by carbonization of a proprietary polymer followed by activation with a gaseous stream to develop optimal pore structure. *Figure 2* shows a comparison of pore structures for various activated CMS materials.

The slit model and a more complex strip models which includes both structural and chemical heterogeneity were applied in order to investigate isotherms and isosteric heats of adsorption. Grand Canonical Monte Carlo (GCMC) simulations were performed. Isotherms and isosteric heats of adsorption were calculated from the fluctuations in the number of molecules and energy⁶. Figure 3 shows a heterogeneous surface of the strip model reduces the adsorption amount as compared to the homogeneous slit model. Figure 4 shows that the heterogeneous materials have isosteric heats that decrease with the coverage due to occupation of lower energy adsorption sites as coverage increases. The theoretical work shows that homogeneity of the material will enhance adsorption greatly.

2.2 Preparation and Evaluation of Carbon Molecular Sieves

The preparation of the polymer-derived carbon molecular sieves consists of four basic steps: preparation of the polymer precursor, pelletization or shaping of the precursor, carbonization, and activation of the resulting carbon molecular sieve. For the development of a high capacity adsorbent for natural gas storage, all these four process steps are investigated and optimized for volumetric storage efficiency.

2.2.1 Precursor Synthesis: A number of polymeric materials were initially screened for the ability to form microporous carbon structures with proper pore size/ pore distribution and with high carbon yield. Results of this study showed very conclusively that only a small number of polymer candidates are potentially promising. These materials include polyvinylidene chloride (PVDC), polyvinylidene fluoride, polyacrylonitrile, polychlorotrifluoroethylene, and phenolic resins. Copolymers incorporating these monomers are also potentially effective. Among these potential precursor materials, we chose to focus on the PVDC system.

Not only is the chemical nature of the monomer important but also the physical chemical properties of the polymer material. The effects of polymer molecular weight, polymer particle size and size distribution, and the density of the polymer particle were extensively studied. Synthesis method, initiation catalyst and polymerization temperature are all critical in the synthesis of the best precursor⁷.

2.2.2 Pelletization and shaping of the precursor: Parameters that were found to be important for the synthesis of the adsorbent for natural gas storage are pellet configuration, pellet piece density and the uniformity of the void space throughout the pellet. During the pelletization of PVDC precursors, there were no shape additives since this may cause decreases in the volumetric/gravimetric efficiency of the resulting CMS.

2.2.3 Carbonization of the Pellet during Thermal Transformation: The PVDC precursor goes through softening, decomposition, and carbon structure formation at various temperatures. The formation of the pore structure and the density of the resulting adsorbent are critically determined by the temperature program used for the precursor pellet. Of particular importance is the fact that the PVDC precursor loses 50% of its total HCl at about 200°C and the rest of the HCl at about 500°C. The control of the kinetics of HCl evolution determines the pore size of the resulting CMS and the packing density of the adsorbent for natural gas storage.

2.2.4 Activation: The volumetric efficiency of the natural gas adsorbent is optimized by increasing the gravimetric efficiency and maintaining high packing density of the adsorbent through activation. Oxidizers such as carbon dioxide, air, and steam, and their combinations were investigated. The activation process increases the total micropore volume and modifies the pore size and pore distribution. Differences in the activation process are illustrated in Table 1.

2.2.5 Evaluation of the activated CMS: The storage efficiency of the activated carbon molecular sieves was evaluated gravimetrically. The adsorbent material was packed in a 40 mL test cell. The material was heated at 150°C under vacuum (less than 25mTorr) for a period of greater than 2 hours. Methane gas was used throughout the study to simulate the natural gas storage. The methane is introduced to the test cell at 25°C at various

pressures and the amount of methane stored was determined by weight uptake at equilibrium. The total volumetric gas storage delivery was calculated by using the total amount of methane stored per unit volume less the methane volumetric density at the delivery condition of 746 mmHg and 26.3°C, which is 0.000643 g/mL. The V/V value was determined by dividing the total deliverable gas volume with the volume of the empty test cell which was volumetrically calibrated with methane. Results of the storage measurements at 300 psig are summarized in Table 2 for comparisons with other carbon adsorbents.

2.2.6 Improvement of Storage Capacity by Packing: As shown in Table 2, the volumetric efficiency of ACMS for methane storage is affected by the packing density of the absorbent material. A packing technique employing at least two sizes of absorbent particles having nominal diameters differing by at least 7:1 was developed⁸. Table 3 illustrates the improvement of deliverable V/V capacity with a binary packing system.

3. CONCLUSION

Through careful screening and parametric process optimization, a class of activated carbon molecular sieves has been developed for the on-board storage of natural gas. A deliverable volumetric capacity of 150 V/V has been achieved at 500 psig. The commercialization of this class of absorbent depends on the market need. Further studies are required to further improve the efficiency and economics of the adsorbent.

REFERENCES

1. J. Wegrzyn, H. Weismann, and T. Lee, Low Pressure Storage of Natural Gas on Activated Carbon Proceedings: Annual Automotive Tech. Develop, Dearborn, MI (1992).
2. C. R. Nelson, Physical Sciences NGV Gas Storage Research, Gas Research Institute, Chicago, IL (1993).
3. D. F. Quinn, J. A. McDonald, and K. Sosin, 207th ACS National Meeting, San Diego, CA (1994).
4. K. Matranga, A. Stella, A. Myers, and E. Glandt, Sep. Sci. and Tech. (1992) **27**, 1825-1836.
5. A. Stella, "Adsorption on Activated Carbon: Comparison of Molecular Simulation with Experiment", Ph.D. Thesis, University of Pennsylvania, 1993.
6. D. Nicholson, N. G. Parsonage, "Computer Simulation and the Statistical Mechanics of Adsorption", Academic Press, London, 1982.
7. C. H. Chang, and G. J. Seminara, "Preparation of Hydrophobic Carbon Molecular Sieves", U. S. Patent #4,820,681, April 11, 1989.
8. C. H. Chang, "Packing Adsorbent Particles for Storage of Natural Gas", U. S. Patent #5,308,821, May 3, 1994.

Table 1. The Effect of Activation on the Properties of PVDC-derived CMS

| Sample # | Activating gas | Activation condition (°C) | Yield after activation (%) | Packing density (g/mL) | BET surface area (m ² /g) | Micropore volume (mL/g) |
|----------|-----------------|---------------------------|----------------------------|------------------------|--------------------------------------|-------------------------|
| 1 | None | None | 100 | 0.633 | 1484 | 0.45 |
| 2 | Steam | 825 | 65.8 | 0.435 | 1861 | 0.56 |
| 3 | Steam | 850 | 25.0 | 0.240 | 2280 | 1.82 |
| 4 | CO ₂ | 800 | 73.0 | 0.469 | 1864 | 0.56 |
| 5 | CO ₂ | 854 | 21.4 | 0.559 | 2145 | 0.65 |

Table 2. Storage Efficiency of Activated CMS for Methane at 25°C and 300 psig

| Carbon Absorbent | Packing density (g/mL) | Storage temperature (°C) | Gravimetric efficiency (g/g) | Volumetric efficiency (V/V) |
|------------------|------------------------|--------------------------|------------------------------|-----------------------------|
| Norit carbon | 0.387 | 24 | 0.1138 | 69 |
| Calgon PCB | 0.445 | 23 | 0.1095 | 76 |
| Calgon PCB | 0.500 | 27 | 0.0108 | 79 |

-Continued (Table 2)

| | | | | |
|----------------|-------|----|--------|-----|
| Nuchar WV-B | 0.259 | 25 | 0.1142 | 46 |
| Anderson AX-21 | 0.355 | 25 | 0.1569 | 87 |
| Saran carbon | 0.320 | 25 | 0.070 | 51 |
| CMS-1 | 0.633 | 25 | 0.1031 | 112 |
| ACMS-1-1 | 0.545 | 25 | 0.133 | 122 |
| ACMS-1-2 | 0.544 | 25 | 0.1401 | 128 |
| ACMS-1-3 | 0.492 | 25 | 0.1363 | 115 |
| CMS-2 | 1.022 | 25 | 0.1001 | 158 |
| ACMS-2-1 | 0.837 | 25 | 0.1334 | 173 |

Table 3. Storage Efficiency of Activated CMS Systems with Binary Packing

| Adsorbent | 1 | 2 | 3 | 4 |
|--|--------------|--------------------|--------------|--------------------|
| Particles | 2.3mm pellet | 2.3mm pellet/beads | 1.6mm pellet | 1.6mm pellet/beads |
| Test cell (mL) | 39.89 | 39.89 | 39.60 | 39.60 |
| Pellet wt.(g) | 21.08 | 21.02 | 21.41 | 21.44 |
| Beads wt.(g) | - | 5.74 | - | 5.43 |
| Total dry wt (g) | 20.72 | 26.23 | 21.05 | 26.33 |
| Packing density (g/mL) | 0.519 | 0.658 | 0.532 | 0.665 |
| CH ₄ adsorbed (g/g) @ 0psig | 0.65 | 0.77 | 0.61 | 0.79 |
| 100 | 2.12 | 2.64 | 2.14 | 2.62 |
| 200 | 2.78 | 3.43 | 2.82 | 3.38 |
| 300 | 3.28 | 3.89 | 3.29 | 3.88 |
| 400 | 3.61 | 4.22 | 3.63 | 4.24 |
| 500 | 3.88 | 4.54 | 3.89 | 4.56 |
| 600 | 4.12 | 4.79 | 4.13 | 4.80 |
| 700 | 4.32 | 4.95 | 4.37 | 4.99 |
| 800 | 4.51 | 5.16 | 4.53 | 5.16 |
| 900 | 4.68 | 5.32 | 4.70 | 5.32 |
| Deliverable V/V @ 0 psig | 0 | 0 | 0 | 0 |
| 100 | 57.33 | 72.92 | 60.11 | 71.89 |
| 200 | 83.06 | 103.73 | 86.82 | 101.75 |
| 300 | 102.56 | 121.67 | 105.28 | 121.39 |
| 400 | 115.43 | 134.54 | 118.64 | 135.53 |
| 500 | 125.96 | 147.02 | 128.28 | 148.10 |
| 600 | 135.32 | 156.77 | 138.28 | 157.53 |
| 700 | 143.12 | 163.01 | 147.71 | 164.99 |
| 800 | 150.53 | 171.20 | 153.99 | 171.69 |
| 900 | 157.16 | 177.44 | 160.67 | 177.96 |

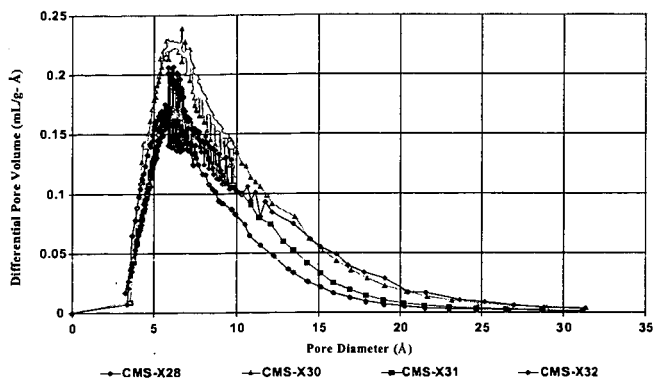


Figure 2 Horvath-Kawazoe Plot for pore structure of CMS materials

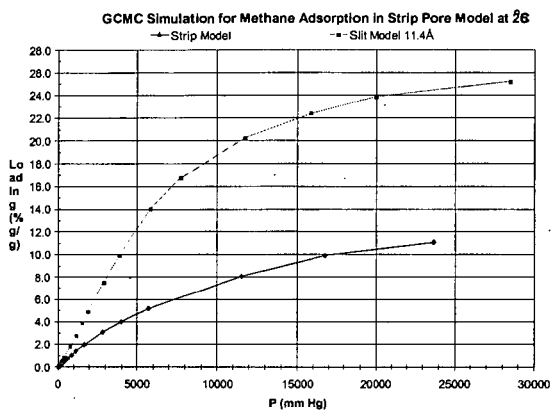


Figure 3. GCMC Simulation for Methane Adsorption in Strip Pore Model at 25°C

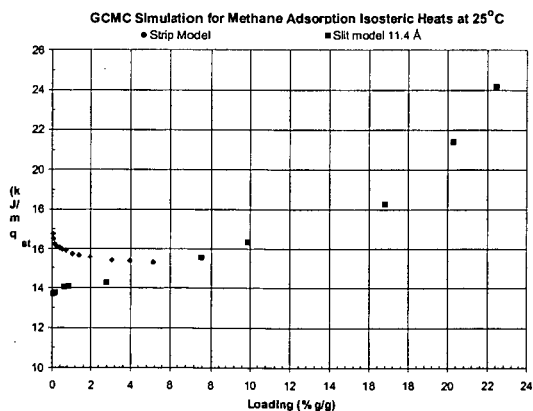


Figure 4. GCMC Simulation for Methane Adsorption Isothermic Heats at 25°C

GAS-STORAGE CARBONS PREPARED BY ALTERNATING OXYGEN CHEMISORPTION AND THERMAL DESORPTION CYCLES

Marek A. Wójciewicz, Brian L. Markowitz, Girard A. Simons*, and Michael A. Serio

Advanced Fuel Research, Inc., 87 Church Street, East Hartford, CT 06108-3742

*Simons Research Associates, 3 Juniper Road, Lynnfield, MA 01940-2416

Keywords: gas storage, activated carbon, chemisorption, desorption

ABSTRACT

The desirable characteristics of activated carbons for gas-storage applications are: (1) high microporosity (pores smaller than 2 nm); and (2) low voidage in the storage container (e.g., the use of shaped sorbent elements). A transient chemisorption-desorption char activation technique was used to maximize micropore formation and minimize mesoporosity. Several carbons were prepared at different degrees of burn-off, and the BET surface areas were found to be up to 2000 m²/g. The carbons were prepared in the form of pellets to show that the future use of shaped elements can lead to the reduction of voidage in the storage container by up to 40%. The adsorption isotherms of the produced carbons showed high microporosity and no appreciable mesoporosity, even at high burn-offs.

INTRODUCTION

Gas storage by adsorption on activated carbon is possible at relatively low pressures using activated carbons with a well developed microporosity, i.e., with pores whose radius, r_p , is less than $r_{\text{lim}} \approx 10 \text{ \AA}$. The generation of microporosity requires a uniform surface phenomenon, such as steady-state gasification in the limit of kinetic control or an alternating adsorption-desorption process in which a reactant gas is chemisorbed on the active sites of a carbon surface and then allowed to desorb, removing the carbon from the walls of the pores [1,2]. A model was presented [3] to describe pore growth in microporous carbons and was used to relate the potential micropore volume to the characteristics of the starting material (initial char). Modeling results show that the microporosity can be maximized by choosing an initial char with minimum initial open porosity and significant initial blind porosity within angstrom-size pores. As a spatially uniform surface recession may be obtained via char gasification in the limit of kinetic control, the microporosity-evolution model [3] has been coupled to a pore structure/pore-transport model [4] capable of describing the simultaneous action of diffusive and kinetically-controlled processes. The integrated model [5] was used to determine the conditions under which diffusion-control may be avoided and the char microporosity maximized. Predicted steady-state activation times are extreme for millimeter-size particles (10⁴ hours), and faster processes are sought. One such process is that of alternating oxygen chemisorption and desorption [1,2]. Rapid adsorption of oxygen onto the char surface in the absence of desorption (via low-temperature chemisorption), followed by rapid high-temperature desorption in the absence of oxygen, may be used to cyclically remove carbon from the walls of the pores.

In this paper, theoretical analysis of the cyclic chemisorption-desorption process is carried out to assess the time scales of: (1) the oxygen chemisorption step; and (2) the thermal desorption of surface oxides. In addition to the results of the modeling effort, microporosity evolution is reported for chars prepared using the above activation technique.

MATERIALS AND EXPERIMENTAL TECHNIQUES

A sample of granular polyvinylidene chloride (PVDC), provided by Solvay Polymers, Inc., Houston, Texas, was used as a carbon precursor. PVDC was first pressed into pellets, using a ten-ton press, and then subjected to carbonization. The initial dimensions of the pellets were 13 mm in diameter and ~5 mm in thickness, and the initial weight of each pellet was approximately one gram. The PVDC-carbonization procedure consisted of the following steps: (1) heating from room temperature to 170 °C at 5 °C/min; (2) heating to 230 °C at 0.1 °C/min; (3) heating to $T_f = 900 \text{ °C}$ at 2 °C/min; (4) holding at T_f for time $\tau_f = 240 \text{ min}$; and (5) cooling down to room temperature at -22 °C/min. After carbonization, the samples were activated to the desired degree of burn-off using a thermogravimetric analyzer (TGA), and the following routine was performed cyclically: (1) purging the system at 200 °C for 17 minutes in helium; (2) heating at 100 °C/min to $T_a = 900 \text{ °C}$ (He); (3) holding for 5 minutes (He); (4) cooling at -22 °C/min to $T_{\text{ch}} = 200 \text{ °C}$ (He); and (5) switching from the flow of helium to oxygen and holding for $\tau_{\text{ch}} = 15 \text{ minutes}$ in O₂. At specified levels of burn-off, samples were taken out of the TGA, weighed, and nitrogen adsorption isotherms were determined using a Micromeritics Digisorb 2600 analyzer.

RESULTS AND DISCUSSION

Modeling of the Kinetics of Oxygen Chemisorption and Surface-Oxide Desorption

The primary limitation of the adsorption process is the time required for oxygen to reach the smallest pores in the char. The high chemisorption rate will generate large oxygen gradients within the particle, but diffusion along these gradients is still responsible for delivering the oxygen to the smallest pores. A model has been developed to describe this transient chemisorption process. A chemisorption "front", coupled with gas-phase diffusion, progresses into the pore structure and deposits chemisorbed oxygen on carbon active sites. This model has been used to determine the time required for complete chemisorption of oxygen onto the walls of the smallest pores.

For phenol-formaldehyde char, chemisorbed oxygen loadings of the order of 12 mg O₂/g C were obtained at 300 °C in one atmosphere of oxygen [6]. The chemisorption time was about 80 minutes, the BET surface area of the char was about 400 m²/g C, and the char particle diameter was of the order of 100 microns. A primary concern is how the chemisorption time scales with particle size and oxygen partial pressure. The model described above has been used to predict this scaling. If s_p represents the internal surface area of the carbon (m²/g C), and σ_w represents the chemisorbed oxygen loading per unit surface area (g O₂/m²), then $s_p\sigma_w$ is the chemisorbed oxygen loading in g O₂/g C. Oxygen loadings of the order of 12 mg/g and an internal surface area of 400 m²/g are consistent with surface loadings (σ_w) of 3×10^{-9} g/cm². Using this set of chemisorption parameters, model predictions for the chemisorption times are illustrated in Figure 1. In the limit of kinetic control (small particles), increased gas pressure significantly reduces the chemisorption time. However, in the limit of diffusion control (large particles), increased gas pressure does not enhance diffusion. It is clear that operating in one atmosphere of oxygen on up to 7 mm particles will maintain chemisorption times of the order of one hour.

The desorption process is just the reverse from the adsorption process. A desorption "front," coupled with gas phase diffusion and viscous convection, progresses into the pore structure and desorbs the oxygen from the carbon active sites. As the particle temperature is raised, the internal gas pressure increases and viscous convection of the gas from the pore structure becomes rate limiting. This is illustrated in Figure 2. Internal gas pressures in excess of a few hundred pounds per square inch are sufficient to create desorption times less than one tenth of an hour per cycle for centimeter-size particles. As the desorption temperature, and therefore pressure, may be arbitrarily increased, the alternating chemisorption-desorption process is readily limited by the chemisorption step. As each chemisorption-desorption cycle will chemisorb only ~12 mg O₂/g C, and desorption will remove only 9 mg carbon per gram of carbon, up to 100 cycles may be required to fully activate the carbon. As temperature cycling may require less than one hour per cycle, it is apparent that this activation process is much faster than kinetically controlled gasification and may be used to activate particles up to one centimeter in diameter on time scales of the order of 100 hours.

Preparation and Characterization of Gas-Storage Carbons

An important consideration in gas-storage applications is the degree of sorbent packing within the storage container. To achieve maximum volumetric storage density, the voidage in the container needs to be minimized. Although some amount of voidage is desirable to ensure adequate gas transport within the sorbent-filled container, the 30-40% voidage typical of randomly packed particles is excessive. Thus, an ideal gas-storage system would consist of a nearly 100% microporous sorbent in the form of tightly packed, shaped elements, e.g., discs 5-10 mm in thickness.

The traditional char-activation methods, which are based on steady-state carbon gasification, usually lead to pore-mouth widening and to the creation of the undesirable mesoporosity. The problem is caused by mass-transfer limitations that occur within the char particle, and this phenomenon is increasingly more severe for particles of larger sizes. Thus, the steady-state activation methods are incapable of producing large elements of highly microporous sorbent. This is in contrast to the cyclic chemisorption-desorption method, which, by obviating the mass-transfer limitations, should allow to obtain large elements of microporous sorbent. This presumption is tested below by analyzing the pore structure of sorbent pellets activated using the cyclic method.

Adsorption isotherms of the PVDC char pellets activated to different burn-offs are shown in Figure 3. It is evident that all the curves have the shape of a Type I isotherm, which is characteristic of highly microporous materials [7]. It is remarkable that even the pellets with as much as 87% burn-off do not show mesopore formation (transition to a Type IV isotherm).

Although the BET surface-area analysis is not quite applicable to highly microporous materials [7], the results can nevertheless serve as an index of sample microporosity. In other words, BET surface areas reported for microporous solids will not have physical meaning, but larger values will indicate a higher degree of microporosity. Another measure of microporosity is the micropore volume evaluated using the Dubinin-Radushkevich equation [8,7]. BET surface areas and micropore volumes of the PVDC char pellets are presented in Figure 4. It can be seen that both variables increase with the increasing burn-off, which indicates that the sorbent becomes more and more microporous as activation progresses.

Additional insights into the morphology of sorbent pellets can be provided by Scanning Electron Microscopy (SEM). SEM pictures of an activated PVDC char pellet are shown in Figure 5. It can be seen the PVDC granules that were initially present within the pellet have changed their original spherical shape (uncompressed PVDC polymer) to a more pentagonal or hexagonal pattern (PVDC char pellet). These particles have an approximate size of 170 microns. The change in particle shape drastically decreases the ~40% voidage typically found in spherical particles. Another interesting observation is the 5-10 micron spaces between individual granules within each pellet. It is expected that these spaces will make gas transport into and out of the storage container far less restricted than in the case of "solid" pellets. Preliminary calculations carried out for the above material show that mass transfer within a bed of shaped sorbent elements should not be a serious problem for gas-storage applications. A more detailed analysis of this result will be discussed in a future publication.

Figure 5 also shows one-micron pits, which are most likely formed during the evolution of pyrolysis gas. Modifications in the PVDC pyrolysis routine may lead to a change in the size and the number of these structural features.

CONCLUSIONS

- Theoretical analysis of the cyclic chemisorption-desorption process shows that char particles up to one centimeter in size can be activated on time scales of the order of 100 hours.
- All PVDC-derived carbons, activated to burn-offs of up to 87% using the cyclic technique, were found to exhibit Type I adsorption isotherms. This is indicative of a high degree of microporosity. Nitrogen BET surface areas and Dubinin-Radushkevich micropore volumes were found to be up to 2000 m²/g and 0.84 cm³/g, respectively. It can be concluded that the concept of producing large, shaped elements of microporous carbon has been experimentally validated. This finding is associated with the benefit of an increased volumetric storage density (by up to 40%) due to improved sorbent packing. First tests of hydrogen-storage capacity of the above sorbents have been carried out, and the results look very encouraging [2].
- SEM micrographs show that sorbent pellets are composed of nested pentagonal or hexagonal particles about 170 μm in size. Spaces between the particles are 5–10 μm wide, and they should provide a good medium for hydrogen transport without creating excessive voidage.

ACKNOWLEDGMENTS

This research was supported by the NASA Johnson Space Center under SBIR contract No. NAS9-19470. The authors also acknowledge helpful comments contributed by Dr. David F. Quinn of the Royal Military College of Canada and Professor Eric M. Suuberg of Brown University.

REFERENCES

- 1 Quinn, D. F. and Holland, J. A., U.S. Patent No. 5,071,820, 1991
- 2 Wójtowicz, M. A., Smith, W. W., Serio, M. A., Simons, G.A. and Fuller, W. D., in *Carbon '97* (Ext. Abstr. 23rd Biennial Conf. Carbon), The Pennsylvania State University, State College, PA, 1997, vol. I, pp. 342-343
- 3 Simons, G. A. and Wójtowicz, M. A., in *Carbon '97* (Ext. Abstr. 23rd Biennial Conf. Carbon), The Pennsylvania State University, State College, PA, 1997, vol. I, pp. 328-329.
- 4 Simons, G.A., in *Nineteenth Symposium (International) on Combustion*, The Combustion Institute, Pittsburgh, PA, 1982, pp. 1067-1076.
- 5 Simons, G. A. and Wójtowicz, M. A., in *Proc. 9th Int. Conf. on Coal Science*, DGMK, Hamburg, Germany, 1997, pp. 1783-1786.
- 6 Wójtowicz, M. A., *Thermogravimetric Study of Active Sites in the Process of Low-Temperature Oxidation of Char*, Ph.D. thesis, Brown University, Providence, RI, 1988.
- 7 Gregg, S. J. and Sing, K. S. W., *Adsorption, Surface Area and Porosity*, Academic Press, London, 1982.
- 8 Dubinin, M. M. and Radushkevich, L. V., *Proc. Acad. Sci. USSR* **55**, 331, 1947; Dubinin, M. M., *Russ. J. Phys. Chem.* **39**, 697, 1965.

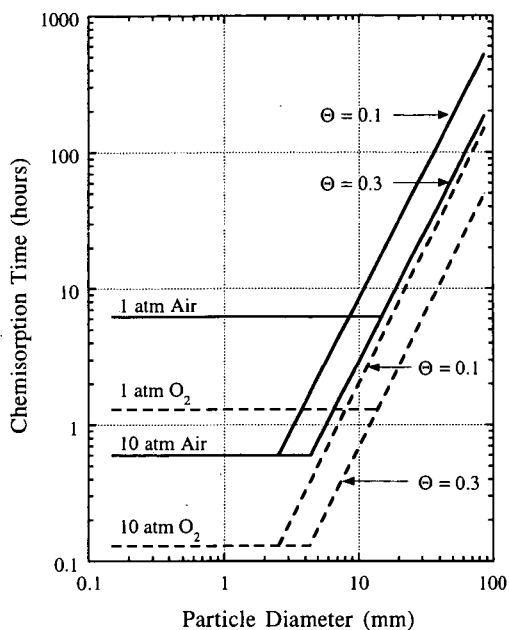


Figure 1. Scaling of chemisorption time with particle size and gas pressure (phenol-formaldehyde resin char carbonized at 1000 °C for 2 hours; Θ is char porosity).

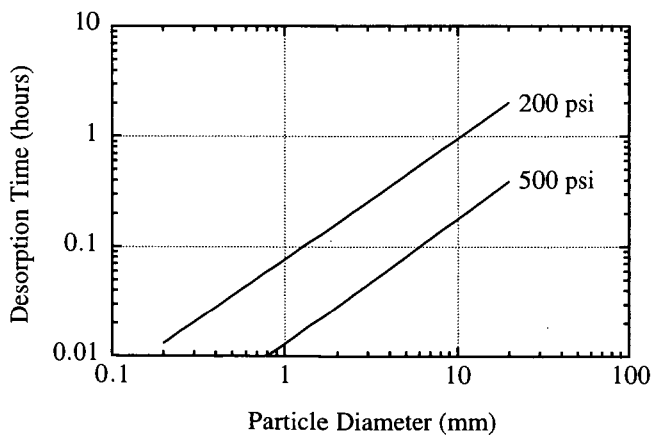


Figure 2. Scaling of desorption time with particle size and internal gas pressure (convection limited, 200 psi and 500 psi).

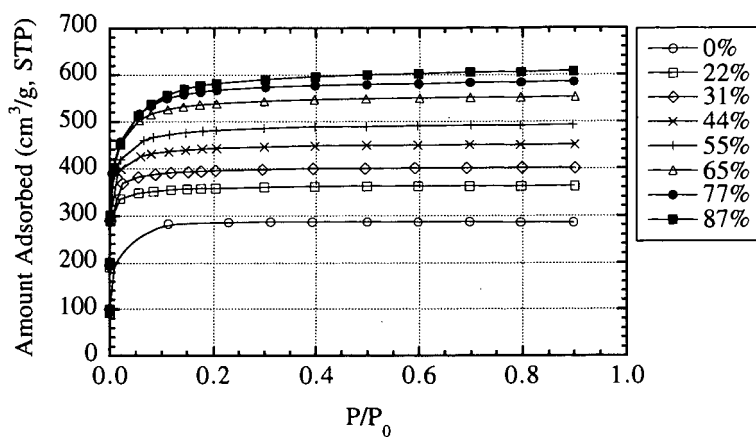


Figure 3. Nitrogen adsorption isotherms for PVDC-char pellets activated to various degrees of burn-off.

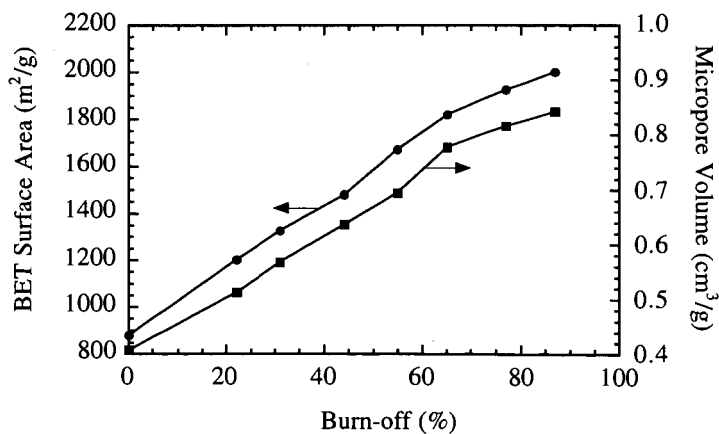


Figure 4. Nitrogen BET surface area and Dubinin-Radushkevich micropore volume versus per cent burn-off for PVDC char pellets.

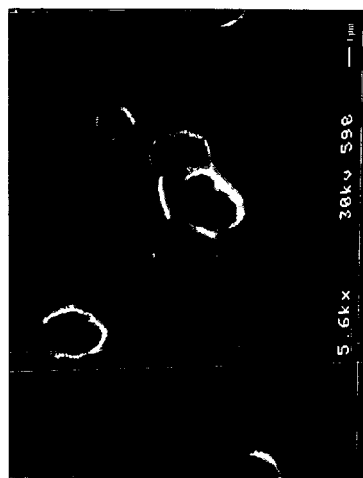
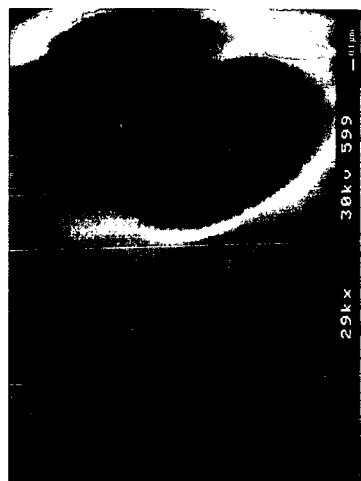
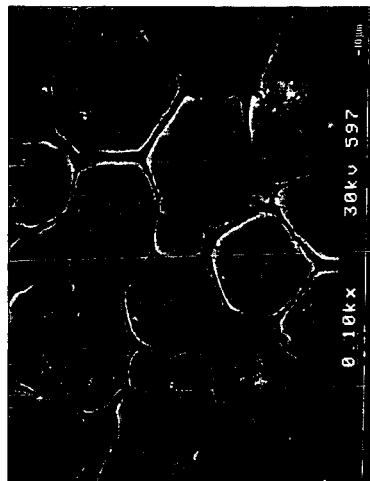


Figure 5. SEM micrographs of a PVDC char pellet ($T_i = 905^\circ\text{C}$, $\tau_i = 5\text{ min}$, $T_{ch} = 200^\circ\text{C}$, $\tau_{ch} = 15\text{ min}$, $T_c = 900^\circ\text{C}$, $BO = 64\%$).

CH₄ STORAGE ON COMPRESSED CARBONS

Aurora M. Rubel and John M. Stencel

Center for Applied Energy Research, University of Kentucky, Lexington, KY 40511

ABSTRACT

The uptake of CH₄ in three commercially-produced carbons before and after physical and chemical modification were studied using a specially designed cell within a high pressure TGA. The uptake capacities in non-compacted and compacted carbons and their pore size distributions were compared. After compaction, a carbon having 75-38 μ m particles adsorbed more CH₄ than the same carbon having larger particles of 1700-425 μ m even though the resultant density of the later sample was greater. Compaction of graphite powder produced significant microporosity, imparting capacities of 25 ml CH₄ at STP/ml carbon. Even though greater microporosity in carbons increases CH₄ storage capacities, high microporosities usually leads to low piece densities and difficulties during compaction. Hence, methods to improve piece density while maintaining CH₄ capacities were investigated. One method involved the mixing a highly microporous carbon with graphite and then compacting the mixture. A blend of 75:25 by volume (carbon : graphite) contained the same adsorption capacity on a volume CH₄/volume carbon basis as did the pure carbon sample; the blend had better compaction properties. Another method involved chemical deposition on and within the carbon. Diethylsilane was impregnated on and in a highly microporous carbon resulting in greater piece density and increased CH₄ uptake capacity.

INTRODUCTION

The commercial utilization of microporous carbons to store natural gas at low pressures will require the optimization of many factors including: maximizing the pore volume around 1.1 nm³; minimizing adsorption/desorption cycle times²; and, increasing the volume-per-volume (v/v) storage capacities, i.e. volume of CH₄ stored-per-volume of carbon used. Optimization and production of suitable carbons has been studied by several researchers³⁻⁶. In transportation applications, the CH₄ sorbent will ultimately need to be contained within a fixed volume, thereby requiring relatively high densities which produce desirable v/v storage capacities.

Previous work has shown that treating activated carbons with surfactants can improve their compressibility and reduce the work needed for densification⁷. However, the CH₄ storage capacities of these carbons were not determined. The present study investigated changes in the compressibility and CH₄ uptake of microporous carbons when physical modifiers were added before compaction.

EXPERIMENTAL

The compaction properties of three carbons and their CH₄ uptake were studied. Three commercially-made carbons, including Barnebey-Sutcliffe A207 (two particle size fractions, 75-38 μ m and 1700-425 μ m), Amoco Super A, and Alfa Aesar graphite were used. The N₂ BET surface areas of these materials were 850, 3000, and 5 m²/g, respectively. Mixtures of Amoco Super A with graphite were also densified and studied; these mixtures were 100:0, 75:25, and 50:50 Amoco: graphite on a volume basis.

In order to prevent expansion of the carbons after compaction, a special reactor was designed for use in the Cahn C1100 high pressure thermal analyzer (HPTGA). Two reactor configurations, shown in Figure 1, were used depending on whether CH₄ storage on compacted or non-compacted (loose) carbons was being measured. The sides and bottom of the cylindrical reactor were made of porous (2 μ m) stainless steel, the top of which was a solid, 3.1 mm thick disk. For loose carbons, this closing disk was placed above and supported by the hanger rod; for compacted carbons, the disk was placed over the carbon and then secured by the hanger rod, thereby preventing expansion during the HPTGA measurements. The procedures of Sosin and Quinn⁸ were used to calculate CH₄ storage capacities and pore size distributions. The densities of loose and compacted carbons were determined by knowing the weights of the carbons contained in the known reactor volume.

Densification of the Amoco carbon was studied after deposition of diethylsilane (DES). DES was chosen because it is a starting material for microporous thin films; a porous coating on the carbon would be desirable during CH₄ adsorption and desorption⁹. Two procedures were used to deposit

the DES on the carbon. In each case, two grams of Amoco carbon were treated. In one case, the carbon was soaked in 5 ml of DES for 2 hours and in the other case the carbon was soaked in a 30% solution of DES in CCl_4 for 30 minutes. Excess DES was decanted and the DES plus carbon were filtered using #1 qualitative filter paper. The carbon was subsequently air dried for 30 minutes, and then heated to 300°C in air for 15 minutes.

RESULTS

Compaction studies on two different particle size distributions, 75-38 μm and 1700-425 μm , of the Bamebey - Sutcliffe A207 carbon were performed. Larger particles have a higher nascent density than finer particles and were anticipated to have higher compaction densities; larger particles in a loose packing situation were anticipated to have a lower density because of the voids due to irregular particle shapes. These anticipations were qualified by the data where loosely packed 75-38 μm and 1700-425 μm particles had densities of 0.49 and 0.44 g/ml, respectively, whereas compressed samples had maximum attainable densities of 0.82 and 0.91 g/ml, respectively. For each particle size distribution, the CH_4 storage capacity increased with increased packing density of the carbon (Figure 2). However, the highest storage capacity obtained for the A207 carbon was for the compressed 75-38 μm powder even though it did not have the highest packing density.

Maximum compaction densities of only 0.34 g/ml were attainable using 100% of the Amoco carbon. It was very difficult to compact. Graphite, however, has a relatively high bulk density and is easily compacted to 1.22 g/ml. The CH_4 uptake on loose graphite is very low but compaction increases it significantly (Figure 3). In an attempt to improve the compaction properties of pure Amoco carbon, varying mixtures of carbon and graphite were prepared and subjected to CH_4 uptake determinations. Figure 4 shows the results for these blends in comparison to the pure Amoco carbon. With the 50:50 Amoco : graphite mixture, the maximum attainable density was 0.63 g/ml, almost twice that of the compacted pure Amoco carbon. The CH_4 uptake capacities increased with increased compaction densities for all blends. Interestingly, the CH_4 uptake on the compacted 75:25 Amoco : graphite mixture was the same as for 100% Amoco carbon.

The possibility of using chemical deposition on and within the pores of the Amoco carbon as a way to increase compressibility was also explored. Maximum compaction densities of 0.38 and 0.44 g/ml were attained for the high and low concentrations of DES, respectively. Even though these densities were only slightly greater than for the pure Amoco, the CH_4 uptake on the DES treated carbons was greater than on the pure carbon (Figure 5). The data suggest that DES impregnation warrants further investigation.

Pore size distributions were determined from the CH_4 isotherms. Comparison of the pore size distribution of compressed Amoco carbon relative to the loose, pure carbon indicated that compression significantly enhanced the pore volume for pores having diameters around 1.1 nm (Figure 6); pores of this dimension are believed to be optimum for CH_4 storage¹. Pore size distributions were also determined for compressed mixtures of Amoco : graphite and for the DES treated Amoco carbon (Figure 7). The total pore volume from pores with dimensions of 0.38-2.0 nm correlated well with the total CH_4 uptake (Figure 8). Plotted in Figure 8 are the average values of all replicates for the untreated and each different physically modified compressed carbon. These data also indicated similar pore volumes for the compressed, pure Amoco and for the 75:25 Amoco:graphite samples. The DES treated Amoco, especially the less severely treated material, had the highest pore volumes which was consistent with their highest CH_4 uptake capacities.

SUMMARY AND DISCUSSION

During this study, methods were explored to improve the compaction properties of porous carbons to increase the amount of CH_4 stored per unit volume of carbon. The particle size of the starting material was important and it appears that, even though larger particle can be compacted to higher densities, greater microporosity was developed during the compaction of fine powders.

Amoco Super A, a highly micro-porous carbon with low bulk density, has been shown to have a higher CH_4 uptake capacity compared to all other carbons studied during this work¹⁰. Maximum compaction densities of this carbon under the experimental conditions were low (0.34 g/ml) in comparison to graphite (1.22 g/ml). Compaction of pure graphite resulted in the development of some microporosity, which is considered responsible for uptake of 25 ml (STP) CH_4 per ml graphite. The compaction properties of a blend of graphite with the Amoco carbon were improved over those of the carbon alone and a blend of 75 : 25 carbon : graphite on a volume basis resulted

in the same amount of CH_4 adsorption as the pure carbon. These results have important implications for improving the economics of CH_4 storage on activated carbon, i.e. inexpensive graphite was substituted for the expensive activated carbon and yet the CH_4 uptake capacity was not compromised.

The role of the graphite and DES has yet to be elucidated. The data in Figure 4, where the 0.20 g/ml density sample from the 75:25 mixture has a CH_4 uptake capacity of 29 v/v, the 0.20 g/ml density sample from the 50:50 mixture has a CH_4 uptake capacity of 14 v/v and the pure Amoco carbon has a capacity of 37 v/v, suggest that in loose mixtures the effect of graphite is nearly linear in graphite concentration where it plays the role of a diluent, i.e. less Amoco carbon implies less CH_4 storage. In compressed mixtures, the diluent effect is still observant but not as predominant. Under compaction, the graphite could occupy macro-voids and provide some microporosity.

The DES coating method was chosen because of its potential to provide a porous micro-coat on and in the carbon. Quite interestingly, the data indicate that the DES treatment improved the carbon's compressibility and increased its microporosity. The DES coating did not appear to change the microporosity of non-compacted carbon.

CONCLUSIONS

The two methods for improving the compaction properties of a highly microporous carbons appear worthy of further investigation relative to fundamental and applied areas of study. Both blending carbons with a material having a higher bulk density and the chemical deposition on or within the carbon improved compaction properties and increased CH_4 uptake. Both methods appear to enhance the microporosity only after sample compaction.

REFERENCES

1. Matranga, K.R., Myers, A.L., and Glandt, E.D. *Chem. Eng. Sci.*, **47**, 1569 (1992)
2. Sheikh, M.A., Hassan, M.M., and Loughlin, K.F., *Gas Sep. Purif.*, **10**, 161 (1996)
3. MacDonald, J.A.F. and Quinn, D.F., *Carbon*, **34**, 1103 (1996)
4. MacDonald, J.A.F. and Quinn, D.F., *Fuel*, **77**, 61 (1998)
5. Alcaniz-Monge, J., De La Casa-Lillo, M.A., Cazorla-Amoros, D., and Linares-Solano, A., *Carbon*, **35**, 291 (1997)
6. Wojtowicz, M.A., Smith, W.W., Serio, M.A., Simons, G.A., and Fuller, W.D., Extended Abstracts, 23rd Biennial Conference on Carbon, Univ. Park, PA, USA, 342, 1997
7. Stewart, M.L. and Stencel, J.M., *Preprints Symposium on Alternate Uses for Fossil Fuels*, ACS, Division of Fuel Chem., Denver, CO Meeting, 408, March., 1993
8. Sosin, K.A. and Quinn, D.F., *J. Porous Materials*, **1**, 111 (1995)
9. Levy, R.A., Ramos, E.S., Krasnoperov, L.N., Datta, A., and Grow, J.M., *J. Mater. Res.*, **11**, 3164 (1996)
10. Stencel, J.M., Ban, H., Li, T.-X., Neathery, J.K., Rubel, A.M., and Schaefer, J.L., Annual Report, NASA/EPSCoR, Materials Processing for Space Mission Energy Needs, April 1, 1996 - March 31, 1997

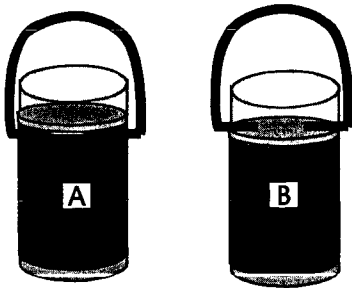


Figure 1. Reactor configurations for CH₄ storage determinations on loose (A) and compressed (B) carbons.

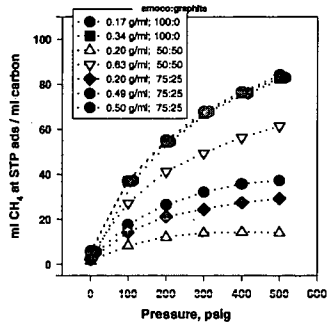


Figure 4. CH₄ storage on loose and compressed mixtures of Amoco Super A and graphite.

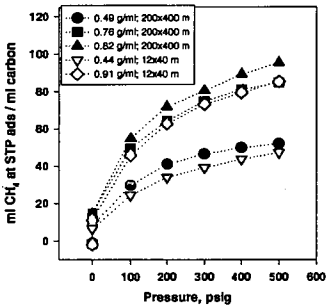


Figure 2. CH₄ storage on loose and compressed 75-38µm and 1700-425µm particle fractions of an activated carbon.

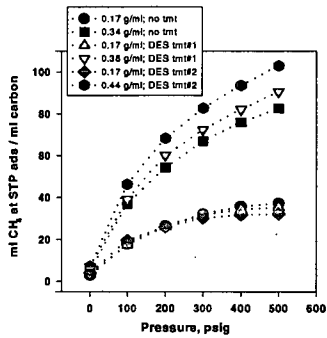


Figure 5. CH₄ storage on loose and compressed untreated and DES treated Amoco Super A carbon.

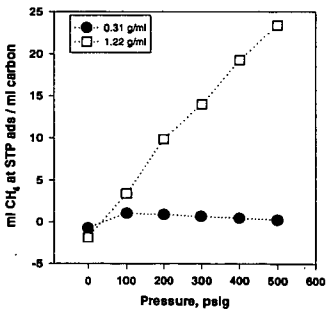


Figure 3. CH₄ storage on loose and compressed graphite.

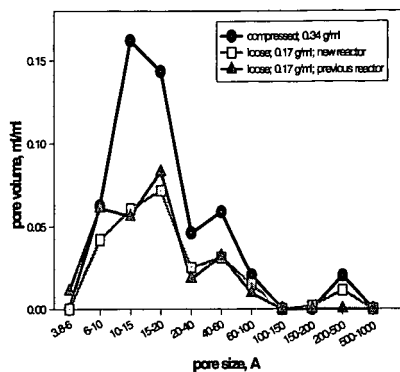


Figure 6. Pore size distributions for loose and compressed Amoco Super A carbon.

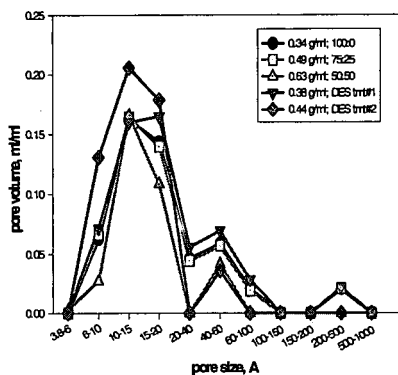


Figure 7. Comparison of the pore size distributions of compressed untreated carbon, carbon-graphite mixtures, and DES treated carbons.

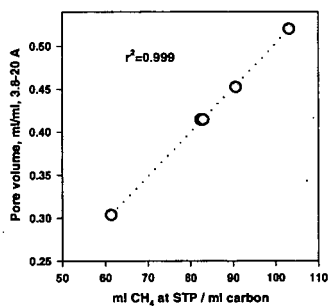


Figure 8. Correlation of pore volume of 3.8-20 Å pores with CH₄ storage capacity.

PREDICTING CH₄ ADSORPTION CAPACITY OF MICROPOROUS CARBON USING N₂ ISOTHERM AND A NEW ANALYTICAL MODEL

Jian Sun,¹ Scott Chen,² Massoud Rostam-Abadi^{1,2} and Mark J. Rood,^{*1}

¹ Department of Civil and Environmental Engineering, University of Illinois at Urbana-Champaign (UIUC), 205 North Mathews Avenue, Urbana IL 61801, USA

² Illinois State Geological Survey (ISGS), 615 East Peabody Drive, Champaign IL 62810, USA

ABSTRACT

A new analytical pore size distribution (PSD) model was developed to predict CH₄ adsorption (storage) capacity of microporous adsorbent carbon. The model is based on a 3-D adsorption isotherm equation, derived from statistical mechanical principles. Least squares error minimization is used to solve the PSD without any pre-assumed distribution function. In comparison with several well-accepted analytical methods from the literature, this 3-D model offers relatively realistic PSD description for select reference materials, including activated carbon fibers. N₂ and CH₄ adsorption data were correlated using the 3-D model for commercial carbons BPL and AX-21. Predicted CH₄ adsorption isotherms, based on N₂ adsorption at 77 K, were in reasonable agreement with the experimental CH₄ isotherms. Modeling results indicate that not all the pores contribute the same percentage V_m/V_s for CH₄ storage due to different adsorbed CH₄ densities. Pores near 8-9 Å shows higher V_m/V_s on the equivalent volume basis than does larger pores.

INTRODUCTION

Activated carbon usually has a heterogeneous pore structure due to the structural complexity and randomness.¹ The distribution of pore sizes is a critical parameter for characterizing the adsorbent, when the adsorption potential is a dominant factor. Adsorption density is strongly dependent on the adsorbent's pore size (w). For instance, adsorption is enhanced in micropores ($w < 20$ Å) due to overlap of the force field created by the opposing pore walls. For applications such as natural gas storage, the adsorbent should be prepared in such a way that it has minimum mesopore ($20 \text{ Å} < w < 500 \text{ Å}$) and macropore ($w > 500 \text{ Å}$) volume and maximum micropore volume. In particular, w for micropores should be near 8 Å; the optimal pore size for CH₄ adsorption.² In this study w is defined as the distance between the edges of the carbon atoms in opposite pore walls. The pores are modeled as slits consisting of two infinite graphite planes.

A number of PSD models have been developed on the basis of N₂ adsorption at 77 K. Although the models provide great insights, there is apparent lack of consistency in the modeled PSD results³ due to their different theoretical foundations and assumptions. Well-accepted PSD characterization methods include MP,⁴ DRS,⁵ JC,⁶ HK⁷ and, more recently, SNAP^{8,9} and DFT.¹⁰ SNAP is one of the latest PSD methods based on numerical results from Mean-Field Density Functional Theory (MFT).^{8,9} SNAP uses a pre-assumed log normal distribution function to model N₂ adsorption at 77 K. DFT (Micromeritics) is one of the latest PSD methods based on Non-local MFT.¹⁰ DFT employs a Regularization technique to solve the generalized adsorption isotherm (GAI)^{8,11} which results in a discrete PSD. Another version of DFT (Quantachrome) is based on Local MFT, which neglects the adsorbate-adsorbate interactions.

The objective of this study is to model and correlate N₂ and CH₄ adsorption on microporous carbon through an analytical approach. A PSD model is developed on the basis of a 3-D isotherm equation without pre-assumed distribution functions. Prediction of CH₄ adsorption isotherm is carried out by correlating the N₂ and CH₄ adsorption for select adsorbents.

MODEL DESCRIPTION

Taking an approach similar to Chen and Yang's 2-D adsorption isotherm equation,¹² a 3-D adsorption isotherm equation was developed,¹³

$$\ln \frac{\rho'}{\rho^g} + \frac{8\eta - 9\eta^2 + 3\eta^3}{(1-\eta)^3} + \frac{1}{k_B T} \frac{a}{b} \left(\ln(1+4\eta) - \frac{4\eta}{1+4\eta} \right) + \frac{\Phi}{k_B T} = 0 \quad (1)$$

for a given pore size and geometry (slits), with a mean force field Φ . The classical Dubinin-Stoeckli (DS) inverse relationship,¹⁴ is used for its simplicity to evaluate the mean force field as a function of pore size. ρ^g and ρ' are volume number densities of the gas and adsorbed phases,

respectively. η is the pore filling fraction. The second term in Eq. 1 describes the short-range repulsive force between adsorbate molecules, while the third term represents the long-range attractive force between adsorbate molecules. The fourth term refers to the interaction between adsorbate and adsorbent. For low adsorption density (close to bulk gas density), the packing fraction is close to zero (so are the second and third terms in Eq. 1), thus the equation reduces to Henry's law. In comparison with the 2-D equation,¹² 3-D adsorption density can be obtained with the 3-D equation. Therefore, N_2 and CH_4 adsorption density and PSD based on N_2 adsorption can be determined.

For N_2 adsorption at 77 K, phase transition from gas to liquid takes place in micropores when adsorption density increases substantially due to pore filling. To include this feature and assure a realistic adsorption density, a modified DR equation is used to calculate adsorption density after pore filling.¹⁵

$$\rho = \rho_l \exp \left[- \left(\frac{A}{\beta E_0} \right)^2 \right] \quad (2)$$

where ρ is the density of adsorbed phase. ρ_l is the density of saturated liquid N_2 . A is the differential molar work, β is the affinity coefficient and E_0 is the adsorption characteristic energy. The pore filling fraction θ can be expressed as ρ/ρ_l .

Correlation between pore filling pressure and critical pore size in the 3-D model was obtained from MFT^{8,9} to describe the discontinuous jump in the N_2 adsorption isotherm.¹³ In other words, the adsorption densities prior to and after pore filling are calculated by the 3-D equation and by the modified DR equation, respectively.

To obtain the PSD, the GAI is formulated as:^{8,11}

$$n(P') = \int_0^{\infty} \rho(P', w) f(w) dw \quad (3)$$

$n(P')$ is the amount of adsorbed N_2 at a relative pressure P' ($= P/P_0$) obtained directly from the experimental adsorption isotherm, $\rho(P', w)$ is the adsorbate density calculated using the 3-D adsorption isotherm (Eq. 1) and modified DR equation (Eq. 2), and $f(w)$ is the distribution of pore volume as a function of w . Eq. 3 is broken down into a set of linear equations solved using least squares error minimization.¹³

MATERIALS USED

Two activated carbon fiber (ACF) samples (ACF-15 and ACF-25) obtained from American Kynol, Inc. (New York, NY) were used as adsorbents for PSD modeling. ACF-15 has the shorter activation time (lower burn-off and higher yield) compared to ACF-25. Norit Row (American Norit) is used to compare PSD results by DFT and the 3-D model. N_2 adsorption data and DFT results for Norit Row were obtained from Kruk.¹⁶ Other commercial carbons used are BPL (Calgon Carbon), and AX-21 (Amoco). The 77 K N_2 adsorption isotherm of BPL and AX-21 was measured with a Micromeritics ASAP2400 (P/P_0 : 10^{-3} to 1).

RESULTS AND DISCUSSION

Optimal Pore Size for CH_4 Adsorption

Multiple layer adsorption does not occur at ambient temperature for CH_4 because it is a supercritical gas. Therefore, there must be an optimal pore size associated with the maximum CH_4 adsorption density. Densities of adsorbed CH_4 at 3.4 MPa (500 psia) and 300 K on an ideal adsorbent with various pore sizes are calculated using Eq. 1. The affinity coefficient β for CH_4 is calculated using the following equation

$$\beta = \frac{[P']}{[P']_0} = 0.353 \quad (4)$$

$[P']$ and $[P']_0$ are the parachors of CH_4 and benzene, respectively, which can be obtained from standard references.¹⁷ Dependence of adsorbed CH_4 density on pore size is plotted in Figure 1. The optimal pore size with a maximum adsorption capacity is ≈ 8.0 Å, closely matching the results obtained by computer simulation.²

PSD Characterization of Activated Carbon Fibers

PSDs for ACF-15 and ACF-25 obtained by the 3-D model are presented in Figure 2. The

micropore volume and pore volume for $w < 100 \text{ \AA}$ from the 3-D model are 0.363 and 0.988 cm^3/g respectively (Table 1). Increased pore volume and pore widening are expected for ACF-25 compared to ACF-15. These features are well illustrated in Figure 2. Calculated N_2 isotherms using the 3-D model and the corresponding experimental isotherms for the two ACF samples are also presented in Figure 2. Good agreement exists in all cases.

Comparisons of PSD results for ACF-25 by MP, JC, HK and the 3-D model are summarized in Figure 3. In contrast to the PSDs by JC and HK, a multiple modal PSD for ACF-25 is revealed by the 3-D model, which corresponds to the inflections in the experimental isotherm. MP method indicates the PSD maximum is about 8 \AA (Table 1). This is due to the MP method not considering the enhanced adsorption in micropores. The adsorption film thickness (related directly to estimated pore size in the MP method) should be greater in micropores than for non-porous materials at a given relative pressure. MP method tends to underestimate the pore size for micropores. The PSD obtained by JC method predicts a single mode and extends further into the mesopore region (maximum at 16 \AA). Such result is presumably caused by use of the DR equation and the initial constraint associated with the pre-assumed normal distribution for the PSD. Compared with the others, HK method gives the smallest PSD maxima for both ACF samples (Table 1). It does not appear to respond well to pore widening brought about by the extent of activation for ACF-25. HK method underestimates the pore size due to the progressive pore filling mechanism.

Comparison of PSDs by DFT and 3-D Model

PSD results using the DFT method¹⁰ for Norit Row is provided in Figure 4. The PSD results by DFT are reproduced by normalizing the pore volumes to the corresponding pore size intervals and taking the center point of each size interval as the corresponding pore size. PSD by DFT is usually presented as a discrete bar chart.^{18,19} PSD results by the 3-D model based on the same N_2 isotherm is also plotted in Figure 4. Reasonable agreement can be observed between the two methods, although the PSD maximum by DFT is 0.5 \AA larger than that by the 3-D model.

Prediction of CH_4 Adsorption Isotherm

Prediction of CH_4 adsorption isotherm at 296 K is carried out with BPL and AX-21 (Figure 5), whose experimental CH_4 adsorption isotherms were obtained from Sosin.²⁰ The 3-D equation is used to calculate the CH_4 adsorption densities (with volume exclusion but no pore filling because CH_4 is supercritical), which are then combined with the modeled PSDs to obtain CH_4 adsorption isotherms at 296 K. It is noticed that CH_4 adsorption is overestimated in the low pressure region and underestimated in the high pressure region by the 3-D model. This is possibly due to the use of the DS inverse relationship to calculate the adsorption potential energy for CH_4 adsorption. In comparison with experimental results based on a molecular probe study,²¹ the DS inverse relationship overestimates the adsorption potential. The potential by the DS relationship also decreases rapidly as the pore size increases,²² resulting in underestimated adsorbed CH_4 density. Using the DS relationship for N_2 adsorption cannot offset this effect, since the modified DR equation is used to calculate the adsorption density after complete pore filling. At high adsorptive pressures, the adsorption density is close to the value of liquid N_2 , when the DS relationship has negligible contribution to the adsorption density. The prediction may be improved by using other more sophisticated yet more complicated correlation like the HK relationship for carbon and CH_4 .

Modeling results indicate that not all the pores contribute the same percentage Vm/Vs for gas storage due to different adsorbed CH_4 densities. Micropores near 8-9 \AA shows greater volumetric CH_4 capacity (Vm/Vs) on the equivalent volume basis than does larger pores. Figures 6 and 7 plot the percentage of pore volume and percentage of Vm/Vs contributed by the pores of ~8, ~9 and ~20 \AA as functions of activation weight loss for a coal-based carbon series.²³ Around 75% weight loss, volume of ~8 \AA pores represents only 22% of the total pore volume (percentage pore volume = 22%), but contribute 39% of the total adsorbent's Vm/Vs . The ratio of percentage Vm/Vs to percentage pore volume is 1.8 for ~8 \AA pores. Similar results can be observed for ~9 \AA pores. The ratio of % Vm/Vs to % pore volume is 1.6 for ~20 \AA pores. The ratio is reduced for mesopores and macropores due to the sharp decrease of adsorbed CH_4 density in these pores.

SUMMARY AND CONCLUSIONS

A new analytical PSD model has been developed by solving the GAI for N_2 adsorption at 77 K using least squares error minimization. Local isotherms for each single pore size is calculated

using a 3-D adsorption isotherm equation, derived from statistical mechanical principles. In comparison to select analytical methods from the literature, this 3-D model offers a relatively realistic PSD description for select reference materials. N₂ and CH₄ adsorption is correlated using the 3-D model for BPL and AX-21. Predicted CH₄ adsorption isotherms are in reasonable agreement with experimental CH₄ isotherms.

Acknowledgments. AX-21 was provided by Mega-Carbon Co. N₂ isotherms for ACFs and Norit Row were provided by Drs. Mark Cal and Anthony Lizzio of ISGS and Drs. Michal Kruk and Mietek Jaroniec of Kent State University.

REFERENCES

1. Gregg, S.J. and Sing, K.S.W. *Adsorption, surface area and porosity* Academic, London, 1984
2. Matranga, K.R.; Stella, A.; Myers, A.L.; Glandt, E. D. *Chem. Eng. Sci.* **1992**, *47*, 1569.
3. Russell, B.P.; LeVan, M.D. *Carbon* **1994**, *32*, 845.
4. Mikhail, R.Sh.; Brunauer, S.; Bodor, E.E. *J. Colloid Interface Sci.* **1968** *26* 45
5. Stoeckli, H.F. *J. Colloid Interface Sci.* **1977**, *59*, 184.
6. Jaroniec, M.; Choma, J. *Mater. Chem. Phys.* **1986**, *15*, 521.
7. Horvath, G.; Kawazoe, K. *J. Chem. Eng. Jpn.* **1983**, *16*, 470.
8. Seaton, N.A.; Walton, J.P.R.B.; Quirke, N. *Carbon* **1989**, *27*, 853.
9. Lastoskie, C.; Gubbins, K.E.; Quirke, N. *J. Phys. Chem.* **1993**, *97*, 4786.
10. Olivier, J.P. *J. Porous Mater.* **1995**, *2*, 9.
11. McEnaney, B. *Carbon* **1988**, *26*, 267.
12. Chen, S.G.; Yang, R.T. *Langmuir* **1994**, *10*, 4244.
13. Sun, J.; Rood, M.J.; Rostam-Abadi, M. in *Extended Abstract the 23rd Biennial Conference on Carbon*, State College, PA, 1997, pp. 348
14. Dubinin, M.M. in *Progress in Surface and Membrane Science* Academic 1-70, 1975
15. Sun, J.; Brady, T.A.; Rood, M.J.; Lehmann, C.M.; Rostam-Abadi, M.; Lizzio, A.A. *Energy and Fuel* **1997**, *11*, 316. (b)
16. Kruk, M.; Jaroniec, M. *Adsorption* **1996**, *3*, 209.
17. Quayle, O.R. *Chem. Rev.* **1953**, *53*, 439.
18. Kruk, M.; Jaroniec, M. in *Extended Abstract the 23rd Biennial Conference on Carbon*, State College, PA, 1997, pp. 106
19. Olivier, J.P.; Conkin, W.B.; Szombathely, M.V. in *Characterization of Porous Solids III* Elsevier Amsterdam, 1994
20. Sosin, K.A.; Quinn, D.F. *J. Porous Material* **1995**, *1*, 111.
21. McEnaney, B. *Carbon* **1987**, *25*, 457.
22. Chen, S.G.; Yang, R.T. *J. Colloid Interface Sci.* **1996**, *177*, 298.

Table 1 Summary of PSD information for ACFs-15 and 25 by MP, JC, HK and the 3-D Model

| Method | PSD Max. [Å] | ACF-15 | | PSD Max. [Å] | ACF-25 | |
|--------|-----------------|---|--|-----------------|---|--|
| | | Micropore volume [cm ³ /g] | Pore volume [cm ³ /g] | | Micropore volume [cm ³ /g] | Pore volume [cm ³ /g] |
| MP | 5.1 | 0.318 | 0.322 | 7.7 | 1.066 | 1.109 |
| JC | 9.5 | 0.343 | 0.343 | 15.5 | 0.504 | 0.865 |
| HK | 5.3* | 0.333 | 0.336 | 5.8 | 0.801 | 0.843 |
| 3-D | 7.0 | 0.363 | 0.363 | 9.0 | 0.988 | 1.070 |

* Actual maximum should be less.

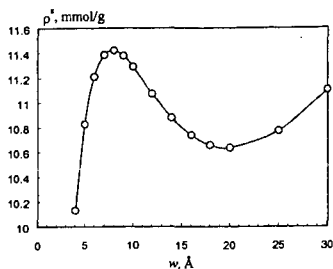


Figure 1 The optimal pore size for CH_4 adsorption.

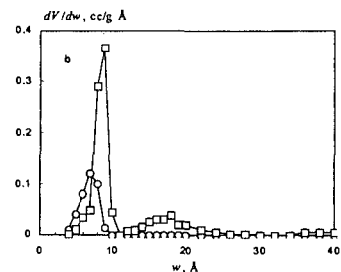
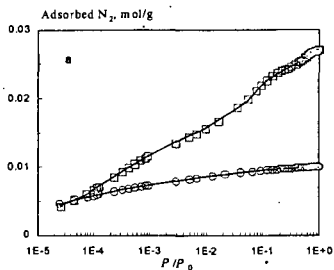


Figure 2 Experimental (symbols) and calculated (lines) N_2 adsorption isotherm at 77 K (a) and PSDs for ACFs-15 (circles) and 25 (squares) by the 3-D model (b).

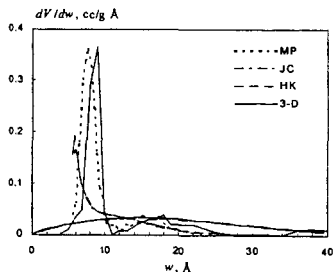


Figure 3 Comparison of PSDs for ACF-25 by MP, JC, HK and the 3-D model.

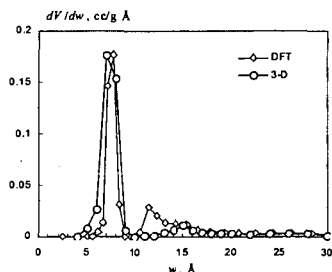


Figure 4 PSD results for Norit Row by DFT and the 3-D model.

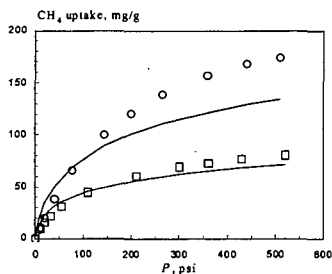


Figure 5 Experimental (symbols) and predicted (lines) CH_4 adsorption isotherms for AX-21 (circles) and BPL (squares).

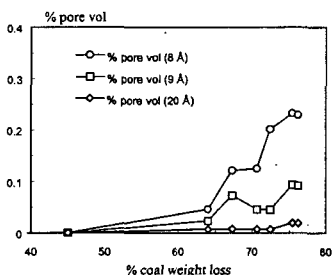


Figure 6 Percentage pore volume vs weight loss in the preparation of a serial coal-based steam-activated carbon at 800°C.

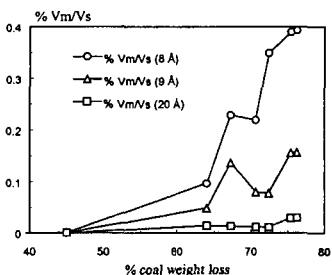


Figure 7 Percentage V_m/V_s vs weight loss.

MULTICOMPONENT DISCHARGE DYNAMICS OF ADSORBED NATURAL GAS STORAGE SYSTEMS

José P. B. Mota

Departamento de Química, Faculdade de Ciências e Tecnologia, Universidade Nova de Lisboa,
2825 Monte de Caparica, Portugal

ABSTRACT

Adsorption storage on highly microporous activated carbon is the most promising low-pressure alternative for storing natural gas. A detailed mathematical model has been developed in order to study the impact of natural gas composition on cycling efficiency of adsorption storage systems. Results show that net deliverable capacity is substantially decreased by heavy hydrocarbons which are present in small amounts in natural gas. Economical means of removing them from the gas stream before charge need to be identified and evaluated.

INTRODUCTION

Natural gas (NG) has always been considered a potentially attractive fuel for vehicle use. It is cheaper than gasoline and diesel, the technical feasibility of NG vehicles is well established, and they have a less adverse effect on the environment than liquid-fueled vehicles. For example, NG can be burnt in such a way as to easily minimize NO_x and CO emissions [1]. In fact, NG outperforms petroleum based fuels in every aspect except on-board storage [2].

A large effort has been devoted to replacing NG high-pressure compression by an alternative storage method working at pressures up to 3.5 MPa. Besides allowing the use of lighter and safer on-board storage reservoirs, this upper pressure limit is easily achieved with a single-stage compressor or, alternatively, the vehicle can be refueled directly from a high-pressure pipeline. As a result, a significant decrease in the capital and operating costs of refuelling stations would be obtained.

A general consensus has been reached regarding adsorption as the most promising low-pressure alternative for storing NG. Extensive experimental work has shown that highly microporous activated carbon is the adsorbent best suited for this task. Quinn and co-workers [1] have given a detailed review of the subject and an update will be published soon [3].

Several operational problems that influence the success of adsorbed natural gas (ANG) storage have been addressed in the literature [1,2]. The one of concern here is the storage capacity loss due to the gradual contamination of the adsorbent with hydrocarbons higher than methane, which are present in trace amounts in NG. If these are not removed from the gas stream before charge, they can adsorb preferentially to high equilibrium residual levels and substantially decrease the net deliverable capacity. This is a consequence of their higher adsorption potential and of the infeasibility of operating an on-board storage reservoir at sub-atmospheric pressures.

Although some work, both analytical and experimental, has been conducted to design and test economical means of controlling the contaminants [4], very little effort has been devoted to the study of their impact on cycling efficiency. This has prompted the author to conduct the work presented here.

PROBLEM FORMULATION

In order to assess the impact of NG composition on net deliverable capacity, the dynamic behaviour of an on-board storage cylinder is modeled as a series of consecutive cycles, each consisting on charge with a fixed gas mixture followed by discharge at constant molar rate until depletion pressure is reached.

Gas adsorption.

Multicomponent adsorption equilibrium is predicted by a formalism combining Adsorption Potential [5] and Ideal Adsorbed Solution (IAS) [6] theories. The same idea has been applied by Stoeckli *et al.* [7] to the binary adsorption of vapours using the Dubinin-Radushkevich isotherm.

Recently, Chang and Talu [8] studied theoretically and experimentally the performance of adsorbed methane storage cylinders under discharge conditions. Their experimental adsorption isotherms are shown in figure 1a. The analysis of these data on the basis of the potential theory results in a characteristic curve of adsorption on the carbon which is depicted in figure 1b. The constructed curve is temperature-independent, this fact corroborates the applicability of the theory. Saturation pressure and adsorbed molar volume, V_A , were calculated according to expressions proposed by Ozawa *et al.* [9].

In many cases, the theory can be generalized if an affinity coefficient, β , is used as shifting factor to bring the characteristic curves of all gases on the same adsorbent into a single curve. This is assumed to apply to all the species under consideration here. Based on the author's past

experience on light hydrocarbon adsorption, the liquid molar volume of the adsorbate at the normal boiling point was used as the affinity coefficient.

Although the functional form of the characteristic curve is adsorbent dependent, expressing the logarithm of the adsorbed phase volume, W , as a truncated series development of the scaled adsorption potential, ϵ/β , provides good fitting of the experimental data [9]. A second-order polynomial is usually enough, as can be seen in figure 1b.

Multicomponent adsorption equilibrium prediction using the IAS method requires values of spreading pressure, Π , for adsorption of single gases. According to the potential theory, if this variable is scaled by V_A/β then it becomes a function of ϵ/β only, and can be computed from a single curve for all intervening adsorbates:

$$A\Pi_i^* \equiv (V_A/\beta)_i A\Pi_i = \int_{\epsilon_i/\beta_i}^{\infty} W(\epsilon^*) d\epsilon^* \quad (i = 1, \dots, N). \quad (1)$$

If the development of $\ln W$ as a power series of ϵ/β accurately describes the experimental data, then eq. (1) suggests that $A\Pi^*$ can also be expressed as a series development of the form

$$\ln(A\Pi_i^*/A\Pi_0^*) = \sum_{n=1}^{n=\infty} k_n (\epsilon_i/\beta_i)^n, \quad k_1 < 0, \quad (2)$$

where $A\Pi_0^*$ is the value of $A\Pi^*$ at saturation. As shown in figure 2a, a truncated second-order polynomial expansion describes very accurately the experimental data under consideration. Furthermore, the truncated series is easily invertible,

$$\epsilon_i/\beta_i = \frac{k_1}{2k_2} \left[\sqrt{1 + (4k_2/k_1^2) \ln(A\Pi_i^*/A\Pi_0^*)} - 1 \right], \quad (3)$$

which is critical in speeding up the computations.

Discharge phase.

The model employed for the discharge phase is an extension to multicomponent adsorption of a prior model [10,11] that has been proven experimentally to describe successfully the discharge dynamics of methane adsorptive storage cylinders [8].

In an on-board storage reservoir the discharge rate is controlled by vehicle power requirements. This process is slow enough for pressure to be uniform within the cylinder and for the inexistence of intraparticle gradients. Hence, an equilibrium model can be employed at the particle level. Moreover, the cylinder is considered sufficiently long so that the small axial temperature gradient induced by the front and rear faces has negligible impact on the overall dynamics. These assumptions drastically reduce the spatial dimensionality of the problem, since only the radial profile needs to be taken into account. The implication of these assumptions on model performance is discussed to further length elsewhere [10].

The differential material balance for component i on a cylindrical shell element of the reservoir located at radial position r , can be written as

$$\epsilon \frac{\partial c_i}{\partial t} + \rho_b \frac{\partial q_i}{\partial t} - \frac{\epsilon}{r} \frac{\partial}{\partial r} \left(r D_{e,i} c \frac{\partial y_i}{\partial r} \right) + y_i F = 0 \quad (i = 1, \dots, N), \quad (4)$$

where c_i and q_i are the concentrations in gas and adsorbed phase, respectively, y_i is the mole fraction in gas, ϵ and ρ_b are the porosity and bulk density of the carbon bed, and $F(t, r)$ is the local contribution to the overall molar discharge rate per unit reservoir volume.

These balances are subjected to boundary conditions

$$\partial y_i / \partial r = 0 \quad \text{for} \quad r = 0, R_0 \quad (i = 1, \dots, N), \quad (5)$$

where R_0 is the cylinder radius.

As discharge proceeds, the consumed heat of adsorption is only partially compensated by the wall thermal capacity and by the heat transferred from the outside air. As a result, a radial temperature profile develops in the medium, the major temperature drop occurring at the centre of the bed. Given that pressure remains uniform within the cylinder, the temperature profile induces radial concentration gradients in both adsorbed and gas phases. The latter tend to be lessened by bulk diffusion which is taken into account in the third term of eq. (4).

Accordingly, the local contribution F must also vary along r in order to ensure uniform pressure in the cylinder and to satisfy the following integral constraint over the cross section of the cylinder:

$$2\pi L \int_0^{R_0} F(t, r) r dr = Q, \quad (6)$$

where L is the cylinder length and Q is the imposed overall molar discharge rate.

The energy equation, applied to the same differential volume, yields

$$\left[\rho_b C_s + C_g (\varepsilon c + \rho_b q) \right] \frac{\partial T}{\partial t} - \varepsilon \frac{dP}{dt} + \rho_b \sum_i (-\Delta H)_i \frac{\partial q_i}{\partial t} - \frac{1}{r} \frac{\partial}{\partial r} \left(r \lambda_e \frac{\partial T}{\partial r} \right) = 0, \quad (7)$$

where C_s and C_g are the carbon and gas heat capacities, respectively, T is temperature, P is gas pressure, $-\Delta H_i$ is the heat of adsorption for species i , and λ_e is the effective thermal conductivity of the carbon bed.

Equation (7) is subjected to boundary conditions

$$\partial T / \partial r = 0 \quad \text{for } r = 0, \quad (8)$$

$$\left(1 + \frac{e_w}{2R_o} \right) e_w C_w \frac{\partial T}{\partial t} + \lambda_e \frac{\partial T}{\partial r} = \left(1 + \frac{e_w}{R_o} \right) h_w (T_{\text{amb}} - T) \quad \text{for } r = R_o. \quad (9)$$

The latter condition is an energy balance on the steel cylinder wall, it cannot be neglected due to its large thermal capacity. Symbols e_w , C_w and h_w represent wall properties (thickness, volumetric heat capacity, and natural convection heat transfer coefficient at the external surface, respectively) and T_{amb} is ambient temperature.

Charge phase.

Heat effects during the charge phase are neglected mainly because adequate solutions have been proposed to eliminate them. For example, at a refuelling station the gas can be cooled before charging the reservoir or an external NG recycle loop can remove the heat and reject it to the environment across an air-cooled heat exchanger [12]. Alternatively, fleet vehicles can be charged over a long period, e.g. overnight, which provides enough time to dissipate the heat of adsorption. The interested reader is referred to Mota [10] for rigorous modeling work on heat effects in the fast charge of ANG storage cylinders.

According to these assumptions, a lumped-based model can be adopted for the charge phase. At the end of the discharge, the residual amount of each component left in storage per unit reservoir volume is computed from

$$S_i = (2/R_o) \int_0^{R_o} (\varepsilon c_i + \rho_b q_i) r dr \quad \text{at depletion} \quad (i = 1, \dots, N). \quad (10)$$

Then, the following set of lumped material balances is solved in order to compute the new discharge initial conditions:

$$\varepsilon c_i + \rho_b q_i = S_i + z_i F_c \quad \text{with } P = P_{\text{charge}} \text{ and } T = T_{\text{amb}} \quad (i = 1, \dots, N), \quad (11)$$

where F_c is the amount of gas admitted to the cylinder during charge and z_i is its mole fraction composition. F_c is an unknown which is computed along with the new initial discharge conditions.

RESULTS AND DISCUSSION

Unfortunately, due to lack of space most of the paper has been spent describing the theoretical model, leaving room for a limited amount of results. The discharge phase model is validated for single-gas adsorption by comparison with the experimental temperature history in an adsorbed methane cylinder during discharge. As shown in figure 2b, model results are in close agreement with the experimental data.

Multicomponent discharge dynamics is summarized in figures 3a and 3b. It is a complex function of the adsorption potential of each component and its mole fraction in the charge gas. Depletion pressure is 1.4 atm while charge pressure is 35 atm. The discharge flow rate considered, 6.7 l/min, produces a methane discharge duration of about 4 hours under non-isothermal conditions. Table 1 lists the values of the main parameters employed in the numerical simulations. The gas composition considered in this study is given in table 2, it characterizes the NG from the Hassi R'Mel well supplying Portugal.

The net deliverable capacity is measured in terms of dynamic efficiency, which for component i is defined as

$$\eta_i = \frac{\text{amount of species } i \text{ delivered under dynamic conditions}}{(\text{amount of pure methane delivered isothermally}) \cdot z_i}, \quad (12)$$

where z_i is its mole fraction in the charge gas (table 2). This way, the η values converge to a common point at the cyclic steady state (figure 3a). The dynamic efficiency decreases gradually with the number of cycles to the cyclic steady-state value, although it attains a maximum at intermediate cycles for the higher hydrocarbons if their mole fractions in the charge gas are high enough. Until steadiness is reached, the total hydrocarbon capacity loss ($C_1 - C_5$) depends linearly on the logarithm of the number of cycles. This is agreement with the experimental observations of Golovoy and Blais [13] for 100 cycles of operation of an ANG cylinder.

The temperature and mole fractions shown in figure 3b are lumped values obtained from averaging the variable over the cross section of the cylinder. The same figure shows that the discharge duration is reduced as the number of cycles is increased since the micropore volume is gradually occupied by the higher hydrocarbons which tend to remain adsorbed at depletion pressure. The temperature history is approximately linear, because the discharge is carried out at constant molar rate, and is nearly insensitive to the cycle number.

CONCLUSIONS

A detailed mathematical model has been developed in order to study the impact of NG composition on cycling efficiency of ANG reservoirs. Although the model has been applied to a single NG, other gas compositions should produce the same qualitative behaviour. The results emphasize the need to identify and evaluate economical means of removing the contaminants from the gas stream before charge. The solution could be either a gas clean-up system installed at the refueling station [4,12] or a guard bed placed in front of the on-board storage reservoir [14].

ACKNOWLEDGEMENTS

Financial support received from PRAXIS XXI (PCEX/C/QUI/109/96) and from FLAD is gratefully acknowledged.

REFERENCES

1. N. D. Parkyns and D. F. Quinn, In *Porosity in Carbons* (Edited by J. Patrick), pp. 291–325. Edward Arnold, London (1995).
2. O. Talu, Proceedings 4th International Conference on Fundamentals of Adsorption, Kyoto, Japan, pp. 655–662 (1993).
3. T. L. Cook, C. Komodromos, D. F. Quinn and S. Ragan, In *Carbon Materials for Advanced Technologies* (Edited by T. Burchell). Elsevier, in press.
4. M. Sejnoha, R. Chahine, W. Yaïci, and T. K. Bose, Paper presented at AIChE Meeting, San Francisco (1994).
5. S. Brunauer, *The adsorption of gases and vapours*. Oxford University Press, Princeton (1945).
6. A. L. Myers and J. M. Prausnitz, *AIChE J.* **11**, 121–127 (1965).
7. F. Stoeckli, D. Wintgens, A. Lavanchy, and M. Stöckli, *Adsorp. Sci. Technol.* **15**, 677–683 (1997).
8. K. J. Chang and O. Talu, *Appl. Thermal Engng* **16**, 359–374 (1996).
9. S. Ozawa, S. Kusumi, and Y. Ogino, *J. Coll. Int. Sci.* **56**, 83–91 (1976).
10. J. P. B. Mota, *Modélisation des transferts couplés en milieux poreux*, Ph.D. Thesis, Institut National Polytechnique de Lorraine, France (1995).
11. J. P. B. Mota, A. E. Rodrigues, E. Saadjan, and D. Tondeur, *Carbon* **35**, 1259–1270 (1997).
12. W. E. BeVier, J. T. Mullhaupt, F. Notaro, I. C. Lewis, and R. E. Coleman, Paper presented at 1989 SAE Future Transportation Technology Conference and Exposition, Vancouver (1989).
13. A. Golovoy and E. J. Blais, In *Alternate Fuels for Special Ignition Engines*, p. 47. SP-559 SAE Conference Proceedings, Warrendale, PA 15096 (1983).
14. T. L. Cook, C. Komodromos, D. F. Quinn, and S. Ragan, Paper presented at Windsor Workshop on Alternative Fuels, Toronto (1996).

| | |
|---|--|
| $C_g = 355.5 \text{ atm}\cdot\text{cm}^3\cdot\text{mol}^{-1}\cdot\text{K}^{-1}$ | $P_{\text{depletion}} = 1.4 \text{ atm}$ |
| $C_s = 10.38 \text{ atm}\cdot\text{cm}^3\cdot\text{g}^{-1}\cdot\text{K}^{-1}$ | $R_o = 10 \text{ cm}$ |
| $C_w = 38.68 \text{ atm}\cdot\text{K}^{-1}$ | $T_{\text{amb}} = 20^\circ\text{C}$ |
| $e_w = 0.55 \text{ cm}$ | $\varepsilon = 0.5$ |
| $L = 74 \text{ cm}$ | $\lambda_e = 1.26 \text{ atm}\cdot\text{cm}^2\cdot\text{min}^{-1}\cdot\text{K}^{-1}$ |
| $P_{\text{charge}} = 35 \text{ atm}$ | $\rho_b = 0.481 \text{ g}\cdot\text{cm}^{-3}$ |

Table 1: Data employed in numerical simulations.

| Component | CH ₄ | C ₂ H ₆ | C ₃ H ₈ | C ₄ H ₁₀ | C ₅ H ₁₂ | N ₂ |
|---------------|-----------------|-------------------------------|-------------------------------|--------------------------------|--------------------------------|----------------|
| Mole fraction | 0.840 | 0.076 | 0.020 | 0.007 | 0.003 | 0.054 |

Table 2: Composition of natural gas from the Hassi R'Mel well (Algeria) supplying Portugal.

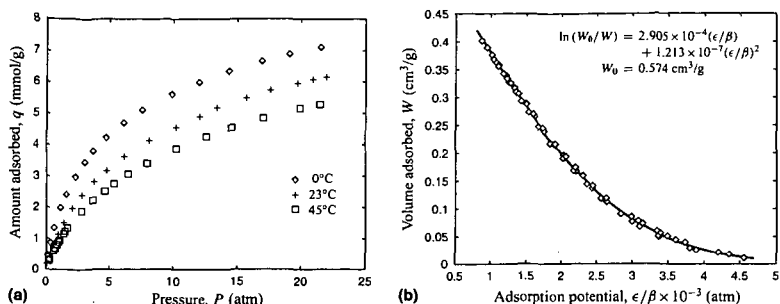


Figure 1: Methane adsorption on an activated carbon. (a) Experimental isotherms reported by Chang and Talu [8]; (b) corresponding characteristic curve of adsorption plotted according to the potential theory.

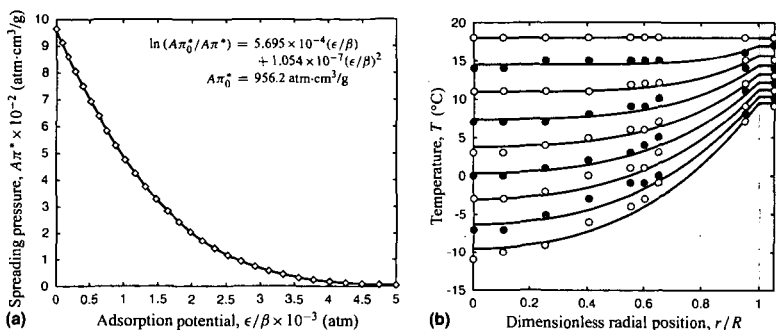


Figure 2: (a) Spreading pressure as a function of scaled adsorption potential for the carbon under study. (b) Radial temperature profiles in an adsorbed methane cylinder as a function of time during discharge. Comparison between experiments [8] (points) and model predictions (lines). Sampling interval = 20 min; $L = 74$ cm, $R = 10$ cm, carbon weight = 15.78 kg, discharge rate = 6.7 l/min, charge pressure = 21 atm, depletion pressure = 1.6 atm.

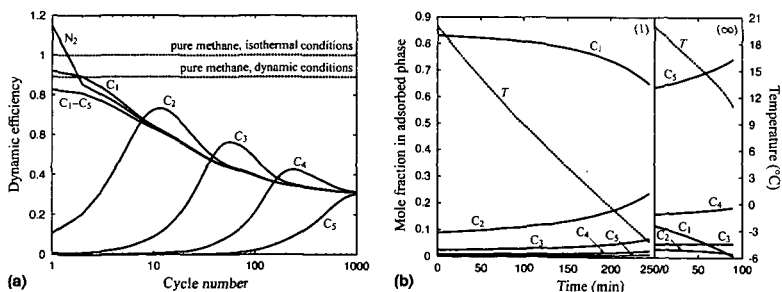


Figure 3: (a) Dynamic efficiency, η_i , as a function of cycle number for an ANG cylinder. (b) Histories of temperature and mole fractions in adsorbed phase for (1) first and (∞) cyclic steady-state discharges in an ANG cylinder.

Block Copolymer Electrolytic Membranes for All Solid-state Rechargeable Lithium Batteries

P.P. Soo, B.Y. Huang, D.R. Sadoway, and A.M. Mayes

Department of Materials Science and Engineering
Massachusetts Institute of Technology
Cambridge, MA 02139-4307

For nearly 20 years, poly(ethylene oxide)-based materials have been researched for use as electrolytes in solid-state rechargeable lithium batteries. Technical obstacles to commercial viability derive from the inability to satisfy simultaneously the electrical and mechanical performance requirements -- high ionic conductivity along with resistance to flow. Here we report the synthesis of poly(lauryl methacrylate)-*b*-poly(oligo(oxyethylene) methacrylate) block copolymer electrolytes in which *both* components have glass-transition temperatures well below room temperature. Microphase separation of the polymer blocks imparts the dimensional stability necessary for thin-film, solid-state battery applications. Electrolytes prepared with these materials display conductivities near 10^{-5} S/cm and are electrochemically stable over a very wide potential window. Cycle testing in prototype batteries demonstrate excellent cyclability and capacity retention.

The lithium solid polymer electrolyte (SPE) battery is arguably the most attractive technology for rechargeable electric power sources, boasting the highest predicted energy density, the fewest environmental, safety and health hazards, low projected materials and processing costs, and greatest freedom in battery configuration. Poly(ethylene oxide) (PEO)-based materials are favored candidates for polymer electrolytes.¹ Although PEO-salt complexes are highly conductive at elevated temperatures ($>10^{-4}$ S cm^{-1} at 70°C), their conductivities drop precipitously at temperatures below the melting point ($T_m = 65^\circ\text{C}$ for PEO). Common strategies to improve conductivity involve modifying the molecular architecture of PEO to suppress crystallization.² While such approaches have resulted in materials whose room-temperature conductivity exceeds 10^{-5} S cm^{-1} , their liquid-like nature typically requires a separator or supporting matrix to allow them to be deployed in a battery configuration. Gel polymer electrolytes combine high ionic conductivity with dimensional stability by infusing a liquid electrolyte into a nonconducting polymer network.^{3,4} However, these systems require suitable packaging of the volatile organics.

Block copolymers offer a novel means to achieve both high ionic conductivity and dimensional stability. These materials consist of two chemically dissimilar polymers covalently bonded end-to-end. At low temperatures or in the absence of solvent, a net repulsion between the polymer blocks induces their local segregation into periodically spaced nanoscale domains. This "microphase separation" event, analogous to crystallization, confers solid-like mechanical properties to the material at macroscopic scales, *even when both polymer blocks are above their respective glass transition temperatures, T_g .*^{5,6} At local scales, however, when $T > T_g$ the mobility

of the polymer chains remains high, even comparable to that in the disordered state.⁷ By choosing an amorphous PEO-based polymer as one block component, continuous ion conducting pathways can be formed in the material upon microphase separation.

For this study, diblock copolymers consisting of a poly(lauryl methacrylate) (PLMA) block ($T_g \sim -40^\circ\text{C}$) and a poly(oligo(oxyethylene) methacrylate) (POEM) block ($T_g \sim -65^\circ\text{C}$) were prepared. POEM employs a PEO side chain with a length of approximately 9 [EO] units, sufficiently low that crystallization does not occur.⁸ The block copolymers were anionically synthesized at -78°C by the sequential addition of lauryl methacrylate (Aldrich) and OEM macromonomer (Polysciences) to a diphenylmethyl potassium initiator in tetrahydrofuran. Upon termination of the reaction with degassed methanol, the copolymer solution was concentrated on a rotary evaporator, precipitated in hexane, and finally centrifuged to isolate the colorless polymer. For comparison purposes, POEM homopolymer was also anionically synthesized following a similar procedure. Molecular weights and compositional characteristics of the polymers are given in Table 1.

Rheological characterization of this system was performed using a Rheometrics ARES rheometer with a parallel plate fixture. The polymer was pressed to a gap width below 1 mm and a stable normal force of approximately 1000 g. The complex shear modulus, $G = G' + iG''$, was then measured as a function of frequency by dynamically shearing the polymer at a fixed strain of 1.5% over the frequency range 0.1 to 250 rad s^{-1} at temperatures from 25°C to 90°C .

Table 1. Molecular weight characteristics of synthesized POEM-based polymers.

| | Composition (v:v) | Molecular weight (g/mol) | Polydispersity (M_w/M_n) |
|----------------------|-------------------|--------------------------|------------------------------|
| PLMA- <i>b</i> -POEM | 47:53 | 64,700 | 1.1 |
| PLMA- <i>b</i> -POEM | 32:68 | 77,800 | 1.2 |
| PLMA- <i>b</i> -POEM | 23:77 | 62,900 | 1.2 |
| POEM | — | 100,000 | 1.3 |

The rheological behavior of block copolymer varies dramatically depending on whether the material resides in the ordered or disordered state. In the PLMA-*b*-POEM block copolymers, the storage modulus reaches a plateau value at low frequencies while the loss modulus assumes a limiting power law in which $G'' \sim \omega^{0.5}$. This low-frequency scaling behavior is characteristic of a microphase-separated system,⁵ and verifies its solid-like nature. Even after blending with significant amounts (23 wt%) of poly(ethylene glycol) dimethyl ether (PEGDME, Polysciences, $M=430 \text{ g mol}^{-1}$), the low-frequency scaling behavior is preserved, indicating that these short PEO chains stay confined to the POEM domains of the copolymer morphology. The formation of nanoscale domains was further verified by direct imaging with transmission electron microscopy. By contrast, the POEM homopolymer exhibits the low frequency scaling behavior $G'' \sim \omega$, indicative of a polymer in its molten state.

Conductivity measurements were performed on the POEM homopolymer and the PLMA-*b*-POEM block copolymers at fixed salt concentration $[\text{EO}]:\text{Li}^+ = 20:1$. Specimens for

conductivity measurements were initially dried in a vacuum oven at 70°C for 24 hours. LiCF_3SO_3 (lithium triflate) was dried *in vacuo* at 130°C for 24 hours. The materials were then transferred to an inert atmosphere, dissolved in dry THF, and solution cast on a glass die. The polymer/salt complex was then annealed *in vacuo* for 48 hours at 70°C. Under dry nitrogen, the polymer electrolyte was loaded between a pair of blocking electrodes made of type 316 stainless steel, pressed to a thickness of 250 μm , and annealed *in situ* at 70°C for 24 hours. Over the temperature interval spanning -20°C to 90°C electrical conductivity was measured by impedance spectroscopy using a Solartron 1260 Impedance Gain/Phase Analyzer.

Figure 1 illustrates that at room temperature the doped 32:68 PLMA-*b*-POEM block copolymer displays ionic conductivities similar to that of pure POEM. As expected, increasing the POEM content of the copolymer had the effect of increasing conductivity. Significantly higher conductivities were achieved by blending the block copolymer with 23 wt% PEGDME, resulting in σ values exceeding $10^{-5} \text{ S cm}^{-1}$ at room temperature.

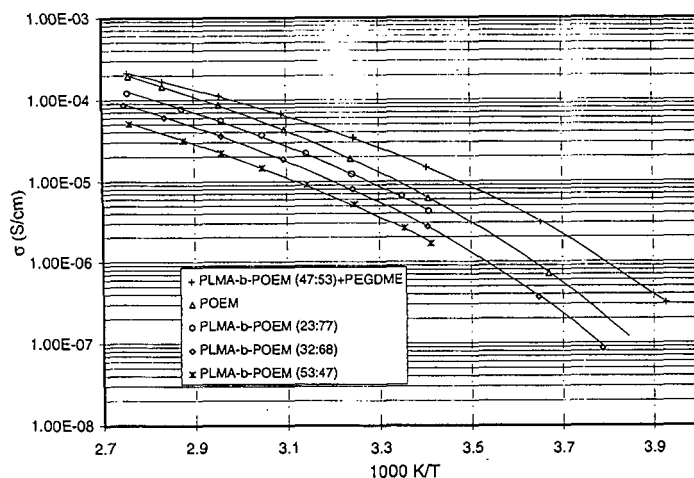


Figure 1. Compositional dependence of conductivity in PLMA-*b*-POEM diblock copolymers doped with LiCF_3SO_3 ($[\text{EO}]:[\text{Li}^+] = 20:1$).

Cyclic voltammetry was performed on a block copolymer electrolyte (BCE) composed of 87 wt% 32:68 PLMA-*b*-POEM and 23 wt% PEGDME at a salt concentration of $[\text{EO}]:\text{LiCF}_3\text{SO}_3 = 20:1$ to investigate the range of electrochemical stability of the material. Films were prepared under an inert atmosphere by casting the BCE onto lithium foil from dry THF solution. The resulting films were placed under vacuum at room temperature overnight to remove excess solvent. The BCE was sandwiched between a counter electrode of lithium and a working electrode of aluminum, with a film thickness of approximately 150 μm . A lithium reference electrode was extruded into the cell through the side and positioned near the working electrode. Using a 1286 Solartron Electrochemical Interface, potential was scanned from +2.0 to +5.0 V vs. Li/Li^+ at a sweep rate of 0.5 mV s^{-1} . Current levels below 0.6 $\mu\text{A cm}^{-2}$ were measured between

2.0 and 5.0 V, indicating that the material is electrochemically stable over this voltage interval, which brackets that used in commercial lithium-ion batteries.

The composite cathode of the solid-state battery was prepared by casting a suspension of a mixture of $\text{LiAl}_{0.25}\text{Mn}_{0.75}\text{O}_2$ (45 wt%), carbon black (7 wt%), graphite (6 wt%), and BCE (42%) in dry THF solution onto an Al foil heated to 60°C. Evaporation of the THF produced a cathode film ~150 μm in thickness. The resulting cathode film was placed under vacuum for 48 hours at 60°C to remove any moisture present. This material was cut into square electrodes measuring 1 cm on a side. The $\text{LiAl}_{0.25}\text{Mn}_{0.75}\text{O}_2$ powder, which serves as the intercalation compound in the cathode, was produced by co-precipitation of hydroxides followed by firing in air at 945°C. Details of oxide synthesis and characterization are published elsewhere¹². The $\text{Li/BCE/LiAl}_{0.25}\text{Mn}_{0.75}\text{O}_2$ solid state battery was then fabricated by laminating lithium metal, BCE, and the composite cathode film containing $\text{LiAl}_{0.25}\text{Mn}_{0.75}\text{O}_2$ together in an argon-filled glove box. Cycle testing was conducted between 2.0 and 4.4 V with a MACCOR Series 4000 Automated Test System at a current density of 0.05 mA cm^{-2} .

Room temperature cycle testing of the $\text{Li/BCE/LiAl}_{0.25}\text{Mn}_{0.75}\text{O}_2\text{-C-BCE}$ cell is shown in figure 2. Fig. 2(a) shows the first cycle which begins with lithium removal from $\text{LiAl}_{0.25}\text{Mn}_{0.75}\text{O}_2$ over the voltage range spanning 3.0 to 4.4 V. A single charging plateau at ~3.6 V is observed, and the initial charging capacity was found to be 136 mAh/g . The first discharge exhibited a capacity of 108 mAh/g and featured the emergence of two voltage steps, one at ~4.0 V and another at ~3.0 V, indicating lithium intercalation at two distinct sites. This behavior is characteristic of the spinel phase $\text{Li}_x\text{Mn}_2\text{O}_4$ for which it is reported that the 3.0 V plateau corresponds to lithium insertion into octahedral sites and the 4.0 V plateau corresponds to lithium

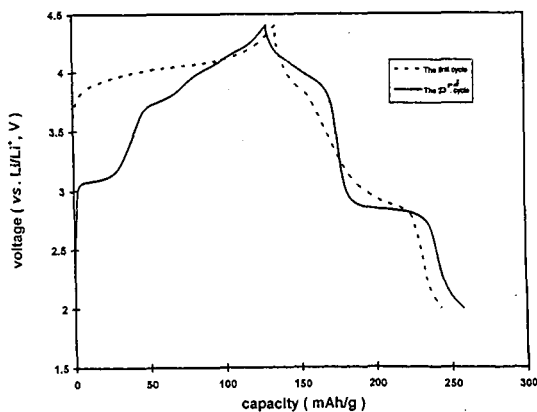


Figure 2. Charge/discharge cycling of the $\text{LiAl}_{0.25}\text{Mn}_{0.75}\text{O}_2\text{/BCE/Li}$ cell with a current density of 0.05 mA/cm^2 cycled between 2.0 and 4.4 V. (a) first cycle; (b) 23rd cycle.

insertion into tetrahedral sites.¹³ After further cycling, the voltage steps became more distinct as can be seen in Fig. 2(b), which shows the 23rd cycle. After ~12 cycles, the intercalation oxide reached its optimal capacity of ~125 mAh/g . This result indicates that the cell has demonstrated

good cyclability when cycled over both 4.0 V and 3.0 V plateaus. Further discussion of the oxide characteristics is reported in a separate manuscript.¹²

Although several groups had previously investigated PEO-based block copolymers as candidate electrolytes for rechargeable Li batteries,⁹⁻¹¹ the conductivities and temperature window of operation of those materials were not optimized because one block component either crystallized or underwent a glass transition above room temperature. Here we demonstrate that by joining two non-crystallizing polymers with T_g s well below 0°C, a dimensionally stable electrolyte can be prepared with conductivities near that of the POEM homopolymer. We expect that moving to block components with higher room temperature conductivities and/or lower glass transitions should further improve both the ambient temperature performance and temperature window of operation.

Acknowledgments

This project has been funded by Furukawa Electric Co., Ltd. and by the INEEL University Research Consortium. We are thankful to Y.-I. Jang and Y.M. Chiang for providing cathode materials. The technical assistance of M.J. Fasolka, M.E. King, M. Nakajima, and Y.-I. Jang is also gratefully acknowledged as are helpful discussions with Professors G. Ceder and Y.-M. Chiang.

References

1. Armand, M.B. *Polymer Electrolyte Reviews* **1**, Ch. 1 (1987).
2. Gray, F.M. *Solid Polymer Electrolytes: Fundamentals and Technological Applications*, Ch. 6 (VCH Publishers, New York, 1991).
3. Scrosati, B. (ed.) *Applications of Electroactive Polymers* (Chapman and Hall, London, 1993).
4. Abraham, K.M. and Jiang, Z. *J. Electrochem. Soc.* **144**, 1136 (1997).
5. Bates, F.S. *Macromolecules* **17**, 2607 (1984); Rosedale, J.H. and Bates, F.S. *Macromolecules* **23**, 2329 (1990).
6. Russell, T.P., Karis, T.E., Gallot, Y. and Mayes, A.M. *Nature* **368**, 729 (1994).
7. Ehlich, D., Takenaka, M. and Hashimoto, T. *Macromolecules* **26**, 492 (1995).
8. Yan, F., Dejardin, P., Frere, Y. and Gramain, P. *Makromol. Chem.* **191**, 1197 (1990).
9. Gray, F.M., MacCallum, J.R., Giles, J.M., and Vincent, C.A., *Macromolecules* **21**, 392 (1988).
10. Khan, I.M., Fish, D., Delaviz, Y. and Smid, J. *Makromol. Chem.* **190**, 1069 (1989).
11. Lobitz, P., Reiche, A. and Fullbier, H. *J. Power Sources* **43**, 467 (1993).
12. Y.I. Jang, B.Y. Huang, Y.M. Chiang, and D.R. Sadoway, *J. Electrochem. Soc.*, in press.
13. M.M. Thackeray, W.I.F. David, P.G. Bruce, and J.B. Goodenough, *Mat. Res. Bull.*, **18**, 461 (1983).

TIME-TEMPERATURE HISTORIES OF BITUMINOUS COAL PARTICLES IN A DROP-TUBE REACTOR

Jonathan P. Mathews, Patrick G. Hatcher, Semih Eser, Peter M. Walsh[†], and Alan W. Scaroni
Fuel Science Program and Energy Institute, 211 CUL, The Pennsylvania State University,
University Park, PA 16802

[†]Sandia National Laboratory, PO Box 969, Livermore, CA 94551

Keywords: drop-tube, particle size and shape.

Abstract

A device often used to simulate pulverized coal combustion conditions is the drop-tube reactor. It can adequately simulate residence times, heating rates, temperatures and flow conditions. Nevertheless, derived Arrhenius pre-exponential factors for devolatilization studies can span several orders of magnitude (1), probable due to difficulties in repeating time-temperature histories for different coals (2). CFD modeling of a simple drop-tube reactor incorporating coal particles as a second phase permitted time-temperature histories to be obtained for narrow size cuts for two bituminous vitrinites. Despite a narrow particle size distribution and the rank of the vitrinites being the same, significant differences were obtained in the time-temperature histories, among the size cut and between the vitrinite samples. Furthermore, the common and simplifying assumption of spherical particles for coal was found to underestimate the characteristic heating time by 22%, in comparison to the more reasonable "house brick" particle shape obtained from microscopic observations with video capture and computational analysis.

EXPERIMENTAL

The vitrain samples were collected from *Sigillaria* (a type of Lycopod) tree remains in the roofs of coal mines in the Upper Freeport (UF) and Lewiston-Stockton (LS) coal seams. The samples were first crushed in an adjustable plate mill to reduce the topsize to approximately 2mm, then comminuted in a Holmes 501XLS pulverizer. Particle size separation was achieved by wet sieving. For shape analysis, polished pellets were prepared using a modified ASTM method. Size and shape analyses were performed using a digital image analysis system (IMAGIST, PGT, Princeton, NJ), in conjunction with a Nikon Microphot-FXA microscope and a workstation. The particle size distributions were determined with a Malvern laser light scattering instrument.

The drop-tube reactor consists of a single zone furnace operated at a maximum temperature of 1,400 °C, and is similar to previously described units (3). The reactor core is a high-purity alumina refractory tube, positioned vertically. The preheater temperature was 830 °C, and secondary nitrogen entered the top of the preheater from two inlets. The injector is water-cooled and also has a ceramic sheath for additional thermal protection. Coal is fed by an Acrison GMC-60 feeder at a rate of 0.33 g/min and is assumed to be entrained by the primary nitrogen. The tip of the injector is positioned level with the bottom of a mullite flow-straightener. Secondary nitrogen exited the flow-straightener with the primary nitrogen. The particle residence times are determined by the particle size, shape and the temperature and fluid-flow through the reactor.

FluentTM, a commercially available computational fluid dynamics (CFD) code, was used to model the gas and particulate flows within the furnace. The drop-tube was modeled in one dimension using symmetry around the centerline axis with a non-uniform grid consisting of 300 cells in length and 22 cells in radius. This grid covers the tip of the injector to the outlet of the ceramic reactor. The wall of the computational grid was arbitrarily split into eight sections and the temperature was assigned based on the average value (for that wall section) obtained experimentally using a suction pyrometer. The temperature of the wall was initially set to 50 °C above the average gas temperature for that section, this value being obtained from the difference between the reactor temperature (from the internal reactor thermocouple) and the gas temperature in the center of the hot zone of the reactor. Refinements were made to the wall temperatures until good agreement < 50 °C was obtained between the CFD and experimentally-determined temperature profile.

RESULTS

Particles were introduced into the CFD calculation as a second phase assuming perfectly spherical particles with densities of 1.4 g/cm³. Five particles were used to span the radius of the injector. The particles fall faster than the fluid; and hence are influenced by the particle diameter (mass is proportional to the radius³, but drag is proportional to the radius²), and changes in mass, volume and shape (which influences drag). A very narrow size cut of vitrinite (as measured by laser light scattering) was achieved by wet sieving. The difference between the D_v[0.1] and the D_v[0.9] (the volumetric weighted particle diameters such that 10 % and 90 % of the volume of the particles is in particles of greater diameters, respectively) was 66 and 53 μm for the Upper Freeport and Lewiston-Stockton vitrinites, respectively. The mean volumetric weighted particle diameters for the 200x400 US Standard Sieve cuts were 65 and 61 μm, for the Upper Freeport and Lewiston-Stockton vitrinites, respectively. Thus, a narrow distribution of time-temperature histories should be obtained for the vitrinites. However, this was not the case. The particle temperatures and residence times for the two extreme cases; the largest particle falling close to the centerline (particle 1) and the smallest particle falling closer to the wall (particle 5), are shown in Table 1. Cold flow experiments and initial CFD modeling indicated that the coal particles would fall in a narrow stream. Some radial growth in the coal stream occurs due to the expansion of the cold primary

nitrogen. However, under rapid-heating conditions, the coal particles fell as a cloud, presumably because of the "jet release" phenomenon (4) altering the particle trajectory. To better represent the particle trajectories a slight axial velocity was imposed on the particles. Particle 5 temperatures are higher at all sampling locations due to the closer proximity of the hot reactor wall (higher local gas temperature). At the 33 cm sampling location (distance from the injector) all the particles are close to the hot zone temperature (wall temperature of 1,400 °C), however, there are significant temperature differences between particles 1 and 5 at distances closer to the injector. The maximum observed difference in temperature between particles 1 and 5 is 320 K at the 23 cm sampling location for the UF case. These differences are, however, the extreme cases; visual observation indicated that the majority of the particles fell closer to the centerline than to the outer radius of the reactor. However, it is plausible that some of the collected particles can have quite different time-temperature histories despite the initially narrow particle size distribution and a drop-tube configuration designed for uniform time-temperature histories. Changes in particle size, mass and shape also influence the drag on the particle and hence the time-temperature history. The reactor temperature profile and morphological changes occurring to the LS 200x400 cut are shown in Figure 1. Significant swelling occurs for both vitrinites (2.5 and 1.8 times the mean particle diameters for the UF and LS vitrinites, respectively). This difference in swelling and a slight difference in mass loss resulted in slightly different time-temperature histories for the two vitrinites (Table 1).

Heat transfer and particle fluid-flow calculations often assume spherical particles. This is a reasonable assumption for both cases at the 33 cm location where the particles are almost exclusively cenospheric, but is a poor assumption for the initial vitrinite sample and the subsequent chars until the 23 cm sampling location (Figure 1). The silhouette of particles from the UF 200x400 cut is shown in Figure 2. Clearly there was a range of particle shapes; however, a sphere was not a good general shape representation. From >500 particle measurements the average aspect ratios are 1.7 for both vitrinite 200x400 cuts. This indicates that for a rectangular silhouette, the breadth is the length divided by 1.7. From SEM micrographs it was determined that to a first approximation, the depth could be assumed to be equal to the breadth. Thus, a square ended rectangular brick of length a and width and breadth of $a/1.7$ is a superior general shape descriptor than a sphere for these bituminous rank vitrinites. This shape descriptor has implications for both the particle residence time and the particle temperature. With a rectangular brick shape, the particle velocity is influenced by the particle orientation in the fluid. In comparison to a sphere of the same volume, the particle falling in the equilibrium position (oriented largest face down) has a similar coefficient of drag to that of a sphere (determined from terminal velocity measurements in an oil of known viscosity using square-ended bricks and spherical playdoh particles of the same mass). In contrast, the end-on orientation has a lower coefficient of drag and hence falls at a higher terminal velocity.

The non-spherical shape of coal particles has implications for commonly employed heating models. Deviation from spherical particles is reported to be responsible for the underestimation of radiative heating rate models (for 106-125 μm particles) by as much as 50% (5). In contrast, spherical carbon particles give a reasonable correlation between observed (optical pyrometry) and calculated heating rates. Combined convective and radiative models were also found to underestimate the heating rate for the same particles. Although there are uncertainties in many of the coal-related parameters and the effects of particle dispersion within the reactor in these calculations, the shape factors may also contribute significantly to the difference. Assuming that a vitrinite particle is adequately represented by a square ended rectangular brick, then equating the diameter of a sphere (d_p), of the same volume as the brick, to the length (a) yields equation 1.

$$Vol = \frac{a^3}{1.7^2} = \pi \frac{d_p^3}{6} \quad \text{or} \quad d_p = 0.87a \quad (1)$$

Sphericity (ϕ_s), the ratio of the surface area of a sphere to the surface area of the particle (of the same volume), yields equation 2, and substituting for d_p in equation 2 yields $\phi_s = 0.78$. Incorporating this term in the commonly employed convective heating calculation yields equation 3, where Nu is the Nusselt number, λ is the thermal conductivity of the gas and T_g and T_p are the temperature of the gas and particle, respectively.

$$\phi_s = \frac{\pi d_p^2}{\left(\frac{2}{1.7^2} + \frac{4}{1.7}\right) a^2} \quad (2) \quad \frac{dQ}{dt} = \frac{Nu\lambda}{d_p} (T_g - T_p) \pi \frac{d_p^2}{\phi_s} \quad (3)$$

The sphericity term is in essence a corrective term for non-spherical particles. Incorporation of the energy gradient terms in equation 4 yields equation 5, where C_p is the specific heat of the particle, and ρ_p is the particle density.

$$\frac{\pi d_p^3}{6} \rho_p C_p \frac{dT_p}{dt} = \frac{Nu\lambda}{d_p} (T_g - T_p) \pi \frac{d_p^2}{\phi_s} \quad (4)$$

Rearranging equation 4 yields equation 5 and defining the characteristic heating time as τ yields equation 6.

$$\frac{dT_p}{dt} = \frac{6Nu\lambda}{d_p^2 \phi_s \rho_p C_p} (T_s - T_p) \quad (5)$$

$$\tau = \frac{d_p^2 \phi_s \rho_p C_p}{6Nu\lambda} \quad (6)$$

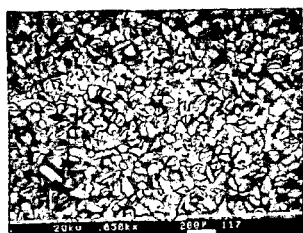
As $\phi_s=0.78$ and assuming $Nu=2$, the τ for the rectangular block is 22% greater than for the sphere. The $Nu=2$ assumption is valid for spheres in quiescent gas. A more accurate comparison would incorporate the influence of the square ended rectangular block geometry on the Nusselt number. Constant sphericity values of 0.73 for pulverized coal dusts and have been reported (6-7) based on microscopic and sieve analyses. A sphericity of 0.38 is also reported for fusain fibers (6), unfortunately the coal classification was not reported. A consistent shape factor (using surface areas as determined by liquid permeability and sieve sizes) has also been reported for various size cuts (11 fractions between 16 to 325 US mesh), although particle shape was found to be rank dependent (9). Aspect ratios of 1.39 to 1.55 have been determined for Pittsburgh seam coal dusts (less than 75 μm diameter) generated within the mine and by a variety of pulverizers (10). The sphericity factor reported here is consistent with some of the early work on coals (9).

CONCLUSIONS

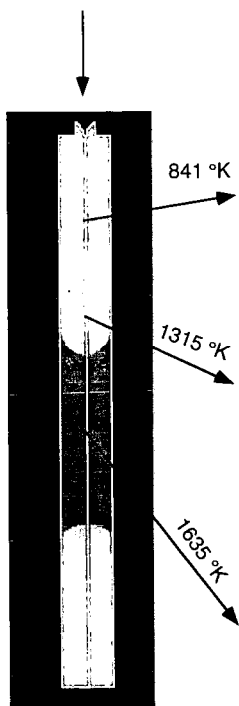
Significant variations were found in time-temperature histories between two narrow cuts of bituminous vitrinites in a drop-tube reactor. This was partially due to the influence of volatiles release, which alters the particle trajectory, but also to differences in mass loss and degree of swelling. The single particle shape descriptor of a sphere was significantly improved upon by using a square-ended rectangular brick. This shape can account for a 22% decrease in the characteristic heating time. The shape influences the drag and hence the particle residence-time.

REFERENCES

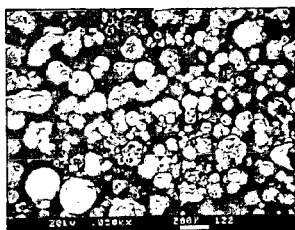
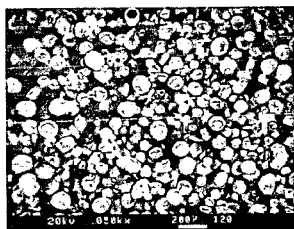
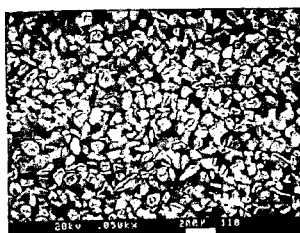
1. Smith, I. W., Nineteenth Symposium (Int) on Combustion, The Combustion Institute, Haifa, Israel, 1982, 1045.
2. Flaxman, R. J., and Hallett, L. H., *Fuel*, 1987, **66**, (5), 607.
3. Artos, V., and Scaroni, A. W., *Fuel*, 1993, **72**, (7), 927.
4. Grey, V. R., *Fuel*, 1988, **67**, (9), 1298.
5. Maloney, D. J., Monazam, E. R., Woodruff, S. D. and Lawson, L. O., *Combustion and Flame*, 1991, **84**, (1), 210.
6. Sakiadis, B. C., Fluid and Particle Mechanics, in Perry's Chemical Engineer's Handbook, Perry, R. G. and Green, D., 1984, McGraw, New York, Chapter 5.
7. Carman, P. C., *Trans. Inst. Chem. Eng. (London)*, 1937, **15**, 150.
8. Heywood, H., *I. Mech E.*, 1933, **125**, 383.
9. Austin, L. G., Gardner, R. P., and Walker, P. L., *Fuel*, 1963, **42**, (2), 319.
10. Li, J., Size shape and chemical characteristics of mining generated and laboratory-generated coal dusts, 1990, MS Thesis, The Pennsylvania State University.



SEM Micrograph of
wet-sieved coal



Drop-tube Reactor
Temperature Profile



Char Morphology

Figure 1. Fluid Temperature Profile and Char Morphology Changes for the Lewiston-Stockton Vitrinite

Table 1. Particle Residence Times and Temperatures at Various Sampling Locations

| Distance from the injector / cm | Time / s | | | |
|------------------------------------|----------------|----------------|----------------|----------------|
| | Particle 1(UF) | Particle 5(UF) | Particle 1(LS) | Particle 5(LS) |
| 13 | 0.062 | 0.140 | 0.068 | 0.152 |
| 23 | 0.146 | 0.333 | 0.174 | 0.332 |
| 33 | 0.242 | 0.462 | 0.281 | 0.471 |
| Temperature / K | | | | |
| 13 | 645 | 938 | 726 | 956 |
| 23 | 1090 | 1410 | 1230 | 1400 |
| 33 | 1600 | 1640 | 1630 | 1640 |

Table 2. Numbered Particle Silhouette Data

| No. | Diam | Circ | E/R | A/R |
|-----|-------|------|------|------|
| 1 | 27.3 | 3.21 | 0.37 | 2.70 |
| 2 | 102.8 | 2.87 | 0.43 | 2.33 |
| 3 | 61.9 | 1.74 | 0.77 | 1.30 |
| 4 | 58.0 | 7.83 | 0.19 | 5.26 |
| 5 | 105.2 | 1.83 | 0.62 | 1.61 |
| 6 | 61.8 | 1.78 | 0.85 | 1.18 |
| 7 | 70.6 | 1.52 | 0.90 | 1.11 |
| 8 | 69.3 | 1.74 | 0.64 | 1.56 |
| 9 | 91.3 | 4.90 | 0.28 | 3.57 |
| 10 | 57.5 | 2.08 | 0.65 | 1.54 |
| 11 | 85.5 | 2.94 | 0.50 | 2.00 |
| 12 | 89.5 | 2.11 | 0.55 | 1.82 |
| 13 | 16.1 | 2.83 | 0.43 | 2.33 |
| 14 | 87.0 | 1.42 | 0.82 | 1.22 |
| 15 | 56.8 | 2.07 | 0.64 | 1.56 |

Diam is the particle diameter in μm , Circ is the circularity, E/R the elongation ratio, A/R the aspect ratio.

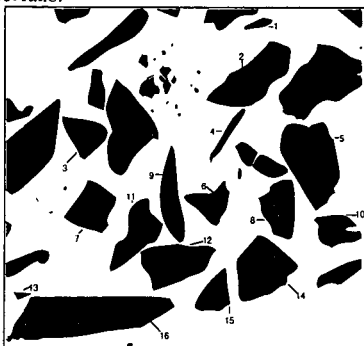


Figure 2. Silhouette of the 200x400 UF Vitrinite Cut

ALTERNATIVE SOLUTION BY ORTHOGONAL COLLOCATION IN THE REGENERATION SYSTEM

L. M. F. LONA BATISTA and R. MACIEL FILHO

Univer. Estadual de Campinas - Fac. Eng. Química - Dep. Processos Químicos
Campinas, SP, Brazil, CEP 13081-970 - CX postal 6066, email: liliane@feq.unicamp.br

KEYWORDS: Orthogonal Collocation, Regeneration System, Modelling and Simulation

1. INTRODUCTION

Orthogonal collocation (OC) methods have been used in many chemical engineering problems such as calculation of effectiveness factors, packed bed analyses and fluid flow problems. In Finlayson (1971), the equations governing a packed bed reactor with radial temperature and concentration gradients are solved using the OC method. The method is shown to be faster and more accurate than finite difference calculations.

In this work, an industrial catalytic cracking regeneration system was simulated. The model equations form a system of non linear integro differential equations. In Maciel Filho *et al.* (1996), the Runge Kutta (RK) method and Trapezoidal Rule are used to solve the model equations, but in this present work, OC method is adopted. Generally, integrals calculation by quadrature is not made simultaneously with differential and algebraic equation, but in this work, this is the case. So, a new methodology is proposed to solve the integrals, based on an approximation of quadrature formula. The simulation results obtained through OC and RK are compared with industrial data from Petrobrás (Brazilian Oil Company).

2. PROCESS DESCRIPTION

The diagram for the catalytic cracking industrial unit is depicted in Figure 1. Deactivated catalyst flows from catalytic cracking reactor (CCR) into regeneration system, composed by fluidized bed reactor (FBR) followed by riser (R) and freeboard (FR). The fluidized bed consists on jet and bubble bed zones. The jet region is idealised as a fully mixed zone, as can be seen in Maciel *et al.* (1996). In the riser exit, the solid flow is divided in such way that part of particle goes to freeboard and part returns to tank A, with solids collected by cyclones. A certain amount of catalyst present in vase A returns to bubble bed, and the rest is transported to the cracking reactor.

3. ORTHOGONAL COLLOCATION ON REGENERATION SYSTEM SIMULATION

First, the riser and freeboard are simulated, and latter, the fluidized bed reactor. In this last reactor, the bed is split into jet and bubbling phase (Maciel Filho *et al.*, 1996). It was assumed C, H and CO combustion. Details about kinetic parameters can be seen in Maciel *et al.* (1996).

3.1 Orthogonal Collocation on Riser and Freeboard

It is assumed PFR heterogeneous model to simulate these both reactors. The model equations form a system of ordinary differential equations, which can be seen in Maciel Filho and Lona Batista (1995). When OC method is adopted, a discretized equation system is generated. The material balances are formulated for solid compounds (Carbon and Hydrogen), as well as for the four gaseous compounds i (O_2 , CO , CO_2 , H_2O). Thus, the following equations can be written:

$$\text{gas compound } i: \quad \sum_p A_{jp} C_{R,i} = \frac{\sum_n K_{\text{car},n}(x_j) \times (1 - E_j) + \sum_l K_{\text{ox},l}(x_j) \times E_j}{U_{\text{tr}}}$$

$$\text{carbon balance:} \quad \sum_p A_{jp} C_{C,p} = \frac{K'_{\text{car,bub}}(x_j) \times PM_{\text{car}} \times (1 - E_j) \times A_R}{Q_{\text{tr}}}$$

$$\text{hydrogen balance:} \quad \sum_p A_{jp} C_{H,p} = \frac{K'_{\text{hd,bub}}(x_j) \times PM_{\text{hd}} \times (1 - E_j) \times A_R}{Q_{\text{tr}}}$$

$$\text{solid phase thermal balance:} \quad \rho_s C_p v_s \left(\sum_p A_{jp} T_{s,p} \right) = \sum_n K'_{\text{car},n}(x_j) \times (-\Delta H_{R,n})_j - h a_s (T_{s,j} - T_{g,j})$$

$$\text{gas phase thermal balance:} \quad \frac{Q_{\text{tr}} C_{p,g}}{A} \left(\sum_p A_{jp} T_{g,p} \right) = h a_s (T_{s,j} - T_{g,j}) f_s + K'_{\text{ox},l}(x_j) \times (-\Delta H_{R,l})_j$$

Figure 2 shows O_2 profiles along the riser, when RK and OC with 4 internal collocation points (ICP) are considered. It can be noticed an agreement in results. This behaviour is also observed in the freeboard (not shown).

3.2 Comparison between the Broyden and Newton

The algebraic equation system presented is solved using 2 different procedures. Initially, the Newton method is used to linearize the equations, that are solved by LU decomposition method, latter, the Broyden method is also adopted.

Figure 3 depicts gas temperature profile along riser length. For the OC method, it is assumed 1 and 2 ICP. Newton and Broyden methods are used to solve algebraic equations when 1 ICP is adopted. It can be concluded that Broyden and Newton method present similar accuracy, but the first one is more efficient. When it is assumed error lower than 10^{-8} , the convergence is achieved after 15 iterations to the Newton method and after 5 iterations to the Broyden method. So, Broyden method will be adopted in this work.

3.3. Orthogonal Collocation on the Fully Mixed Zone

The system of equations that models the fully mixed zone in the fluidized bed can be seen in Maciel *et al.* (1996). When OC is applied, the differential equations are discretized, and the algebraic equations remain unchanged.

$$\begin{aligned} \text{gas compound i:} & \quad \frac{F_i R}{P} (T_0 C_{0,i} - T_{FMZ} C_{FMZ,i}) = \sum_k K_{FMZ,k} \\ \text{carbon balance:} & \quad V_s (C_{C_0} - C_{C_{FMZ}}) = K_{cor,FMZ}(x_j) PM_{cor} \\ \text{hydrogen balance:} & \quad V_s (Ch_0 - Ch_{FMZ}) = K_{hid,FMZ}(x_j) PM_{hid} \\ \text{solid phase energy balance:} & \quad \rho_s C_p V_s \left(\sum_p A_{jp} T_{s,p} \right) = \sum_m K_{het,m}^s(x_j) \times (\Delta H_{R,m})_j - h(T_{s,j} - T_{g,j}) \alpha_v \\ \text{gas phase energy balance:} & \quad \frac{Q_g C_p}{A} \left(\sum_p A_{jp} T_{g,p} \right) = h \alpha_v (T_{s,j} - T_{g,j}) f_s + K_{tmm}^g(x_j) \times (-\Delta H_{R,1})_j \end{aligned}$$

The generated profiles from RK and OC method are divergent (Figure 4). As greater is the number of collocation point, more accurate are the results, but the same results are obtained when 4 or 5 points are used. This means that 4 points are enough.

The divergence between RK and OC method occurs due to the presence of algebraic equations. In the methodology presented in Maciel Filho and Lona Batista (1995) to solve the system of equation through RK method, the inlet condition for the second integration step represents the exit condition for the first one. Algebraic equations idealise perfectly mixed behaviour, and differential equations represent plug flow. When RK method is applied, the algebraic equations are solved in a sequential way, so it is assumed several CSTRs, and consequently a PFR behaviour. On the other hand, when OC is used, the model equations are solved simultaneously for all collocation points, so the algebraic equations always represent perfectly mixed behaviour. The inlet concentration or temperature are always assumed in $x = 0$. In Figure 5, the jet region is splitted of into 2, 4 and 40 sections, and each of them is solved through OC method. This approach tries imitate the methodology applied in the RK method. As greater is the number of sections, closer are the profiles obtained via RK and OC. When there is division on jet phase, C_{co} represents the carbon concentration in the exit of previous section, similarly to the RK methodology.

3.4. Orthogonal Collocation in the Bubbling Bed

The equation system generated from heterogeneous modelling of bubbling bed can be seen in Maciel *et al.* (1996). When OC method is adopted the equation system become:

Gas compound i, emulsion phase

$$\sum_k K_{B,k}(x_j) = \frac{F_B R}{P} (T_{FMZ} C_{FMZ,i} - T_{D,j} C_{B,i,j}) + \frac{F_B K_{mb} R T_{D,j}}{U_B P} \left(\sum_j w_j C_{B,i,j} - \sum_j w_j C_{B,i,j} \right) \quad (1)$$

$$\text{Gas compound i, bubbling bed:} \quad \sum_{p=1}^{N+2} A_{jp} C_{B,i,p} = -\frac{K_{mb}}{U_B} (C_{B,i,j} - C_{B,i,j}) + \frac{\sum_k K_{B,k}(x_j)}{U_B}$$

$$\text{Carbon balance:} \quad V_s (C_{C_{FMZ}} - C_{C_{B,j}}) = K_{cor,B}(x_j) PM_{cor}$$

$$\text{Hydrogen balance:} \quad V_s (Ch_{FMZ} - Ch_{B,j}) = K_{hid,B}(x_j) PM_{hid}$$

$$\text{Solid phase Thermal balance:} \quad \rho_s C_p V_s \left(\sum_p A_{jp} T_{s,p} \right) = \sum_m K_{het,m}^s(x_j) \times (\Delta H_{R,m})_j - h(T_{s,j} - T_{g,j}) \alpha_v$$

$$\text{Gas Phase Thermal balance:} \quad \frac{Q_g C_p}{A} \left(\sum_p A_{jp} T_{g,p} \right) = h \alpha_v (T_{s,j} - T_{g,j}) f_s + K_{tmm}^g(x_j) \times (-\Delta H_{R,1})_j$$

$$\text{Eq. (1) in its original form is: } \sum_k K_{B,k} = \frac{F_B R}{P} (T_{FMZ} C_{FMZ,i} - T_{D,j} C_{B,i,j}) + \frac{F_B K_{mb} R T_{D,j}}{U_B P} \int_{h_j}^H (C_{B,i,j} - C_{B,i,j}) dx$$

The integral limits h_j and H must be normalised between 0 and 1 before applying quadrature formula. Initially, it was assumed that fluidized bed length is 1 m. By simplicity, it was considered

initially only one ICP. So, concentration and temperature must be calculated on $x = 0.5$ m and $x = 1$ m (the inlet conditions are known).

When equations are solved at $x = 0.5$ m, the integral in the emulsion phase balance have limits 0 and 0.5. By quadrature formula it can be written:

$$\int_0^{0.5} W(x)y(x)dx = \sum_{i=1}^N y_i w_i$$

After changing integral limits from 0 - 0.5 to 0 - 1, another problem is found. When the calculations are made in the bed centre, it is necessary to know the concentration in bubble and emulsion phase at point $x = 0.25$, in order to solve the integrals by quadrature. Meanwhile, these concentrations are unknown.

So, in this work, it is developed an approach to resolve this problem. For that, it is considered that the integral of a function between 0 and r is equal to the product between r (root of Jacobi polynomial) and integral of function over limits 0 and 1. So, if it is considered $W(x) = 1$, we have:

$$\int_0^r y(x)dx = r \int_0^1 y(x)dx \quad (2)$$

As smaller is the variation of function with the co-ordinate (x), more real is this approach. For constant functions this is really true.

It can be noticed that RK and OC method promote similar results along 1 m of bed (not shown). Figure 6 shows that carbon monoxide concentration profiles from RK and OC method are different when the simulation is made considering all length of fluidized bed. The approach expressed in equation (2), in this case, is less accurate because the bed is longer.

The bubbling bed simulation was made assuming that the bed is composed of sections of 1 m each. The results are shown in Figure 7. It can be noticed that the profiles obtained from RK and OC are more similar (this behaviour was also observed when the jet region was sectioned).

In this work, it is also proposed a second approach to calculate the integral in the internal collocation points based on the quadrature formula. It can be written that:

$$\int_0^1 y(x)dx = \sum_{i=1}^N y_i w_i \quad (3)$$

If it is assumed 5 collocation points, this integral can be expressed by summation of 5 terms:

$$\int_0^1 y(x)dx = w_1 y(r_1) + w_2 y(r_2) + w_3 y(r_3) + w_4 y(r_4) + w_5 y(r_5)$$

where: r_2, r_3, r_4 are roots in the internal collocation points, $r_1 = 0$ and $r_5 = 1$.

In this second approach, it is assumed that integral between 0 and r_p may be approximate by:

$$\int_0^{r_p} y(x)dx = \sum_{i=1}^p y_i w_i \quad (4) \quad \text{where: } p = \text{collocation point and } r_p = \text{root in point } p$$

Expression (4) is true for $r_p = 0$ and $r_p = 1$, and it represents an approximation for ICP. Table 1 shows the equation (4) applied in the integral calculation for the function $f(x) = 5x$ (function arbitrarily chosen). It is obtained better results when r_p is close to 1.

Figure 8 shows the results using this second approach. The concentration profiles in the emulsion phase become oscillatory. This oscillation is due to inaccuracy in equation (4), mainly when integrals are calculated near root 0. So, in bubbling bed simulation it was used the first approach (equation 2), and the bed was divided in sections of 1 m each.

4. MODELLING APPLIED TO THE INDUSTRIAL SYSTEM

Operation conditions and dimensions for the regeneration system are shown in Tables 2 and 3 respectively. In order to verify if equation (2) is accurate to represent the integral when the superior limit is a ICP, a test is proposed. The bubble region is divided into sections of 1 m each. In order to facilitate the calculations, it is used only one ICP for each section. Simulations using 1, 2 or 3 ICP are made, but they indicate that there are no appreciable divergence in results (not shown), so this hypothesis does not represent limitation in this test.

In this procedure, initially, the integral in $x = 0.5$ is calculated according to equation 2. After solution of material and energy equations, concentration and temperature are obtained in the collocation points. The interpolation is done, and concentration and temperature in $x = 0.25$ are obtained. With the emulsion and bubble phase gas concentration at $x = 0.5$ and 0.25 , the integrals may be calculated in an exact way. So, the values of integrals are compared with that obtained in the last iteration. If difference between them are greater than the allowed error, the actual integral calculation is used to determine concentration and temperature profiles.

This procedure is repeated until the difference in the integral calculation between 2 consecutive iteration does not exceed the allowed error.

By using this procedure, concentration and temperature profiles are obtained. These results are compared with that obtained when only equation (2) is used to calculate the integrals in the internal collocation points. It can be noticed that the profiles are coincident (not shown). So, the approach represented by equation 2 is adequate when the model equations are calculated for an specific length of the bubble bed. Figure 9 shows the gas compounds profiles in dry base obtained

from RK and OC methods, and Figure 10 presents the solid temperature profiles. The industrial data are also shown. Through these figures it can be noticed that the second method is more adequate to simulate the industrial regeneration system.

5. CONCLUSIONS

In this work, an alternative solution methodology based on OC, was adopted to simulate an industrial catalytic cracking regeneration system.

Concentration and temperature profiles from RK and OC method present different behaviours if there exist algebraic equation in the equation system. In the OC method, algebraic equation represents a perfectly mixed behaviour. In the methodology presented by Maciel *et al.* (1996), algebraic equations represent a sequence of perfectly mixed cells, when RK is adopted.

In the bubble bed simulation, the equation system presents integrals. When the integration is made in internal collocation points (r), it is proposed an approach at which the integral between 0 and r is equal the integral between 0 and 1 multiplied by root of Jacobi polynomial. It is observed that when this approach is used, the results are the same to that obtained if integral calculation is carried out.

Comparison with industrial data shows that RK method can predict well the concentration values, meanwhile the temperatures stay subpredicted. It can be noticed that OC is adequate in simulation of regeneration system, and the results agree with industrial data from Petrobrás. The bubble region of fluidized bed was divided in sections of 1 m each during simulation. This height can be used as an adjustable parameter of model in order to solve industrial problems.

Acknowledgements – The authors thank the industrial data provided by Petrobrás.

NOTATION

A = area of the reactor, m^2 , matrix elements
 a_v = interfacial area gas-solid, l/m
C = gas molar concentration, $kmol/m^3$
Cc = carbon concentration, kg carb/kg catal
Ch = hydrogen concentration, kg hyd / kg cat
Cp = specific heat, $kJ/kg K$
E = porosity of the bed
fs = volumetric fraction of solid
H, h_j = bed height, jet height (m)
h = heat transfer coefficient $kJ/K s m^2$
 k_{be} = bubble-emulsion mass transfer coefficient
K = reaction rate group, $kmol/s$
 K' = reaction rate group, $kmol/s m^3$
 K'' = reaction rate group, $kmol/m_p^3 s$
P, PM = pressure, atm; molecular weight

Q = mass flow rate, kg/s
R = ideal gas constant
T = temperature, K
U = superficial velocity, m/s
 ΔH = reaction heat, $kJ/kmol$
 ρ = specific mass, kg/m^3
indices
0 = initial
B, car = bubble, carbon phase
E, D = emulsion, dense phase
FMZ, g = fully mixed zone, gas phase
het, hid, hom = heterogeneous, hydrogen, homogeneous
i, l, m = gas component, reaction l, m
R, s, t = riser, solid phase, total

REFERENCES

- Finlayson, B.A., Chem. Eng. Sci., V. 26, pp. 1081-1091 (1971).
Maciel Filho R. and Lona Batista L. M. F., Modelagem Heterogênea de Regeneradores Industriais Considerando a Recirculação de Sólidos", *Anais do Iberian Latin American Conference on Computational Methods for Engineering*. (1995)
Maciel Filho R., Lona Batista L. M. F., Mozart Fusco, Chem. Eng. Sci., Vol. 51, N. 10 (1996)

TABLES AND FIGURES

Table 1: Analyses of the second approach

| roots | $\int_0^r f(x)$ | |
|----------------|------------------|--------------|
| | analytic results | approach (4) |
| $r_1 = 0$ | 0 | 0 |
| $r_2 = 0.1127$ | 0.03175 | 0.1677 |
| $r_3 = 0.5$ | 0.625 | 0.6438 |
| $r_4 = 0.8873$ | 1.968 | 1.964 |
| $r_5 = 1$ | 2.5 | 2.5 |

Table 3: Dimension of regeneration system

| Section / Dimension | Length (m) | Diameter (m) |
|---------------------|------------|--------------|
| Combustor | 6.71 | 5.18 |
| Riser | 20.09 | 2.74 |
| Freeboard | 8.12 | 7.67 |

Table 2: Operation data to regeneration

| Variable / case | I | II |
|----------------------------------|-------|------|
| Air flow rate (kg/s) | 28.08 | 25.3 |
| Catalyst flow rate (kg/s) | 326.5 | 307. |
| Recirculation (kg/s) | 107.8 | 225. |
| Pressure (atm) | 2.88 | 2.65 |
| Retificator temperature (K) | 534 | 560 |
| Air regeneration temperature (K) | 217 | 202 |
| Coke in catalyst (% weight) | 0.78 | 0.60 |
| H / Coke (% weight) | 7.5 | 4.50 |

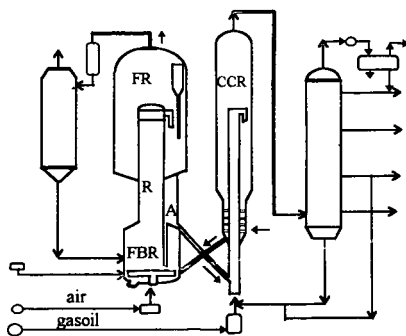


Figure 1: Diagram for a catalytic cracking industrial unit

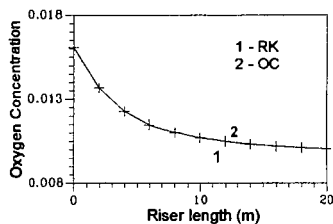


Figure 2: Oxygen Profiles

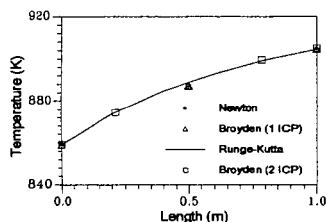


Figure 3: Gas temperature profile.

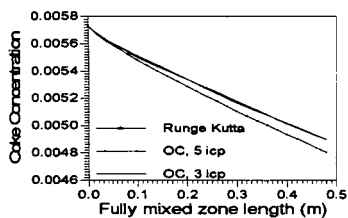


Figure 4: Carbon profiles

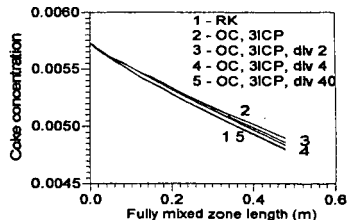


Figure 5: Carbon profiles in jets.

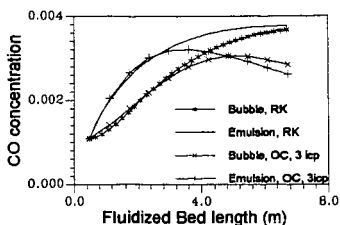


Figure 6: CO profile along bubbling bed

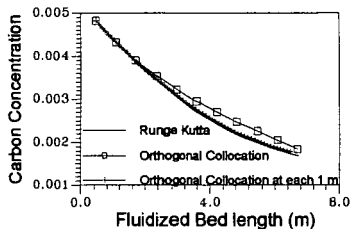


Figure 7: Carbon profile

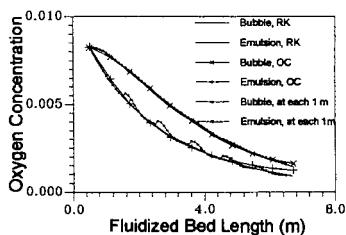


Figure 8: Oxygen profile

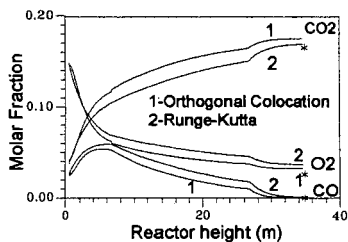


Figure 9: Gas molar fraction

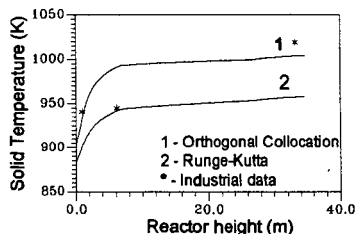


Figure 10: Solid temperature profiles

REACTOR MODELING AND PHYSICAL-CHEMICAL PROPERTIES CHARACTERIZATION IN POLYETHYLENE FLUIDIZED-BED REACTOR

Fabiano A.N. Fernandes & Liliame M.F. Lona Batista
Chemical Engineering Institute
Universidade Estadual de Campinas - UNICAMP
13081-970, Campinas - SP, BRAZIL

KEYWORDS: modeling, polyethylene, fluidized-bed reactor

INTRODUCTION

Although the fluidized-bed reactor technology for producing polyethylene has been invented on the 50s, and its commercial use has been growing since the last decade, little is still known about its behavior regarding to temperature, concentration, production and polyethylene physical-chemical properties characterization gradients inside the reactor.

In the past years, some researchers have focused their attention to the modeling of these polyethylene gas-phase processes (Choi & Ray, 1985; McAuley et al., 1994) but, even though, these models are based on strong assumptions such as a well-mixed emulsion phase, which can be easily brought down when considering low degree or no pre-polymerization. In the latter cases, heat and mass transfer resistances become significant and the polymerization rate of young particles can lead to over-heating.

In order to create a more reliable model for the fluidized-bed reactor, a steady-state model incorporating interactions between separate bubble and emulsion phases inside the reactor bed has been developed. A polymer physical-chemical characterization model has also been developed and the linkage of these two models has been studied.

MODEL DEVELOPMENT

The assumptions that have been made in the development of the model are summarized below.

- The fluidized bed comprises two phases: bubble and emulsion phases.
- The polymerization reactions occur only in the emulsion phase.
- The emulsion phase is at minimum fluidizing conditions.
- The emulsion phase is not well-mixed.
- The gas in excess of that required for maintaining the minimum fluidizing condition passes through the bed as bubble phase.
- The bubbles are spherical and of uniform size throughout the bed, reaching a maximum stable size. The bubbles travel up through the bed at a constant velocity in a plug-flow regime.
- There are a negligible radial gradient of temperature and concentration in the bed, due to the agitation produced by the up flowing gas.
- There is negligible resistance of heat and mass transfer between gas and solids in the emulsion phase.
- There is no agglomeration between polymer particles throughout the bed.
- Elutriation of fines from the bed are not considered.
- The polymer particle grows and segregates inside the reactor.
- The gas-phase is composed by ethylene, 1-butene, 1-hexene, nitrogen and hydrogen

All mass and energy balances were given in the differential form, in order to account for gas concentrations (ethylene, 1-butene, 1-hexene, hydrogen and nitrogen) and temperature axial gradients along the reactor in both phases. This means that the reagent gases are in a plug-flow regime but at different velocities for bubble and emulsion phases.

Bubble-phase material and energy balances

$$\frac{dC_{bi}}{dz} = \frac{K_{mi}}{U_b} \cdot (C_{ei} - C_{bi})$$
$$\frac{dT_b}{dz} = \frac{H_m}{U_b \cdot C_{bT} \cdot c_{pgT}} \cdot (T_b - T_e)$$

Emulsion-phase material and energy balances

$$\frac{dC_{ei}}{dz} = \frac{Rp' \cdot (1 - \varepsilon_{mf})}{\varepsilon_{mf} \cdot A \cdot U_e} + \frac{K_{mi} \cdot (C_{bi} - C_{ei}) \cdot \delta}{(1 - \delta) \cdot \varepsilon_{mf} \cdot U_e}$$

$$\frac{dT_e}{dz} = \frac{\left[\sum_{i=1}^{NC} \dot{c}_{pgi} \cdot K_{mi} \cdot (C_{bi} - C_{ei}) + Hm \right] \cdot (T_b - T_e) \cdot \delta}{U_e \cdot (1 - \delta) \cdot \varepsilon_{mf} \cdot \dot{c}_{pgT} \cdot C_{eT}}$$

$$\frac{Rp' \cdot (1 - \varepsilon_{mf}) \cdot M_w \cdot \left[-\Delta H - (c_{ps} - c_{pgT}) \cdot (T_e - T_{ref}) \right] + \pi \cdot D \cdot U_h \cdot (T_e - T_\infty)}{U_e \cdot \varepsilon_{mf} \cdot \dot{c}_{pgT} \cdot C_{eT}}$$

The new approach given by this study relies on the average weight fraction of catalyst in the polymer, which is not constant along the reactor and has been equated also in a differential form depending mainly on the polyethylene production. In this way it is possible to simulate that there is a high catalyst/polymer mass weight fraction at the top of the reactor and a low mass weight fraction at the base, what is in accordance with the fact that there exists a degree of segregation of the different polyethylene particle sizes in the fluidized-bed reactor.

Average mass weight fraction of catalyst in the polyethylene

$$\frac{d\chi}{dz} = \frac{Rp' \cdot A \cdot (1 - \delta) \cdot (1 - \varepsilon_{mf}) \cdot M_w}{\chi \cdot q_{cat}}$$

The great advantage in having this new variable is that it allows the usage of a more complex reaction mechanism, which is summarized in Table 1. Not only that but it gives strong support to predict the growth of polyethylene particles along the fluidized-bed.

It is important to state that the mathematical resolution of the model followed the physical design of the reactor, where the gas and polymer particles flow in countercurrent, the gas is fed at the base and the catalyst at the top portion of the reactor. This design configuration implies on having contour conditions at the base and top of the reactor, what resulted in an iterative resolution of the system till all base and top contour conditions were satisfied. The final reactor model was composed of 10 differential equations, plus accessories equations for the calculation of the particle growth throughout the reactor.

The reaction mechanism used in this work is the same described by Kissin (1987), de Carvalho et al (1989) and McAuley et al (1990). In general, this mechanism is based upon the coordination copolymerization of ethylene using Ziegler-Natta catalyst with two different types of catalyst sites. Each site type is associated with different rate constants for formation, initiation, propagation and chain transfer. Only the effects of the terminal monomers were considered on the reaction rates.

Alongside to the reactor model, the method of moments (Zabisky et al, 1992) has been used to create a new mathematical model capable of predicting the physical-chemical characteristics of the polyethylene (average molecular weight, density, polydispersity, melt index, etc.) been build up along the reactor height and also to predict the polymer particle growth. The guidelines followed by Zabisky et al (1992) were adapted to the case of the coordination copolymerization reaction mechanism outlined by McAuley et al (1990) and to the dynamics along the reactor height. The model consisted of 36 differential equations corresponding to the components material balances and the life and dead polymers moments, plus accessories equations to account for calculation of polydispersity, density, comonomer incorporation in the polymer chain and others calculated characteristics.

To connect the results from the reactor model (temperature, concentration and production profiles obtained in function of the height position) with the results from the method of moments' predictions (concentration, production and quality profiles obtained in function of the time) an iterative process was created. Outputs from the reactor model served as inputs for the physical-chemical model, and vice-versa, so that adjustments on operational parameters could be done in both models, till the profiles obtained from both models matched in terms of ethylene and comonomers concentrations and production of polyethylene. The difficulty of this operation had relied on the different integration variables (time and position) of the two models, what complicates the convergence of the system to a single matching result.

RESULTS

The data that have been obtained with the reactor model have shown interesting results concerning to the temperature and concentration gradients in the reactor, specially at the catalyst feeding region, where the reaction rate is greater due to the higher temperature and to the higher influence of the catalyst in the formation and early development of young polymer particles. The case illustrated by figure 1 shows a typical temperature and concentration gradient profiles given for the production of polyethylene in a fluidized bed reactor with no prepolymerization. The data used in the models simulations are shown in table 2.

As it can be observed from figure 1, the top portion of the reactor requires special attention in order to not present hot spots or even the melting of the polymer. According to the parametric study of the system, this situation can be avoided by controlling the gas feed velocity and temperature. In terms of polyethylene production, it can be enhanced by elevating the gas feed temperature, and by decreasing the gas feed velocity. It was observed that an increase of 15K in the gas feed temperature can multiply the production of polyethylene by up to 50% (not shown), without compromising the polyethylene characteristic and integrity.

The physical-chemical model, alone, shows that the average molecular weight of the polymer increases more intensely at the beginning of the polymerization period and slows down after a while. The polydispersity follows the same increase profile. Density and comonomer incorporation on the polymer remains practically constant during the entire polymerization process (not shown).

The figure 2 shows the simulation of the polyethylene physical-chemical characteristics build up inside the fluidized bed reactor, obtained by the link of the reactor and the physical-chemical characterization models. The simulation shows that there is a highly active reaction zone in the top of the reactor, what is in accordance to the reactor model. Beneath this highly active zone, follows a less active zone responsible for the refining of the polymer characteristics.

The upper and highly reaction active zone tends to be less evident when prepolymerization of the polyethylene particles are employed (not shown).

The assumption that the polymer particles segregates inside the reactor still holds up, with fine particles being at the reactors' top and heavier particles being distributed along the reactor height.

CONCLUSION

In this work a new reactor and physical-chemical characterization models were developed and linked together to give a complete understanding of the fluidized bed reactor for polyethylene production.

The reactor model developed permits the usage of a more complex reaction mechanism and the prediction of the polymer average particle diameter and polymer/catalyst weight fraction. But more than all, it also extends the possibility of simulation of the reactor operating with low degree or no prepolymerization, case which the models based on the well-mixed emulsion phase theory are incapable to predict correctly.

The two models when linked together become very useful tool to perform a complete optimization of the fluidized bed reactor for the production of polyethylene, since it makes possible to optimize the reactor conditions looking for an enhancement on the polyethylene production rate and at the same time check how the changes on the operational conditions of the reactor influence on the grade of polymer being produced.

From the industrial point of view, these more reliable copolymerization models are capable of simulating the synthesis conditions of the polyethylene and permit the study of new copolymers previously to industrial tests. In this way, new polymer grades can be developed more easily, and existents grades can be optimized in order to produce high quality resins.

NOTATION

| | |
|------------|---|
| A | sectional area of the reactor |
| C_{ij} | concentration of the component j in the i phase |
| $C_{p,gj}$ | molar heat capacity of the gas component j |
| $C_{p,s}$ | mass heat capacity of the solids |

| | |
|-----------------|--|
| D | fluidized bed reactor diameter |
| ΔH | heat of reaction |
| H^* | molecular hydrogen |
| H_m | heat transfer coefficient |
| K_{mj} | mass transfer coefficient of the component j |
| M_w | ethylene molecular weight |
| NC | number of components |
| $P(r)$ | non-reactive polymer with chain length size r |
| q_{cat} | catalyst feeding rate |
| R^* | potential active site |
| $R_i(r)$ | live polymer with terminal monomer i and chain length size r |
| R_p' | polyethylene production rate |
| T_i | temperature of the i phase |
| T_{ref} | reference temperature |
| U_i | velocity of the i phase |
| U_h | wall heat transfer coefficient |
| X | cocatalyst |
| z | height above the distributor |
| δ | bubble volumetric fraction in bed |
| ϵ_{mf} | minimum fluidized porosity |
| χ | catalyst/polymer average weight fraction |

subscripts

| | |
|----|-------------------------------|
| 1 | ethylene |
| 2 | 1-butene |
| b | bubble phase |
| e | emulsion phase |
| mf | minimum fluidizing condition |
| T | total (sum of all components) |

ACKNOWLEDGEMENTS

The authors would like to thanks the São Paulo State Research Aid Foundation - FAPESP, for the award of a scholarship and for the financial support of this research.

REFERENCES

- Choi, K.Y. & Ray, W.H. The dynamic behaviour of fluidized bed reactors for solid catalyzed gas phase olefin polymerization. *Chem. Eng. Sci.*, **40**: 2261-2279, 1985.
- deCarvalho, A.B., Gloor, P.E. & Hamielec, A.E. A Kinetic Mathematical Model for Heterogeneous Ziegler-Natta Copolymerization, *Polymer*, **30**: 280, 1989.
- Kissin, Y.V. *Isospecific Polymerization of Olefins with Heterogeneous Ziegler-Natta Catalysts*, Springer-Verlag, New York, 1987.
- McAuley, K.B., MacGregor, J.F. & Hamielec, A.E. A kinetic model for industrial gas-phase ethylene copolymerization. *A.I.Ch.E.J.*, **36**(6): 837-850, 1990.
- McAuley, K.B., Talbot, J.P. & Harris, T.J. A comparison of two-phase and well-mixed models for fluidized-bed polyethylene reactors. *Chem. Eng. Sci.*, **49**(13): 2035-2045, 1994.
- Zabisky, R.C.M.; Chan, W.M.; Gloor, P.E. & Hamielec, A.E. A kinetic model for olefin polymerization in high-pressure tubular reactors: a review and update. *Polymer*, **33**: 2243-2262, 1992.

TABLES AND FIGURES

Table 1. Reaction Mechanism and Kinetic Parameters

| Reaction | | | Catalytic Site 1 | Catalytic Site 2 |
|---------------------------------------|---|------------------|------------------|------------------|
| formation [s^{-1}] | $R^* \xrightarrow{k_f} R_0$ | kf | 1 | 1 |
| initiation [$L.mol^{-1}.s^{-1}$] | $R_0 + C_i \xrightarrow{ki} R_i(I)$ | ki ₁ | 1 | 1 |
| | $H^* + C_i \xrightarrow{khi} R_i(I)$ | ki ₂ | 0.14 | 0.14 |
| | | kh ₁ | 1 | 1 |
| | $H^* + X \xrightarrow{khr} R_X(I)$ | kh ₂ | 0.1 | 0.1 |
| propagation | | kh _r | 20 | 20 |
| | $R_i(r) + C_k \xrightarrow{kpi k} R_k(r+1)$ | kp ₁₁ | 85 | 85 |

| | | | | |
|---|--|------------------|--------|--------|
| [L.mol ⁻¹ .s ⁻¹] | | kp ₁₂ | 2 | 15 |
| | | kp ₂₁ | 64 | 64 |
| | | kp ₂₂ | 1.5 | 6.2 |
| chain transfer | $R_i(r) + C_k \xrightarrow{kfmik} P(r) + R_k(l)$ | kf ₁₁ | 0.0021 | 0.0021 |
| [L.mol ⁻¹ .s ⁻¹] | | kf ₁₂ | 0.006 | 0.11 |
| | | kf ₂₁ | 0.0021 | 0.001 |
| | | kf ₂₂ | 0.006 | 0.11 |
| | $R_i(r) + H_2 \xrightarrow{kfh1} P(r) + H^*$ | kfh ₁ | 0.088 | 0.37 |
| | | kfh ₂ | 0.088 | 0.37 |
| | $R_i(r) + X \xrightarrow{kfr1} R_X(l) + P(r)$ | kfr ₁ | 0.024 | 0.12 |
| | | kfr ₂ | 0.048 | 0.24 |
| | $R_i(r) \xrightarrow{kfs1} P(r) + H^*$ | kfs ₁ | 0.0001 | 0.0001 |
| | | kfs ₂ | 0.0001 | 0.0001 |
| deactivation [s ⁻¹] | $R_i(r) \xrightarrow{kds} P(r) + R_D$ | kds | 0.0001 | 0.0001 |

Table 2. Operational conditions and reactor data used in the simulations

| | | | |
|----------------------|------------------------|----------------------|------------|
| Ethylene feed rate | 0.50 mol/L | 1-Butene feed rate | 0.20 mol/L |
| Hydrogen feed rate | 0.05 mol/L | Inert feed rate | 0.00 mol/L |
| Catalyst feed rate | 0.20 g/s | Cocatalyst feed rate | 0.01 mol/L |
| Gas feed temperature | 316 K | Room temperature | 340 K |
| Catalyst density | 2.38 g/cm ³ | Catalyst diameter | 0.05 mm |
| Activation energy | 37620 J/mol | ΔH | -3829 J/g |
| Reactor diameter | 396 cm | Reactor height | 1097 cm |
| δ | 0.214 | ε _{mf} | 0.50 |
| U _{mf} | 7.0 cm/s | U _c | 34.8 cm/s |
| U _b | 114.0 cm/s | Bubble diameter | 15 cm |

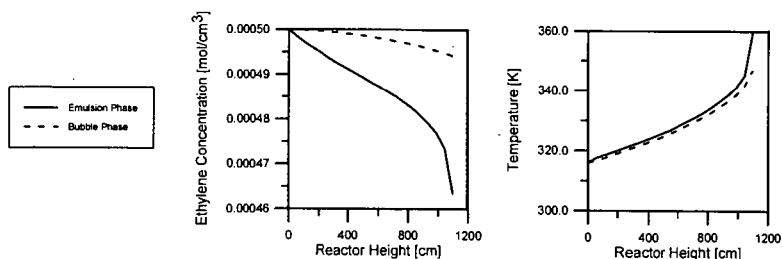


Figure 1. Ethylene concentration and temperature gradients for the production of polyethylene in a fluidized bed reactor with no prepolymerization. Simulation data from table 2.

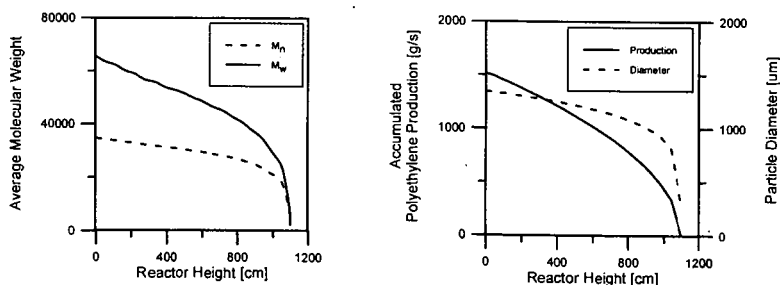


Figure 2. Average molecular weight (M_n and M_w), accumulated polyethylene production and particle diameter build up profiles inside the fluidized bed reactor. Simulation data from table 2.

MODELING OF METHYLCYCLOHEXANE TRANSFORMATION OVER A USHY ZEOLITE

Henrique S. Cerqueira, Patrick Magnoux, Dominique Martin and Michel Guisnet, Université de Poitiers, Fac. Sci. Fond. Et Appliquées, UMR CNRS 6503, 40, avenue du Recteur pineau, 86022 Poitiers Cedex, FRANCE

Key words: USHY zeolite, modeling, methylcyclohexane

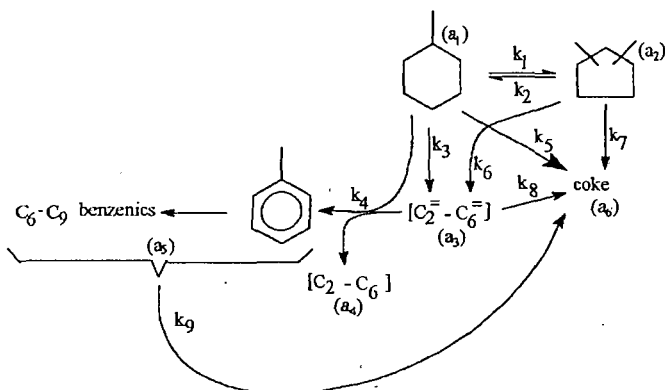
ABSTRACT

A kinetic model with functions of deactivation by coke has been developed for the transformation of methylcyclohexane (isomerization, cracking, hydrogen transfer and coking) in a fixed bed reactor at 450°C over a USHY zeolite. A good fitting is obtained showing that the function of deactivation by coke depends on contact time.

INTRODUCTION

Although naphthenes are important constituents of feedstocks and products of FCC (fluid catalytic cracking) little work has been reported in the literature [1,2]. This study concerns the transformation of methylcyclohexane over an USHY zeolite in a fixed bed reactor at 450°C.

From the effect of contact time the following reaction scheme was proposed to explain the formation of various products over the fresh catalyst.



Methylcyclohexane (a_1) is isomerized into dimethylcyclopentanes (a_2). C_2 - C_6 alkenes (a_3) are formed from double cracking of a_1 and a_2 followed by oligomerisation cracking steps. Methylcyclohexane is also transformed into toluene through hydrogen transfer towards a_3 with formation of C_7 - C_9 alkanes (a_4), three moles of a_3 being transformed per mole of a_1 . Toluene undergoes disproportionation with formation of benzene, xylenes and trimethylbenzenes. Coke results mainly from C_3 products (which are not observed) of the simple cracking of a_1 and a_2 but is also formed from a_3 and from aromatics (a_5).

A kinetic model with deactivation functions was developed allowing the complete description of the transformation of methylcyclohexane.

MATERIALS AND METHODS

The USHY zeolite ($Na_{3.4}H_{34.5}Al_{34.5}Si_{157.1}O_{841}$, 17.8 extra framework aluminium) resulted from calcination under air flow, at 500°C for 12 h of an ultrastable NH_4 zeolite (CBV 500 from PQ). Methylcyclohexane transformation was carried out in a fixed bed reactor at 450°C $p/V_1 = 0.9$ bar, $p_{methylcyclohexane} = 0.1$ bar at various contact times. Reaction products were analyzed on-line by gas chromatography with a 50 m fused silica capillary column Plot Al_2O_3/KCl .

The mathematical model has been previously described [3]. From the reaction scheme, assuming elementary steps, a plug flow behaviour uniform porosity and quasi-steady-state, the following equations may be written:

$$\frac{\partial a_1}{\partial Z} = \frac{P}{WHSV \cdot R \cdot T \cdot \sum_{i=1}^5 a_i} \cdot [k_2 \cdot a_2 \cdot \phi_1 - (k_1 \cdot \phi_1 + k_3 \cdot \phi_3 + k_4 \cdot a_3 \cdot \phi_3 + k_5 \cdot \phi_{\text{coke}}) \cdot a_1] \quad (1)$$

$$\frac{\partial a_2}{\partial Z} = \frac{P}{WHSV \cdot R \cdot T \cdot \sum_{i=1}^5 a_i} \cdot [k_1 \cdot a_1 \cdot \phi_2 - (k_6 \cdot \phi_3 + k_2 \cdot \phi_1 + k_7 \cdot \phi_{\text{coke}}) \cdot a_2] \quad (2)$$

$$\frac{\partial a_3}{\partial Z} = \frac{P}{WHSV \cdot R \cdot T \cdot \sum_{i=1}^5 a_i} \cdot [(v_1 \cdot k_3 \cdot a_1 + v_2 \cdot k_4 \cdot a_2) \cdot \phi_3 - (3 \cdot k_4 \cdot a_1 \cdot \phi_3 + k_5 \cdot \phi_{\text{coke}}) \cdot a_3] \quad (3)$$

$$\frac{\partial a_4}{\partial Z} = \frac{P}{WHSV \cdot R \cdot T \cdot \sum_{i=1}^5 a_i} \cdot (3 \cdot k_4 \cdot a_1 \cdot a_3 \cdot \phi_4) \quad (4)$$

$$\frac{\partial a_5}{\partial Z} = \frac{P}{WHSV \cdot R \cdot T \cdot \sum_{i=1}^5 a_i} \cdot [(k_4 \cdot a_1 \cdot a_3 \cdot \phi_4) - k_9 \cdot a_5 \cdot \phi_{\text{coke}}] \quad (5)$$

$$\frac{\partial a_6}{\partial Z} = \frac{P}{WHSV \cdot R \cdot T \cdot \sum_{i=1}^5 a_i} \cdot (v_3 \cdot k_3 \cdot a_1 + v_4 \cdot k_7 \cdot a_2 + v_5 \cdot k_8 \cdot a_3 + v_6 \cdot k_9 \cdot a_5) \cdot \phi_{\text{coke}} \quad (6)$$

$$\frac{\partial a_7}{\partial t} = \frac{P}{R \cdot T \cdot \sum_{i=1}^5 a_i} \cdot (v_3 \cdot k_3 \cdot a_1 + v_4 \cdot k_7 \cdot a_2 + v_5 \cdot k_8 \cdot a_3 + v_6 \cdot k_9 \cdot a_5) \cdot \phi_{\text{coke}} \quad (7)$$

Where, a_i is the concentration of the a_i species [mols of lump i / g gas], $a_7 = C_c$ is the coke content on catalyst [wt%], k_i is the kinetic constant for the reaction i , t is the time-on-stream, Z is the dimensionless axial position, $v_1 = v_2$ is the ratio between the molecular weight of methylcyclohexane and olefins, $v_3 = v_4$ is the molecular weight of methylcyclohexane, v_5 is the molecular weight of olefins, v_6 is the molecular weight of aromatics, ϕ_i is the deactivation function for reactions leading to the correspondent a_i specie and ϕ_{coke} is the deactivation function for reactions leading to coke.

The mathematical solution was performed by finite difference discretization of the reactor with respect to the axial position. For a given set of kinetic constants and deactivation parameters, the system solution was obtained by backward finite differences formula with variable step, implemented in the DASSL code [4,5]. The initial condition is that the reactor is full of nitrogen. Although numerical convergence for a relative tolerance of 10^{-7} was obtained only for 120 discretization elements, satisfactory results are obtained for 10 discretization elements.

RESULTS AND DISCUSSION

Deactivation Functions

The deactivation functions may be related to the true deactivating agent, i.e., coke itself [6,7]. One parameter functions (eq. 8) which provide results very similar to those obtained with multiparameter functions [8] were chosen for all the reaction steps except for coke formation. However as coke may alter the product distribution, the deactivation parameter (α) should depend on the step.

It is generally found that at short time-on-stream, which corresponds to the formation of the first coke molecules, coke formation itself is not deactivated. Deactivation becomes very pronounced when the coke molecules attain a size comparable to that of zeolite cages because the access of the coke-maker molecules becomes difficult. In order to consider this particular mode of deactivation the deactivation function given in equation 9 was used for all reactions leading to coke.

The limit coke content (C_{lim}) above which the coke affects its formation was obtained from the change in coke content as a function of time-on-stream. Many values were considered for the A constant, a value of 180 being finally found to be appropriate.

$$\phi_i = \exp(-\alpha_i \cdot C_c) \quad (8)$$

$$\phi_{\text{coke}} = \frac{1}{\exp[A \cdot (C_c - C_{\text{lim}})] + 1} \quad (9)$$

Parameter Estimation

Different approaches were tested to improve the convergence of a maximum likelihood method [9]. Sequential parameter estimation, centering [10], model reformulation, using only either initial or iso-coke data and also trial and error change of initial values. Experimental error estimation was made with five replicates for one time-on-stream of 30 min and a WHSV (weight hourly space velocity) of 62.

Firstly, relations between the deactivation parameters (α) were established. To achieve this goal the residual activities as a function of coke on catalyst should be determined for all the reaction steps, the initial activities (at zero coke content) being estimated by extrapolation of the curves giving the product yield vs. time-on-stream. The following relations between parameters were obtained.

$$\alpha_1 = \alpha_2 = \alpha \quad (10)$$

$$\alpha_3 = 1.6 \cdot \alpha \quad (11)$$

$$\alpha_4 = \alpha_5 = 1.8 \cdot \alpha \quad (12)$$

Good fitting is obtained for each contact time but the value of α seems to depend on contact time, which indicates that the location of coke, hence its deactivating effect changes with this parameter (α). Indeed when coke molecules are located near the pore mouth, their blockage effect is more significant than when they are homogeneously distributed in the crystallite [11].

The values of α which give the best results increase with contact time from 3 (WHSV = 500) to 12 (WHSV = 62), i.e. the longer the contact time, the less homogeneous the coke distribution in the zeolite crystallites. With these values of α a good agreement is found between experimental results and model curves (figs. 1 to 3). The objective likelihood function presented a relative reduction of 25%.

The kinetic constant values are presented in Table 1. For isomerization of methylcyclohexane the k_1/k_2 ratio is determined from thermodynamic data [12].

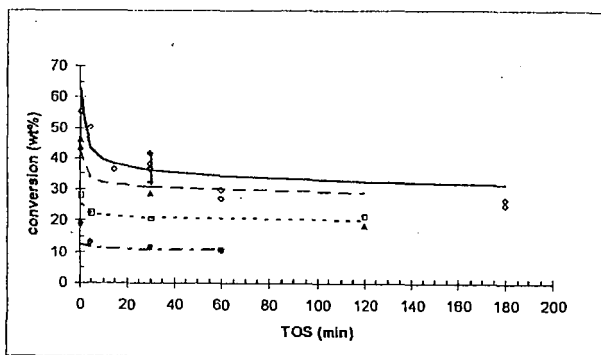


Figure 1: Conversion of methylcyclohexane versus time-on-stream (TOS). Calculated curves and experimental data for 4 different contact times.

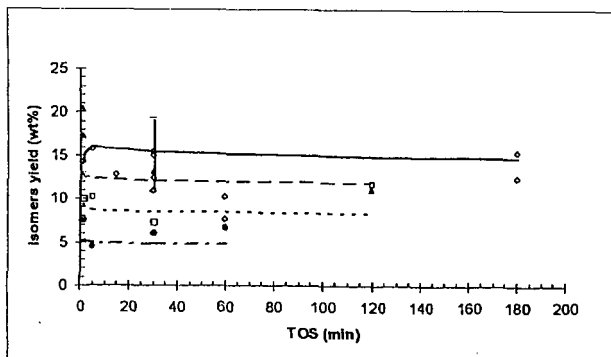


Figure 2: Isomers yield versus time-on-stream (TOS). Calculated curves and experimental data for 4 different contact times.

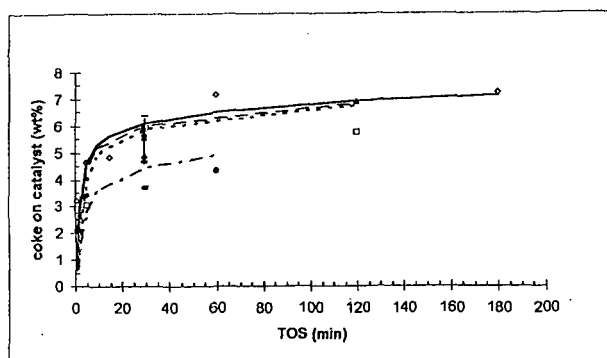


Figure 3: Coke on catalyst versus time-on-stream (TOS). Calculated curves and experimental data for 4 different contact times.

Table 1 : Kinetic constants

| kinetic constant | value | kinetic constant | value |
|---|-------------------|---|-------------------|
| k_1 [(g ca/cm ³) ⁻¹ ·h ⁻¹] | 8.5×10^4 | k_6 [(g ca/cm ³) ⁻¹ ·h ⁻¹] | 1.7×10^3 |
| k_2 [(g ca/cm ³) ⁻¹ ·h ⁻¹] | $0.417 \cdot k_1$ | k_7 [(g ca/cm ³) ⁻¹ ·h ⁻¹] | 3.5×10^4 |
| k_3 [(g ca/cm ³) ⁻¹ ·h ⁻¹] | 7.0×10^4 | k_8 [(g ca/cm ³) ⁻¹ ·h ⁻¹] | 8.5×10^3 |
| k_4 [(g ca/cm ³) ⁻¹ ·(g/mol)·h ⁻¹] | 3.3×10^9 | k_9 [(g ca/cm ³) ⁻¹ ·h ⁻¹] | 5.7×10^3 |
| k_5 [(g ca/cm ³) ⁻¹ ·h ⁻¹] | 2.0×10^3 | | |

CONCLUSIONS

The reaction scheme of methylcyclohexane transformation over a USHY zeolite was established. A kinetic model was developed to represent the change versus time-on-stream of the product yields. A good fitting is obtained showing that the function of deactivation by coke depends on contact time and then on the coke location inside the zeolite.

ACKNOWLEDGEMENTS

The support of CAPES foundation (Brazilian government), FCC S.A. and UMR CNRS 6503 is gratefully acknowledged.

REFERENCES

- [1] Lin, L., Gnep, N. S. and Guisnet, M., Am. Chem. Soc. Div. Petro. Chem., Miami meeting, September 10-15, 687-693 (1989).
- [2] Corma, A., Mocholi, F., Orchilles, V., Koerner, G. S. and Madon, R. J., Appl. Catalysis A: General, 67, 307-324 (1991).
- [3] Cerqueira, H. S., Falabella S-Aguiar, E. and Biscaia Jr., E. C., Appl. Catalysis A: General, 164, 1-2 (1997).
- [4] Petzold, L. R., "DASSL code", version 1989, Computing and Mathematics Research Division, Lawrence Livermore National Laboratory, L316, PO Box 808, Livermore, California, USA.
- [5] Brennan, K. E., Campbell, S. L. and Petzold, L. R., "Numerical Solution of Initial Value Problems in Differential-Algebraic Equations", Elsevier Sc. Publishing Co., Inc., New York (1989).
- [6] Froment, G. and Bischoff, K. B., Chem. Eng. Sci., 16(3) 189-201 (1961).
- [7] Froment, G. and Bischoff, K. B., Chem. Eng. Sci., 17(4) 105-114 (1962).
- [8] Cerqueira, H. S., Falabella S-Aguiar, E. and Biscaia Jr., E. C., Studies in Surface Science Catalysts, catalyst deactivation 1997, 303-310, Elsevier Science B.V. (1997).
- [9] Pinto, J. C., "Estima code", version 1997, Chemical Engineering Program, COPPE/UFRJ, CP 68502, CEP 21945-970, Rio de Janeiro, Brazil.
- [10] Watts, D. G., The Can. Journal of Chem. Eng., 74, August, 701-710 (1994).
- [11] Doka Nassionou, G. A., Magnoux, P. and Guisnet, M., Microporous and Mesoporous Materials, (1998) in press.
- [12] Stull, D. R., Westrun Jr., E. F. and Sinke, G. C., "The Chemical Thermodynamics of Organic Compounds", John Wiley and Sons, Inc. (1969).

INVESTIGATION OF THERMOLYSIS PATHWAYS FOR DIARYLMETHANE MODEL COMPOUNDS UNDER RESTRICTED DIFFUSION

A. C. Buchanan, III* and Phillip F. Britt

Chemical and Analytical Sciences Division
Oak Ridge National Laboratory
1 Bethel Valley Road
P. O. Box 2008
Oak Ridge, Tennessee 37831-6197

Submitted For Publication in ACS, Division of Fuel Chemistry, Preprints

* To whom correspondence should be addressed
phone: (423) 576-2168
fax: (423) 576-5235
e-mail: buchananac@ornl.gov

This research was sponsored by the Division of Chemical Sciences, Office of Basic Energy Sciences, U.S. Department of Energy, under contract No. DE-AC05-96OR22464 with Oak Ridge National Laboratory, managed by Lockheed Martin Energy Research, Corp.

"The submitted manuscript has been authored by a contractor of the U.S. Government under contract No. DE-AC05-96OR22464. Accordingly, the U.S. Government retains a nonexclusive, royalty-free license to publish or reproduce the published form of this contribution, or allow others to do so, for U.S. Government purposes."

INVESTIGATION OF THERMOLYSIS PATHWAYS FOR DIARYLMETHANE MODEL COMPOUNDS UNDER RESTRICTED DIFFUSION

A. C. Buchanan, III and Phillip F. Britt

Chemical & Analytical Sciences Division
Oak Ridge National Laboratory
1 Bethel Valley Road
P.O. Box 2008, MS-6197
Oak Ridge, Tennessee 37831-6197

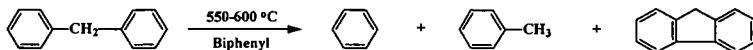
Keywords: Model compounds, pyrolysis, restricted diffusion, diphenylmethane

ABSTRACT

Diarylmethane linkages are important structural units in coals and Kraft lignins that contain only strong carbon-carbon bonds. Studies of the thermolysis of the model compound, diphenylmethane, in fluid phases have demonstrated an important retrograde cyclization pathway that forms the polycyclic aromatic hydrocarbon, fluorene, as a major product. We have now prepared a silica-immobilized form of diphenylmethane ($\approx \text{SiOC}_6\text{H}_4\text{CH}_2\text{C}_6\text{H}_5$; $\approx \text{DPM}$) to investigate the influence of restricted mass transport on this retrogressive pathway. Initial studies at 425-450 °C indicate that at high surface coverages, the cyclization pathway remains the dominant thermolysis pathway. In addition, restricted diffusion leads to the production of significant quantities of triphenylmethanes (ca. 8-10 %) generated by a competing radical displacement pathway involving diphenylmethyl radicals. The impact of lower $\approx \text{DPM}$ surface coverages and the structure of neighboring spacer molecules on the retrogressive pathways is under investigation.

INTRODUCTION

The thermal decomposition of diarylmethane structures has drawn considerable attention as they are models for related linkages present in coals and Kraft lignin.¹⁻¹² These linkages are important due to their refractory nature, which makes it difficult to cleave them except at high temperatures. For example, diphenylmethane (DPM) is typically reported to be thermally stable at 400-430 °C even in the presence of a hydrogen donor solvent such as tetralin.^{8,9} Petrocelli and Klein reported that thermolysis of DPM in biphenyl solvent at 1.8-6.2 MPa (nitrogen) and 550-600 °C gave benzene, toluene, and fluorene as major products, as shown below, with fluorene yields of ca. 25-30 % and material balances of 81-85 %.¹⁰



The main products are consistent with an earlier report of Sweeting and Wilshire, who examined the thermolysis of DPM at 700 °C in the vapor phase under short contact time, flow conditions.¹¹ However, Suzuki, et. al. have reported that thermolysis of liquid DPM in the absence of solvent, catalyst, or hydrogen atmosphere can occur slowly at temperatures as low as 425 °C to produce benzene and toluene at a rate of about 1 % h⁻¹ (formation of fluorene was not reported).¹²

In our research, we have been exploring the effects of restricted mass transport on thermolysis reactions of model compounds for related structural units in fossil and renewable energy resources.¹³ Restricted mass transport, which can be important in the thermochemical processing of macromolecular energy resources, has been simulated through the use of model compounds that are covalently linked to a silica surface through a thermally robust Si-O-C_{aryl} linkage. This research has uncovered examples where product selectivities and reaction rates

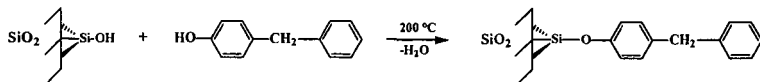
are significantly altered compared with corresponding fluid phase models. In particular, retrogressive rearrangement and cyclization pathways can be promoted under restricted mass transport conditions. In this paper, we report our first investigations of the thermolysis of a silica-immobilized diphenylmethane, indicated by \approx DPM, to examine the nature of the cyclization pathway under diffusional constraints.

Experimental

The DPM model compound was attached to the silica surface through both a *para*- and *meta*- linkage. The precursor phenol, *p*-HOC₆H₄CH₂C₆H₅, was commercially available. Purification involved elution from a silica gel column with benzene, followed by multiple recrystallizations from hot benzene:hexane (1:4) to give the desired phenol in 99.9 % purity by GC. The isomeric phenol, *m*-HOC₆H₄CH₂C₆H₅, was synthesized by the reaction of benzene with *m*-HOC₆H₄CH₂OH in the presence of AlCl₃. Following addition of water and then additional benzene, the benzene layer was separated, washed with saturated NaCl solution, dried over Na₂SO₄, filtered, and the solvent removed on a rotovap. Distillation under vacuum (135-140°C at 0.25 torr) gave the desired phenol with a purity of 99.6 % by GC.

Chemical attachment of the precursor phenol to the surface of a nonporous silica (Cabosil M-5; 200 m² g⁻¹; ca. 1.5 mmol SiOH g⁻¹) was accomplished as described below for the *p*-DPM isomer. *p*-HOC₆H₄CH₂C₆H₅ (6.085 g; 33.0 mmol) was dissolved in dry benzene (distilled from LiAlH₄) and added to a benzene slurry of silica (9.57 g; 14.4 mmol SiOH) that had been dried at 200°C for 4 h in an oven. Following stirring and benzene removal on a rotovap, the solid was sealed in a pyrex tube evacuated to 4 × 10⁻⁶ torr. The attachment reaction was conducted in a fluidized sand bath at 200°C for 1 h. Unattached phenol was removed by temperature-ramped sublimation under dynamic vacuum (250-375°C; 1 h; 0.02 torr). Surface coverage analysis was accomplished by dissolution of the solid (ca. 200 mg) in 30 mL of 1 N NaOH overnight. 4-Phenylphenol was added as an internal standard. The solution was neutralized by the addition of HCl, and extracted thoroughly with CH₂Cl₂. The solution was dried over MgSO₄, filtered, the solvent removed on a rotovap, and the resulting material silylated with *N,O*-bis-(trimethylsilyl)trifluoroacetamide (BSTFA) in pyridine (2.5 M). The corresponding trimethylsilyl ether derivative was analyzed by GC (HP 5890) on a J&W Scientific 30 m × 0.25 mm i.d. (0.25 μm film thickness) methyl silicone column with flame ionization detection. GC analysis gave a surface coverage of 0.43 mmol g⁻¹ for the *para*- isomer (purity of 99.8 %), and a surface coverage of 0.29 mmol g⁻¹ for the *meta*-isomer (purity of 98.2%).

Attachment Reaction

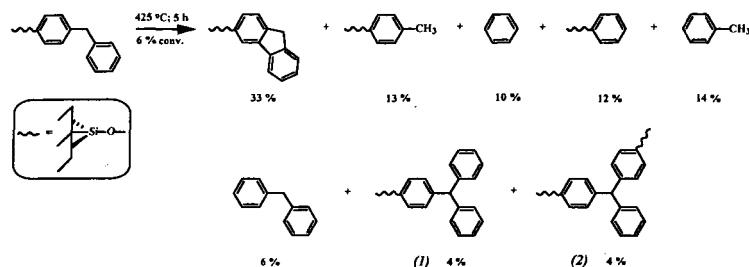


Thermolyses were conducted in sealed, evacuated (2 × 10⁻⁶ torr) T-shaped pyrex tubes in a temperature controlled furnace. Volatile products were collected as they were produced in a liquid nitrogen cold trap, and subsequently analyzed by GC and GC-MS with the use of internal calibration standards. Surface-attached products were similarly analyzed after digestion of the silica in aqueous base, and silylation of the resulting phenols to the corresponding trimethylsilyl ethers as described above for the surface coverage analysis.

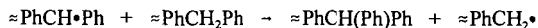
Results and Discussion

Our initial studies of the thermolysis of the *para*-isomer of silica-immobilized diphenylmethane (\approx *p*-DPM, 0.43 mmol g⁻¹) indicate that a slow reaction occurs at 425°C (conversion rate of ca. 1.2 % h⁻¹). The principal products are shown in the scheme below, and the selectivities are insensitive to the extent of \approx *p*-DPM conversion over the range

studied (1.8 - 18.0 %). Numerous higher molecular weight products can be detected in the GC trace, particularly at higher conversions. As expected, mass balances which are good (ca. 98% at low conversions) become progressively poorer at the higher conversions (ca. 87 % at 18 % conversion).

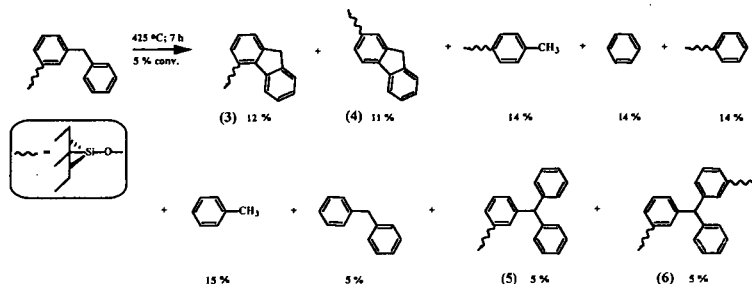


The major reaction path observed for *p*-DPM is cyclization-dehydrogenation to form silica-immobilized fluorene, which is formed in a slightly higher yield (33 mol %) than reported in the liquid phase.¹⁰ This is accompanied by hydrogenolysis of *p*-DPM to form benzene and toluene products (both gas-phase and surface-attached), which is induced by hydrogen atoms released from the cyclization step. This suggests that the dominant reaction chemistry observed in fluid-phase studies of DPM can similarly occur under restricted mass transport conditions. Hydrogen atoms are also found to induce cleavage of the $\equiv\text{SiO}-\text{PhCH}_2\text{Ph}$ bond which produces the PhCH_2Ph product. Diphenylmethyl radicals, $\approx\text{PhCH}\cdot\text{Ph}$, are thought to be the key intermediates in the cyclization to form fluorene, which are principally generated through hydrogen transfer propagation steps with gas-phase and surface-immobilized benzyl radicals. The initiation step for this radical chain process is not currently known, but a molecular disproportionation step seems most likely.^{1,2} The efficiency of this radical chain pathway should be sensitive to the *p*-DPM surface coverage as well as the structure of neighboring molecules on the surface, which is under current investigation. The formation of unexpectedly significant amounts of triphenylmethane products 1 and 2 (totaling 8 mol % of the products) is also consistent with the formation of diphenylmethyl radical intermediates, that undergo an aromatic substitution reaction on a neighboring molecule of $\approx\text{PhCH}_2\text{Ph}$ in competition with cyclization. This process appears



to be promoted compared with fluid phases as a result of the restricted mass transport. Reduced rates for radical termination on the surface as well as the close proximity of the species at high surface coverages contribute to the emergence of this pathway.

To see if the orientation of the DPM molecule on the surface would impact the pyrolysis rate and product selectivities, we have prepared the *meta*- isomer of surface-attached DPM, *m*-DPM. As we observed previously for other molecules, the *meta*- surface linkage leads to a lower saturated surface coverage (0.29 mmol g⁻¹) compared with the *para*-linkage (0.43 mmol g⁻¹) due to less efficient packing on the surface. Initial thermolyses indicate a slightly lower thermolysis rate for *m*-DPM (ca. 0.7 % h⁻¹) at 425 °C, but the principal products shown below are quite similar. Cyclization occurring through the benzylic radical, $\approx m\text{-PhCH}\cdot\text{Ph}$, can lead to two possible isomeric fluorene products, and the two isomers 3 and 4 are detected in comparable yields. The identification of 4 has been confirmed with an authentic sample of the corresponding 2-hydroxyfluorene (the product formed after detaching 4 from the silica surface) that was independently synthesized as described previously.^{13a} The combined yield of fluorene formation, 23 mol %, is somewhat less than the yield observed for the *para*- isomer. The origin of this effect remains under investigation. The radical displacement chemistry that formed the triphenylmethanes, 1 and 2, in the thermolysis of *p*-DPM occurs with similar effectiveness for the *meta*- isomer and results in significant yields of triphenylmethanes 5 and 6.



CONCLUSIONS

Thermolysis of diphenylmethane under restricted mass transport conditions has been found to occur slowly at 425 °C by an apparent radical chain process cycling through diphenylmethyl radicals. At high surface coverages, these free-radical intermediates undergo competitive cyclization to form the polycyclic aromatic hydrocarbon, fluorene (major), and radical displacement on another diphenylmethane molecule to form triphenylmethanes (minor). The selectivity for these two pathways is 4.1 for the *para*- isomer of DPM and 2.3 for the *meta*- isomer indicating some sensitivity to orientation of DPM molecules on the surface. The hydrogen liberated from these processes results, as expected, in the unselective hydrocracking of DPM to form benzene and toluene products, and both material and hydrogen balances are good at the low conversions investigated. Future studies will examine the effect of surface coverage on the pyrolysis rates and product selectivities, and will explore the impact of a co-attached hydroaromatic spacer molecule such as tetralin.

ACKNOWLEDGMENTS

The authors express appreciation to K. B. Thomas for technical support. This research was sponsored by the Division of Chemical Sciences, Office of Basic Energy Sciences, U.S. Department of Energy, under contract No. DE-AC05-96OR22464 with Oak Ridge National Laboratory, managed by Lockheed Martin Energy Research, Corp.

REFERENCES

1. Poutsma, M. L. *Energy & Fuels* **1990**, *4*, 113, and references therein.
2. Murata, S.; Nakamura, M.; Miura, M.; Nomura, M. *Energy & Fuels* **1995**, *9*, 849.
3. Futamura, S.; Koyanagi, S.; Kamiya, Y. *Fuel* **1988**, *67*, 1436.
4. (a) McMillen, D. F.; Malhotra, R.; Chang, S.-J. *Fuel* **1987**, *66*, 1611. (b) Malhotra, R.; McMillen, D. F. *Energy & Fuels* **1990**, *4*, 184.
5. Autrey, T.; Alborn, E. A.; Franz, J. A.; Camaioni, D. M. *Energy & Fuels* **1995**, *9*, 420.
6. Mitchell, S. C.; Lafferty, C. J.; Garcia, R.; Snape, C. E.; Buchanan, III, A. C.; Britt, P. F.; Klavetter, E. *Energy & Fuels* **1993**, *7*, 331.
7. Shi, B.; Ji, Y.; Guthrie, R. D.; Davis, B. H. *Energy & Fuels* **1994**, *8*, 1268.
8. McMillen, D. F.; Ogier, W. C.; Ross, D. S. *J. Org. Chem.* **1981**, *46*, 3322.
9. Benjamin, B. M.; Raaen, V. F.; Maupin, P. H.; Brown, L. L.; Collins, C. J. *Fuel* **1978**, *57*, 269.
10. Petrocelli, F. P.; Klein, M. T. *Macromolecules* **1984**, *17*, 161.
11. Sweeting, J. W.; Wilshire, J. F. K. *Aust. J. Chem.* **1962**, *15*, 89.
12. Suzuki, T.; Yamada, H.; Sears, P. L.; Watanabe, Y. *Energy & Fuels* **1989**, *3*, 707.
13. (a) Buchanan, III, A. C.; Britt, P. F.; Thomas, K. B.; Biggs, C. A. *J. Am. Chem. Soc.* **1996**, *118*, 2182. (b) Buchanan, III, A. C.; Britt, P. F.; Thomas, K. B. *Energy & Fuels* **1998**, in press. (c) Buchanan, III, A. C.; Biggs, C. A. *J. Org. Chem.* **1989**, *54*, 517. (d) Britt, P. F.; Buchanan, III, A. C. *J. Org. Chem.* **1991**, *56*, 6132. (e) Britt, P. F.; Buchanan, III, A. C.; Malcolm, E. A.; Biggs, C. A. *J. Anal. Appl. Pyrolysis* **1993**, *25*, 407. (f) Buchanan, III, A. C.; Britt, P. F.; Biggs, C. A. *Energy Fuels* **1990**, *4*, 415.

PREDICTING THE LIFE OF SKIRT SUPPORTS IN PRESSURIZED REACTORS UNDER CYCLIC CONDITIONS

Marcos Sugaya
Petrobras S.A., Cenpes
Rio de Janeiro 21910-900, Brazil

Colin McGreavy
The University of Leeds, Chem. Eng. Dept.
Leeds LS2 9JT, UK

KEYWORDS: pressure vessel, skirt support, thermal stresses

ABSTRACT

A common problem with skirt support is the occurrence of cracks originating at the outer boundaries of the welded junction. In order to understand the background on this, a study of the changes in temperatures and stress profiles has been undertaken by placing strain gages and thermocouples near the attachment region of an existing delayed coking reactor. Stresses arising from the differential thermal expansion, junction momentum and other contributions have been examined in terms of the Weil-Murphy analysis of the problem to provide a basis for validating models of stress failure.

INTRODUCTION

Mechanical designs of reactors are usually based on steady-state operating conditions and ignore stresses which arise during process transients, such as in emergencies or at start-up and shut-down. For continuous processes this is not a major problem because transients occur only infrequently. In the case of batch operations, however, transients are a normal part of the production cycle and so the effect need to be examined in more detail.

In particular, welded skirt supports of the type commonly used in vertical pressurized reactors are often subject to fatigue failure. The cycling causes abnormal transient thermal stresses in the vessel near these joints which tend to progressively weaken the structure. It is therefore important to look into ways in which this deterioration in the structural integrity can be mitigated by looking at the effect of transient changes occurring during batch operations particularly in terms of how the frequency and magnitude of the changes can be accommodated to ensure safer designs and how this might have to be reflected in operating policies which will maximize equipment life.

DIFFERENTIAL STRESS ANALYSIS

The main stress components at the skirt junction can be calculated using beam on elastic foundation theory (1) applied to a three-cylinder junction, as suggested by Weil and Murphy (2).

To assess fatigue, the stresses of major concern are those arising in the outer skirt region, since the weld is much more susceptible to this kind of failure than the vessel plates as has been verified in studies of the origins of cracks occurring in operational units. All the evidence suggests that the outer surface of the attachment weld is the starting point.

During the normal operation of the drums, heat flows from the hot vessel walls to the skirt attachment. When the reactor is cooled, the flux is in the opposite direction. The calculation of thermal stresses (which are the major components) requires thermal gradients to be estimated in the skirt, shell and conic sections. The largest gradients occur near the junction because the flow of heat to or from the skirt is by conduction through, although radiation and convection between the conic and skirt sections are important if there is no insulation. Heat accumulates as a result of the axial heat flow and causes the magnitude of the gradients to decrease away from the region.

In this study, thermocouples were placed close to the weld at the skirt, shell and conic sections and are spaced at short intervals (Figure 1). At low heat flux, the temperature differences between neighboring points are similar but because the gradients are estimated by finite difference approximation, the numerical estimate is subject to noise (Figure 2). Mean gradients for the shell, skirt and conic sections can be calculated using the temperature readings over wider intervals. It can be seen that this represents the average behavior fairly well (Figure 2) and effectively filters out the noise. Consistency in the results can be verified by comparing these

values with those estimated for adjacent thermocouples then computing an average gradient (for example, calculating the average gradient at the shell both with $(NE1-NE5)/4$ and $(NE2-NE5)/3$).

RESULTS AND DISCUSSION

During the cooling operation, the reactor full of coke is quenched with water. Figures 3-6 present the temperature change at four angular positions. Before switching the reactor (10.47 h), heat flows axially from the shell to the skirt and cone (Figures 7-10). This is consistent with the assumption of a main flow channel located centrally inside the vessel. The furnace effluents flow up through this channel to the top of the coke bed where the hot liquid accumulates. The coke deposited around the walls of the shell and conic sections acts as an insulating layer, limiting heat flow to the axial direction. As the drum fills up, the highest wall temperatures gradually move upwards. The lower part of the wall gradually cools down because heat is lost through the external insulation, but the temperatures are maintained at somewhat lower levels by axial and radial heat transfer. The temperature at the inlet nozzle is 490 C with the wall temperatures gradually falling from 390-435 C (a few hours after the drum starts to fill) to 300-325 C (before the next switch).

The temperatures in the lower left quadrant before the switch are somewhat higher than in the other positions, which are fairly uniform (Figures 3-6). This suggests that the main channel is located off-center and close to this quadrant. However, during cooling, the upper right quadrant cools faster. Had the channel being located closer to the lower left, it would have cooled faster, since quench water could be expected to spread radially from the central channel towards the walls. The most difficult zone to cool is the first quadrant, only being active after 9.6 hours. This means that this region behaves as if no cooling has taken place.

In Figures 3-6 it can also be seen that the switch and the steam stripping stages (both the 'small', 5 t/h, initiated immediately after the switch and the 'large', 15 t/h, initiated at ~ 11.85 h) do not seem to contribute to cooling of the reactor walls, since the temperatures remain unchanged during these operations. The heat transfer between the steam and the coke is poor, since convective heat transfer coefficients are known to be much smaller than boiling coefficients. It is also difficult for the steam to flow through the parts of the coke bed closer to the vessel walls. Strictly, an enthalpy balance on the steam during the stripping cycle is necessary to clarify this point but the top temperature is not accessible. The temperature of the gasoil quench remains constant during steaming, which suggests that only the central portions of the coke bed are exchanging heat.

It should also be noted that the production of lighter fractions due to thermal cracking is still significant even a long time after the switch has been made. The steam mixes with the vapors resulting only in a small temperature drop at the top. This requires estimating the oily fractions recovered from the blowdown system in order to compare the relative flow rates of hydrocarbons and steam at the top.

Increasing the pressure in the drum during the stripping operation would be beneficial to make it possible to penetrate deeper into the coke bed and so reduce the partial pressure in the zones closer to the walls. This increases the removal of hydrocarbons and cools the coke bed.

The important features contained in Figures 3-6 relate to the differences in the local curves, not the trend suggested by the general rate of change in temperature reflected in the different quadrants. Thus, the local spatial gradients in NW do not change much with time and the average value of temperature changes little. On the other hand, there is a significant change in average local temperature in SW ~200 C but little change in the local temperature differences, so the local gradient remains more or less constant. In the case of NE and SE, the local gradients are larger during part of the transient because of increases in local temperature differences. It is clear that the rate of change of temperature with time is not therefore in itself an indicator of significant changes in temperature gradient and by implication the local stress.

The calculated stresses are all very small (Figure 11 shows the longitudinal stresses at the outer skirt as an example) and far from the yield limit (~ 210 MPa). This is to be expected considering the modest thermal gradients observed. In the third quadrant the forces are slightly lower and decline faster than at other positions. On the other hand, in the first quadrant there is change from tension to compression at a certain point, which is important in fatigue assessment if fast quench rates results tend to exacerbate this. Generally, no residual forces seem to remain as the vessel is cooled down, apart from those due to the weight of coke and water.

As water evaporates, the pressure rises and if care is not taken, it can result in activation of the safety valve, causing a shut-down. A delay occurs in the response of the pressure to the water flow rate and the pressure sometimes rises, even after the water flow rate has been reduced, and requires careful attention to ensure it does not cause problems.

One strategy used is to close the top valve a little in order to increase the pressure in the vessel. This practice has originated in a plant where the delayed coking units tend to be a

As water evaporates, the pressure rises and if care is not taken, it can result in activation of the safety valve, causing a shut-down. A delay occurs in the response of the pressure to the water flow rate and the pressure sometimes rises, even after the water flow rate has been reduced, and requires careful attention to ensure it does not cause problems.

One strategy used is to close the top valve a little in order to increase the pressure in the vessel. This practice has originated in a plant where the delayed coking units tend to be a production bottleneck. Experience has shown that restraining the top valves promotes radial flow of water through the coke bed, which accelerates cooling.

Successive runs show that parts which appear to be difficult to cool change randomly, indicating that the main channel is deviating from the center. Before the cooling stage, heat flows towards the junction at the shell and away from the junction at the skirt and conic sections. This is followed by heat flow in the opposite direction in the shell and skirt immediately after the cooling phase. The gradients in the conic section are initially positive then decrease soon after the start of the cooling cycle. Sometimes they are negative or increase again after a short drop.

The skirt and cone generally have more similar temperatures. The slower cooling rates and the gradients which develop in the conic section are caused by competition between the heat removed from the wall to the coke bed and heat supplied by the skirt attachment through the welded joint, as well as by radiation and convection. The form of the weld can also cause the heat which is retained in the skirt to move into the conic section which would explain why the shell cools faster than the conic section.

Figures 12-20 show that for rapid preheating (sometimes the cycle is delayed and requires heating the drum at a fast rate), variations of 1.6 C/min are obtained, which compare with the 1.6-1.8 C/min reported by Lieberman for a fast warm-up operation where one third of the vapors from the full drum are by-passed to the empty one (3). The high temperature gradients result in higher thermal stresses than those found in any of the cooling runs analyzed, but are still less than the yield limit.

CONCLUSIONS

The results indicate that the stresses that define the life of the skirt attachment weld on a fatigue basis are mainly established during warm-up or perhaps shortly after switching on. The inversion of stresses observed during the cooling operation at the outer region is mild and does not seem to be significant as far as fatigue assessment is concerned.

Switching to a cold drum should be avoided if at all possible. The results reported here suggest that this event could give rise to significant stresses in the coke drum, higher than for any other case and probably above the yield limit. To assemble useful information, it is necessary to have access to a suitable model since collection of experimental data on an extended experimental program is not feasible.

The results illustrate the importance of operational practices. Policies designed to increase the life of the skirt attachment weld should focus on warm-up and switch conditions or factors that could reduce the available time for warm-up (such as a delay in cutting the coke or an excessively slow cooling operation). Design should ensure sufficient drum capacity.

REFERENCES

1. Hetenyi M. Beams on Elastic Foundations 1946.
2. Weil N. A.; Murphy J. J. Journal of Engineering for Industry 1960, Feb., 1.
3. Lieberman N. P. Oil & Gas Journal 1983, Aug.29, 39.

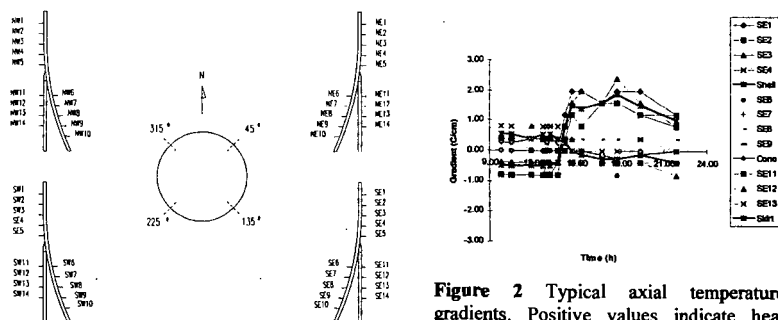


Figure 1 Location of thermocouples at the shell-skirt junction.

Figure 2 Typical axial temperature gradients. Positive values indicate heat flowing from the junction, dark lines represent average values.

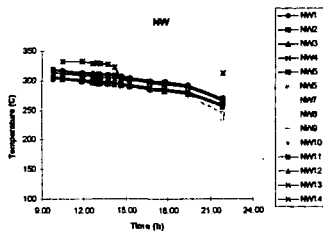


Figure 3 Skin temperatures at NW.

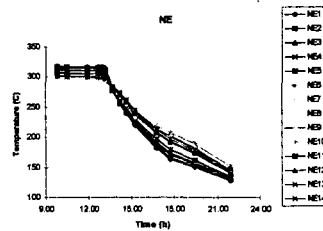


Figure 4 Skin temperatures at NE.

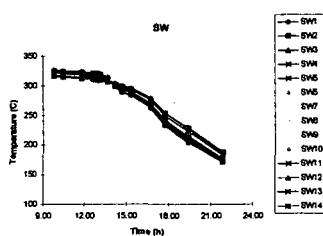


Figure 5 Skin temperatures at SW.

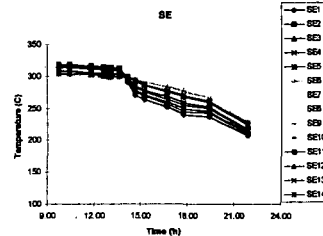


Figure 6 Skin temperatures at SE.

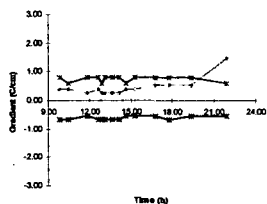


Figure 7 Axial gradients at NW.

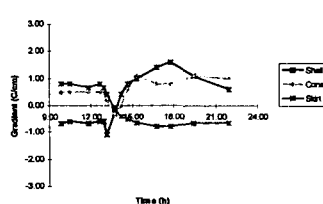


Figure 8 Axial gradients at NE.

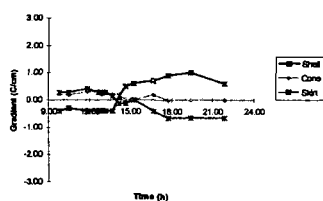


Figure 9 Axial gradients at SW.

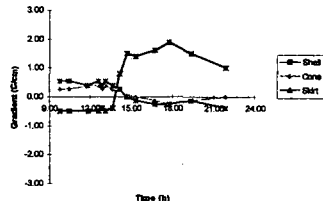


Figure 10 Axial gradients at SE.

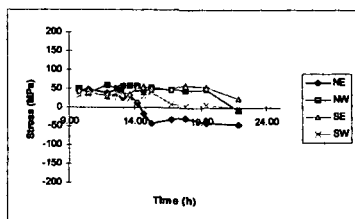


Figure 11 Longitudinal stresses at the (outer) skirt during cooling.

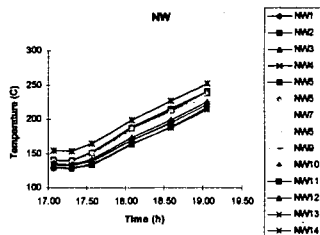


Figure 12 Temperatures at NW.

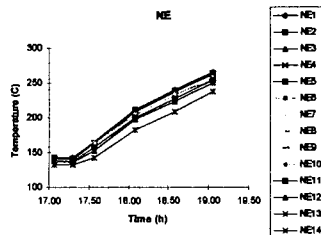


Figure 13 Temperatures at NE.

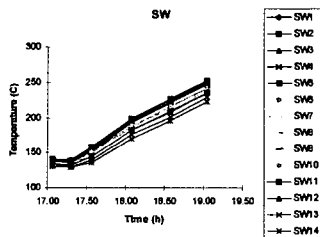


Figure 14 Temperatures at SW.

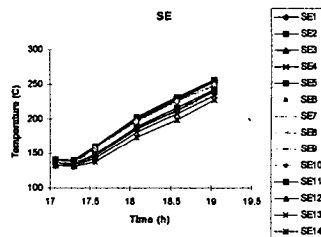


Figure 15 Temperatures at SE.

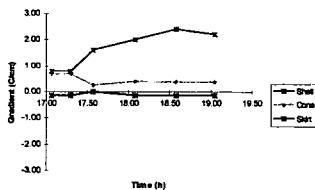


Figure 16 Axial gradients at NW.

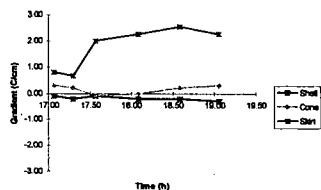


Figure 17 Axial gradients at NE.

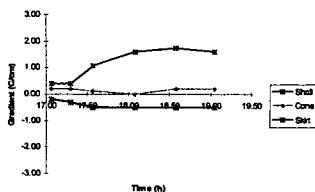


Figure 18 Axial gradients at SW.

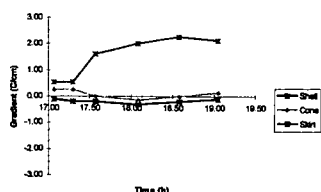


Figure 19 Axial gradients at SE.

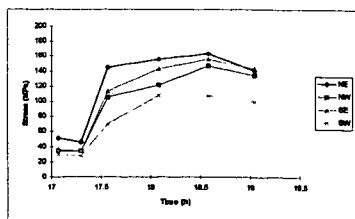


Figure 20 Longitudinal stress at the (outer) skirt during a fast pre-heating operation.

COST EFFECTIVE EVALUATION TECHNIQUES FOR FCC ATOMIZING NOZZLES

Edson José Joaquim de Souza
Aurélio Medina Dubois
Petrobras Rod. Br 476, Km 143
São Mateus do Sul-PR
83900-000 Brazil

KEYWORDS: FCC NOZZLES; NOZZLES EVALUATION; FCC FEEDING
IMPROVEMENT

INTRODUCTION

The improvement of gasoline yields and quality on FCC plants has been a must on the field of oil industry research and development over the last several years. The high inlet processing volumes make any improvement either in conversion or product quality result in very high levels of financial savings. There is an important relationship between the oil feeding quality and the oil-catalyst interaction which leads to such better yield and quality upgrade⁽²⁾.

The complete uniform mixing of catalyst and oil has become a challenging target for FCC plant engineers and designers around the world. Besides the usage of heavier input oil makes such a mixing even more important. The oil-catalyst contact, vaporisation and residence times in the riser environment are all involved with inlet oil spray pattern. Some of the most important figures on feeding quality such as the droplet diameter, mass flow distribution on spray and momentum depend on the FCC atomisation nozzle. This paper discusses some on plant, cost-effective evaluation techniques, which may be applied by FCC plant engineers in order to choose a good feeding tip for their needs. High-speed photography, mass distribution measurements and other simple but effective evaluation procedures are discussed. Also a nozzle case study is shown, whose evaluation was carried out by such a set of techniques under several conditions.

FCC FEEDING NOZZLES

There are many commercial feeding nozzles types available on FCC technology world-wide. However about a dozen of such a models have been mostly used on plants lately. Some devices have registered marks and they are protected under patents.

The most used nozzle atomizer type is the twin-fluid atomizer. Those devices use a high velocity atomizing fluid, which impinges on a liquid traverse flow. The high relative velocity between the two fluids causes a very rapid deformation of the liquid film, the sheet break up, the formation of ligaments, drops and droplets.

In order to select a good tip for any specific need a FCC engineer may carry out an evaluation plan. The feeding oil physical and chemical properties, the atomizing steam availability, the pumping power and other operating conditions must be considered.

An effective evaluation plan must focus on the main known features of a good tip. As a matter of fact a good nozzle must fulfil a set of features as follows: Small droplet diameter under a narrow distribution⁽³⁾; uniform flow rate on spray; symmetrical flat shaped spray; stability; easy manufacturing and maintenance; life-span; turndown and performance.

EVALUATION PLAN

A challenging target in testing FCC nozzles on test rigs is the safe scale up and down process and the usage of test fluids instead of oil and steam. The usage of actual fluids on test rigs is difficult and even dangerous, due to the hazardous oil properties. Besides the test cost may increase considerable so a good choice is to replace oil by water and steam by compressed air.

Another well-used method is the tip scale up and down process to avoid the high mass flow rates used by the full-scale nozzle. Both methods may be used under strict theory rules otherwise the results from test rig fail. Above all there are some important

parameters and dimensionless numbers must be checked.

| | Liquid | Gas |
|---|--|----------|
| Density (ρ_L) | ρ_L | ρ_G |
| Viscosity (ν) | ν_L | ν_G |
| Surface tension (σ) | σ | |
| Relative velocity ($U_r = U_G - U_L$) | U_L | U_G |
| Reynolds Number (Re) | $Re = \rho_L \cdot U_L \cdot d_0 \cdot \nu^{-1}$ | |
| Weber Number (We) | $We = \rho_L U_r^2 \cdot d_0 \sigma^{-1}$ | |
| Initial jet diameter d_0 | | |

On twin fluid atomizer theory the most important parameter is the Weber number⁽¹⁾. The feeding oil and atomizing steam under their operating conditions must have the above parameters as close as possible to the testing fluids, i.e. air and water at ambient temperature⁽⁴⁾. Also tips scale up and down cannot properly succeed without such a set of parameters relationship. Furthermore scale down process using mass flow ratio by a factor over say, four times are not recommended as well. Fortunately FCC feedstock and steam have atomizing parameters quite similar to water and air at test rig conditions.

SOME EVALUATION TECHNIQUES

Some of the most effective measurement techniques for FCC atomizers are related to the oil spray pattern analysis. There are many quantitative and qualitative methods that may vary in cost, applicability and reliability. This paper discusses some cost effective "on plant" techniques that may be used by FCC plant engineers. They are: the nozzle test rig and apparatus; droplet sizing by high-speed photography; mass flow rate distribution and pressure profile measurement.

NOZZLE TEST RIG

A simple but effective test rig can be built up beside any utility facility on a FCC plant. All need utilities can be easily found such as water and compressed air. The rig flow capacity may be designed to test full-scale nozzles or scaled down model tips. Measurements of water and air flow rates can be easily achieved by conventional flow meters.

DROPLET SIZING

One of the most famous droplet sizing technique is the laser scattering. Some good overall advantages are:

- It is a non-intrusive method so the spray pattern is not disturbed⁽¹⁾.
- There is a fast, quantitative result such as the droplet distribution and mean diameters (SMD, the Sauter Mean Diameter, for instance).

Some few, but not less important disadvantages are:

- Scattering light devices are not suitable for dense sprays⁽¹⁾ (FCC nozzles produces typically dense sprays, even using a scale down model).
- The scattering light principle considers a droplet a globular shaped body. This is not true because the surrounding areas downstream the tip contains ligaments with typically non-globular shape.
- It demands investments on lab-like test rigs, equipment and high qualified technical staff.

HIGH-SPEED PHOTOGRAPHY

An alternative droplet sizing technique is the high-speed photography. It is not a quantitative method but it can give us a good idea about the spray pattern and droplet size (comparison). The high cost and difficult to use old spark flashes are not effective anymore. Nowadays a high-speed photographic system can be built up using only almost conventional devices (fig. 1). A simple set was successfully used to carry out tests on a group of FCC nozzles.

The camera does not need to have high speed shutter capabilities⁽⁵⁾. As matter of fact

even special high-speed shutters are enable to "stop" the spray image because the droplets velocity stream. The shutter is kept open while the trigger is pressed (on the "B" setting). The photo is taken in the darkness and the exposition time is the flash duration. An EG&G high-speed flash may produce a lightning as fast as 1/50,000 of a second. The speed film such as ISO 400 B&W is satisfactory (fig.2). Some conventional amateur electronic flash may be also used but the light is not powerful enough for quality photos.

MASS FLOW RATE DISTRIBUTION

A flat shaped spray may produce several mass flow rate patterns even with the same droplet mean diameter. Basically one of the oil/catalyst mixing goals is to inject the feedstock where the catalyst is and so a uniform mass flow distribution is required. Some commercial nozzles have good droplet mean diameter but poor mass flow distribution. Using a simple cell box device the mass flow distribution measurement can be carried out (fig 3). Also a distribution histogram of the collected water is shown. Many nozzles release much flow at the spray centre producing a non-ideal pattern(fig. 4).

STATIC PRESSURE DOWNSTREAM THE SPRAY

The pressure profile downstream the feeding nozzle used to be negligible in the early days of FCC feeding development. However low pressure zones downstream the atomization chamber may induce dangerous backward catalyst flow (inside Riser). The catalyst may impinge on the nozzle top at high velocity by means of backward stream. Sometimes the erosion is so hard that whatever the tip material is it may last only few hours. The pressure profile along the nozzle chamber and in the first feet downstream the top may vary under different operating conditions. A good nozzle should keep positive pressure on its turndown range. Using mercury U gauges such a pressure can be easily measured.

The pressure profile (example on fig.5) on tips is strongly dependent on geometry and pressure drops. Sometimes the chamber geometry, liquid injection angle, and mass flow liquid/gas ratio result in different pressure levels.

CASE STUDY

The set of techniques shown on this paper was successfully applied on a group of nine up to date FCC nozzles. The main target was to carry out a comparison study between the Petrobras UltraMist[®] FCC nozzle and other commercial tips. All evaluation techniques discussed on this paper were successfully applied. Although the droplet sizing by high-speed photos results qualitative analysis, some good points and bad points were highlighted. Such a nozzle has got a good and uniform mass flow distribution, small droplet mean diameter and stability. Other commercial nozzles achieve good standard features as well. However there are some conflicting features they should be managed, such as droplet diameter and pressure profile.

REFERENCES

- 1) Yule, A.J. et al, 1996, "Atomizer and spray technology", notes in support of the 10th UMIST short course, University of Manchester.
- 2) Wrench, R.E. et al, "FCC Hardware Options for the Modern Cat Cracker", AIChE Symposium Series.
- 3) Sapre, A.V. et al, "Design Methods for FCC Feed Atomization", AIChE Symposium Series, no 291, vol.88
- 4) Simmons, H.C., Harding C.F., 1981, "Some Effects of Using Water as a Test Fluid in Fuel Nozzle Spray Diagnostics", transactions of the ASME, Vol. 103, Jan/81.
- 5) Winters, L.M., 1996, "High Speed Flash Photography for Amateur Photographers"; North Carolina School of Mathematics Science.

FIGURES

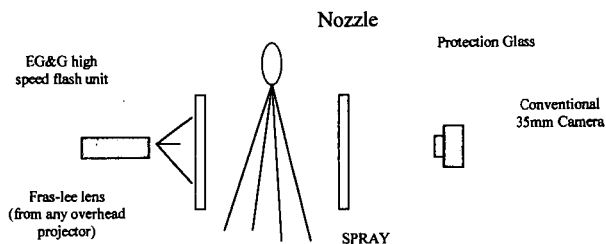


fig1. High-speed photography system-Schematic of apparatus



Fig.2 High speed photography (liquid flow rate=3230 Kg/h; air flow rate 100 Nm³/h)

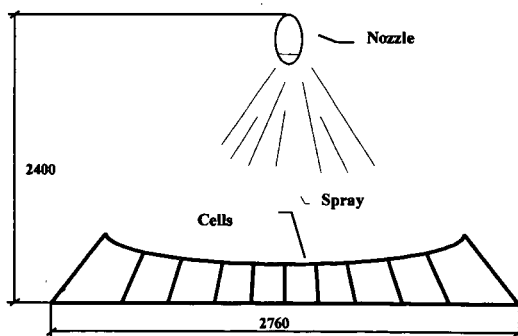


Fig.3 Cell box for flat spray flow distribution

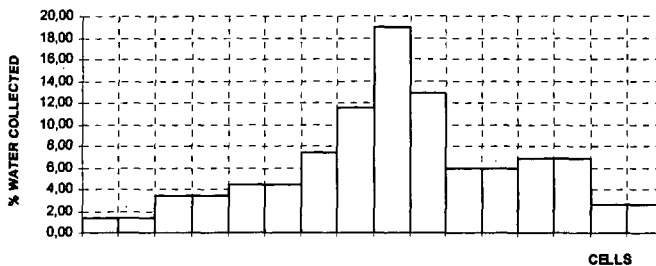


Fig.4 Mass flow rate on the spray-Histogram from the cell box

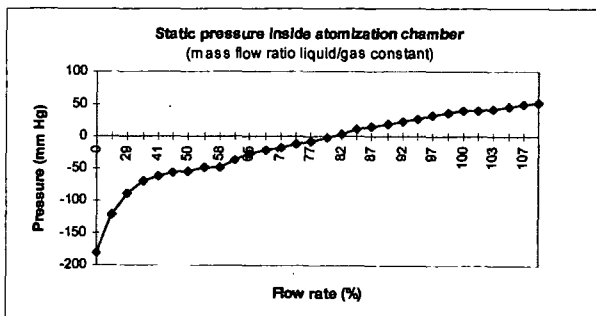


Fig.5. Pressure profile example

ULTRASONIC CHARACTERIZATIONS OF SLURRIES IN BUBBLE COLUMN REACTORS

Y. Soong*, A. G. Blackwell, F. W. Harke, E. P. Ladner, and M. F. Zaroachak, U.S. Department of Energy, Federal Energy Technology Center, P.O. Box 10940, Pittsburgh, PA 15236, U.S.A.

Key words: ultrasound, solid holdup, bubble columns

INTRODUCTION

For the optimum design and operation of gas-liquid-solid three-phase reactors, the degree of dispersion of the solid (catalyst) in the reactor must be understood and controlled. Recently, a method involving the measurement of ultrasound transmission has been reported in a slurry-phase stirred-tank reactor which offers the possibility of using the ultrasonic technique to measure solid holdup in a three-phase slurry reactor (1-3). The ultrasonic transmission uses measurements of the velocity and attenuation of the sound wave which travels directly through the slurry sample. When an acoustic wave strikes the boundary between two different media (liquid and solid) and the acoustic impedances of the two media are different, some acoustic energy will be reflected, absorbed, and some will be transmitted. The reflected wave travels back through the incident medium (liquid) at the same velocity. The transmitted wave continues to move through the new medium (solid) at the sound velocity of the new medium. When the velocity of sound in a liquid is significantly different from that in a solid, a time shift (a velocity change) in the sound wave can be detected when solid particles are present relative to that for the pure liquid. The amplitude of the sound wave is also reduced when a solid particle is present since the wave is partially scattered and absorbed. Therefore, a change in amplitude of the sound wave can also be detected when solid particles are present relative to that for the pure liquid. Okamura et al. (1) and Soong et al., (2-4) used a continuous stirred-tank reactor to correlate the solid holdup to the relative time shift $[(t_s - t_0)/t_0]$. Furthermore, the application of the measurement of ultrasound transmission for gas holdup (5-7) and for gas holdup as well as low concentration of solid (up to 1 wt. %) under limited superficial gas velocities (up to 3 cm/s) in a slurry-bubble-column reactor has been reported (8,9). This leads to the initial study of using the ultrasonic technique for the measurement of solid holdup in a three-phase gas-liquid-solid bubble column reactor over a wide range of superficial gas velocities and solid holdup.

EXPERIMENTAL

A schematic representation of the bubble-column-reactor in which the ultrasonic investigation was conducted is shown in Figure 1. The transparent acrylic bubble-column-reactor has an internal diameter of 8.89 cm and a height of 290 cm. The column has six different axial locations for data collection. The ultrasonic signals are transmitted at 33 cm above the bottom of the gas distributor, which is a perforated-plate gas distributor with 15 x 1 mm diameter holes, along the center of the bubble-column-reactor. Experiments were conducted in batch-mode operation (stationary liquid-water and continuous flow of gas-nitrogen). Nitrogen bubbles were introduced through the gas distributor plate located at the bottom of the reactor. The nitrogen flow was controlled electronically to a maximum of 12 cm/s through a mass-flow controller. Glass beads from Cataphote, Inc., (10-37 μ m in diameter with density of 2.46 g/cm³) were used as the solid in the slurry. The solid holdup (solid weight/total slurry weight) was varied from 5 to 30 wt. % for each nitrogen flow in the reactor. To evaluate the accuracy of the ultrasonic technique for solid holdup measurement, an independent slurry sampling device was installed. The measurement was conducted by inserting a stainless steel tubing (0.775 cm. I.D.) horizontally into the center of the column at 0.635 cm above the path of the ultrasonic transmission. For each sampling, a 10 cm³ of slurries sample was collected and analyzed for solid holdup characterization. The ultrasonic transmitter/receiver and the solid sampling device are positioned such that both means are measuring approximately the same hydrodynamic phenomena as shown enlarged areas in Figure 1. The detailed information of the ultrasonic unit has been reported elsewhere (2-4). Data were obtained with longitudinal waves at a frequency of 1 MHz using lithium niobate transducers. Both the transmitter and receiver were mounted directly inside the reactor wall at 33 cm above the gas distributor.

RESULTS & DISCUSSION

Figure 2 illustrates the effects of the superficial gas velocity (SGV) on the transit time [an arbitrary first distinct zero crossing time in the ultrasonic signal; the details have been described elsewhere (2)] and on the gas holdup in the reactor. The average gas holdup was determined by visual observations of the expanded bed height versus the static bed height. During this process, we have visually identified the various flow regimes since our bubble column is transparent. Basically, three flow regimes were identified in the bubble column. The homogeneous flow regime was observed when the SGV is 2.4 cm/sec or less. The average gas holdup in this regime was found to increase linearly from 0.015 at a gas velocity of 0.26 cm/sec to 0.093 at a SGV of 2.4 cm/sec. A transition flow regime exists between the SGV of 2.4 and 4 cm./sec. A slug flow regime is established when the velocity is 4 cm/sec or higher. The average gas holdup increased from 0.1 to 0.148 when the flow regimes changed from transition to slug flow. The transit time does not have an apparent correlation with the SGVs. It was approximately 72 μ s at all SGVs and all flow regimes. Because what we measured was the signal that not transmitted through the nitrogen. Chang et al. (5) also reported that the amplitude of the transmitted sound pulses depends significantly on the number of bubbles; however, the transit time does not change with the void fraction. Uchida et al. (8) also measured the gas holdup in a bubble column for a gas-liquid system through determining the variation in transit time ratios. More recently, Warsito et al. (9) reported the measurement of gas holdup in a bubble column using the ultrasonic method. A change in transit time of 0.09 μ s as the gas holdup increased from 0.05 to 0.1 was reported from their system. In current study, we did not observe such a change in transit time as the gas holdup increased from 0.05 to 0.1 in our system. The discrepancy may be due to different experimental setup or other factors. The small variation in transit time in this study is probably due to the experimental errors rather than the effect of nitrogen flow.

Figure 3 shows the change in the amplitude ratio of the transmitted ultrasonic signals A/A_0 and the local gas holdup in the reactor as a function of the SGV. A and A_0 are the amplitudes of the transmitted signals with and without the presence of nitrogen, respectively. Figure 3 suggests that the amplitude ratio is approximately an inverse exponential function of the SGV when the column is operated in the homogeneous flow regime (SGV of 2.4 cm/sec or less). No discernible relationship between A/A_0 and SGV could be found when the latter is higher than 2.4 cm/sec, i.e., while the column is operating in transition or slug flow regimes. When a large nitrogen bubble (slug) passes across the ultrasonic transmitted path, the transmitted signal will be reduced significantly. The transmitted signal will regain some amplitude immediately after the slug has passed through the transmitted path. Therefore, a large scatter of the A/A_0 ratio is observed at SGV of 2.4 cm/sec or higher. These phenomena could be observed while the column was operated in the transition or slug flow regimes. Chang et al. (5) measured void fractions up to 20% in bubbly air-water two phase flow using an ultrasonic transmission technique. Their results also showed that the A/A_0 ratio has exponential relationship with the void fraction and a function dependent on the bubble diameter. The effect of air bubble diameters on A/A_0 ratio was found to be significant where A/A_0 decreased with increasing bubble size. Bensler et al.(6) also conducted the measurement of interfacial area in bubbly flows in air-water systems by means of an ultrasonic technique. Their observations suggest that the A/A_0 ratio has an exponential relationship with the interfacial area and the scattering cross section, which depends on the bubble radius (a) and the wave number (k) of the ultrasonic wave surrounding the bubble. Our observations of A/A_0 in the nitrogen/water system are in qualitative agreement with those reported by Chang et al. (5) and Bensler et al.(6).

Figure 4 shows the effect of gas velocity (SGV) on amplitude ratio (A/A_0), transit time, and average gas holdup in three-phase systems (30 wt. % of glass bead/nitrogen/water) in the bubble column reactor. A and A_0 are the transmitted signals with and without the presence of solids, respectively. The similar flow regimes' patterns were also observed in the three-phase system (Figure 4) as those in a two-phase system (Figures 2 and 3). The fluctuation patterns of the A/A_0 along with different flow regimes in Figure 4 are similar to that in Figure 3. Unlike the constant transit time observed in Figure 2 for a two-phase system, the transit time in a three-phase system is related to the flow regimes operated and the presence of solids. The transit times were 70.56 and 70.52 μ s, respectively, for superficial gas velocities of 0.537 and 1.611 cm/sec when the column is operated in the homogeneous flow regime. In the transition flow regime, the transit time increased from 70.8 to 70.88 μ s as the SGV changed from 0.537 to 12.05 cm/sec suggests that there was variation in the concentration of solids in the ultrasonic path. For example, partial sedimentation occurred when the SGV was 2 cm/sec or less. Thus the concentration of solids

should be high under these conditions. The detected constant transit time of approximately 70.88 μ s in the slug flow regime suggests that there is a complete suspension of solids when the SGV is 4 cm/sec or higher. Kölbel and Realek (10) indicate that sedimentation will occur when the bubble column is operated under 2 cm/sec or less and the complete suspension of the solid will be established when the column is operated at 4 cm/sec or higher. Our ultrasonic observations are in good agreement with this finding.

Figure 5 illustrates the effects of solid holdup on the transit time measured at 33.65 cm above the gas distributor in the glass beads/nitrogen/water system at different SGVs. In this experiment, the SGV was systematically varied at any given initial solid holdup of 5, 10, 20, and 30 wt. % in the bubble column reactor. In general, the transit time varies with the variation of the superficial gas velocity for the SGV of 4 cm/sec or less at any given initial constant solid holdup loading in the reactor. The transit time was relative constant when the SGV is 4 cm/sec or higher. The transit times are around 71.96, 71.6, 71.12 and 70.88 μ s for the solid holdup of 5, 10, 20, and 30 wt. % respectively, when the SGV is 4 cm/sec or higher. Therefore, the transit time can be utilized to determine the solid holdup when the column is operated in a complete suspension mode. The fluctuation of the transit time when the SGVs is 4 cm/sec or less may attribute to the both partial sedimentation and other factors which is under investigation

The fractional change of transit time [$\square t/t_0 = (t_a - t_b)/t_0$] can be calculated on each individual transit time in Figure 5. From the fractional change of transit time, the solid holdup can be determined from the previous calibrated curve obtained from a stirred tank reactor [Figure 11. in (2)]. The determined solids holdup from these procedures and the solid holdup determined by the direct sampling are illustrated in Figure 6. The solid holdup measurements by the ultrasonic technique compared reasonably well with results obtained by the direct sampling techniques. Some discrepancies observed between these two techniques are probably due to the nature of these techniques. The ultrasonic technique measures the average solid holdup in the ultrasound path while direct sampling determines the collected local solid holdup.

CONCLUSIONS

An ultrasonic transmission technique has been developed to measure solid holdup in a gas-liquid-solid bubble column reactor. The results presented in this study show that the transit time of an ultrasonic signal is influenced by the variation of solid holdup and the operating conditions in the bubble column. The transit time can be correlated to the solid holdup. The variation of nitrogen flow has little influence on the observed transit time within the two-phase flow conditions studied. The ultrasonic technique is potentially applicable for solid holdup measurements in slurry-bubble-column reactors.

REFERENCES

1. Okamura, S., Uchida, S., Katsumata, T., Iida, K., *Chem. Eng. Sci.*, **1989**, 44, 196.
2. Soong, Y., Blackwell, A. G., Schehl, R. R., Zarochak, M. F., Rayne, J. A., *Chem. Eng. Com.*, **1995**, 138, 213.
3. Soong, Y., Gamwo, I. K., Blackwell, A. G., Schehl, R. R., Zarochak, M. F., *Chem. Eng. J.*, **1995**, 60, 161.
4. Soong, Y., Gamwo, I. K., Blackwell, A. B., Harke, F. W., Schehl, R. R., Zarochak, M. F., *Ind. Eng. Chem. Res.*, **1996**, 35, 1807.
5. Chang, J. S., Ichikawa, Y., Irons, G. A., Morala, E. C., Wan, P. T., *Measuring Techniques in Gas Liquid Two-Phase Flows*, Delhay, J. M. and Cognet, G., Eds, Springer-Verlag: New York, **1984**, p319.
6. Bensler, H. P., Delhay, J. M., Favreau, C., *Proc. ANS Natl. Heat Transfer Conf.*, **1987**, 240.
7. Soong, Y., Gamwo, I. K., Blackwell, A. B., Harke, F. W., Schehl, R. R., Zarochak, M. F., *Chem. Eng. Comm.*, **1997**, 158, 181.
8. Uchida, S., Okamura, S., Katsumata, T., *Can. J. of Chem. Eng.*, **1989**, 67, 166.
9. Warsito, A., Maezawa, A., Uchida, S., Okamura, S., *Can. J. of Chem. Eng.*, **1995**, 73, 734.
10. Kölbel, H., Realek, M., *Catal. Rev-Sci. Eng.*, **1980**, 21, 225.

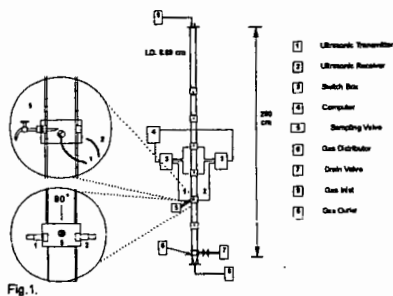


Fig. 1.

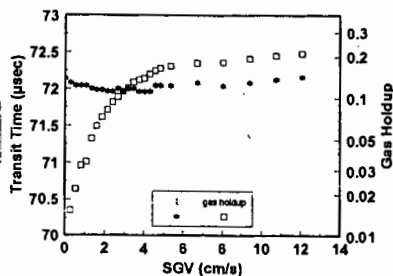


Fig. 2. Effect of superficial gas velocity (SGV) on transit time and gas holdup in nitrogen-water system.

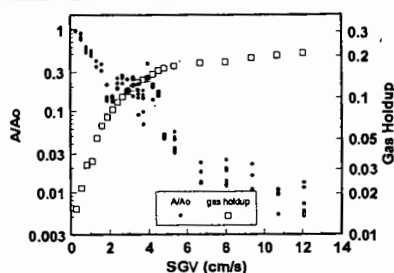


Fig. 3. Effect of superficial gas velocity (SGV) on amplitude ratio (A/A_o) in nitrogen-water system.

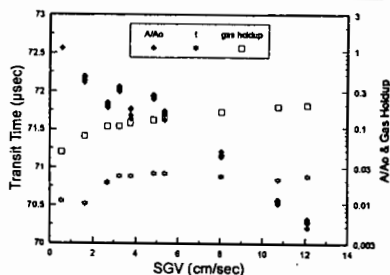


Fig. 4. Effect of superficial gas velocity (SGV) on amplitude ratio (A/A_o), transit time, and gas holdup in glass beads (30 wt %)/water system.

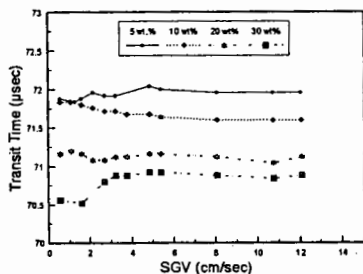


Fig. 5. Effects of solids concentration on the transit time in the glass beads/water system.

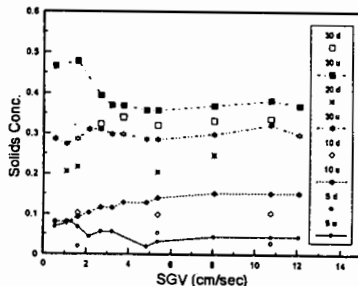


Fig. 6. Solid Conc. determined by ultrasonic and direct sampling.

Selection of Optimized Vessel Geometries for Coiled Stirred Tank Reactors

S. M. C. Peixoto and J. R. Nunhez *

Faculdade de Engenharia Química – UNICAMP

Departamento de Processos Químicos

Cidade Universitária Zeferino Vaz

Cx Postal 6066 – Campinas – SP –Brazil – 13090-010

Keywords

Heat transfer in stirred tanks; computational fluid dynamics, helical coils, reactor design.

Abstract

Stirred Tank Reactors are extensively used in chemical industries. It is common to use either jackets or internal coils when the reaction inside these reactors is highly exothermic. Both arrangements have positive influence and drawbacks in controlling the bulk temperature.

The design of coiled vessels today follows very much the geometry by Oldshue and Gretton [4] which has been criticized since it affects the flow. Street and McGreavy [6, 5] and Nunhez and McGreavy [3, 7, 2] indicated that if coils are placed in the same height of the impeller blades, internal flow circulation is restricted, even though there is an excellent local heat transfer in the impeller region.

This work aims to show by simulating the momentum, mass and energy equations inside the reactor, that there is great gain in performance if small alterations in the internals location are made. The idea is to simulate the flow for both the experimental apparatus cited above and some proposed geometries to indicate how internal flow can be improved. Preliminary simulations have already shown that there is great gain by avoiding to place any coil at the impeller height.

1 Introduction

It is common to use either jackets or internal coils when the reaction inside stirred tank reactors is highly exothermic. Both arrangements have positive influence and drawbacks in controlling the bulk temperature and they should be weighed carefully before deciding which arrangement should be chosen in any design. Reactor performance is greatly affected by the location of the internals and reactor mode of operation. Coiled vessels are even more affected because the coils drag the flow circulation. Important design parameters are coil helix and tube radius, as well as the number and location of coils. All these factors have an influence on the final flow and heat transfer inside the tank.

For laminar flows, when jacketed vessels are employed, there is a maximum of temperature inside the vessel at the centers of the recirculation zones of the secondary flow, since heat transfer in stirred tanks in these circumstances are dominated by the secondary flow. If coils are used, the temperature peak is not necessarily anymore at the center of the recirculation

The primary concern of this research is to show that there are mechanical limitations for flow circulation and heat transfer in the geometry suggested by Oldshue and Gretton [4]. Even though this computational work is only for laminar flow, the results for the flow can be extended to turbulent conditions because similar flow patterns are present for both laminar and turbulent conditions. The same mechanical limitations which are present for laminar flow are also present for turbulent flow. Therefore, studying the fluid circulation inside the coiled tank laminar flow will be of benefit for both flow regimes.

2 Modeling and simulation

The problem under investigation is three dimensional and can be for both Newtonian and non-Newtonian flow. For a preliminary investigation however, it will be considered a two-dimensional axis-symmetric model, even though the radial, axial and angular velocities will be determined on a two-dimensional grid, making this a pseudo three-dimensional model.

The critical part and weakest link of the axis-symmetric model is the application of the boundary conditions for the impeller blades in order to give a reasonable representation of the blades effect. The approach used by Kuncewics [1] was adopted. This approach was followed by Nunhez and McGreavy [3, 7] and results show it gives a good representation for the flow patterns and serves as a basis for geometry selection which can be further refined at a later stage by a three dimensional model.

The governing equations for the axis-symmetric model are:

2.1 Momentum balance

radial

$$\rho \left(u_r \frac{\partial u_r}{\partial r} - \frac{u_\theta^2}{r} + u_z \frac{\partial u_r}{\partial z} \right) = \frac{1}{r} \frac{\partial}{\partial r} (r \sigma_{rr}) - \frac{1}{r} \sigma_{\theta\theta} + \frac{\partial \sigma_{rz}}{\partial z} \quad (1)$$

angular

$$\rho \left(u_r \frac{\partial u_\theta}{\partial r} + \frac{u_r u_\theta}{r} + u_z \frac{\partial u_\theta}{\partial z} \right) = \frac{1}{r^2} \frac{\partial}{\partial r} (r^2 \sigma_{r\theta}) + \frac{\partial \sigma_{z\theta}}{\partial z} \quad (2)$$

axial

$$\rho \left(u_r \frac{\partial u_z}{\partial r} + u_z \frac{\partial u_z}{\partial z} \right) = \frac{1}{r} \frac{\partial}{\partial r} (r \sigma_{rz}) + \frac{\partial \sigma_{zz}}{\partial z} \quad (3)$$

2.2 Mass conservation

$$\frac{1}{r} \frac{\partial}{\partial r} (r u_r) + \frac{\partial}{\partial z} (u_z) = 0 \quad (4)$$

2.3 Energy conservation

$$\rho C_p \left(u_r \frac{\partial T}{\partial r} + u_z \frac{\partial T}{\partial z} \right) = \frac{1}{r} \frac{\partial}{\partial r} \left(k_l r \frac{\partial T}{\partial r} \right) + \frac{\partial}{\partial z} \left(k_l \frac{\partial T}{\partial z} \right) + \Delta H \quad (5)$$

The stress tensors are:

$$\sigma_{rr} = -p + 2\mu \frac{\partial u_r}{\partial r} \quad (6)$$

$$\sigma_{\theta\theta} = -p + 2\mu \frac{u_r}{r} \quad (7)$$

The equations are solved numerically by the finite volume method and the simulations are performed using the CFX-4 package by AEA which has been successfully used for many flow problems. The boundary conditions are the same used by Street and McGreavy [6, 2] and Nunhez and McGreavy [3, 7].

3 Preliminary results and discussion

Preliminary results have already been obtained and show that there is great gain in modifying coils position inside the vessel and show it is beneficial to avoid placing any coil at the impeller height. This happens because if there are coils at this height, the average flow velocity is reduced when the fluid which leaves the impeller encounter the coils and, as a consequence of the velocity being reduced, there is a tendency of fluid stagnation between the coils and wall of the vessel. Figure 1 shows the velocity vector plot for an axial section of the reactor¹ for the experimental arrangement suggested by Oldshue and Gretton. As already commented, there is a limitation in the fluid circulation because the flow which is generated by the impeller encounters the coils which are present at the impeller blades height. As a consequence, those two coils drag the flow in the intire tank which, of course, impaire the flow in the tank. Figure 2 shows an arrangement having no coils at the impeller blades height. It is apparent from the figure that fluid circulation is greatly improved if the coils at the impeller region are removed. It is specially true for the circulation between the coils and the wall. The two figures are for the same angular velocity of the impeller of 30rpm.

In the actual stage, heat transfer and a non-Newtonian model have been introduced into the model. Reaction is considered as a source of heat in the bulk which has to be removed by either a jacket and/or coils. Several arrangements are being analysed to demonstrate how computational fluid dynamics can be used as a tool for reactor design.

At a later stage, a three dimensional and a turbulent model is aimed to be considered.

References

- [1] C. Kuncewicz. Three-dimensional model of laminar liquid flow for paddle impellers and flat-blade turbines. *Chem. Eng. Sci.*, 47(15/16):3959-3967, 1992.
- [2] J. R. Nunhez. *The Influence of geometric factors on the optimum design of stirred tank reactors*. PhD thesis, The University of Leeds, 1994. in preparation.
- [3] J. R. Nunhez and C. McGreavy. A comparison of the heat transfer in helical coils and jacketed stirred tank reactors. *Brazilian Journal of Chemical Engineering*, 12(1), 1995.
- [4] J. Y. Oldshue and A. T. Gretton. helical coil heat transfer in mixing vessels. *Chem. Eng. Progress*, 50(12):615 -621, 1954.
- [5] D. A. Street. *Computational Modelling of Stirred Reaction Vessels*. PhD thesis, The University of Leeds, 1991.
- [6] D. A. Street and C. McGreavy. A model of the heat transfer in internally cooled reaction vessels. In E. A. Foumeny and P. J. Heggs, editors, *Heat Exchange Engineering*, volume 2, pages 279-302. Ellis Horwood Ltd., 1991.
- [7] G. Tatterson, editor. *Industrial Mixing Technology: Chemical and Biological Applications. Title of the Chapter: The Influence of Geometric Factors on The Optimum Design of Stirred Tank Reactors*, volume 89 of *AIChE Symposium Series*. AIChE, 1994.
- [8] V. Uhl and Gray. *Mizing: theory and practice*, volume I. Academic Press, London, 1966.

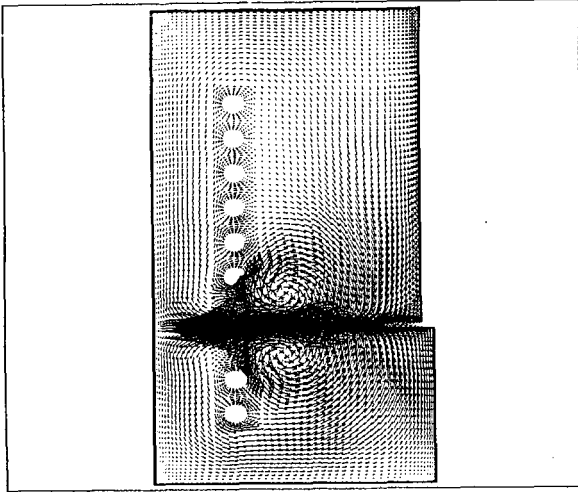


Figure 1: Experimental coiled arrangement by Oldshue and Gretton

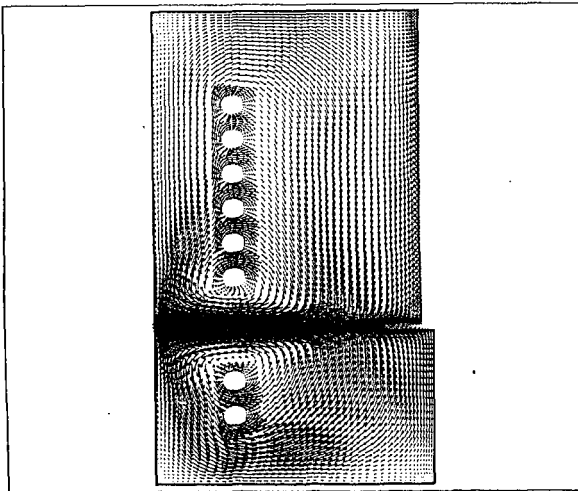


Figure 2: Alternative arrangement having no coils at the impeller height

THE CHARACTERIZATION OF RESIDUAL HYDROCARBON FRACTIONS WITH MODEL COMPOUNDS RETAINING THE ESSENTIAL INFORMATION

Giulia Bozzano, Mario Dente

Politecnico di Milano, CIIC Department, Piazza L. Da Vinci, 32, 20133 Milan, Italy - email:
Mario.Dente@polimi.it

Marcos Sugaya

Petrobras S.A., Cenpes, Ilha do Fundao QD7, Rio de Janeiro 21910-900, Brazil

Colin McGreavy

The University of Leeds, Chemical Engineering Department, Leeds LS2 9JT, UK

KEYWORDS: Heavy residues characterization, model compounds, lumping

ABSTRACT

A characterization method for heavy residues is proposed. It has been specifically studied for the characterization of high molecular weight mixtures, with the aim of modeling thermal conversion processes such as thermal cracking, Eureka, visbreaking and delayed coking. Only essential commonly available information is necessary. Extensive data based on the use of the Boduszynski-Altgelt methodology based on short-path molecular distillation (DISTACT), sequential elution fractionation technique (SEF) and vapor phase osmometry analyses (VPO), are surprisingly well reproduced. The results also match ^1H and ^{13}C NMR analyses. The proposed model is a valuable tool when complex and lengthy analyses are unavailable as is usually the case.

INTRODUCTION

The use of model compounds and mechanistic kinetic schemes has significantly improved the quality of product characterization when modeling the pyrolysis of high molecular weight mixtures.

Good characterization of the feed is crucial if reliable predictions of yield and quality of products based on mechanistic models are required. The availability of suitable data for heavy fractions is often a problem. In general, only a single density and average molecular weight (or kinematic viscosity) together with the initial boiling point range are available, while the whole distribution of these properties is actually required.

The higher the boiling point of a hydrocarbon fraction, the more difficult its characterization becomes. While the composition of naphthas can be determined, middle distillates can only be described in terms of their constituent groups and for heavy fractions the situation is far more complicated.

Since petroleum products are usually specified by their distillation properties, the boiling range often becomes more important than the actual molecular composition. Thermal cracking limits the cut points in commercial atmospheric and vacuum distillations to 350 and 540 C, respectively. In the laboratory, the use of high-vacuum short-path 'molecular' distillation (DISTACT) allows atmospheric equivalent boiling points (AEBP) of 700 C to be obtained.

Researchers often rely on solubility relations to characterize streams. These are arbitrary in the sense that the results depend on the solvents chosen, the temperatures, contact time, the relative quantities used in the treatment and on the agitation conditions, which results in obvious difficulties when comparing results of different scientists.

Distillation followed by a sequential elution fractionation (SEF) has been proposed by Boduszynski (1). This constitutes a better alternative because it avoids the problems derived from the strictly operational and therefore vague definition of asphaltenes, maltenes and resins (2).

Dente and Bozzano recently developed a global kinetic mechanism for visbreaking and delayed coking. A basic point of their activity has been the definition of model compounds in order to reduce the extremely large number of reactions and involved components in a sufficiently representative kinetic scheme. Using a combination of statistical methods, model compounds have been defined which give a good representation of the dominant phenomena involved.

Starting from the resulting distribution curves of the boiling point, kinematic viscosity or molecular weight, specific gravity and sulfur content, reactants and products can be lumped into a discrete number of pseudocomponents having fixed or varying properties. Alternatively, they can be represented as a mixture of model compounds (3).

METHOD

The feed (atmospheric and vacuum distillation residues) has been characterized by Dente and Bozzano (4) as a mixture of paraffinic, naphthenic and aromatic model compound. The relative amounts can be derived from the above mentioned macroscopic properties.

Once the total amounts of the three different classes of components have been estimated, it is possible to deduce the relative amounts of the pseudocomponents in the class. In fact, a careful elaboration of the data published in the literature (see, for instance, ref. 5), has shown that the statistical distribution of the single pseudocomponents with n_c carbon atoms (in every class) takes the form:

$$\frac{df}{dn_c} = k \exp[-k(n_c - n_{c_{\min}})] \quad \text{Equation 1}$$

where k is obtained from the average number of carbon atoms of the distribution

$$k = \frac{1}{n_{c_{\text{med}}} - n_{c_{\min}}} \quad \text{Equation 2}$$

where:

- f = fraction of the single component on the total of the class
- $n_{c_{\text{med}}}$ = average number of carbon atoms of the class
- $n_{c_{\min}}$ = minimum number of carbon atoms of the class
- the index k depends on the class (paraffins, "aromatics", etc.) of components involved

The lumping rule typically groups 5 by 5 carbon atoms, from the minimum number to 58 carbon atoms; above this the splitting rule is 10 by 10 carbon atoms. For more than 98 carbon atoms an equivalent pseudocomponent is assumed to be representative of all the rest. A similar grouping rule can also be applied to the pyrolysis products. Of course, more complicated intrinsic rules are implied for multiple ring components (such as condensed rings polyaromatics and so on). The model compound characteristics can be summarized as follows:

- PAREQ - paraffin with 20% of methylation (i.e. 20% of carbon atoms is in a methyl group). The methylation degree has been deduced by assuming a prevalent polyisoprenoid structure for i-paraffins and a relative amount of n-paraffins into equivalent paraffinic pseudocomponent of about 20%.
- ARO0 - polyaromatic sheet with 50% of methylation at the boundaries and a single alkyl side chain with 20% of methylation. A distribution of all such possibilities includes a proportionality assumption between the molar fractions and the number of aromatic atoms in the molecules. The side chain size of this distribution is averaged and a single average aromatic molecule results which is defined solely by the number of carbon atoms. NMR data of some residues satisfactorily confirm the assumed methylation degree on the aromatic sheet boundary (typically in the range of 0.4-0.5). A direct proportionality between carbon atoms number and aromatic rings in the molecule is present.
- NAFTO0 - a polynaphthenic sheet with 50% of methylation at the boundaries and a single alkyl side chain with 20% of methylation. As in the case of aromatics, an internal distribution into the molecules is assumed. Contrary to the case of aromatic components, the major probabilities are in favor of structures with few rings and long side chains (as is possible to deduce from the API Research Project 60 where naphthenes contained in vacuum gasoil fractions extracted by chromatography are reported). There is, in consequence, an inverse proportionality between number of C atoms and number of rings in the molecule.

The relative amounts of paraffins, aromatics and naphthenes can be estimated from other feed properties and if the carbon distribution for each of the ARO0, NAFTO0 and PAREQ classes is known, the feed is completely characterized. The average number of carbon atoms of each compound class can be calculated to satisfy the global molecular weight and H/C relation. The minimum number of carbon atoms is calculated from the initial boiling point of the feed (Equation 3). For a given number of carbon atoms, the aromatic molecules will boil at higher temperatures than the paraffins, since their specific gravity is higher.

$$MW_{AEBP>500F} = 140 + 3.40 \times 10^{-7} \frac{AEBP^3}{SPGR^{2.5}} \quad \text{Equation 3}$$

$$MW_{AEBP<500F} = MW_{AEBP>500F} \left[1 - 1.4 \times 10^{-4} (600 - AEBP) \right]$$

Partial volumes at 20 C can be calculated using the group contribution method of Hirsch (6). These have been adjusted to 15.5 C with the Rackett equation modified by Yamada and Gunn (7). The additive methods of Schroeder (8) and Le Bas (9), which give surprisingly good values for the molal volume of small hydrocarbon molecules at saturation temperature, show strong discrepancies when compared with the method of Hirsch, which has been developed for heavy fractions.

Dente and Bozzano (4) have pointed out the importance of performing corrections for sulfur before appropriate estimates of the content of paraffins, naphthenes and aromatics (and the H/C ratio) are possible. An equivalent hydrocarbon density is defined as

$$\rho_{eq} = \rho - 0.0066(S\%) \quad \text{Equation 4}$$

RESULTS AND DISCUSSION

The predictions of the procedure are compared with experimental data (available only up to C₁₇) and (calculated) results from the API Research Project 44 (1972) (Figure 1). The agreement is good with the PAREQ curve fitting the data for paraffins fairly well and the ARO0 curve located somewhere between the paraffins and the pure aromatics compounds (the ARO0 compounds are alkyl substituted aromatics). The aromatic curve in Figure 1 results from applying the methodology described above for purely aromatic structures. In this case, the agreement can be seen to be also good.

In Figure 2, a comparison is made with experimental data for Kern River petroleum (2), which is a highly biodegraded crude. As can be seen, its constituents can be considered to be a mixture of paraffinic, naphthenic and aromatic model compounds up to 700 C, which is the current experimental limit. This figure also implies that fractions up to 400 C are mainly paraffinic.

The corresponding molecular weight distribution matches the experimental data of Boduszynski (10) remarkably well, as can be seen in figure 3. The actual matching can be even better than that presented here, since the molecular weight for the last fraction has been measured with vapor pressure osmometry (VPO) using two different solvents. While the results differ, the true MW for this fraction is probably lower than the value measured with the most efficient solvent shown in Figure 3.

Figure 4 presents the molecular weight distribution obtained for an atmospheric residue of an Arabian Heavy crude. The agreement between calculated and experimental results is also good.

Since equation 3 has been developed using a series of petroleum distillations, including Kern River and Arabian Heavy crudes (11,12), the agreement in AEBPs is implicitly good.

Table 1 provides a comparison in terms of some functional groups determined from ¹H and ¹³C NMR analyses applied to a vacuum residue of Baiano petroleum (a light paraffinic crude).

CONCLUSIONS

The methodology described here gives a fairly good characterization of boiling points and molecular weights for residual fractions based on initial boiling point, sulfur content, average specific gravity and molecular weight (or kinematic viscosity).

The feed characterization predicted reproduces the results of NMR and VPO-DISTACT analyses and seems to constitute a viable route for investigating the composition of residual fractions. An important application would be in the modeling of typical resid upgrade processes such as visbreaking and delayed coking (13). In this case, a good definition of residence times for the liquid phase, where the most reactive components are concentrated is necessary.

Since the maximum temperature in these processes is around 500 C, fractions boiling above this will remain mainly in the liquid phase and precise definition of the true boiling point is not required.

Nevertheless, the molecular weight distribution (number of carbon atoms) is of great importance because it affects flash calculations, solubility relations (for precipitation of precursors in coking) and defines the system reaction state and residence time.

REFERENCES

1. Boduszynski M. M. Energy & Fuels 1987, 1, 2.
2. Altgelt K. H.; Boduszynski M. M. Comp. and Analysis of Heavy Petroleum Frac. 1994.
3. Astarita G.; Ocone R. Chemical Engineering Science 1992, 47, 2135.
4. Bozzano G. Tesi di dottorato in ingegneria chimica 1994, Politecnico di Milano.
5. Ali M. F.; Hasan M.; Bukhari A.; Saleem M. Oil & Gas Journal 1985, Aug. 12, 71.
6. Hirsch E. Analytical Chemistry 1970, 42, 1326.
7. Yamada T.; Gunn R. D. J. Chem. Eng. Data 1973, 18, 234.
8. Partington J. An Adv. Treat. on Phys. Chem., V. 1, Fund. Princ.: The Prop. of Gases 1949.
9. Le Bas G. The Molecular Volumes of Liquid Chemical Compounds 1915.
10. Boduszynski M. M. Energy & Fuels 1988, 2, 597.
11. Altgelt, K. H.; Boduszynski, M. M. Energy & Fuels 1992, 6, 68.
12. Altgelt, K. H.; Boduszynski, M. M. Energy & Fuels 1992, 6, 72.
13. Dente M.; Bozzano G.; Bussani G. Computers & Chem. Eng. 1997, 21, 1125.

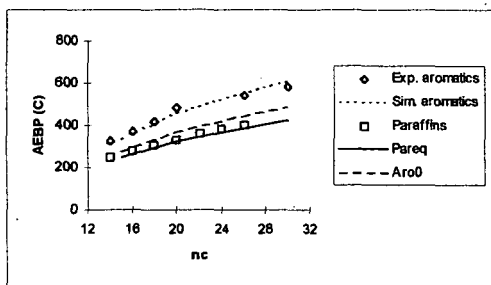


Figure 1 Atmospheric equivalent boiling points as a function of the number of carbon atoms for the model compounds of Dente and Bozzano (1994).

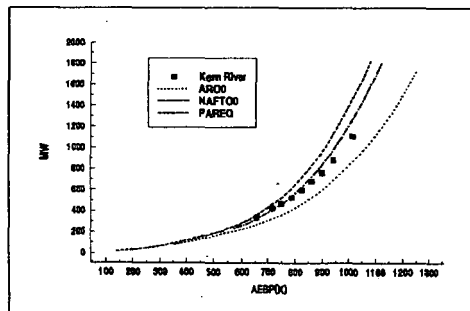


Figure 2 MW vs. AEBP representation of PAREQ/ARO0/NAFT00 model compounds.

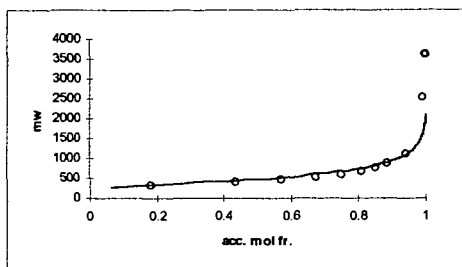


Figure 3 Molecular weight distribution for Kern River residue.

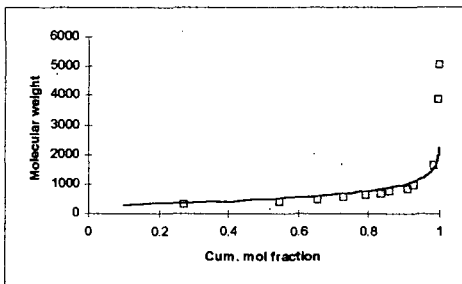


Figure 4 Molecular weight distribution for atmospheric residue of Arabian Heavy crude.

Table 1 Results for VR Baiano.

| | Model | NMR data |
|--------------------------|-------|----------|
| H/C | 1.89 | 1.80 |
| C _{ar} | 11.1 | 15.4 |
| C _{Ar,H} | 4.0 | 4.3 |
| C _{Ar,CH3} | 3.1 | 4.0 |
| avg. size of side chains | 22.2 | 26.5 |
| C _{sat} | 88.9 | 84.6 |
| (H/C) _{sat} | 2.05 | 2.02 |

CONTINUOUS-DISTRIBUTION KINETIC MODEL FOR MACROMOLECULAR CONVERSION: ASPHALTENE AND POLYMER

Yoichi Kodera, Yoshiki Sato, Tohru Kamo
National Inst. for Resources & Environment, AIST
16-3 Onogawa, Tsukuba, Ibaraki, 305-8569, Japan

KEYWORDS: continuous-distribution kinetics, asphaltene, polymer

ABSTRACT

One of the important purposes of macromolecular processing is to lower its molecular weight in cases of heavy oil processing or of feedstock recycling of plastic wastes. Molecular-weight distributions (MWDs) of macromolecular feedstocks and the reaction products at the early stage of conversion continuously span wide ranges of molecular weights. Continuous-distribution analysis is a convenient method to evaluate macromolecular conversion based on time-dependent changes of MWDs of reaction mixtures, which are readily monitored by HPLC-GPC. Kinetic models of macromolecular conversion are derived from simplified reaction schemes to interpret experimental results giving kinetic parameters, rate of conversion and activation energy. The kinetic modeling is useful to the evaluation of reaction conditions of processing regarding rate of conversion. In this presentation, kinetic models are proposed to interpret asphaltene hydrocracking and polymer degradation of polyolefin and phenolic (resole) resin. Details of experimental results will be discussed in the presentation.

INTRODUCTION

We have been studied asphaltene hydrocracking to improve heavy oil processing [1]. The similar experimental strategy is effective on phenolic resin degradation using tetralin or co-processed polystyrene acting as a hydrogen donor [2]. Kinetic models by continuous-distribution kinetics have been proposed in this presentation. Rate of reaction is defined as a rate of increase or decrease of molar concentration of chemical species. For macromolecules, the rate are given by moment method using time-dependent changes of MWDs. Mathematical model using continuous-distribution kinetics expresses macromolecular conversion by simplified schemes at the point of MW-lowering and is useful for evaluation of the reaction conditions.

Many kinetic models have been proposed based on lumping or continuous function of measurable properties. Rice-Herzfeld and the derived mechanism are quite useful for the kinetic analysis for petroleum processing. Recently, a general kinetic model for polymer degradation based on continuous-distribution kinetics using simplified schemes of radical mechanism was reported [3,4]. This model is illustrating kinetics of polymer (especially, polyolefin) degradation and polymerization based on reversible radical-chain reaction. However, reaction mechanism is sometimes different in the reaction of each substrate due to the nature of chemical structures. The major difference of kinetic models for each substrate are derived from the amounts of hydrocarbon chains which undergo β -scission promoting radical chain reaction. Such chain reaction have a minor role in the macromolecular conversion such as asphaltene hydrocracking and phenolic resin degradation. The absence of the radical chain reaction at thermal treatment is a general property of thermoset plastics.

We propose kinetic models for different types of macromolecular feedstocks, i.e., phenolic resin (resole resin) with aromatic matrix, polyolefins with linear main chains of hydrocarbons, and asphaltene with fused aromatics linked by hydrocarbon chains and hydrocarbon side-chains attached to the aromatic rings. For modeling such reactions, physical issues such as diffusion and vaporization sometimes have the significant effect in an individual reactor system. As a first step, we build general kinetic models regarding chemistry of macromolecules.

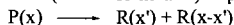
KINETIC MODEL

Continuous-distribution kinetics consists of two technique. One is simplified notation of reaction schemes and another is moment method for converting MWDs of GPC chromatograms into amounts of moments (e. g., first moment means molar concentration). In the simplified schemes, some lumped groups of chemical species are chosen to examine the changes of amounts of moments in the function of time. A lumped group is a group of compounds which behave in the similar manner chemically and those compounds should be analytically distinguished from the other groups. For example, asphaltene from Arabian Light consists of

two types of chemical moieties, fused aromatics and hydrocarbon chains attached to the fused rings. Asphaltene hydrocracking gives asphaltene component with the lower MWs and aliphatic hydrocarbon as the major products. What we want to examine is the quantity of asphaltene component. Then, asphaltene and aliphatic hydrocarbons are the two chemical species to be described in the reaction schemes. For polyolefin degradation, chain-scission occurs along the main chain to give monomer, dimer, trimer, and oligomers. Any polymer gives oligomers via random chain-scission and some polymers give some specific products (monomer, dimer, and trimer) in high yields by specific chain-scission following to random-chain scission. Phenolic resin degradation gives only random chain-scission products. Phenols are given by the results of the random chain-scission not the reaction via β -scission or chain-end scission as found in polyolefin degradation.

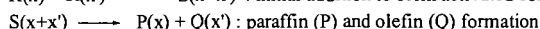
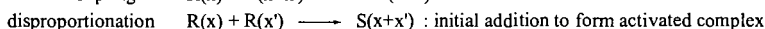
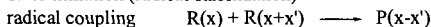
General notation. Rice-Herzfeld and related mechanism gave the following steps as the major radical reactions of hydrocarbons in petroleum processing. In continuous-distribution kinetics, each reaction is described as follows:

1. initiation (radical formation) of polymer $P(x)$ with an arbitrary MW of x .



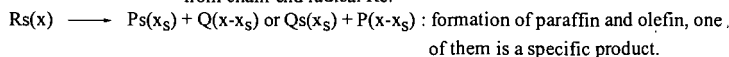
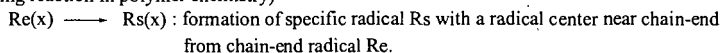
This step always gives end-radical, which has a radical center at the chain-end. The other path to form radical is radical-promoted intermolecular hydrogen-abstraction below.

2. termination (radical stabilization)



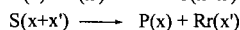
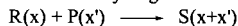
Initiation and termination step have negligible contribution to the increase of molar concentration because the major contribution is given by β -scission and intermolecular hydrogen-abstraction, which are the main route of radical chain reaction increasing molar concentration of the products. This concept (Long Chain Assumption) is valid only for polyolefin degradation and aliphatic components in asphaltene hydrocracking and not valid for phenolic and asphaltene components.

3. intramolecular hydrogen-abstraction by Rice-Kossiakoff mechanism (this is called as back-biting reaction in polymer chemistry)



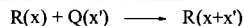
This step is important step for the formation of specific products. End-radical is unstable to abstract a hydrogen at around fifth carbon via cyclic transition state. The resulting radical then undergo β -scission to give specific products, dimer or trimer.

4. Intermolecular hydrogen-abstraction



Radical also promotes intermolecular hydrogen-abstraction. This gives mostly random radical $Rr(x)$, where radical center randomly distributes along a main chain. β -Scission of random radical gives the corresponding olefin and chain-end radical of random MWs.

5. Radical addition to olefins



When olefin are abundant in a reaction, radical addition is important. Some researchers report the importance of addition in liquid phase compared with that in vapor phase [5]. Using this scheme, it is possible to describe simple kinetics of polymerization [3].

Catalytic reaction involves some different mechanisms such as alkyl-group transfer and cyclization of olefin to form aromatics. These have no big change in MWs. However, one may describe lumped groups in schemes when the chemical species plays important role in the chemical or physical properties one interested in at the processing.

Asphaltene hydrocracking. In asphaltene hydrocracking, the conversion is evaluated at the point that decreasing rate of asphaltene component $A(x)$. The simplified schemes shown in Schemes (A, B, C) are for the evaluation under the experimental conditions with no coking and enough supply of hydrogen[1]. Random bond-scission is assumed for the cleavage of linkages between fused-ring units (Scheme (A)), the side-chain cleavage from a fused ring (Scheme (B)), and bond-scission of aliphatic hydrocarbons (Scheme (C)) because of the possible random-distribution features of MWDs of fused-rings and linkages. Each component $A(x)$ and $P(x)$ separate by precipitation with hexane and is analyzed by GPC.



Polyolefin degradation is expressed as Scheme (C) due to the absence of $A(x)$ and phenolic resin degradation is expressed as scheme (A) because of the negligible contribution of hydrocarbon linkage to the overall degradation. The detailed kinetic model for polyolefin degradation was reported in ref. [3], where reversible radical mechanism is considered.

Phenolic resin degradation. Presence of a hydrogen donor in phenolic resin degradation is the essential factor to proceed the degradation. One may need to know the effect of hydrogen source. The schemes including radicals are required to describe the interaction between radical intermediates and hydrogen source. Phenolic resin degradation is described as follows:



where phenolic resin is $A(x)$ and radical is $R(x)$.

Scheme (D) expresses radical formation (k_T) and stabilization (k_R). Radical formation is given by Scheme (F) and stabilization is a simplified scheme of the bimolecular reactions of a radical with a hydrogen donor such as tetralin T in Schemes (G) and (H) under the assumption of quasi-stationary state of radical [3].



Another radical formation is radical-promoted intermolecular hydrogen-abstraction, which have no contribution to the increase of concentration of radical and it is a competitive reaction to radical addition to aromatic rings. It is a determining factor to characterize phenolic resin degradation from polyolefin degradation that the resulting radical given by the hydrogen-abstraction is not expected to proceed radical chain reaction giving olefin and another radical due to the aromatic structure.

Schemes (D) and (E) gives integro-differential equations (1) and (2) according to continuous-distribution kinetics.

$$\partial a / \partial t = -k_T a(x) + k_R r(x) - k_a a(x) \int_0^\infty r(x') dx' + k_A \int_x^\infty r(x') \Omega(x, x') dx' \quad (1)$$

$$\begin{aligned} \partial r / \partial t = & k_T a(x) - k_R r(x) - k_a r(x) \int_0^\infty a(x') dx' + k_a \int_0^\infty a(x') r(x-x') dx' \\ & + k_A \int_x^\infty r(x') \Omega(x, x') dx' - k_A r(x) \end{aligned} \quad (2)$$

Applying the moment operation (McCoy [6], McCoy and Wang [7]), $\int_x^\infty [] x^n dx$, to the integro-differential equations (1) and (2) yield

$$da^{(n)} / dt = -k_T a^{(n)} + k_R r^{(n)} - k_a a^{(n)} r^{(0)} + k_A Z_{n0} r^{(n)} \quad (3)$$

$$dr^{(n)} / dt = k_T a^{(n)} - k_R r^{(n)} + k_a \left[\sum_{j=0}^n \binom{n}{j} a^{(j)} r^{(n-j)} - a^{(0)} r^{(n)} \right] + k_A r^{(n)} (Z_{n0} + 1) \quad (4)$$

where $Z_{n0} = 1, 1/2$, or $1/3$ for $n = 0, 1$, or 2 .

Zeroth moments ($n=0$) are governed by the differential equations (5) and (6),

$$da^{(0)} / dt = -k_T a^{(0)} + k_R r^{(0)} - k_a a^{(0)} r^{(0)} + k_A r^{(0)} \quad (5)$$

$$dr^{(0)} / dt = k_T a^{(0)} - k_R r^{(0)} \quad (6)$$

Applying quasi-stationary state assumption (QSSA) of radical $dr(0)/dt \approx 0$ to equation (6) gives

$$r^{(0)} = (k_r / k_R) a^{(0)} \quad (7)$$

Then,

$$da^{(0)}/dt = (k_A - k_a a^{(0)}) (k_r / k_R) a^{(0)} \quad (8)$$

Integration of equation (5) with the initial condition $a^{(0)}(t=0) = a_0^{(0)}$ gives

$$a^{(0)} = \exp[(k_A k_r / k_R) t] / \{1/a_0^{(0)} + (k_a/k_A) [\exp[(k_A k_r / k_R) t] - 1]\} \quad (9)$$

$$a^{(0)}(t \rightarrow \infty) = k_A/k_a$$

First moments ($n=1$) are given as follows:

$$da^{(1)}/dt = -k_r a^{(1)} + k_R r^{(1)} - k_a a^{(1)} r^{(0)} + (k_A/2) r^{(1)} \quad (10)$$

$$dr^{(1)}/dt = k_r a^{(1)} - k_R r^{(1)} + k_a a^{(1)} r^{(0)} - (k_A/2) r^{(1)} \quad (11)$$

The summation of first moments for polymer and radical gives

$$d[a^{(1)} + r^{(1)}]/dt = 0 \quad (12)$$

confirming the conservation of reactant polymer mass.

This is a kinetic model for resole resin in solution. Phenolic resin is its cured form with filler and other additives. Solubility of phenolic resin provide the interesting physical issues to the modeling, which will be examined in the near future.

EXPERIMENTAL TREATMENTS FOR THE KINETICS

Sample preparation. Macromolecular substrates for kinetic analysis has to have a smooth distribution of MWDs because of the overlap of reaction products with the original peaks. Typically, an original resole resin contains some low MW components, which are easily removed by reprecipitation with THF and hexane. After resole resin was dissolved with THF, hexane was added with stirring. Low MW components in THF/hexane were readily removed by decantation. The residual solvent was evaporated under reduced pressure to give resole resin to be used in experiments (Fig. 1). The similar pretreatment is required in some polymers such as polystyrene.

Analysis. HPLC-GPC is a major apparatus to determine MWDs of reaction mixtures in this kinetics. Light scattering measurement or GC are alternative methods depending on the properties of substrates. MWDs thus obtained are converted into the corresponding amounts of moments. Mass of chemical species versus retention time of a chromatogram is calculated to give moments defined as equation (13).

$$m^{(n)} = \int_0^\infty x^n m(x) dx \quad (13)$$

where $m(x)$ is molar concentration of component m in the MW range of $[x, x + dx]$. In GPC chromatogram using a refractive index detector have coordinates of mass concentration as intensity and retention time giving MWs. Different types of chemical species gives different intensity even if they have the same mass concentration whereas the similar chemical species of the same mass concentration gives the same peak area. For example, polystyrene samples of different MWs gives the same peak area if they are the same concentration whereas 1 g/L polystyrene and 1 g/L polyethylene give different peak area depending their refractive index. In product analysis of asphaltene hydrocracking, separate analysis is required for asphaltene components and aliphatic hydrocarbons. Asphaltene is defined as a hexane(or heptane)-insoluble component and, actually, the most parts of chemical species which have asphaltene structure do not dissolve in reaction mixtures after precipitation with hexane or heptane. Asphaltene components are analyzed by using the precipitation. MWDs of another products (aliphatic hydrocarbons) are obtained by subtracting MWDs of asphaltene components from MWDs of reaction mixtures.

Careful treatment is required to evaluate experimental results of macromolecular conversion by comparing them with a kinetic model. Some MW-standards such as asphaltene and phenolic resin are not available. Especially, it is impossible to obtain absolute MWs of asphaltene even by light scattering method due to its color. Then, molar concentration of a substrate does not change linearly with time despite to linear relation of kinetic discussion. However, we can still get the reaction rate, i.e. slope of the line, at the very early periods of the conversion and can compare the rates at different reaction conditions.

CONCLUSION

Kinetic models by continuous-distribution kinetics for asphaltene hydrocracking, phenolic resin degradation, olefin degradation were discussed. The kinetic treatment using time-dependent changes of MWDs of reaction mixtures provide a convenient method to evaluate macromolecular conversion. Depending the nature of a macromolecule, reaction schemes should be selected carefully.

REFERENCES

- [1] Y. Kodera, et al., Preprints of International Conference on Refinery Processes, AIChE Spring Meeting, New Orleans, March 1998, p. 321. In preparation for submission.
- [2] Sato, Y., Kodera, Y., Kamo, Y., Matsumoto, T., 7th EPF Symposium on Polymeric Materials, European Polymer Federation/Polish Chemical Society, Poland, Sept. 21, 1998. (scheduled).
- [3] Kodera, Y., McCoy, B. J., *AIChE J.*, 1997, 43, 3205.
- [4] Kodera, Y., Cha, W. S., McCoy, B. J., *Prep. Div. Fuel Chem., ACS*, 1997, 42, 1003.
- [5] Wu, G. Katsumura, Y., Matsuura, C., Ishigure, K., Kubo, J., *Ind. Eng. Chem. Res.*, 1996, 35, 4747.
- [6] McCoy, B. J., *AIChE J.*, 1993, 39, 1827.
- [7] McCoy, B. J., Wang, M., *Chem. Eng. Science*, 1994, 49, 3773.

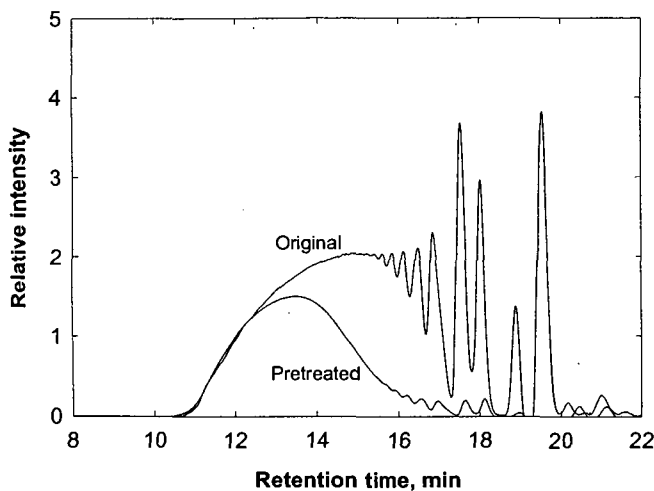


Figure 1.- RI chromatogram of resole resin before and after pretreatment
GPC analysis was performed with a HPLC (Shimadzu LC-9A pump, RID-6A RI detector) using Polymer Laboratories GPC columns (50x7.5 mm-guard column and two 300x7.5 mm columns of 3 μ m-Mixed E) at 40 °C. THF was used as an eluent at flow rate of 1.0 mL/min.

HYDRODESULFURIZATION OF A VACUUM GAS OIL IN A SLURRY BED AND IN A TRICKLE-BED REACTOR: A COMPARATIVE STUDY

C.G. Yiokari and C.G. Vayenas
Department of Chemical Engineering
University of Patras
26500 Rio, Patra Greece

KEYWORDS: Trickle-Bed Reactors, Hydrodesulfurization, Wetting Efficiency

INTRODUCTION

Partial wetting of catalyst pellets is an important characteristic of trickle-bed reactors (Satterfield, 1975; Herskowitz and Smith, 1983; Gianetto and Specchia, 1992). Two kinds of wetting must be considered for porous catalysts, internal wetting, defined as the ratio between the wetted pellet volume and the total pellet volume and external effective wetting that is the fraction of the external area of the pellet effectively wetted. Many investigations have dealt mostly with external wetting efficiency by tracer (Mills and Dudukovic, 1981) and reaction (Herskowitz et al., 1979; Ring and Missen, 1989; Morita and Smith, 1978) methods and by computational simulations (Ring and Missen, 1986; Yentekakis and Vayenas, 1987). Total internal wetting of the catalyst pellets is normally assumed due to capillary effects.

With the exception of few studies aiming at the determination of catalyst wetting under industrial reaction conditions (Ruecker and Akgerman, 1987; Ring and Missen, 1989; Al-Dahhan and Dudukovic, 1995), reaction methods used have determined wetting efficiencies at low pressures and temperatures (Herskowitz et al., 1979; Morita and Smith, 1978).

In this investigation effective catalyst wetting was estimated for a trickle-bed reactor for the HDS of a vacuum gas oil at high pressure (60atm) and temperatures (280-330°C). The wetting efficiencies were accounted for by expressing the global rate in terms of an overall effectiveness factor, which is a function of internal and external wetting efficiencies, internal diffusion and intrinsic kinetics. External mass and heat transfer limitations were negligible. The modified Thiele modulus proposed by Dudukovic was used and intrinsic kinetics were determined by batch experiments.

EXPERIMENTAL

The 15%MoO₃-4.5%NiO/ γ -Al₂O₃ catalyst was prepared by incipient wetness co-impregnation of 1/16" γ -Al₂O₃ extrudates with the appropriate solutions. The catalyst was calcined at 110°C overnight and at 500°C for 5h. The presulfidation of the catalyst was accomplished by exposure to a H₂S/H₂ mixture at 360°C, preceded and followed by a 1h He purge. The presulfation time was adjusted accordingly so that the total amount of H₂S passed over the catalyst contained approximately 6 times more sulfur than the stoichiometric amount needed for the sulfidation of the Mo, Ni oxides. The feedstock used was a vacuum distillate obtained from the refinery of LPC Hellas with a total sulfur content of 0.45% wt. The density of the lube oil was 0.86 g/ml at 20°C, the kinematic viscosity at 40 and 100°C was 39 and 6.14cSt respectively giving a viscosity index of 103. The sulfur content of the feed and product oils were determined by an ASOMA sulfur analyzer (200T-series) based on X-ray fluorescence analysis.

The HDS of the vacuum gas oil was carried out in both a stirred batch autoclave and a concurrent downflow trickle-bed reactor. The batch autoclave had a volume of 300ml and the catalyst to oil mass ratio was equal to 1/10. The reactor operating time was counted from the moment the temperature of the reactor reached the desired value and the pressure was fixed at 880psi (\approx 60atm). A more detailed description of the setup and performance of the batch reactor is given elsewhere (Yiokari et al., 1997). The trickle-bed reactor was a stainless steel tube of 15mm i.d. and 300mm length arranged inside a heater. The 15ml catalyst bed was placed at the bottom of the reactor while the rest of the tube was filled with γ -Al₂O₃ extrudates. The flow rates of the gases were controlled by mass flowmeters and controllers. The viscous liquid feed, which was placed in a piston, was driven into the reactor by pumping distilled water into the other side of the piston with the help of a common HPLC pump. The reactants, both liquid and gas, were mixed and heated before entering the reactor at 150°C. The reactor effluent flowed into a stainless steel cylinder acting as a gas-liquid separator. The liquid product flowed continuously into a sample tank with the help of a solenoid valve whereas the scrubbed gas product flowed into the vent. Control for the pressure and temperature of the catalyst bed were provided. All results were obtained under steady state conditions which were reached approximately 4h after the reaction conditions were applied. According to the work of Fukushima and Kusaka (1977a,b) regarding the boundaries of hydrodynamic flow regions, the range of Reynolds numbers experimentally covered in this work belonged to the trickle flow region ($1 \times 10^{-4} < Re_L < 1.5 \times 10^{-3}$).

RESULTS

Hydrodesulfurization Kinetics: One of the most important set of reactions that take place during the hydrotreatment of residual oils is the hydrodesulfurization (HDS) of its various sulfur compounds. Since there is a great number of different sulfur compounds in industrial feedstocks, the actual mechanism of the HDS reaction is quite complex. Kinetic studies have shown that the HDS of an industrial feedstock could be described satisfactorily if it is considered as a mixture of two sulfur containing pseudocompounds, which differ considerably in HDS reactivity (Schuit and Gates, 1973). The first pseudocompound represents a reactive group that consists of thionaphthenes, mercaptans and sulfides (S_1), while the second hypothetical compound consist of the less reactive thiophenoaromatics (S_2). Each pseudocompound is assumed to react at a rate proportional to its sulfur concentration. Therefore the HDS reactions can be written simply,



Gel permeation chromatography of the gas oil (Varotsis and Pasadakis, 1997) used in this investigation determined 40% of sulfur pertaining to the less reactive thiophenoaromatics (S_2). Hence the remaining 60% of the gas oil total sulfur content was assumed to be the more reactive pseudocomponent S_1 . The two straight lines illustrated in Figure 1 indicate first order reaction of each sulfur containing pseudocomponent adding up to the curve fitting the data. This type of kinetic behavior can be mistaken for second order reaction kinetics. The distinction between the two parallel first order reactions and one second order reaction was made according to the procedure proposed by Wei and Hung (1974) for sulfur conversions above 97%.

Schuit and Gates (1973) reported that the kinetics regarding hydrogen are dependent on catalyst composition and on the nature of the feedstock. Hence the effect of hydrogen partial pressure on the HDS reaction was investigated. Figure 2 shows that sulfur conversion practically remains constant for hydrogen partial pressures over 20atm, independent of total gas flow rate. Thus the experiments performed in this study were in the region of zero-order kinetics regarding hydrogen.

Assumptions: The absence of external mass and heat transfer limitations was verified in the batch autoclave by choosing the appropriate stirring speed and in the trickle-bed reactor by confirming that the sulfur conversion remained constant when the volume of the catalyst bed and liquid flow rate where both doubled (constant LHSV). The 1/16" diameter pellets assured no internal mass and heat transfer by performing batch experiments with pellets of different sizes. First-order isothermal, irreversible reactions with respect to the reactants in the liquid are considered and the gaseous H_2 is present in great excess so the liquid is always saturated with gas. The catalyst pellets are completely wetted in the batch autoclave. Under these conditions the rate constants derived from the batch autoclave are assumed to be intrinsic rate constants.

Batch Reactor Performance: In the case of the batch reactor, one has:

$$\frac{dC_{S,i}}{dt} = \left(\frac{v_{cat}}{v_{liq} + v_{cat}} \right) \cdot r_i \quad (2)$$

where r_i is the reaction rate and $C_{S,i}$ the concentration of the sulfur-containing pseudocomponent i and v_{cat} and v_{liq} are the volume of the catalyst bed and the extra liquid in the batch autoclave respectively. For first order reaction regarding the sulfur component and zero order reaction regarding H_2 , one has:

$$r_i = k_{B,i} \cdot C_{S,i} \quad (3)$$

where $k_{B,i}$ is the rate constant of the sulfur containing pseudocomponent i . Substituting equation (3) in equation (2) and integrating, one obtains:

$$C_{S,i} = C_{S0,i} \cdot \exp\left(-\frac{k_{B,i}}{ELHSV}\right) \quad (4)$$

where ELHSV is an equivalent liquid hourly space velocity and can be defined for the batch autoclave as:

$$ELHSV^{-1} = \left(\frac{v_{cat}}{v_{liq} + v_{cat}} \right) \cdot t \quad (5)$$

Therefore the total sulfur concentration is:

$$C_S = C_{S,1} + C_{S,2} = \frac{C_S}{C_{S0}} = \alpha_1 \cdot \exp\left(-\frac{k_{B,1}}{ELHSV}\right) + \alpha_2 \cdot \exp\left(-\frac{k_{B,2}}{ELHSV}\right) \quad (6)$$

where α_1 and α_2 express the percentage of the pseudocompounds S_1 and S_2 and depend on the feedstock used. In this study α_1 and α_2 are 0.6 and 0.4 respectively as discussed above.

Trickle-bed Reactor Performance: Considering a differential volume element across the reactor, one has:

$$F \cdot C_{S0,i} \cdot dx_S = r_i \cdot dV \quad (7)$$

where F is the liquid flow rate, x_S is the sulfur conversion and V is the volume of the catalyst bed. Considering first order reaction regarding the sulfur component and zero order reaction regarding H_2 we substitute equation (3) in equation (7) to obtain:

$$C_{S,i} = C_{S0,i} \cdot \exp\left(-\frac{k_{T,i}}{\text{LHSV}}\right) \quad (8)$$

where LHSV is the liquid hourly space velocity and is defined for the trickle-bed reactor as:

$$\text{LHSV}^{-1} = \frac{V}{F} \quad (9)$$

and $k_{T,i}$, $i=1,2$, are the apparent first order kinetic constants for trickle-bed operation. Therefore the total sulfur concentration for the trickle-bed reactor is:

$$C_S = C_{S,1} + C_{S,2} \Leftrightarrow \frac{C_S}{C_{S0}} = \alpha_1 \cdot \exp\left(-\frac{k_{T,1}}{\text{LHSV}}\right) + \alpha_2 \cdot \exp\left(-\frac{k_{T,2}}{\text{LHSV}}\right) \quad (10)$$

Figures 3 and 4 illustrate the kinetic behavior of the batch and trickle-bed reactors, for the four temperatures studied, respectively. As expected sulfur concentration decreases with increasing LHSV⁻¹ and temperature. The total gas flow rate for the trickle-bed reactor is equal to 200ml/min. The removal of sulfur from the vacuum gas oil is greater in the batch reactor for given reaction conditions. The values of the rate constants derived for both the batch autoclave and the trickle-bed reactor are summarized in Table 1. The rate constants of group S₁ are 5-35 times greater than those of group S₂ depending on the reaction temperature. It is important to note that the ratios $k_{T,1}/k_{B,1}$ and $k_{T,2}/k_{B,2}$ remain practically constant with temperature and that the latter is larger since it corresponds to the slower reaction.

DISCUSSION

In the absence of mass transfer effects one would expect that the rate constants derived from equation (10), $k_{B,i}$, would be equal to the ones derived from equation (6), $k_{T,i}$, but this is not the case (Table 1). The essential difference of the two reactors is illustrated in Figure 5, where one can see that the rate of the HDS reactions is affected only by the partial wetting of the catalyst in the case of the trickle-bed reactor since other factors which affect it are the same (hydrogen excess, feed, etc.) and internal and external mass and heat transport limitations are negligible.

For a non ideal trickle-bed reactor, equation (10) can be written again by substituting $k_{T,i}$ with ($k_{B,i} \cdot \eta_{T,i}$), as:

$$\frac{C_S}{C_{S0}} = \alpha_1 \cdot \exp\left(-\frac{k_{B,1} \cdot \eta_{T,1}}{\text{LHSV}}\right) + \alpha_2 \cdot \exp\left(-\frac{k_{B,2} \cdot \eta_{T,2}}{\text{LHSV}}\right) \quad (11)$$

where $\eta_{T,i}$, $i=1,2$ are overall catalyst effectiveness factors for trickle-bed reactor for reactions (1). Therefore $k_{T,i}/k_{B,i}$ is equal to $\eta_{T,i}$ ($i=1,2$).

For particles of irregular shape and in two-phase systems, it has been established by Aris (1957) that the effectiveness factor can be approximated by:

$$\eta_i = \frac{\tanh \Phi_i}{\Phi_i} \quad (12)$$

$$\text{where } \Phi_i = \frac{V_p}{S} \sqrt{\frac{k_{B,i}}{D_{\text{eff},i}}} \quad (13)$$

V_p is the catalyst volume, S is the catalyst external surface and $D_{\text{eff},i}$ is the diffusivity of pseudocomponent i . Diffusivities of the sulfur-containing pseudocompounds were calculated using the Wilke-Chang correlation with $V_{S_1}=80.8 \text{ cm}^3/\text{mole}$ and $V_{S_2}=190 \text{ cm}^3/\text{mole}$ (Reid et al., 1977). Effective diffusivities were computed assuming a porosity/tortuosity factor of 0.1 (Yitzhaki and Aharoni, 1977). The dynamic viscosity of the lube oil at a given temperature was calculated by multiplying the kinematic viscosity with the density of the lube oil at that temperature. The variances of density and dynamic viscosity with temperature were calculated with the Watson-Gamson and Guzman-Andrade equations respectively.

To account for the partial external wetting of the catalyst particles one can use the modified Thiele modulus for trickle-bed reactors proposed by Dudukovic (1977). This modulus is based on the effective wetted external area, S_{eff} , and wetted internal volume of the pellet, $V_{p,\text{eff}}$, and can be written as:

$$\Phi_{T,i} = \frac{V_{p,\text{eff}}}{S_{\text{eff}}} \sqrt{\frac{k_{B,i}}{D_{\text{eff},i}}} \Rightarrow \Phi_{T,i} = \frac{f_{\text{int}}}{f_{\text{ext}}} \cdot \Phi_i \quad (14)$$

where f_{int} and f_{ext} are the internal and external wetting efficiencies respectively, defined as:

$$f_{\text{int}} = \frac{V_{p,\text{eff}}}{V_p} \quad \text{and} \quad f_{\text{ext}} = \frac{S_{\text{eff}}}{S_p} \quad (15)$$

From the values of the overall catalyst effectiveness factors $\eta_{T,i}$ (Table 1) and equation (12) the Thiele modulus of the trickle-bed reactor, $\Phi_{T,i}$ (Table 2) is calculated. Using equation (13) we compute Φ_i (Table 2). Therefore from equation (14) the ratio $f_{\text{int}}/f_{\text{ext}}$ is calculated and is summarized for the four temperatures studied and for the two sulfur pseudocomponents in Table 2. Total internal wetting of the catalysts pellets is normally assumed due to capillary effects, hence f_{int} could be considered unity and the external wetting efficiencies are estimated and presented in

Table 2. The computed values of the external wetting efficiencies slightly decrease with decreasing temperature. It is reassuring that similar values are extracted from both pseudocompounds for the preceding analysis. The mean values are 0.45 and 0.39 for pseudocomponents S_1 and S_2 respectively. These values of wetting efficiency are somehow smaller than the ones usually reported in the past (Satterfield, 1975; Gianetto and Specchia, 1992). This could be related to the low liquid flow rates used in the present investigation.

CONCLUSIONS

The HDS kinetics of an industrial feedstock were studied in the temperature range of 280-330°C in both a stirred batch autoclave and a trickle-bed reactor. The feed was considered as a mixture of two sulfur containing groups each reacting according to first order kinetics regarding their sulfur content. Reaction kinetics for hydrogen were zero order in the region of the present investigation.

The rate constants derived from the trickle-bed reactor are smaller than the ones obtained from the batch autoclave. The latter must correspond to intrinsic kinetic constants since internal and external mass and heat limitations were absent and total catalyst wetting was attained. The ratio of the rate constants extracted from the batch autoclave and trickle-bed experiments can be used to estimate the effectiveness factors during trickle-bed operation and thus also estimate the wetting efficiency under reaction conditions.

REFERENCES

Al-Dahhan, M.H. and Dudukovic, M.P., 1995, *Chem. Eng. Sci.* **50**, 2377.
Aris, R., 1957, *Chem. Eng. Sci.* **6**, 262.
Dudukovic, M.P., 1977, *A.I.Ch.E. J.* **23**, 940.
Fukushima, S., and Kusaka, K., 1977, *J. Chem. Eng. Jpn.* **10**, 461.
Fukushima, S., and Kusaka, K., 1977, *J. Chem. Eng. Jpn.* **10**, 468.
Gianetto, A., and Specchia V., 1992, *Chem. Eng. Sci.* **47**, 3197.
Herskowitz, M., Carbonell, R.G., and Smith, J.M., 1979, *A.I.Ch.E. J.* **25**, 272.
Herskowitz, M., and Smith, J.M., 1983, *A.I.Ch.E. J.* **29**, 1.
Llano, J.J., Rosal, R., Sastre, H., and Diez, F.V., 1997, *Ind. Eng. Chem. Res.* **36**, 2616.
Mills, P.L. and Dudukovic, M.P., 1981, *A.I.Ch.E. J.* **27**, 893.
Monta, S., and Smith J.M., 1983, *Ind. Eng. Chem. Fundam.* **17**, 113.
Reid, R.C., Prausnitz, J.M. and Sherwood, T.K., 1977, *The Properties of Gases and Liquids*, 3rd edn. McGraw-Hill, New York.
Ring, Z.E., and Missen, R.W., 1986, *Can. J. Chem. Eng.* **64**, 117.
Ring, Z.E., and Missen, R.W., 1989, *A.I.Ch.E. J.* **35**, 1820.
Ruecker C.M., and Akgerman, A., 1987, *Ind. Eng. Chem. Res.* **26**, 164.
Satterfield, C.N., 1975, *A.I.Ch.E. J.* **21**, 209.
Schuit, G.C.A. and Gates, B.C., 1973, *A.I.Ch.E. J.* **19**, 417.
Varotsis, N., and Pasadakis, N., 1997, *Ind. Eng. Chem. Res.* **36**, 5519.
Wei, J., and Hung, C.W., 1980, *Ind. Eng. Chem. Process Des. Dev.* **19**, 197.
Yentekakis, I.V. and Vayenas, C.G., 1987, *Chem. Eng. Sci.* **42**, 1323.
Yiokari, C., Morphi, S., Siokou, A., Satra, F., Bebelis, S., Vayenas C.G., Karavassilis C., and Deligiorgis G., 1997, Proceedings of the 1st International Symposium/6th European Workshop "Hydrotreating and hydrocracking of Oil fractions", Oostende, Belgium.
Yitzhaki, D., and Aharoni, C., 1977, *A.I.Ch.E. J.* **23**, 342.

TABLE 1- Kinetic rate constants for batch autoclave and trickle-bed reactor.

| Temperature, °C | Batch Reactor | | Trickle-bed Reactor | | | |
|-----------------|-----------------------------|-----------------------------|-----------------------------|-----------------------------|------------------------------|------------------------------|
| | $k_{B,1}$, h ⁻¹ | $k_{B,2}$, h ⁻¹ | $k_{T,1}$, h ⁻¹ | $k_{T,2}$, h ⁻¹ | $\eta_1 = k_{T,1} / k_{B,1}$ | $\eta_2 = k_{T,2} / k_{B,2}$ |
| 330 | 23.50 | 1.43 | 3.52 | 0.74 | 0.150 | 0.517 |
| 315 | 12.50 | 0.59 | 1.88 | 0.33 | 0.150 | 0.559 |
| 300 | 9.00 | 0.25 | 1.50 | 0.15 | 0.167 | 0.600 |
| 280 | 1.93 | 0.21 | 0.52 | 0.12 | 0.269 | 0.571 |

TABLE 2- Thiele moduli calculated from equations (12) and (13).

| Temperature, °C | Φ_1 (eq. 13) | Φ_2 (eq. 13) | $\Phi_{T,1}$ (eq. 12) | $\Phi_{T,2}$ (eq. 12) | $f_{int,1}/f_{ext,1} = \Phi_{T,1}/\Phi_1$ | $f_{int,2}/f_{ext,2} = \Phi_{T,2}/\Phi_2$ | $f_{ext,1}$ | $f_{ext,2}$ |
|-----------------|-------------------|-------------------|-----------------------|-----------------------|---|---|-------------|-------------|
| 330 | 3.79 | 0.94 | 6.67 | 1.84 | 1.76 | 1.87 | 0.57 | 0.54 |
| 315 | 2.84 | 0.66 | 6.67 | 1.67 | 2.35 | 2.53 | 0.43 | 0.40 |
| 300 | 2.66 | 0.47 | 5.99 | 1.51 | 2.25 | 3.21 | 0.44 | 0.31 |
| 280 | 1.41 | 0.50 | 3.71 | 1.62 | 2.63 | 3.24 | 0.38 | 0.31 |

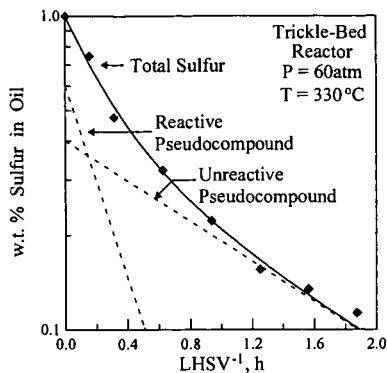


FIGURE 1 - Effect of inverse LHSV on sulfur content of vacuum gas oil and kinetic analysis.

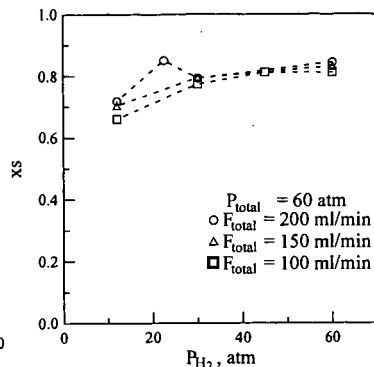


FIGURE 2 - Dependence of sulfur conversion on hydrogen partial pressure. Trickle bed reactor.

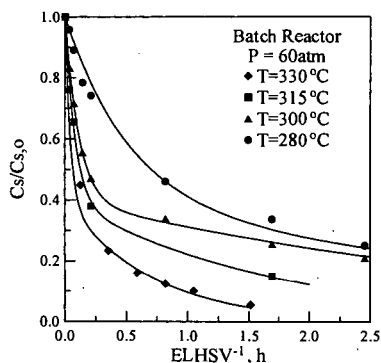


FIGURE 3 - Dependence of sulfur content on the inverse equivalent liquid hourly space velocity and temperature (Batch Reactor).

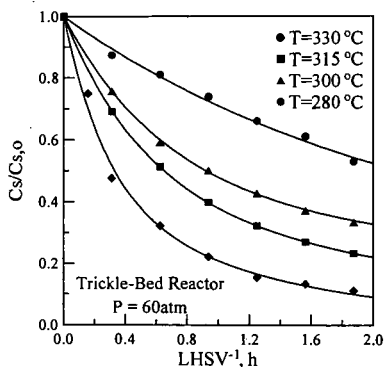
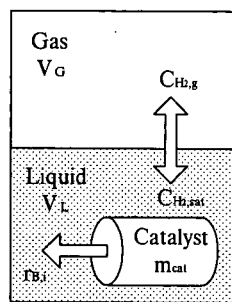
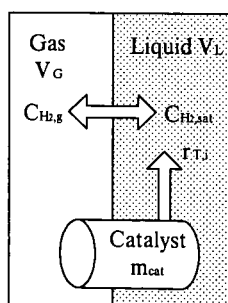


FIGURE 4 - Dependence of sulfur content on the inverse liquid hourly space velocity and temperature (Trickle-Bed Reactor).



Batch Reactor



Trickle-Bed Reactor

FIGURE 5 - Schematic representation of the particle environment in the batch autoclave and the trickle-bed reactors.

REACTION CHARACTERISTICS AND MECHANISM OF RESIDUUM HYDROCRACKING

Chaohe Yang, Hai Zheng, Feng Du, Chunming Xu, State Key Laboratory of Heavy Oil Processing, University of Petroleum, Dongying City, Shandong Province, China, 257062

Key words: residuum, hydrocracking, reaction mechanism

ABSTRACT

The Gudao vacuum residuum (GDVR) was hydrocracked in a 100 mL autoclave with crushed commercial Ni-Mo Catalyst within a temperature range of 390-420°C. The characteristics of series reaction remains obviously in the residuum hydrocracking. The relationship of coke yield and conversion for catalytic hydrocracking is different from thermal cracking and non-catalytic hydrocracking. The presence of catalyst and hydrogen can significantly inhibit the coking reaction, but simultaneously decreases the cracking rate to a certain extent. The apparent activation energy of residuum catalytic hydrocracking is close to that for thermal cracking. It can be derived that rate limiting step of the residuum catalytic hydrocracking is essentially thermal activation.

INTRODUCTION

The residuum hydrocracking is a very complex reaction system because the feed and product contain innumerable compounds and various reactions occur simultaneously. So it is difficult to study kinetics for every component in this system. Catalytic hydrocracking is more complicated than the non-catalytic hydrocracking. In residuum hydrocracking there often exist three phases of gaseous, liquid, and solid. The catalytic reactions occur on the surface of catalyst and the thermal reactions take place in the interspace of catalyst particles. The reactions not only occur in the liquid phase, but also happen in gaseous phase. Residuum thermal cracking is a free radical chain reaction, but there are different views for the mechanism of heavy oil catalytic hydrocracking due to the various feed, catalysts, and method used by different investigators.

Through the comparison of the chemical analogies of visbreaking, hydro-thermal cracking, catalytic cracking and catalytic hydrocracking, Le Page^[1-2] found that the driving force of the conversion reactions is essentially thermal activation in the temperature range applied. The catalyst, the hydrogen present, and the sophistication of the various techniques are merely expediences, which basically participate in limiting, indeed controlling, the condensation side reactions involving the heavy resin and asphaltene molecules.

De Jong^[3] (1994) investigated the hydroconversion of heavy vacuum gas oil in a trickle-bed reactor at about 450°C and moderate hydrogen pressure (30atm). He found that the cracking reactions are hardly affected by the presence of the metal active component of the catalyst and thought the cracking reactions are not acid-catalyzed but mainly thermally induced under the prevailing conditions. Through the studies of atmospheric residuum^[4], it is observed that catalytic cracking and thermal cracking take place simultaneously, the lighter distillates are mainly produced from the thermal cracking and the effect of catalyst is to offer active hydrogen to the heavy component in order to controlling coking. That is to say, the hydrogen captured by the light component come directly from the heavy component (the large molecule to be hydrocracked).

In the kinetic model of hydrocracking developed by De Jong^[5], the vapor-liquid equilibrium of the reaction mixture was considered. For fitting the experimental data, it was assumed that the cracking of molecules in the vapor phase is 25 times faster than for those present in the liquid phase. In other words it seems as if activated hydrogen in the liquid phase inhibit the radical cracking reaction, while the acceleration is apparent in the vapor phase. This assumption is in line with comments in the investigation of Sanhanen^[6] and Shabtai^[7]. The residuum hydrocracking made by Xu^[8] showed that the conversion of catalytic hydrocracking is greater than that of non-catalytic hydrocracking, which is ascribed to the inhibition of a great number of active hydrogen on the polymerization and coking reactions involving the heavy components.

As a whole, the recognition for heavy oil catalytic hydrocracking has been being semi-theoretical and no consistent conclusion has been drawn about the reaction mechanism and the effect of catalyst and hydrogen. For instance, active hydrogen capturing the large molecular radical can inhibit coking reaction and will be of help for enhancing the distillate yields, but the cracking rate will be decreased and distillate yield declined when the small and medium radicals are captured. The final result would depend upon the concrete situations. In the present paper, hydrocracking characteristics of GDVR will be investigated and the reaction mechanism discussed.

EXPERIMENTAL

The Gudao vacuum residuum was hydrocracked in a 100mL autoclave with crushed ICR-130H Catalyst of 0.35mm average diameter at the initial hydrogen pressure 8.5 MPa, with agitation speed at 850rpm and in the temperature range of 390-420. After hydrocracking, gas, liquid and coke were separated and analyzed. The yield of gas, liquid and coke were determined and the simulated distillation data of feed and liquid product were obtained.

RESULTS AND DISCUSSION

Product Distribution of GDVR Hydrocracking

The yields of gasoline and diesel increase gradually with the reaction time. The increasing rate is slow at the initial period of reaction and become faster and faster toward the end of reaction. The yield of vacuum gas oil (VGO) increases firstly at a faster rate and then slackens gradually. It passes through a maximum at certain time and then declines slowly. The phenomena mentioned above shows that residuum hydrocracking has an obvious characteristic of series reaction. The gas yield increase gradually with time at constant temperature except in the case of 390°C. The coke yield increase quickly at the initial period and slowly with increasing reaction time.

The relationships of product yields and conversions are showed in figure 1. Gas, gasoline and diesel increases gradually with the conversion of >500°C portion, and the increasing rate is slow when the conversion is lower and becomes faster with the increase of conversion. This is because the heavy distillate must be cracked at first into middle distillate and the formation rate of light distillates becomes gradually faster with the increase of middle distillate. The middle distillate content increases at first and reaches to a maximum at a certain conversion, and then decreases gradually.

The relationship of coke yield and conversion for catalytic hydrocracking is obviously different from thermal cracking and non-catalytic hydrocracking^[9-12]. For the latter two cases the coke yield increases slowly at the initial period and grows seriously when the conversion passes a critical value (about 55—65% for GDVR), which is similar as the relationship of gas yield

versus conversion in figure 1. For residuum hydrocracking, the coke yield increases quickly when the conversion is low, and the increasing rate slows down gradually with further conversion, which is consistent with the conclusion derived by most investigators on catalyst deactivation. For the present study, the initial quickly coking may be caused by the promotion of acid catalysis on the surface of catalyst, and the hydrogenation function becomes stronger relative the cracking function when the acid sites are gradually covered by the deposition of coke, which can inhibit greatly the coking reaction.

The product selectivity versus conversion of $>500^{\circ}\text{C}$ portion is illustrated in figure 2. The selectivity of gasoline and diesel increase gradually with the conversion. The selectivity of VGO reaches a maximum at 30% conversion and then decrease gradually. The selectivities of gas and coke decrease seriously at a low conversion range and then tend to a constant. Therefore, residuum catalytic hydrocracking differs from thermal cracking and hydrocracking mainly in serious inhibition of coking and gas formation. The data points of selectivity of gas and coke versus conversion at different temperatures all fall on the corresponding curves respectively. This supports that the temperature has no effect on the selectivity of gas and coke at the conditions used in this study.

Simple kinetic model of GDVR hydrocracking

Whether the driving force of residuum catalytic hydrocracking is essentially the thermal activation can be checked by comparing the activation energy of catalytic cracking with that of thermal cracking. Residuum hydrocracking has ever been described successfully by simple first-order or second-order kinetics. The experimental results have been correlated in terms of the simple kinetic equations, with the plots of $\ln[1/(1-x)]$ and $x/(1-x)$ (x is conversion) versus reaction time, t . It is found better to describe the catalytic hydrocracking of GDVR by first-order kinetics than second-order kinetics. But the second-order kinetics is feasible

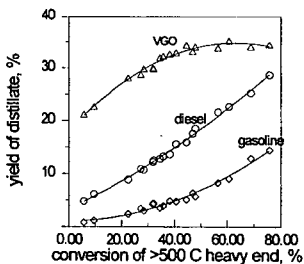


Fig.1A Yields of liquid products versus conversion

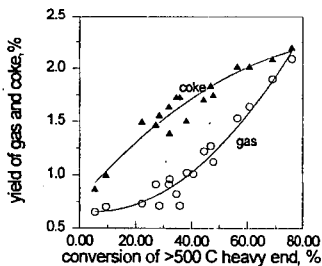


Fig.1B yield of coke and gas versus conversion

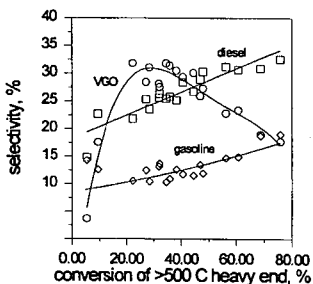


Fig.2A Selectivity of liquid products versus conversion

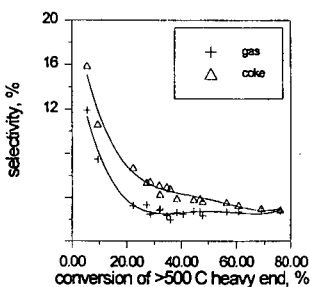


Fig.2B Selectivity of coke and gas versus conversion

when the conversion is not too high, especially for the hydroconversion of $>350^{\circ}\text{C}$ portion. It could be thought that the reaction order is affected by the lumping method when using power kinetic equations to describe hydrocracking. The rate constants (k) at different temperature were calculated according to the first-order kinetics, a linear relationship exists between $\ln(k)$ and $1/T$ (reciprocal of temperature) and the correlation coefficient is 0.9994. The activation energy of GDVR hydrocracking is listed in Table 1.

Table 1 Kinetic reactions of hydrocracking

| Feed | Reaction | Catalyst | Temp($^{\circ}\text{C}$) | E (KJ/mol) | Reference |
|-----------------------|--------------------------------|--------------|----------------------------|------------|-----------|
| Maya VR | VR+H ₂ →Products | Dispersed Mo | 397-438 | ~290 | 10 |
| Athabasca asphaltene | Bitumen→ Products | No | 370-538 | 130 | 13 |
| Athabasca asphaltene | Bitumen→ Products | No | 375-420 | 150 | 14 |
| Huanxiling asphaltene | VR→ Products | No | 385-430 | 260 | 15 |
| Distillate | VGO+H ₂ → Products | NiW/SiAl | 300-430 | 88.2 | 16 |
| Coal tar | Tar+H ₂ → Products | NiW/SiAl | 400-500 | 73.6 | 17 |
| GDVR | VR+H ₂ → Products | No | 400-420 | 216 | 18 |
| GDVR | GDVR+H ₂ → Products | ICR130H | 390-420 | 260-285 | This work |

Some kinetic results of heavy oil hydrocracking are summarized in table 1. From these results the activation energy of residuum hydrocracking in the presence of catalyst is very close to that for thermal cracking, whereas the activation energy of distillate catalytic hydrocracking is obviously smaller than that of residuum hydrocracking. This may be explained as the cracking active sites of catalyst play an important role in the distillate hydrocracking, while in the residuum catalytic hydrocracking thermal activation is predominating. The catalysts just create active hydrogen to inhibit coke deposition and simultaneously decrease the cracking rate to a certain extent.

CONCLUSION

From the present study a number of conclusions emerge.

- (1) Series reaction model is consistent with the reaction process of residuum catalytic hydrocracking.
- (2) The relationship of coke yield versus conversion is obviously different from thermal cracking and non-catalytic hydrocracking. Catalyst and hydrogen can significantly inhibit the coke deposition and simultaneously control the cracking reaction.
- (3) The initiation and rate controlling step of residuum catalytic hydrocracking is thermal activation in essence.
- (4) GDVR hydrocracking is described very well by the first-order kinetics and reaction order is affected by the lumping method.

REFERENCES

1. Le Page J F. Preprints, Div of Petrol Chem, ACS. 1987, 32(2):470
2. Le Page J F. Chemical and Physico-chemical Problems Involved in the Catalytic Hydroconversion of Heavy Feedstocks. Proceedings of International Conference on Petroleum Refining and Petrochemical Processing. Sept. 1991, Beijing, China. Volume 1, p185.
3. De Jong K P. Ind Eng Chem Res. 1994, 33:821
4. Translation proceedings on Heavy Oil Processing(Chinese), Sino-Petroleum Chem. Press 1990, P.47
5. De Jong K P. Ind Eng Chem Res. 1994, 33:3141
6. Sachanen A N. Conversion of Petroleum. Reinhold, Ney York. 1984, p390
7. Shabtai J, et al. Adv Chem Ser. 1979, 183:297
8. Xu chunmin, lin shixon. Petroleum Processin and Petrochemicals(Chinese), 1995, 26(9):52

9. Liu Chenguang. Hydrocracking of Gudao Residue using Dispersed phase catalysts. Doctoral thesis, University of Petroleum, China. 1991
10. Heck K H, et al. Preprints, Division of Petro.Chem., ACS. 1993, 38(2):417
11. Del Bianco A ,et al. Fuel, 1993, 72(1):75
12. Liu Chenguang, Que Guohe, et al. Petroleum Processing(Chinese). 1993,24(3):57
13. Barbour R V, et al. 172nd Nat Meeting, Am. Chem. Soc, San Francisco, 29 August-3 September, 1976, 21(6):278.
14. Köseoglu R ,Phillips C R. Fuel, 1987, 13(6):56.
15. Yang Jiamo, Liang Wenjie, et al. Journal. of university of Petroleum(Chinese), 1989, 13(6):56
16. Qader S A and Hill G R. IEC Proc Des .Dev. 1969, 8(1):98.
17. Qader S A and Hill G R. IEC Proc Des .Dev. 1969, 8(4):465.
18. Sun Bojun, Que Guohe, et al. Petroleum Processing(Chinese), 1991, 22(4):62

A LUMPING MODEL FOR KINETICS OF RESIDUUM HYDROCRACKING

Chaohe Yang, Chunming Xu, Feng Du, Shixiong Lin, State Key Laboratory of Heavy Oil Hydroprocessing, University of Petroleum, Dongying City, Shandong Province, China, 257062

Key words: residuum, hydrocracking, kinetic model

ABSTRACT

The Hydrocracking reaction kinetics of Gudao Vacuum Residuum was investigated in a 100 ml autoclave with crushed ICR-130H Catalyst in a temperature range of 390-420°C. A lumping model with five parameters for the prediction of the product distribution curve for residuum hydrocracking was proposed as modification of the narrow-boiling point lumping model developed originally for distillate hydrocracking by Stangeland. A major advantage to this kinetic model is that its establishment and application don't need the complete distillation data of residua and products. The results predicted by this model agree satisfactorily with the experimental observation.

INTRODUCTION

The hydrocracking of residuum is a very complex reaction system in which thousands of organic species participate in a highly coupled mode. For this reaction system, it is not possible to establish kinetic equation for every reaction species by the conventional method used in reaction kinetics studies. Such a complex reaction system must be simplified so that the kinetics characteristics of residuum hydrocracking could be elucidated with mathematical equation, that is to say, the lumping method would be used. Lumping method for reaction kinetics is to build a lumping kinetic model in which the innumerable chemical compounds in reaction system is classified as a number of lumps by means of the kinetic characteristics of molecule reaction. The strategy of modeling a given reaction system usually varies with the specific goal to be attained. For example, a large number of chemical compound could be lumped by the total content of a component or a kind of component, by the boiling point range (compounds having similar boiling point grouped into a lump), by the chemical structure (compound having similar chemical structure as a lump), or sometimes by the combination of boiling point range and the chemical structure similarity.

Considerable effort has been focused worldwide on investigating the hydrocracking kinetics of distillates^[1] and a better narrow-boiling point lumping model has been proposed by Stangeland (1974)^[2] which can be used to predict the product distribution for distillate hydrocracking. There are a few studies on the kinetic model of residuum hydrocracking, and most of them were product lumping models which is not flexible enough to cope with various operation conditions and product scheme, although some investigators have tried to apply such model to commercial operation. Once the product scheme is subject to change, the parameters of product lumping model should be recalculated so as to approach the new product scheme.

Most of studies on the narrow-boiling point lumping model are based on the Stangeland model developed for distillate hydrocracking which requires the complete distillation data of feed and product and characterizes each lump by its final boiling point. These models have not been applied successfully to residuum hydrocracking for lack of the complete distillation curve of heavy oil feed and product. The prediction results is greatly different from the experimental observation in high boiling point range, even if these model are applied to heavier distillate hydrocracking^[3].

In the present study, based on the flexibility of the rate distribution and production distribution functions in the Stangeland narrow-boiling point lumping model, a lumping kinetic model suitable for residuum hydrocracking was proposed by combination of the correlation results on SFEF (Super Fluid Extraction Fractionation) fraction hydrocracking^[1].

EXPERIMENTAL

The Gudao Vacuum residuum was hydrocracked in a 100mL autoclave with crushed ICR-130H Catalyst of 0.35mm average diameter at the initial hydrogen pressure 8.5 MPa, with agitation speed at 850rpm and in the temperature range of 390-420°C. After hydrocracking, gas, liquid and coke were separated and analyzed. The yield of gas, liquid and coke were determined and the simulated distillation data of feed and liquid product were obtained.

KINETIC MODEL

The kinetic model is based on the concept of pseudo-components (narrow fractions) and is similar to one proposed by Stangeland (1974). Assumptions in the present model are as follows:

- (1) The feed and products are represented by a series of continuous mixture which are pseudo-components of boiling range of 28°C and could be characterized by its final boiling point. The lightest pseudo-component is gas lump of boiling point below 10°C. The residual part of boiling point above 537.8°C. was treated as a lump, the heaviest pseudo-component, and characterized by a pseudo-boiling point (TBP_p).
- (2) Each pseudo-component is assumed to undergo a first order irreversible reaction. Polymerization reaction is neglected and no coking reaction is supposed.
- (3) The rate constant of hydrocracking of any lump is assumed to be relative to the heaviest lump in the model.
- (4) A lump can be hydrocracked into any lighter lump, but no conversion occurs among the lightest four lumps.

The reaction kinetic model of residuum hydrocracking is given by the following differential equations:

$$\frac{dF_i}{dt} = -k_i F_i + \sum_{j=i+1}^n k_j p_{ij} F_j \quad i=1,2, \dots, n$$

where k_i is the constant of lump i hydrocracking (hr^{-1}), t is reaction time (hr), and p_{ij} is the fraction of the cracked products from a heavier component, j , that become a lighter component i .

The calculation methods of k_i and p_{ij} have a great influence on the validity of the model. It is too difficult to derive a mathematical model if the number of model parameter is too great. But if the model parameters are not sufficient, the model would be lack of flexibility in application. Equations for calculating k_i was selected as follows:

$$k_i = k_0 \exp\left(-\frac{E}{RT_i}\right) \cdot [T_i + A(T_i^3 - T_i)] \quad T_i = \frac{TBP_i}{TBP_p}$$

where R is the gas constant ($8.314 \text{ J} \cdot \text{K}^{-1} \cdot \text{mol}^{-1}$), T_i is the temperature (K), T_i is the temperature parameter of lump i , TBP_i is the final boiling point of lump i (°F) and TBP_p is the pseudo-boiling point of the heaviest component (°F). k_0 is frequency factor (hr^{-1}) and E represents the apparent activation energy. Li (1994) proved that the relative deviation of

$k_0 \exp\left(-\frac{E}{RT_r}\right)$ is not greater than 3% when k_0 and E vary in a reasonable range. So the apparent activation energy was set to a constant value ($E=108\text{KJ/mol}$)^[4].

Because there is a strong decreases in cracking rate as the boiling point of hydrocarbon is less than 250°F and the heaviest lumping in residuum hydrocracking has a dominant amount, the rate constant k_i was modified in terms of the following relations:

$$k_i = \begin{cases} 0.0 & TBP_i \leq 250 \\ 0.33k_i & TBP_i = 300 \\ 0.78k_i & TBP_i = 350 \\ 3.0k_i & TBP_i = TBP_f \end{cases}$$

and the product distribution function was represented by the equations as follows:

$$p_{ij} = \begin{cases} 0.0 & i \leq j \\ C \cdot \exp[-0.00693 \cdot (TBP_j - 250)] & i = n, j \leq i-1 \\ P(Y_{ij}) - P(Y_{i+1,j}) & i < n, j \leq i-1 \end{cases} \quad P(Y_{ij}) = [Y_{ij}^2 + B(Y_{ij}^3 - Y_{ij}^2)](1 - p_{ij})$$

$$Y_{ij} = \frac{TBP_i - 50}{TBP_j - 100}$$

So, kinetic parameters (k_i and p_{ij}) in residuum hydrocracking reaction can be represented by five model parameters (k_0 , A , B , C , TBP_p). The distinction of this model and Stangeland model lies in:

- (1) Suitable for the cases lacking complete TBP distillation data of feed and product.
- (2) The pseudo-boiling point (TBP_p) is proposed to characterize the heaviest lump and the rate constant distribution function is modified.
- (3) Any lump may be hydrocracked into any lighter lump. this is especially important when the heaviest lump accounts for a dominant amount.
- (4) The pseudo-boiling point, TBP_p , was set by the correlation of SFEF fraction hydrocracking.

Estimation of model parameters is done by algorithm according to Herbest (1968)^[5]. The objective function is defined as the sum of the squares of the differences between the observed and calculated composition of the pseudo-component.

DISCUSSION

Through the estimation of model parameters, TBP_r at different reaction temperature were found approximately the same value, 1100°F . It could be thought that the properties of feed at the zero reaction time are similar no matter what reaction temperature was set, although the cracking reaction may occur already to a certain extent. Thus, TBP_r was fixed invariably to be equal to 1100°F , the deviation due to this decision can be compensated by adjusting other parameters. The relations of other model parameters and reaction temperature are given as follows,

$$\left. \begin{aligned} A &= 11881.8 - 88.0901\text{Tr} + 0.217577\text{Tr}^2 - 0.000179023\text{Tr}^3 \\ B &= 2329.12 - 17.6345\text{Tr} + 0.0445643\text{Tr}^2 - 3.75908\text{E} - 005\text{Tr}^3 \\ C &= 28180.1 - 210.262\text{Tr} + 0.522687\text{Tr}^2 - 0.000432817\text{Tr}^3 \\ k_0 &= 11960.5 - 88.8419\text{Tr} + 0.219754\text{Tr}^2 - 0.000180983\text{Tr}^3 \end{aligned} \right\}$$

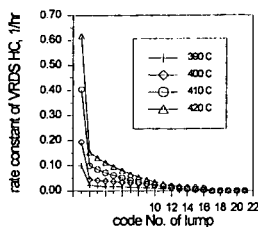


Fig. 1 Rate constant of each lump hydrocracking

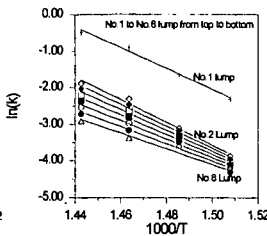


Fig 2 Rate constant of lumps v.s. temperature

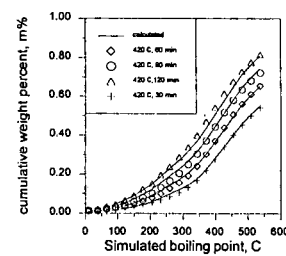
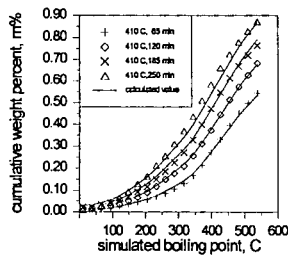
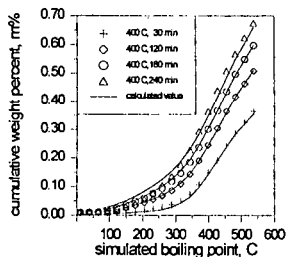
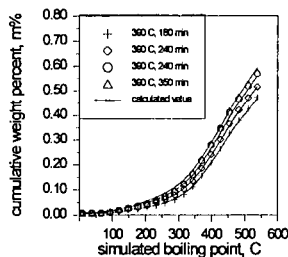


Fig. 3 Comparison of calculated and observation distillation curves

The rate constants of each lump hydrocracking were illustrated in Figure 1. The rate constant of the heaviest lump is far larger than those of any other lumps. At the same temperature, hydrocracking rate decreases gradually with the lowering of boiling point of lump component. The rate constant of the heaviest pseudo-component is 3.6–4.1 times as large as that of the next lump and 3–4 orders of magnitude larger than that of the lightest pseudo-component which is supposed to have been undergone hydrocracking. The methods chosen for calculating the cracking rate and product distribution of 1 to 8 lumps pave the way to the success of the model.

The cracking rate constants of the lump with higher boiling point are presented in Arrhenius plots in Figure 2. For each lump a straight line was obtained, especially for the heaviest four lumps. This suggests that the present model represents adequately the kinetic characteristics of GDVR hydrocracking.

The observed and calculated product yields at different reaction conditions are summarized in Table 1. The relative deviation between observed and predicted yields of the distillate products are not greater than 1.5% which is just the same as the permitted error of simulated distillation except for reaction condition at 410°C and 120 min.^[6] As shown in figure 3, the predicted yields based upon those model parameters mentioned above are represented as solid lines and the discrete observed data as points of different form. In general, the agreement is quite good and

probably closed to experimental error, which shows that it is feasible to characterize residuum-hydrocracking reaction by this narrow-boiling point lumping model.

CONCLUSION

A lumping model suitable for residuum hydrocracking was proposed by modifying the Stangeland model, and the agreement of the calculated yields with the observed ones is quite good. But there is much work to be done in order to check the suitability of this model for different hydrocracking feedstocks and various reaction conditions.

Table 1 The observed and calculated distillate product yield at different reaction conditions (m%)

| Temperature, Time | 390°C, 180min | | | 390°C, 240min | | | 390°C, 300min | | |
|-------------------|---------------|--------|--------|---------------|--------|--------|---------------|--------|--------|
| | Obs. | Calcd. | Diff.. | Obs. | Calcd. | Diff.. | Obs. | Calcd. | Diff.. |
| gas | 0.73 | 0.43 | 0.30 | 0.71 | 0.39 | 0.12 | 0.82 | 0.76 | 0.06 |
| 38—204°C | 2.34 | 2.64 | -0.30 | 3.11 | 3.41 | -0.30 | 3.73 | 4.13 | -0.40 |
| 204—343°C | 8.20 | 8.25 | -0.05 | 9.85 | 9.69 | -0.16 | 11.62 | 11.02 | 0.60 |
| 343—537°C | 36.08 | 35.53 | 0.55 | 37.93 | 37.95 | -0.02 | 40.74 | 40.08 | 0.66 |
| >537°C | 52.65 | 53.14 | -0.49 | 48.40 | 48.36 | 0.04 | 43.09 | 44.0 | -0.91 |
| Temperature, Time | 390°C, 350min | | | 400°C, 30min | | | 400°C, 120min | | |
| | Obs. | Calcd. | Diff.. | Obs. | Calcd. | Diff.. | Obs. | Calcd. | Diff.. |
| gas | 0.71 | 0.90 | -0.19 | 0.70 | 0.95 | -0.25 | 0.91 | 0.66 | 0.25 |
| 38—204°C | 4.04 | 4.71 | -0.67 | 1.06 | 1.05 | 0.01 | 3.43 | 3.81 | -0.38 |
| 204—343°C | 12.11 | 12.05 | 0.06 | 5.49 | 5.05 | 0.34 | 9.91 | 9.79 | 0.12 |
| 343—537°C | 40.90 | 41.66 | -0.76 | 29.17 | 28.68 | 0.49 | 36.46 | 36.83 | -0.37 |
| >537°C | 42.23 | 40.68 | 1.55 | 63.58 | 64.36 | -0.78 | 49.29 | 48.91 | 0.38 |
| Temperature, Time | 400°C, 120min | | | 400°C, 240min | | | 410°C, 65min | | |
| | Obs. | Calcd. | Diff.. | Obs. | Calcd. | Diff.. | Obs. | Calcd. | Diff.. |
| gas | 1.02 | 1.08 | -0.06 | 1.12 | 1.46 | -0.34 | 0.91 | 0.73 | 0.18 |
| 38—204°C | 4.92 | 5.50 | -0.58 | 5.48 | 6.76 | -1.28 | 4.61 | 5.03 | -0.42 |
| 204—343°C | 12.52 | 12.60 | -0.08 | 16.14 | 14.65 | 1.49 | 11.18 | 11.89 | -0.71 |
| 343—537°C | 41.25 | 40.70 | 0.55 | 44.76 | 43.21 | 1.55 | 37.66 | 35.85 | 1.84 |
| >537°C | 40.29 | 40.12 | 0.17 | 32.50 | 33.92 | -1.42 | 45.64 | 46.53 | -0.89 |
| Temperature, Time | 410°C, 120min | | | 410°C, 185min | | | 410°C, 255min | | |
| | Obs. | Calcd. | Diff.. | Obs. | Calcd. | Diff.. | Obs. | Calcd. | Diff.. |
| gas | 1.22 | 1.35 | -0.13 | 1.64 | 2.08 | -0.44 | 2.09 | 2.86 | -0.77 |
| 38—204°C | 5.70 | 8.14 | -2.44 | 9.92 | 10.91 | -0.99 | 14.21 | 13.17 | 1.04 |
| 204—343°C | 14.65 | 16.68 | -2.03 | 21.21 | 20.76 | 0.45 | 27.31 | 25.87 | 1.44 |
| 343—537°C | 43.57 | 41.41 | 2.16 | 44.56 | 45.48 | -0.92 | 43.48 | 45.12 | -1.64 |
| >537°C | 34.86 | 32.15 | 2.71 | 22.66 | 20.77 | 1.89 | 12.91 | 12.97 | -0.06 |
| Temperature, Time | 420°C, 35min | | | 420°C, 60min | | | 420°C, 120min | | |
| | Obs. | Calcd. | Diff.. | Obs. | Calcd. | Diff.. | Obs. | Calcd. | Diff.. |
| gas | 0.96 | 0.34 | 0.42 | 1.27 | 0.93 | 0.34 | 1.90 | 1.90 | 0.00 |
| 38—204°C | 4.45 | 5.35 | -0.90 | 6.55 | 7.19 | -0.64 | 13.42 | 13.21 | 0.21 |
| 204—343°C | 11.59 | 11.96 | -0.37 | 16.42 | 16.72 | -0.30 | 24.62 | 22.99 | 1.63 |
| 343—537°C | 37.13 | 37.38 | -0.25 | 41.17 | 40.54 | 0.30 | 41.81 | 43.23 | -1.42 |
| >537°C | 45.87 | 44.74 | 1.10 | 34.59 | 34.61 | -0.02 | 18.25 | 18.67 | -0.42 |

REFERENCES

1. Yang, Chaohe. Characteristics and Kinetics of Heavy Oil Hydroconversion. Doctoral Thesis, University of Petroleum, Beijing, China, 1997
2. Stangeland, B. E., et al. IEC Pro. Des. Dev. 1974, 13(1):71.
3. Raychaudhuri, U., et al. Fuel Sci Techn Int'l, 1994, 12(2):315
4. Li dongsheng, Sun wei, Petroleum Processing and Petrochemicals, (Chinese)1994, 25(5):29.
5. Herbst, J. A., Fuerstenau, D. W. AIIME Trans., 1968, 241:538.
6. ASTM Standard: D5307, Standard Test Method for Determination of Boiling Range Distribution of Crude Petroleum by Gas Chromatography, Annual Book of ASTM Standards, Vol.05.02, P564, 1993.

Pyrolysis Kinetics and Mechanism for Average Molecular Structures of Heavy Oil Crudes,

Iván Machín, Edgar Cotte

PDVSA-Intevep, Process Department, P.O. Box 76343, Caracas 1070A, VENEZUELA

Keywords: Heavy Crude Oils, Pyrolysis, Kinetics, Molecular Models

ABSTRACT

A molecular kinetic model named PYRO2, for pyrolysis of heavy crude oils, has been developed. This model uses average molecular structures (AMS) derived from experimental analytical data obtained from heavy crude oils. The PYRO2 model consists of about 50 reactions associated with homolytic C-C, C-S, C-N and C-H bond breaking over saturated chains, bridges and cycles bounded to condensed rings. This model was applied to average molecules of Athabasca and Boscan crude oils in order to reproduce thermal conversion and product distribution data. The dependence of conversions to volatile products and coke yields on temperature and time of reaction are reproduced within a 10 % deviation from the experimental results. Variations in the distribution of gas and liquid components of volatile products follow the same tendencies as experimental results; but they depart significantly from the absolute values. This may indicate that new reaction paths and/or additional corrections in the AMS's are necessary. Two such factors, one of each, were identified..

INTRODUCTION

In very complex systems, like crude oils, the reaction mechanism and associated kinetics are not directly accessible for individual molecular entities. Kinetic models are thus based on different representations of molecular aggregations or the key properties of interest. According to the methodology used, kinetic models can be divided in three categories: (a) Pseudokinetic Models, in which the reaction schemes are associated with transformations of pseudocomponents that represent the crude oil fraction. Due to the fitting parameters they contain, their predictive capacity is limited to the specific crude oil and/or the process to which they were defined [1]. (b) Kinetics of model compounds, which use simple molecules to simulate reactions associated with substructures of very complex systems. These models assume similar behavior in the substructures they intend to represent [2]. (c) Kinetic models of complex systems, in which it is given explicit molecular structure of reactants and intermediates used to represent the crude oil or its components. The reactants can be represented by a distribution of individual molecules, stochastically generated by a Monte Carlo methodology, or by an average molecule [3-5]. In this work the kinetic model PYRO2 uses average molecular representations of crude oil. They were obtained based on elemental analysis, proton NMR and VPO molecular weights using a methodology described in the literature [6-9].

MODEL DEVELOPMENT

In its most simple form, it is possible to associate the pyrolysis process with homolytic C-X (X=C, S, N, H) bond scissions in the molecules R-R' of crude oil to produce two free radicals:



To start with, we build up our kinetic model with the minimum set of elemental reactions necessary to produce results comparable with experimental data from our own work or from the literature. In future work, complexity will be increased as necessary according to the results of this comparison. Therefore the PYRO2 model only considers neutral molecules and does not contain the evolution of radical fragments. Accordingly, we assumed stabilization of the free radicals in reaction (1) with hydrogen from any internal hydrogen transfer mechanism and use the generalized reaction:



where each bond breaks in R-R' according to the Arrhenius expression of kinetic rate constant (k):

$$\ln(k) = \ln(A') + E_a/RT \quad (3)$$

The pre-exponential factor A' was obtained from Gavalas et al. [10]. The activation energy E_a was calculated based on the Bell-Evans-Polanyi principle (BEP) [11,12]. This principle associates the change of energy between the reactants and the transition state (E_a) with the reaction enthalpy for a given elemental step in the kinetic mechanism. In our case the rate determining step depends on the difference in energy between the bond breaking step BS(C-X) and the bond formation step for RH and R'H, represented by a constant c. We found a practical way to evaluate the E_a parameter of (3) for reaction (2) for any C-X bond scission according to the expression:

$$E_a \sim \text{BS}(\text{C-X}) - c \quad (4)$$

where $c=49.40; 44.97; 49.40$ for $X=\text{C}, \text{S}, \text{H}$ and BS(C-X) are the C-X bond strengths.

We found a linear correlation between the experimental BS parameter and the theoretical quantum parameter known as Diatomic Energy (DE) for a series of very different compounds:

$$\text{BS}(\text{A-B}) = a + b \text{DE}(\text{A-B}) \quad (5)$$

This equation allowed us to evaluate the BS parameter for any other compound or structure of interest. Correlation (5) was obtained as follows:

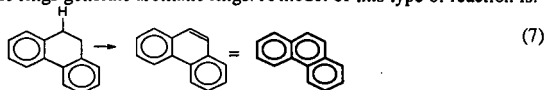
We selected simple model molecules whose BS parameters were tabulated in the CRC Handbook [13] and evaluated the Diatomic Energy (DE). The linear regression parameters a and b were then obtained. The Diatomic Energies (DE) were calculated using an energy partitioning scheme presented by Kollmar [14] for the analysis of *ab initio* and semi-empirical SCF calculations. The resulting value can be associated with the bond strength Ruette and Sanchez[15] have proposed this parameter as a tool for bond analysis. Based on semi-empirical methods, the following expression was obtained:

$$\text{DE}(\text{A-B}) = \sum_{i,j \in \text{A,B}} p_{ij} (h_{ij} + f_{ij}) \quad (6)$$

Where h_{ij} , p_{ij} and f_{ij} are the one electron matrix, bond order matrix and Fock matrix elements, as obtained from the INDO1 calculations [16]. DE(A-B) contains contributions of the resonance energy and of the electron exchange energy to the bond and does not contain electrostatic energy terms which are included by the one-center energy terms. The second purpose of using the DE parameter is to establish an increasing order for Energy Dissociation of bonds in the reactant AMS of interest. We associated each bond breaking in the molecule to an elemental step in our kinetic model, obtaining schemes like that depicted in Table 1. Afterwards, we compared the theoretical products distribution with the experimental distribution derived from the pyrolysis. This allowed us (a) to check the practical consistency of the kinetic model, and, (b) to check the molecular structure proposed as model for the fractions here considered. Table 1 shows the parameters obtained from the best linear fit of the calculated ED (in Hartrees) to the experimental dissociation energy BS for C-C, C-S and C-H bonds.

Afterwards we introduced the following conditions in the kinetic model:

a) Hydroaromatic rings generate aromatic rings. A model of this type of reaction is:



The activation energy (Kcal/Mol) was defined as:

$$E_a = \text{BS}(\text{C-H}) - 166.92 - 23.8 n \quad (8)$$

where n is the number of aromatic rings generated in the reaction; in this case, $n = 1, b$) The sequence of bond breakings in each molecular structure was organized by increasing C-X bond energies from quantum mechanical calculations. c) The aromatic C-C, C-S and C-N bonds are not broken.

3. RESULTS

We applied the PYRO2 kinetic model to the pyrolysis of the AMS depicted by Cotte [17] for Boscan asphaltene (Fig. 1) and Sanford [18] for Athabasca residue (Fig. 2). The differential equations associated to the rate laws of the elementary reactions proposed in this study were solved using a Fortran program developed by Braum and coworkers [19]. Boscan asphaltene pyrolysis can be represented by the cracking of the aliphatic side chains (some could be bridges) and naphthenic cycles. This process leaves the peri-condensed aromatic rings system as coke, represented by a black circle in the compact representation of Fig. 1. This cracking progresses according to the increasing bond energy values. Aliphatic C-C bonds γ to the aromatic rings break first, followed by β bonds, naphthenic and possibly α aliphatic bonds, in all cases following the increasing bond strength. Branches from the opening of naphthenic rings, once formed, crack according to this sequence. The conversion to volatile products measured by weight yield and the coke yield in a thermogram (Fig. 3) and the light product yields (Fig. 4) can be predicted in a reasonable way from the model in this peri-condensed representation of Boscan asphaltene AMS (Fig. 1). However, for the open kata-condensed Athabasca molecular representation (Fig. 2), this trend did not work. The kinetic model invariably went to zero coke due to the complete fragmentation of the Fig. 2 molecule to volatile products. The calculation by quantum mechanical methods of bond energies indicated that the weakest bonds were not the γ or further away aliphatic bonds of aromatic side chains, but instead the C-H bonds in the hydroaromatic substructures to the right side of Fig. 2. When this bond rupture order was allowed, the very first process that occurred was the aromatization of the right side of the molecule in Fig. 2, according to the first six steps in Table 1. This aromatized part was represented by a black circle in Table 1. From this step on, this structure remains as a coke precursor not originally present. The left side totally cracked to produce gases and liquids, as depicted in Table 1 after step 6.

From this kinetic model results, we concluded that this very early aromatization, that introduces a coke precursor nucleus in the molecule, even before liquids and gases are formed, is a very important principle that governs the natural tendency to form coke in complex hydrocarbon systems. It could also explain the increased coke yield of heavy petroleum fractions pretreated by extended periods of time at low temperatures (below 300°C), as reported by Cotte et. al. [20]. Present tendency is toward the consideration of kata-condensed structures, like that of Fig. 2, as more representative of heavy petroleum fractions [18], than those peri-condensed as in Fig. 1. This principle indicates a likely path to coke formation in these open systems, and the expansion of the reaction network in pyrolysis to include it, together with other non-conventional reactions like the retrograde reactions proposed by Mc. Millen and Malhotra [21]. The reasonable agreement between the tendencies in products formation and the conversion and coke yields proposed by Sanford for the AMS of Fig. 1 (Fig. 6), indicates the usefulness of the PYRO2 kinetic model and its predictive capability for gross results, in spite of the very simple assumptions it contains. The disagreement with gas and liquid yields, we believe, indicates mainly the failure of the AMS to contain certain reactivity information. This was particularly evident in the CO yield for Boscan asphaltene. Experimentally, this is one of the first gas product to be formed at about 400 °C, before the bulk of gases peak [17], but the model indicated its formation at about 600 °C, after the bulk gases formation in Fig. 6 (does not appear due to the Y-scale). This disagreement indicates that although the AMS is consistent with the analytical data from which it was built up, its reactivity is not consistent, and the position of the CO group should be modified accordingly. Improvements in reaction networks and in the AMS's can be made with the use of this model. This should give a deeper knowledge of the chemistry of heavy petroleum fractions, which was the main objective of the development of the PYRO2 model.

4. SUMMARY AND CONCLUSIONS

A kinetic model was developed to study the thermal reactivity of average molecular structures representative of heavy petroleum fractions. This model is based on the application of the Arrhenius equation to the rupture of C-X bonds, arranged by increasing activation energies estimated through quantum mechanical principles and correlations. Reasonable gross agreement was obtained with experimental data and with chemical intuition as applied to the pyrolysis of a crude residue and an asphaltene. This application indicated that:

-The reproduction of the experimental thermogram of the boscan asphaltenes, indicated that the theoretical considerations to obtain the activation energies associated with each step of kinetic model are in reasonable agreement with experimental data.

-The PYRO2 model did not reproduce the distribution of volatile products relieved from the thermogravimetric pyrolytic experiments of the fraction considered. This mismatch of some kinetic model results with experimental data indicated that further improvements or corrections are necessary in the average molecular structures representative of heavy petroleum fractions.

-Early aromatization of certain hydroaromatic moieties, during the thermal treatment of very complex kata-condensed hydrocarbon systems, appears to be an important factor in the natural tendency of heavy crude oil fractions to produce coke. This aromatization should be included as an important further reaction in the networks representative of hydrocarbon systems under pyrolysis conditions.

REFERENCES

- [1] Trauth D., Yasar M., Neurock M., Nigam A., Klein M., Kukes S.; *Fuel Sc. and Tech. Intl.*, **10**, 1161-1179 (1992).
- [2] Savage P. E.; *Am. Chem. Soc. (ACS), Div. Fuel Chem.*, **42**, 13-17, 1997.
- [3] Savage P. E., Klein M. T.; *Chem. Eng. Sc.*, **44**, 393-404 (1989).
- [4] Neurock M., Libanati C., Klein M., *AIChE Symposium Series*, No. 273, **85**, 7 (1989).
- [5] Scott M. S., Neurock M. and Klein M. T., *Chem. Eng. Sc.*, **48**, 4081-4096 (1993).
- [6] Dickinson E. N.; *Fuel*, **59**, 290-294, 1980.
- [7] Speight J. G.; Moschopedis S. E. Bunger J. W. and Li N. C. Ed.; *Adv. Chem Ser.* **195**, 1-15, Washington D.C., 1981.
- [8] Yen T. F.; Wu W. H.; Chilingarian G. V.; *Energy Sources*, **7**(3), 275-305, 1984.
- [9] Leon V.; *Fuel* **66**, 1445-1446, 1987.
- [10] Gavalas, G., Cheong, P., Jain, R., *Ind. Eng. Chem., Fundam.*, **20**, 113-122, 1981.
- [11] Dewar M., Dougherty R.; "The PMO Theory of Organic Chemistry", Edit. Plenum Press, New York, (1975), 65-69, 212-220.
- [12] Neurock M., Klein M. T.; *Chemtech*, 26-32, September (1993).
- [13] *CRC Handbook of Chemistry and Physics*, 76th Edition (1995-1996) pag. 9-64.
- [14] Kollmar H.; *Theoret. Chim. Acta (Berl.)*, **50**, 253 (1992).
- [15] Sánchez M., Ruete F.; *J. Mol. Struct. (Theochem)*, **254**, 335 (1992).
- [16] ZINDO Code Molecular Simulations, Inc.
- [17] (a) Cotte E.; MSc Thesis; Venez. Inst. of Sc. Res. (IVIC). 1977. (b) Cotte E., Calderón J. L.; *Rev. Tec. Intevep*, **1**(2):109-117, 1981.
- [18] Sanford E.; *Ind. Eng. Chem. Res.*, **33**, 109 (1994).
- [19] Braum W., Herron J., Kahaner K.; *Int. J. Chem. Kinetics*, **29**, 51 (1988).
- [20] Cotte E., Ovalles C., Scaglioni G., Castro W.; *Thermal Reactivity of Venezuelan Heavy Crude Fractions*, 5th Chem. Cong. of Nth. Am. Cancun, Mexico, 11-15 Nov., 1997.
- [21] McMillen, D. F.; Malhotra, R.; *Am. Chem. Soc. (ACS), Div. Fuel Chem.*, v.42, No.1, April 13-17, 1997.

Table 1. Pyrolysis scheme derived from the PYRO2 kinetic model for a cracked Athabasca residue Average Molecular Structure.

| Step | Molecule | Ea Kcal/ Mol | Step | Molecule | Ea Kcal/ Mol | Step | Molecule | Ea Kcal/ Mol |
|------|----------|--------------------|------|----------|--------------------|------|----------|--------------------|
| 0 | | - | 12 | + C2 | 19 | 24 | + 2 Cl | 22 |
| 1 | | 30 | 13 | + C2 | 19 | 25 | | 22 |
| 2 | | 38 | 14 | | 19 | 26 | + 2 Cl | 23 |
| 3 | | 33 | 15 | | 19 | 27 | + | 23 |
| 4 | | 30 | 16 | | 20 | 28 | + + | 24 |
| 5 | | 30 | 17 | | 22 | 29 | + | 24 |
| 6 | | 29 | 18 | | 22 | 30 | + 2 | 24 |
| 7 | | 19 | 19 | + Cl | 22 | 31 | + 2 | 26 |
| 8 | | 19 | 20 | + C2 | 22 | 32 | + Cl + | 27 |
| 9 | + Cl | 19 | 21 | | 22 | 33 | | - |
| 10 | | 19 | 22 | + C2 | 22 | | | |
| 11 | | 19 | 23 | | 22 | | | |

Table 2. Fitting parameters, correlation factor r^2 , and standard deviation s for the correlations: $BS(A-B) = a + b DE(A-B)$

| Bond (A-B) | a (Kcal) | b (Kcal/Hartree) | r^2 | s (Kcal) |
|------------|-------------|---------------------|-------|-------------|
| C-C | -95.371 | 1339.273 | 0.95 | 16.8 |
| C-S | -31.952 | 998.201 | 0.94 | 5.7 |
| C-H | -414.488 | 4837.562 | 0.94 | 5.7 |

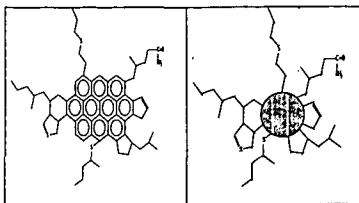


Fig.1. The Boscan Asphaltene Average Molecular Structure (from Ref. 17) and its Compact Representation

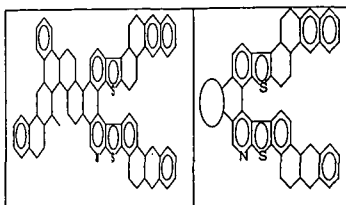


Fig.2. The Average Molecular Structure of an Athabasca Cracked Residue (from Ref.18) and its Compact Representation.

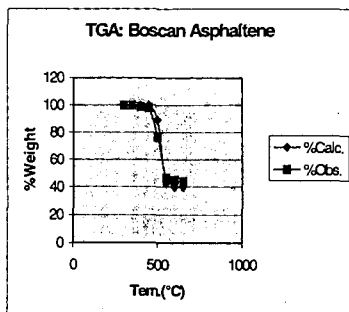


Fig.3. Calculated (from PYRO2 model) and Observed (form Ref. 17) TGA of Boscan Asphaltene.

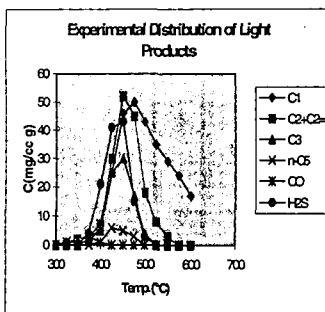


Fig.4. Experimental Distribution of Light Products from the pyrolysis of Boscan Asphaltenes. Data from Ref. 17

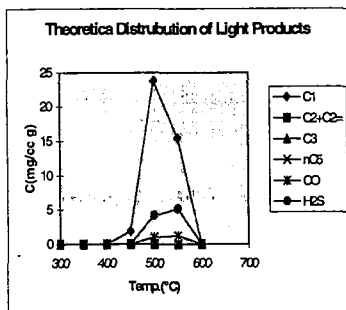


Fig.5. Theoretical Distribution of Light Products from the pyrolysis of Boscan Asphaltenes obtained from PYRO2 Model.

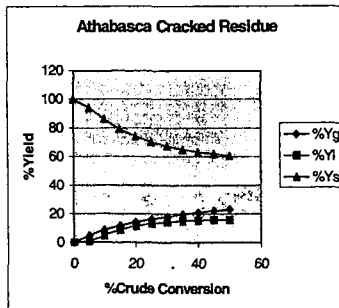


Fig.6. Gas (Yg), liquid (Yl) and residue plus solids (Ys) yields calculated from the PYRO2 kinetic model for the Athabasca Residue.

THE TWO PHASE, TWO PLUG REACTOR THE SEPARATE PHASE RESIDENCE TIMES EFFECT

Colin McGreavy
The University of Leeds, Chem. Eng. Dept.
Leeds LS2 9JT, UK

Marcos Sugaya
Petrobras S.A., Cenpes
Rio de Janeiro 21910-900, Brazil

KEYWORDS: Delayed coking, visbreaking, pyrolysis

ABSTRACT

The two phase, two plug flow reactor (2TP-R) is a distinctive example which highlights the problems in modeling complex multiphase flows where the different phases can have well-defined and independent residence times which need to be taken into account. As a case study, the pyrolysis of distillation residues in a 2TP-R scheme is examined to illustrate some of the issues in characterizing such systems which include practical applications such as visbreaking and delayed coking furnaces and other residue upgrading processes. Kinetic parameters for the lumped pseudocomponents system have been derived from isothermal pilot plant runs. Operating parameters and geometric considerations have been examined aiming at maximization of the light derivatives in the pyrolysis of residues. It is important to balance the conversion between the furnace and the soaking drums downstream to optimize the yield of products and the overall operation.

INTRODUCTION

Delayed coking furnaces are designed to postpone chemical transformations in the feed to the soaking drums downstream so as to avoid deposition of coke in the furnace tubes which would limit the campaign time. High velocities, moderate heat fluxes and large surface/diameter ratios are necessary to accomplish this.

Generally, a box geometry with two radiant sections connected to a single convection section is used. The tubes are horizontal and, in the radiant section, they are often located adjacent to the walls but separated on a large pitch in order to improve the distribution of heat. More recently the distribution of heat has been enhanced by placing the tubes in a double fired zone at the center of the radiant boxes with the feed flowing downwards in a direction opposite to the flow of combustion gases. This has the advantage of reducing the maximum wall temperatures.

Not all of the tube length is used for heat exchange. Dead end sections are usually connected by 'mule-ear' heads to one side of the furnace with 'U' sections at the opposite side. These configurations give rise to significant pressure drops while adding to the soaking volume. A variety of tube lengths, diameters and pitches is also used.

Kinetic constants for chain initiation reactions in the liquid and vapor phases are related by the equation

$$K_{liq} = k_{vap} \cdot \exp\left(\frac{\Delta S^\circ}{R} - \frac{\Delta H^\circ}{RT}\right) \quad \text{Equation 1}$$

where ΔS° and ΔH° are the differences in the entropy and enthalpy of the activated complex and reactants in the liquid and vapor phases (1). Since ΔH° is negative, reactions in the vapor phase can be neglected at the low temperatures used in delayed coking, visbreaking and similar processes.

The generation of vapor in the process influences the residence time of the liquid phase because it effectively reduces the volume. Steam can be used to reduce the partial pressure of the hydrocarbons in the vapor phase and hence increase the vaporization which enables the residence times to be controlled. This arrangement results in increased flexibility for a particular geometry. When estimating residence times, it is therefore important to consider a distinction between the liquid holdup in the coil and the vapor/liquid ratio which is determined by phase equilibrium.

APPROACH

The model uses lumped kinetic parameters derived from pilot plant experiments. The liquid phase holdup can be estimated using the method due to Hughmark (2). As the hydrocarbon vaporizes, the flow regime along the tubes changes. Baker's map (3) can be used to follow the changes. Phase equilibrium is based on the Redlich-Kwong equation as modified by Soave (4). The physical properties have been estimated using the method due to Dean-Stiel (vapor viscosity), Twu (liquid viscosity), Mallan *et al.* (liquid conductivity), Stiel-Thodos (vapor conductivity) and Gunn-Yamada-Rackett (liquid density). The temperature dependence of liquid viscosities is obtained from the ASTM procedure modified by Wright (5), using appropriate mixing rules. Single phase pressure drop is calculated using the equation due to Chen (6). For two phase flow, the method of Dukler (7) and a proprietary correlation (8) have been used.

A mass balance is given by

$$\frac{dc_{i,T}}{dx} = -\frac{h_L A_T \rho_L}{W_T} k_i c_{i,L} \quad \text{Equation 2}$$

where c_i stands for the concentration of species i , h the holdup, A the cross-sectional area, W the mass flow rate, ρ the density, k the kinetic constant and the subscripts L and T denote the liquid phase and the total stream respectively.

Enthalpies are calculated based on the Lee-Kesler equations and the heat of reaction is taken as 800 J/kg for products boiling below 204 °C (ASTM D-86). Wall temperatures are estimated from the heat flux and adopting the definition of heat transfer coefficients and the methodology described in API RP-530 (1988).

The 2TP model used here has been extended to take account of the transfer line between the furnace and the coking drums with pipe fittings accounted for by using appropriate equivalent lengths.

Change in the static head is based based on the following equation

$$\left(\frac{dP}{dx}\right)_d = (h_L \rho_L + h_V \rho_V) \sin \theta \quad \text{Equation 3}$$

where P is the pressure and θ is the inclination to the vertical. The flow regime is taken from the zones defined by Griffith and Wallis (9).

RESULTS AND DISCUSSION

The furnaces at Petrobras Gabriel Passos Unit 52 have two radiation chambers connected to a single convection section with the feed being split into four passes per furnace. Tubes in the radiation boxes are in two horizontal lines near the walls fired from the center and each furnace feeds a pair of coke drums. Geometric data are presented in Table 1, operating conditions in Table 2. Table 3 contains a geometric description of the transfer line.

Table 4 compares the simulation results with process data. Furnace B generates more coke than A, as indicated by the measured pressure drop, which is 30 % higher. The campaign time is not reported, although furnace A has recently been decoked. The calculated pressure drop in B needs to be increased by 23% to reproduce this effect. Correspondingly, A needs to be reduced by 31% to match the plant pressure drop. This means that the pressure drop correlation is conservative as far as design is concerned.

The heat duty and fuel gas consumption matches the plant data very well (Table 4). In Figures 1-2 the temperature of the tubes predicted by the model compare well with the plant and the agreement between the model output and the process data is generally good.

In Figure 3, the composition profile in furnace A is represented by the fraction of products boiling below 350 °C. As can be seen, reaction is significant only in the final third of the tubes, where the temperature is above 400 °C. No significant reaction occurs in the convection zone. Higher coke drum temperatures favor condensation reactions at the expense of cracking, because of the different activation energies. However this also increases the vaporization in the drums causing in a net decrease in coke production.

The choice of appropriate operating conditions is crucial in seeking to increase the production of liquids and needs to be anticipated at the design stage because more options are available at this time. In particular, a low operating pressure is very desirable since it decreases the production of coke.

Table 5 shows that an important fraction of the conversion and pressure drop arise in the transfer line between the furnace and the coking drums. In fact, most of the conversion and pressure drop takes place at the last third of the coil in the furnace. Clearly, efforts to reduce the

system pressure should be directed to these sections in particular by minimizing the length of the transfer lines and the number of pipe fittings, which depend on plant layout.

CONCLUSIONS

Good delayed coking furnace performance is generally seen as meeting the specified outlet temperatures for the lowest possible conversion since this would mean that the campaign time is maximized. However, the energy required for the endothermic chemical reactions and vaporization of products in the coke drums is supplied by the furnace. If the conversion upstream the drums is low, the temperature needs to be increased to ensure that a similar yield of liquids is obtained. In practice this increases the tendency of coking in the furnace tubes, since higher wall temperatures have to be expected. It can also result in shot coke formation (10).

The goal should not be to minimize conversion in the furnace but to reduce the pressure drop. This vaporizes products at the lowest possible temperature, transferring energy to the drums as latent rather than sensible heat. Tube coking is minimized by using high velocities while not reducing residence times, e.g., by using small diameters and longer coil lengths.

The scope for gaining maximum benefit using this approach is obviously increased if the process models can be further developed. This requires a good representation of the angular distribution of heat in the tubes.

REFERENCES

1. Bozzano G. Tesi di Dottorato in Ingegneria Chimica 1994, Politecnico di Milano.
2. Hughmark G. A. Chemical Engineering Progress 1962, 62.
3. Baker O. Oil & Gas Journal 1954, July 26, 185.
4. Soave G., Chemical Engineering Science 1972, 27, 1197.
5. Wright W. A. Journal of Materials 1969, 4, 1, 19.
6. Chen N. H. Ind. Eng. Chem. Fund. 1979, 18, 296.
7. Dukler A. E.; Wicks M.; Cleveland R. G. AIChE Journal 1964, 44.
8. Sugaya M. F.; Maciel R. Petrobras Internal Report 1994.
9. Griffith P.; Wallis G. B. Journal of Heat Transfer 1961, Aug., 307.
10. Ellis P. J.; Bacha J. D. Light Metals 1996, 477.
11. Dean D. E.; Stiel L. I. AIChE Journal 1965, 526.
12. Gunn R. D.; Yamada T. AIChE Journal 1971, 17, 1341.
13. Mallan G. M.; Michaelian M. S.; Lockhart F. J. J. Chem. Eng. Data 1972, 17, 412.
14. Stiel L. I., Thodos G., AIChE Journal 1964, Jan., 26.

Table 1 Geometric data for tubes in furnaces 52-F-1 A/B. Dead ends are 2 x 225 mm.

| Section | Part | L_{eff} (m) | d_i (mm) | d_o (in) | Avg. pitch (mm) | Tubes (per pass) |
|------------|------|------------------|---------------|---------------|--------------------|---------------------|
| Convection | 1-4 | 10.364 | 74 | 89 | 189 | 38 |
| Radiation | 1 | 10.364 | 65 | 83 | 199 | 34 |

Table 2 Operating data for furnaces 52-F-1 (including a 10 % heavy gasoil recycle).

| Furnace | Pass | Combined feed (m ³ /d) | Water (m ³ /d) |
|---------|------|--------------------------------------|------------------------------|
| A | 1 | 320 | 3.5 |
| | 2 | 316 | 3.5 |
| | 3 | 318 | 3.4 |
| | 4 | 313 | 3.4 |
| B | 1 | 315 | 3.5 |
| | 2 | 316 | 3.5 |
| | 3 | 315 | 3.5 |
| | 4 | 316 | 3.5 |
| total | | 2530 | 27.8 |

Table 3 Transfer line geometry up to the switch valve.

| Part | Type | d _{in} (in) | d _{out} (in) | Length (m) | Inclination (degrees) | Passes |
|------|-----------|-------------------------|--------------------------|---------------|--------------------------|--------|
| 1 | nozzle | 3 | 3 | - | - | 4 |
| 2 | expansion | 3 | 4 | - | - | 4 |
| 3 | line | 4 | 4 | 2.2 | 0 | 4 |
| 4 | cross | 4 | 4 | - | - | 4 |
| 5 | line | 4 | 4 | 1.2 | 0 | 4 |
| 6 | expansion | 4 | 6 | - | - | 4 |
| 7 | cross | 6 | 6 | - | - | 2 |
| 8 | line | 6 | 6 | 1.0 | 90 | 2 |
| 9 | cross | 6 | 6 | - | - | 2 |
| 10 | line | 6 | 6 | 2.0 | 0 | 2 |
| 11 | expansion | 6 | 8 | - | - | 2 |
| 12 | cross | 8 | 8 | - | - | 1 |
| 13 | line | 8 | 8 | 11.7 | 0 | 1 |
| 14 | cross | 8 | 8 | - | - | 1 |
| 15 | line | 8 | 8 | 7.7 | 90 | 1 |
| 16 | cross | 8 | 8 | - | - | 1 |
| 17 | line | 8 | 8 | 2.3 | 0 | 1 |

Table 4 Results of the model in comparison with industrial data. Pressures in bars, temperatures in C, duties in 10⁶ kcal/h and fuel gas consumption in Nm³/d.

| | 52-F-1 A | Model | 52-F-1 B | Model |
|------------------------------|----------|-------|----------|-------|
| T _{in, convection} | 238 | 238 | 238 | 238 |
| T _{out, convection} | 396 | 396 | 372 | 372 |
| Duty _{convection} | n.a. | 6.2 | n.a. | 5.2 |
| T _{out, radiation} | 502 | 502 | 502 | 503 |
| Duty _{radiation} | n.a. | 5.7 | n.a. | 6.5 |
| Duty _{furnace} | 11.1 | 11.9 | 11.5 | 11.7 |
| Fuel gas | 1380 | 1470 | 1420 | 1450 |
| T _{switch valve} | n.a. | 490 | n.a. | 490 |
| P _{in, furnace} | 16.2 | 16.2 | 19.9 | 19.9 |
| P _{in, convection} | 14.7 | 14.7 | 18.4 | 18.4 |
| P _{out, convection} | n.a. | 13.6 | n.a. | 16.8 |
| ΔP _{convection} | n.a. | 1.1 | n.a. | 1.6 |
| P _{in, radiation} | n.a. | 13.6 | n.a. | 16.8 |
| P _{out, radiation} | n.a. | 8.5 | n.a. | 10.1 |
| ΔP _{radiation} | n.a. | 5.1 | n.a. | 6.7 |
| ΔP _{furnace} | n.a. | 7.7 | n.a. | 9.8 |
| P _{switch valve} | 4.0 | 4.1 | 4.3 | 4.2 |
| ΔP _{transfer line} | n.a. | 4.4 | n.a. | 5.9 |
| ΔP _{furnace+tr.in} | 12.2 | 12.1 | 15.6 | 15.7 |

Table 5 Distribution of conversion and pressure drop in the system.

| | 52-F-1 A | 52-F-1 B |
|-----------------------------|----------|----------|
| conversion in furnace | 83 % | 81 % |
| conversion in transfer line | 17 % | 19 % |
| ΔP _{furnace} | 64 % | 62 % |
| ΔP _{transfer line} | 36 % | 38 % |

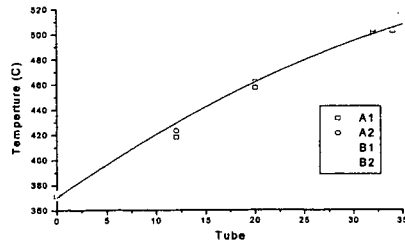


Figure 1 Fluid temperatures in the radiation zones A/B of F-1 A.

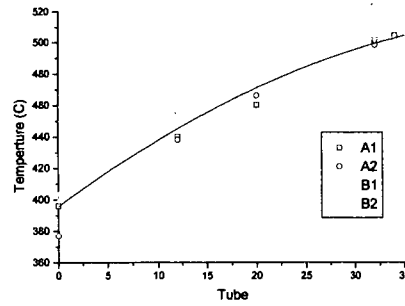


Figure 2 Fluid temperatures in the radiation zones A/B of F-1 B.

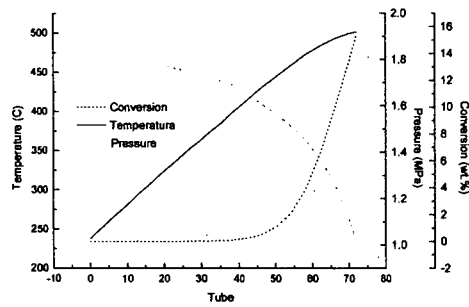


Figure 3 Conversion in F-1 A. The radiation section starts after tube 34.

HETEROGENEOUS MODELING OF AN ADIABATIC PACKED BED REACTOR WITH CATALYST DECAY. INTRAPARTICLE DIFFUSION EFFECTS

M. Chocrón^{1,2}, N. E. Amadeo², and M. A. Laborde²

1. Unidad de Actividad Química, Centro Atómico Constituyentes, Comisión Nacional de Energía Atómica. Av. del Libertador 8250 (1429), Buenos Aires, Argentina.

2. Depto. de Ingeniería Química, Facultad de Ingeniería, Universidad de Buenos Aires Pabellón de Industrias, (1428) Ciudad Universitaria, Buenos Aires, Argentina. e-mail: miguel@di.fcen.uba.edu.ar (Address to which correspondence should be submitted).

KEYWORDS : Fixed bed reactor, heterogeneous modeling, catalyst deactivation.

INTRODUCTION

Reactor models for catalytic reactions overlaid with transport restrictions and with catalyst deactivation are still not completely developed. The interrelation between internal diffusion and deactivation in a catalytic pellet was previously examined [1,2].

In the present work, an algorithm for simulation of an adiabatic fixed bed reactor subjected to catalyst deactivation by poisoning is developed applying the heterogeneous model. An irreversible first order reaction is considered for modeling purposes. The integral packed bed reactor is nodalized by N state equations corresponding to the N differential continuous stirred tank reactors into which the whole reactor is divided. For each differential reactor the energy and mass balances are solved and the concentration value at the center of the catalyst pellet is found using the shooting technique.

MATHEMATICAL MODEL

For an adiabatic fixed bed reactor and considering the one dimensional heterogeneous model nodalized as a series of differential CSTR's, the dimensionless mass balances for the main reactant and poison at the jth reactor are:

$$(C_{ij} - C_{oj}) = N_j \text{av} \frac{V_i}{Q} \quad (1)$$

$$(C_{p_{ij}} - C_{p_{oj}}) = N_{p_j} \text{av} \frac{V_i}{Q} \quad (2)$$

and the dimensionless energy balance is:

$$T_{oj} = T_{ij} + \beta (C_{ij} - C_{oj}) \quad (3)$$

In equation (3) it was assumed that the only contribution to the temperature rise is given by the main reaction, since the poison is highly diluted in the feed.

On the other hand, for an isothermal, cylindrical catalyst pellet with constant properties and ignoring the external diffusional effects, the mass conservation equations for the reactant and poison are:

$$\frac{1}{r} \frac{d}{dr} \left(r \frac{d\xi}{dr} \right) = \phi_p^2 a_p(r, t) \exp \left[\gamma_1 \frac{(T-1)}{T} \right] \xi \quad (4)$$

$$\frac{1}{r} \frac{d}{dr} \left(r \frac{d\xi_p}{dr} \right) = \phi_{p^2}^2 a_p(r, t) \exp \left[\gamma_{p2} \frac{(T-1)}{T} \right] \xi_p \quad (5)$$

An irreversible first order reaction is assumed for the main reaction, like :

$$r_m = k_0 \exp \left[-\frac{\gamma_1}{T} \right] \xi a_p(r, t) = k \xi(r, t) a_p(r, t) \quad (6)$$

while a kinetic expression such as:

$$r_p = k_{20} \exp \left[-\frac{\gamma p_2}{T} \right] \xi_p a_p(r, t) = k_2 \xi_p(r, t) a_p(r, t) \quad (7)$$

is considered for the poison.

The boundary conditions for equations (4) and (5) are:

$$\text{at } r=0, \quad d\xi / dr = 0 \quad \text{and} \quad d\xi_p / dr = 0 \quad (8)$$

at $r=1$:

$$(C_{ij} - C_{oj}) = \frac{Deff \, av \, V_i}{R_p Q} \left(\frac{\partial \xi}{\partial r} \right) \quad (9)$$

$$(C_{pj} - C_{poj}) = \frac{Dpeff \, av \, V_i}{R_p Q} \left(\frac{\partial \xi_p}{\partial r} \right) \quad (10)$$

where:

$$N_j = \frac{Deff}{R_p} \left(\frac{\partial \xi}{\partial r} \right) \quad (11)$$

$$N_{pj} = \frac{Dpeff}{R_p} \left(\frac{\partial \xi_p}{\partial r} \right) \quad (12)$$

The deactivation rate into the pellet is given by:

$$\frac{da_p(r, t)}{dt} = -k_{10} \exp \left[-\frac{\gamma p_1}{T} \right] \xi_p a_p(r, t) = -k_1 \xi_p a_p(r, t) \quad (13)$$

The system of equations (1)-(13) is solved assuming a quasi-steady state for the reactant and poison profiles into the pellet because the deactivation rate is relatively slow.

Beginning from $t=0$ and $j=1$ (the first CSTR), the reactant and poison profiles into the pellet are found using the shooting technique. The pellet is deactivated a given period of time and the procedure is repeated until the final operating time of the reactor is achieved. The same method is applied to the other differential reactors.

RESULTS

The plots shown in Figures 1 to 6 were obtained for the following reactor inlet conditions: $T^0 = 503 \text{ K}$, $C^0 = 8.5 \text{ mol/m}^3$, $C_p^0 = 8.3 \cdot 10^{-9} \text{ mol/m}^3$. Feed rate, reactor volume and specific area of the bed are $Q = 1.13 \text{ m}^3/\text{sec}$, $V = 14 \text{ m}^3$ and $av = 950 \text{ m}^2/\text{m}^3$ respectively. The reaction enthalpy is $\Delta H = -41190 \text{ J/mol}$. The specific heat and density of the feed mixture are, $C_{pg} = 2576 \text{ J/Kg}^\circ\text{C}$ and $\rho_g = 8.46 \text{ Kg/m}^3$.

The parameters of the pellet are: $R_p = 0.0022 \text{ m}$; $Deff = 4.3 \cdot 10^{-7} \text{ m}^2/\text{sec}$; $Dpeff = 6 \cdot 10^{-6} \text{ m}^2/\text{sec}$.

In figures 1 to 3 the evolution of the profiles of reactant, poison and activity into the pellet is presented for poison and reactant Thiele modulus values such that strong diffusional effects exist. It can be seen that, at $t = 0$, the reactant and poison profiles are pronounced and became flatter along the time. Consequently, at short operating time the activity is almost nulle in the pellet surface and remain high toward the center.

The evolution of the poison and activity profiles along the fixed bed reactor is shown in figures 4 and 5. It is observed that, in agreement with the highly diffusional effects achieved into the pellet, the reactor is deactivated as a plug flow. This effect is frequently observed in industrial reactors; for instance in the case of CO converters [4].

Finally, reactant profiles along the reactor for two different poison Thiele modulus are presented in figure 6. It can be appreciated that as higher the poison Thiele modulus, higher is the fixed bed life.

CONCLUSIONS

The simulation of a fixed bed undergoing catalyst deactivation by poisoning was presented by means of the heterogeneous one-dimensional model. The parameter values of the model and the operating conditions were chosen such that relatively high diffusional effects appeared into the pellet for the poison as well as for the main reactant.

Activity and concentration profiles into the pellet and along the reactor and their evolution with the operating time are presented. The effect of the reaction rate of the poison is examined. It is proved that the performance of the reactor and the life of the catalyst improve when diffusional resistance for the poison increases.

ACKNOWLEDGMENTS

Support of this work provided by the Consejo Nacional de Investigaciones Científicas y Técnicas (CONICET), Universidad de Buenos Aires and the Comisión Nacional de Energía Atómica (C.N.E.A.) is gratefully acknowledged.

NOTATION

| | |
|---|--|
| a_p : activity by poison. | z : dimensionless axial position |
| a_v : specific area of the catalytic bed | <i>Greek Symbols</i> |
| C : dimensionless reactant concentration (bed) | $\phi_p^2 : R^2 r_p^S / D_{peff} \xi_p^S$ |
| C_p : dimensionless poison concentration (bed) | $\phi^2 : R^2 r_m^S / D_{eff} \xi^S$ |
| C_{pg} : specific heat of the mixture | γ_{p1} : dimensionless activation energy, eq.(13) |
| D_{eff} : effective diffusion of the reactant. | γ_1 : dimensionless activation energy, eq. (6) |
| D_{peff} : effective diffusion of the poison | γ_{p2} : dimensionless activation energy, eq. (7) |
| k : kinetic coeff. of the main reaction | ξ : dimensionless reactant concentration into the pellet |
| k_1 : kinetic coeff. of the deactivation rate | ξ_p : dimensionless poison concentration into the pellet |
| k_2 : kinetic coeff. of the poison reaction | ΔH : enthalpy of reaction |
| N : reactive flux toward the pellet | ρ_g : feed density |
| N_p : poison flux toward the pellet | $\beta : (-\Delta H) C^0 / \rho_g C_{pg} T^0$ |
| Q : volumetric flow rate | |
| r_m : main reaction velocity | <i>Superscripts</i> |
| r : dimensionless radial position into the pellet | S : pellet surface value |
| r_p : poison reaction velocity | 0 : conditions at the bed entrance |
| R_p : Pellet radius | <i>Subscripts</i> |
| T : dimensionless temperature | i : differential reactor inlet value |
| t : time | j : differential reactor number |
| V : reactor volume | o : differential reactor outlet value |

REFERENCES

- [1] M. Chocrón, Ma. del C. Raffo Calderón, N. Amadeo, M. Laborde. "Effect of intraparticle diffusion on catalyst decay". Chem. Eng. Sci., **51**, (1996), pp. 683.
- [2] M. Chocrón, N. Amadeo, M. Laborde. "Catalyst decay by simultaneous sintering and poisoning. Effect of intraparticle and interfacial gradients". Catalyst Deactivation 1997. Studies in Surface Science and Catalysis, Vol. 111, pp. 311. Elsevier.
- [3] Froment G., Bishoff K., "Chemical Reactor Analysis and Design", J. Wiley & Sons, 1979.
- [4] González Velasco J., Gutiérrez Ortiz M., González Marcos J., Amadeo N., Laborde M.A., Paz M., "Optimal inlet temperature trajectories for adiabatic packed beds reactors with catalyst decay". Chem. Eng. Sci., **47**, (1992), pp. 1945.

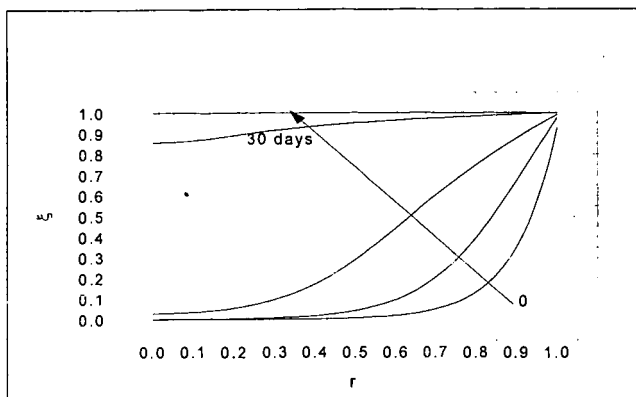


Figure 1 : Main reactant profile into the catalyst. First CSTR, $\phi = 10$, $\phi_p = 6$, $k_1 = 0.2 \text{ l/h}$

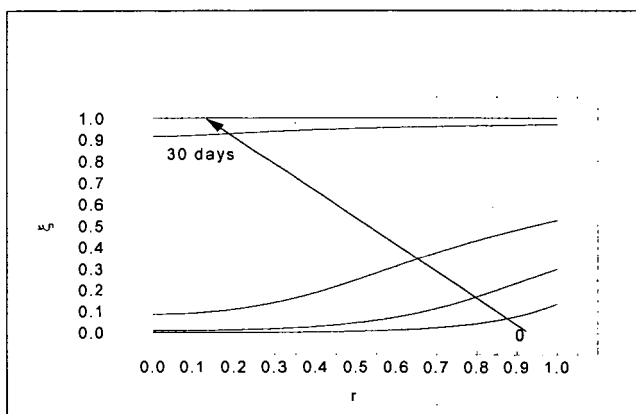


Figure 2: Poison profile into the catalyst. First CSTR, $\phi = 10$, $\phi_p = 6$, $k_1 = 0.2 \text{ l/h}$

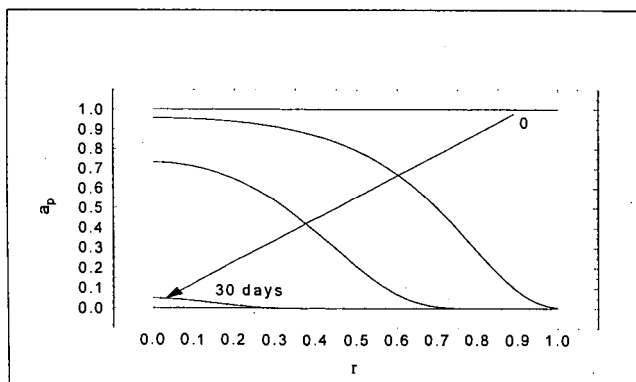


Figure 3 : Activity by poison into the catalyst. First CSRT, $\phi = 10$, $\phi_p = 6$, $k_1 = 0.2 \text{ l/h}$

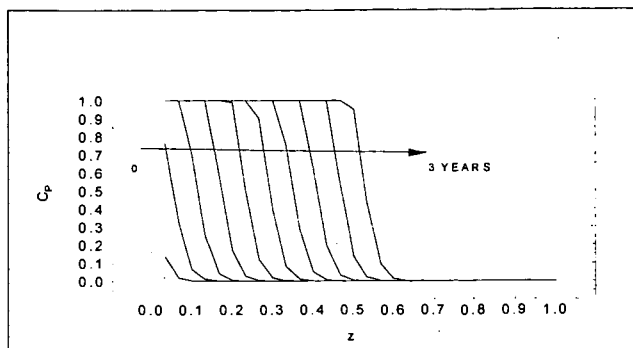


Figure 4: Dimensionless poison concentration vs. axial position. $\phi_p = 6$, $k_I = 0.2 \text{ l/h}$

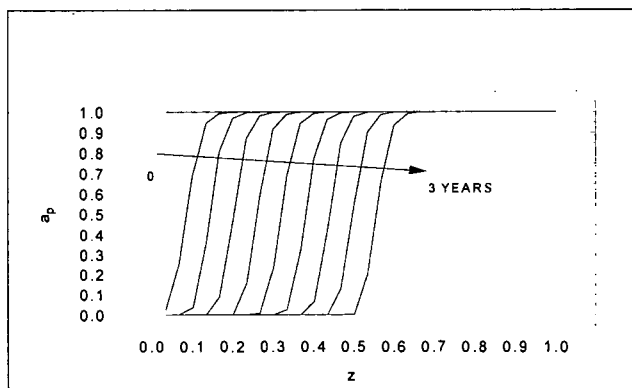


Figure 5: Activity by poison vs. axial position. $\phi_p = 6$, $k_I = 0.2 \text{ l/h}$

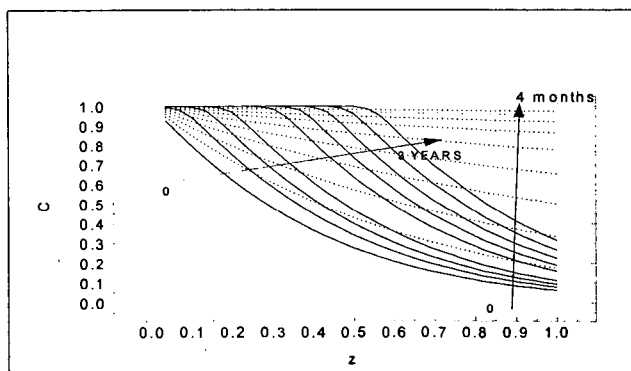


Figure 6: Main reactant profile vs. axial position. Solid line: $\phi = 10$, $\phi_p = 6$; Dots line: $\phi = 10$, $\phi_p = 3 \times 10^{-2}$.

THE EFFECT OF CATALYST, HYDROGEN PRESSURE, AND SOLVENT IN COAL LIQUEFACTION UNDER SIMULATED PREHEATER CONDITIONS

J. P. Ferrance, R. P. Warzinski, and B. Bockrath
Federal Energy Technology Center
P. O. Box 10940
Pittsburgh, PA 15236

Keywords: Coal liquefaction preheater simulation, NMP extraction, Thermogravimetric analysis

INTRODUCTION

The purpose of a preheater in a coal liquefaction plant is to raise the temperature of a coal slurry to the reaction temperature before entering the reactor chain. In practice, the preheater actually serves as the first reactor because significant chemical and physical changes take place in the coal slurry as it heats to the reaction temperature. Investigations of these changes were carried out at the Fort Lewis and HRI pilot plants.¹⁻³ In addition to the actual preheaters, microautoclave experiments were used to simulate the HRI preheater as well as the preheater at the Wilsonville pilot plant.^{2,4} These studies have shown that much of the conversion of the coal into initial products is complete by the time the slurry exits the preheater.

All of the preheater studies described above were carried out in the absence of dispersed catalysts; the coal did not contact the catalyst until it entered the first packed-bed reactor. In this arrangement, the slurry was at reaction temperature when it contacted a preactivated catalyst. With dispersed catalysts, the catalyst precursor is added to the initial slurry and travels through the preheater with the coal. For the precursor used in this investigation, no work has been performed which shows whether the short time in the preheater is sufficient to form an active catalyst. If the catalyst did activate, would it have any effect on the coal breakdown reactions taking place in the preheater? The purpose of this study was to look at these issues. Microautoclave experiments were employed in which the loadings of coal, solvent, hydrogen, and catalyst were similar to those used in large-scale coal liquefaction preheaters and in which the heat-up was performed in a manner that reasonably approximated the time/temperature histories of the large units. In addition to routine microautoclave liquefaction product characterization procedures, extraction with N-methyl-pyrrolidone and thermogravimetric analysis were used to gain more insight into the reactions occurring as coal dissolves and begins to liquefy.

EXPERIMENTAL

The reactor used in these experiments was a previously described microautoclave system modified to allow controlled submersion of the reactor into the heated sand bath.⁵ This was accomplished by restricting the airflow to the pneumatic lift on the sand bath. A fairly reproducible internal time/temperature profile was obtained that resembled the available data from the Fort Lewis and Wilsonville pilot plant preheaters. A comparison of these data is shown in Figure 1. The solids concentration of 36.6% and slurry fraction loading of 0.4 used in these experiments were also representative of values used in these preheaters. For the microautoclaves used in these experiments, 7.0 g of coal and 11.0 g of solvent were used. In experiments without solvent, only 7.0 g of coal was placed in the reactor.

The coal used in this study was DECS-17 (Blind Canyon) coal, a bituminous coal from the Penn State Sample bank. The solvent used was a coal-derived vacuum gas oil (VGO) produced by Exxon in its bench-scale coal liquefaction reactor; this material had a boiling range of 274 - 510°C and was 100% soluble in cyclohexane.⁶ The catalyst used in this study was a dispersed MoS₂ formed by the decomposition of Mo(CO)₆ in the presence of H₂S.⁵ The precursor was added at a concentration of 1000 ppm Mo relative to the daf coal in the catalytic experiments. A H₂/3%H₂S gas mixture was used in most experiments at a cold pressure of 7.1 MPa (6.9 MPa hydrogen). One experiment was performed with an equivalent pressure of nitrogen. Also, thermal and catalytic experiments were carried out without solvent at higher (13.8 MPa) and lower (3.4 MPa) hydrogen pressures.

Experiments consisted of filling the reactor then raising the temperature to 425°C, along the profile given in Figure 1, followed by an immediate quench. Several experiments were performed in which the reactor was held at 425°C for 60 minutes following heat-up before being quenched. The products were initially fractionated by sequential extraction with THF and cyclohexane. The THF-insoluble fractions were further fractionated using a modification of published NMP extraction procedures.^{7,8} Small amounts (0.6-0.7 g) of the THF insolubles were refluxed under nitrogen with 90 ml of NMP (BASF) for 1 hour. The solution was centrifuged at

500xg for 60 minutes. The supernatant was collected and the residue resuspended in 90 ml of fresh NMP. The refluxing/centrifugation was repeated 4 times. The combined supernatants were filtered through a 5 μ m Mitrex Teflon filter. The residue was washed onto the filter paper with acetone then the filter cake was washed with water and dried overnight in a vacuum oven. The filtrate was concentrated to about 20 ml volume by rotary evaporation. Acidified water (500 ml of 0.002 N) was then added dropwise overnight with stirring to precipitate the NMP-soluble material. This solution was filtered through a second Teflon filter, which was then washed with acetone and dried overnight in a vacuum oven.

TGA experiments were carried out on the cyclohexane-insoluble, NMP-soluble, and NMP-insoluble fractions using a DuPont 951 TGA. An open quartz pan was suspended from the end of the balance arm and filled with 10-15 mg of sample. The TGA was purged with nitrogen then held at 150°C to remove adsorbed water. The temperature was then raised to 900°C at a rate of 10°C/min. At that point, air was introduced into the TGA and the temperature held at 900°C until a constant weight was achieved. The amount of volatile material in the sample was equal to the weight lost as the sample was heated to 900°C. The weight loss following the introduction of air represented the loss of fixed carbon from the sample through oxidation. The weight of the material remaining in the pan following oxidation was the ash content of the sample. Figure 2 shows a typical curve generated by the TGA from an NMP-insoluble fraction.

RESULTS

The list of experiments, conditions, and conversions is given in Table 1. Cyclohexane, THF, and NMP conversion results are reported on a %daf coal basis. The TGA results for the NMP insoluble fractions are also given in Table 1. Because of the differences in conversions and the presence or absence of catalyst, there are large differences in ash contents of the NMP insoluble fractions. For easier comparisons the percentages of volatile matter and fixed carbon are reported on an ash-free basis.

Catalyst Activation Experiments

The $\text{Mo}(\text{CO})_6$ precursor has been extensively investigated in the microautoclave system. Under slow heat-up conditions (approximately 1 h), hydrogen transfer to the DECS-17 coal was shown by a corresponding increases in THF conversion. This occurred at temperatures as low as 325°C, with a pronounced increase in activity at 370°C.⁵ These experiments were performed without an added solvent, which would tend to mask the effect of the catalyst. Whether similar activation occurs under preheater simulation conditions was addressed by performing both thermal and catalytic experiments, again in the absence of solvent.

Solvent-free/Thermal Experiments The first series of experiments listed in the table are the solvent-free experiments. Hydrogen for the liquefaction reactions could only come from either the coal structure or the hydrogen gas phase in these experiments. Since coal conversion is known to be dependent on the amount of available hydrogen, the results should be dependent on the hydrogen pressure in the reactor if hydrogen gas is used in the reactions. For the thermal case, increasing (JF449) or decreasing (JF451) the hydrogen pressure in the reactor had no effect on conversions over the base pressure experiments (JF412, JF450). The fixed carbon content of the NMP insolubles was also the same in all three cases, further indicating that the reactions taking place are independent of hydrogen pressure. Holding the reactor at the reaction temperature for an additional 60 minutes (JF420) resulted in no additional conversion to NMP soluble material, showing that the initial coal decomposition takes place rapidly. The slower secondary reactions continue to take place during the additional time at reaction temperature with a minor increase in THF conversion and a significant increase in cyclohexane conversion. The fixed carbon content of the NMP insolubles increases as these secondary reactions take place, again showing that hydrogen from the coal structure is used in these reactions rather than gas-phase hydrogen.

Solvent-free/Catalytic Experiments The corresponding set of experiments in which $\text{Mo}(\text{CO})_6$ was included in the reaction show much different results from the thermal set. At the base hydrogen pressure, experiments JF413 and JF447 show greater conversion to NMP, THF, and cyclohexane soluble products compared with the thermal experiments. This immediately indicates that the catalyst precursor has become at least partly active when exposed to only this short heat-up profile. This is important, because it shows that a preactivation step may not be needed for certain dispersed catalysts in large-scale liquefaction processes. The large disparity between the NMP and THF conversions for these two experiments carried out under identical conditions has not yet been resolved.

In addition to determining if the catalyst was activated, the hypothesis that the role of the catalyst was to make gas-phase hydrogen available for the liquefaction reactions was also tested. This was accomplished by performing experiments at both a lower (3.4 MPa, JF448) and a higher (13.8 MPa, JF445) hydrogen pressure. The drastic increases in NMP and THF conversion in going to the higher pressure indicate that this hypothesis is probably correct, but the wide variance in the intermediate pressure experiments must be considered. Even at the lowest pressure, however, the NMP conversion is greater than those found in all thermal experiments.

The presence of the catalyst continues to have an effect on conversions, as seen from the 60-minute catalytic experiment (JF417). The NMP conversion has been affected by the longer reaction time showing a small increase; this was not seen in the thermal experiments. As was seen in the thermal 60-minute experiment, however, there is an increase in the fixed carbon content of the NMP insoluble fraction and greatly increased THF and cyclohexane conversions.

One additional insight can be gained by comparing the TGA results of the thermal and catalytic experiments. The fixed carbon content of the NMP insolubles was $58\% \pm 2\%$ regardless of the amount of NMP conversion. This shows that the volatile matter in the NMP insolubles is not preferentially broken down into soluble product, but that the more condensed structures are equally reactive.

Microautoclave Simulations of a Preheater

The second set of experiments listed in Table 1 are those performed using the VGO solvent. These experiments represent the actual simulations of a liquefaction preheater, where a slurry of coal and a coal-derived solvent are in contact with a hydrogen gas phase as the mixture is pumped through the preheater. In an initial set of experiments, not reported in the table, the VGO was tested under thermal and catalytic conditions without coal present. Elemental analysis, average molecular weights, ^1H NMR, and ^{13}C NMR of the treated and untreated VGO showed no differences, indicating that the VGO itself is not reactive under these conditions. As discussed below, however, there is adduction of the VGO to the coal material in some of the coal plus solvent experiments.

The solvent serves as an additional source of hydrogen for the liquefaction reactions. The dramatic increases in NMP and THF conversions over both the thermal and catalytic solvent-free experiments show how important this source of hydrogen is for these reactions. The importance of having good hydrogen transferring solvents during the heat-up phase of the coal liquefaction process has long been recognized.

Thermal Simulations Thermal experiments were carried out under three sets of conditions in which VGO solvent was used. The baseline preheater simulations (JF410, JF415, JF453, JF455) had an average of 88% conversion to NMP solubles and 68% conversion to THF solubles within the five minute heat-up to 425°C. Cyclohexane conversions for these experiments are lower than those for the solvent free experiments, however. The reason for this is that the amount of VGO present is subtracted out of the cyclohexane solubles collected at the end of the experiment. Some of the VGO solvent adducts to larger molecular weight coal molecules, however, and becomes insoluble in cyclohexane. This type of solvent behavior has been reported before with complex solvents.⁹

Performing the same experiment under 6.9 MPa of nitrogen, with no hydrogen gas present (JF414), produces the same NMP and THF conversions. This again shows that the presence of the hydrogen gas is not important in the thermal experiments. An experiment was also performed holding the coal and solvent at 425°C under 6.8 MPa of hydrogen for 60 minutes following the heat-up (JF459). A disproportionation occurs over time, with retrograde reactions causing a decrease in the NMP conversion while secondary reactions increase the THF and cyclohexane conversions. The cyclohexane conversion, however, remains lower than that achieved in the solvent-free experiments held for 60 minutes due to reaction of the solvent with the coal. The NMP insoluble material is also becoming more condensed, with the fixed carbon content increasing almost 20%.

Catalytic Simulations From the previous solvent-free results, it is presumed that the catalyst makes hydrogen gas more readily available for liquefaction reactions. Interestingly, however, this has no effect on the NMP conversion catalytic preheater simulation experiments (JF452, JF454, JF456). The presence of the solvent alone provides sufficient hydrogen for this phase of coal dissolution. The additional hydrogen provided by the catalyst does increase the THF and cyclohexane conversions. The catalyst, however, does not prevent solvent adduction reactions because the solvent-free experiments had greater cyclohexane conversions. Fixed carbon

contents of the NMP insolubles from the catalytic and thermal experiments are the same, indicating that the presence of the catalyst does not change the amount of hydrogen extracted from the coal structure during the liquefaction reactions.

In the 60-minute experiment with catalyst present (JF460), the retrograde reactions which took place without catalyst are prevented. There remains some use of hydrogen from the NMP insoluble material, because the amount of fixed carbon in this fraction still increases. In terms of conversion relative to the zero-minute experiment, there is a slight increase in the NMP solubles with larger increases in both the THF and cyclohexane solubles when the reaction is continued for 60 minutes.

CONCLUSIONS

This study confirmed two conclusions from earlier preheater and preheater simulation experiments: 1) The initial coal breakdown reactions occur very rapidly, and 2) greater than 90% of the total conversion for a system is achieved in the preheater.

For its own objectives, this study showed that dispersed catalyst precursor added to the slurry becomes active as it passes through the preheater. Experiments under different hydrogen pressures indicate that hydrogen gas does not participate in liquefaction reactions under thermal conditions, but seem to indicate that the molybdenum catalyst makes hydrogen from the gas phase available for these reactions. Hydrogen provided by the solvent is more easily used than hydrogen supplied by the catalyst, but the coal itself remains a significant source of hydrogen.

The use of NMP extraction to determine conversion is a valuable method for analyzing liquefaction results. NMP's ability to solubilize more of the coal material than THF gives insights into the formation and breakdown of this material. Especially important is the fact that no NMP-soluble material is formed above what would be produced in the preheater even after 60 minutes of additional reaction. The occurrence of retrograde reactions is also easily detected by increases in the NMP insoluble material.

The usefulness of thermogravimetric analysis to characterize solid products from the liquefaction reactions is also demonstrated. Determination of the fixed carbon contents showed that volatile material in the insoluble fraction is not preferentially converted to lighter products in the initial reactions. The use of hydrogen from the coal structure in the initial and secondary reactions was also identified through the TGA work.

Further work needs to be performed, first to determine the cause of the large variation between experiments JF413 and JF447, and second to apply this analysis to coals of lower rank, which would be more susceptible to retrograde reactions.

ACKNOWLEDGMENTS

Support for one of the investigators (JPF) was provided by an ORISE Fellowship through the Department of Energy's Oak Ridge National Laboratory. We also wish to thank J. Foster for his work on the microautoclave reactions.

REFERENCES

1. DOE/ET/10104-46 1981, 1 & 2
2. Yu, R.K., Comolli, A.G., Johanson, E.S., Hippo, E.J., *Proc. 17th, Inter. Ener. Conv. Eng. Conf.*, 1982, 844
3. DOE/ET/10152-86, 1982.
4. Brandes, S.D., Lancet, M.S., Robbins, G.A., Winschel, R.A., Burke, F.P., DOE/PC/89883-53, 1992.
5. Warzinski, R.P.; Bockrath, B.C. *Energy & Fuels*, 1996, 10, 612.
6. Coless, L.A., Poole, M.C., Wen, M.Y., Exxon Report, 1995, ERLA.2KW.95.
7. Renganathan, K., Zondlo, J.W., Stiller, A.H., Phillips, G., Mintz, E.A., *Int'l. Conf. Coal Sci.*, 1987, 367.
8. Cagniant, D., Gruber, R., Lacordaire-Wilhelm, C., Schulten, H.R., *Fuel*, 1990, 69, 902.
9. McNeil, R.I., Young, D.C., Cronauer, D.C., *Fuel*, 1983, 62, 806.

Table 1
Preheater Simulation Experiments - Conditions and Results

| ID | SOLVENT | GAS | COLD PRESSURE (MPa) | CATALYST PRECURSOR | TIME (min) | CONVERSION | | | NMP INSOLUBLES (daf%) | TGA RESULTS | |
|-------|---------|--------------------------------|---------------------------|-----------------------|---------------|-----------------------|---------------|---------------|-----------------------------|----------------------------|--------|
| | | | | | | Cyclohexane (daf%) | THF (daf%) | NMP (daf%) | | NMP INSOLUBLES Volatile | Fixed |
| JF412 | NONE | H ₂ /3% <i>H</i> 2S | 7.1 | NONE | 0 | 20.3 | 35.4 | | | | Carbon |
| JF450 | NONE | H ₂ /3% <i>H</i> 2S | 7.1 | NONE | 0 | 15.1 | 28.4 | 44.3 | 55.7 | 39.2 | 60.8 |
| JF451 | NONE | H ₂ /3% <i>H</i> 2S | 3.4 | NONE | 0 | 17.8 | 29.4 | 39.6 | 60.4 | 39.3 | 60.7 |
| JF449 | NONE | H ₂ /3% <i>H</i> 2S | 13.8 | NONE | 0 | 14.7 | 27.6 | 40.7 | 59.3 | 42.9 | 57.1 |
| JF420 | NONE | H ₂ /3% <i>H</i> 2S | 7.1 | NONE | 60 | 31.8 | 33.6 | 40.2 | 59.8 | 31.7 | 68.3 |
| JF413 | NONE | H ₂ /3% <i>H</i> 2S | 7.1 | Mo(CO) ₆ | 0 | 22.5 | 34.1 | 55.3 | 44.7 | 42.8 | 57.2 |
| JF447 | NONE | H ₂ /3% <i>H</i> 2S | 7.1 | Mo(CO) ₆ | 0 | 22.4 | 45.7 | 84.6 | 15.4 | 44.2 | 55.8 |
| JF448 | NONE | H ₂ /3% <i>H</i> 2S | 3.4 | Mo(CO) ₆ | 0 | 17.6 | 36.8 | 50.6 | 49.4 | 39.8 | 60.2 |
| JF445 | NONE | H ₂ /3% <i>H</i> 2S | 13.8 | Mo(CO) ₆ | 0 | 22 | 52.4 | 81.7 | 18.3 | 44.4 | 55.6 |
| JF417 | NONE | H ₂ /3% <i>H</i> 2S | 7.1 | Mo(CO) ₆ | 60 | 47.9 | 63.5 | 75.4 | 24.6 | 32.6 | 67.4 |
| JF410 | VGO | H ₂ /3% <i>H</i> 2S | 7.1 | NONE | 0 | 11.7 | 67 | 90.3 | 9.7 | 45.4 | 54.6 |
| JF415 | VGO | H ₂ /3% <i>H</i> 2S | 7.1 | NONE | 0 | 7.4 | 68.9 | 91.3 | 8.7 | 52.0 | 48.0 |
| JF453 | VGO | H ₂ /3% <i>H</i> 2S | 7.1 | NONE | 0 | 2 | 58.4 | 89.6 | 10.4 | 50.0 | 50.0 |
| JF455 | VGO | H ₂ /3% <i>H</i> 2S | 7.1 | NONE | 0 | 4.1 | 68.6 | 81.7 | 18.3 | 47.4 | 52.6 |
| JF414 | VGO | N ₂ | 6.9 | NONE | 0 | 18.9 | 66.5 | 89.5 | 10.5 | 49.9 | 50.2 |
| JF459 | VGO | H ₂ /3% <i>H</i> 2S | 7.1 | NONE | 60 | 24.7 | 71.4 | 82 | 18 | 32.0 | 68.0 |
| JF452 | VGO | H ₂ /3% <i>H</i> 2S | 7.1 | Mo(CO) ₆ | 0 | 9.2 | 69.7 | 84.9 | 15.1 | 43.7 | 56.3 |
| JF454 | VGO | H ₂ /3% <i>H</i> 2S | 7.1 | Mo(CO) ₆ | 0 | 13.6 | 71.4 | 92.6 | 7.4 | 49.7 | 50.3 |
| JF456 | VGO | H ₂ /3% <i>H</i> 2S | 7.1 | Mo(CO) ₆ | 0 | 7.1 | 73.8 | 87.9 | 12.1 | 48.8 | 51.4 |
| JF460 | VGO | H ₂ /3% <i>H</i> 2S | 7.1 | Mo(CO) ₆ | 60 | 38.4 | 84.8 | 91.5 | 8.5 | 36.6 | 63.4 |

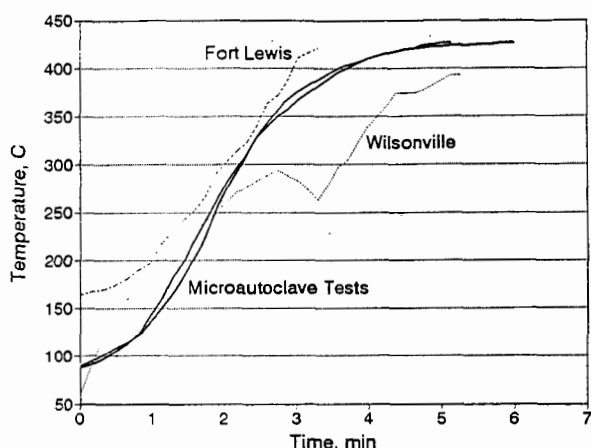


Figure 1. Comparison of microautoclave heating profiles with those from the Fort Lewis and Wilsonville pilot plants.

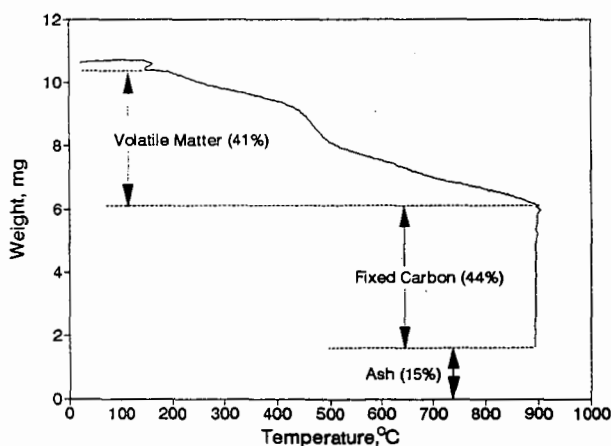


Figure 2. TGA curve of the NMP-insoluble material from experiment JF456 which contained both solvent and catalyst.

ACID CATALYZED DEPOLYMERIZATION OF COAL UNDER MILD CONDITIONS WITH SUPERACID HF/BF₃

Kiyoyuki Shimizu*, Ikuo Saito, Hiroyuki Kawashima
National Institute for Resources and Environment, AIST.
16-3 Onogawa, Tsukuba, Ibaraki 305-8569, Japan.

Shinsuke Sasaki, Akira Suganuma
Science University of Tokyo, Noda, Chiba 278-8510, JAPAN

Keywords: Coal solubilization, Superacid, Depolymerization

1. INTRODUCTION

Acid-catalyzed coal depolymerization has been widely studied as a way to liquefy coal under milder conditions¹⁻⁴. However, it is usually very difficult to recover completely the acid catalyst from solids or products. HF/BF₃, which has been recognized as a Bronsted/Lewis superacid catalyst for Friedel-Crafts reactions: isomerization and separation of m-xylene, and formylation of aromatic compounds on an industrial scale (Mitsubishi Gas Chemical Co., Ltd.). HF/BF₃ mixtures are fully recoverable from the product by distillation only, and can be reused, because their boiling points are very low (HF: 19.9°C, BF₃: -101°C). Olah studied coal liquefaction using the HF-BF₃-H₂ system and HF-BF₃-isopentane⁵. We also reported that HF and HF/BF₃ in the presence of toluene depolymerized coal more efficiently at 100-150°C through the acid-catalyzed transalkylation reaction of coal⁶.

In the present study, solubilization of coals of different rank were carried out at 50-150°C in order to evaluate recyclable superacid HF/BF₃ as catalyst for efficient depolymerization of coal of different rank via an ionic reaction. The depolymerization of coals in the acid-catalyzed reaction process was considered in terms of the chemical structure of coals and behaviors of oxygen containing functional groups.

Table 1 Elemental analyses of the treated coals.

| Run | Elemental analyses (wt%, daf base) | | | | ash (wt%) |
|----------|------------------------------------|-----|-----|------------------|-----------|
| | C | H | N | O _{air} | |
| Yallourn | 65.6 | 4.6 | 0.6 | 29.20 | 1.3 |
| Taiheiyo | 73.3 | 6.4 | 1.2 | 19.1 | 13.7 |
| Miike | 82.0 | 6.7 | 1.2 | 10.1 | 14.7 |

2. EXPERIMENTAL

Yallourn lignite, Taiheiyo subbituminous and Miike bituminous coal were used, ground to a diameter of 0.25mm less and dried in a vacuum at 110°C for 24h (Table 1). The liquefaction was carried out in a hastelloy-C microautoclave of 100 ml capacity. Coal (5 g) and toluene or isopentane (20ml) were placed in the dry ice-methanol cooled autoclave. First, the reactor of autoclave was evacuated by vacuum pump; then the HF (0.582 g/g-coal) and BF₃ (0.219 g/g-coal) were introduced to the coal-solvent slurry while dry ice-methanol cooling continued. Gaseous hydrogen (5.1 MPa) was introduced to autoclave after BF₃ when instead of toluene or isopentane. The autoclave was then heated to 50-150°C at a heating rate of 1.5°C/min for 3 h under autogenous pressure with vigorous stirring. After the reaction, gaseous HF/BF₃, solvent and volatile fraction from toluene in the autoclave were depressurized and absorbed into ice-water at 90-110°C under flowing nitrogen gas (100-150 mL/min) with stirring (300rpm) for 2h. The contents of the autoclave were slowly poured into cool water, and then were gradually neutralized with an cool aqueous solution (5 wt%) of Na₂CO₃. The products were filtered and washed in water with sonication. Washing with an aqueous methanol solution (30-50 vol%) was repeated 3 times in order to remove small

amount of neutralized product NaF and dimer of toluene. The solid product was vacuum-dried at 110°C for 24h. Reaction conditions are summarized in Table 2. Calculation to obtain the yield of solubles and weight increase has been described in detail elsewhere⁸.

The products were extracted with benzene, THF and pyridine in a sequential Soxhlet extractor. Oxygen-containing functional groups were determined by the method of Hatami et al. This determination has been described in detail elsewhere⁶.

The ¹³C-CP/MAS solid-state NMR spectra were measured with a chemagnetics at 75.58 MHz. The following operating parameters were used: a spectral width of 30 kHz, a 90 proton pulse of 5 μs, an acquisition time of 34.130 ms, a pulse repetition time of 4 s and an accumulation of 4000 scans.

3. RESULTS AND DISCUSSION

3.1 Effects of reaction temperature

The effects of reaction temperature on coals solubilization in the presence of HF/BF₃ (7 mol%) are shown in Figure 1. The reaction at even 50°C showed higher extractability than original coals. The reaction at 100°C greatly increased extractability, especially Miike bituminous coal could solubilize almost completely. The reaction at 150°C resulted in high extractability as described. Pyridine soluble yield in the treated coals at the lower reaction temperature of 50 and 100 °C was increased with increasing of carbon content in coal. However, the extractability of product from any coal was not changed at the reaction temperature of 150°C.

3.2 Effects of stabilizer

The extractability of the products treated with different kinds of stabilizer are shown in Figure 2. Extractability of products from Yallourn lignite depend very much upon the kinds of stabilizer. Although it can solubilize nearly completely by the reaction with toluene isopentane and hydrogen showed lower extractability such as 49 and 20 wt%, respectively. Differences of extractability in the case of Taiheiyō subbituminous coal was smaller than Yallourn lignite. And the products from Miike bituminous coal was not significantly changed with kind of stabilizer.

3.3 Oxygen containing functional groups

The distribution of oxygen-containing functional groups in the original coals and the treated coals is summarized in Table 3. Oxygen-containing functional groups were divided into 4 groups(carboxylic, hydroxyl, carbonyl group and Orest). Orest is mostly ascribed to ether groups such as Ar-CH₂-O-R, Ar-O-Ar and Ar-O-R. Most of the oxygen-containing functional groups decreased after the reaction. Decreasing of ether bonds, carboxylic and hydroxyl groups were increased with increasing of reaction temperature. This highly deoxygenation during reaction at 150°C would be cause of high extractability of products. The reaction with isopentane under HF/BF₃ at 150 °C retained more hydroxyl groups and ether bond in the products than did the reaction with toluene, indicating that these oxygen containing functional groups remained restricted extractability, leading that lower coal depolymerization. In contrast, Miike bituminous coal inherently have small amount of oxygen containing functional groups, and their decreasing after reaction was substantially small, therefore behaviours of oxygen containing functional groups in Miike coal did not contribute the solubilization reaction.

These results indicated that Miike bituminous coal comparatively easy to produce highly soluble products even at any reaction conditions because of small amount of oxygen containing functional groups. In contrast, Yallourn lignite which have more amount of their functional groups and its content in products depend on the reaction condition such as kind of stabilizer and reaction temperature.

3.4 CP/MAS-¹³C NMR spectra

Table 4 summarizes the carbon distributions of original coals and treated coal from the reaction with HF/BF₃ under gaseous hydrogen. The carbon atoms were classified into

7 categories as shown. Original Yallourn lignite have more aromatic carbons bound to oxygen (phenolic-OH), oxygen functional groups C=O, COOH and other bond (-O-CH₂-), but less methylene bridges and terminal CH₃ content when compared with those of Taiheiyo subbituminous and Miike bituminous coal. After the reaction, decreasing of methylene bridges in the Yallourn treated coal was the lowest by less 5 %. In contrast, Taiheiyo and Miike coal showed more reduction of methylene bridge. The Yallourn treated coal have more aromatic carbons bound to oxygen and oxygen containing functional groups than those of products from others. These results indicated that the improvement of extractability of Taiheiyo and Miike coal was ascribed to the cleavage of methylene and other bridges in their coal, while lower extractability of Yallourn treated coal was caused by small cleavage of methylene bridge and a significant amount of oxygen containing functional groups.

4. CONCLUSIONS

1. Solubilization of higher-rank coals, Miike bituminous coal, by any reaction conditions was almost higher than those of lower rank coals.
2. Solubilization of lignite, Yallourn coal, depend upon reaction conditions, it was greatly changed by the stabilizer and reaction temperature.
3. The reaction with toluene as stabilizer significantly solubilized even Yallourn lignite coal because of more cleavage of ether groups and deoxygenation.

5. REFERENCES

1. Heredy, L.A. and Neuworth, M.B. Fuel 1962, 41, 21
2. Larsen, J.W. and Kuemmerle, E.W. Fuel 1976, 55, 162
3. Kumagai, H., Shimomura, M. and Sanada, Y. Fuel Process. Technol. 1986, 13, 97
4. Farcasiu, M. Fuel Process. Technol. 1986, 14, 161
5. Olah, G.A., Bruce, M.R., Edelson, E.H. and Husain, A. Fuel 1984, 63, 1130
6. Shimizu, K. and Saito, I. Energy & Fuels, 1997, 11, 115.

Table 2 Reaction condition of the treated coals.

| Run | Temp. (°C) | HF (g) | BF ₃ (g) | solvent | W1 (%) |
|-----|---------------|-----------|------------------------|----------------|-----------|
| Y-1 | 50 | 5.8 | 1.10 | toluene | 37 |
| Y-2 | 100 | 5.8 | 1.18 | toluene | 44 |
| Y-3 | 150 | 5.8 | 1.26 | toluene | 97 |
| Y-4 | 150 | 5.8 | 1.24 | isopentane | 32 |
| Y-5 | 150 | 5.4 | 1.38 | H ₂ | -7 |
| T-1 | 50 | 5.10 | 1.38 | toluene | 18 |
| T-2 | 100 | 4.92 | 1.28 | toluene | 35 |
| T-3 | 150 | 5.8 | 1.39 | toluene | 71 |
| T-4 | 150 | 5.5 | 1.38 | isopentane | 24 |
| T-5 | 150 | 5.82 | 1.38 | H ₂ | -14 |
| M-1 | 50 | 5.46 | 1.4 | toluene | 11 |
| M-2 | 100 | 5.46 | 1.4 | toluene | 9 |
| M-3 | 150 | 5.82 | 1.4 | toluene | 113 |
| M-4 | 150 | 6.06 | 1.25 | H ₂ | -3 |

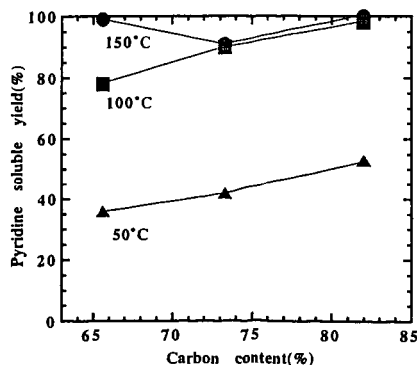


Figure 1 Effect of reaction temperature on extractability of treated coal with HF/BF₃.

Reaction condition: 3 h, toluene

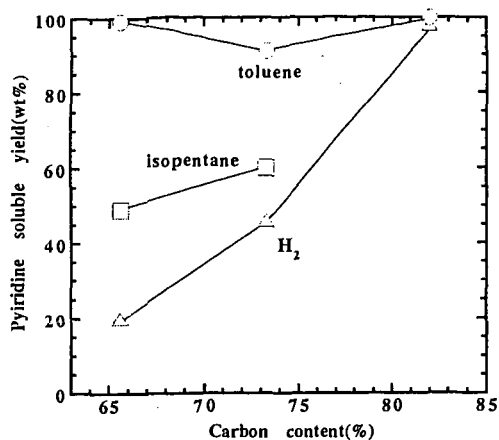


Figure 2 Effect of stabilizer on extractability of treated coal with HF/BF₃.

Reaction condition: 150°C, 3h

Table 3 Distribution of oxygen containing functional group in original coal and the treated coals.

| Run | Reaction conditions | | | | wt% | | | | |
|----------|---------------------|--------|---------------------|------------|------|-----|-----|-------------------|-------|
| | Temp. (°C) | HF (g) | BF ₃ (g) | solvent | COOH | OH | C=O | O _{rest} | Total |
| Yallourn | | | | | 4.1 | 5.7 | 4.5 | 14.9 | 29.2 |
| Y-1 | 50 | 5.8 | 1.10 | toluene | 1.9 | 5.0 | 2.8 | 12.8 | 22.5 |
| Y-2 | 100 | 5.8 | 1.18 | toluene | 2.3 | 2.9 | 4.2 | 8.4 | 17.8 |
| Y-3 | 150 | 5.8 | 1.26 | toluene | 0.6 | 1.8 | 4.5 | 6.5 | 13.4 |
| Y-4 | 150 | 5.8 | 1.24 | isopentane | 0.8 | 3.9 | 4.5 | 9.0 | 18.0 |
| Taiheiyo | | | | | 0.6 | 5.3 | 3.4 | 9.8 | 19.1 |
| T-1 | 50 | 5.10 | 1.38 | toluene | 1.0 | 5.1 | 2.8 | 3.7 | 12.6 |
| T-2 | 100 | 4.92 | 1.28 | toluene | 0.5 | 6.1 | 2.9 | 3.0 | 12.5 |
| T-3 | 150 | 5.8 | 1.39 | toluene | 0.7 | 3.4 | 2.8 | 1.7 | 8.6 |
| T-4 | 150 | 5.5 | 1.38 | isopentane | 1.2 | 4.6 | 3.4 | 4.3 | 13.5 |
| Miike | | | | | 0.1 | 3.3 | 1.1 | 3.6 | 8.1 |
| M-2 | 100 | 5.46 | 1.4 | toluene | - | 1.7 | 1.9 | 3.8 | 7.4 |
| M-3 | 150 | 5.82 | 1.4 | toluene | - | 0.7 | 2.5 | 3.4 | 6.6 |

Content of oxygen functional groups and total oxygen were corrected with weight increase.

O_{rest}: ether or ester groups

Table 4 Carbon distribution in original and treated coals by NMR.

| (ppm) | COOH, C=O (220-171) | Phenolic C-O (171-149) | Ar-C (149-128) | Ar-H (128-93) | -CH ₂ -O- (75-50) | -CH ₂ -CH (55-22) | -CH ₃ (22-0) |
|----------|---------------------|------------------------|----------------|---------------|------------------------------|------------------------------|-------------------------|
| Yallourn | 7.1 | 12.9 | 17.2 | 27.2 | 9.4 | 22.3 | 3.9 |
| Y-5 | 8.5 | 14.6 | 18.7 | 26.0 | 6.6 | 18.8 | 6.8 |
| Taiheiyo | 4.3 | 8.2 | 15.3 | 24.4 | 7.0 | 34.1 | 6.7 |
| T-5 | 3.7 | 9.6 | 18.4 | 29.7 | 7.8 | 22.9 | 7.9 |
| Miike | 4.3 | 8.3 | 15.7 | 24.4 | 5.9 | 32.5 | 8.9 |
| M-4 | 3.6 | 10.0 | 21.7 | 31.5 | 6.5 | 18.6 | 8.1 |

PYROLYSIS OF COAL WITH HYDROGEN ATOMS

J. Bi, T. Kamo, Y. Kodera, H. Yamaguchi, and Y. Sato

Energy Resources Department,
National Institute for Resources and Environment
16-3 Onogawa, Tsukuba-city, Ibaraki, 305-8569 Japan

Keywords: coal hydropyrolysis, hydrogen atom, low pressure

ABSTRACT

The reactions of coal directly with hydrogen atoms are very important for understanding the mechanisms of coal liquefaction and coal hydrogasification. In the present study, Taiheiyo coal was reacted in a low pressure TG with hydrogen atoms(induced by microwave discharge cavity) and hydrogen gas under a pressure range of 1.0 - 50.0 torr, and a temperature range of 20 -1000°C, with heating rates of 5-20 °C/min. The yields of char, gas and liquid were measured and analyzed by TG-MS and GC-MS respectively. The results showed that the conversion of coal with hydrogen atoms was higher than that under low pressure of hydrogen gas. More liquid and gas products were obtained in the reaction with hydrogen atoms. It was observed that in the presence of hydrogen atoms, CO was more produced at a relative low temperature. Alkylated naphthalene compounds in the liquid yield were less produced in the reaction with hydrogen atoms than in the atmosphere of hydrogen gas.

INTRODUCTION

It is recognized that reactions of coal hydropyrolysis has a significant effect on the yield and distribution of end products such as coal-derived liquids, gases, coke, or pollutant emissions in the processes of coal liquefaction and coal hydrogasification under various conditions. In usual coal hydropyrolysis, thermal decomposition of coal occurs first and tar and some light carbonhydrogen compounds release at/around 400-500 °C. After the temperature is increased to that hydrogen decomposes, then the hydrogen atoms react with coal, coal-derived pyrolysates and char, yielding products with a rather wide molecular distribution. Therefore the mechanism in hydropyrolysis is much more complex comparing with in pyrolysis. To investigate the reactions of coal directly with hydrogen atoms are very important for understanding the mechanism of hydropyrolysis. However, the information on reaction of coal directly with hydrogen atoms is limited. Amano et al.¹⁾ investigated reactions between carbonized coal and hydrogen atoms using a discharge flow apparatus in a temperature range of 130-250 °C under 1Torr pressure. They found that oil yielded in the presence of hydrogen atoms has a different composition from that in the absence of hydrogen atoms , while a similar composition with that of middle fraction of petroleum distillate. In their another study²⁾, it was found that the liquid products contain more monocyclic alkanes, which is rather different from the liquid products yielded in conventional coal liquefaction. In addition, the liquid products contain little compounds of heteroatoms.

Hydropyrolysis require more detailed chemical information to predict the distribution of final products. Especially the reactions of coal directly with hydrogen atoms are needed to be further investigated under a wide conditions. The present study investigated coal reactions in the presence and absence of hydrogen atoms by means of vacuum TG/MS. Gas components of CH₄, CO and CO₂ were quantitatively measured and their variations with temperature were observed. The liquid products obtained at different temperatures were analyzed and compared in different atmospheres.

EXPERIMENTAL

A vacuum thermogravimetry(TG, Rigaku, Thermo plus TG8120) was used to observe the variation of coal weight, as shown in Figure 1. About 4.0 mg(-100 mesh) of Taiheiyo coal was placed in a quartz pan(Φ5mm) which was inserted into a quartz tube reactor. The pan was heated from ambient temperature to 1000 °C at a linear heating rate of 5 °C/min. The oven temperature was measured and controlled at the bottom of the pan by using a thermocouple. The pressure in the TG balance chamber was evacuated and controlled at less than 1.0 torr by a rotary vacuum pump and an adjustable valve.

Ultimate analysis data of Taiheiyo coal are 74.1 C, 6.4 H, 1.3 N, 18.0 O (by difference), 0.2 S(wt%, daf) and 14.2% ash(dry base).

Hydrogen gas was introduced to the TG chamber at a flow rate of $1.0\text{cm}^3/\text{min}$ (standard temperature and pressure, STA). Hydrogen atoms were induced by passing hydrogen gas through a microwave discharge cavity (2450 MHz). The discharge cavity was located at an introduction tube which was 10cm above the quartz reactor. Total distance between the discharge cavity and the coal sample was about 20cm which ensured the influence of plasma and UV from the discharge on the coal sample could be negligible. To prevent recombination of the hydrogen atoms, boric acid solution was coated in the inner surface of the reactor. For comparison, helium gas was also used under the same conditions as hydrogen gas was used.

The produced gas were analyzed by a mass spectrometer (MS, Balzers QMG112A). A turbomolecular pump (Balzers TMH/U 260) was used for evacuating the MS chamber up to 10^{-7} torr. MS conditions were set as follows: electron ionization voltage 70eV, mass range scanned 1-110 amu, scan sweeping time 52s. Each spectrum scanned was recorded and stored by computer through a MS interface (VTI, Aere Scan 1600MS/RGA).

Argon gas at a flow rate of $0.01\text{cm}^3/\text{min}$ (STA) was used as internal standard. Relation between ion intensity and flow rate of CH_4 , CO and CO_2 was calibrated. Therefore the gas products could be quantitatively measured through the ion intensity ratios of argon to CH_4 , CO and CO_2 . Before the experiment began, the background ion intensity was recorded and then subtracted during data treatment.

The liquid products were collected in a sample tube packed by Tenax powder. The sample tube was inserted in a U-tube immersed in a dry ice trap. Using a flash thermal desorption cold trap injector, the liquid products were analyzed by a gas chromatography (GC, HP-6890).

RESULTS AND DISCUSSION

1) Coal conversion

Coal weight variations with temperature in different atmospheres are described in Figure 2. It can be seen that the differences of weight variations in hydrogen gas, helium gas and discharged helium gas atmospheres are not so significant, where the weights decrease rapidly at around 400°C and the coal conversions at 800°C are about 50%. It reflects that hydrogen gas almost does not affect the pyrolysis reactions under low pressure. It also reflects that the discharge has scarce effect on pyrolysis in the present experiment, comparing the profiles between in the helium gas and in the discharged helium gas. However, the weight decreases rapidly at around 300°C in the hydrogen atom atmosphere and remarkable higher coal conversion, more than 60% at 800°C , is observed with temperature increase. This result suggests that hydrogen atoms promote significantly the pyrolysis reaction at a lower temperature.

2) Gas products

CH_4 , CO and CO_2 gas yield rate profiles with temperature in the absence and presence of hydrogen atoms are shown in Figure 3. In the hydrogen atmosphere, as shown in Figure 3(a), CH_4 reaches the maximum at around 500°C , CO has an increase tendency with temperature and CO_2 increases to the maximum before 400°C then decreases. In the reaction with hydrogen atoms, as shown in Figure 3(b), the profile patterns are quite different comparing with Figure 3(a). CH_4 has two peaks at around 200°C and 400°C . In particular, CO has a sharp increase at 200°C then a small peak at 400°C . CO_2 increases to the maximum at 200°C then decreases.

Mechanism is not exactly understood why CO increases so much. It is not likely that the shift reaction should be responsible for much CO yielded, since CO_2 increases not so dramatically as CO in the present experiment. The clarification of the mechanism is needed.

3) Liquid products

Figure 4 shows total amounts of BTX or monocyclic hydrocarbon compounds obtained at different temperatures in the absence and presence of hydrogen atoms. It can be seen that the amounts in the reaction with hydrogen atoms are much more than those in the hydrogen atmosphere with temperature increase. Comparing the amounts at 400°C and 600°C in different atmospheres, the amount increases about 5 times at 400°C while about 2 times at 600°C . Combining the gas yields produced before 300°C as shown in Figure 3(b), this reflects partly that why coal weight decreases rapidly at 300°C in the reaction with hydrogen atoms as shown in Figure 2. It can also be seen that relatively more BTX compounds are produced at 800°C in the reaction with hydrogen atoms. From the liquid product distribution, more monocyclic compounds and less naphthalene compounds were yielded in the reaction with hydrogen atoms than in the hydrogen atmosphere.

In the reaction of coal with hydrogen atoms, it was observed that tar was less produced comparing with in hydrogen atmosphere under the same conditions.

Exact amount of hydrogen atoms generated are not known. It was estimated¹⁾ about 10% of the hydrogen was in atomic state near the discharge cavity when 2450 MHz microwave discharge was applied. Even less amount of hydrogen atoms exist, the impact on the pyrolysis is profound from the present experiment.

4) Effects of pressure and heating rate

Pyrolysis was also carried out in a wider experimental conditions in the hydrogen atmosphere. Increasing the pressure from 1 torr to 10, 20 and 45 torr showed a decrease in gas products. Increasing the heating rate from 5 °C/min to 10 and 20 °C/min resulted in an increase in gas products. It implies that the effect of heating rate on the gas products of small molecules is probably different from the effect on the larger molecular compound products (amu values larger than 50) as observed by Yun et al.³⁾ where they found that the pyrolysate distributions of primary pyrolysis reactions in Pittsburgh No. 8 coal are independent of heating rate over a magnitude of 10^{-2} - 10^4 °C/s when monitoring the 50-200 amu mass range.

CONCLUSIONS

Pyrolysis of Taiheiyō coal in the reaction with hydrogen atoms was investigated and compared with pyrolysis in the hydrogen atmosphere. The result showed that the conversion of coal with hydrogen atoms was higher than that with hydrogen gas, and more liquid and gas products were obtained in the former case. It was observed that in the presence of hydrogen atoms, CO was more produced at a relative low temperature. More monocyclic compounds and less naphthalene compounds were yielded in the reaction with hydrogen atoms than in the hydrogen atmosphere.

REFERENCES

- 1) Amano, A., Yamada, M., Shindo, T., Akakura, T., Yotsusuji, S., *Inst. of Chem. Soc. of Jpn*, 1984, No. 10, 1648-1655
- 2) Amano, A., Yamada, M., Shindo, T., Akakura, T., *Fuel*, 1984, Vol. 63, May
- 3) Yun, Y., Maswadeh, W., Meuzelaar, H.L.C., Simmleit, N., Schulten, H.R., *Energy & Fuels*, 1991, 5, 22-29

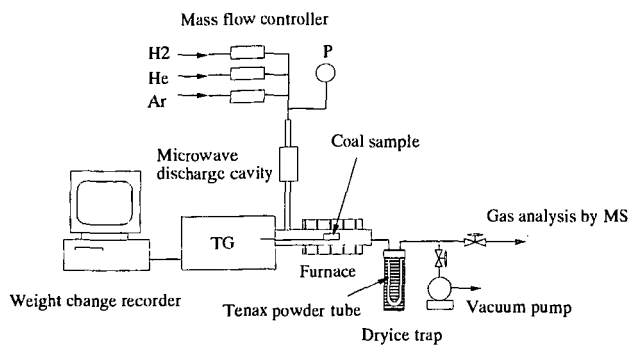


Figure 1. Experimental apparatus

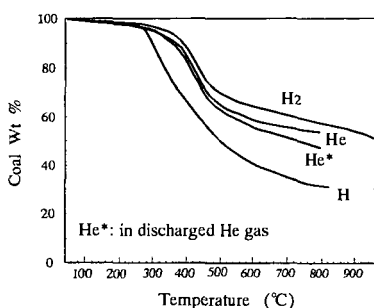


Figure 2. Coal weight decrease with temperature in various gas atmospheres

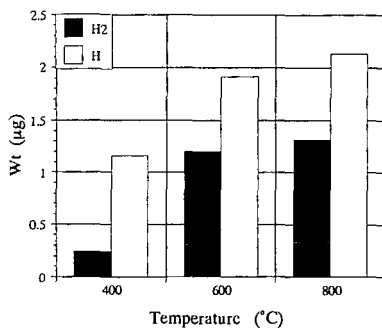


Figure 4. Weight variation of BTX compounds with temperature

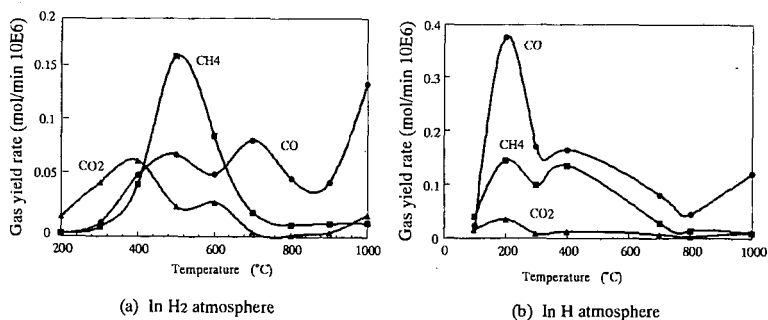


Figure 3. Main gas yield rate with temperature

STUDY ON INTERACTION BETWEEN COAL AND MODEL PLASTICS DURING LIQUID-PHASE CATALYTIC COLIQUEFACTION

H. Yamaguchi^a, Y. Okuyama^a, K. Matsubara^b, J. Bi^c, Y. Kodera^c, T. Kamo^c and Y. Sato^c

^a NKK Corp., 1-1 Minamiwatarida-cho, Kawasaki, 210 Japan

^b NK Techno Service, 1-1 Minamiwatarida-cho, Kawasaki, 210 Japan

^c National Institute for Resources and Environment, 16-3 Onogawa, Tsukuba, 305 Japan

ABSTRACT

Coliquefaction of Tanitoharum coal with PP, PS, high-density PE was carried out using red mud plus sulfur as the catalyst, at 430 °C for 60 min under 7 MPa initial pressure of hydrogen. There existed almost linear relationship of coal concentration in coal/plastics mixture with conversion to THF-soluble (THFS) or oil yield for the mixture of coal/PP, coal/PS or coal/PE in case of tetralin. Observed oil yield at 75 % of coal concentration for any coal/plastics mixture was slightly larger than that calculated. The use of decalin gave lower values of conversion, yields of THFS in VR and oil, particularly at coal concentration of 75% for the coal/PE mixture, compared to those calculated, while a similar tendency as to interaction in respect of conversion, yields of THFS in VR, oil, and gas was observed for the mixture of coal/PP and coal/PS. However, when the coal was reacted with mixed plastics of PP, PS and PE at coal concentration of 50 %, the interaction observed for the coal/PE mixture disappeared, and higher oil yield than that calculated was obtained. The results suggested interaction between PE and the other plastics (PP, PS) is larger than that between coal and PE. It is also suggested from the results for the coal/PP mixture that radicals from PP cracking was used for stabilization of radicals from the coal and PP, instead of hydrogen donated from gas and solvent. Higher values of conversion and oil yield for the use of decalin were obtained, compared to tetralin. The results indicated that a good hydrogen donor solvent would not be necessary in case of the use of catalyst for coliquefaction of coal with waste plastics.

Keywords: coal liquefaction, model compounds, waste plastics

1. INTRODUCTION

Under conventional direct coal liquefaction process, large amount of hydrogen gas is consumed to stabilize radical fragments from thermal cracking of coal. At present the price of produced coal liquid does not compete with that of crude oil, due to not only the severe operating conditions, but also the expensive production cost of hydrogen gas. Coprocessing of coal with heavy oil containing high concentrations of sulfur and heavy metals, has been investigated to improve the economical feasibility¹⁾. On the other hand, large amounts of waste plastics is being generated in Japan, mostly not recycled. The shortage of landfilling site has become more serious in recent years. Thus, coliquefaction of coal with heavy oil and waste plastics would be an attractive process of overcoming environmental problems and further enhancing economical feasibility. However, few studies have reported on this reaction, due to the complicated reaction system²⁾. We have conducted a model experiment of coliquefaction of coal with waste plastics using dibenzyl as a coal model compound to clarify the reaction mechanism, and investigated interactions between coal and plastics, and between the plastics, in respect of conversion, product distribution and composition of distillate oil³⁾.

In this study, catalytic coliquefaction of coal with model plastics was conducted under the same reaction conditions as those for the model experiment. Interaction between the coal and plastics was investigated in respect of conversion, product distribution, and H₂ transferred from gas or solvent, and the reaction mechanism involved was discussed.

2. EXPERIMENTAL

Catalytic coliquefaction of Tanitoharum coal (-100 mesh, C 75.91, H 5.66, N 1.62, S 0.37, O 16.44 (wt% daf (dry ash free) base)) with model plastics (PP, PS, high-density PE) and their mixture (1/1/1 by weight) was carried out at 430 °C for 60 min in a 500-ml magnetically stirred autoclave. Tetralin or decalin was used as the solvent. Red mud (total Fe 28.37 wt%) plus sulfur (1/1 by weight) was used as the catalyst. Weight ratio of (daf coal + plastics)/solvent/red mud was 100/150/3/3. Gas atmosphere was 7 MPa initial pressure of hydrogen gas. After the reaction, the measurement of gas volume and GC analysis were conducted for the product gas. Main part of the product liquid (plus any unconverted solid reactant and catalyst) was separated into distillate oil (-538 °C) and vacuum residue (+538 °C, VR) by vacuum distillation. The product liquid in part was subjected to Soxhlet extraction with hexane, tetrahydrofuran (THF) sequentially. Conversion to hexane & THF-soluble (THFS), yields of oil, hexane & THF-soluble in vacuum residue (THFS in VR), gas, and hydrogen gas consumption were measured, based on the weight of daf coal plus plastics by conventional methods. The composition of the distillate oil was analyzed using FID/GC. H₂ transferred from solvent was calculated from mass balance of naphthalene, decalin for the use of tetralin as the solvent

or tetralin, naphthalene for the use of decalin, before and after the coliquefaction⁴⁾.

3. RESULTS AND DISCUSSION

Coliquefaction of coal with PP, PS or PE using tetralin

In Fig.1, conversion to THFS, yields of oil, THFS in VR, and gas for coliquefaction of Tanitoharum coal with each of PP, PS or PE using tetralin were plotted against coal concentration in coal/plastics mixture.

Without any coexisting reactant, for each of the coal, PP, PS and PE, conversion of 99.7, 100, 100, 31.9 wt%, oil yield of 37.4, 76.4, 94.0, -1.2 wt%, yield of THFS in VR of 41.1, 13.9, 2.9, 28.8 wt%, and gas yield of 11.9, 10.1, 4.0, 3.9 wt%, respectively were obtained. PE was most difficult to be converted to THFS and oil among the reactants, while PS was almost converted to oil. For PP, conversion was very high, and larger yield of THFS in VR was produced, compared to PS. Gas produced from PP was largest among the plastics. For the coal, oil yield was much lower than those for PP and PS, in spite of very high conversion, and production of THFS in VR was largest among the reactants.

In case of coliquefaction, there existed almost linear relationship of coal concentration with conversion to THFS or oil yield. Oil yield at 75 % of coal concentration for the mixture of coal/PP, coal/PS or coal/PE was higher by 4.9, 4.8, 3.3 wt% respectively than that calculated (arithmetic mean value of results for each reactant). As to THFS in VR, almost linear relationship against coal concentration was obtained for the mixture of coal/PS or coal/PE, but observed values for the coal/PP mixture were higher than those calculated. As to gas yield, observed values for any coal/plastics mixture were lower than those calculated. The difference between the calculated value and the observed value was very large for the coal/PP mixture, compared to the other coal/plastics mixture.

Fig.2 shows H_2 transferred from gas and solvent in this reaction as a function of coal concentration in coal/plastics mixture.

H_2 transferred from gas or tetralin (mmol/g-daf reactant) was 15.5, 4.6 for the coal, 4.4, 1.9 for PP, 6.6, 3.1 for PS, and 0.94, 0.62 for PE, respectively. H_2 transferred from gas or tetralin for coal was largest among the reactants. It was observed that larger amounts of H_2 from gas or tetralin was transferred for PS than for PP. The amounts of H_2 transferred was small for PE. However, it is thought by considering the difference in conversion between PP and PE that the values for PE would become similar to those for PP when 100 wt% of conversion is obtained for PE.

For the coal/PE mixture, almost linear relationship of H_2 transferred with coal concentration was recognized. For the coal/PS mixture, H_2 transferred from gas were a little larger than those calculated, while H_2 transferred from tetralin were a little lower than those calculated. No difference in total of H_2 transferred between the observed value and the calculated value was observed. For the coal/PP mixture, H_2 transferred from gas or tetralin was lower than that calculated. The results from Figs. 1 and 2 for the coal/PP mixture suggest that radicals from PP cracking would be used for stabilization of radicals from the coal and PP, instead of hydrogen donated from gas and solvent.

Decomposition of PE proceeds as radical chain reaction. In the model experiment of coliquefaction of dibenzyl (DB) as a coal model compound with model plastics using tetralin and the same catalyst, conversion and yield of THFS in VR were higher than those calculated, suggesting that radicals from DB decomposition would secondarily attack PE³⁾. However, the tendency for the coal/PE mixture as seen in Figs. 1 and 2 is different from that in the model experiment. On the other hand, the mixtures of coal/PP and coal/PS showed almost the same tendencies as those from the model experiment.

Coliquefaction of coal with PP, PS or PE using decalin

In Fig.3, conversion to THFS, yields of oil, THFS in VR, gas, and H_2 transferred for coliquefaction of the coal with each of PP, PS or PE using decalin were plotted against coal concentration in coal/plastics mixture.

Without any coexisting reactant, for each of the coal, PP, PS and PE, conversion of 96.6, 100, 100, 77.3 wt%, oil yield of 42.6, 83.3, 92.5, 15.6 wt%, yield of THFS in VR of 36.4, 3.7, 3.5, 57.8 wt%, gas yield of 12.9, 14.5, 5.0, 3.9 wt%, and total of H_2 transferred from gas and decalin of 18.8, 9.8, 7.7, 2.1 mmol/g-daf reactant, respectively were obtained. Here, (H_2 transferred from gas)/(total H_2 transferred) were 3-7 %. Thus, H_2 transferred from decalin were small, compared to tetralin. The use of decalin instead of tetralin remarkably accelerated PE decomposition. This result indicates that the increase in hydrogen donorability of solvent inhibits PE decomposition, probably due to more rapid stabilization of radicals from PE cracking by hydrogen donation from solvent. For PP, yield of THFS in VR decreased, while yields of oil and gas increased a little. For PS, there was no large difference observed between decalin and tetralin, in respect of conversion, yields of THFS in VR, oil and gas. For the coal, the use of decalin instead of tetralin gave a little lower conversion, while oil yield became a little larger.

In case of decalin, considerably different coliquefaction behavior was obtained for the

coal/PE mixture, compared to tetralin. Conversion, yields of oil and THFS in VR were lower than those calculated, although there existed linear relationship of coal concentration with gas yield and total of H₂ transferred. The differences in conversion, yields of oil and THFS in VR between the observed value and the calculated value were very large at coal concentration of 25 %. The differences were not observed in case of tetralin. Hydrogen donation from hydrogen donor solvent to radicals is much faster than that from hydrogen gas even for catalytic coal liquefaction. For the use of decalin, radicals from cracking of the coal and PE would exist for longer time, compared to tetralin, resulting in larger interaction between radicals to polymerize to give THF-insoluble fraction. On the other hand, in the model experiment of coliquefaction of DB with model plastics using decalin and the same catalyst, PE decomposition proceeded more effectively with coexistence of the coal model compound, giving higher values of conversion and oil yield⁹. Thus, the results in Figs. 1-3 indicate that the coal would interacted with PE in a different way, compared to the coal model compound of DB. In case of coliquefaction of the coal with PP, almost linear relationship of coal concentration with conversion or oil yield was obtained. Yield of THFS in VR were higher than those calculated, while gas yield and total of H₂ transferred were lower than those calculated. The tendency for the coal/PP mixture was same, compared to that for the use of tetralin. The differences in total of H₂ transferred between the observed value and the calculated value became larger than those for the use of tetralin. From the results, more effective use of radicals from PP cracking for stabilization of radicals from the coal and PP instead of hydrogen could be expected. For the coal/PS mixture, there existed almost linear relationship of coal concentration with conversion, yield of THFS in VR. Oil yield and total of H₂ transferred were a little higher than those calculated, while gas yield was lower than that calculated. The tendency in respect of conversion, yields of oil, THFS in VR and gas was similar to that for the use of tetralin.

Coliquefaction of coal with mixed plastics of PP, PS and PE

Table 1 shows results of coliquefaction of the coal with mixed plastics of PP, PS and PE using tetralin or decalin and the same catalyst. Coal/mixed plastics was 1/1 and PP/PS/PE was 1/1/1. Two kinds of calculated value (cal¹ : arithmetic mean value of results from the coal/PP, the coal/PS and the coal/PE (1/1 mixture), cal² : arithmetic mean value of results for each reactant) are also shown in this table.

Coliquefaction using tetralin gave a little higher gas yield, lower values of conversion and yield of THFS in VR, compared to cal¹. On the other hand, conversion and THFS in VR also became lower, compared to cal² but gas yield was larger. There existed almost no difference in oil yield between the observed value and the calculated value, not depending on the way of calculation. Coliquefaction using decalin gave the same gas yield, higher values of conversion and oil yield, and a little lower yield of THFS in VR, compared to cal¹. On the other hand, almost the same conversion, lower yields of THFS in VR and gas, and higher oil yield were observed, compared to cal². The results indicate that PE decomposition proceeded more effectively with the coexistence of PP and/or PS during coliquefaction of the coal with the mixed plastics, although PE decomposition inhibited by coexistence of the coal in case of coliquefaction of the coal with PE alone. It is also suggested that the results reflected larger interaction between PE and the other plastics (PP, PS) than that between coal and PE. Lower gas yield in case of tetralin or decalin, compared to cal², as seen in Table 1 was probably due to inhibition of gas production by the coexistence of PP, also shown in Figs.1 and 3. Total of H₂ transferred for the use of tetralin or decalin was only a little lower, compared to cal², due to the low concentration of PP in coal/plastics mixture.

As also seen in Table 1, higher values of conversion and oil yield for the use of decalin were obtained, compared to tetralin. The results indicate that a good hydrogen donor solvent would not be necessary in case of the use of catalyst for coliquefaction of coal with waste plastics.

ACKNOWLEDGEMENT

This study was supported by the Original Industrial Technology R&D Promotion Program from NEDO of Japan.

References

1. Cugini, A.V. and Lett, R.G., *Energy and Fuels*, Vol.3, 120 (1989)
2. Rothenberger, K.S. et al., *ACS Div. Fuel Chem. Preprints*, Vol.40, No.1, 38 (1995)
3. Yamaguchi, H. et al., *Proc. of the 1998 Int. Symposium on Advanced Energy Technology*, 163 (1998)
4. Curtis, C.W and Cassell, F.N., *Energy and Fuels*, Vol.2, 1 (1988)

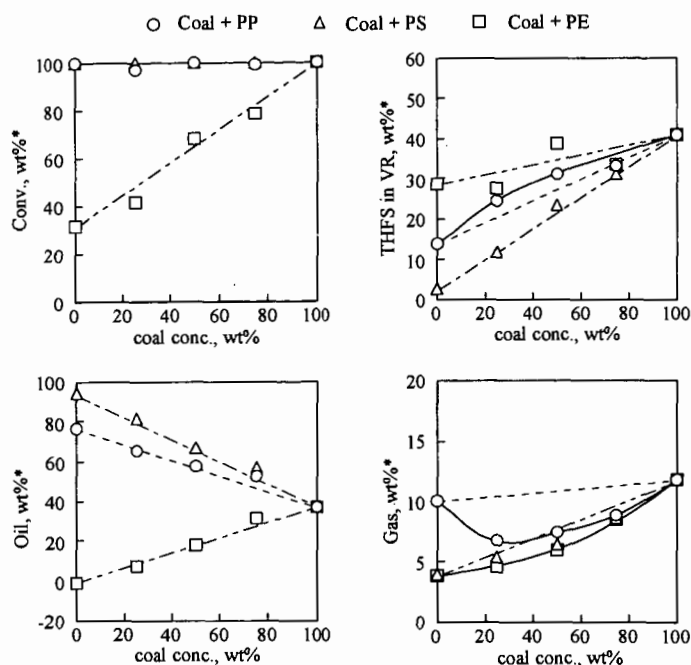


Fig.1 Coliquefaction of Tanitoharum coal with plastics using tetralin as the solvent at 430 °C for 60 min under 7 MPa initial pressure of hydrogen gas

* based on daf reactant

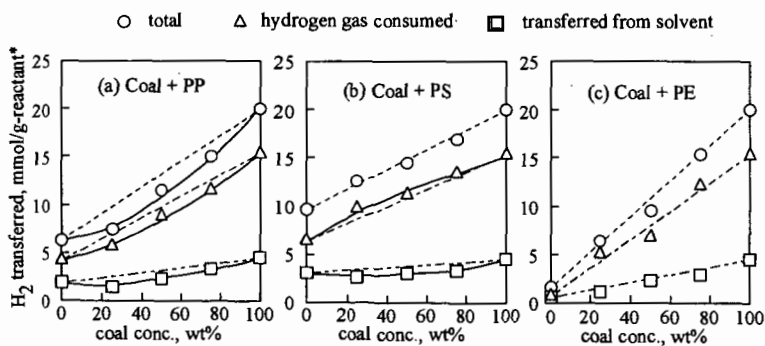


Fig.2 Hydrogen transfer under coliquefaction of Tanitoharum coal with plastics using tetralin as the solvent at 430 °C for 60 min under 7 MPa initial pressure of hydrogen gas

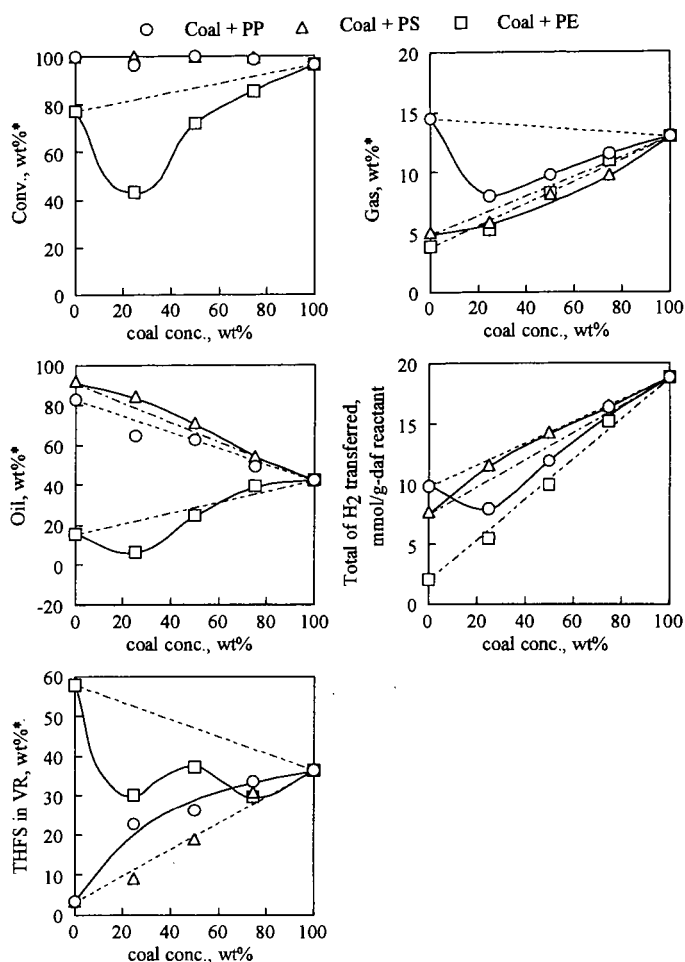


Fig.3 Coliquefaction of Tanitoharum coal with plastics using decalin as the solvent at 430 °C for 60 min under 7 MPa initial pressure of hydrogen gas

* based on daf reactant

Table 1 Coliquefaction of Tanitoharum coal with mixed plastics of PP, PS and PE at 430 °C for 60 min
(coal/mixed plastics = 1/1, PP/PS/PE = 1/1/1 (by weight))

| Solvent | Conv. (wt%) | THFS in VR (wt%) | Oil (wt%) | Gas (wt%) | Total of H ₂ transferred (mmol/g-daf reactant) | |
|----------|----------------|---------------------|--------------|--------------|--|------------------|
| Tetralin | 85.31 | 26.65 | 47.75 | 7.50 | 12.41 | observed |
| | 89.31 | 31.38 | 47.38 | 6.64 | 11.80 | cal ¹ |
| | 88.52 | 28.17 | 46.90 | 8.92 | 12.95 | cal ² |
| Decalin | 93.31 | 25.39 | 57.57 | 8.84 | 12.04 | observed |
| | 90.64 | 27.43 | 53.12 | 8.77 | 12.08 | cal ¹ |
| | 94.53 | 29.02 | 53.22 | 10.37 | 12.70 | cal ² |

¹ arithmetic mean value of results for the coal/PP, the coal/PS or the coal/PE (1/1 mixture)

² arithmetic mean value of results for each reactant

EFFECT OF VARIOUS ADDITIVES ON COAL EXTRACTION WITH CARBON DISULFIDE / *N*-METHYL-2-PYRROLIDINONE MIXED SOLVENT

Masashi Iino, Hideyuki Kurose, E. Sultan Giray, and Toshimasa Takanohashi
Institute for Chemical Reaction Science, Tohoku University,
Katahira, Aoba-ku, Sendai 980-8577, JAPAN

KEYWORDS: Coal extraction, additive, carbon disulfide / *N*-methyl-2-pyrrolidinone mixed solvent

INTRODUCTION

We have reported (1) that the extraction yield with carbon disulfide / *N*-methyl-2-pyrrolidinone (CS₂ / NMP) mixed solvent (1:1 by volume), which gave very high extraction yields for bituminous coals at room temperature (2), increases by the addition of a small amount of tetracyanoethylene (TCNE) to the solvent. The yield of the room temperature extraction of Upper Freeport coal with the 1:1 CS₂ / NMP mixed solvent increases from 59 wt% (daf) to 85 wt% (daf) by adding only 5% (based on coal) of TCNE to the mixed solvent. *p*-Phenylenediamine(PDA) is also an effective additive for the mixed solvent extraction (3).

We have also found (4) that when the extracts obtained with the CS₂/NMP mixed solvent were fractionated with pyridine to yield pyridine insoluble (PI) and soluble fractions, part of PI became insoluble in the mixed solvent. The addition of a small amount of TCNE, tetracyanoquinodimethane (TCNQ) or *p*-phenylenediamine to the mixed solvent, PI became soluble in the mixed solvent.

While, swelling and viscoelasticity behaviors of coal shows that coal has a kind of macromolecular network structure. The changes of this network structure were often quoted to explain the changes of reactivity and product selectivity of coal by heat or solvent treatment. But the nature of the macromolecular network structure are still unknown. Although covalently connected crosslinking structures are often assumed, the evidences for them are not enough. Recent works, including our results, suggest that for some bituminous coals, large associates of coal molecules i.e., non-covalent (physical) network are a better network model, than the covalent one. Coal extracts and coal-derived liquids are known to readily associate between themselves to form complex associates (5-8).

Solubility limit of coals, i.e., how high extraction yields can be obtained without the breaking of covalent bonds is one of the key points to clarify a kind of network bonds, i.e., covalent or non-covalent (physical) networks. If coal consists of highly developed covalent networks and low molecular weight substances occluded in them, coal extractability is low, as observed in the extraction with conventional solvents such as pyridine. However, 85wt% of the extraction yield obtained for CS₂ / NMP / TCNE solvent system described above suggests that Upper Freeport coal has little covalent networks. The reversibility of the effect of TCNE on the solubility increase for coal extracts (PI) was observed, indicating that no covalent bond breakings occur during this extraction(8).

In this study the effect of electron acceptors and donors on extraction yield of coal, and solubility of the extract component (PI) in the mixed solvent was studied. Formation of charge-transfer complex of TCNE with coal extracts was also investigated. Mechanisms for the enhancement of the extraction yield and the solubility by the additives are discussed.

EXPERIMENTAL

Extraction of coals with CS₂ / NMP mixed solvent

Six Argonne coals were used. The as-received coal samples (2.5 g) were extracted with 60 ml CS₂ / NMP mixed solvent (1:1, volume ratio) and an electron donor under ultrasonic irradiation for 30 min at room temperature (2). PDA, *N,N,N',N'*-tetramethyl-*p*-phenylenediamine (TMPDA), aniline and melamine were used as an electron donor. The quantity of electron donor was 10 - 100 mg/g-coal. For exhaustive extraction the extraction was repeated (usually 3 times) until the color of the extract solution almost disappeared. Extraction yields were determined from the amount of the residue, after the correction for water content in the coals.

Solubility of PI in CS₂ / NMP Mixed Solvent

The extracts obtained by the extraction of Upper Freeport (Argonne Premium coal, 86.2 wt% C(daf)) and Zao Zhuang (Chinese coal, 87.8 wt% C(daf)) coals with the CS₂ / NMP mixed solvent were fractionated to acetone soluble (AS), pyridine soluble/acetone insoluble (PS) and pyridine insoluble (PI) fractions, with acetone and pyridine, respectively (2). The yields of PI are about 30 and 40 wt% (daf coal base), for Upper Freeport and Zao Zhuang coals, respectively.

Solubility of PI in the mixed solvent with or without an electron acceptor was determined using 0.4g of PI and 50ml of the mixed solvent at room temperature under ultrasonic irradiation. The quantity of an electron acceptor added is 8×10^{-5} mol to 0.4g of PI. This quantity corresponds to

2.5wt% (10mg) to 0.4g of PI for TCNE. After the irradiation a centrifugation and filtration of the mixture were carried out, and the amount of the insoluble PI was determined. In the solubility experiments under nitrogen atmosphere all the procedures before a centrifugation were carried out in a glove box filled with nitrogen. The CS₂/NMP mixed solvent were also deaerated by passing nitrogen gas before use. While, solubility of PS and PI in THF or the mixed solvent with and without PDA were examined using 0.2 g of fraction and 50 ml of solvent at room temperature under ultrasonic irradiation. The amount of PDA added is 25 mg/g-PS.

Synthesis of Pyridinium 1,1,2,3,3-pentacyanopropenide (PPCP)

Pyridinium 1,1,2,3,3-pentacyanopropenide (PPCP) was synthesized from TCNE with water in the presence of a base (pyridine) in acetone at -50 °C (9).

RESULTTA AND DISCUSSION

Effect of a Kind of Electron Acceptors on Solubility of PI

Table 1 shows the solubility of PI from Zao Zhuang coal in the mixed solvent when various electron acceptors were added, together with their electron affinities, which are a measure of their electron acceptabilities, i.e., the degree of charge-transfer (donor-acceptor) complex formation with an electron donor. Table 1 shows that only TCNE and TCNQ gave high solubility as expected from their high electron affinities. The three electron acceptors which contain chlorine atom, i.e., DDQ, *p*-chloranyl and 2, 6-dichloro-*p*-benzoquinone shows much lower solubilities than those expected from their electron affinities. It could not clarify from this experiment whether charge-transfer interactions are responsible for the solubility enhancement by the addition of TCNE and TCNQ or not.

IR Study on Interaction of PI with TCNE

Figure 1 shows the result of the solubility experiments of PI from Zao Zhuang and Upper Freeport coals in the 1:1 CS₂ / NMP mixed solvent with or without TCNE. For Zao Zhuang coal a part (40.4%) of PI becomes insoluble in the mixed solvent, though PI is a part of the mixed solvent extract, but almost completely (97.6%) soluble in the mixed solvent containing TCNE, as already reported (4). For Upper Freeport coal (the data shown in the parenthesis in Figure 1) a similar result was obtained.

Figure 2 shows that FT-IR spectra of soluble and insoluble fractions of PI from Zao Zhuang coal in the CS₂ / NMP / TCNE solvent indicate the peak at 2200cm⁻¹ due to nitrile group of TCNE. The peak is much greater for the soluble PI than the insoluble PI. We also reported that the peak was almost disappeared by washing with pyridine(1). The removal of TCNE retained in the soluble PI, by washing with pyridine, resulted in the insolubilization in the CS₂ / NMP mixed solvent again i.e., 31.6% of PI became insoluble, but by the addition of TCNE 99.0% of PI became again dissolved in the mixed solvent (8).

The peak at 2200cm⁻¹ is considered to be that due to a charge-transfer complex of TCNE with the aromatic rings of coal (10, 11). Flowers et al. (11) proposed the formation of TCNE (and TCNQ) - coal complex in which TCNE accepts an electron from cooperated delocalized state of structure, not from individual independent aromatic structures of coal, since the shift of the nitrile peak from pure TCNE, about 36cm⁻¹ is unusually large, compared to that for TCNE - model aromatic compounds complex such as phenanthrene.

Figure 3(a) shows IR spectra of the solid obtained by the filtration of the mixture of PS with TCNE in acetone. Figure 3(a) shows the peak at 1500cm⁻¹ in addition to that at 2200cm⁻¹, as indicated in the literature (10). When this sample was washed several times with acetone, acetone soluble component was obtained. Its IR spectrum (Figure 3(b)) shows that the two peaks at 1500cm⁻¹ and 2200cm⁻¹ became predominant, suggesting that they come from some stable compound, which is not a charge transfer complex, since the peaks due to PS appeared in Figure 3(a) drastically decreased in Figure 3(b). Figure 3(c) shows that synthesized pyridinium 1,1,2,3,3-pentacyanopropenide (PPCP) has a similar spectrum as that of Figure 3(b). According to Middleton et al. (9), the hydrate of free PPCP acid, i.e., 1,1,2,3,3-pentacyanopropene dihydrate is a strong acid with pK_a of 1.9, and has also the peaks at 1500cm⁻¹ and 2200cm⁻¹ like PPCP. Although pyridine and water which need to get PPCP from TCNE are usually present in coal, we can not deny the possibility that other derivatives of PPCP has a similar peaks at 1500cm⁻¹ and 2200cm⁻¹.

PPCP was found to have a similar enhancement effect on the solubility of PI as TCNE, as shown in Figure 4. At present we consider that PPCP or its acid is formed through interaction of TCNE with coal molecules, resulting in the solubility increase of coal molecules.

Effect of Oxygen on Solubility of PI in CS₂ / NMP Mixed Solvent

Figure 4 shows that the removal of oxygen drastically decreases the solubility of PI, regardless of the presence of TCNE. Figure 4 further shows that the addition of PPCP increases the solubility to a similar degree as TCNE, and also decreases it under nitrogen atmosphere. Mechanisms of the enhancement of solubility by oxygen are not clear, but change of association state, i.e., change to smaller associates by the presence of oxygen, like TCNE, is conceivable. In

fact, oxygen is known to have charge transfer interaction with electron donors, and with strong donor oxygen radical anion forms. The occurrence of some chemical reaction such as covalent bond breaking by oxygen is unlikely, since PI was already in enough contact with oxygen during the extraction and subsequent solvent fractionation procedure through which PI was obtained, before this solubility experiment.

Effect of the Addition of Electron Donors on the Extraction Yield.

In Table 2, the yields of the exhaustive extraction of coals studied in the mixed solvent with and without PDA are given. It indicates that the addition of only 25 mg/g-coal of PDA increased extraction yield of Upper Freeport coal from 51.4% to 81.3%. The addition of PDA slightly increased the extraction yield of high-volatile coals. Increasing the amount of PDA to 100mg/g-coal did not increase the extraction yield.

In Table 3, the extraction yields of Upper Freeport coal when an electron donor added into the mixed solvent together with their ionization potentials are given. Table 3 indicates that there is no correlation between the ionization potential of the donors and the extraction yield. According to the ionization potential of TMPDA, it is expected to show higher extraction yield than those of PDA and aniline. However, it doesn't show a significant increase in the extraction yield.

Effect of PDA on the Solubility of Extract Fractions of Upper Freeport Coals.

The solubility of PS fraction of Upper Freeport coal increased 10% in the presence of PDA. PDA is also effective on the solubility of PI fraction of Upper Freeport coal. When we added only 5 mg / 0.2 g-PI of PDA into the mixed solvent, solubility of PI increased from 75.4 to 90.2%.

ACKNOWLEDGMENT

This work was supported by "Research for the Future" project of Japan Society for the Promotion of Science (JSPS).

REFERENCES

1. Liu, H., Ishizuka, T., Takanohashi, T. and Iino, M., *Energy Fuels*, **1993**, 7, 1108-1111.
2. Iino, M., Takanohashi, T., Osuga, H. and Toda, K., *Fuel*, **1988**, 67, 1639-1647.
3. Ishizuka, T., Takanohashi, T., Ito, O. and Iino, M. *Fuel*, **1993**, 72, 579-580.
4. Sanokawa, Y., Takanohashi, T. and Iino, M. *Fuel*, **1990**, 69, 1577-1578.
5. Sternberg, H. W., Raymond, R. and Schweighardt, F. K., *Science*, **1975**, 188, 49-51.
6. Stenberg, V. I., Baltisberger, R. J., Patel, K. M. et al., *Coal Science* (ed Gorbarty, M. L., Larsen, J. W., Wender, I.), Academic Press, New York, **1983**, pp 125-171.
7. Nakamura, K., Takanohashi, T., Iino, M. et al., *Energy Fuels*, **1995**, 9, 1003-1010.
8. Iino, M., Liu, H., Hosaka, N., Kurose, H. and Takanohashi, T., *Prepr. Pap. Am. Chem. Soc., Div. Fuel Chem.* **1997**, 42(1), 248-252.
9. Middleton, W. J., Little, E. L., Coffman, D. D. and Engelhardt, V. A. *J. Amer. Chem. Soc.* **1958**, 80, 2795-2806.
10. Schwager, I., Kwan, J. T., Miller, J. G. and Yen, T. F., *Prepr. Pap. Am. Chem. Soc., Div. Fuel Chem.* **1978**, 23(1), 284-289.
11. Flowers, II, R. A., Gebhard, L., Larsen, J. W. et al., *Energy Fuels*, **1994**, 8, 1524-1525.

Table 1. The effect of the addition of electron acceptors on the solubility^{a)} of PI from Zao Zhuang coal in CS₂/NMP mixed solvent at room temperature

| Electron acceptor | Solubility of PI (wt%) | Electron affinity ^{b)} (eV) |
|---|------------------------|--------------------------------------|
| None | 51.0 | — |
| Tetracyanoethylene(TCNE) | 99.5 | 2.2 |
| 7,7,8,8-Tetracyanoquinodimethane(TCNQ) | 81.0 | 1.7 |
| 2,3-Dichloro-5,6-dicyano- <i>p</i> -benzoquinone(DDQ) | 53.8 | 1.95 |
| 1,2,4,5-Tetracyanobenzene | 47.7 | 0.4 |
| <i>p</i> -Benzoquinone | 44.1 | 0.77 |
| 2,6-Dichloro- <i>p</i> -benzoquinone | 37.0 | 1.2 |
| <i>p</i> -Chloranil | 34.8 | 1.37 |

^{a)} Wt% of PI soluble in the mixed solvent when 8×10^{-3} mol of an electron acceptor was added to 0.4g of PI in 50ml of the mixed solvent ^{b)} Electron affinity of the electron acceptors

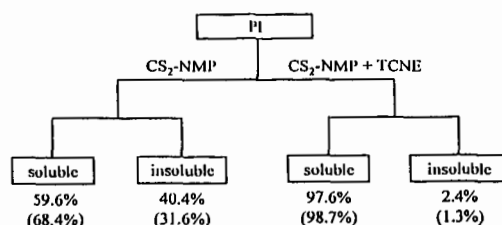


Figure 1. Solubility of PI from Zao Zhuang and Upper Freeport (shown in parenthesis) coals in CS₂/NMP mixed solvent with or without TCNE

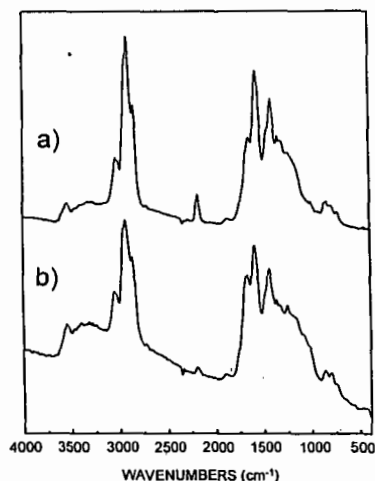


Figure 2. FT-IR spectra of soluble(a) and insoluble(b) fractions of PI from Zao Zhuang coal

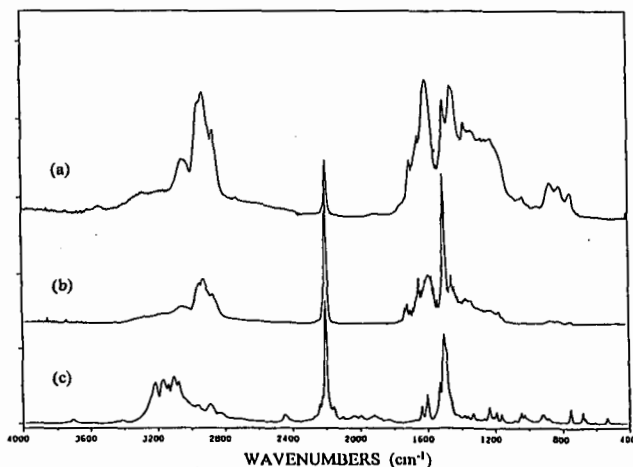


Figure 3. FT-IR spectra of the mixture(a) of PS from Upper Freeport coal with TCNE, its acetone soluble fraction (b), and Pyridinim 1,1,2,3,3-pentacyanopropenide(c)

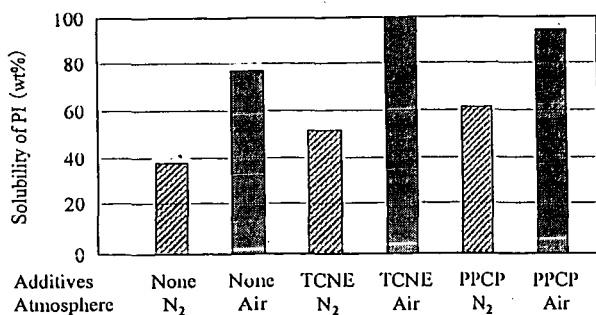


Figure 4. Solubility of PI from Upper Freeport coal in the CS₂/NMP mixed solvent under various conditions

Table 2. Effect of addition of *p*-phenylenediamine(PDA) on exhaustive extraction of Argonne coals with CS₂/NMP mixed solvent

| coal ^a | PDA (mg/g-coal) | extraction yield (wt%,daf) |
|-----------------------|--------------------|-------------------------------|
| Upper Freeport | none | 51.4 |
| | 25 | 81.3 |
| Blind Canyon | none | 36.3 |
| | 25 | 40.4 |
| Lewiston- Stockton | none | 24.6 |
| | 25 | 29.2 |
| Pittsburgh No.8 | none | 41.5 |
| | 25 | 44.4 |
| Illinois No.6 | none | 29.7 |
| | 35 | 34.8 |
| Wyodak- Anderson | none | 7.3 |
| | 50 | 11.9 |

^aas received

Table 3. Effect of addition of electron donors^a on single and exhaustive extraction of Upper Freeport coal with CS₂/NMP mixed Solvent

| electron donor | extraction yield (wt%,daf) | | ionization potential (eV) |
|----------------|-------------------------------|------------|------------------------------|
| | single | exhaustive | |
| none | 31.5 | 51.4 | |
| PDA | 61.2 | 81.3 | 6.87 |
| aniline | 32.5 | 72.3 | 7.7 |
| TMPDA | 42.3 | 61.4 | 6.5 |
| melaniline | 62.6 | - | - |

^a Amount of electron donors used is 25 mg/g-coal

CHARACTERIZATION OF UNSUPPORTED MoS_2 CATALYSTS BY CONTROLLED-
ATMOSPHERE PROGRAMMED-TEMPERATURE OXIDATION

B. BOCKRATH, R. LaCOUNT*, D. KERN*, D. PARFITT, E. FROMMELL, and
M. KELLER, III

US DEPARTMENT OF ENERGY
FEDERAL ENERGY TECHNOLOGY CENTER
PO BOX 10940
PITTSBURGH, PA 12356

*VIROLAC INDUSTRIES
403 ARBOR COURT
WAYNESBURG, PA 15370

Keywords: MoS_2 catalyst, CAPTO analysis, sulfur forms

INTRODUCTION

Controlled-atmosphere programmed-temperature oxidation, CAPTO, has been used as an effective tool for the quantitative determination and characterization of carbon, hydrogen, and sulfur in coal¹ and related materials.² This technique now has been applied here to provide unique, new information on the oxidation reactivity of sulfur in a variety of unsupported MoS_2 catalysts and of the carbonaceous deposits sometimes associated with them. In this application, the CAPTO analysis provides quantitative determination of three of the key elements in the structure of the working catalysts: sulfur, carbon, and hydrogen. Further, interpretation of the temperature profiles for the evolution of the oxides of these elements provides valuable information on the chemical state of these elements in the particular catalyst under study. This combination of information can shed more light on the structural differences among catalysts prepared by different methods and on the changes that may result from exposure to the processing conditions found under typical hydrotreating applications. To assess the potential of this analytical technique, a series of dispersed catalysts prepared by a variety of widely different methods was analyzed by CAPTO. The results indicate that the method is a useful, new means to characterize these materials.

Molybdenum disulfide has been used for a long time as the basis for many unsupported catalysts used for hydrotreating and related processing applications including direct coal liquefaction.³ Unsupported catalysts of this type have been prepared by various methods using any one of several molybdenum compounds as precursors. Promoted MoS_2 catalysts have been prepared by introducing minor amounts of other metals, primarily cobalt, nickel, or iron. In many cases, the catalyst is prepared *in situ* by the addition of a catalyst precursor just prior to the introduction of the feedstock to the hydrotreating reactor. Typically, this mode of preparation leads to a catalytic material that contains MoS_2 in close contact with a carbonaceous deposit.⁴ Alternatively, the MoS_2 may be generated separately and introduced to the reactor as a pure compound. Both approaches have been used in this work to generate a small set of catalysts of different crystallite sizes and with different degrees of crystallinity. In particular, the exfoliation and restacking technique^{5,6,7,8} has proven to be very valuable as a means to manipulate the structure of MoS_2 . Analysis of these materials by CAPTO provided "fingerprints" of the susceptibility of the sulfur in these catalysts to oxidation. Comparison of the different fingerprints from each sample indicated that the relative prominence of characteristic peaks may be related to the individual history of the catalyst's preparation and use.

EXPERIMENTAL

The CAPTO apparatus has been described previously.¹ Briefly, the sample is mixed with an inert diluent, WO_3 , and packed in a quartz tube. The device heats the sample according to a programmed temperature ramp, typically 3°C min^{-1} . In these analyses, a stream of 100% oxygen was passed through the sample plug. The gas flow was regulated by a mass flow controller. Complete combustion of the gases from the primary reactor was obtained by passage through a secondary catalytic reactor held at 1050°C . An FTIR was used to monitor the exit stream for CO_2 , SO_2 , and H_2O . The detector response was calibrated, allowing the final output to be plotted in terms of the mass of each element evolved as a function of sample temperature. Integration of the area under the curves provided the total mass of each element evolved from a sample, and thus the elemental analysis for carbon, hydrogen, and sulfur. Information

about the chemical forms in which these elements exist in the sample was available from the recorded temperature profiles. The total envelope for each gas was resolved by a peak fitting program into a set of individual peaks, each centered about a characteristic temperature. Experience obtained from the analyses of a wide variety of coals and well-characterized reference materials has made possible the association of the various characteristic temperatures with different chemical forms of the elements. For example, aromatic carbon is readily distinguished from other forms of carbon, and may be quantitatively determined.

CAPTO analysis was carried out on a series of fresh and used catalysts prepared by different methods. Exfoliation techniques were used as one means to manipulate the physical and chemical properties of MoS₂ catalysts. This method has been used to disassemble highly crystalline MoS₂ to form single layers suspended in water, followed by restacking of the layers to regenerate MoS₂ in a less-ordered crystalline form. The experimental procedures used here have been reported in a study of the application of this technique to generate MoS₂ catalysts for use in coal liquefaction and petroleum resid upgrading.^{7,8}

The exfoliated/restacked catalysts used here were prepared by first intercalating a commercial sample of MoS₂ (Alpha) with Li by reduction with 2.5 M n-butyllithium in hexanes (Aldrich) for two or three days in a glove box. The intercalated solid was filtered, dried, then removed from the glove box and added to water agitated by an ultrasonic bath. On addition to water, a suspension developed which is typically associated with the formation of single layer MoS₂. The suspension settled on standing as the restacking of MoS₂ proceeded. The restacked material was filtered, washed, and dried under vacuum.

An *in situ* preparation method was used as another route to MoS₂. A mixture of 4 g dodecane, 2 g pyrene, 0.3 g sulfur, and 0.5 g ammonium molybdate (2.43 mmole Mo) dissolved in 3 g water was added to a 40 mL high-pressure microautoclave. The vessel was pressurized with 500 psig hydrogen, heated to 380 °C over the course of about 1 h, then held at this temperature for another 1 h. Agitation was provided by shaking the reactor. After cooling, the catalyst was recovered by filtration, washed with tetrahydrofuran, and dried under vacuum.

An example of a used catalyst was obtained by recovering it after a standard test for hydrotreating activity.⁸ A mixture of 0.32 g exfoliated/restacked MoS₂, 3.23 g tetralin, and 3.0 g Hondo resid was added to a 40 mL microautoclave. The reactor was charged with 1000 psig hydrogen and heated over the course of about 1 h to 425 °C, then held at this temperature for another 1 h. The reactor was quenched in water, and the product analyzed by determination of heptane solubility using a pressure filtration method. The catalyst was recovered by washing the heptane insoluble portion with tetrahydrofuran, again using the pressure filtration method. The recovered catalyst was dried in a vacuum oven.

The catalysts were also examined by other methods to obtain comparative data, including SEM, X-ray diffraction, BET surface areas, and elemental analyses.

RESULTS AND DISCUSSION

Sulfur Profiles. The same highly crystalline sample of MoS₂ used as the starting material for the exfoliation/restacking method of catalyst preparation was analyzed by CAPTO to provide a reference. The sulfur profile is shown in Fig. 1A. SO₂ evolved producing a broad envelope of peaks beginning about 220 °C and ending by 580 °C. The shape of the whole complex envelope was well simulated by a combination of four peaks. The central temperature and relative area associated with each peak is given in Table 1. The majority of sulfur in this sample lies under the peak at highest temperature, centered around 507 °C. The general appearance and wide breadth of the total sulfur profile reflects considerable variability in sulfur oxidation reactivity. The separation of the total envelope into a series of separate peaks gives evidence that the sulfur contained in the single compound, MoS₂, may be consist of several distinct populations, each associated with a characteristic oxidation temperature.

The sulfur profile for the exfoliated/restacked sample of MoS₂ is given in Fig. 1B. The considerable change in physical structure induced by this treatment is reflected by a profoundly different sulfur profile. The broad envelope of this new profile begins at about 220 °C, just as it does with the highly crystalline starting material. However, the majority of sulfur dioxide from the restacked material evolves at comparatively lower temperatures and the profile already returns to baseline by about 500 °C rather than 580 °C. That means the major oxidative event was complete before

reaching the temperature of the maximum rate of SO_2 evolution observed for the highly crystalline starting material. The large envelope was again very broad and could be resolved into four individual peaks. The pronounced shift to lower oxidation temperatures after exfoliation/restacking implies that the degree of crystallinity of the catalyst is a major factor governing the reactivity of sulfur in MoS_2 toward oxidation. In addition, a small isolated peak centered at 628°C now also appears. Peaks in this area are often associated with metal sulfates.

A third sample was investigated to determine the effect of exposure to hydrotreating conditions on the exfoliated/restacked catalyst. An exfoliated/restacked catalyst sample prepared in the same way as described above was used in hydrotreating Hondo resid⁸ under the conditions summarized in the experimental section. The sulfur profile is given in Fig. 1C. Compared to the fresh catalyst, the center of gravity of the major peak has moved to a higher temperature. However, the endpoint of the major peak still comes at about 500°C , just as with the fresh exfoliated/restacked catalyst. The major envelope of the used catalyst could be resolved using three peaks rather than the four required for fresh catalyst. The three peaks of the used catalyst correspond rather well with three peaks of the fresh catalyst in terms of temperature and width. Comparison of the areas under the peaks reveals that the exposure to hydrotreating conditions for even only a single activity test made the recovered catalyst somewhat more resistant to oxidation. It should be noted that the CAPTO analysis for carbon demonstrated negligible amounts of coke were deposited on this sample. The possibility that sulfur in coke laid down by the Hondo resid contributed to the CAPTO profile for sulfur may be dismissed in this case.

The sulfur evolution profile of the catalyst prepared from ammonium molybdate by the *in situ* method was also obtained (not shown) for comparison to the previous samples. In contrast to both the highly crystalline and the exfoliated/restacked catalysts, the sulfur evolution profile for the MoS_2 catalyst derived from ammonium molybdate is dominated by a low temperature envelope. Again, individual peaks were resolved, five in this case. A difference was found in the atypical breadth of the peak centered at 429°C , which extensively overlapped two neighboring major peaks with widths more typical of the narrow peaks seen in the analyses of other samples of MoS_2 . These four CAPTO analyses demonstrate that there is a wide variation in the reactivity of sulfur in MoS_2 toward oxidation. Furthermore, the fingerprint characteristics obtained by CAPTO are related to the method of catalyst preparation and its history under processing conditions.

Table 1 contains the temperature and the relative amount of sulfur evolved for each peak for all four samples. When the resolved peaks are arranged in this way, it is apparent that there are corresponding peaks among the samples that have similar temperatures for peak maxima and generally similar widths. The CAPTO analyses give evidence that differences in the physical structure of MoS_2 are associated with differences in the distribution of sulfur among several characteristic types. Correlation with X-ray diffraction data, discussed below, shows that the relative amount of sulfur under peaks at higher oxidation temperatures increases with the degree of crystallinity.

Profound differences in crystallinity among the four MoS_2 catalysts became readily evident on comparison of their X-ray diffraction patterns. The highly ordered, three-dimensional structure of the original MoS_2 was apparent from the narrow peaks that compose the diffraction pattern. The 002 line was particularly prominent and narrow. The diffractogram of the exfoliated/restacked material was markedly different. Its broad lines were consistent with a turbostratic structure, indicating that order along the dimension of the stacking plane had been lost. The width of the 002 line at half-height was used to estimate the stacking heights of the crystallites for each sample. The changes in line width indicated that the exfoliation/restacking process reduced the average stacking height from 325 \AA to 185 \AA . An increased degree of crystallinity (loss of turbostratic disorder) was observed for the exfoliated/restacked catalyst recovered after hydrotreatment. However, the changes were modest, and the stacking height remained essentially unchanged at 185 \AA . The catalyst prepared *in situ* presented yet another picture. The 002 peak was the broadest of the four samples, yielding an estimate for average stacking height of 27 \AA . The XRD data thus confirmed that this set of four catalysts exhibits a wide range of crystallinity. When the XRD results are compared with the distributions of sulfur among the various CAPTO peaks, it is evident that the MoS_2 samples of lesser crystallinity and composed of smaller crystallites also have a larger portion of more readily oxidized sulfur.

CONCLUSIONS

The CAPTO technique provides important information about dispersed molybdenum sulfide catalysts. First, the method provided useful basic information in the form of the quantitative determination of the elements sulfur, carbon, and hydrogen, although these data were not discussed here. More importantly, the various patterns for sulfur oxidation with temperature observed for dispersed catalysts prepared by different means and of different crystalline structure indicate the method is quite sensitive to physical characteristics of each catalyst sample. This technique offers the potential for following changes in catalyst structure throughout the course of its preparation and use. Detailed correlation of the shapes of the SO_2 evolution profiles with catalyst activity is not yet possible with the small set of samples investigated so far. However, higher activity has been observed for the exfoliated/restacked catalysts as opposed to the highly crystalline sample¹⁰. The catalyst prepared by the *in situ* method appears to be as active as the exfoliated/restacked example. In general, it appears that higher activity may be associated with a less ordered and more easily oxidized structure.

REFERENCES

- * E-mail: bockrath@fetc.doe.gov
- (1) LaCount, R. B.; Anderson, R. R.; Friedman, S.; Blaustein, B. D. *Fuel* **1987**, *66*, 909-913.
 - (2) LaCount, R. B.; Kern, D. G.; King, W. P.; LaCount, R. B. Jr.; Miltz, D. J.; Stewart, A. L.; Trulli, T. K.; Walker, R. K. *Prepr. Pap.-Am. Chem. Soc., Div. Fuel Chem.* **1991**, *36*, 1217-1224.
 - (3) LaCount, R. B.; Kern, D. G.; King, W. P.; Trulli, T. K.; Walker, D. K. *Prepr. Pap.-Am. Chem. Soc., Div. Fuel Chem.* **1992**, *37*, 1083-1086.
 - (4) Weller, S. W. *Energy Fuels* **1994**, *8*, 415-420.
 - (5) Bearden, R.; Aldridge, C. L. *Energy Prog.* **1981**, *1*, 44-48.
 - (6) Miremadi, B. K.; Morrison, S. R. *J. Catal.* **1987**, *103*, 334-345.
 - (7) Joensen, P.; Frindt, R. F.; Morrison, S. R. *Mat. Res. Bull.* **1986**, *21*, 457-461.
 - (8) Yang, D.; Frindt, R. F. *Prepr. Pap.-Am. Chem. Soc., Div. Petr. Chem.* **1994**, *39*, 612-617.
 - (9) Bockrath, B. C.; Parfitt, D. S. *Catal. Letts.* **1995**, *33*, 210-207.
 - (10) Bockrath, B. C.; Parfitt, D. S. *Proc. Int. Conf. Coal Sci.* **1995**, *2*, 1343-1346.
 - (11) LaCount, R. B.; Kern, D. G.; King, W. P.; LaCount, R. B. Jr.; Miltz, D. J. Jr.; Stewart, A. L.; Trulli, T. K.; Walker, D. K.; Wicker, R. K. *Fuel* **1993**, *72*, 1203-1208.

DISCLAIMER

Reference in this work to any specific commercial product is to facilitate understanding and does not necessarily imply endorsement by the United States Department of Energy.

Table 1. Characteristic Temperatures of Sulfur Evolution for MoS_2 Catalysts.¹

| DESCRIPTION | PEAK TEMPERATURES, °C | | | | | |
|---|-----------------------|---------------|---------------|--------------------------------|---------------|--------------|
| | 1 | 2 | 3 | 4 | 5 | 6 |
| CRYSTALLINE MoS_2 | | 301 (2.7) | 384 (3.0) | 440 (28.5) | 507 (65.7) | |
| EXFOLIATED/ RESTACKED | 244 (2.1) | 299 (2.2) | 371 (15.4) | 417 (76.6) | | 628 (3.7) |
| RECOVERED AFTER HYDROTREATMENT | | 289 (9.1) | 381 (2.0) | 425 (86.3) | | 600 (2.6) |
| PREPARED IN-SITU FROM AmMo | | 272 (50.8) | 382 (23.9) | 429 (10.1) 456 (14.2) | | 575 (1.0) |

1. Central temperature of peaks from curve-fit. Area per cent in parentheses.

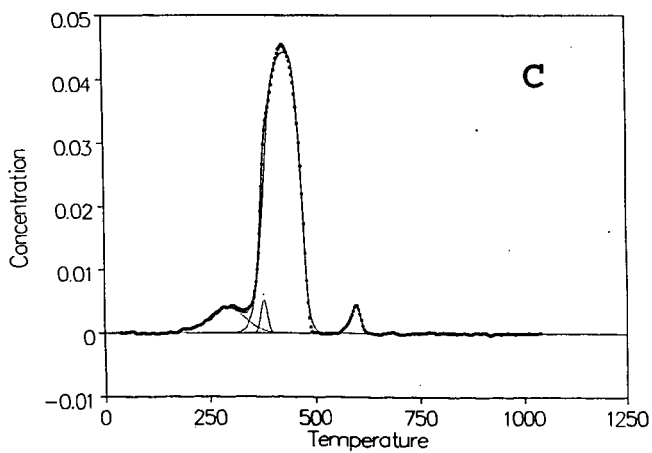
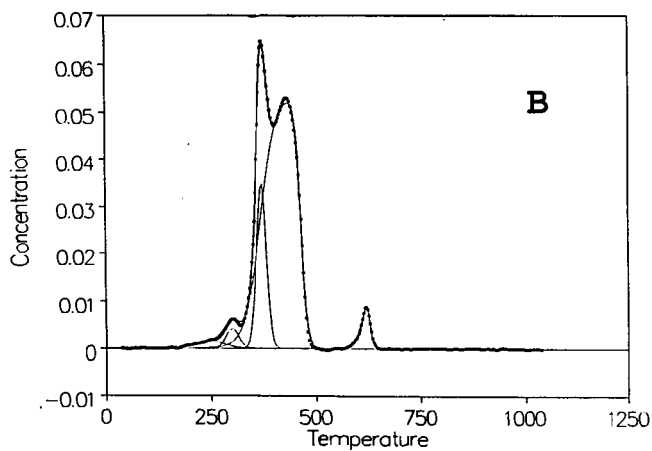
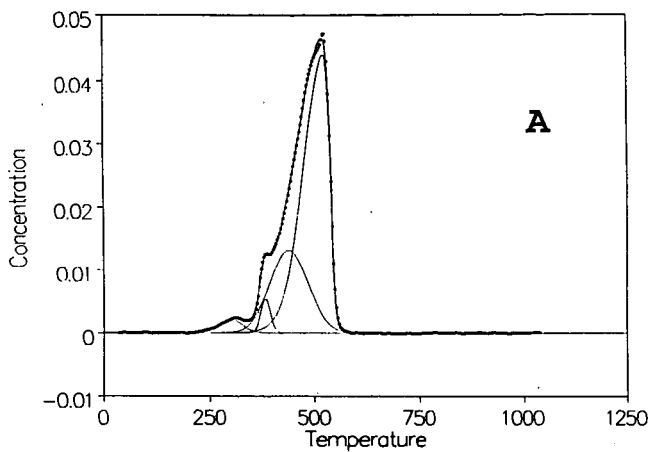


Fig. 1. CAPTO profiles of SO_2 evolution from MoS_2 . **A.** Crystalline MoS_2 . **B.** Exfoliated/restacked catalyst derived from sample A. **C.** Exfoliated/restacked catalyst recovered after use in hydrotreating Hondo resid.

HYDROCARBON SYNTHESIS FROM DIMETHYL ETHER OVER ZSM-5 CATALYST

Abhay Sardesai and Sunggyu Lee
Department of Chemical Engineering
The University of Missouri-Columbia
Columbia, MO 65211

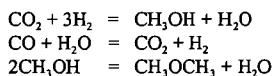
ABSTRACT

The liquid phase synthesis of dimethyl ether from syngas has significant advantages over the liquid phase methanol synthesis in the areas of syngas conversion and reactor productivity. The merits of this dual catalytic process allows dimethyl ether to be utilized as a viable feedstock for petrochemical synthesis. In particular, dimethyl ether can be converted to hydrocarbons using H-ZSM-5 type zeolite catalysts. Appropriate choice of the acidity of the zeolite catalyst as well as the operating parameters such as reaction temperature, partial pressure and space velocity of dimethyl ether dictate the product spectrum, ranging from lower olefins (ethylene and propylene) to gasoline-range hydrocarbons. The focus of this paper is to thoroughly study the aforementioned details of this process and compare its merits with methanol conversion.

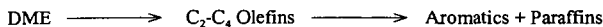
INTRODUCTION

The synthesis of petrochemicals from syngas via methanol has been the focus of research in the chemical industry for several decades. Methanol synthesis from syngas is a well established technology (Lee, 1990). However, the methanol synthesis technology faces a serious impediment because the reaction is severely limited by chemical equilibrium. Due to the reversible nature of the methanol synthesis reaction, the maximum per-pass conversion of syngas is restricted. However, the potential of the reverse reaction and the chemical equilibrium limitation can be alleviated by chemically converting methanol into another chemical species that is not affected by the equilibrium constraint. The in-situ dehydration of methanol to dimethyl ether (DME) is based on this approach.

Of particular interest is the novel process that has been developed by Lee and his co-workers for the co-production of dimethyl ether and methanol from syngas (Lee, 1992). This liquid phase dimethyl ether (LPDME) process consists of a dual-catalytic synthesis in a single reactor stage. Methanol is synthesized over coprecipitated Cu/ZnO/Al₂O₃ catalyst, whereas dimethyl ether synthesis takes place over γ -alumina catalyst. The reactions take place in a liquid phase system involving inert hydrocarbon oil such as Witco-40, Witco-70, Freccene-100, etc. Various aspects of the methanol synthesis reaction and the co-production of dimethyl ether reaction have been assessed for commercialization of the process (Gogate, 1992). The process merits such as reactor productivities, catalyst life and activity, etc. were significantly higher in the co-production case. For high productivity cases using very high weight hourly space velocities of syngas, the single-stage productivity can be increased by as much as 70%. In terms of catalyst deactivation, the rate of thermal aging of methanol synthesis catalyst becomes slower when it is used in a co-production mode along with γ -alumina. Moreover, the process exhibits excellent control because it is possible to co-produce dimethyl ether and methanol in any desired proportion, from 5% DME to 95% DME, by varying the mass ratios of the methanol synthesis catalyst to the methanol dehydration catalyst. From the economic point of view, dimethyl ether produced from syngas is substantially cheaper than methanol synthesis on a methyl productivity basis. This cost benefit and enhanced effectiveness provides an alternative route to produce a variety of petrochemicals from DME as a starting raw material. The process chemistry is as follows:



Synthesis of lower olefins from methanol over ZSM-5 catalyst has been investigated in detail (Chang, 1983). Lower olefins synthesis from methanol over smaller pore size ZSM-34 catalyst has also been studied (Givens, 1978). Selective conversion of dimethyl ether to lower olefins is a process of growing potential in the chemical industry. Lower olefins are intermediates in the conversion of dimethyl ether to hydrocarbons over ZSM-5 type zeolite catalysts. The reaction pathway can be represented as follows:



Of particular interest is the synthesis of ethylene and propylene from dimethyl ether because of their growing demand as raw materials for a number of petrochemicals. Besides chemicals like ethylene oxide, ethylene glycol, propylene oxide, etc. these olefins are the building blocks for the production of their respective polymers, polyethylene and polypropylene. These polymers are widely used in everyday life applications such as molded plastic items, plastic packaging films, etc. Increasing demand for isobutene is inevitable since isobutene is used as the raw material for MTBE (methyl tert-butyl ether), a high octane gasoline blending oxygenate. Isobutene is also used in the manufacture of methyl methacrylate and isoprene. 1-Butene and 2-Butenes are important ingredients in the synthesis of methyl ethyl ketone. Thus, lower olefins have varied usage in the chemical industry, and so the research devoted toward their production from non-petroleum sources is of economic interest.

EXPERIMENTAL

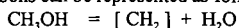
A schematic of the DME-to-hydrocarbons experimental system is shown in Figure 1. The system can be divided into several sections: feed gas blending section, reaction section, and product separation and analysis section. The feed gas section consists of three mass flow controllers for DME, nitrogen, and carbon dioxide, respectively. A fixed bed reactor 18" in length and 0.5" I.D., manufactured by Autoclave Engineers has been utilized for this study. An axial thermowell runs the entire length of the tube and allows for measurement of the temperature profile in the reactor. The reactor tube is completely filled with 1/16" inert ZrO₂ beads. These beads are highly thermally stable and facilitate heat transfer from the beaded heater to the catalyst. Use of the beads in the reaction zone also helps dilute the reaction exotherm and therefore helps maintain a uniform temperature profile.

The feed gas analysis (DME, nitrogen and in some cases, carbon dioxide and methanol) as well as the analysis of the hydrocarbon product (C₁-C₅ range) was carried out using gas chromatography. The gas samples were withdrawn from the system using a constant rate 50 µl Hamilton syringe, as well as gas sampling bags. The liquid hydrocarbon product (C₅⁺ paraffins and aromatics) was analyzed using gas chromatography/mass spectrometry.

RESULTS AND DISCUSSION

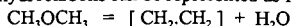
The assessment of process feasibility of DME conversion to lower olefins, particularly ethylene and propylene, has been carried out over ZSM-5 type zeolite catalysts (Sardesai, 1997). The results obtained from this research have revealed important relevant information about this process. Over the conventional ZSM-5 catalyst (SiO₂/Al₂O₃ ratio of 150), lower olefin (C₂-C₄) selectivity of 70 wt.% of total hydrocarbons was achieved. One of the salient features of this process is that it can be customized to target an individual olefin in the C₂-C₄ range at the expense of the other lower olefins. Process parameters such as operating temperature, partial pressure of DME, contact time, and catalyst acidity were evaluated over a limited range in light of maximizing lower olefin selectivity at optimal conditions. The results indicated that the temperature of the reaction has to be kept high, the partial pressure of DME has to be kept low, and the contact time of the reactants with the catalyst has to be kept low as shown in Figures 2-4. The concentration of strong Bronsted acid sites on the ZSM-5 catalyst has to be kept low by maintaining a lower SiO₂/Al₂O₃ ratio as shown in Figure 5. Also, the pore size of the catalyst has to be small enough to control the product spectrum on the higher end, and has to be large enough not to be a target of rapid deactivation by coking. Optimum results for lower olefin synthesis were obtained using the following parameters: Temperature = 430C, vol% Nitrogen in Feed = 65%, weight hourly space velocity of DME = 30 h⁻¹, SiO₂/Al₂O₃ ratio of ZSM-5 catalyst = 150.

Methanol conversion to hydrocarbons can be represented as follows:



where [CH₂] is the average representation of the hydrocarbon product. The conversion is essentially complete and stoichiometric. The above reaction shows a 44% selectivity by weight toward hydrocarbons, and a 56% selectivity toward water.

Dimethyl ether conversion to hydrocarbons can be represented as follows:



where [CH₂, CH₂] is the average representation of the hydrocarbon product. The conversion is essentially complete and stoichiometric. The above reaction shows a 60.8% selectivity by weight toward hydrocarbons, and a 39.2% selectivity toward water. Thus at nominally identical conditions, the selectivity toward hydrocarbons is 38% higher in the dimethyl ether conversion case as compared to the methanol conversion process (Lee, 1996).

In the methanol to hydrocarbons process, methanol formed from syngas first dehydrates to dimethyl ether in the first, and then an equilibrium mixture of methanol, dimethyl ether, and water is converted in the second reactor to form hydrocarbons. The exothermic of reaction is -398 cal/g methanol converted. The

methanol dehydration step of the reaction liberates 15% of the reaction heat, whereas the rest is given off in the latter step. In the dimethyl ether to hydrocarbons process, the exothermic heat liberated is only 85% of that of the methanol conversion process. This is because dimethyl ether is produced in the syngas reactor, whereas, in the methanol case, dimethyl ether is produced in the dehydration reactor. Thus, the heat management is better in the dimethyl ether conversion process. In addition to this, it obviates the need of a dehydration reactor thereby causing considerable saving in capital investments and working capital.

Dimethyl ether can also be converted to gasoline-range hydrocarbons using ZSM-5 catalysts of very high acidity ($\text{SiO}_2/\text{Al}_2\text{O}_3$ ratio of 30). The experimental and testing results have been very promising from a commercial standpoint. A U.S. patent for the process has been issued (Lee, 1995).

CONCLUSIONS

As a long term commodity chemical, dimethyl ether is proving to be one of the chemical industry's most dynamic product. It can be produced from any fossil fuel source. It finds use as an alternate fuel, as well as a chemical feedstock. Technical and market application efforts are proceeding at a great pace on both its production and uses on an international basis. Dimethyl ether can be easily converted to ethylene and propylene, the building blocks of the chemical industry, using this process which has distinct advantages over methanol conversion. Thus, natural gas-based syngas can be converted to hydrocarbons via dimethyl ether as an intermediate using zeolite catalysts. The merits of this process are very attractive and have been investigated in detail for pre-scale up assessment. The demonstrated process feasibility and excellence are novel and very promising in developing alternative sources for lower olefins.

REFERENCES

- Chang, C. D., "Hydrocarbons from Methanol", Catal. Rev. Sci. Eng., vol. 25, n 1, pp 1-118, 1983.
 Givens, E., U. S. Patent, 4,079,096. 1978.
 Gogate M., "A Novel Single-Step Dimethyl Ether Synthesis from Syngas", Ph.D. Dissertation, The University of Akron, 1992.
 Lee, S., "Methanol Synthesis Technology", CRC Press, Boca Raton, FL, 1990.
 Lee, S., "A Novel DME Synthesis process in a three phase Slurry Reactor from CO-rich Syngas", Chem. Eng. Sci., vol. 47, n 13/14, pp 3769-3776, 1992.
 Lee, S., U.S. Patent, 5,459,166. 1995.
 Lee, S., "Methanol-to-Gasoline vs. DME-to-Gasoline. II. Process Comparison and Analysis", Fuel Science & Technology International, vol. 13, n 8, pp 1039-1058, 1995.
 Sardesai, A., "Catalytic Conversion of Dimethyl Ether to Lower Olefins: Process and Catalyst Deactivation Studies", Ph.D. Dissertation, The University of Akron, 1997.

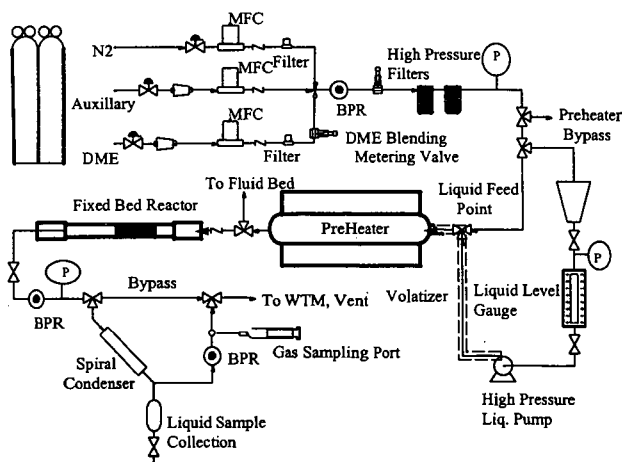


Figure 1. Schematic of the Dimethyl Ether (DME) to Hydrocarbons Experimental Unit.

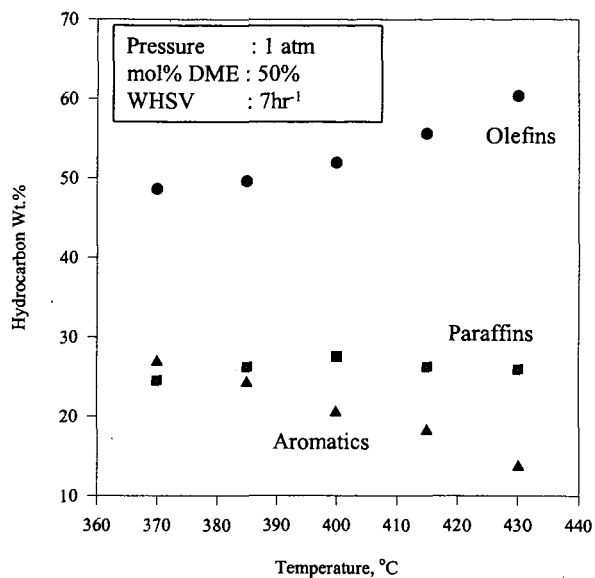


Figure 2. Effect of Reaction Temperature on Hydrocarbon Selectivity

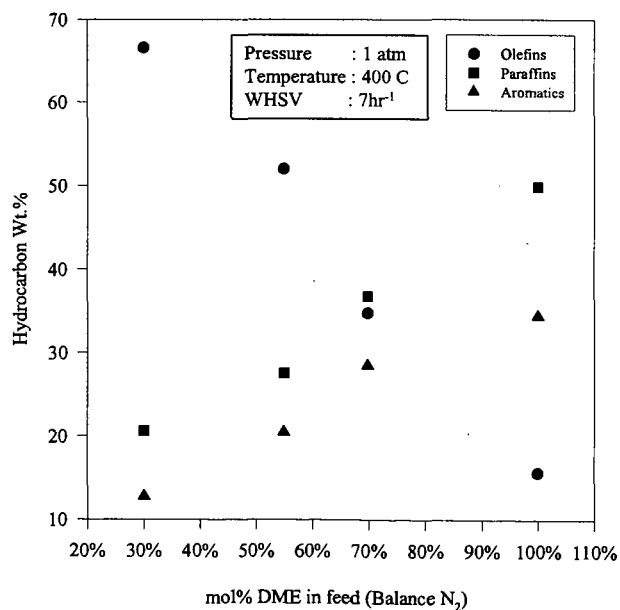


Figure 3. Effect of Feed Dilution on Hydrocarbon Selectivity

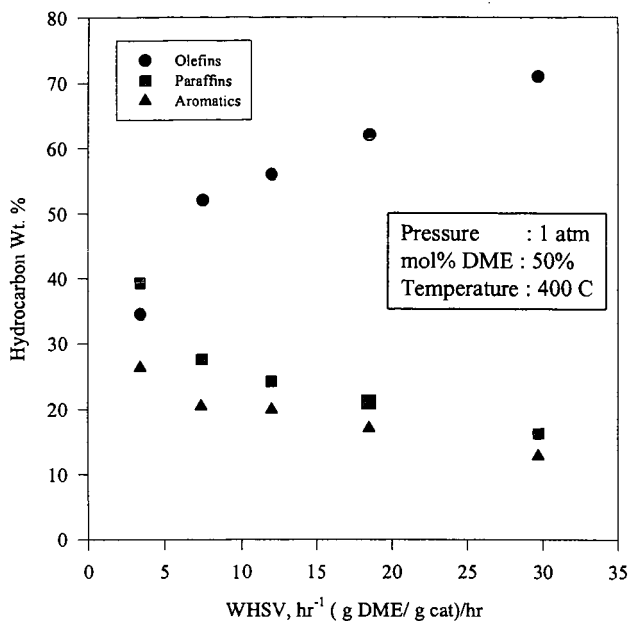


Figure 4. Effect of Space Velocity on Hydrocarbon Selectivity

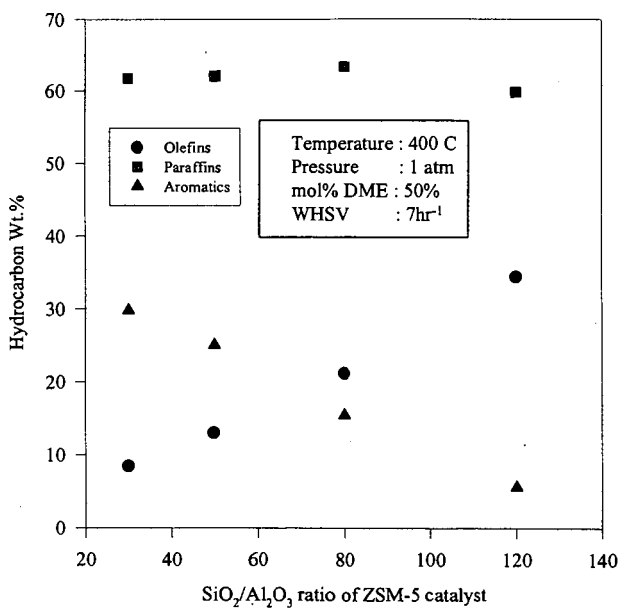


Figure 5. Effect of Zeolite Acidity on Hydrocarbon Selectivity

BIAS TESTING OF MECHANICAL AUTOMATIC SAMPLING SYSTEM INSTALLED AT LAXT FOR LOADING EXPORT COALS AND PETROLEUM COKES

Jun M. Lee, Jeffrey G. Rolle, James J. Baker, Robert Llerena
A. J. Edmond Co., 1530 West 16th Street, Long Beach CA 90813
Jim Holland, Los Angeles Export Terminal, Inc., San Pedro, CA 90731
Robert White, Pacific Carbon Services, Inc., San Pedro, CA 90731
Wendell Cook, Hall-Buck Marine, Inc., San Pedro, CA 90731

Keywords: coal, bias test, mechanical sampling

ABSTRACT

A new modern LAXT (Los Angeles Export Terminal) facility was built in September 1997 and has been operational for export shipment of coals and petroleum cokes. Recently on March 16-18, 1998, bias testing of the mechanical automatic sampling system, which is installed at LAXT for representative sampling, was performed by A. J. Edmond Company to evaluate the performance of the mechanical sampler. The bias test was carried out loading 86600 metric tons of coal in M/V Noshiro Maru. Thirty sets of system (crushed), reference (stopped-belt) and secondary cutter reject (backup) samples were collected for bias analysis. Paired test batch design is employed for sample collection procedure and Walsh averages, non-parametric method is selected for statistical analysis. Test batch size was 2670 metric tons and target coal transfer rate was 4500 metric-tons/hr. Coal characteristics analyzed for the bias test are moisture and dry ash content. In addition size consist analysis will be performed, if necessary to identify sources causing biases. Based on the statistical analysis, bias test results are presented.

INTRODUCTION

The LAXT is a coal and petroleum coke receiving, handling and exporting facility located at the Port of Los Angeles' Pier 300 on Terminal Island. The facility is owned by LAXT, Inc., a consortium of 37 shareholders representing the entire coal chain from the coal mines to power plants and operated by Pacific Carbon Services and Hall-Buck Marine. Throughput capacity is 10 million metric tons of product per year with expansion potential to 18 million metric tons.

Export quality of coals was reported at the ACS Las Vegas Meeting (September 7-11, 1997), based on bituminous coal properties determined for M/V ship samples and subbituminous coal properties from western coal round robin samples [1].

Theory involved in non-parametric statistical method for bias analysis can be found in the literature [2,3,4]. Walsh averages, non-parametric method has been practiced in bias analysis of mechanical coal sampling [5,6,7] and methods for mechanical sampling from moving streams of coal are available in American Society for Testing and Materials (ASTM) Standard [8] and International Standard [9].

The objective of this study is to determine the absence or presence of bias of the mechanical automatic sampling system located at the LAXT facility, based on matched-pair experimental designs. Coal sample collection and statistical evaluation procedures must be chosen before the bias test is conducted. The overall bias of the mechanical sampling system is determined. After collection, the test samples (reference, system and backup) are prepared and analyzed using applicable ASTM test methods for coal characteristics such as moisture, dry ash and size consist.

Details of statistical analysis methodology, experimental data obtained from the bias test, and bias test operating conditions are described in the following sections.

SELECTION OF BIAS TEST METHOD

Paired-test batch design is selected for sample collection procedure. The procedure is designed for the overall system test at normal mode of operation. Test batch size was approximately 2670 metric-tons interval. Thirty (30) sets of test samples including stopped-belt reference, mechanically collected system and secondary cutter reject (for backup) were collected for this bias study, loading 86600 metric tons of coal in M/V Noshiro Maru.

The Walsh averages non-parametric method is used for statistical analysis. The median of sorted differences is taken as the point estimate of bias. Two-sided confidence limits for multivariate analysis for two variables, moisture and dry ash are obtained based on the Bonferroni

inequality [10]. Interpretation of the results depends on whether or not the confidence interval of any one of the variables encompasses zero for the multivariate case. Ten (10) statistical analyses calculating Walsh averages were performed for this bias test, comparing bias among three collected samples (reference, system and backup). Two (2) statistical calculations for moisture and dry ash content were made comparing mechanical system samples against stopped-belt reference samples; two (2) calculations comparing secondary cutter reject (backup) samples against stopped-belt reference samples; two (2) calculations comparing mechanical system samples against secondary cutter reject samples (as a new reference); and four (4) additional calculations to evaluate outliers arbitrarily defined for this bias test.

GUIDELINE USED IN TEST PREPARATION

The bias test was prepared considering the following guideline and criteria.

- (1) Coal to be tested with consistent quality
- (2) Coal characteristics to be analyzed (ASTM Methods)

| | |
|--------------|--------|
| Moisture | D 3302 |
| Dry Ash | D 3174 |
| Size Consist | D 4749 |
- (3) No change in sampler operation mode and coal transfer rate
- (4) Same width of stopped-belt (SB) divider plates ($\geq 6"$)
- (5) Minimum 20 minutes interval between SB reference increments
- (6) Approximately equal amount of laboratory sample prepared from both system and reference samples
- (7) Number of paired data sets, initially 20-40 sets of data
- (8) Approximately same batch size throughout the entire test period

TEST OPERATING CONDITIONS AND PROCEDURE

Each test batch was carefully controlled to meet operating criteria set for the test. Daily operating log was prepared for the test and actual operating data were recorded for test monitoring. Planned target conditions are listed below.

| | |
|-----------------------------|---|
| Coal type: | fuel-grade bituminous coal |
| Feed rate: | 4500 metric-tons/hr (4000-6000 range) |
| Test batch size: | 2670 metric-tons/hr (approximately every 36 min operation) |
| Test lot size: | 86600 metric tons |
| Stopped-belt (SB) interval: | once per batch |
| SB sampling time: | 10-15 min at each stop |

As planned thirty (30) sets of samples were collected for the entire test period. SB reference samples were collected within 15 min using a sampling divider as soon as the main conveyor stopped. SB sampling location was about 30 feet downstream after the mechanical automatic sampler. Samples of secondary cutter reject stream (backup) accumulated three times of separate collections for each test batch duration. Mechanical system samples were automatically collected in carousel cans. Each test batch consists of approximately 20-25 lbs of mechanical system, 80-100 lbs of SB reference, and 80-100 lbs secondary cutter reject (backup) sample.

During the bias test coal transfer rate maintained most of time in the range of 3500 to 5500 metric-tons/hr. The test was occasionally interrupted due to unavoidable hold changes and lunch breaks. Other than that the operation was very smooth with exception for one major plugging in the mechanical sampler occurred in Test Batch No. 6 and several minor operational problems experienced for the entire test period. The bias test was successfully complete in five 8-hrs shifts.

During startup of Test Batch No. 6, the mechanical sampler was plugged due to buildup of crushed material from the secondary cutter to crusher and further to carousel can. This buildup was caused by the main conveyor stop at the end of Test Batch No. 5 to collect the stopped-belt reference sample while the mechanical sampler was purging the sampling system. Approximately two (2) hours was spent to clear the plug. In addition the conveyor gate was not properly operational for the test. Test Batch No. 6 aborted and declared as not-for-bias-test (NBT) and sampling was continued for lot analysis only.

In Test Batch No. 19 the first portion of the period loading 1515 metric-tons was not included for the bias test and declared as NBT due to the morning shift break from 0300 to 0800 in the middle

of the test. Sampling was continued for lot analysis only. However, the second portion of the period loading 1316 metric-tons was included for the bias test and officially designated as Test Batch No. 19, which is used for statistical analysis.

Between Test Batch No. 28 and 29 the period loading 331 metric tons was not included for the bias test due to hold change. Sampling was discontinued for this period.

Test Batch No. 31 and 33 were not for bias test (NBT) although test serial numbers were given for convenience identifying samples for lot analysis only. The main conveyor was not stopped during these periods to collect the stopped-belt reference sample. Test Batch No. 32 was official for the bias test.

Operating conditions of the mechanical sampler was set as typical, normally practiced for ship loading at LAXT, at timer settings, 42 sec for primary, 7 sec for secondary and 14 sec for tertiary cutter, respectively. All operating data indicated that ASTM D 2234 ("Standard Test Methods for Collection of a Gross Sample of Coal") minimum increment requirement for individual cutter was met. The ASTM minimum requirements for the consignment lot of 8830 short tons are 104 increments for primary and 624 increments for secondary cutter, respectively.

ANALYTICAL DATA FOR COAL CHARACTERISTICS

Laboratory analysis samples for thirty (30) collected samples, total ninety different samples were prepared following the procedures listed in the ASTM D 2013, "Standard Method of Preparing Coal Samples for Analysis." Analyses of each sample were performed to determine air-dried loss, residual moisture and ash content following the procedures listed in the ASTM D 3302 and D 3174. Then total moisture and dry ash were calculated and reported for statistical analysis. Repeatability and reproducibility checks for ash content was carried out for samples from Test # 27, 28 and 30 (stopped-belt, stopped-belt and secondary cutter reject sample, respectively). For the first raw data with these samples showed significant deviation (difference) of ash content by 2 to 5% compared to 0 to 1.5% normally observed with other samples. Test # 30 sample (secondary cutter reject) was also rechecked and reported although the deviation (difference) of first raw data was smaller (1.3%).

STATISTICAL ANALYSIS DATA (WALSH AVERAGES)

Three different cases were evaluated for statistical bias analysis as described below. Selection of pairs from thirty (30) available pairs was based on 95% confidence interval ($\pm 2\sigma$). This initial screening of the data (reducing # of pairs) was done for the purpose of eliminating outliers. Test for independent differences was performed in each analysis. The sample differences must be independent to correctly draw inference about system bias using this method. So far all cases evaluated for this bias study has passed the test for independent differences.

The Walsh averages non-parametric method is based on creating a super-set of the population of differences by differencing every possible combination of the observed differences and sorting them in ascending order. For instance with a set of thirty ($n=30$) pairs of differences Walsh averages are 465 values [$w = n(n+1)/2$].

Mechanical System Vs. Stopped-Belt Reference Samples

Using raw data screened at a 95% confidence level (29 pairs of moisture and 28 pairs of dry ash values), statistical analysis and bias test results of mechanical system samples against stopped-belt reference samples are summarized below. An example of the Walsh averages method procedure (steps) is shown in Tables 1-4 comparing moisture content.

| | |
|----------|--|
| Table 1: | Observed Data, Difference, Run #, Median |
| Table 2: | Test for Independence Differences |
| Table 3: | Sorted Walsh Averages |
| Table 4: | Point Estimate of Bias (Median) and Confidence Interval (Concluding Statements for Bias Test) |

Bias test results with these samples are:

- A) If a chance error with a maximum probability prior to the test of no more than about 1 out of 20, did not occur, biases of mechanically collected samples against stopped-belt reference samples lie within the closed intervals given below:
- Moisture $-0.300 < B(m) < 0.345$

Dry Ash (data under evaluation)

where $B(m)$ and $B(da)$ are point estimates of bias for moisture and dry ash, respectively. $B(m) = 0.005$, $B(da) =$ (data under evaluation).

- B) The confidence interval for moisture includes the value zero. Thus, this test offers insufficient evidence to reject a hypothesis of no bias of system samples against stopped-belt reference samples.

Secondary Cutter Reject (Backup) Vs. Stopped-Belt Reference Samples

Using raw data screened at a 95% confidence level (29 pairs of moisture and 27 pairs of dry ash values), statistical analysis and bias test results of secondary cutter reject (backup) samples against stopped-belt reference samples are:

- A) If a chance error with a maximum probability prior to the test of no more than about 1 out of 20, did not occur, biases of secondary cutter reject (backup) samples against stopped-belt reference samples lie within the closed intervals given below:

| | |
|----------|--------------------------|
| Moisture | $-0.315 < B(m) < 0.245$ |
| Dry Ash | $-0.150 < B(da) < 0.480$ |

where $B(m)$ and $B(da)$ are point estimates of bias for moisture and dry ash, respectively. $B(m) = -0.030$, $B(da) = 0.1875$.

- B) The confidence interval for each coal characteristic includes the value zero. Thus, this test offers insufficient evidence to reject a hypothesis of no bias of secondary cutter reject (backup) samples against stopped-belt reference samples.

Mechanical System Vs. Secondary Cutter Reject (New) Reference Samples

Using raw data screened at a 95% confidence level (28 pairs of moisture and 29 pairs of dry ash values), statistical analysis and bias test results of mechanical system samples against secondary cutter reject (new) reference samples are:

- A) If a chance error with a maximum probability prior to the test of no more than about 1 out of 20, did not occur, biases of mechanical system samples against secondary cutter reject (new) reference samples lie within the closed intervals given below:

| | |
|----------|--------------------------|
| Moisture | $-0.215 < B(m) < 0.165$ |
| Dry Ash | $-0.050 < B(da) < 0.520$ |

where $B(m)$ and $B(da)$ are point estimates of bias for moisture and dry ash, respectively. $B(m) = -0.0025$, $B(da) = 0.238$.

- B) The confidence interval for each coal characteristic includes the value zero. Thus, this test offers insufficient evidence to reject a hypothesis of no bias of mechanical system samples against secondary cutter reject (new) reference samples.

EVALUATION OF OUTLIERS

Two different statistical analyses were additionally performed to evaluate outliers arbitrarily defined for this bias test (95% confidence level). Sources of variability are coal quality, loading rate and operating conditions, analysis sample preparation, analytical methods, sample handling and storage, etc.

Using revised data from repeated ash values for Test # 27, 28, 30 and 32 (30 pairs of dry ash values), outliers for dry ash content were evaluated with secondary cutter reject samples and mechanical system samples against stopped-belt reference samples, respectively. The evaluation was designed to sensitivity affected by reducing laboratory analytical errors and increasing # of pairs. Additional outlier evaluation was performed with mechanical system samples against stopped-belt reference samples, using raw data screened with difference less than 1% (25 pairs of moisture and 24 pairs of dry ash values). The additional evaluation was designed to sensitivity affected by reducing # of pairs using majority of data, 80 to 85%, with smaller differences. Implication is to see sensitivity affected by reducing combined process operational and laboratory analytical errors.

The outlier evaluation shows a significant band reduction in the bias confidence interval by 0.045 to 0.135% absolute (about 10-20% of magnitude). Improvement in accuracy and precision can be achieved by eliminating or minimizing process operational and/or laboratory analytical errors.

SUMMARY OF TEST RESULTS

The following is a summary of major findings obtained from the bias test:

- Five out of six statistical analysis results include no bias in the confidence interval calculated.
- Bias analysis result with moisture content includes no bias when compared mechanical system samples against stopped-belt reference samples.
- Both bias analysis results with moisture and dry ash content include no bias when compared secondary cutter reject samples against stopped-belt reference samples.
- Both bias analysis results with moisture and dry ash content include no bias when compared mechanical system samples against secondary cutter reject (new) reference samples.
- Evaluation of outliers indicates that a significant band reduction in the bias confidence interval can be achieved by eliminating or minimizing process operational and/or laboratory analytical errors. This results in better accuracy and precision of bias test. The observed reduction of confidence interval varies in the range of 0.045 to 0.135% absolute (by about 10-20% of magnitude).

Based on the above findings, the following is recommended for future additional bias test.

- To perform dynamic (improved) bias test around secondary cutter and crusher components using paired increment design. This test will not require stopping the main conveyor; thus no interruptions will occur in loading. Specifically ash content will be analyzed for bias test. If necessary, size consist analysis will be performed additionally to pinpoint biases.
- To calculate biases for comparison using different statistical analysis methods such as ISO 9411, parametric methods, etc.

ACKNOWLEDGMENT

A. J. Edmond Company and Hall-Buck Marine staff, who participated in this bias test, are acknowledged.

REFERENCES

1. J. M. Lee, J. J. Baker, R. Llerena, J. G. Rolle, 214th American Chemical Society National Meeting, Las Vegas, Preprints of Symposia, Division of Fuel Chemistry, Vol. 42, No. 3, 844-853 (1997).
2. R. H. Randles, Encyclopedia of Statistical Sciences, Vol. 9, Wiley, New York, NY, 124-129 (1988).
3. N. L. Johnson and F. C. Leone, Statistics and Experimental Design, Vol. I, 2nd Ed., New York, NY, Chapter 9 (1977).
4. M. Holland and D. A. Wolfe, Non-parametric Statistical Methods, Wiley, New York, NY, 35-38 (1973).
5. A. M. Long, J. B. Long Company, private communication.
6. P. Reagan, Sampling Associates International, private communication.
7. C. D. Rose, The Journal of Coal Quality, Vol. 9, No. 4, 124-129 (1990).
8. ASTM D 2234.
9. International Standard, ISO 9411-1:1994(E).
10. F. B. Alt, Encyclopedia of Statistical Sciences, Vol. 1, Wiley, New York, NY, 294-300 (1982).

Table 1. Observed Moisture Values

| Run # | Mech | | Above + Below - | Ordered Sample Differences |
|-------|--------|-------|--------------------|----------------------------------|
| | SB Ref | Systm | Sys-Ref Median | |
| 1 | 8.81 | 10.45 | 0.64 | 1 |
| 2 | 10.47 | 10.13 | -0.34 | 2 |
| 3 | 10.66 | 10.06 | -0.68 | 2 |
| 4 | 11.87 | 11.04 | -0.83 | 2 |
| 5 | 11.95 | 11.53 | 0.48 | 3 |
| 6 | 11.96 | 11.16 | 0.10 | 4 |
| 7 | 10.76 | 10.81 | -0.14 | 4 |
| 8 | 10.33 | 10.72 | -0.21 | 4 |
| 9 | 10.16 | 10.63 | 0.47 | 6 |
| 10 | 10.81 | 10.66 | -0.35 | 6 |
| 11 | 10.24 | 10.80 | 0.56 | 7 |
| 12 | 11.95 | 10.81 | -1.14 | 8 |
| 13 | 10.30 | 10.68 | 0.28 | 8 |
| 14 | 10.31 | 10.16 | -0.13 | 10 |
| 15 | 12.99 | 11.37 | -1.62 | 10 |
| 16 | 11.20 | 12.70 | 1.50 | 11 |
| 17 | 12.80 | 11.92 | -0.88 | 12 |
| 18 | 11.27 | 10.69 | -0.58 | 12 |
| 19 | 11.16 | 10.63 | -0.53 | 12 |
| 20 | 10.11 | 10.54 | 0.43 | 13 |
| 21 | 11.00 | 10.90 | -0.20 | 14 |
| 22 | 11.01 | 10.44 | -0.57 | 14 |
| 23 | 11.00 | 11.53 | 0.53 | 15 |
| 24 | 10.81 | 11.22 | 0.81 | 15 |
| 25 | 10.76 | 11.31 | 0.66 | 15 |
| 26 | 11.33 | 11.49 | 0.16 | 15 |
| 27 | 10.79 | 11.80 | 1.01 | 15 |
| 28 | 11.14 | 11.52 | 0.38 | 15 |
| 29 | 11.37 | 11.84 | 0.47 | 15 |

Median 11.000 10.800 0.100
Average 10.886 11.001 0.005
STDEV 0.705 0.616 0.873

Table 2. Test for Independent Differences

| Test criteria are: If $r < -u$, passed and the sample differences are independent. If $r < l$, or $r > u$, failed and the process is viewed as inconclusive. | | | | | | | | | |
|---|-------|-------|-------|-----|-----|------------|--------|--|--|
| r | 0.1 | 0.2 | 0.5 | 1 | u | P or F | | | |
| 15 | 14 | 14 | 14 | 2 | 10 | 20 | passed | | |

Legend: r = number of runs
 p = number of coal characteristics tested
 n_1 = number of forest like signs
 n_2 = number of most like signs
 l = lower significance value
 u = upper significance value

Table 4. Point Estimate of Bias (Median) and Confidence Interval

| Point estimate of bias = 0.005 median = 218th ordered value | | | | |
|--|-----|-----|--------|-------|
| Confidence Interval | | | | |
| d = counting value | | | | |
| L_d = the d th smallest value = 114th ordered value = -0.300 | | | | |
| U_d = the d th largest value = 322th ordered value = 0.345 | | | | |
| n | p | d | L_d | U_d |
| 28 | 2 | 114 | -0.300 | 0.345 |
| Closed Confidence Interval [L_d, U_d] | | | | |
| [-0.300, 0.345] | | | | |

Table 3. Sorted Walsh Averages for Moisture

| <u>Order</u> | <u>W</u> | <u>Order</u> | <u>W</u> | <u>Order</u> | <u>W</u> | <u>Order</u> | <u>W</u> | <u>Order</u> | <u>W</u> |
|--------------|----------|--------------|----------|--------------|----------|--------------|----------|--------------|----------|
| 1 | -1.620 | 54 | -0.570 | 107 | -0.335 | 160 | -0.130 | 213 | -0.010 |
| 2 | -1.380 | 55 | -0.490 | 108 | -0.335 | 161 | -0.125 | 214 | -0.010 |
| 3 | -1.250 | 56 | -0.555 | 109 | -0.330 | 162 | -0.125 | 215 | -0.010 |
| 4 | -1.140 | 57 | -0.550 | 110 | -0.330 | 163 | -0.120 | 216 | -0.005 |
| 5 | -1.125 | 58 | -0.545 | 111 | -0.310 | 164 | -0.105 | 217 | 0.000 |
| 6 | -1.105 | 59 | -0.545 | 112 | -0.305 | 165 | -0.100 | 218 | 0.005 |
| 7 | -1.100 | 60 | -0.540 | 113 | -0.305 | 166 | -0.100 | 219 | 0.010 |
| 8 | -1.095 | 61 | -0.540 | 114 | -0.300 | 167 | -0.095 | 220 | 0.010 |
| 9 | -1.075 | 62 | -0.535 | 115 | -0.295 | 168 | -0.095 | 221 | 0.010 |
| 10 | -1.010 | 63 | -0.530 | 116 | -0.290 | 169 | -0.090 | 222 | 0.015 |
| 11 | -0.985 | 64 | -0.530 | 117 | -0.280 | 170 | -0.080 | 223 | 0.015 |
| 12 | -0.980 | 65 | -0.520 | 118 | -0.275 | 171 | -0.080 | 224 | 0.015 |
| 13 | -0.915 | 66 | -0.510 | 119 | -0.275 | 172 | -0.080 | 225 | 0.015 |
| 14 | -0.910 | 67 | -0.505 | 120 | -0.270 | 173 | -0.075 | 226 | 0.020 |
| 15 | -0.885 | 68 | -0.505 | 121 | -0.265 | 174 | -0.075 | 227 | 0.020 |
| 16 | -0.880 | 69 | -0.490 | 122 | -0.265 | 175 | -0.075 | 228 | 0.025 |
| 17 | -0.880 | 70 | -0.490 | 123 | -0.265 | 176 | -0.070 | 229 | 0.030 |
| 18 | -0.875 | 71 | -0.485 | 124 | -0.250 | 177 | -0.065 | 230 | 0.040 |
| 19 | -0.865 | 72 | -0.470 | 125 | -0.245 | 178 | -0.060 | 231 | 0.040 |
| 20 | -0.860 | 73 | -0.465 | 126 | -0.245 | 179 | -0.060 | 232 | 0.045 |
| 21 | -0.855 | 74 | -0.465 | 127 | -0.240 | 180 | -0.060 | 233 | 0.060 |
| 22 | -0.835 | 75 | -0.460 | 128 | -0.240 | 181 | -0.055 | 234 | 0.080 |
| 23 | -0.760 | 76 | -0.460 | 129 | -0.240 | 182 | -0.055 | 235 | 0.060 |
| 24 | -0.755 | 77 | -0.455 | 130 | -0.235 | 183 | -0.055 | 236 | 0.065 |
| 25 | -0.745 | 78 | -0.440 | 131 | -0.235 | 184 | -0.055 | 237 | 0.065 |
| 26 | -0.740 | 79 | -0.440 | 132 | -0.235 | 185 | -0.050 | 238 | 0.065 |
| 27 | -0.735 | 80 | -0.435 | 133 | -0.215 | 186 | -0.050 | 239 | 0.065 |
| 28 | -0.730 | 81 | -0.420 | 134 | -0.215 | 187 | -0.050 | 240 | 0.065 |
| 29 | -0.730 | 82 | -0.415 | 135 | -0.210 | 188 | -0.050 | 241 | 0.070 |
| 30 | -0.725 | 83 | -0.400 | 136 | -0.210 | 189 | -0.050 | 242 | 0.085 |
| 31 | -0.705 | 84 | -0.395 | 137 | -0.205 | 190 | -0.050 | 243 | 0.090 |
| 32 | -0.680 | 85 | -0.395 | 138 | -0.205 | 191 | -0.045 | 244 | 0.090 |
| 33 | -0.675 | 86 | -0.390 | 139 | -0.205 | 192 | -0.045 | 245 | 0.095 |
| 34 | -0.670 | 87 | -0.390 | 140 | -0.205 | 193 | -0.045 | 246 | 0.095 |
| 35 | -0.640 | 88 | -0.390 | 141 | -0.200 | 194 | -0.040 | 247 | 0.100 |
| 36 | -0.635 | 89 | -0.385 | 142 | -0.200 | 195 | -0.040 | 248 | 0.100 |
| 37 | -0.630 | 90 | -0.385 | 143 | -0.185 | 196 | -0.035 | 249 | 0.100 |
| 38 | -0.620 | 91 | -0.380 | 144 | -0.186 | 197 | -0.030 | 250 | 0.105 |
| 39 | -0.615 | 92 | -0.380 | 145 | -0.175 | 198 | -0.030 | 251 | 0.105 |
| 40 | -0.610 | 93 | -0.370 | 146 | -0.175 | 199 | -0.030 | 252 | 0.110 |
| 41 | -0.610 | 94 | -0.365 | 147 | -0.170 | 200 | -0.025 | 253 | 0.110 |
| 42 | -0.605 | 95 | -0.365 | 148 | -0.170 | 201 | -0.025 | 254 | 0.115 |
| 43 | -0.600 | 96 | -0.360 | 149 | -0.170 | 202 | -0.025 | 255 | 0.120 |
| 44 | -0.595 | 97 | -0.360 | 150 | -0.165 | 203 | -0.025 | 256 | 0.125 |
| 45 | -0.590 | 98 | -0.360 | 151 | -0.165 | 204 | -0.020 | 257 | 0.130 |
| 46 | -0.585 | 99 | -0.355 | 152 | -0.165 | 205 | -0.020 | 258 | 0.130 |
| 47 | -0.580 | 100 | -0.355 | 153 | -0.180 | 206 | -0.020 | 259 | 0.130 |
| 48 | -0.580 | 101 | -0.355 | 154 | -0.180 | 207 | -0.020 | 260 | 0.130 |
| 49 | -0.580 | 102 | -0.350 | 155 | -0.155 | 208 | -0.020 | 261 | 0.135 |
| 50 | -0.575 | 103 | -0.350 | 156 | -0.140 | 209 | -0.015 | 262 | 0.135 |
| 51 | -0.575 | 104 | -0.345 | 157 | -0.135 | 210 | -0.015 | 263 | 0.135 |
| 52 | -0.575 | 105 | -0.340 | 158 | -0.135 | 211 | -0.015 | 264 | 0.135 |
| 53 | -0.670 | 106 | -0.335 | 159 | -0.135 | 212 | -0.015 | 265 | 0.140 |

Table 3. Sorted Walsh Averages for Moisture (continued)

| <u>Order</u> | <u>W</u> | <u>Order</u> | <u>W</u> | <u>Order</u> | <u>W</u> | <u>Order</u> | <u>W</u> |
|--------------|----------|--------------|----------|--------------|----------|--------------|----------|
| 266 | 0.145 | 319 | 0.330 | 372 | 0.505 | 425 | 0.985 |
| 267 | 0.150 | 320 | 0.330 | 373 | 0.505 | 426 | 0.985 |
| 268 | 0.160 | 321 | 0.335 | 374 | 0.505 | 427 | 0.990 |
| 269 | 0.160 | 322 | 0.345 | 375 | 0.510 | 428 | 1.010 |
| 270 | 0.165 | 323 | 0.345 | 376 | 0.510 | 429 | 1.015 |
| 271 | 0.165 | 324 | 0.360 | 377 | 0.510 | 430 | 1.020 |
| 272 | 0.165 | 325 | 0.355 | 378 | 0.515 | 431 | 1.025 |
| 273 | 0.165 | 326 | 0.355 | 379 | 0.515 | 432 | 1.030 |
| 274 | 0.170 | 327 | 0.360 | 380 | 0.515 | 433 | 1.055 |
| 275 | 0.170 | 328 | 0.365 | 381 | 0.520 | 434 | 1.255 |
| 276 | 0.170 | 329 | 0.365 | 382 | 0.520 | 435 | 1.500 |
| 277 | 0.170 | 330 | 0.370 | 383 | 0.530 | | |
| 278 | 0.170 | 331 | 0.380 | 384 | 0.535 | | |
| 279 | 0.175 | 332 | 0.385 | 385 | 0.540 | | |
| 280 | 0.175 | 333 | 0.395 | 386 | 0.540 | | |
| 281 | 0.175 | 334 | 0.400 | 387 | 0.540 | | |
| 282 | 0.180 | 335 | 0.400 | 388 | 0.540 | | |
| 283 | 0.180 | 336 | 0.405 | 389 | 0.545 | | |
| 284 | 0.180 | 337 | 0.405 | 390 | 0.545 | | |
| 285 | 0.190 | 338 | 0.405 | 391 | 0.545 | | |
| 286 | 0.195 | 339 | 0.410 | 392 | 0.550 | | |
| 287 | 0.200 | 340 | 0.425 | 393 | 0.550 | | |
| 288 | 0.200 | 341 | 0.425 | 394 | 0.555 | | |
| 289 | 0.200 | 342 | 0.430 | 395 | 0.555 | | |
| 290 | 0.205 | 343 | 0.430 | 396 | 0.560 | | |
| 291 | 0.205 | 344 | 0.435 | 397 | 0.570 | | |
| 292 | 0.205 | 345 | 0.435 | 398 | 0.575 | | |
| 293 | 0.210 | 346 | 0.435 | 399 | 0.575 | | |
| 294 | 0.210 | 347 | 0.440 | 400 | 0.580 | | |
| 295 | 0.210 | 348 | 0.450 | 401 | 0.580 | | |
| 296 | 0.210 | 349 | 0.450 | 402 | 0.585 | | |
| 297 | 0.215 | 350 | 0.455 | 403 | 0.585 | | |
| 298 | 0.215 | 351 | 0.455 | 404 | 0.610 | | |
| 299 | 0.220 | 352 | 0.455 | 405 | 0.635 | | |
| 300 | 0.235 | 353 | 0.460 | 406 | 0.645 | | |
| 301 | 0.240 | 354 | 0.460 | 407 | 0.650 | | |
| 302 | 0.240 | 355 | 0.465 | 408 | 0.680 | | |
| 303 | 0.240 | 356 | 0.465 | 409 | 0.685 | | |
| 304 | 0.280 | 357 | 0.470 | 410 | 0.695 | | |
| 305 | 0.265 | 358 | 0.470 | 411 | 0.720 | | |
| 306 | 0.270 | 359 | 0.470 | 412 | 0.740 | | |
| 307 | 0.285 | 360 | 0.470 | 413 | 0.740 | | |
| 308 | 0.285 | 361 | 0.475 | 414 | 0.745 | | |
| 309 | 0.290 | 362 | 0.475 | 415 | 0.770 | | |
| 310 | 0.295 | 363 | 0.480 | 416 | 0.775 | | |
| 311 | 0.310 | 364 | 0.480 | 417 | 0.760 | | |
| 312 | 0.315 | 365 | 0.485 | 418 | 0.765 | | |
| 313 | 0.315 | 366 | 0.485 | 419 | 0.800 | | |
| 314 | 0.315 | 367 | 0.490 | 420 | 0.810 | | |
| 315 | 0.320 | 368 | 0.495 | 421 | 0.830 | | |
| 316 | 0.320 | 369 | 0.495 | 422 | 0.880 | | |
| 317 | 0.320 | 370 | 0.500 | 423 | 0.940 | | |
| 318 | 0.325 | 371 | 0.500 | 424 | 0.985 | | |

STRUCTURAL ANALYSIS OF ASPHALTENES IN PETROLEUM HEAVY OILS BY LASER DESORPTION MASS SPECTROMETRY

M. Fujii, Y. Sanada and T. Yoneda,
Advanced Catalysts Research Laboratory, Petroleum Energy Center
KSP D-1237, 3-2-1, Sakato, Takatsu-ku, Kawasaki, Kanagawa 213-0012, Japan

M. Sato
Center for Advanced Research of Energy Technology
Hokkaido University, Kita-13, Nishi-8, Kita-ku
Sapporo, 060-8628, Japan

Key words: laser desorption mass spectrometry, asphaltenes, type analysis

INTRODUCTION

Asphaltenes are obtained as the precipitates when adding alkane to heavy oil such as vacuum residue, which are defined as n-heptane insoluble-toluene soluble, for example. For the reason of their heavy characteristics, they are a major component that occurs the deactivation of catalyst under the hydrotreating reaction, and make troubles such as the pipe plugging by forming sludges at the transportation. A number of analyses have been made by using many kinds of measurements, and many structure models have been proposed(1,2). In spite of these efforts, there have not been well-defined structures yet. Having the strong interaction of molecules for its chemical structure, they aggregate to form micelles as high-dimension structure in oil(3). Therefore, this would make difficult to measure the molecular weight of a unit molecule.

In this study, we have attempted to measure the molecular mass and the distribution for asphaltenes in Arabian heavy vacuum residue (AH-VR), Sumatra light vacuum residue (SL-VR) and hydrotreated oil of Arabian heavy atmospheric residue (AH-AR) by laser desorption time of flight mass spectrometry (LDMS). LDMS techniques have been applied to many kinds of heavy oils by the capability of larger mass range, but there are few observations of molecular mass above 2000 Da, especially for asphaltenes(4,5). We found that useful mass spectra were obtained from the selected measuring conditions, and compared the average molecular weight with those measured by vapor pressure osmometry (VPO) and gel permeation chromatography (GPC). Then, we made the structure analysis of asphaltenes which were fractionated by solvent or GPC separation. Furthermore, the type analysis of the homologous peaks observed at increasing the laser power was provided the difference of aromatic skeleton structures in asphaltenes.

EXPERIMENTAL

Asphaltenes were prepared from AH-VR and SL-VR by precipitation with n-heptane according to the procedure of Japan Petroleum Institute Standard (JPI-5S-22). Maltene (n-heptane soluble) was separated to 3 fractions (saturate, aromatic and resin) by column-chromatography. LDMS were measured with Thermoquest Co., Ltd. Vision 2000 Spectrometer, using angiotensin as a calibration standard. Samples were dissolved in solution of toluene(1 or 0.1 mg/ml), and 1 μ l of the solution was dropped on the laser target, then dried in air. Laser beams were shot on the sample surface with changing the place as every shot. Spectra were

gained by averaging about 20 shots. VPO measurements were made using UIC Inc. Osmomat 070-SA with toluene as the solvent at 333K and with nitrobenzene at 373K, calibrating by benzil. GPC measurements were made using Sensyu Scientific Co., Ltd. SSC-7100 (column : Shodex K-802.5 and K-805L, 8mmI.D.300mmL) in nitrobenzene for the eluent at 373K, calibrating by polystyrene.

AH-VR asphaltene was fractionated into 4 parts (S-1~S-4) by solvent separation using mixtures of methanol / toluene. The toluene solution of asphaltene of 1/30 wt/vol% was precipitated by addition of methanol, ratio of 30/70 vol/vol. The precipitant was settled for 5 hr at 283 K, and separated by centrifugation. The soluble, then, was separated stepwise by addition of methanol / toluene mixtures of 40/60 and 45/55, respectively. GPC separation was made using Toso Co., Ltd. Model SC-8020 (column : TSKgel G 3000H, 55 mmI.D.600 mmL) in chloroform for the eluent at room temperature, and 4 fractions (G-1~G-4) were obtained.

Hydrotreating was performed in a bench-scale fixed-bed continuous flow reactor system, using the demetallization catalyst. Five reactors having 18 mmI.D.560 mmL each were connected in series. The reaction conditions were: temperature at 653 K; pressure of 12 MPa; LHSV of 0.5 hr⁻¹, and H₂/oil ratio of 800 vol/vol. The feedstock was Arabian heavy atmospheric residue (AH-AR) (b.p. of 616°K). The product oil samples were obtained from the bypass line of each reactor outlet by 2% of the flow rate. These oils were distilled, and asphaltenes were prepared from the distillation residue.

RESULTS AND DISCUSSION

LDMS spectra of asphaltenes

The LDMS spectra of AH-VR and SL-VR asphaltenes are shown in Figure 1, where broad distribution profiles were observed up to m/z 6000. Some peaks below 200 might be assigned to metals, such as Na, K and Fe. Peak intensities grew up with the laser power increasing, and many fragments appeared in lower mass range. The addition of matrix, for example, 2,5-dihydroxybenzoic acid showed no effects to suppress the fragmentation. We extracted the spectrum with stronger intensity and less fragment to calculate the weight average molecular weight (Mw) and number average molecular weight (Mn). It showed a broad peak in the range from m/z 200 to 6000 with a maximum near 1500 and a shoulder peak near 400. The spectral shape was almost the similar for AH and SL. Mw and Mn for AH and SL with those by GPC and VPO are summarized in Table 1. It was noted that Mw or Mn obtained by LDMS was the smallest in value. It was reported that the polar solvent such as nitrobenzene was preferable to minimize the aggregation of asphaltene in measuring molecular weight, except for the calibration standard problem(6). However, the LDMS results indicated that asphaltene was measured at the stage of less aggregation. It means the values of almost an unit molecule, assuming that the whole molecules could be desorped or ionized without cracking. Again, it was noted that the average molecular weight of AH-VR asphaltene was almost the same as that of SL-VR, though the difference between AH-VR and SL-VR were appeared by means of GPC and VPO. This implies that the substantial molecules consisting of asphaltenes are not dependent upon kinds of crude oil.

Figure 2 shows the LDMS spectra of AH-VR saturate, aromatic and resin compared with the asphaltene. The saturate showed many sharp peaks below m/z 200 and a broad one from 200 to 1000, the aromatic had a broad peak from 200 to 2000, and the resin had a bimodal peak from 200 to 6000. The shoulder peak near 400 appeared in the asphaltene seems to coincide with that of aromatic or resin. It would be caused by the drawing of the partial components of aromatic or resin due to the structure similarity at the precipitation. Asphaltenes were further separated into 4 fractions by solvent and GPC. The LDMS spectra of solvent separated fractions (S-1~S-4) are shown in Figure 3. The fraction, S-1, behaves bimodal peaks having 2 tops near m/z 400 and 1500. The peak near 400 decreased and the peak near 1500 increased for the heavy fractions, S-2 and S-3. As for S-4, a peak near 1500 was observed only. The fraction is thought to be heavier or more polar in order from S-1 to S-4 standing upon the solvent separation mechanism(7). Therefore, the major part of S-1 is found to be aromatic or resin which might be drawn at the precipitation. There was no change in these profiles in the vicinity of 1500. This suggests that the asphaltene becomes separated as a function of solubility of micelles except for the drawn fraction, S-1 as contaminants. Figure 4 shows the LDMS spectra of GPC fractions. Their molecular weight distributions were shifted to larger in order from G-1 to G-4. While G-1 showed a bimodal spectrum in the range from m/z 200 to 6000, the others were almost the same of the broad one from 200 to 6000. The profile of G-1 seems to coincide with aromatic or resin. So, it can say again that the drawn component of asphaltene would be aromatic or resin. As asphaltenes are thought to be aggregated in solvent as described earlier, they would be separated by the solubility difference of micelles, not that of molecular structure due to no differences in the LDMS spectra. This suggests that they might have the other properties related to forming micelles.

Next, we tried to analyze the asphaltenes in the hydrotreated oils to make sure the structural changes by the reaction. Figure 5 shows the LDMS spectra of those asphaltenes (Rx-1, Rx-3 and Rx-5), prepared from the product oils of the first, the third and fifth reactor, respectively. It was observed that the profiles became flat and the peak of m/z 1500 in the profiles shifted to smaller mass near 600 with increasing the reaction pass. As there occurred the transfer from asphaltenes to maltenes, and the decrease of asphaltene contents under hydrotreating, it is hard to estimate the structural changes from analyzing the residual oil. But, we could insist that the molecular weight lowering of asphaltenes molecules would occur under hydrotreating.

Type analysis of homologous LDMS peaks

When increasing the laser power for the sample prepared by the solution of 0.1 mg/ml, many sharp homologous peaks appeared in the range from 200 to 5000, together with a lot of fragment peaks. The spectra of AH-VR asphaltene are shown in Figure 6. This phenomenon implies that the cracking of side chains attached to aromatic cluster and skeleton in asphaltenes was caused by the laser abrasion resulting the homologous compounds series with cracked fragments. The prominent series with a Δm of 24 interval is assigned to cata-type aromatic compounds. The ring number increases with one by two carbons. The proposed structural change of condensed aromatic rings is shown in Figure 7. The appearance of homologous peaks was also

observed in SL-VR as well as hydrotreated oils. We make sure the type analysis for these series of an interval of m/z 24 for AH-VR and SL-VR. The analysis is that (1) general formula of hydrocarbons is expressed as C_nH_{2n+z} , and (2) separation of hydrocarbons belonging to a given group with the definite z -value from the spectrum having lots of sharp peaks in LDMS. Calculation was computed by a personal computer system. The plots of the various types in the sample shown in Figure 8 provide "finger printing" of asphaltene. The notations mean that each series are classified by the component of the initial mass. It is clear that the type distribution in the asphaltene is dependent upon the kind of crude oils, while the average molecular weight and its distribution are the almost same. That is, the type analysis provides one of characterization of mixture of hydrocarbon and asphaltenes. LDMS is a useful tool for the structure analysis of asphaltenes with complexity and will be applied to obtaining deep insight of structure such as shape and size of aromatic skeleton.

CONCLUSIONS

The structures of the asphaltene in petroleum heavy oils were investigated from molecular weight distribution by LDMS. It was observed that the mass spectrum of asphaltene in AH-VR was in the range from m/z 200 to 6000 having two peaks, and that the former was small near 400 and the latter was large and broad near 1500. This distribution was almost the same for that in SL-VR, but not for that in the hydrotreated oil, which showed the shifting of the peak to the lower mass. From the results of fractions by solvent fractionation and GPC for AH-VR asphaltenes, it is found that the peak near 400 is assigned to aromatic or resin fraction drawn at the separation and that asphaltenes in micelles are comprised from the same molecular weight distribution.

Type analysis was made for the homologous peaks of a Δm of 24 in the range from 200 to 5000, which appeared by increasing the laser power. The appearance of these peaks might be suggested the number of aromatic cata-condensed ring system, that is, asphaltene would be association of compounds with the similar aromatic ring structures.

ACKNOWLEDGMENTS

This work has been carried out as a research project of the Petroleum Energy Center with the subsidy of the Ministry of International Trade and Industry.

LITERATURE CITED

- (1) Speight, J. G., *The Chemistry and Technology of Petroleum*, Marcel Dekker Inc.
- (2) Yen, T. F. and Chilingarian, G. V., *asphaltenes and asphalts*, I, Elsevier Science
- (3) Moschopedis, S. E., Fryer, J. F. and Speight, J. G., *Fuel*, **55**, 227(1976)
- (4) Parker, J. E., et al., *Fuel*, **72**, 1381(1993)
- (5) Hunt, J. E., Lykke, K. R. and Winans, R. E., *Pre. Pap. ACS. Div. Fuel Chem.*, **36**, 1325(1991)
- (6) Nali, M. and Manclossi, A., *Fuel Scie. and Tech. Int'l*, **13**, 1251(1995)
- (7) Andersen, S. I., Keul, A. and Stenby, E., *Petr. Scie. and Tech.*, **15**, 611(1997)

Table 1. Properties of asphaltenes

| Sample | LDMS | | GPC | | VPO | (Mn) | density | fa | H/C |
|--------|------|------|------|------|----------------------|-----------------|-------------------|---------|------|
| | Mw | Mn | Mw | Mn | nitrobenzene 373K | toluene 333K | g/cm ³ | III-NMR | - |
| AH-VR | 2040 | 1560 | 2280 | 1840 | 2870 | 12710 | 1.165 | 0.52 | 1.05 |
| SL-VR | 1980 | 1490 | - | - | 3170 | 12870 | 1.115 | - | 1.03 |

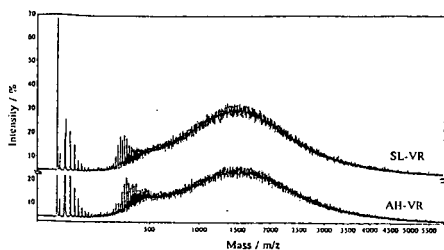


Figure 1. LDMS spectra of asphaltenes

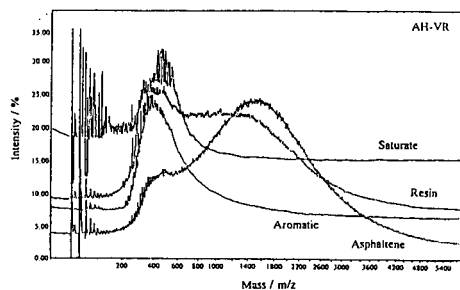


Figure 2. LDMS spectra of fractions by column chromatography

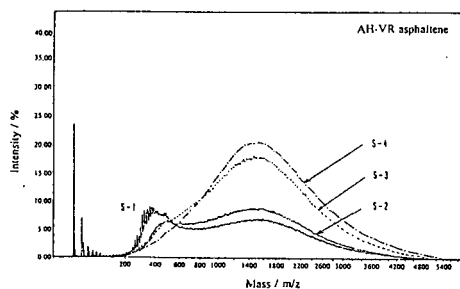


Figure 3. LDMS spectra of fractions by solvent separation

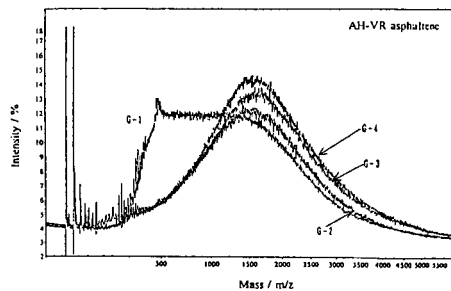


Figure 4. LDMS spectra of GPC fractions

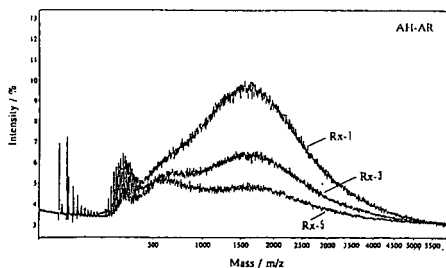


Figure 5. LDMS spectra of asphaltenes in the hydrotreated oils

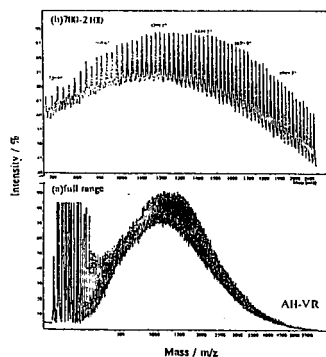


Figure 6. Homologous peaks of LDMS spectrum

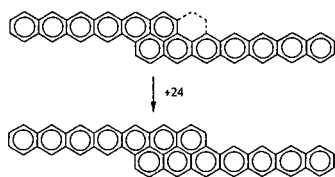


Figure 7. A model of structural changes with a Δm of 24

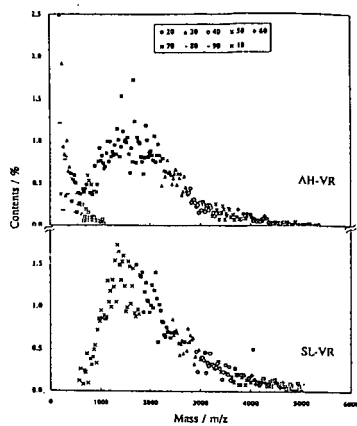


Figure 8. Type analyses of homologous peaks

UPGRADING OF BITUMEN WITH SUPERCRITICAL WATER FOR A SYSTEM COMBINED WITH SAGD.

H. Kamimura*, S. Takahashi†, A. Kishita*, T. Moriya†, C.X. Hong*, and H. Enomoto*

* Tohoku University, Dept. of Geoscience and Technology, Sendai 980-8579 Japan

† Japan National Oil Corp., Technology Research Center, 1-2-2 Hamada, Mihama-Ku, Chiba-Shi, 261-0025 Japan

‡ Tohoku Electric Power Co., Research and Development Center, 7-2-1 Nakayama, Aoba-Ku, Sendai, 981-0952 Japan

Key words: Upgrading, Bitumen, Supercritical Water

INTRODUCTION

Recent development of Steam Assisted Gravity Drainage (SAGD), which is believed to be an economically feasible recovery method of bitumen from oil sand deposits, is now asking for a new upgrading technology. In the operation of SAGD, mixture of bitumen and hot water at the temperature above 500 K is continuously recovered, so that the mixture recovered can be fed into a ground reactor. Then, the on-site upgrading by hydrothermal reaction could be a new technology as a combined system with SAGD.

Functions of water in hydrothermal reactions have been studied, and it was found by NMR analysis that hetero-atoms contained in low molecular compounds were easily substituted by hydrolysis and polymers were easily cracked to useful low molecular compounds with the supply of hydrogen from water [1].

On the basis of these fundamental studies, studies on the upgrading of bitumen in supercritical water were carried out.

EXPERIMENTAL

Batch-type autoclaves of 45 cm³ in volume were used. The autoclave and the induction furnace used for heating are shown in Fig.1. Experimental conditions of hydrothermal treatment are shown in Table 1. The sample oil was prepared by extraction from athabasca oil sands with toluene and subsequent evaporation of toluene. The viscosity of original oil (bitumen) is over 10⁵ mPa·s at 303 K.

In each experiment, 5 g of the bitumen was put into an autoclave with a certain amount of alkali aqueous solution and a stirring ball made of the same alloy as that of inner vessel of the autoclaves (Inconel 600). The autoclave was inserted horizontally at the center of the furnace and was heated up to a reaction temperature at the heating rate of 40°C/min. The content of autoclave was stirred with the stirring ball by rocking the furnace. After keeping the temperature for a certain time, the autoclave was taken out of the furnace and was cooled down to the room temperature at the similar cooling rate to the heating rate. Then the oil product was separated from water with separation funnel, but when the fractions of product were measured, toluene was used to wash the inner wall of the autoclave to ensure the recovery.

A rotational viscometer was used for measuring the viscosity of oil products at 303 K. Molecular weight distribution of oils was obtained with HPLC, which was calibrated with standard polystyrenes. Sulfur content was analyzed by CNS analyzer. Light oil components were analyzed with GC/MS and GC/AED (Atomic Emission Detector).

RESULTS AND DISCUSSION

Products

In all cases of hydrothermal treatment, bitumen was converted to much lighter oil. Fig.2 shows that the viscosity of oil products decreases with increasing temperature, and the reaction condition of 703 K for reaction temperature and 15min for reaction time is enough to produce sufficiently light oils for pipeline transportation.

Figure 3 shows the viscosity reduction with the reaction time as well as the water loading which is the ratio of the volume of water loaded into the reaction chamber to that of the reaction chamber. Drastic reduction was achieved in first 5 min. And the effect of water loading, that is water density, is also seen.

Figure 4 shows the influence of KOH concentration. As the KOH concentration increased, the viscosity of oil product slightly decreased, but when the KOH concentration is more than 5 mol/dm³ (M), the viscosity reduction is less. The viscosity

of oil product in case of without alkali is slightly lower than those with around 1 M alkali. In kinds of alkali, KOH was most effective.

Figure 5 shows normalized molecular weight distributions of oil products and original oil. Because of the characteristics of the separation column used, the distribution in the region of molecular weight less than 100 ($\text{LogMw}=2$) is not accurate. But, it is seen that the heavy components are diminished as the reaction proceeds.

Figure 6 shows the fraction of products by weight at different temperatures. Fractions of coke (toluene-insoluble), and gas and water-soluble organic compounds are increased with increasing temperature. But, the fraction of gas and water-soluble organic compounds is obtained as difference, and about a half of it is estimated to be lighter oil components which are evacuated in evaporating toluene used as the extractant. Therefore, it can be said that the fraction of asphaltene (n-pentane-insoluble but toluene-soluble) for the original oil is roughly equal to the sum of those of others than malten (n-pentane-soluble), that is to say, the fraction of malten does not change much.

Fraction of coke produced at 703 K is ca. 5%, which is much less than that in the thermal cracking. This may imply that hydrogen is supplied from water and/or the water prevents polymerization. The original vanadium content of 160 ppm was reduced to 12 ppm by the 15 min reaction at 703 K.

As to the gas composition, H_2 and CH_4 were produced, but CO_2 and H_2S gases did not exist when alkali solution was used. However, when pure water was used instead of alkali solution, CO_2 and H_2S as well as H_2 and CH_4 were produced.

Desulfurization

Figure 7 shows the desulfurization at various temperatures. The sulfur content of oil product at 703 K decreased to 2.0% from 4.5% (original). Fig.8 shows the variation of sulfur content with the reaction time. The sulfur content decreased to a half of the original value in first 5 min in all cases of water loading. After first 5 min, influence of water loading appears, but 30% of sulfur still remains even in the case of 40% water loading. In the case of thermal cracking without water, sulfur removal was less.

Figure 9 shows the GC/MS total ion chromatogram of oil product after 100 min reaction. The parent peaks of a series of paraffin and low molecular aromatic compounds were mainly detected. Fig.10(A) shows a S atom chromatogram of the oil product obtained with GC/AED. These peaks are grouped as C_1 to C_3 alkyl benzothiophenes and dibenzothiophenes with the help of GC/MS selected ion chromatograms. As examples, selected m/e number chromatograms corresponding to the parent peaks of C_1 to C_3 alkyl dibenzothiophenes are shown in Fig.10(B) to (D). The parent peaks of benzothiophene and dibenzothiophene were not detected.

As shown in Fig.8, it was difficult to decrease the sulfur content of oil products further by increasing the reaction time. Table 2 shows results of GC/MS and GC/AED analysis of oil products in long time reactions. It is seen that the concentrations of benzothiophenes (BTs) and dibenzothiophenes (DBTs) increased with reaction time and/or reaction temperature, though the total sulfur content changes little. This means that these BTs and DBTs are produced by breaking aliphatic C-C bonds in high molecular aromatic sulfur compounds and these aromatic compounds are hardly decomposed. Table 2 also shows the effect of water loading, which implies more breakage of C-S bonds with high water loading, probably in aromatic structures.

Decomposition of benzothiophenes and dibenzothiophenes

Figures 11 and 12 show results of hydrothermal decomposition of BT and DBT. BT was easily decomposed in the region of subcritical water. 5-Methyl BT is less reactive than BT but it was decomposed in the subcritical region. DBT was hardly decomposed in the near-critical region of water but was decomposed in the supercritical region of water as shown in Fig.12. However, only 50% of 2,8-dimethyl DBT was decomposed at the reaction condition of 703 K, 120 min, 40% water loading and 5 M KOH, at which 96% of DBT was decomposed.

These results show that low molecular aromatic sulfur compounds themselves, at least BTs, can be decomposed by hydrothermal reaction in the supercritical region of water, but they are hardly decomposed when mixed with other oil products.

DISCUSSION ON THE HYDROTHERMAL CRACKING

From the results so far described, it may be summarized that the viscosity reduction occurs simultaneously with desulfurization, but the dominant mechanisms in the first 5 min and subsequent reactions are different each other. In the first 5 min reaction, the thermal cracking may be dominant and the breakage of C-S bonds in aliphatic structures may occur. In this process, increase of water loading may cause hindering the thermal cracking, which proceeds by radical reactions, because of the enhancement of ionic character of water. At the next stage of cracking, the slow thermal cracking of C-C bonds and the hydrothermal cracking of C-S bonds probably in aromatic structures may lead to the reduction of viscosity and sulfur content. Through the whole process of cracking, water acts to suppress the production of coke. Data are not shown here, but experimental results of hydrothermal cracking of polymers show that hydrogen is supplied from water, which may prevent coking, where oxygen goes mostly into water-soluble compounds and some form CO_3^{2-} . Similar mechanisms may act in the hydrothermal cracking of bitumen, but it does not accelerate the reaction.

CONCLUSIONS

Fundamental studies on the hydrothermal cracking of oil sands in the region of supercritical water were carried out to clarify the reaction condition for developing a new on-site upgrading method. Reaction conditions of temperature of 700K reaction time of 5-15min, water loading of 20% (pressure \approx 3.1MPa) and 0.1-1 M KOH give us upgraded oils of viscosity of 10-20 mPa·s, sulfur content of less than a half and vanadium content of less than 10%, with less coke. It should be also emphasized that neither hydrogen gas nor catalyst was used, and neither CO_2 nor H_2S was issued. A combined system with SAGD can utilize the waste water to generate steam for injection.

ACKNOWLEDGMENT

The authors are grateful to Japan Petroleum Exploration Co., Ltd. (JAPEX) for financial support of a part of this work.

REFERENCE

- [1] Nakahara, M., Tennen, T., Wakai, C., Fujita, E., and Enomoto, H., ^{13}C -NMR Evidence for Hydrogen Supply by Water for Polymer Cracking in Supercritical Water. *Chemistry Letters* 1997, 163-164.

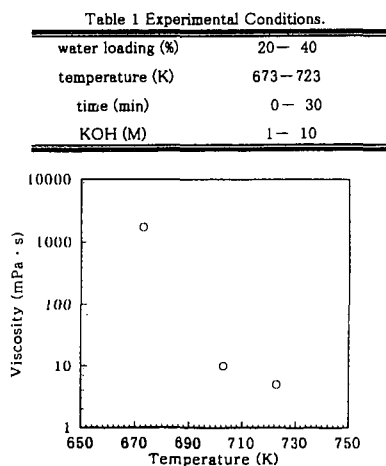


Fig. 2 Viscosity of oil products.
(1M KOH, 20% water loading)

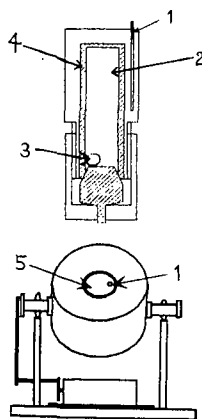


Fig. 1 A batch type autoclave (top) and the induction furnace (bottom).
1: thermocouple, 2: chamber
3: stirring ball, 4: inner vessel,
5: autoclave

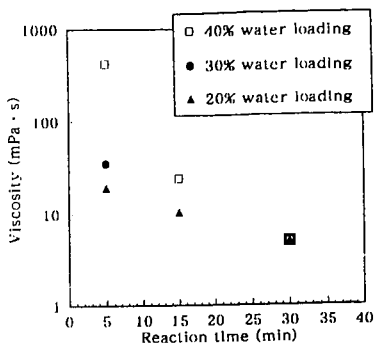


Fig.3 Viscosity of oil products with reaction time.

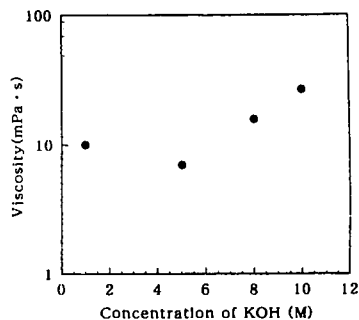


Fig.4 Influence of KOH concentration on the Viscosity of oil products. (Reaction temperature: 703K, Reaction time: 15min, 20% water loading,)

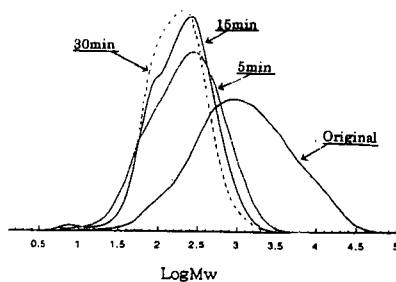


Fig.5 Comparison of molecular weight distribution. (Reaction temperature: 703K, 1M KOH, 20% water loading)

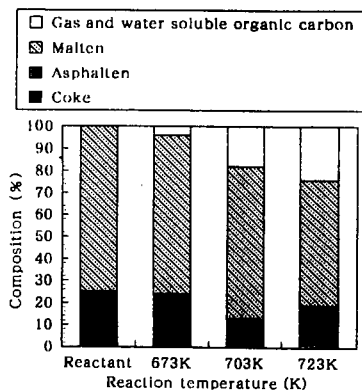


Fig.6 Fraction of products. (Reaction time: 15min, 1M KOH)

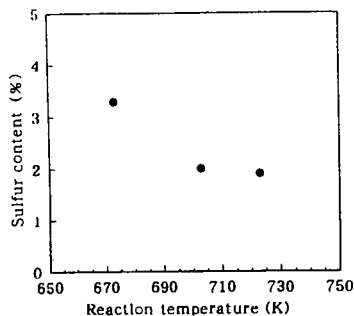


Fig.7 Sulfur content of oil products. (Reaction time: 15min, 1M KOH 20% water loading)

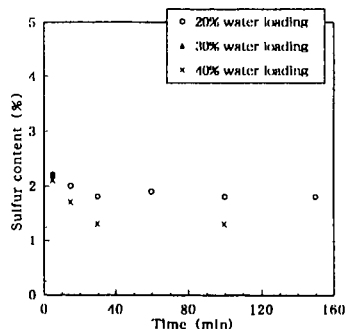


Fig.8 Influence of reaction time on sulfur contents of oil products. (1M KOH)

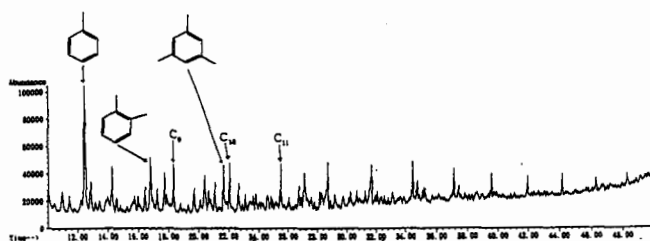


Fig.9 GC/MS chromatogram of n-hexane soluble oil products.
(Reaction temperature: 703K, Reaction time: 100min,
1M KOH, 20% water loading)

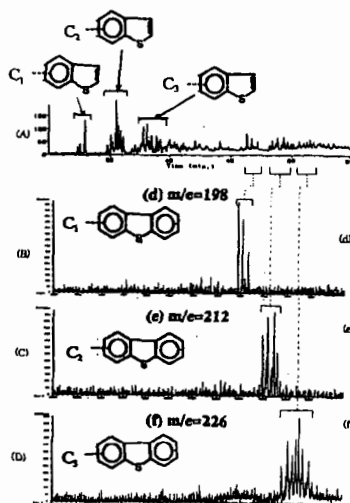


Fig.10 Chromatograms of low molecular sulfur compounds.

Table 2 Concentration of sulfur compounds.

| No. | 1 | 2 | 3 | 4 | 5 | 6 |
|-------------------------|------|------|------|------|------|------|
| Temperature(K) | 430 | 430 | 430 | 450 | 430 | 430 |
| Time(min) | 60 | 100 | 150 | 100 | 100 | 100 |
| KOH (M) | 1 | 1 | 1 | 1 | 1 | 5 |
| Water Loading(%) | 20 | 20 | 20 | 20 | 40 | 20 |
| Sulfur content(%) | 1.9 | 1.8 | 1.8 | 1.7 | 1.3 | 1.5 |
| C ₁ -BT(wt%) | 0.03 | 0.05 | 0.06 | 0.10 | 0.02 | 0.02 |
| C ₂ -BT | 0.06 | 0.10 | 0.12 | 0.17 | 0.06 | 0.07 |
| C ₃ -BT | 0.07 | 0.11 | 0.12 | 0.15 | 0.08 | 0.11 |
| C ₄ -DBT | 0.02 | 0.03 | 0.04 | 0.06 | 0.02 | 0.02 |
| C ₅ -DBT | 0.04 | 0.07 | 0.08 | 0.10 | 0.03 | 0.04 |
| C ₆ -DBT | 0.03 | 0.07 | 0.08 | 0.10 | 0.03 | 0.02 |
| SUM | 0.25 | 0.43 | 0.50 | 0.68 | 0.24 | 0.28 |

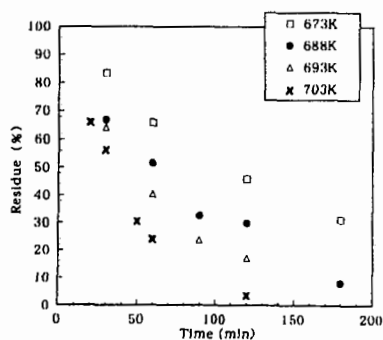


Fig.12 Decomposition of Dibenzothophene
by hydrothermal reaction.
(5M KOH)

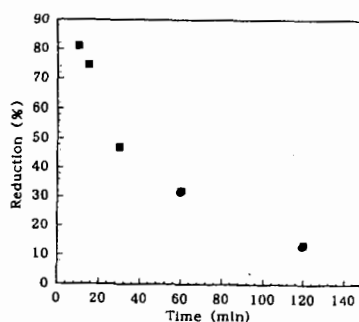


Fig.11 Decomposition of Benzothophene
by hydrothermal reaction.
(Reaction Temperature:573K,5M NaOH)

HYDROCONVERSION CHARACTERISTICS ON NARROW FRACTIONS OF RESIDUA

Chaohe Yang¹, Jianfang Zhang, Chunming Xu, Shixiong Lin
State Key Laboratory of Heavy Oil Processing, University of Petroleum
Dongying city, Shandong province, China, 257062

ABSTRACT

An atmospheric residuum from Dagang crude of China(DGAR) and two vacuum residua from Arabian Light crude and Arabian Medium crude(SQVR and SZVR) were fractionated into 7-8 cuts by supercritical fluid extraction fractionation (SFEF) technique developed by State Key Laboratory of Heavy Oil Processing. The major properties of these fractions were measured, and each fraction was catalytically hydroprocessed in a 100 mL autoclave with crushed commercial Ni-Mo catalyst at the same reaction conditions. Removal of sulfur and nitrogen decreases with increase of the average molecular weight(AMW) of the feedstock, but the total conversion of heavy portion greater than 500 for every fraction is similar. The yield of coke increases with increasing AMW of feed, especially for the several heavier fractions, and the SFEF residue inhibits the HDS and HDN of other SFEF fractions to a certain extent.

INTRODUCTION

Due to increasing use of heavy oils and bitumen as refinery feedstock and the growing demand of light distillate oils, catalytic hydroprocessing of heavy oil plays an increasingly important role in modern petroleum deeply processing. Considerable effort has been focused worldwide on characterizing oils from the points of view of feedstock properties and the resultant kinetic properties. Much of this effort, however, has been directed at characterizing the reaction kinetics of whole oils, and the investigations about the hydroconversion features of narrow fractions of heavy oils are scarce. Hoog(1950)^[1] upgraded two narrow-boiling fractions and a whole gas oil, all at 375°C with a Co/Mo catalyst. The rate of desulfurization decreased with increasing boiling point. Yitzhaki and Aharoni(1988)^[2] processed a whole gas oil and fractionated the feed and products into narrow-boiling cuts. The desulfurization kinetics were estimated for each fraction based on the assumption that no sulfur compounds migrated between fractions. Their modeled kinetics showed that the HDS rate decreases with the increase of average boiling point of the feed. Constantine Philippopoulos and Nickos Papayannakos(1988)^[3] investigated the hydrocracking reaction of asphaltene from an atmospheric residuum and the HDS kinetics and diffusion properties of asphaltene and deasphaltene oil(DAO) of the atmospheric residuum in a small trickle-bed reactor. The hydrocracking of asphaltene and the HDS of DAO were elucidated very well with second order kinetic equations, the HDS reaction of asphaltene was represented by third order kinetics. The effective diffusivity of DAO is 5.85 times as big as that of asphaltene and the HDS rate of DAO is obviously faster than that of asphaltene. Trytten and Gray(1990)^[4] fractionated a heavy gas oil, produced by thermal cracking of Athabasca bitumen, into six narrow boiling cuts of nominal 50° width and a high boiling residue, and catalytically hydroprocessed them in a 150 mL CSTR with a commercial Ni/Mo catalyst. The AMW of the fractions range from 197 for the lightest one to 653 for high-boiling residue. The reaction conditions were $P_{H_2}=13.9\text{MPa}$ $V_{H_2}=1.05\text{L/min}$ $HSV=12.5\text{ml/(hg)}$. Reaction results were treated by first order kinetics. The removal of sulfur and nitrogen as well as conversion of aromatic carbon decrease with the increase of feed AMW. The intrinsic activation energies of HDN and HDS do not change significantly with increasing feed AMW, but the apparent activation energies increase gradually. The estimated effectiveness factors increase with the increase of feed AMW for both reactions and pass through a maximum at a molecular weight of 362 for the feed. The reactivity decreasing of the sulfur and nitrogen with increasing feed AMW due to the steric effects or inhibition by components in the mixture plays a dominant role on the decrease of effectiveness factors for lighter fractions, although the estimated diffusivity decreases gradually.

Dai^[5] fractionated the Shengli Vacuum residuum into 14 cuts by the SFEF technique and separated each fraction into saturate, aromatics and resin by SARA method. Every resin in different fraction was catalytically cracked in a small reactor designed oneself. When the total yield of extract oil in SFEF is not greater than 78%, the resin in each fraction can be

cracked easily with a liquid yield of 65-75%. The reactivity of resin is greatly affected by its AMW, the greater the AMW of resin is, the poorer its cracking reactivity.

As a whole, the reaction features of feed vary with the AMW, or molecular size. Now there are not investigations about the hydroconversion characteristics of narrow fractions of residuum reported for lack of proper separation method. The SFEF technique developed by State Key Laboratory of Heavy Oil Processing affords the possibility to do such a work. In this paper, three residua were fractionated into narrow fractions by the SFEF method and all fractions were catalytically hydroprocessed at the same conditions.

EXPERIMENTAL

Feedstocks. Two vacuum residua of Arabian Light crude and Arabian medium crude were provided by Fushun Research Institute of Petroleum Processing, and Dagang atmospheric residuum came from Dagang refinery. Such three residua were separated respectively into 8 fractions by the SFEF method. The main properties of each fraction were measured and summarized in table 1.

Table-1 SFEF fraction properties of residua

| DGAR, iso-butane as solvent in SFEF | | | | | | | | | |
|---|--------|--------|--------|--------|--------|--------|--------|--------|---------|
| Fraction No. | 1 | 2 | 3 | 4 | 5 | 6 | 7 | 8 | residue |
| Fraction, m% | 10.26 | 11.10 | 10.30 | 10.65 | 9.98 | 10.27 | 10.07 | 10.54 | 16.83 |
| Sum, m% | 10.26 | 21.36 | 31.66 | 42.31 | 52.29 | 62.56 | 72.63 | 83.17 | 100.0 |
| 20° density, g/cm ³ | 0.8721 | 0.8793 | 0.8855 | 0.8905 | 0.8960 | 0.9027 | 0.9103 | 0.9267 | 1.0616 |
| Molecular weight | 353 | 379 | 407 | 420 | 443 | 467 | 505 | 582 | 1473 |
| S m% | 0.101 | 0.112 | 0.149 | 0.152 | 0.176 | 0.197 | 0.234 | 0.315 | 0.780 |
| N µg/g | 436 | 1119 | 1430 | 1770 | 2066 | 2398 | 2940 | 3841 | 12979 |
| H/C, mol/mol | 1.81 | 1.80 | 1.78 | 1.77 | 1.75 | 1.73 | 1.71 | 1.66 | 1.39 |
| SQVR, normal pentane as solvent in SFEF | | | | | | | | | |
| Fraction No. | 1 | 2 | 3 | 4 | 5 | 6 | 7 | 8 | residue |
| Fraction, m% | 9.9 | 10.2 | 10.1 | 10.0 | 10.1 | 10.1 | 10.0 | 12.0 | 18.3 |
| Sum, m% | 9.9 | 20.1 | 30.2 | 40.2 | 50.3 | 60.4 | 70.4 | 80.4 | 98.7 |
| 20° density, g/cm ³ | 0.9432 | 0.9559 | 0.9634 | 0.9714 | 0.9789 | 0.9947 | 1.0232 | 1.0606 | |
| Molecular weight | 558 | 610 | 644 | 653 | 690 | 744 | 900 | 1128 | 3047 |
| Carbon residue m% | 2.2 | 6.1 | 6.2 | 6.5 | 8.4 | 12.6 | 15.4 | 26.8 | 33.1 |
| S m% | 2.55 | 2.60 | 2.94 | 3.20 | 3.48 | 4.11 | 4.74 | 5.56 | 5.89 |
| N µg/g | 1845 | 2088 | 2550 | 2823 | 3000 | 3863 | 5356 | 6100 | 8100 |
| H/C, mol/mol | 1.67 | 1.62 | 1.63 | 1.63 | 1.59 | 1.55 | 1.46 | 1.38 | 1.14 |
| SZVR, normal pentane as solvent in SFEF | | | | | | | | | |
| Fraction No. | 1 | 2 | 3 | 4 | 5 | 6 | 7 | 8 | residue |
| Fraction, m% | 10.2 | 10.2 | 10.2 | 10.0 | 10.2 | 10.0 | 9.9 | 5.0 | 24.6 |
| Sum, m% | 10.2 | 20.4 | 30.6 | 40.6 | 50.8 | 60.8 | 70.7 | 75.7 | 100.3 |
| 20° density, g/cm ³ | 0.9369 | 0.9484 | 0.9610 | 0.9740 | 0.9937 | 1.0056 | 1.0320 | 1.0533 | 1.1405 |
| Molecular weight | 498 | 611 | 657 | 711 | 802 | 826 | 1079 | 1124 | 3394 |
| Carbon residue m% | 3.0 | 4.0 | 4.8 | 6.8 | 10.3 | 14.5 | 21.3 | 27.0 | 44.8 |
| S m% | 2.70 | 2.71 | 2.92 | 3.54 | 4.18 | 4.41 | 4.83 | | 6.40 |
| N µg/g | 2169 | 2490 | 3280 | 3950 | 4600 | 5803 | 7132 | | 9700 |
| H/C, mol/mol | 1.69 | 1.66 | 1.64 | 1.63 | 1.56 | 1.51 | 1.47 | | 1.19 |

Catalyst. A key catalyst used in Chevron VRDS process(CAT1) and another catalyst(CAT2) produced in China were chosen in this research, their major properties were listed in table 2. The average pore diameter of both catalysts is 30Å - 40Å, pore volume is 0.39 - 0.45mL/g, and specific surface area is 203 - 275 m²/g. The main metal active components are molybdenum and nickel. Catalyst was crushed and sieved into 60/80 mesh particles (average diameter of 0.35mm), and the catalyst particles were presulfurized before use in reaction.

table-2 Major properties of catalysts

| | CAT1 | CAT2 |
|--|----------------------------------|----------------------------------|
| Particle size/ mm | 0.79 | 0.84 |
| Particle density/ g/cm ³ | 1.52 | 1.50 |
| Bulk density/ g/cm ³ | 0.89 | 0.88 |
| Specific area/ m ² /g ⁻¹ | 275 | 203 |
| Pore volume/ mL/g ⁻¹ | 0.45 | 0.39 |
| Pore radius/ Å | 33 | 38 |
| Active components | Mo, Ni, Fe, Co | Mo, Ni, Fe, |
| support | γ-Al ₂ O ₃ | γ-Al ₂ O ₃ |

Hydroconversion and Separation.

The flowsheet of heavy oil hydroconversion and separation was shown in figure 1. The crushed catalyst was presulfurized firstly, washed with solvent and dried in a vacuum drying oven. The presulfurized catalyst and sample were charged into the autoclave with the ratio of 1 to 10. After loading the catalyst and sample, the system was purged with hydrogen three times, then the temperature was increased gradually and the agitator was switch on when the temperature reached from 100°C - 150°C. Standard reaction conditions include a temperature of 400°C, initial hydrogen pressure(IHP) of 8.5Mpa at ambient temperature, and stirring rate of about 850rpm. After reaction, the autoclave was taken out from the heating furnace and put it into cooling water. When the temperature reaches to about 200°C, the reactor was placed into an isothermal water bath of 60°C in order to assure the consistency of sampling conditions and avoid or reduce the evaporation of light components in liquid product. While the autoclave comes to about 60°C, reactor was connected to a gas ration and sampling system for collecting gas product. The in-situ temperature, atmospheric pressure and the collected gas volume were recorded. Then the gas product was transferred into a gas sample bag for composition analysis. After sampling gas, the reactor was cooled down to ambient temperature, opening the reactor and taking immediately a little liquid product into a centrifugal test tube. The catalyst contained in the liquid product was deposited on the bottom of the test tube by centrifugation separation in a centrifugal machine at 5000rpm for 5 minutes. The upper oil in test tube was transferred to a sealed vial for simulated distillation analysis.

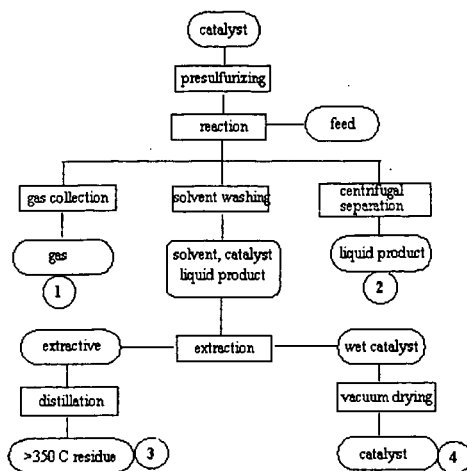


Fig.1 Hydroconversion and separation flowsheet

When the temperature reaches to about 200°C, the reactor was placed into an isothermal water bath of 60°C in order to assure the consistency of sampling conditions and avoid or reduce the evaporation of light components in liquid product. While the autoclave comes to about 60°C, reactor was connected to a gas ration and sampling system for collecting gas product. The in-situ temperature, atmospheric pressure and the collected gas volume were recorded. Then the gas product was transferred into a gas sample bag for composition analysis. After sampling gas, the reactor was cooled down to ambient temperature, opening the reactor and taking immediately a little liquid product into a centrifugal test tube. The catalyst contained in the liquid product was deposited on the bottom of the test tube by centrifugation separation in a centrifugal machine at 5000rpm for 5 minutes. The upper oil in test tube was transferred to a sealed vial for simulated distillation analysis.

The remaining liquid product and catalyst in reactor was diluted with solvent and transferred into a Soxhlet apparatus, then extracted with dichloro-ethane for one hour, finally the extracted liquid should be not color. The wet catalyst in the extractor was taken out and placed into a vacuum drying oven to dry for coke content and other properties analysis. The extractive was distilled at atmospheric pressure to recover the solvent, then the liquid product was transferred into a small distillation flask of 150mL and subjected to vacuum distillation to obtain the high boiling residue of >350°C for analyzing the sulfur and nitrogen contents, molecular weight, and hydrocarbon group composition.

In the present study, the loss in experiment could be ignorable and sum of yields of gas, coke and liquid product accounted as 100%. Once the gas and coke yields are determined, the yield of any distillate can be calculated according to the simulated distillation data of liquid product.

RESULTS AND DISCUSSION

Hydroconversion of DGAR fractions. It is shown in table 3 that the removal of sulfur and nitrogen are similar for both catalysts. The HDS conversions are very high for No.1 to No. 8 fractions, all greater than 90%. The HDN conversion is greater than 75% for fraction lighter than No.7 fraction. HDS and HDN conversions decrease obviously with the increase of AMW of feed, and the declining rate for HDN is greater than that for HDS. The removal of sulfur and nitrogen in the SFEF residue is more difficult than other fractions, the conversion of HDS and HDN are only 44.3% and 16.4% respectively.

From the distribution of cracked product, the gas yield of each fraction do not change obviously except for the SFEF residue. In the latter case, the short side chains may be directly cracked into gas product, which results in the high gas yield. The yields of gasoline and diesel distillates lower with increasing the AMW of SFEF fractions. The distribution of product trends towards two ends for the SFEF residue, than is, gas and coke are produced greatly, which is same as the

features of polyaromatics cracking. It also can be seen that the coke yield increases gradually with the fraction becoming heavier. The coke yield of SFEF residue is about 4 times larger than that of No.8 fraction and 13 times as big as that of No.1 fraction.

Hydroconversion of SZVR and SQVR fractions. It is shown from the data in table 3 that the reactivity of HDS and HDN for SFEF fractions of SZVR and SQVR is obviously poorer than that of DGVR. Most of HDS conversions is less than 70%, and the HDN conversion is less than 60% for all fractions. This could be ascribed to the higher boiling point, larger molecular weight and stronger aromaticity of SZVR and SQVR compared with DGAR and most of sulfur and nitrogen atoms existing in the heterocyclic structures, which results in the difficulty of HDS and HDN reactions.

In general, the gas and coke yields increase with the fraction becoming heavier, although some experimental points fluctuate due to experiment and analysis errors. There is not coincident trend for the distribution of liquid product. The gas and coke yields increase seriously compared with other fractions.

Table-3 Hydroconversion results (400°C, 240 min, IHP of 8.5MPa)

| SFEF fractions of DGAR | | | | | | | | | |
|------------------------|--------|--------|--------|--------|---------|--------|--------|---------|---------|
| feed | DGAR-1 | DGAR-3 | DGAR-5 | DGAR-7 | DGAR-2 | DGAR-4 | DGAR-6 | DGAR-8 | residue |
| catalyst | CAT1 | CAT1 | CAT1 | CAT1 | CAT2 | CAT2 | CAT2 | CAT2 | CAT1 |
| S removal, % | 96.3 | 95.0 | 94.7 | 91.6 | 95.8 | 94.4 | 93.4 | 90.7 | 44.3 |
| N removal, % | 95.2 | 87.6 | 79.1 | 60.9 | 94.9 | 84.8 | 76.1 | 48.3 | 16.4 |
| Material balance, % | | | | | | | | | |
| gas | 1.13 | 0.87 | 1.18 | 0.71 | 1.18 | 1.07 | 0.96 | 0.96 | 1.58 |
| <200°C | 7.76 | 6.94 | 5.37 | 3.96 | 5.37 | 4.93 | 3.65 | 3.89 | 7.21 |
| 200-350°C | 37.81 | 24.86 | 19.76 | 14.49 | 22.94 | 18.92 | 14.28 | 12.76 | 10.47 |
| 350-500°C | 53.10 | 60.65 | 59.66 | 49.14 | 61.89 | 58.51 | 52.51 | 39.27 | 27.01 |
| >500°C | 0.00 | 6.41 | 13.75 | 31.36 | 8.35 | 16.23 | 28.23 | 42.58 | 51.12 |
| coke | 0.20 | 0.27 | 0.29 | 0.33 | 0.27 | 0.36 | 0.38 | 0.56 | 2.60 |
| SFEF fractions of SZVR | | | | | | | | | |
| feed | SZVR-1 | SZVR-3 | SZVR-5 | SZVR-7 | SZVR-2 | SZVR-4 | SZVR-6 | residue | DGAR |
| catalyst | CAT1 | CAT1 | CAT1 | CAT1 | CAT2 | CAT2 | CAT2 | CAT1 | CAT1 |
| S removal, % | 92.5 | 70.9 | 51.1 | 31.0 | 85.9 | 75.7 | 54.0 | 27.4 | 78.1 |
| N removal, % | 59.8 | 42.2 | 20.2 | 13.3 | 53.7 | 38.0 | 19.7 | 7.4 | 41.9 |
| Coke on Cat, % | 4.56 | 5.59 | 10.74 | 15.69 | 6.06 | 8.19 | 11.78 | 23.74 | |
| Coke amount, g | 0.22 | 0.27 | 0.54 | 0.84 | 0.29 | 0.40 | 0.60 | 1.40 | |
| Coke yield, % | 0.49 | 0.60 | 1.22 | 1.87 | 0.64 | 0.89 | 1.33 | 3.11 | |
| Material balance, % | | | | | | | | | |
| gas | 1.22 | 1.18 | 2.24 | 3.13 | 0.49 | 0.93 | 2.07 | 3.16 | |
| <200°C | 8.70 | 7.14 | 11.24 | 12.32 | 7.83 | 8.61 | 9.60 | 2.95 | |
| 200-350°C | 22.69 | 17.46 | 22.34 | 20.43 | 18.62 | 18.87 | 17.96 | 12.90 | |
| 350-500°C | 42.72 | 31.02 | 29.18 | 21.32 | 32.92 | 29.54 | 24.65 | 15.90 | |
| >500°C | 24.18 | 42.60 | 33.79 | 40.92 | 39.50 | 41.16 | 44.38 | 61.98 | |
| coke | 0.49 | 0.60 | 1.20 | 1.87 | 0.64 | 0.89 | 1.33 | 3.11 | |
| SFEF fractions of SQVR | | | | | | | | | |
| feed | SQVR-2 | SQVR-4 | SQVR-6 | SQVR-8 | residue | SQVR | SQVR | | |
| catalyst | CAT1 | CAT1 | CAT1 | CAT1 | CAT1 | CAT1 | CAT2 | | |
| S removal, % | 78.3 | 70.8 | 61.0 | 48.2 | 23.8 | 48.1 | 52.3 | | |
| N removal, % | 31.2 | 24.8 | 15.3 | 5.5 | | | | | |
| Coke on Cat, % | 8.01 | 7.34 | 9.94 | 13.84 | 28.75 | 18.45 | 14.77 | | |
| Coke amount, g | 0.44 | 0.40 | 0.55 | 0.80 | 1.81 | 1.02 | 0.78 | | |
| Coke yield, % | 0.88 | 0.80 | 1.10 | 1.60 | 4.02 | 2.27 | 1.73 | | |
| Material balance, % | | | | | | | | | |
| gas | 1.02 | 0.98 | 1.34 | 2.04 | 2.89 | 1.29 | 1.47 | | |
| <200°C | 9.04 | 8.32 | 6.57 | 11.00 | 2.81 | 6.28 | 5.14 | | |
| 200-350°C | 16.88 | 16.00 | 16.79 | 14.57 | 11.46 | 14.43 | 12.91 | | |
| 350-500°C | 31.35 | 29.43 | 28.17 | 19.47 | 12.33 | 25.73 | 22.21 | | |
| >500°C | 40.83 | 44.47 | 46.03 | 51.32 | 66.49 | 50.01 | 56.54 | | |
| coke | 0.88 | 0.80 | 1.10 | 1.60 | 4.02 | 2.27 | 1.73 | | |

Relation of coke yield and feed properties. Coking trend is an important factor of feed processing characteristics, it affects not only the activity and selectivity of catalyst and the distribution of product, but also the increase of bed pressure drop of reactor, energy consumption and the operation period. Coke yield increases with the increase of aromatic carbon fraction, f_a , in the average molecule, and is directly proportional to the content of resin and asphaltene in

feed, x_{RA} . The fitting equations are as follows,

$$y_{\text{coke}} = 8.076 \cdot f_a^{1.495} \quad (1)$$

$$y_{\text{coke}} = 0.05049 \cdot x_{RA} + 0.1776 \quad (2)$$

Where y_{coke} is the coke yield, wt%. The coking characteristics can also be represented by the heavy oil characteristic parameter, K_H , which is defined as,^[6]

$$K_H = 10 \cdot \frac{H/C}{AMW^{0.1236} \cdot d_4^{20}} \quad (3)$$

Where H/C is the atomic ratio of hydrogen to carbon, d_4^{20} is the relative density. With the decrease of feed K_H , coke yield increases slowly when $K_H=6.0-8.0$, the increasing rate of coke yield rises gradually with decreasing the feed K_H value, and grows seriously for $K_H < 6.0$. Such a relationship can be represented by the following equation,

$$y_{\text{coke}} = 444.5 \cdot K_H^{-3.23} \quad (4)$$

Relations of HDS & HDN reactivity and feed properties. The HDS and HDN conversions decrease quickly with the increase of the content of resin and asphaltene, and the decrease of atomic ratio of hydrogen to carbon. This suggests that it is more difficult to remove the sulfur and nitrogen atom in the heavier component. Figure 2 shows the relationships between the percentages of sulfur and nitrogen removal and the heavy oil characteristic parameter. With decreasing the K_H value, the removal of nitrogen decreases quickly when the K_H is bigger, and gradually tends towards a constant level which approximates the conversion for thermal cracking reaction. While $K_H > 8.0$, the declining rate of HDN reaction is faster than that of HDS reaction. This relationship behaves as S-type curve for HDS and as an ice stick for HDN. The HDS conversion is always greater than that of HDN for any fraction at the same reaction conditions. This implies that the reactivity of HDS and HDN lowers obviously with the increase of fraction AMW, and the removal of nitrogen is more difficult than that of sulfur.

The solid circle and bold plus sign are the data points of whole DGAR HDN and HDS. The K_H value of DGAR is 9.1, the responding HDS and HDN conversions predicted from the curves in figure 2 are 94% and 77% respectively, but the real HDS and HDN conversion are 71.0% and 41.9% respectively. This shows that the heavy components in residuum may inhibit the HDS and HDN reaction of lighter components to a certain extent. Due to the strong adsorptivity and high coking trend, these heavy components would affect the activity of catalyst and then decrease the catalytic reaction rate.

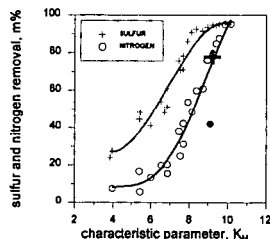


Fig.2 sulfur and nitrogen removal versus K_H

Comparing the HDS and HDN results for CAT1 catalyst with those for CAT2 catalyst shown in table 3, it is found that CAT1 has a similar HDS and HDN activity with CAT2 for lighter SFEF fractions, but for heavier fractions the latter has stronger catalytic activity than the former. This phenomenon may be attributed to the larger pore size of the CAT2 catalyst.

REFERENCE

1. Hoog H. J Inst Petro. 1950,36:738
2. Yitzhaki D, Aharoni C. AIChE J. 1988,23:342
3. Philippopoulos C, Papayannkos N. IEC Res. 1988,27(3):415
4. Trytten L C, Gray M R. IEC Res. 1990,29(5):725
5. Dai wenguo. The catalytic cracking characteristics of resins in different narrow fractions of Shengli vacuum residuum. Master thesis, University of Petroleum, China. March 1993
6. Si Tiepan, Hu Yunxiang, et al. Acta Petrolei Sinica(Petroleum Processing Section).1997, 13(2):1

CHARACTERISTICS ON HDS AND HDN KINETICS OF NARROW FRACTIONS FROM RESIDUA

Chaohe Yang, Feng Du, Chunming Xu
State Key Laboratory of Heavy Oil Processing, University of Petroleum
Dongying city, Shandong province, 257062 China

ABSTRACT

An atmospheric residuum from Dagang crude of China(DGAR) and two vacuum residua from Arabian Light crude and Arabian Medium crude(SQVR and SZVR) were fractionated into 7-8 cuts by supercritical fluid extraction fractionation (SFEF) technique developed by State Key Laboratory of Heavy Oil Processing. These SFEF fractions were catalytically hydroprocessed in a 100 mL autoclave with crushed commercial Ni-Mo catalyst. The HDS and HDN diffusion-reaction model of residue in autoclave reactor was established. The diffusion and HDS and HDN characteristics of these fractions were discussed.

KEYWORDS: heavy oil, diffusion, HDS and HDN

INTRODUCTION

Because of the increase of heavy oils and bitumen as refinery feedstock and the growing demand of amount and quality for light distillate oils, catalytic hydroprocessing of heavy oil plays a growingly important role in modern petroleum deeply processing. Considerable effort has been focused worldwide on characterizing oils from the points of view of feedstock properties and the resultant kinetic properties. Much of this effort, however, has been directed at characterizing the reaction kinetics of whole oils, and the investigations about the hydroconversion features of narrow fractions of heavy oils are scarce. Hoog(1950)^[1], Yitzhaki and Aharoni(1988)^[2], Papayannakos(1988)^[3], and Trytten & Gray(1990)^[4] studied the hydroconversion of narrow fractions from distillates. The removal of sulfur and nitrogen as well as conversion of aromatic carbon decreases with the increase of average molecular weight(AMW) of feed. Although the hydroconversion is affected by its intrinsic reactivity and diffusion property, the intrinsic reactivity is the controlling factor of reaction rate, especially for the heavier fractions. In a small reactor designed oneself, Dai^[5] investigated the resin catalytic cracking of each SFEF fraction from Shengli Vacuum residuum. When the total yield of extract oil in SFEF is not greater than 78%, the resin in each fraction can be cracked easily with a liquid yield of 65-75%. The reactivity of resin is greatly affected by its AMW, the greater the AMW of resin is, the poorer the cracking reactivity.

As a whole, the reaction feature of feed varies with the AMW, or molecular size. Now there is not investigation about the hydroconversion characteristics of narrow fractions of residuum reported for lack of proper separation method. The SFEF technique developed by State Key Laboratory of Heavy Oil Processing affords the possibility to do such a work. In this paper, three residua were fractionated into narrow fractions by the SFEF method and the hydroconversion characteristics of every fraction were studied at the same conditions.

EXPERIMENTAL

Feedstocks Two vacuum residua of Arabian Light crude and Arabian medium crude were provided by Fushun Research Institute of Petroleum Processing, and Dagang atmospheric residuum came from Dagang refinery. Such three residua were separated respectively into 8 fractions by the SFEF method. The main properties of each fraction were measured, density at 20°C is of 0.8721 to 1.1405/g/cm³, AMW of 353-3394, sulfur of 0.101-6.40 m%, nitrogen of 436-9700 µg/g, H/C atomic ratio of 1.40-1.81.

Catalyst A key catalyst used in Chevron VRDS process(CAT1) and another catalyst(CAT2) produced in China were chosen in this research. The average pore diameter of both catalysts is 33Å and 38Å, pore volume is 0.45 and 0.39mL/g, and specific surface area is 275 and 203m²/g. The main metal active components are molybdenum and nickel. Catalyst was crushed and sieved into 60/80 mesh particles (average diameter of 0.35mm), and the catalyst particles were presulfurized before use in reaction.

Hydroconversion and Separation The crushed catalyst was presulfurized firstly, washed with solvent and dried in a vacuum drying oven. The presulfurized catalyst and sample were charged into the autoclave with the ratio of 1 to 10. Reaction conditions were set as follows: 400°C 8.5Mpa of initial hydrogen pressure, 4 hours and 850rpm of agitation rate. After loading the catalyst and sample, the system was purged with hydrogen three times, then the temperature was increased gradually and the agitator was switched on when the temperature reached from 100° - 150°C. After reaction, the autoclave was taken out from the heating furnace and put it into cooling water. When the temperature reaches to about 200°C, the reactor was placed into an isothermal water bath of 60°C in order to assure the consistency of sampling conditions and avoid or reduce the evaporation of light components in liquid product. While the autoclave comes to about 60°C, reactor was connected to a gas ration and sampling system for collecting gas product. The in-situ temperature, atmospheric pressure and the collected gas volume were recorded. Then the gas product was transferred into a gas sample bag for composition analysis. After sampling gas, the reactor was cooled down to ambient temperature, opening the reactor and taking immediately a little liquid product into a centrifugal test tube. The catalyst contained in the liquid product was deposited on the bottom of the test tube by centrifugation separation in a centrifugal machine at 5000rpm for 5 minutes. The upper oil in test tube was transferred to a sealed vial for simulated distillation analysis.

The remaining liquid product and catalyst in reactor was diluted with solvent and transferred into a Soxhlet apparatus, then extracted with dichloro-ethane for one hour, finally the extracted liquid should be not color. The wet catalyst in the extractor was taken out and placed into a vacuum drying oven to dry for coke content and other properties analysis. The extractive was distilled at atmospheric pressure to recover the solvent, then the liquid product was transferred into a small distillation flask of 150mL and subjected to vacuum distillation to obtain the high boiling residue of >350°C for analyzing the sulfur and nitrogen contents, molecular weight, and hydrocarbon group composition.

In the present study, the loss in experiment could be ignorable, and sum of yields of gas, coke and liquid product accounted as 100%. Once the gas and coke yields are determined, the yield of any distillate can be calculated according to the simulated distillation data of liquid product.

DIFFUSION-REACTION MODEL

Reaction Kinetic Model The non-homogenous catalytic reaction with order of n can be described generally as follows:

$$r = - \frac{dN}{dt} \cdot \frac{1}{w_c s_g} = k_s c_m^n \quad (1)$$

Where, r--amount consumed on unit surface area of catalyst in unit time, mol/(m²·s);

N--amount of reactant, mol

t--reaction time, s;

w_c--catalyst weight, g;

s_g--specific surface area of catalyst, m²/g

c_m--concentration of reactant, mol/m³;

k_s--apparent rate constant for first-order reaction based on the surface area of catalyst, m³ⁿ/(mol⁽ⁿ⁻¹⁾·m²·s)

If the volume of reaction mixture is thought changeless in reaction process, the right end of equation above can be written as,

$$\frac{dN}{dt} \cdot \frac{1}{w_c s_g} = \frac{d(c_m \cdot v_r)}{dt} \cdot \frac{1}{w_c s_g} \approx \frac{v_r dc_m}{w_c s_g \cdot dt}$$

That is,

$$- \frac{dc_m}{dt} = \frac{w_c \cdot s_g}{v_r} \cdot k_s \cdot c_m^n \quad (2)$$

When v_r is the volume of reaction mixture(m³). The molar concentration of reactant is converted

into mass fraction, $c = \frac{c_m \cdot M}{\rho_r}$

Where, c--the mass fraction of reactant ;

M--molecular weight of reactant/g mol;

ρ_r--density of reaction mixture at reaction temperature/gm³.

Substitution of the above relation in equation (2) gives,

$$-\frac{dc}{dt} = \frac{w_c \cdot s_g}{v_r} \cdot \left(\frac{\rho_r}{M}\right)^{n-1} \cdot k_i \cdot c^n \quad (3)$$

In the special case of $n=1$, equation (3) reduces to

$$-\frac{dc}{dt} = \frac{w_c \cdot s_g}{v_r} \cdot k_i \cdot c \quad (4)$$

Integrating equation (4), we get,

$$\ln \frac{c_0}{c} = \frac{w_c \cdot s_g}{v_r} \cdot k_i \cdot t \quad (5a)$$

or

$$-\ln(1-x) = \frac{w_c \cdot s_g}{v_r} \cdot k_i \cdot t \quad (5b)$$

Where x is the conversion of reactant $x = (c_0 - c) / c_0$. Solving the k_i From equation (5b) gives

$$k_i = -\frac{v_r \cdot \ln(1-x)}{w_c \cdot s_g \cdot t} \quad (6)$$

Many investigators^[6] have correlated their experimental data with first-order kinetics for the HDS and HDN reactions of residua. In general, the conversions of HDS and HDN are not greater than 90% in this study, and the feed with narrow range has similar reactivity for all compounds contained in it. For simplicity, HDS and HDN are treated as first-order irreversibly reactions, so the apparent rate constants can be calculated by equation (6).

Diffusion Effect The external diffusion effect on reaction rate is ignorable in the stirred autoclave with high agitation speed^[7]. The effect of reactant migration through catalyst micropores on reaction rate can be described by the effectiveness factor,

$$\eta = \frac{\text{actual reaction rate within pore}}{\text{rate of not slowed by pore diffusion}} \quad (7)$$

For first-order reaction, the relationships between effectiveness factor and Thiele modulus have been proposed for different catalyst shape.

$$\text{Single cylindrical pore}^{[8]} \quad \eta = \frac{\tanh(\phi)}{\phi} \quad (8)$$

$$\text{Long cylinder particle}^{[9]} \quad \eta = \frac{1}{\phi} \frac{I_1(2\phi)}{I_2(2\phi)} \quad (9)$$

$$\text{Sphere particle}^{[10]} \quad \eta = \frac{1}{\phi} \left[\frac{1}{\tanh(3\phi)} - \frac{1}{3\phi} \right] \quad (10)$$

$$\phi = \frac{V_p}{A_p} \cdot \left(\frac{\rho_p \cdot s_g \cdot k_i}{D_e} \right)^{1/2} \quad (11)$$

Where, ϕ —Thiele modulus, dimensionless

V_p —volume of catalyst particle, m^3

A_p —external surface area of catalyst particle, m^2

ρ_p —particle density of catalyst, g/m^3

k_i —intrinsic rate constant based on the surface area of catalyst, m/s

D_e —effective diffusion coefficient of reactant, m^2/s .

Although the forms of three equations above for different shape of catalyst particle are different, the predicted values of η at the same ϕ are similar, especially for the case of $\phi < 4$. In the present study, equation(10) for sphere particle was selected to describe the relationship of effectiveness factor of HDS and HDN reactions and Thiele modulus.

Assuming no temperature gradient exists between the external surface and the center of catalyst particle, for first-order irreversible reaction we have,

$$\eta = \frac{k_i}{k_i} \quad (12)$$

$$\text{for sphere catalyst particle} \quad \frac{V_p}{A_p} = \frac{d_p}{6} \quad (13)$$

where d_p is the equivalent sphere diameter(m). Substitution of equation (11), (12) and (13) in

$$\text{equation (10) gives, } \frac{k_s}{k_i} = \frac{3}{Ak_i^{0.5}} \left[\frac{1}{\tanh(Ak_i^{0.5})} - \frac{1}{Ak_i^{0.5}} \right] \quad (14)$$

$$\text{where, } A = \frac{d_p}{2} \left(\frac{\rho_p \cdot s_g}{D_e} \right)^{1/2} \quad (15)$$

If the parameter d_p , ρ_p , s_g , v_r , w_c , t and x in equation (6), (14), (15) are obtained, the apparent rate constant k_3 can be calculated by equation (6), parameter A can be determined once the effective diffusivity is given. Instituting k_s and A into equation (14), the intrinsic rate constant, k_i , can be calculated by Newton iteration, and the effectiveness factor, η , will be determined by equation (12).

Estimation of Effective Diffusivity For heavy oil hydroconversion, three phases of gas, liquid and solid exist simultaneously, the reactant must firstly migrate through the micropores filled with liquid to the internal surface of catalyst, and then the catalytic reactions take place there. The transport in liquid-filled pores is usually described by a Fickian diffusion relation with a

effective diffusion coefficient^[11] ($D_e = \frac{\epsilon}{\tau} D_b$). When the size of diffusion molecules and the pores are of the same order of magnitude, the interaction between the walls and coefficient tends to decrease the effective diffusivity. It belongs to the configuration diffusion and the effective diffusivity can be computed by the equation,

$$D_e = \frac{\epsilon}{\tau} D_b \cdot F(\lambda) \quad (16)$$

Where D_e —effective diffusion coefficient, m^2/s ;

D_b —bulk diffusion coefficient, m^2/s ;

ϵ —catalyst porosity, $\epsilon = V_g \cdot \rho_p$;

V_g —pore volume of catalyst, m^3/g

τ —catalyst tortuosity which have a value of 1-6, For catalysts in this study, τ was set to be equal to 4 according to the reference^[10].

$F(\lambda)$ is named as restricted diffusion Factor, $F(\lambda) = k_p \cdot k_r$ ^[12]. k_p is the ratio between the concentration of diffusion molecules inside and outside the pore and depends on λ , the ratio of pore to molecule diameter. For small solvent molecules, k_p satisfies the relation:

$k_p = (1 - \lambda)^2$. When either the solute or the solvent absorb on the surface of pore, there is a resistance caused by drag exerted on the moving molecules by the walls. This influence is expressed through the drag coefficient, k_r . Some relation of $F(\lambda)$ and λ were summarized in chapter 1 of reference [13], which are illustrated schematically in figure 1. Figure 1 shows that the theoretical model proposed by Renkin is very close to the experimental model developed by Lee through the kinetic experiment. Here the Renkin's relation was chosen to computer the restricted diffusion factor.

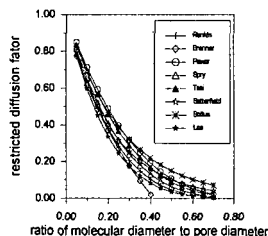


Fig.1 $F(\lambda)$ versus λ

$$F(\lambda) = (1 - \lambda)^2 \cdot (1 - 2.104\lambda + 2.09\lambda^3 - 0.95\lambda^5), \quad \lambda < 0.5 \quad (17)$$

Bulk diffusion coefficient is calculated by Stokes-Einstein equation^[14],

$$D_b = \frac{kT}{3\pi \cdot \mu \cdot d_r} \quad (18)$$

Where, k —Boltzmann constant, $1.38 \times 10^{-23} J/K$;

T —absolute temperature, K ;

d_r —diameter of spherical solute, m ;

μ —viscosity of solvent, $Pa \cdot s$.

The empirical relation between the equivalent spherical diameter and the molecular weight was selected to estimate the size of reactant^[13],

$$d_r = 0.403 \cdot M^{0.537} \quad (19)$$

In industrial process, all molecules with different size exist in one system with the same viscosity of solvent. The viscosity of reactant mixture was estimated to be $1.24 \times 10^{-4} \text{ Pa} \cdot \text{s}$ under 390°C , 7.6MPa in the study of residuum hydroprocessing. In the present study, every SEFE fraction was subject to hydroconversion, then the viscosity of reaction system may be different for different fraction. The viscosity of feed and product at reaction conditions was calculated using ASPEN software, and the viscosity in equation (18) was taken as an average of calculated viscosity of feed and product. The deviation of the viscosity for heaviest fractions may be larger for lack of distillation data of feed.

Now, the effective diffusivity can be determined through equations (19), (18), (17) and (16).

RESULTS AND DISCUSSION

The reaction product was classified into two lumps, the heavy lump of $>350^\circ\text{C}$ and the light lump of $<350^\circ\text{C}$. The sulfur and nitrogen in light lump migrated from heavy lump were thought removal by hydrogenation. Therefore, the conversion of HDS and HDN can be calculated according to the distillation data and the element analysis results.

The equivalent spherical diameter, bulk diffusion coefficient, effective diffusivity, effectiveness factor, apparent and intrinsic rate constant of HDS and HDN were obtained for every SEFE fraction in terms of the diffusion-reaction model mentioned above. The result was summarized in table 1.

Table 1A HDS diffusivities and kinetic parameters of SFEE fractions

| feed | $d_r/\text{\AA}$ | $F(\lambda)$ | $D_b/10^{-10}\text{m}^2\text{s}^{-1}$ | $D_r/10^{-10}\text{m}^2\text{s}^{-1}$ | $k_s/10^{-4}\text{ms}^{-1}$ | $k_r/10^{-4}\text{ms}^{-1}$ | η |
|--------------|------------------|--------------|---------------------------------------|---------------------------------------|-----------------------------|-----------------------------|--------|
| DGAR-1 | 9.34 | 0.522 | 112.2 | 10.01 | 9.250 | 9.323 | 0.992 |
| DGAR-2 | 9.71 | 0.507 | 93.53 | 8.109 | 8.894 | 8.978 | 0.990 |
| DGAR-3 | 10.1 | 0.492 | 85.27 | 7.175 | 8.405 | 8.490 | 0.990 |
| DGAR-4 | 10.3 | 0.483 | 76.00 | 6.274 | 8.087 | 8.177 | 0.989 |
| DGAR-5 | 10.6 | 0.474 | 72.30 | 5.858 | 8.242 | 8.341 | 0.988 |
| DGAR-6 | 10.8 | 0.462 | 63.83 | 5.046 | 7.626 | 7.725 | 0.987 |
| DGAR-7 | 11.3 | 0.445 | 51.71 | 3.936 | 6.949 | 7.055 | 0.985 |
| DGAR-8 | 12.2 | 0.413 | 27.55 | 1.946 | 6.664 | 6.862 | 0.971 |
| DGAR residue | 20.2 | 0.198 | 2.116 | 0.072 | 1.641 | 1.997 | 0.821 |
| DGAR | 11.0 | 0.456 | 62.23 | 4.856 | 4.261 | 4.293 | 0.992 |
| SZVR-1 | 11.2 | 0.448 | 38.48 | 2.949 | 7.267 | 7.422 | 0.979 |
| SZVR-2 | 12.5 | 0.402 | 7.207 | 0.495 | 5.496 | 6.045 | 0.909 |
| SZVR-3 | 13.1 | 0.385 | 6.894 | 0.454 | 3.463 | 3.697 | 0.936 |
| SZVR-4 | 13.6 | 0.367 | 5.141 | 0.322 | 3.969 | 4.411 | 0.899 |
| SZVR-5 | 14.5 | 0.339 | 3.415 | 0.197 | 2.007 | 2.189 | 0.916 |
| SZVR-6 | 14.8 | 0.332 | 2.582 | 0.146 | 2.178 | 2.475 | 0.880 |
| SZVR-7 | 17.1 | 0.269 | 1.761 | 0.081 | 1.475 | 1.725 | 0.855 |
| SZVR residue | 31.7 | 0.053 | 0.772 | 0.0069 | 0.785 | 1.839 | 0.426 |
| SQVR-2 | 12.6 | 0.402 | 7.213 | 0.496 | 4.286 | 4.616 | 0.928 |
| SQVR-4 | 13.0 | 0.386 | 5.383 | 0.356 | 3.454 | 3.753 | 0.920 |
| SQVR-6 | 13.9 | 0.356 | 3.295 | 0.201 | 2.642 | 2.957 | 0.893 |
| SQVR-8 | 17.5 | 0.258 | 1.413 | 0.062 | 1.845 | 2.375 | 0.776 |
| SQVR residue | 30.0 | 0.066 | 0.723 | 0.0082 | 0.762 | 1.584 | 0.481 |
| SQVR | 14.7 | 0.335 | 3.134 | 0.179 | 1.840 | 2.009 | 0.915 |
| SQVR | 14.7 | 0.334 | 3.134 | 0.179 | 2.077 | 2.293 | 0.905 |

Table 1B HDN diffusivities and kinetic parameters of SFEE fractions

| feed | $d_r/\text{\AA}$ | $F(\lambda)$ | $D_b/10^{-10}\text{m}^2\text{s}^{-1}$ | $D_r/10^{-10}\text{m}^2\text{s}^{-1}$ | $k_s/10^{-4}\text{ms}^{-1}$ | $k_r/10^{-4}\text{ms}^{-1}$ | η |
|--------------|------------------|--------------|---------------------------------------|---------------------------------------|-----------------------------|-----------------------------|--------|
| DGAR-1 | 9.34 | 0.522 | 112.2 | 10.01 | 8.520 | 8.582 | 0.992 |
| DGAR-2 | 9.71 | 0.507 | 93.53 | 8.109 | 8.350 | 8.423 | 0.991 |
| DGAR-3 | 10.1 | 0.492 | 85.27 | 7.175 | 5.857 | 5.898 | 0.993 |
| DGAR-4 | 10.3 | 0.483 | 76.00 | 6.274 | 5.285 | 5.324 | 0.992 |
| DGAR-5 | 10.6 | 0.474 | 72.30 | 5.858 | 4.392 | 4.420 | 0.993 |
| DGAR-6 | 10.8 | 0.462 | 63.83 | 5.046 | 4.016 | 4.043 | 0.993 |
| DGAR-7 | 11.3 | 0.445 | 51.71 | 3.936 | 2.634 | 2.650 | 0.994 |
| DGAR-8 | 12.2 | 0.413 | 27.55 | 1.946 | 1.851 | 1.866 | 0.991 |
| DGAR residue | 20.2 | 0.198 | 2.116 | 0.072 | 0.502 | 0.533 | 0.941 |
| DGAR | 11.0 | 0.456 | 62.23 | 4.856 | 1.523 | 1.527 | 0.997 |
| SZVR-1 | 11.2 | 0.448 | 38.48 | 2.949 | 2.557 | 2.576 | 0.992 |
| SZVR-2 | 12.5 | 0.402 | 7.207 | 0.495 | 2.160 | 2.217 | 0.974 |
| SZVR-3 | 13.1 | 0.385 | 6.894 | 0.454 | 1.538 | 1.583 | 0.971 |
| SZVR-4 | 13.6 | 0.367 | 5.141 | 0.322 | 1.341 | 1.402 | 0.956 |
| SZVR-5 | 14.5 | 0.339 | 3.415 | 0.197 | 0.833 | 0.650 | 0.973 |
| SZVR-6 | 14.8 | 0.332 | 2.582 | 0.146 | 0.815 | 0.638 | 0.964 |
| SZVR-7 | 17.1 | 0.269 | 1.761 | 0.081 | 0.400 | 0.417 | 0.958 |
| SZVR residue | 31.7 | 0.053 | 0.772 | 0.0069 | 0.215 | 0.281 | 0.766 |
| SQVR-2 | 12.6 | 0.402 | 7.213 | 0.496 | 1.049 | 1.068 | 0.982 |
| SQVR-4 | 13.0 | 0.386 | 5.383 | 0.356 | 0.799 | 0.815 | 0.980 |
| SQVR-6 | 13.9 | 0.356 | 3.295 | 0.201 | 0.465 | 0.475 | 0.980 |
| SQVR-8 | 17.5 | 0.258 | 1.413 | 0.062 | 0.158 | 0.162 | 0.978 |

The molecular size of SFEF fractions is 10-20Å and 20-30Å for the SEFE residue. The largest ratio of diffusion molecule diameter to pore diameter is 0.48, which is less than 0.5. In the present study conditions, bulk diffusivity is $0.7 \sim 112 \times 10^{-10} \text{ m}^2/\text{s}$, and the effective diffusivity is $0.006 \sim 10 \times 10^{-10} \text{ m}^2/\text{s}$. The bulk diffusivity varies within the range of liquid diffusivity for less viscous system. The effective diffusivity belongs to the range of configuration [16]. For less viscous system the diffusivity agrees with that in reference very well [17], but for more viscous system, no published data can be used to compare.

The apparent and intrinsic rate constants are $0.76 \sim 9.25 \times 10^{-12} \text{ m/s}$ and $1.58 \sim 9.32 \times 10^{-12} \text{ m/s}$ for HDS, and $0.15 \sim 8.52 \times 10^{-12} \text{ m/s}$ and $0.16 \sim 8.58 \times 10^{-12} \text{ m/s}$ for HDN. For the same feed, HDS reaction rate is always greater than HDN. Which means that the removal of nitrogen is more difficult than that of sulfur in heavy oil.

The differences of rate constants between HDS and HDN for different feeds are shown in figure 2. Such differences are obviously greater for medium fractions than for lighter and heavier fractions. It may be ascribed to the difficulty for lighter fraction reaching to high conversion of HDS reaction and for the removal of sulfur and nitrogen of heavier fraction with high aromaticity. Therefore, the deeply HDS of lighter fraction is very difficult as the HDS and HDN of heavier fraction.

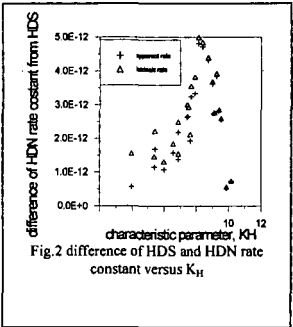


Fig.2 difference of HDS and HDN rate constant versus K_H

Figure 3 and 4 shows the relationships of apparent and intrinsic rate constant of HDS and HDN and the heavy oil characteristic parameter^[18], K_H , and the molecular weight of feed. The apparent and intrinsic rate constants decrease quickly with the increase of AMW, and reach to a stable value. Rate constants vary with the decrease of K_H with the similar mode mentioned above, and the minimum value in close to the level of thermal cracking. It is better to describe the HDS and HDN reactivity of SEFE fractions with the heavy oil characteristic parameter than AMW. The intrinsic reactivity decreases most quickly at $K_H=8.0$ for HDS reaction, and quickly at the startup of $K_H=9.5$. This phenomenon agrees with the common views that the HDS reactivity is obvious greater than that of HDN for lighter distillate.

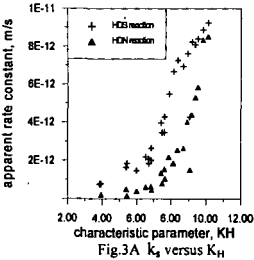


Fig.3A k_a versus K_H

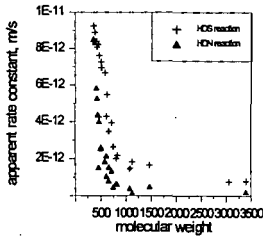


Fig.3B k_a versus AMW

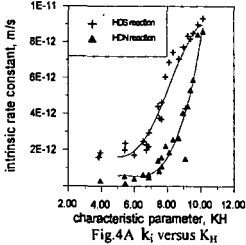


Fig.4A k_i versus K_H

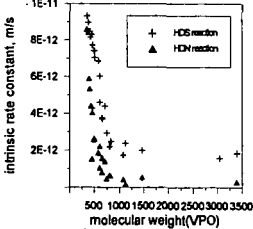


Fig.4B k_i versus AMW

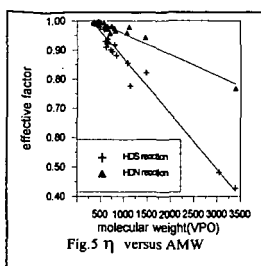


Figure 5 is the plots of relationships of effectiveness factors of HDS and HDN and the molecular weight of feed. The effectiveness factors decrease proportionally with the increase of AMW. This means that diffusion effect exists in the present reaction conditions, and the heavier the fraction is, the larger the molecular size, and the severer the diffusion effect.

With the increase of fraction AMW, the decrease of intrinsic rate constant for HDN is faster than for HDS, but the decrease of effectiveness factor for HDN is slower than for HDS. Therefore, the poorer HDS and HDN reactivity for heavier fractions can be explained by the lower intrinsic reactivity as

well as stronger diffusion resistance, and the decrease of intrinsic reactivity is the controlling factor for HDN reaction.

CONCLUSION

Through the catalytical hydroconversion of SFEF fractions which properties change in a large range, some conclusions were emerged. The diffusion of macromolecule in catalyst micropore filled with liquid belongs to configuration diffusion. The HDS and HDN diffusion-reaction model of residue in autoclave reactor was established. The intrinsic and apparent rate constants of HDS and HDN reaction obtained in terms of the kinetic model decrease quickly and reach to stable values with the increase of average molecular weight. HDN rate constant declines faster than that of HDS, but the effective factor of HDS decreases more quickly than that of HDN. It means that the low conversion of HDS and HDN reaction for heavier SFEF fractions could be ascribed to the poorer reactivity and the stronger diffusion resistance. The heavier the SFEF fraction, the larger the molecular size, and the severer the effect of diffusion on the reaction.

REFERENCES

1. Hoog H. *J Inst Petro.* 1950,36:738
2. Yitzhaki D, Aharoni C. *AIChE J.* 1988,23:342
3. Philippopoulos C, Papayannkos N. *IEC Res.* 1988,27(3):415
4. Trytten L C, Gray M R. *IEC Res.* 1990,29(5):725
5. Dai wenguo. The catalytic cracking characteristics of resins in different narrow fractions of Shengli vacuum residuum. Master thesis, University of Petroleum, China. March 1993
6. Chang Jie, Kinetics and Catalyst Deactivity Model of Residua. Doctoral thesis, Beijing Research Institute of Petroleum Processing, China, August 1997
7. Shah Y T, Paraskas J A. *ICE Press Des.Dev.* 1975, 14(4):368
8. Levenspiel O. *Chemical Reaction Engineering(second edition).* John Wiley & Sons, Inc. 1972, P474
9. Ruckenstein E, Tsai M C. *AIChE J.* 1981, 27(4):697
10. Chen Gantong, *Chemical Reaction Engineering(Chinese).* Chemical Industry Press, July 1981, P182
11. Carberry J J, *Chemical Reaction and Reactor Engineering.* Marcel Dekker, Inc. 1987, P251
12. Renkin E M. *Journal of General Physiology.* 1954, 38:225
13. Yang Chaohe. Characteristics and kinetics of heavy oil Hydroconversion. Doctoral Thesis, University of petroleum, Beijing, China, 1997
14. Shi Jun. *Handbook of Chemical Engineering(section 10)Mass Transfer.* Chemical Industry Press, October 1989, P10-80
15. Chen Y W, Thasi M C. *IEC Res.* 1995, 34:898
16. Weisy P B. *Chem. Techn.* 1973:504
17. Baltus R E. *Fuel Sci & Techn.Intl.* 1993, 11(5&6):52
18. Si Tiepan, Hu Yunxiang, et al. *Acta Petrolei Sinica(Petroleum Processing Section).* 1997, 13(2):1

COKE FORMATION AND CHARACTERIZATION DURING THERMAL TREATMENT AND HYDROCRACKING OF LIAOHE VACUUM RESIDUUM

Zong-xian Wang, Ai-Jun Guo, Guo-he Que
National Heavy Oil Processing Laboratory, University of Petroleum
Dongying, Shandong 257062, P. R. China

The physical and chemical properties and structural compositions of Liaohe residuum were studied. The coke formation in the processes of thermal conversion and slurry catalytic hydrocracking reaction of the residuum was subsequently investigated. Then, the relationship between coke formation tendency and physicochemical compositions of the residuum was studied. The effect of initial coke formation on the propagation of coke formation was also studied. Using high-precision microscope and FTIR, the formed coke was characterized. With increasing processing severity, the coke formed in the bulk of reaction fluid system is changing from fine particulate form to coke cluster form. Initially formed coke seems to promote coke formation and growth of coke clusters during thermal treatment under low pressure. The on-set of coke formation is quite closely related to the ability of reaction system to peptize coke precursors.

KEY WORDS: coke formation, thermal treatment, hydrocracking, vacuum residue.

INTRODUCTION

Coke formation has long been a concern of petroleum refiners and researchers because petroleum residue processing is often limited by coke formation. This limitation is very severe in the cases of visbreaking, catalytic hydrotreating and catalytic hydrocracking, in which no appreciable amount of coke can be tolerated because of the need to flow freely through coils or catalyst-bed and the need to keep catalysts active. In the FCC or RFCC and slurry-bed catalytic hydrocracking (SBCH) processes, coke formation may deactivate catalysts and decrease the depth of upgrading. Even the delayed-coking process would be limited by coke formation in heating coils. Hence, the coke formation is one of key factors influencing petroleum residue upgrading.

In addition to processing conditions, the physical and chemical properties and structural composition of petroleum residues dictate the action of coke formation (1-4). A vacuum residue (VR) with low H/C atomic ratio and high carbon residue may be of high propensity to produce large amount of coke, to which much attention has been paid by RFCC, Coking and SBCH processes. The inducing period of coke formation is not only related to carbon residue value but to the miscibility of residue sub-fractions and particularly to the ability for vacuum residue system to peptize its asphaltene and coke precursors (5-7). Evidently, the long inducing period of coke formation is relevant to visbreaking and hydrotreating processes. Therefore, the study on coke formation is of significance in searching for coke inhibition procedures.

This work is intended to take Liaohe vacuum residue as a specimen to study, in detail, its physical and chemical properties and structural composition, and to investigate coke formation during its thermal, hydrothermal conversion and slurry-bed catalytic hydrocracking.

EXPERIMENTAL

Sample

Liaohe vacuum residue was collected from Liaohe Petrochemical Plant in March 1996; Gudao VR was collected from Shengli Oil Refinery. Their general properties are listed in Table 1.

Analytical Procedures

Isolation of Six Sub-fractions

Liaohe and Gudao vacuum residues were chromatographically separated into six fractions, i.e. light oil (F1), heavy aromatic fraction (F2), light resin (F3), middle resin (F4), heavy resin (F5) and n-pentane asphaltene (F6) by using a procedure described in reference (8)

Ultimate Analysis and Molecular Weight Measurement

Carlo Erba 1160 elemental analyzer was used for C, H, N analysis; atomic absorption method was used to determine Ni, V, Fe and Ca contents. Average molecular weight was measured by using VPO method (benzene as solvent, 45 °C) with Knauer molecular weight analyzer.

FTIR and Microscopic Characterization of Petroleum Coke

FTIR analysis of coke was conducted at Nicolet Magna 750 IR analyzer, a mold flat of coke and KBr mixture as sampling. An OLYMPAS HS-2 microscope was used to visualize the coke formed in the bulk of reaction system.

Liaoh VR Thermal and Hydrothermal Conversion and Catalytic Hydrocracking

The experiments were carried in a 100ml FDW-01 autoclave reactor with an up-and-down stirrer at 120 times of reciprocation per minute. Initial pressure was 5.0Mpa N₂ for thermal conversion and 7.0Mpa H₂ for hydrothermal conversion and catalytic hydrocracking. Catalyst used in hydrocracking reaction was Mo based oil soluble additive (ca.200 PPM Mo in reaction feed), and was pre-sulfided by elemental sulfur at 320°C for 30minute after mixing with Liaoh VR (S/Mo atomic ratio=3/1). Reaction temperature (430°C) was reached within 25minute from room temperature. After 1 hr. reaction time, the reactor was quenched (cooled) to room temperature, the reactor gas was vented, and toluene slurry was prepared from the reactor contents. Any solids adhering to the reactor walls or internals was carefully scraped off. The slurry was centrifuged into the toluene insoluble (TI or coke) and the toluene soluble; the toluene insoluble was then washed (extracted) with boiling toluene and separated by using quantitative filter paper, and then dried and weighed. The toluene soluble was distilled into several fractions. The data are listed in table 4.

RESULTS AND DISCUSSION

Relation Between Feed Properties and Coke Formation

The data in table I show that Liaoh VR, in contrast to Gudao VR, is high in viscosity, CCR, heavy metals, nitrogen content, aromaticity (f_A) and the ratio of aromatic ring number to naphthenic ring number (R_A/R_N). This indicates that Liaoh VR will generates more coke than Gudao VR under high processing severity (e.g. delayed coking and RFCC).

However, the SARA analysis (group composition) is similar for these two VR, for example, the oil fractions (saturates+aromatics) are 47.7% and 49.3% for Liaoh VR and Gudao VR respectively. Even the n-heptane asphaltene (nC7-At) content of Liaoh VR is less than that of Gudao VR. Even the oil fraction of Liaoh VR has lower density, viscosity, pour point, CCR, sulfur, nitrogen and metal contents, contrast to the oil fraction of Gudao VR.

Therefore, it can be inferred that the qualities of resin and asphaltene fractions of Liaoh VR must be much inferior to those of Gudao VR. It is verified by further analysis of six sub-fractions of these two VR, as seen in table 3. The nitrogen, nickel and CCR in heavy resin and asphaltene account for 69.1%, 78.6% and 74.1% respectively of total N, Ni and CCR in Liaoh VR, while the corresponding values are only 61.0%, 61.0% and 63.0% for Gudao VR. The aromaticity and R_A/R_N ratio of Liaoh resin and asphaltene are much higher than those of Gudao resin and asphaltene, indicating that the cracking performance of Liaoh resin and asphaltene must be quite poor.

Besides, there exists a great difference in molecular weight distribution in Liaoh VR six sub-fractions. The ratio of asphaltene molecular weight to oil molecular weight for Liaoh VR is about 9.5, while that for Gudao is only about 4.6. The gap between properties of oil fraction and resin-asphaltene fraction of Liaoh VR is much wider than that of Gudao VR, which implies that the system of Liaoh VR is not harmonious, and its colloidal stability must be very low. All those above show that Liaoh VR is kind of inferior heavy oil; the propensity to coke formation is much higher than Gudao VR during processing. A preliminary thermal treatment test has shown that the inducing period of coke formation of Liaoh VR is shorter than that of Gudao VR.

Distribution of Products in Thermal Treatment and Hydrocracking of Liaoh VR

Table 4 lists 450°C⁻ fraction, 450°C⁺ cracked residue, coke content in reaction products and

pentane asphaltene content in cracked residue. With reaction temperature being increased, 450°C fraction yields increases for all three series of reactions, and the increment is the highest for thermal reaction and the least for catalytic hydrocracking with Mo based catalyst. But the conversion to light products is the highest for the latter process under unit coke formation condition. Under the reaction condition of 430°C and reaction time 1 hr, the coke formation is less than 1% and conversion reaches up to 50% for the latter process; while coke formation is much greater than 1% as conversion reaches 50% for other two series of reactions of Liaohe VR. The coke formation increases rapidly with temperature for thermal treatment of Liaohe VR, but quite slowly for catalytic hydrocracking. The asphaltene contents in three reaction systems are changed in the similar tendency with cracked residue proportions. The molecular weight of asphaltene decreases with increasing reaction temperature for all these three reaction systems. The decrease of asphaltene molecular weight for thermal treatment is most eminent.

Characterization of Coke Formation by Microscopic Analysis

Reacted materials were sampled from the bulk of reaction system with thin glass plate as the samplers and then visualized by using an OLYMPAS HS-2 microscope. Three series of microphotographs (10×40×3.3) were taken of reacted materials from three series of reaction systems of Liaohe VR thermal treatment, hydro-thermal treatment and catalytic hydrocracking. The microscopic analysis showed that there was yet little coke at 420°C for hydrocracking system. With temperature increasing, the coke formed in the bulk of reaction system was changing from fine dispersed particle forms to small clusters(about 0.1-0.2% coke contents), corresponding temperatures being at 425, 415 and 400°C for thermal treatment, hydro-thermal treatment and catalytic hydrocracking respectively; and further to coke clusters corresponding temperatures being at 430, 420, 415°C respectively.

Characterization of Coke by FTIR

Fourier Transition Infrared spectrometry (FTIR) is a useful technique for characterizing organic functional groups of organic substances. Naturally it can be used to characterize the coke formed in reaction system and to describe the changes of different organic function groups, such as aromatic carbon, paraffinic carbon and substitution extent of aromatic ring periphery, of coke with increasing reaction severity.

Aromatic C=C double bond vibrates at 1600 cm^{-1} aromatic C-H bond vibrates at 3030 cm^{-1} , and 750 cm^{-1} , 810 cm^{-1} , 870 cm^{-1} . Paraffinic C-H vibrates at 2920 cm^{-1} , 2860 cm^{-1} , 1460 cm^{-1} and 1380 cm^{-1} . Here, the relative vibrating strength (A_x), i.e., the ratio of vibrating strength (A_x) of function groups to C=C vibrating strength (A_{1600}), was used to describe the relative changes of coke function groups and to reveal the way in which chemical structures change. The relative vibrating strengths of several organic function groups of coke formed at different severity in Liaohe VR reaction systems were tabulated in table 5. With temperature increasing, A_{2920} and A_{2860} seemed gradually decreasing, showing the paraffinic portion of coke decreasing and aromaticity relatively increasing. A_{870} , A_{810} and A_{750} increased with temperature increasing, showing that constitution extent of aromatic ring was decreasing and side chain cracking occurred. Therefore, FTIR is an effective means for characterization of coke formation during VR processing.

Mechanism of Initial Coke Formation and Its Effect

Vacuum residue is a colloidal system with asphaltene and heavy resin as dispersed phase and oil fraction and light resin as media. If physical and chemical properties of dispersed phase were much different from those of media constituents, the media would not properly peptize the asphaltene, and the colloidal system would not be stable. For example, asphaltene can be precipitated by n-pentane because pentane dilutes the colloidal system and makes the media less aromaticity, low average molecular weight and low polarity. When heating disturbs vacuum residue system, the molecules move fast, the micelle made up of asphaltene and media would become loser, some of asphaltene molecules may bump off the micelle cages to coalesce. The vacuum residue colloidal system can also be disturbed by some fine solid polar particles due to the adsorption of asphaltene molecules to these particles. At high heating severity, some weak bonds in asphaltene molecules may crack. Asphaltene micelles may break apart; some asphaltene molecules may physically coalesce or chemically interact to form large molecules. At the same time, the ability for media to peptize asphaltene molecules becomes lower due to light fractions

increasing, thus causing asphaltene molecules to coalesce and to be precipitated.

All these factors can account for the initial coke formation of vacuum residue reaction system. In fact, the initial coke is the physical-chemically-coalescent phase of asphaltene molecules, whose properties are very similar to those of asphaltene-coke precursor. Hence initial coke may have high an affinity for asphaltene molecules and promote coalescence of asphaltene molecules and coke formation.

In order to testify the effect of the initial coke on reaction system, Liaoh VR with some pre-added coke powders was subjected to thermal treatment and hydrocracking tests. The thermal treatment under atmospheric nitrogen gas was conducted in a quartz tube reactor (30 ml) heated by an electric tin bath, other tests were carried out in an autoclave of 100 ml under 7MPa hydrogen gas. The results were tabulated in table 6.

Coke formation was about 0.73% for Liaoh VR thermal treatment under conditions of 406°C 2hr and nitrogen atmosphere. When 0.5% coke was pre-added in the thermal treatment system, total coke was about 1.93%, net coke formation was 1.20%, net coke increment was about 0.47% contrast to blank test without pre-added coke; 1% pre-added coke promoted 1.22% net coke formation compared with the blank thermal treatment. It was obvious that initial coke could considerably promote coke formation during thermal treatment of vacuum residue under low pressure(a relatively open system). In hydrothermal treatment of VR, it seemed, superficially, that pre-added coke was of little influence on coke formation. In fact, the Ni, Fe in pre-added coke might act as hydrocracking catalysts, the catalytically active hydrogen could saturate the coke precursor free radicals and chemically inhibit condensation of these free radicals, thus inhibit the coke formation. The counteraction between the coke promotion by initial coke and the coke inhibition by heavy metals in the coke makes total coke formation similar to the coke formation in virgin hydrothermal treatment. In the catalytic hydrocracking process, pre-added coke could markedly inhibit net coke formation. In addition to activating hydrogen, the pre-added coke and Mo sulfide solid particles were of high affinity for asphaltene free radicals, and made these coke precursor radicals adsorbed around them. Thus, the active hydrogen on catalysts could instantly terminate coke precursor radicals; thus the coke inhibition efficiency was enhanced. The performance for catalyst particles to enrich asphaltene-coke precursors around them and to promote the utilization of active hydrogen may be the important factors for slurry-bed catalytic hydrocracking of heavy oils to effectively inhibit coke formation.

CONCLUSION

The SARA group composition of Liaoh VR is similar to that of Gudao VR, the nature of its oil fraction is even better than that of the Gudao VR counterpart, but its resin and asphaltene fractions are much inferior to those of Gudao VR. The uniformity of Liaoh VR system is lower than that of Gudao VR, its colloidal system is not stable, and the coke formation tendency is high during further processing.

With processing severity increasing, coke formation in VR reaction system is developed from dispersed fine particles to coke clusters. FTIR technique can effectively characterize the evolution of aromatic part and paraffinic part of the coke formed at different severity.

The initial coke could promote coke formation during low-pressure thermal treatment of VR. During hydrothermal and hydrocracking treatments, pre-added coke seems to promote catalysis.

LITERATURE CITED

1. Weihe, I. A., *Ind. Eng. Chem. Res.*, **31**: 530(1992)
2. Weihe, I. A., *Ind. Eng. Chem. Res.*, **32**: 530(1993)
3. Xu, Y.-M., *Acta Petrolei Sinica (Petroleum Processing Section)*, **1**(3): 13(1985)
4. Que, G.-h. *Fuel*, **71**:1483(1992)
5. Weihe, I. A., *PREPRINTS, Div. Petol. Chem., ACS*, **38**: 428(1993)
6. Li, S.-h., Liu, C.-G., Que, G.-H., Liang, W.-J., *Fuel*, **75**:1025(1996)
7. Deng, W.-A., Que, G.-H., *Acta Petrolei Sinica (Petroleum Processing Section)*, **13**(1): 1(1997)
8. Wang, Z.-X., Que, G.-H., Liang, W.-J., *PREPRINTS, Div. Petol. Chem., ACS*, **43**(1): 155(1998)

Table 1 Properties of Liaohe vacuum residue (VR)

| Property | Liaohe VR | Gudao VR |
|---|-----------|----------|
| Density(20°C), g/cm ³ | 0.9976 | 0.9998 |
| Viscosity(100°C)/mm ² .s ⁻¹ | 3375 | 1710 |
| Pour point, °C | 42 | 41 |
| Flash point, °C | 312 | 327 |
| Carbon residue, % | 19.0 | 15.6 |
| Elemental composition | | |
| C, % | 87.0 | 85.4 |
| H, % | 11.4 | 11.4 |
| S, % | 0.43 | 2.52 |
| N, % | 1.08 | 0.80 |
| H/C(Atomic ratio) | 1.50 | 1.60 |
| Total Metal/PPM | 258.6 | 131.6 |
| Ni, PPM | 122.6 | 48.0 |
| V, PPM | 2.9 | 2.2 |
| Fe, PPM | 37.5 | 13.8 |
| Ca, PPM | 95.6 | 33.8 |
| Ash, % | 0.056 | 0.026 |
| SARA fractions: | | |
| Saturates, % | 17.1 | 14.5 |
| Aromatics, % | 30.3 | 34.8 |
| Resins, % | 50.2 | 47.2 |
| nC7-Asphaltene, % | 2.1 | 3.5 |
| Structural Parameters | | |
| F _A | 0.267 | 0.181 |
| F _N | 0.258 | 0.330 |
| R _A /R _N | 0.93 | 0.47 |

Table 2 Properties of oil fraction of Liaohe VR

| Properties | Oil fraction of Liaohe VR | oil Fraction of Gudao VR |
|--|---------------------------|--------------------------|
| Density(20°C), g/cm ³ | 0.9392 | 0.9558 |
| Viscosity(100°C), mm ² .s ⁻¹ | 84.1 | 103.0 |
| Pour point, °C | 36.0 | 39.0 |
| Carbon residue, % | 3.5 | 5.8 |
| MW | 630 | 860 |
| Elemental composition | | |
| C, % | 87.2 | 85.0 |
| H, % | 12.3 | 11.9 |
| S, % | 0.34 | 2.0 |
| N, % | 0.33 | 0.45 |
| H/C(Atomic ratio) | 1.68 | 1.67 |
| Metals | | |
| Ni, PPM | 1.3 | 6.0 |
| V, PPM | 2.4 | / |
| Ca, PPM | 1.1 | 19.8 |

Table 3 Properties and composition of six fractions of Liaohé VR

| Property | F1 | F2 | F3 | F4 | F5 | nC ₅ -At |
|--|------|------|-------|-------|-------|---------------------|
| <i>Liaohé VR:</i> | | | | | | |
| Yield, % | 36.1 | 11.6 | 16.8 | 9.0 | 12.3 | 14.2 |
| MW | 590 | 810 | 1050 | 1380 | 2240 | 5970 |
| f _A | / | / | 0.329 | 0.357 | 0.371 | 0.509 |
| f _N | / | / | 0.201 | 0.153 | 0.151 | 0.082 |
| R _A /R _N | / | / | 1.5 | 2.2 | 2.4 | 6.2 |
| H/C | 1.75 | 1.48 | 1.44 | 1.41 | 1.38 | 1.19 |
| N, % | 0.16 | 0.85 | 1.42 | 1.70 | 1.78 | 1.96 |
| N _f /N _T , % | 2.1 | 10.8 | 18.0 | 21.6 | 22.6 | 24.9 |
| Ni, ppm | 1.3 | | 197.3 | 225.2 | | 502.3 |
| Ni _f /Ni _T , % | 0.2 | | 21.3 | 24.3 | | 54.3 |
| CCR, % | 3.5 | | 23.2 | 31.1 | | 45.3 |
| CCR _f /CCR _T , % | 3.4 | | 22.5 | 30.2 | | 43.9 |
| <i>Gudao VR:</i> | | | | | | |
| Yield, % | 34.9 | 14.2 | 15.6 | 7.9 | 8.8 | 15.9 |
| MW | 800 | 1000 | 1370 | 1760 | 2430 | 3920 |
| f _A | / | / | 0.285 | 0.290 | 0.297 | 0.437 |
| f _N | / | / | 0.149 | 0.182 | 0.166 | 0.128 |
| R _A /R _N | / | / | 1.8 | 1.5 | 1.7 | 3.3 |
| H/C | 1.83 | 1.50 | 1.51 | 1.49 | 1.48 | 1.29 |
| N, % | 0.10 | 0.75 | 1.17 | 1.37 | 1.43 | 1.48 |
| N _f /N _T , % | 4.2 | 12.9 | 21.9 | 13.0 | 19.7 | 28.3 |
| Ni, ppm | 0.6 | 9.7 | 109.1 | 43.7 | 49.6 | 127.3 |
| Ni _f /Ni _T , % | 0.4 | 2.9 | 35.7 | 7.2 | 12.0 | 41.8 |
| CCR, % | 2.4 | 15.9 | 21.7 | 23.6 | 21.7 | 41.8 |
| CCR _f /CCR _T , % | 4.8 | 12.9 | 19.3 | 10.6 | 14.5 | 37.9 |

MW- molecular weight. N_f/N_T-the ratio of nitrogen in fraction to total nitrogen in VRNi_f/Ni_T-the ratio of nickel in fraction to total nickel in VRCCR_f/CCR_T-the ratio of carbon residue of fraction to total carbon residue in VRTable 4 Yields of conversion products under three series of reaction conditions
(Reaction time 1hr)

| Reaction condition | | <450°C product, % | >450°C cracked residue, % | Coke, % | nC ₅ -At in cracked residue | |
|--|-----|----------------------|---------------------------------|---------|---|------|
| | | | | | % | MW |
| N ₂ 5MPa | 400 | 37.7 | 62.2 | 0.1 | / | / |
| | 410 | 44.4 | 54.2 | 1.4 | 24.6 | 3349 |
| | 420 | 67.1 | 32.9 | 10.9 | 15.8 | 2829 |
| | 430 | 62.8 | 17.7 | 19.5 | 9.2 | 1499 |
| H ₂ 7MPa | 400 | 28.27 | 71.68 | 0.05 | / | / |
| | 410 | 40.90 | 59.00 | 0.10 | 23.1 | 3837 |
| | 420 | 50.20 | 46.60 | 3.20 | 17.9 | 2989 |
| | 430 | 61.40 | 30.78 | 7.92 | 13.3 | 1979 |
| H ₂ 7MPa Mo 200ppm | 400 | 18.95 | 81.00 | 0.05 | / | / |
| | 410 | 25.60 | 74.31 | 0.09 | / | / |
| | 420 | 35.54 | 64.24 | 0.22 | 15.8 | 3477 |
| | 430 | 50.19 | 49.13 | 0.68 | 14.8 | 2932 |
| | 440 | 53.79 | 42.0 | 4.21 | 12.2 | 2063 |

Table 5 Relations between coke FTIR Data and reaction conditions

| Coke samples | A ₂₉₂₀ | A ₂₈₆₀ | A ₃₀₃₀ | A ₈₇₀ | A ₈₁₀ | A ₇₅₀ |
|------------------------------|-------------------|-------------------|-------------------|------------------|------------------|------------------|
| N ₂ | | | | | | |
| 410°C | 0.780 | 0.493 | 0.060 | 0.271 | 0.206 | 0.185 |
| 420°C | 0.650 | 0.426 | 0.095 | 0.283 | 0.243 | 0.241 |
| 430°C | 0.273 | 0.210 | 0.098 | 0.349 | 0.312 | 0.294 |
| H ₂ , Mo200ppm | | | | | | |
| 425°C | 0.574 | 0.385 | 0.068 | 0.280 | 0.152 | 0.149 |
| 430°C | 0.375 | 0.256 | 0.058 | 0.278 | 0.210 | 0.184 |
| 435°C | 0.265 | 0.176 | 0.060 | 0.214 | 0.215 | 0.196 |
| 440°C | 0.183 | 0.155 | 0.030 | 0.390 | 0.422 | 0.406 |

Table 6 Effect of initial coke on coke formation of reaction system

| Reaction condition | sample | <450°C product, % | >450°C cracked residue, % | ** coke, % | *** coke increment, % |
|--|---------------|-------------------------|---------------------------------|---------------|-----------------------------|
| * N ₂ (blowing), 2hr | | | | | |
| 406° | LHVR | / | / | 0.73 | |
| 406° | LHVR+0.5%coke | / | / | 1.20 | 0.47 |
| 406° | LHVR+1.0%coke | / | / | 1.95 | 1.22 |
| H ₂ , 7MPa, 2hr | | | | | |
| 412° | LHVR | 53.37 | 43.70 | 2.93 | |
| 412° | LHVR+0.5%coke | 54.06 | 42.50 | 2.94 | 0.01 |
| H ₂ , 7Mpa, 2hr Mo, 200ppm | | | | | |
| 425° | LHVR | 56.87 | 41.50 | 1.63 | |
| 425° | LHVR0.5%coke | 52.96 | 45.40 | 1.14 | -0.49 |

* conducted by using a quartz tube reactor with N₂ as a blowing gas ;

** net coke formation, i.e., total coke minus added coke.

*** coke increment on the base of blank test.

AUTHOR INDEX, VOLUME 43, (ISSUE NUMBER) PAGE NUMBER

| | | | |
|-----------------------------|----------|--------------------------|----------|
| Aceves, S. M. | (3) 570 | Chang, C. H. | (3) 580 |
| Ahmed, S. | (3) 543 | Chang, R. | (4) 871 |
| Ali, M. F. | (4) 1063 | Chavadej, S. | (3) 490 |
| Ali, S. A. | (3) 543 | Chen, S. | (3) 596 |
| Allardice, D. J. | (3) 407 | Chen, S. | (4) 871 |
| Allen, M. | (3) 575 | Cheng, H. | (4) 990 |
| Amadeo, N. E. | (3) 689 | Chinn, M. J. | (4) 885 |
| Amouroux, J. | (4) 890 | Chipps, J. F. | (4) 1057 |
| Anderson, D. A. | (4) 1069 | Chocrón, M. | (3) 689 |
| Andriollo, A. | (3) 563 | Chollar, B. | (4) 1031 |
| Antal, M. J. | (3) 363 | Chollar, B. H. | (4) 1083 |
| Antal, M. J. | (4) 825 | Chollar, B. H. | (4) 1090 |
| Arenillas, A. | (4) 1120 | Chollar, B. H. | (4) 1096 |
| Arenillas, A. | (4) 1133 | Chu, I. | (3) 451 |
| Armour, S. J. | (4) 1115 | Chung, K. | (4) 929 |
| Atha, T. | (4) 1045 | Clarkson, R. B. | (4) 955 |
| Aulich, T. | (3) 383 | Comolli, A. G. | (3) 441 |
| Aurilio, V. | (4) 1031 | Contescu, A. | (4) 833 |
| Badger, M. W. | (3) 461 | Contescu, C. I. | (4) 833 |
| Bahia, H. U. | (4) 1041 | Cook, W. | (3) 727 |
| Baker, J. J. | (3) 727 | Cotte, E. | (3) 678 |
| Baleo, J. N. | (4) 875 | Coulibaly, K. | (4) 890 |
| Ban, H. | (4) 1010 | Crelling, J. C. | (4) 924 |
| Banfield, T. L. | (4) 995 | Cyr, T. | (3) 496 |
| Barnakov, Ch. N. | (4) 1107 | Dai, X. | (4) 825 |
| Barnes, P. A. | (4) 885 | Daly, W. H. | (4) 1075 |
| Bates, D. R. | (3) 575 | Davini, P. | (4) 1129 |
| Beisel, A. J. | (4) 995 | Davison, R. R. | (4) 1057 |
| Belford, R. L. | (4) 955 | Dawson, E. A. | (4) 885 |
| Benedetti, M. F. | (4) 829 | Demirel, B. | (3) 466 |
| Benham, M. | (4) 770 | Demirel, B. | (3) 501 |
| Bermejo, J. | (4) 941 | Dente, M. | (3) 653 |
| Berry, G. D. | (3) 570 | Desai, S. | (4) 814 |
| Beznisko, S. I. | (4) 838 | Dieterle, M. | (3) 501 |
| Bi, J. | (3) 703 | Dongré, R. | (4) 1019 |
| Bi, J. | (3) 707 | Du, F. | (3) 668 |
| Billiter, T. C. | (4) 1057 | Du, F. | (3) 673 |
| Biswas, M. E. | (3) 543 | Du, F. | (3) 751 |
| Blackwell, A. G. | (3) 645 | Dubois, A. M. | (3) 640 |
| Bockrath, B. | (3) 694 | DuBose, S. B. | (4) 796 |
| Bockrath, B. | (3) 717 | Dunham, G. E. | (4) 867 |
| Borole, A. P. | (3) 506 | Dutta, R. | (3) 538 |
| Boudou, J-P. | (4) 829 | Economy, J. | (4) 880 |
| Bozzano, G. | (3) 653 | Embaid, B. P. | (3) 521 |
| Brackman-Danheux, C. | (4) 857 | Enomoto, H. | (3) 741 |
| Branthaver, J. | (4) 1037 | Enqvist, J. | (3) 400 |
| Brasquet, A. | (4) 970 | Enqvist, M. | (3) 400 |
| Bridges, J. L. | (4) 796 | Erdmann, K. | (4) 905 |
| Britt, P. F. | (3) 630 | Eser, S. | (3) 471 |
| Buchanan, A. C. | (3) 630 | Eser, S. | (3) 611 |
| Caldwell, T. A. | (3) 490 | Espino, R. L. | (3) 388 |
| Carrillo Guarin, J. A. | (3) 431 | Fairbridge, C. | (3) 476 |
| Casal, E. | (4) 941 | Fedorak, P. M. | (3) 515 |
| Ceroke, P. | (4) 955 | Fernandes, F. A. N. | (3) 621 |
| Cerqueira, H. S. | (3) 626 | Ferrance, J. P. | (3) 694 |

AUTHOR INDEX, VOLUME 43, (ISSUE NUMBER) PAGE NUMBER

| | | | |
|----------------------------|---------|------------------------------|---------|
| Filgueiras, E. | (3) 521 | Holland, J. | (3) 727 |
| Finseth, D. | (4)1010 | Hong, C. X. | (3) 741 |
| Foght, J. M. | (3) 515 | Howard, B. H. | (4) 862 |
| Fontana, A. | (4) 857 | Hower, J. C. | (4) 975 |
| Frommell, E. | (3) 717 | Hower, J. C. | (4)1014 |
| Fuentes, A. | (3) 563 | Huang, B. Y. | (3) 606 |
| Fujii, M. | (3) 735 | Hudgins, R. R. | (4) 844 |
| Fuller, E. L. | (4) 770 | Hurt, R. | (4) 965 |
| Fuller, E. L. | (4) 775 | Hurt, R. H. | (4) 980 |
| Furutsuka, T. | (4)1125 | Iino, M. | (3) 712 |
| Galiasso, R. E. | (3) 563 | Iglesias, M. J. | (4) 820 |
| Gamble, V. | (4) 913 | Ingram, J. P. | (3) 575 |
| Gao, Y.-M. | (4) 980 | Ishihara, S. | (4)1125 |
| García, A. | (4) 820 | Itoh, Y. | (4) 852 |
| Gentzis, T. | (4) 929 | Iwamatsu, E. | (3) 543 |
| Gentzis, T. | (4) 933 | James, B. D. | (3) 568 |
| Gerlach, T. | (3) 383 | Jaroniec, M. | (4) 780 |
| Gibbins, J. R. | (4)1000 | Joaquim de Souza, E. J. | (3) 640 |
| Gibbins, J. R. | (4)1138 | Johns, M. M. | (4) 805 |
| Giles, K. A. | (4) 995 | Johns, M. M. | (4) 810 |
| Giray, E. S. | (3) 712 | Judd, R. W. | (3) 575 |
| Givens, E. N. | (3) 466 | Kamimura, H. | (3) 741 |
| Givens, E. N. | (3) 501 | Kamo, T. | (3) 658 |
| Gladding, D. T. M. | (3) 575 | Kamo, T. | (3) 703 |
| Glover, C. J. | (4)1057 | Kamo, T. | (3) 707 |
| Gonzalez-Gimenez, F. | (3) 521 | Kaufman, E. N. | (3) 506 |
| Graham, U. M. | (4) 985 | Kawano, S. | (4) 848 |
| Granda, M. | (4) 941 | Kawashima, H. | (3) 699 |
| Gray, M. R. | (3) 515 | Keller, M. | (3) 717 |
| Gray, R. J. | (4) 924 | Kern, D. | (3) 717 |
| Gregoire Padró, C. E. | (3) 353 | Kern, D. G. | (4) 995 |
| Gropppo, J. G. | (4) 985 | King, W. P. | (4) 995 |
| Guisnet, M. | (3) 626 | Kishita, A. | (3) 741 |
| Gülder, Ö. L. | (3) 435 | Kodera, Y. | (3) 658 |
| Guo, A.-J. | (3) 486 | Kodera, Y. | (3) 703 |
| Guo, A.-J. | (3) 530 | Kodera, Y. | (3) 707 |
| Guo, A.-J. | (3) 758 | Kondo, T. | (4)1125 |
| Guran, S. | (4) 990 | Korai, Y. | (4) 848 |
| Hada, T. | (4) 848 | Kornievich, M. V. | (4) 838 |
| Hagaman, E. W. | (4) 951 | Kosbab, S. | (4) 796 |
| Hamid, H. | (3) 543 | Kozlov, A. P. | (4)1107 |
| Hamilton, J. R. | (3) 407 | Krivohlavek, D. D. | (4)1102 |
| Harke, F. W. | (3) 645 | Kroo, E. | (4)1005 |
| Harrigan, E. | (4)1031 | Kruk, M. | (4) 780 |
| Hatcher, P. G. | (3) 611 | Külaots, I. | (4) 980 |
| Hattori, H. | (3) 426 | Kurose, H. | (3) 712 |
| Hawkins, R. W. T. | (3) 496 | Kuvshinov, D. G. | (4) 946 |
| Hequet, V. | (4) 875 | Kuvshinov, G. G. | (4) 895 |
| Herrmann, J.-M. | (4)1112 | Kuvshinov, G. G. | (4) 946 |
| Hidalgo, R. | (3) 368 | Kyotani, T. | (4) 960 |
| Hill, R. L. | (4) 975 | Lablanchy, P. | (4) 829 |
| Ho, K. | (4) 801 | Laborde, M. A. | (3) 689 |
| Ho, S. | (4)1026 | LaCount, R. | (3) 717 |
| Hodrien, R. C. | (3) 575 | LaCount, R. B. | (4) 995 |
| Hogan, E. N. | (3) 416 | Ladner, E. P. | (3) 645 |

AUTHOR INDEX, VOLUME 43, (ISSUE NUMBER) PAGE NUMBER

| | | | |
|-----------------------------|---------|------------------------|---------|
| Laine, J. | (4)1112 | McGreavy, C. | (3) 684 |
| Le Cloirec, P. | (4) 875 | Memom, G. M. | (4)1045 |
| Le Cloirec, P. | (4) 970 | Memom, G. M. | (4)1083 |
| Lebedev, M. Yu. | (4) 895 | Memom, G. M. | (4)1090 |
| Lee, J. M. | (3) 727 | Memom, G. M. | (4)1096 |
| Lee, S. | (3) 722 | Memom, M. | (4)1019 |
| Lee, T. L. K. | (3) 441 | Menéndez, E. M. | (4) 820 |
| Lemberton, J. L. | (3) 547 | Menéndez, J. A. | (4) 820 |
| Lewandowski, M. | (4) 909 | Menéndez, R. | (4) 941 |
| Li, P.-P. | (3) 558 | Mercer, M. | (4) 770 |
| Li, T. X. | (4)1010 | Michaud, P. | (3) 547 |
| Li, X. | (3) 435 | Mikuni, M. | (3) 426 |
| Liang, S. H. C. | (4)1115 | Mill, T. | (4)1053 |
| Lin, S. | (3) 673 | Miller, S. J. | (4) 867 |
| Lin, S. | (3) 746 | Miyamoto, S. | (4) 848 |
| Linkous, C. A. | (3) 358 | Mochida, I. | (4) 848 |
| Linkous, C. A. | (3) 378 | Mogilnykh, Yu. I. | (4) 895 |
| Liu, C. | (3) 481 | Mogilnykh, Yu. I. | (4) 946 |
| Lizzio, A. A. | (4) 814 | Mohan, T. | (4) 905 |
| Lizzio, A. A. | (4) 862 | Mojelsky, T. W. | (3) 526 |
| Llerena, R. | (3) 727 | Mojelsky, T. W. | (4) 917 |
| Lobban, L. L. | (3) 490 | Moliner, R. | (4) 857 |
| Lona Batista, L. M. F. | (3) 616 | Morales, A. | (3) 521 |
| Lona Batista, L. M. F. | (3) 621 | Moriya, T. | (3) 741 |
| López-Linares, F. | (3) 563 | Mota, J. P. B. | (3) 601 |
| Lown, E. M. | (4) 917 | Nagaishi, H. | (3) 426 |
| Machín, I. | (3) 678 | Neathery, J. K. | (4)1010 |
| Maciel Filho, R. | (3) 616 | Negulescu, I. I. | (4)1075 |
| Magnoux, P. | (3) 626 | Ng, F. T. T. | (3) 456 |
| Maier, W. F. | (3) 534 | Nishimiya, K. | (4)1125 |
| Majors, R. K. | (4) 975 | Norman, P. R. | (4) 885 |
| Mallinson, R. G. | (3) 490 | Nowlan, V. | (4) 929 |
| Man, C. K. | (4)1138 | Nunhez, J. R. | (3) 649 |
| Mangun, C. | (4) 880 | Odintsov, B. M. | (4) 955 |
| Marasteanu, M. O. | (4)1069 | Okuyama, Y. | (3) 707 |
| Markowitz, B. L. | (3) 585 | Olah, G. A. | (3) 526 |
| Maroto-Valer, M. M. | (4)1014 | Olson, E. S. | (3) 447 |
| Marran, D. F. | (4)1005 | Olson, E. S. | (4) 867 |
| Marsh, N. D. | (4) 990 | Orikasa, H. | (4) 852 |
| Marshall, W. E. | (4) 805 | Ovalles, C. | (3) 521 |
| Marshall, W. E. | (4) 810 | Páez, D. E. | (3) 563 |
| Martin, D. | (3) 626 | Painter, P. C. | (4) 913 |
| Martin, S. | (3) 538 | Palit, A. K. | (3) 392 |
| Martinez-Alonso, A. | (4) 829 | Panthaky, M. | (4) 844 |
| Mathews, J. P. | (3) 611 | Pantoja, F. | (3) 431 |
| Matos, J. | (4)1112 | Parfitt, D. | (3) 717 |
| Matsubara, K. | (3) 707 | Park, C. | (3) 368 |
| Matsuoka, K. | (4) 852 | Parker, R. J. | (4) 933 |
| Mayes, A. M. | (3) 606 | Parra, J. B. | (4)1120 |
| McCormick, C. J. | (4) 985 | Parra, J. B. | (4)1133 |
| McFarland, S. J. | (4)1090 | Patwardhan, S. R. | (4) 765 |
| McFarlane, R. A. | (3) 496 | Paul, S. F. | (3) 373 |
| McFarlane, R. A. | (4) 933 | Payzant, J. D. | (3) 526 |
| McGreavy, C. | (3) 635 | Peixoto, S. M. C. | (3) 649 |
| McGreavy, C. | (3) 653 | Peng, P. | (4) 917 |

AUTHOR INDEX, VOLUME 43, (ISSUE NUMBER) PAGE NUMBER

| | | | |
|---------------------------|---------|-----------------------|---------|
| Perot, G. | (3) 547 | Satou, M. | (3) 426 |
| Pickard, M. A. | (3) 515 | Scaroni, A. W. | (3) 611 |
| Pignon, H. | (4) 970 | Schaefer, J. L. | (4)1010 |
| Pilawa, B. | (4) 909 | Schobert, H. H. | (3) 461 |
| Pis, J. J. | (4) 820 | Schobert, H. H. | (3) 538 |
| Pis, J. J. | (4)1120 | Schukin, L. I. | (4) 838 |
| Pis, J. J. | (4)1133 | Schwarz, J. A. | (4) 833 |
| Plummer, M. | (3) 538 | Scott, C. E. | (3) 521 |
| Plummer, M. A. | (3) 552 | Serio, M. A. | (3) 585 |
| Poon, R. | (3) 451 | Serio, M. A. | (4)1005 |
| Poonphatanaricha, P. | (3) 490 | Sharma, A. | (4) 960 |
| Popper, G. A. | (3) 441 | Sharma, R. K. | (4) 801 |
| Prada, V. | (4) 941 | Sharma, R. K. | (4) 867 |
| Prakash, G. K. S. | (3) 526 | Shen, R. | (3) 481 |
| Que, G. | (3) 481 | Shi, B. | (3) 558 |
| Que, G.-H. | (3) 486 | Shim, H.-S. | (4) 965 |
| Que, G.-H. | (3) 530 | Shimizu, K. | (3) 699 |
| Que, G.-H. | (3) 558 | Siddiqui, M. N. | (4)1063 |
| Que, G.-H. | (3) 758 | Silveston, P. L. | (4) 844 |
| Quin, J. L. | (4) 900 | Simons, G. A. | (3) 585 |
| Rahimi, P. | (3) 476 | Singh, H. K. | (3) 447 |
| Rahimi, P. | (4) 929 | Slattery, D. K. | (3) 378 |
| Rathbone, R. F. | (4) 975 | Sobkowiak, M. | (4) 913 |
| Renou-Gonnord, M. F. | (4) 890 | Song, C. | (3) 552 |
| Reucroft, P. J. | (4) 785 | Soo, P. P. | (3) 606 |
| Revette, J. A. | (3) 563 | Soong, Y. | (3) 645 |
| Rivin, D. | (4) 785 | Stalzer, R. H. | (3) 441 |
| Robbins, J. L. | (3) 388 | Stastna, J. | (4)1026 |
| Robl, T. L. | (4) 985 | Steinberg, M. | (3) 412 |
| Rodriguez, N. M. | (3) 368 | Stella, A. | (3) 580 |
| Rolle, J. G. | (3) 727 | Stencel, J. M. | (3) 591 |
| Rood, M. J. | (3) 596 | Stencel, J. M. | (4)1010 |
| Rood, M. J. | (4) 814 | Strausz, O. P. | (3) 526 |
| Rostam-Abadi, M. | (3) 596 | Strausz, O. P. | (4) 917 |
| Rostam-Abadi, M. | (4) 871 | Su, M. | (4)1053 |
| Rubel, A. M. | (3) 591 | Subrenat, E. | (4) 875 |
| Rubiera, F. | (4)1120 | Subrenat, E. | (4) 970 |
| Rubiera, F. | (4)1133 | Subrenat, A. | (4) 875 |
| Rudina, N. A. | (4) 946 | Suelves, I. | (4) 857 |
| Russell, N. V. | (4)1000 | Suganuma, A. | (3) 699 |
| Russell, N. V. | (4)1138 | Sugaya, M. | (3) 635 |
| Sadoway, D. R. | (3) 606 | Sugaya, M. | (3) 653 |
| Saito, I. | (3) 699 | Sugaya, M. | (3) 684 |
| Sakanishi, K. | (4) 848 | Sun, J. | (3) 596 |
| Salanov, A. N. | (4) 946 | Suuberg, E. M. | (4) 980 |
| Sanada, Y. | (3) 543 | Takahashi, S. | (3) 741 |
| Sanada, Y. | (3) 735 | Takanohashi, T. | (3) 712 |
| Sánchez-Delgado, R. | (3) 563 | Tam, M. S. | (4) 825 |
| Sardesai, A. | (3) 722 | Tan, C. D. | (3) 368 |
| Sasaki, M. | (3) 552 | Tanner, D. | (3) 476 |
| Sasaki, S. | (3) 699 | Tascon, J. M. D. | (4) 829 |
| Sato, M. | (3) 735 | Taulbee, D. N. | (4)1014 |
| Sato, Y. | (3) 658 | Taylor, R. | (4)1031 |
| Sato, Y. | (3) 703 | Thomas, A. | (3) 466 |
| Sato, Y. | (3) 707 | Tierney, J. W. | (3) 421 |

AUTHOR INDEX, VOLUME 43, (ISSUE NUMBER) PAGE NUMBER

| | | | |
|-------------------------|----------|----------------------|----------|
| Timpe, R. C. | (4) 801 | Yoneda, T. | (3) 735 |
| Toles, C. A. | (4) 805 | Yoshida, T. | (3) 426 |
| Toles, C. A. | (4) 810 | Yoshikawa, M. | (4) 848 |
| Tomita, A. | (4) 852 | Young, B. C. | (3) 407 |
| Tomita, A. | (4) 960 | Youtcheff, J. | (4) 1037 |
| Trahan, A. D. | (4) 796 | Yu, Z. | (4) 905 |
| Vartapetjan, R. S. | (4) 838 | Zanzotto, L. | (4) 1026 |
| Vassilev, S. | (4) 857 | Zarochak, M. F. | (3) 645 |
| Vayenas, C. G. | (3) 663 | Zhai, H. | (4) 1041 |
| Verkade, J. G. | (4) 905 | Zhan, X. | (3) 501 |
| Vladea, R. V. | (4) 844 | Zhang, H.-Y. | (3) 486 |
| Vogel, C. | (3) 403 | Zhang, H.-Y. | (3) 530 |
| Walsh, P. M. | (3) 611 | Zhang, J. | (3) 746 |
| Wang, Z.-X. | (3) 486 | Zhang, S. | (3) 421 |
| Wang, Z.-X. | (3) 530 | Zheng, H. | (3) 668 |
| Wang, Z.-X. | (3) 758 | Zhou, P. | (3) 441 |
| Warzinski, R. P. | (3) 694 | Zondlo, J. | (4) 790 |
| Wender, I. | (3) 421 | | |
| Wertz, D. L. | (4) 796 | | |
| Wertz, D. L. | (4) 900 | | |
| White, R. | (3) 727 | | |
| Wieckowski, A. B. | (4) 909 | | |
| Williams, C. | (4) 1037 | | |
| Williamson, J. | (4) 1000 | | |
| Williamson, J. | (4) 1138 | | |
| Wójtowicz, M. A. | (3) 585 | | |
| Wójtowicz, M. A. | (4) 1005 | | |
| Wornat, M. J. | (4) 990 | | |
| Wu, Q. | (3) 515 | | |
| Xiao, X. | (3) 421 | | |
| Xu, C. | (3) 668 | | |
| Xu, C. | (3) 673 | | |
| Xu, C. | (3) 746 | | |
| Xu, C. | (3) 751 | | |
| Xu, X. | (3) 363 | | |
| Xu, Y. | (4) 790 | | |
| Yagelowich, M. | (3) 447 | | |
| Yamaguchi, H. | (3) 703 | | |
| Yamaguchi, H. | (3) 707 | | |
| Yamane, T. | (4) 1125 | | |
| Yang, C. | (3) 668 | | |
| Yang, C. | (3) 673 | | |
| Yang, C. | (3) 746 | | |
| Yang, C. | (3) 751 | | |
| Yang, M.-G. | (3) 471 | | |
| Yang, N. | (4) 965 | | |
| Yao, D. | (4) 1053 | | |
| Yasutake, A. | (4) 848 | | |
| Yatsunami, S. | (4) 848 | | |
| Yee, E. C. | (4) 1115 | | |
| Yeh, P.-H. | (4) 1075 | | |
| Yermakov, D. Yu. | (4) 946 | | |
| Yermakova, M. A. | (4) 946 | | |
| Yiokari, C. G. | (3) 663 | | |
| Yoneda, T. | (3) 543 | | |